Homogeneous Transition Metal Catalyzed Reactions

Homogeneous Transition Metal Catalyzed Reactions

William R. Moser, EDITOR
Worcester Polytechnic Institute

Donald W. Slocum, EDITOR
Western Kentucky University

Developed from a symposium sponsored
by the Catalysis and Surface Science Secretariat
of the American Chemical Society

American Chemical Society, Washington, DC 1992

The paper used in this publication meets the minimum requirements of American National
Standard for Information Sciences—Permanence of Paper for Printed Library Materials, ANSI
Z39.48–1984.   ∞

American Chemical Society
Library
1155 16th St., N.W.
Washington, D.C. 20036

FOREWORD

The ADVANCES IN CHEMISTRY SERIES was founded in 1949 by the American Chemical Society as an outlet for symposia and collections of data in special areas of topical interest that could not be accommodated in the Society's journals. It provides a medium for symposia that would otherwise be fragmented because their papers would be distributed among several journals or not published at all.

Papers are reviewed critically according to ACS editorial standards and receive the careful attention and processing characteristic of ACS publications. Volumes in the ADVANCES IN CHEMISTRY SERIES maintain the integrity of the symposia on which they are based; however, verbatim reproductions of previously published papers are not accepted. Papers may include reports of research as well as reviews, because symposia may embrace both types of presentation.

ABOUT THE EDITORS
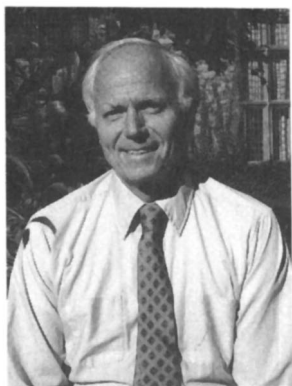
WILLIAM R. MOSER is a professor of chemical engineering at the Worcester Polytechnic Institute (WPI). He received his Ph.D. from the Massachusetts Institute of Technology and a B.S. in chemistry and mathematics from Middle Tennessee State University. He is also a member of the Center for Inorganic Membrane Studies at WPI. During the past 28 years his research interests in the catalytic sciences have included homogeneous and heterogeneous catalysis, novel materials synthesis, and in situ reaction monitoring. He is the inventor of cylindrical internal reflectance reactors (CIR reactors) and optical fiber coupled CIR reactors (OFCIR reactors) for in situ chemical reaction monitoring, and the high-temperature aerosol decomposition process for metal oxide synthesis of ceramics, catalysts, and superconductors. Moser is a fellow of the New York Academy of Sciences and is a co-founder of the Organic Reactions Catalysis Society. He is currently chairman-elect of the ACS Division of Petroleum Chemistry, Inc. He is editor of several books on homogeneous and heterogeneous catalysis and has a variety of publications and patents in the catalysis, zeolite, and materials science fields.
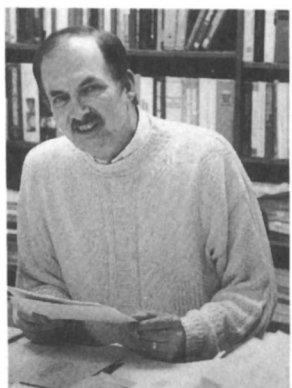
DONALD W. SLOCUM was awarded his Ph.D. in chemistry from New York University after obtaining a B.S. in chemistry and a B.A. in English from the University of Rochester. He served as a research associate at Duke University, assistant professor of chemistry at Carnegie Institute of Technology, full professor of chemistry at Southern Illinois University, and head of the Department of Chemistry at Western Kentucky University. He has been a senior scientist at Gulf Research and Development Company, program director of the Chemical Dynamics Section of the National Science Foundation, and program leader in the Division of Educational Programs at Argonne National Laboratory. His visiting academic appointments include

the University of Illinois, University of Bristol, University of Cincinnati, Carnegie–Mellon University, and University of Pittsburgh. Slocum is the author of many publications. He has organized and coordinated international scientific meetings and has directed a large academic research program and a venture industrial research program. He is a member of the American Association for the Advancement of Science, the American Chemical Society (1991 secretary general of the Catalysis and Surface Science Secretariat), the Chemical Society of Great Britain, Phi Lambda Upsilon, and Sigma Xi.

PREFACE

HOMOGENEOUS CATALYSIS is now a relatively mature field with numerous and diverse reactions being explored alongside informative studies of mechanism and theory. Relationships to important areas such as heterogeneous catalysis, organometallic chemistry, and biocatalysis have been firmly established. From a personal perspective, the field of transition metal homogeneous catalysis has grown dramatically since we organized our first conference and volume in this area (*The Place of Transition Metals in Organic Synthesis*, New York Academy of Sciences, Volume 295, 1977) and has made impressive advances since our last conference and volume for the New York Academy (*Catalytic Transition Metal Hydrides*, New York Academy of Sciences, Volume 415, 1983).

Homogeneous catalysis remains a relatively untapped resource whose importance cannot be overestimated. As industry becomes more oriented toward specialty chemicals, methods to catalyze functional group transformations, hydrocarbon activations, polymerizations, and inductions of asymmetry will be increasingly in demand. Also, catalysis in general needs a wider dissemination in graduate schools, with some introduction to the subject at the advanced undergraduate level. Therefore, we hope that this Advances in Chemistry volume will become a valuable resource not only to practitioners in the field but also to educators not necessarily in the field.

During the organization of the symposium on which this book is based, we contacted and received replies from both Professor John Stille, Colorado State University, and Professor Piero Pino, Eidgenossische Technische Hochschule, shortly before their untimely deaths. Both had been forces in the field of homogeneous catalysis for many years. They shall be missed.

DONALD W. SLOCUM
Western Kentucky University
Bowling Green, KY 42101

WILLIAM R. MOSER
Worcester Polytechnic Institute
Worcester, MA 01609–5250

November 1991

1

Reaction Monitoring by High-Pressure Cylindrical Internal-Reflectance and Optical-Fiber Coupled Reactors

William R. Moser

Department of Chemical Engineering, Worcester Polytechnic Institute, Worcester, MA 01609

The development of high-pressure, well-stirred cylindrical internal-reflectance (CIR) reactors for infrared reaction monitoring provided an unusual capability for examining the contents of high-pressure reactors under typical commercial conditions for many processes. The reactors utilize a crystal of a high-performance ceramic such as zinc selenide, silicon, or zinc sulfide. The crystal is mounted directly within the high-pressure zone of the chemical reaction. Through an IR beam directed into one end of the crystal, an attenuated total reflectance (ATR) analysis of the reactor contents is obtained. The technique was used for reaction monitoring up to 100 atm (10.1 MPa) for the in situ analysis of several homogeneous catalyzed chemical processes, hydrothermal zeolite synthesis, and heterogeneous metal-catalyzed reactions. The most recent development in the technology uses optical-fiber CIR (OFCIR) coupled high-pressure reactors to achieve, in addition, truly remote sensing.

T HE OBJECTIVE OF ANY REACTION-MONITORING TECHNIQUE is to examine the desired chemical reaction under a specific set of reaction conditions without disturbing the contents of the reactor in any way. Some basic parameters that should not be disturbed by the monitoring technique are pressure, temperature, and efficient stirring. For liquid-phase reactions, a general technique must also be able to monitor reactions in corrosive solvents, dilute or concentrated solutions, reactions containing suspended solids, and strongly absorbing solvents. Few reaction-monitoring techniques described in the literature meet these specifications.

High-pressure, well-stirred autoclaves equipped with cylindrical internal-reflectance crystals embedded in their high-pressure reaction zone for infrared analysis (CIR reactors) were first described (*1–3*) in the mid-1980s. Their reaction-monitoring capabilities meet most of these criteria. Following the design, fabrication, and testing of several reactor configurations (*1*), the low-volume (30-mL) reactor shown in Figure 1 was designed and used for most of the reaction-monitoring studies undertaken in this laboratory.

Figure 1. Cylindrical internal-reflectance (CIR) reactor, showing the 50-mL internal-volume autoclave equipped with a high-speed stirrer, thermocouple, high-pressure gauge, base-mounted cartridge heater, and high-pressure seal for the cylindrical internal-reflectance crystal.

The schematic view shown in Figure 2 illustrates the high-speed stirring facilities and pressure closure for the crystal used by the CIR reactors to provide instantaneous in situ analyses. Although CIR reactors have been used mainly for IR analysis, studies of cobalt-catalyzed carbonylation of methanol (*4*) showed that the visible region of the spectrum could also be analyzed to provide information on catalyst compositions.

Techniques previously described in the literature for high-pressure in situ reaction monitoring of homogeneous metal-catalyzed reactions by infrared spectroscopy were mainly based on transmission cells (*5–10*). With this type of equipment, the homogeneous catalyst solution was either purged from a high-pressure autoclave into a high-pressure transmission cell (*5, 8, 10*) or internally recycled from an autoclave through a high-pressure cell of short path length (*7, 9*).
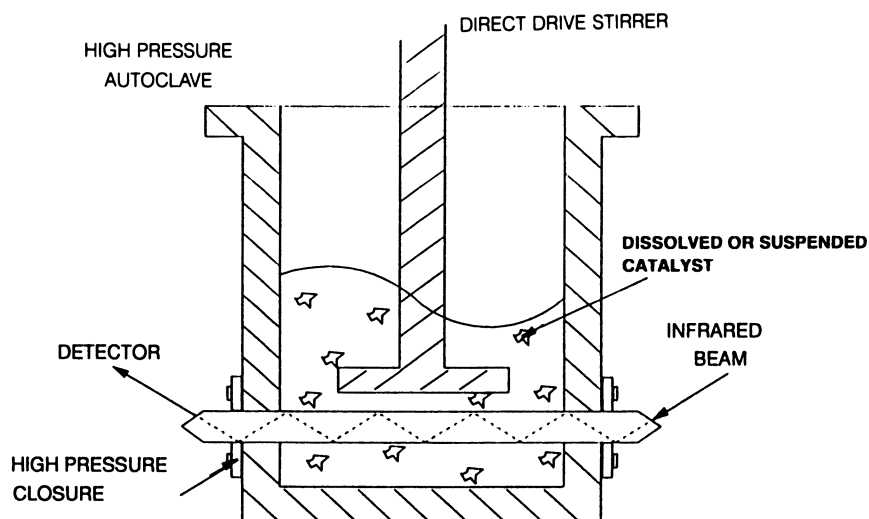
Figure 2. Cross-sectional view of a CIR reactor with high-pressure closure for a cylindrical internal-reflectance crystal. The crystal, commonly fabricated from ZnSe, ZnS, Si, or Ge, is polished and conical at each end.

The transmission method works exceptionally well for reactions in solvents that are not strongly absorbing and for homogeneous catalysis solutions in which the catalyst is in exceptionally low concentration. Often important regions of the spectra are obscured in high-pressure studies by either dissolved gases or gas bubbles. Because the transmission cell is not located directly within the stirred reaction zone, the method may not always give an instantaneous view of the reactor contents.

The wide range of studies using CIR reactors in the monitoring of homogeneous catalyzed reactions, zeolite synthesis, and heterogeneous gas–solid reactions have demonstrated that the reactors

- lead to truly in situ results in equipment that provides excellent mixing;
- are able to provide analyses in strongly absorbing solvents such as water or acetic acid;
- provide analyses that show no path-length dependence on pressure and little on temperature; and
- are exceptionally easy to run and to obtain instantaneous analyses as the reaction parameters are altered.

The CIR reactors have few disadvantages. Most important, the smaller-diameter crystals used in the low-volume reactors shown in Figure 1 are fragile, especially ZnSe, unless they are initially mounted with care and not

heated too rapidly during the catalytic investigation. The only other disadvantage appears in monitoring the synthesis of zeolites or other chemical reactions where the solution pH is above 12. In these cases all of the commonly available crystals become etched, leading to loss of signal. The most corrosive acidic conditions we have employed, HI in aqueous acetic acid–methanol solutions, are easily handled by using a silicon crystal. Zinc selenide works well for most acidic solutions. Its advantage over silicon is its useful IR spectral range (4000–700 cm^{-1}). The range achieved by using silicon is 4000–1400 cm^{-1}.

Experimental Procedure

The CIR reactors used in these studies were fabricated from corrosion-resistant 316 stainless steel and were equipped with a variable-speed direct-drive stirrer, thermocouple within the reacting solution, high-pressure gas valves, and high-pressure gauge. The internal volume of the autoclave was 50 mL, and the total volume of solutions studied was usually 10–15 mL. The autoclave was heated by two cartridge heaters built directly into the body of the reactor, and the temperature was controlled by a thermocouple mounted within this same part of the autoclave.

The CIR crystal was mounted within the reactor by high-pressure closures as shown in Figure 1 and usually used poly(tetrafluoroethylene) (Teflon) O-rings within the fastening mechanism. The autoclaves were fabricated according to our design by Parr Instrument Company (Moline, IL) and were obtained from Spectra-Tech (Stamford, CT). The silicon, zinc selenide, or zinc sulfide crystals used in these studies were obtained from Spectral Systems (Irvington, NY), Harrick Scientific Corporation (Ossining, NY), or Spectra-Tech (Stamford, CT).

Crystals that lose their polish through either long use or chemical attack could be repolished through the application of a commercial toothpaste and polishing with a soft cloth. More corroded surfaces were repolished by the application of a commercial polishing-grade alumina with the crystal mounted on a lathe.

The optical-fiber cylindrical internal-reflectance (OFCIR) reactor (11) was operated by directing an IR beam into a chalcogenide fiber obtained from Galileo Electro-Optics Corporation (Sturbridge, MA). The beam was transmitted in the 4000–850-cm^{-1} spectral region directly into a CIR crystal fabricated out of either zinc selenide or silicon. The opposite end of the crystal was coupled to another optical-fiber cable, which was coupled to a mercury–cadmium telluride (MCT) A detector.

The dried CIR reactors were filled with catalysts, solvents, and any liquid or solid reactants in a dry box; closed; and then mounted within the sampling compartment of a mid-infrared-range spectrometer (Nicolet 60SX). After pressurization of the reactor with gaseous reactants, spectral data were collected at four-wavenumber resolution by using an MCT A or B detector. Spectra were taken at various time intervals, as dictated by the kinetics of the reaction. Instantaneous concentrations of reactants, products, and metal-containing intermediates were usually determined by comparison to calibration standards of these materials, matched to the temperature of the reaction under study. In some cases liquid samples were withdrawn from the reactor under pressurized conditions. This procedure permitted gas chromatographic data to be collected

for species determinations that were not easily done by IR spectroscopy, such as the determination of linear-to-branched aldehyde ratios in the hydroformylation studies.

Reaction Mechanisms and Reaction Monitoring by CIR–FTIR Reactors

Since our initial 1984 description of the design of the CIR reactors and their capabilities for reaction monitoring, they have been used in our laboratory for examining the mechanisms of several homogeneous catalyzed reactions. These studies include

- the phosphine-modified rhodium-catalyzed hydroformylation of olefins (*12*);
- the phosphine-modified palladium-catalyzed carbonylation of aryl halides to aromatic esters (*13*, *14*) and the double carbonylation of aryl halides affording α-keto esters (*15*);
- the mechanism of the cobalt-catalyzed carbonylation of methanol to form methyl acetate (*16*);
- the cobalt-catalyzed hydroformylation of olefins (*17*); and
- the cobalt-catalyzed oxidation of substituted alkyl aromatics (*17*).

The reactors were successfully used in examining synthetic phosphoaluminate (ALPO) molecular sieve syntheses by comparing the effects of templates such as triethanolamine, tripropylamine, dipropylamine, and isopropylamine (*18*) on zeolite formation. In addition, monitoring of the synthesis of the synthetic zeolite, ZSM-5, was successful with a modified synthesis technique that avoids high pH conditions (*1*).

Another design of CIR reactor has a small annular space around the CIR crystal, where the catalyst was tightly packed (*19*). This apparatus made possible high-pressure Fourier transform infrared (FTIR) monitoring of heterogeneous catalyzed reactions, such as the reaction of synthesis gas (syngas) or pure CO with 2% rhodium on alumina or silica. Recently developed high-temperature seals led to high-quality monitoring of the reaction of butane with a solid-state P–V–O catalyst for the formation of maleic anhydride. Finally, the stirred CIR reactors were used to follow the course of the soluble reactants and gel formation in a typical sol–gel synthesis of metal oxides in the formation of solid-state inorganic metal oxides.

Reaction Monitoring of Homogeneous Metal-Catalyzed Reactions.   Mechanistic studies of homogeneous catalyzed reactions by in situ reaction-monitoring techniques such as CIR reactors or transmission reactors

are principally based on the observation of certain coordination compounds under a variety of autogenous reaction conditions. Positive identification of a specific coordination compound under autogenous conditions is taken as evidence of the possibility that it is an intermediate that participates in one of the elementary reactions contained within the catalytic cycle.

However, observation of a specific coordination compound alone does not permit its unequivocal assignment as an intermediate within the catalytic cycle. It may be an exceptionally stable compound that lies outside of the catalytic cycle and merely serves as a reservoir for the intermediates within the cycle. The assignment of a species as a participant in the catalytic cycle must be made with caution. When possible, it must be verified with simultaneous kinetic experiments, parallel stoichiometric reactions that involve the species, and reaction perturbation by altering the reaction parameters to determine whether the slate of observable intermediates changes in a way that can be logically predicted by any proposed reaction mechanism.

In the studies described here the homogeneous catalyzed reaction was conducted under steady-state temperature, pressure, and concentration conditions that are as similar as possible to those used in a commercial process. Then reaction parameters were altered in an attempt to change the slate of observable species. After this information was accumulated, various reaction mechanisms were postulated on the basis of observable intermediates and prior teachings of coordination chemistry.

When several reactants were fed to the reactor, the concentration of each reactant was individually varied from normal to low in an attempt to force the elementary reaction involving that material and metal complex to become the slow step. For an intermediate within the catalytic cycle, the rate of the reaction involving this species is often sufficiently slowed to allow its observation in the reaction solution.

A basic assumption in this analysis is that if a specific coordination compound is observed in solution during the in situ reaction-monitoring experiment, only two conclusions are permissible:

1. The species is not within the catalytic cycle, is catalytically inactive as such, and may serve as a reservoir for the various species within the catalytic cycle.

2. The species is within the catalytic cycle and participates in an elementary reaction. Kinetically, it is either one of the slow steps in the process under the given set of reaction conditions or a complex in equilibrium with a species that participates in the rate-limiting step.

The following examples summarize some of the particular advantages of CIR reactors for in situ reaction monitoring of homogeneous metal-catalyzed processes.

Mechanism of the Palladium-Catalyzed Carbonylation of Aryl Halides. The approach used in the investigation of homogeneous catalytic mechanisms is illustrated by the phosphine-modified carbonylation of bromobenzene in methanol under CO pressure to produce methyl benzoate. Stoichiometric studies with CIR reactors suggested the catalytic cycle shown in Scheme I (*13*). Compounds 1 and 3, two of the stable, well-characterized species shown in the catalytic cycle, were synthesized. Their stoichiometric reactions with each of the compounds were studied under a variety of conditions.
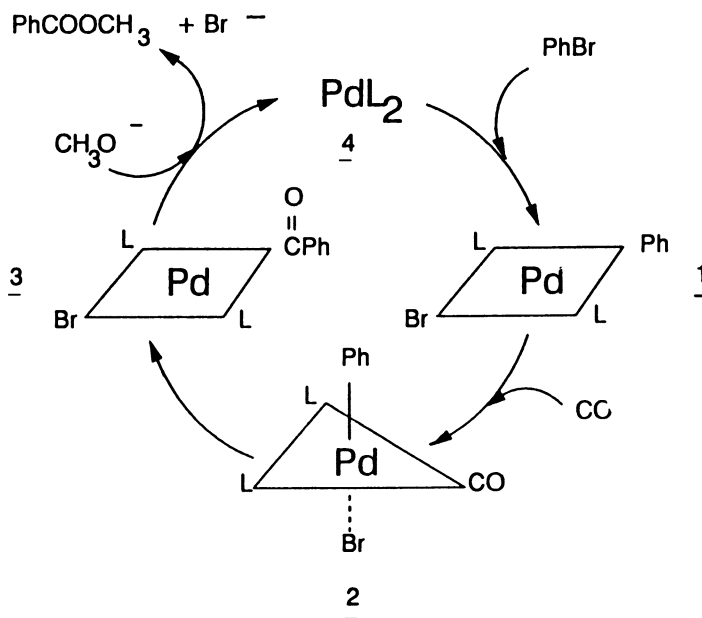
Scheme 1. Proposed mechanism for the phosphine-modified, palladium-catalyzed reaction of CO with aryl halides in alcohols to produce aromatic esters (13–15).

Then the reaction was carried out under typical catalytic conditions with all reactants in large excess and at temperatures and pressures appropriate for obtaining high rates of methyl benzoate formation at steady state. Under these conditions, the steady-state in situ spectrum shown in Figure 3 was obtained. The quality of the displayed spectrum is typical of CIR reactor experiments, even at much higher pressures (100 atm, 10.1 MPa).

An expansion of the spectrum in the 1500–1800-cm^{-1} IR region demonstrated no acyl metal frequencies and showed only bands for bromobenzene at 1578 cm^{-1} and for triphenylphosphine–palladium compounds, PdL$_{(4-x)}$, at 1583 cm^{-1}. When the methanol concentration was reduced from
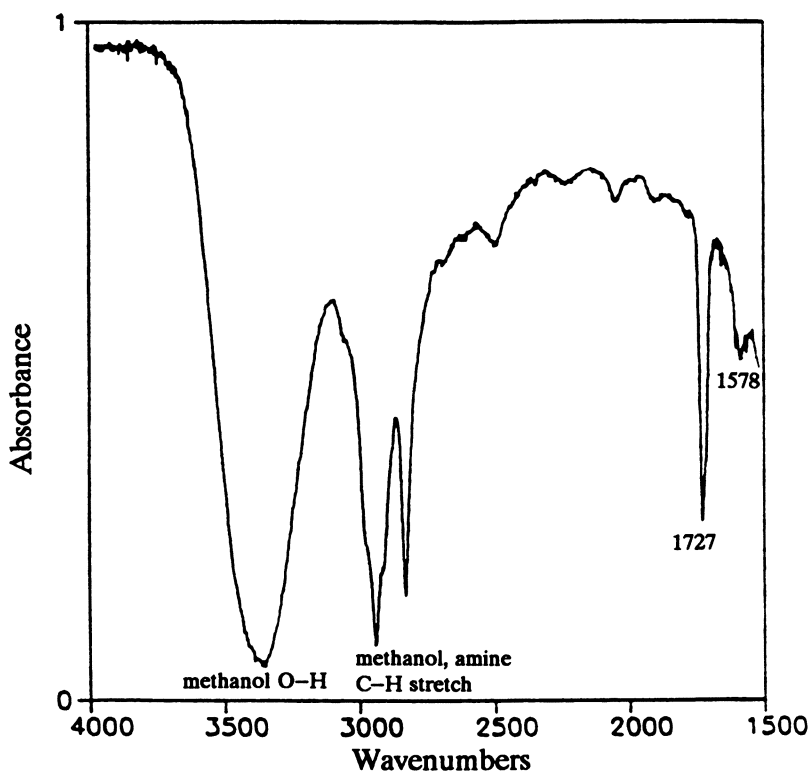
Figure 3. In situ CIR catalytic reaction of a 10-mL solution of bromobenzene, 1 M; triethylamine, 1 M; methanol, 18.7 M; palladium acetate, 0.05 M; and triphenylphosphine, 0.20 M; under 40 psig (0.28 MPa) of carbon monoxide at 90 °C. Spectra were recorded at 4-cm^{-1} spectral resolution using 500 signal-averaged scans. Methyl benzoate appears in the spectrum at 1727 cm^{-1} and bromobenzene at 1578 cm^{-1}.

18.7 to 1 M, the overall rate of methyl benzoate formation decreased and the in situ spectrum exhibited the acyl absorption at 1648 cm^{-1} for the palladium acyl complex 3, as seen in Figure 4. When all of the normal reactant concentrations were used in experiments except for the exclusion of CO, the in situ spectrum (not shown) exhibited only bands for the palladium–aryl complex 1 at 1562 cm^{-1}.

The results of these studies were combined with those of kinetic studies on both stoichiometric and catalytic reactions. Amine and methanol were both clearly required in the step involving the conversion of the metal acyl 3 to methyl benzoate. The kinetic data were gathered by directly observing the concentrations of all of the subject species by the CIR technique. This method usually reveals the instantaneous concentrations of reactants, products, and the dominant or competing catalytic intermediates simultaneously.
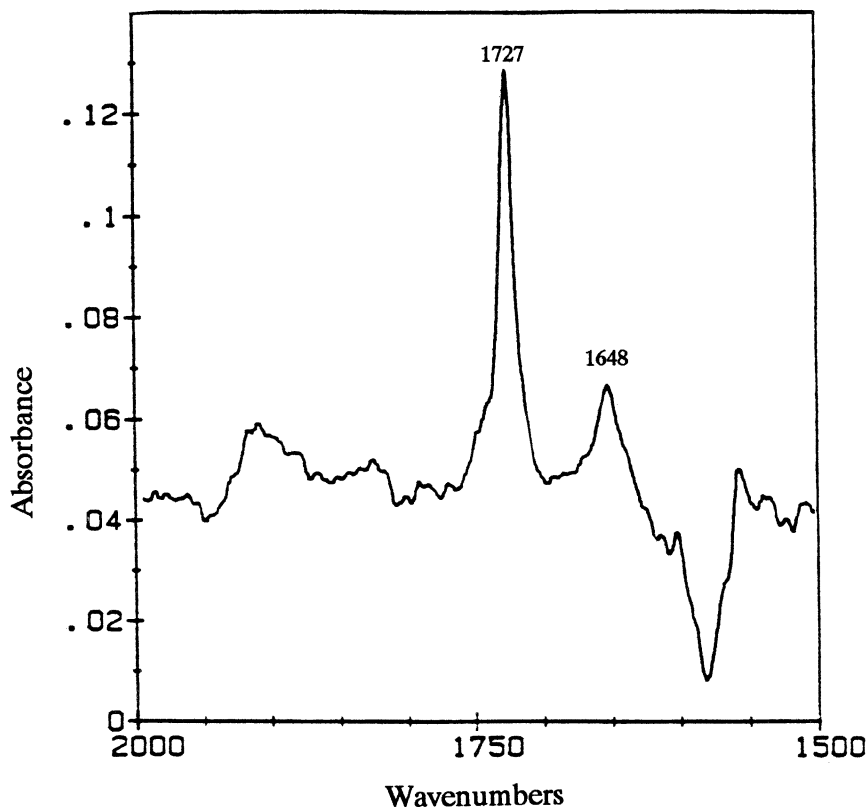
Figure 4. Difference spectrum (ratio of steady state to initial solution) of in situ CIR steady-state catalytic reaction in 1 M methanol (i.e., low concentration); bromobenzene, 1 M; triethylamine, 1 M; palladium acetate, 0.05 M; and triphenylphosphine, 0.20 M; in benzene under 40 psig (0.28 MPa) of carbon monoxide at 90 °C. The CIR reactor spectra were measured as described in Figure 3.

Mechanism of the Phosphine-Modified Rhodium-Catalyzed Hydroformylation of Olefins.

Mechanistic studies of the phosphine-modified rhodium-catalyzed oxo reaction (12) illustrate a particular feature of the CIR reactor analyses that may be either an advantage or a disadvantage. The initial mechanistic study of this system involved a typical hydrocarbon solvent system that had been widely reported in the literature. Its kinetics data, the effects of P/Rh ratios, reactant gas pressures, and structures of various phosphines were related to the activity and selectivity of the rhodium catalyst system.

For our studies of this system we used 1-hexene in an isooctane solvent. The resulting reaction rates were 4.3 times slower when we used triphenylphosphine as a ligand than rates for the identical reaction in dichloroethane.

The in situ CIR results on the isooctane system (Figure 5) show an intensity of IR bands in the carbonylrhodium absorption region of 1950–2150 cm^{-1} for the observable catalyst that was much stronger than the intensity of the bands for either the olefin or the product aldehyde, which were in much higher concentrations. This result is in sharp contrast to the results of reactions carried out in dichloroethane (Figure 6), where the carbonylrhodium bands in the same spectral region were much weaker. At the end of the isooctane study reaction, a careful examination of the crystal revealed a fine layer of crystallized material that was identified as the yellow dimer, [Rh(CO)$_2$L$_2$]$_2$.

This example illustrates a benefit of the CIR technique. In most cases one may detect the presence of a catalyst that becomes insoluble during the reaction because the high concentration of the complex near the face of the crystal leads to unreasonably high absorption bands. This boundary effect is normally not a problem in soluble-system CIR reactor analyses because the depth of penetration per reflection is typically in the range of 1–1.2 μm for most solutions.

On the other hand, a small amount of a complex may crystallize and shield the analysis of the reactor contents. Worse, an inactive complex may appear in the IR spectrum as a normally intense band, which could lead to
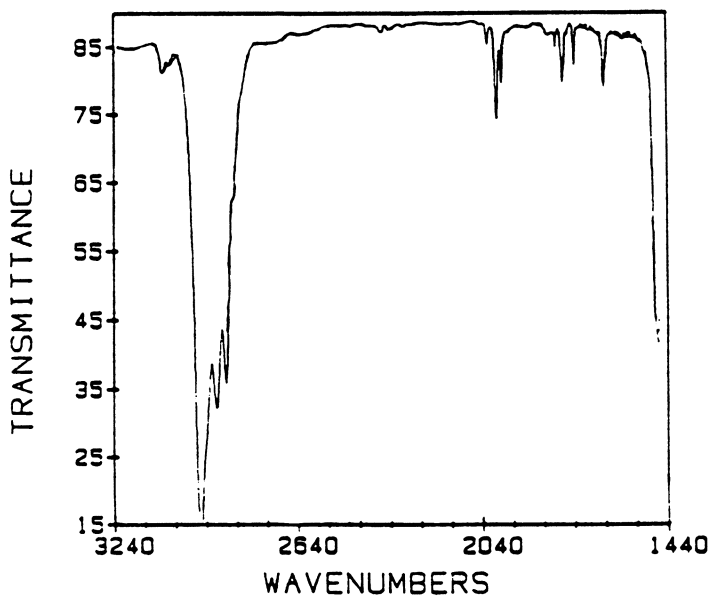

Figure 5. In situ CIR broad-band spectrum of a steady-state, active hydroformylation reaction in isooctane at 70 °C under 200 psi (1.38 MPa) of 1:1 H$_2$–CO at low olefin conversion. The solution charged to the reactor was initially RhH(CO)$_2$(PR$_3$)$_2$, 0.010 M; triphenylphosphine, 0.060 M; and 1-hexene, 1.372 M; in isooctane solvent.
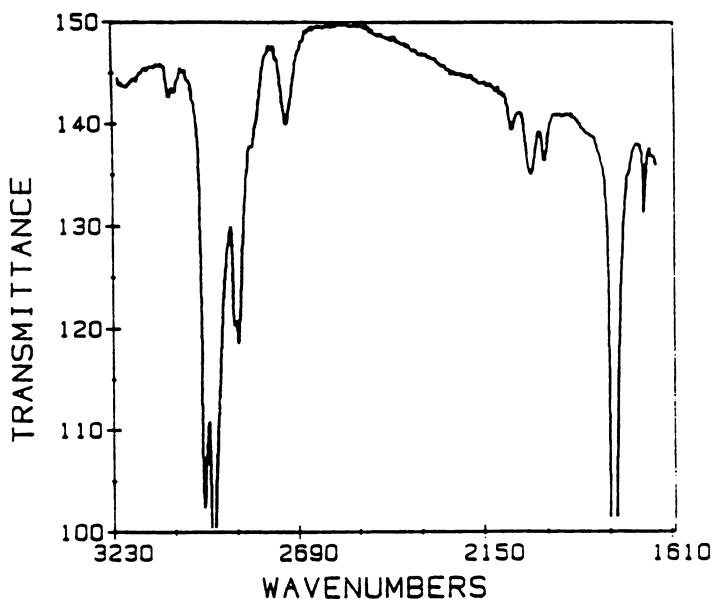
Figure 6. In situ CIR broad-band spectrum of a steady-state, active hydro-formylation reaction in dichloroethane at 70 °C under 200 psi (1.38 MPa) of 1:1 H₂–CO at low olefin conversion. The solution charged to the reactor was initially RhH(CO)₂(PR₃)₂, 0.010 M; triphenylphosphine, 0.060 M; and 1-hexene, 1.372 M; in dichloroethane solvent.

its erroneous assignment as a solution species. This problem can often be solved by a careful examination of all postreaction solutions, alteration of the reaction conditions during the in situ study to observe disappearance of the species, kinetic studies on the stoichiometric reaction using the subject complex, or all of these procedures.

A further example of the advantages of CIR in situ analyses was illustrated in another rhodium-catalyzed oxo study (*20*) of deactivation. It was shown that the kinetics of reactant disappearance and product appearance could be rapidly and reliably monitored while the composition of the catalyst is monitored. By using this technique, the changes in the instantaneous rate of olefin disappearance were monitored while the changes in the rhodium species composition were observed. In this case the rate slowed and eventually became zero after several hours under autogenous conditions while the catalyst made transitions between three complexes that were progressively less active.

Mechanism of the Cobalt-Catalyzed Hydroformylation of Olefins. Data on the cobalt-catalyzed hydroformylation of 1-hexene are presented here to illustrate the point that the contents of the reactor may be

monitored rapidly. The results may be used to answer current mechanistic questions concerning homogeneous catalyzed reactions that are difficult to answer by other means. Figure 7 illustrates the reaction concentration versus time profile for the carbonylcobalt species, olefin disappearance, and aldehyde formation when 1-hexene was converted to heptaldehyde under syngas by cobalt catalysis.
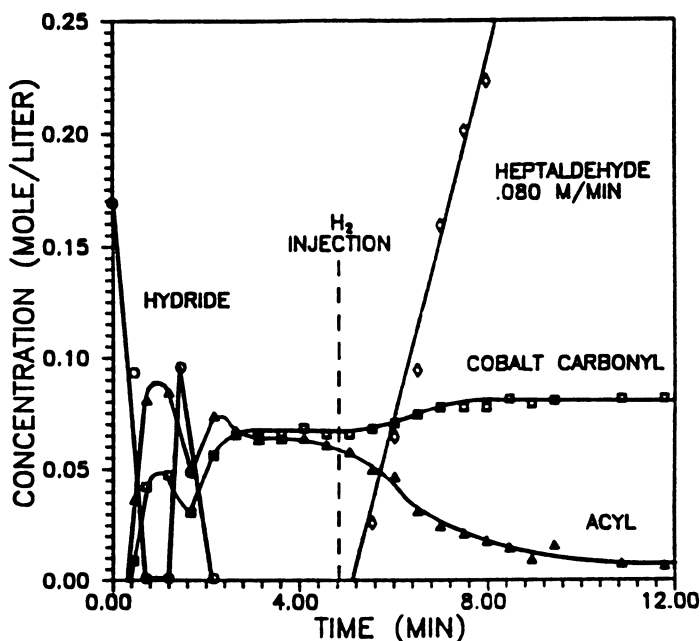

Figure 7. Reaction profile of cobalt-catalyzed hydroformylation of 1-hexene under 600 psi (4.14 MPa) of CO and 400 psi (2.76 MPa) of hydrogen, at 90 °C in a decane solvent. $HCo(CO)_4$ was injected at time zero to provide an initial cobalt concentration of 0.18 M under 600 psi (4.14 MPa) of pure CO. At 1.2 min, an equal amount of $HCo(CO)_4$ was again injected. At 4.8 min, 400 psi (2.76 MPa) of hydrogen was injected under pressure into the reactor.

The experiment reported in Figure 8 was carried out by heating a 1-hexene solution in decane under 600 psi (4.14 MPa) of pure CO at 90 °C in a CIR reactor. Then a solution of $HCo(CO)_4$ in decane was injected into the reactor under these conditions at time zero, and the CIR–FTIR spectra were recorded at 30-s intervals. These data show a rapid decrease in the concentration of $HCo(CO)_4$ with the simultaneous formation of the acyl cobalt species, $C_6H_{13}COCo(CO)_4$ and $Co_2(CO)_8$. At 1.2 min into the reaction another portion of the $HCo(CO)_4$ solution was injected into the reactor. The composition of the autoclave was monitored at 30-s intervals.

The key mechanistic information provided by these experiments was the fact that no heptaldehyde was formed in the two regions of the profile
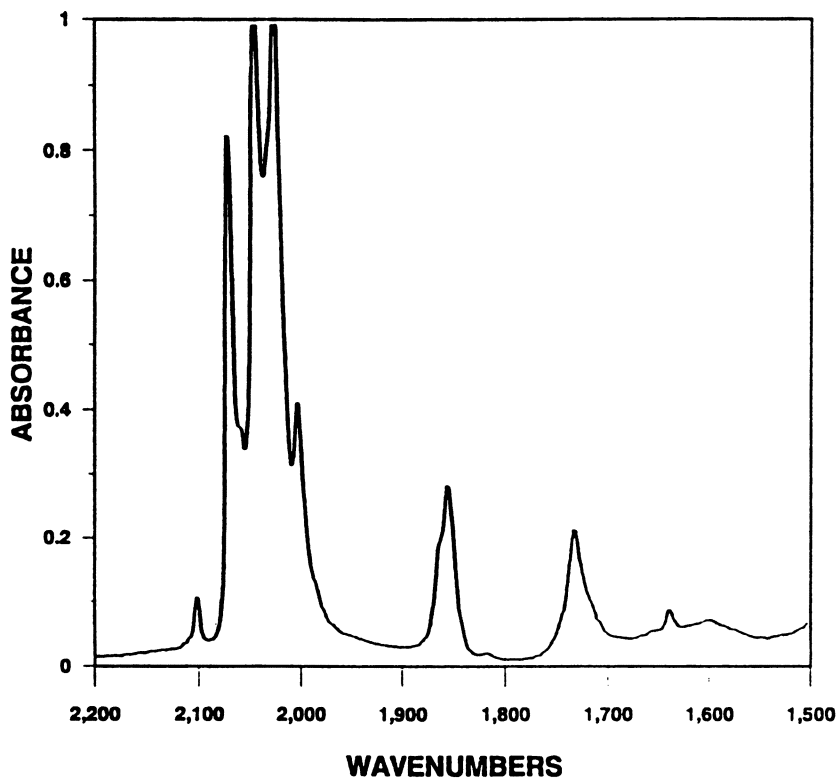
Figure 8. In situ CIR medium-range spectrum of a steady-state, active cobalt-catalyzed hydroformylation reaction at 50 °C and a constant syngas pressure of 1200 psi (8.28 MPa) of 2:1 H_2–CO. 1-Hexene, 1.85 M in decane, 10 mL, was heated to reaction temperature. At that point HCo(CO)$_4$ was injected to give an initial solution of 0.15 M. Absorption bands at 2104 cm^{-1} are due to the acyl tetracarbonylcobalt, those at 1867 cm^{-1} show the bridging carbonyls in octacarbonyldicobalt, heptaldehyde appears at 1724 cm^{-1}, and 1-hexene appears at 1641 cm^{-1}.

where both $HCo(CO)_4$ and $C_6H_{13}COCo(CO)_4$ were observed at high concentrations (i.e., 0.0–0.6 and 1.2–2.0 min). At 4.8 min hydrogen (400 psi, 2.76 MPa) was injected under pressure into the reactor. Heptaldehyde was immediately formed, and its rate remained constant over the next 20 min. Furthermore, in this region where catalysis is rapid, the concentration of $C_6H_{13}COCo(CO)_4$ is low but observable; in contrast, $HCo(CO)_4$ could not be detected. This situation is illustrated in the steady-state spectra at a reaction time of ~12 min into the profile (Figure 8). These data strongly suggest that the reaction of acyl cobalt species with $HCo(CO)_4$ is very slow, compared to the reaction of hydrogen with the acyl complex. Thus, an important step in the formation of aldehyde in cobalt-catalyzed hydroformylation is the direct hydrogenation of the acyl cobalt species.

Reaction Monitoring by OFCIR Reactors.   In collaboration with Galileo Electro Optics, we developed a new method of remote sensing that uses optical fibers coupled to a CIR reactor (*11*). This equipment consists of linking a mid-infrared-transmitting optical-fiber bundle with both the inlet and exit of the CIR crystal. The inlet is connected to the IR source and the exit to the detector. This equipment was used in monitoring the cobalt-catalyzed hydroformylation of 1-hexene, and a typical steady-state spectrum at 50 °C and 1000 psi (6.9 MPa) of syngas (2:1 H_2–CO) is illustrated in Figure 9.
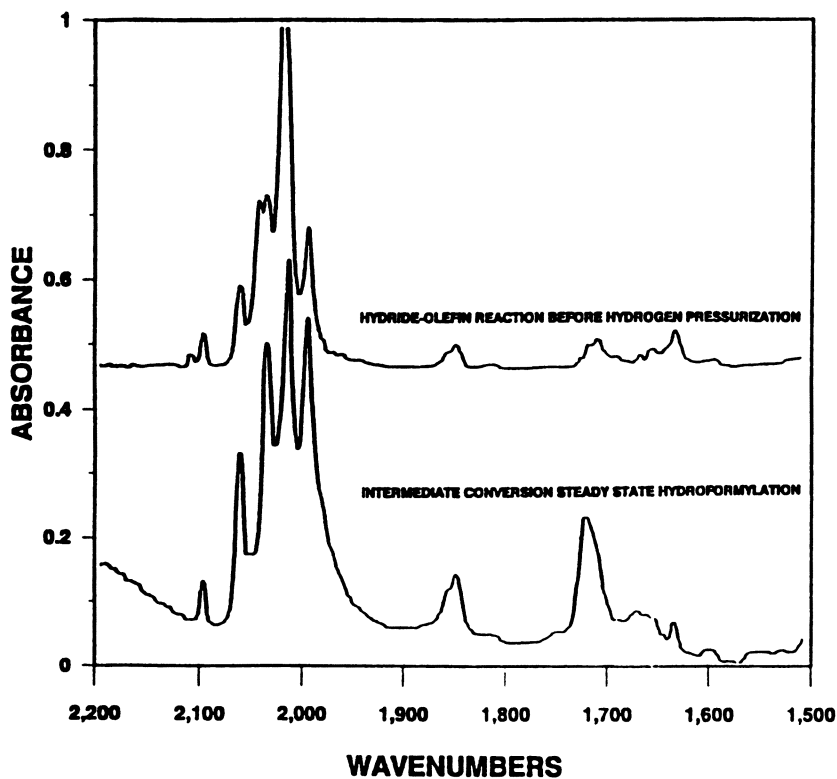
Figure 9. OFCIR coupled reaction of a cobalt-catalyzed hydroformylation of 1-hexene under 400 psi (2.76 MPa) of CO (top), and after addition of 600 psi (4.14 MPa) of hydrogen (bottom), at 50 °C in a decane solvent. The IR beam was directed into one end of an optical fiber, which was coupled to a high-pressure CIR reactor. The exit beam from the CIR crystal was coupled to another fiber and into an MCT A detector. The top curve illustrates the cobalt complex distribution under a pure CO atmosphere after the reaction of $HCo(CO)_4$ with 1-hexene in a decane solvent. The bottom curve was taken after the hydrogen was added after ~40% conversion of the olefin. The reaction contents and conditions were otherwise carried out as described in Figure 8. The additional band seen in the top spectrum at 2114 cm^{-1} is due to $HCo(CO)_4$.

The method gives high-quality midrange IR spectra under autogenous conditions. The equipment can be placed in a remote high-pressure facility, separated from the spectrometer and operators. Thus, this method offers the possibility of multiplexing to monitor several chemical reactions simultaneously with a single spectrometer.

Conclusions

CIR reactors offer an excellent method for the direct observation of homogeneous metal-catalyzed reactions and all other chemical reactions under well-mixed high-temperature and high-pressure conditions. They can reliably and simultaneously measure the concentrations of IR-observable metal complexes and reactant and product concentrations. Thus, the real-time observation of catalytic species can be coupled with kinetic data to provide a more confident assignment of the catalytic roles of observable species.

Acknowledgments

References

1. Moser, W. R.; Cnossen, J. E.; Wang, A. W.; Krouse, S. A. *J. Catal.* **1985**, *95*, 21.
2. Moser, W. R.; Cnossen, J. E.; Wang, A. W.; Krouse, S. A. *Abstracts of Papers*, 187th National Meeting of the American Chemical Society, St. Louis, MO; American Chemical Society: Washington, DC, 1984; INDE 110.
3. Moser, W. R.; Chiang, C. C.; Cnossen, J. E. *Advances in Materials Characterization*; Condrate, R. A., Ed.; Plenum: New York, 1985; p 31.
4. Cnossen, J. E. M.S. Thesis, Worcester Polytechnic Institute, 1989.
5. Alemdaroglu, N. H.; Penninger, J. L. M.; Oltay, E. *J. Mol. Catal.* **1967**, *1*, 27.
6. Noack, K. *Spectrochim. Acta, Part A* **1968**, *24*, 1917.
7. Rigby, W.; Whyman, R.; Wilding, K. *J. Phys. Sci. Instrum.* **1970**, *2*, 572.
8. Morris, D. E.; Tinker, H. B. *Rev. Sci. Instrum.* **1977**, *43*, 1024.
9. King, R. B.; King, A. D., Jr.; Ifbal, M. Z.; Frazier, C. C. *J. Am. Chem. Soc.* **1978**, *100*, 1687.
10. Vidal, J. L.; Walker, W. E. *Inorg. Chem.* **1980**, *19*, 896.
11. Moser, W. R.; Berard, J. F.; Melling,, P.; Berger, R. Presented at PittCon, Chicago, IL, March 1991; paper 973.

12. Moser, W. R.; Papile, C. J.; Brannon, D. A.; Duwell, R. A.; Weininger, S. A. *J. Mol. Catal.* **1987**, *41*, 271.
13. Moser, W. R.; Wang, A. W.; Kildahl, N. K. *J. Am. Chem. Soc.* **1988**, *110*, 2816.
14. Moser, W. R.; Wang, A. W.; Kildahl, N. K. *Catalysis of Organic Reactions*; Blackburn, D. W., Ed.; Dekker: New York, 1990; p 137.
15. Wang, A. W. Ph.D. Dissertation, Worcester Polytechnic Institute, 1990.
16. Moser, W. R.; Cnossen, J. E. *Proceedings of the North American Catalysis Society Meeting*, Detroit, MI; Catalysis Society of North America: Dearborn, MI, 1989; D18.
17. Moser, W. R.; Berard, J. F. *Proceedings of the Canadian Chemical Society*, Halifax, Nova Scotia, Canada; National Research Council of Canada: Ottawa, 1990.
18. Lubas, P. M. B.S. Thesis, Worcester Polytechnic Institute, 1987.
19. Fenstermacher, J. M. B.S. Thesis, Worcester Polytechnic Institute, 1984.
20. Moser, W. R.; Papile, C. J.; Weininger, S. J. *J. Mol. Catal.* **1987**, *41*, 293.

In Situ Spectroscopic Studies
in Homogeneous Catalysis

Robin Whyman

Research and Technology Department, ICI Chemicals and Polymers Ltd., P.O. Box 8, The Heath, Runcorn, Cheshire WA7 4QD, United Kingdom

This chapter describes the various methods that have been developed for in situ spectroscopic studies on homogeneously catalyzed reactions requiring the use of elevated pressures and temperatures for optimum performance. The advantages and disadvantages of the two most commonly used techniques, vibrational and nuclear magnetic resonance spectroscopies, are discussed. A critical evaluation of the types of spectroscopic cells that have been developed for high-pressure infrared studies is presented. Examples of applications of the latter illustrate the ease with which (under favorable circumstances) unstable intermediates can be identified, the level of information that can be extracted from the spectra of relatively complex mixtures by using advanced instrumentation techniques, and the correlations between spectroscopic data and catalytic performance that can be obtained even with multicomponent catalyst systems, harsh and highly IR-absorbing reaction media, and extreme conditions of pressure and temperature.

MANY INDUSTRIALLY IMPORTANT CATALYZED REACTIONS require, for optimum performance, the use of high pressures and high temperatures. To provide as much insight as possible into the nature of the species present under such reaction conditions, it is highly desirable to have available, by the use of appropriate physical techniques, in situ methods of measurement.

Clearly the use of such methods provides a significant advance over the traditional method of withdrawal of samples from high-pressure–high-temperature reactions followed by analysis under ambient conditions. Even if the catalyst precursor and the nature of the species obtained after withdrawal

and depressurization are identical, it is highly likely that they exist in quite different forms under operating conditions.

However, the use of in situ methods per se is extremely unlikely to lead directly to the identification of the actual catalytically active species, particularly with highly active catalysts. As Rooney (1) and others have pointed out, true catalytically active intermediates in solutions are very unstable and transient. Therefore, in most cases it is extremely difficult (by using spectroscopic techniques) to identify them among the much more numerous and more stable complexes that are also frequently present. These more stable complexes only transform, if at all, with a much lower frequency than those that form an intrinsic part of the catalytic cycle.

In situ techniques can provide only a detailed insight into the most stable species present under a particular set of reaction conditions. Nevertheless, even if the results of in situ spectroscopic measurements taken in isolation are less than ideal, more meaningful information can emerge when they are assessed in parallel with kinetic studies and measurements of product distributions. Such a course should therefore provide the maximum benefit from in situ spectroscopic studies on catalyzed reactions.

Techniques for In Situ Studies

For homogeneously catalyzed reactions an assessment of the information provided by appropriate physical techniques, together with factors such as general applicability and ease of experimentation, leads to the conclusion that vibrational spectroscopy and nuclear magnetic resonance spectroscopy are the techniques of choice. Of these, high-pressure infrared (HPIR) spectroscopy has become well established during the past 20 years (2), and the technique has become part of the traditional armory of physical methods, particularly in industrial laboratories. The application of nuclear magnetic resonance (NMR) spectroscopy is of rather more recent vintage, largely as a result of the generally greater degree of difficulty in the experimentation required (3–5).

The two techniques are in many respects complementary. Thus, infrared (IR) spectroscopy has the particular advantages of speed and high sensitivity. The high sensitivity is compatible with the low catalyst concentrations typically used in many catalyzed processes. In contrast, NMR spectroscopy is characterized by slow time scale and low sensitivity. It frequently requires more concentrated solutions than those typically used in catalyzed reactions. In addition, instrumental limitations impose severe restrictions on the upper temperature limits that can be tolerated.

On the positive side, however, NMR data are typified by highly dispersed spectra from which, by the measurement of chemical shifts and couplings and by multinuclear operation, detailed structural information can be derived. This aspect is in sharp contrast to the data obtained from IR

spectroscopy, in which overlapping spectra from closely related species are commonly observed. Such spectra are frequently difficult to separate, even with access to Fourier transform instrumentation.

The quantitative nature of NMR spectra also provides a contrast with vibrational spectroscopy because quantitative IR data can be generated only in favorable circumstances. The ability to operate these two complementary techniques in tandem can provide a distinct advantage.

Following this introduction to the subject of in situ spectroscopic measurements, I shall concentrate on high-pressure IR studies. This chapter describes, in general terms, the key design criteria and the advantages and disadvantages of the various types of cells. I shall use examples taken from our work to illustrate various points such as the level (and limitations) of information that can be extracted by using current instrumentation and the harsh and corrosive chemical environments under which such cells can be used to provide meaningful data.

Design of High-Pressure Infrared Cells

Some key items in the design of a high-pressure cell for in situ spectroscopic measurements are

- the material of construction,
- the nature of the window material,
- the design of the window-sealing arrangement, and
- the ability to operate in a safe manner.

Key requirements for construction material are high mechanical strength and corrosion resistance toward reactants and products. Suitable materials are austenitic stainless steels such as type 316, nickel–molybdenum–chromium alloys such as Hastelloy C–276, and various titanium alloys. Stainless steel is satisfactory for fairly mild pressure and temperature conditions. However, under certain conditions it reacts slowly with carbon monoxide to form small amounts of $Fe(CO)_5$ and $Ni(CO)_4$, which give rise to spurious bands in the IR spectra. Titanium alloys are strong, tough, and inert toward carbon monoxide. However, they are attacked at high temperatures by, for example, primary alcohols such as methanol and related molecules that contain active hydrogen atoms. Hastelloy C has the advantages of high strength and exceptional resistance to a wide variety of chemical process environments including strong oxidizing agents, mineral acids, carboxylic acids, and acetic anhydride. For reactions involving high hydrogen pressures the question of hydrogen embrittlement must also be considered, although this phenomenon generally becomes a problem only at temperatures higher than 200 °C.

The primary requirements for window materials are high mechanical strength and corrosion resistance, together with transparency over the maximum infrared range. The strength of the window material frequently limits the maximum operating pressure of the cell because the window materials available for long-wavelength transmission are generally mechanically weak. A compromise has to be reached. A summary of the properties of a variety of materials suitable for different pressure, temperature, and wavelength ranges is given in Table I. For much of the work with the ICI cells, we have found calcium fluoride windows to be very suitable.

Table I. Window Materials for High-Pressure IR Transmission Studies

Material	Young's Modulus (psi $\times$ 10^6)	Spectral Range (cm^{-1})	Pressure (atm)	Temperature (°C)
Sapphire	50	4000–2000	10,000	>250
ZnS (Irtran 2)	14	4000–700	1,000	250
CaF$_2$	11	4000–1200	650	250
NaCl	5.8	4000–650	200	100

The window-sealing arrangement is also very important and a range of designs has been considered. These are best illustrated by reference to the various cell designs.

Types of High-Pressure Cells.   The many types of high-pressure cells for vibrational spectroscopic studies in homogeneously catalyzed reactions fall into two basic categories. The first includes self-contained units, such as autoclaves fitted with windows, that can be stirred and heated. Thus chemical reactions can be monitored continuously from start to finish without perturbing the system (i.e., a truly in situ experiment). Typical of this category are the cells we have developed in ICI (6) and the Moser cells (7), which take advantage of the data-acquisition method involving cylindrical internal reflectance (the CIRCLE cell).

High-pressure cells comprising the second category are those in which the cell and autoclave are separate components operated in conjunction with one another. Reacting solutions from an autoclave are circulated through the IR cell by means of either gravity or a pump. Typical of these flow cells are the Monsanto cell (8), which can also be used for UV–visible spectroscopic measurements, and the Penninger cell (9), which can be used for the study of slurries and of the gas–solid systems typical of heterogeneous catalysts. The Penninger cell was originally designed for studies of the liquid-phase hydroformylation reaction using $Co_2(CO)_8$ immobilized on cross-linked polystyrene. A modification of the Monsanto cell has been developed by Union Carbide (10) to allow operation under more severe reaction conditions. The operating ranges of these cells are summarized in Table II.

Table II. High-Pressure IR Cells

Reactors	Maximum Operating Pressure (atm)	Maximum Operating Temperature (°C)	Windows
Batch reactors			
ICI cell	1000	250	CaF_2, ZnS
Moser CIR cell	80	160	ZnSe crystal
Flow type reactors			
Monsanto cell	100	200	CaF_2
Penninger cell	600	450	CaF_2

Advantages of Specific Cell Designs.   The various cell designs have their advantages and disadvantages. Although the details are described elsewhere (*2, 6–10*), a few general comments are appropriate.

ICI and Moser cells are complete reaction vessels with integral stirrers. Thus, chemical reactions can be followed from start to finish in a truly in situ manner. In both cell designs the windows are surrounded on all sides by the reaction solution. This arrangement minimizes the possibility of a "stagnant" area between the cell windows that would not be representative of the composition of the bulk solution.

The importance of effective stirring, which is not necessarily a feature of all the reported cell designs, may be easily demonstrated by monitoring the spectrum of a solvent (e.g., *n*-heptane) under pressures of gaseous carbon monoxide. After initial pressurization to about 100 atm, followed by activation of the stirrer, strong absorptions are observed immediately at ca. 2140 cm^{-1}, showing dissolved carbon monoxide. The intensity of these absorptions does not increase significantly with time. In contrast, only very weak peaks are observed when the system is not stirred. The intensity of these peaks increases only slowly with time, and the system requires many hours in which to establish the equilibrium concentration of dissolved gas (*6*).

The advantage of the Monsanto–Penninger-type flow cells is that they are separate small-volume units that can be isolated from the autoclave, which contains the bulk of the reacting fluids. Thus any damage to the spectrometer in the event of a window failure is minimized. Continuous-flow reactions can be monitored easily. Thus these cells can be very useful adjuncts as side stream reactors to monitor, for example, the progressive changes in reacting species or catalyst change–decay on chemical plants.

However, they are not truly in situ experiments. The contents of the autoclave must be circulated through the cell and back again. This process inevitably leads to a pressure drop across the system, which can have two significant consequences. First, dissolved gases may be released. These gases usually tend to accumulate at the narrowest part of the system, namely the gap between the windows of the cell. Such accumulations lead to experimental difficulties, particularly if quantitative measurements are required.

Second, and more seriously, the equilibria between different species in solution can be very sensitive to changes in pressure. This condition is particularly true for reactions involving $CO-H_2$ and carbonylmetals.

A very clear example of this disadvantage is shown in data obtained on the Co–Ru-catalyzed conversion of methanol and CO to methyl acetate (7). A comparison of the spectra obtained under nominally identical conditions shows that the major species, $[Ru(CO)_3I_3]^-$, observed in the in situ cell apparently partially decomposes during the time taken to pump the sample from an autoclave through a flow cell. This observation indicates that caution is required in interpreting data obtained from flow cells where a true instantaneous view of the reacting species is not available.

Identification and Characterization of Unstable Molecules and Reactive Intermediates

Reaction of $Ru(CO)_4PPh_3$ with Dihydrogen.   A classic example of the use of high-pressure infrared spectroscopy for the identification of unstable species derives from a study of the reaction of dihydrogen with hydrocarbon solutions of $Ru(CO)_4PPh_3$ (11). Convincing evidence was obtained for the reversible formation of $Ru(CO)_3(H)_2PPh_3$ according to the equilibrium in reaction 1.

$$Ru(CO)_4PPh_3 + H_2 \rightleftarrows Ru(CO)_3(H)_2PPh_3 + CO \qquad (1)$$
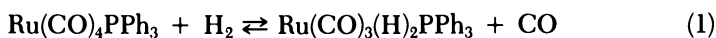
The reasons for the unequivocal nature of this example are as follows:

- both ruthenium-containing species displayed relatively simple well-resolved spectra that were spatially separated and therefore easily distinguishable,

- the spectra were not complicated by strong absorption bands caused by dissolved gases (e.g., CO), and

- the stable osmium analog had been isolated and characterized previously, and spectroscopic data were therefore available for comparison.

Intense interest has recently arisen in the characterization of complexes containing molecular dihydrogen. This system was therefore reexamined, as part of a collaborative exercise with the University of Nottingham, to seek spectroscopic evidence for the formation of $Ru(CO)_3(H)_2PPh_3$ as a possible precursor state to the dihydride. Supercritical xenon was used as the solvent. Although the dihydride was readily obtained by photolysis at ca. 50 atm of hydrogen pressure, no spectroscopic evidence for the intermediacy of the proposed molecular dihydrogen complex was obtained (12).

Reactions of $Rh_4(CO)_{12}$ with Carbon Monoxide and Dihydrogen.
By analogy with the known chemistry of the carbonylcobalts, two key species, interrelated through reactions of $Rh_4(CO)_{12}$ with carbon monoxide and dihydrogen, are likely reactive intermediates.

$$Rh_4(CO)_{12} + 4CO \rightleftarrows Rh_2(CO)_8 \qquad (2)$$
$$2H_2 \qquad 2H_2$$
$$4HRh(CO)_4$$
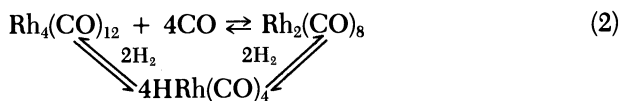
The reversible formation of $Rh_2(CO)_8$ during the reaction of $Rh_4(CO)_{12}$ under pressures of carbon monoxide was first reported 20 years ago (13). Further spectroscopic evidence in support of the bridged form of $Rh_2(CO)_8$ was provided by the matrix isolation experiments of Hanlan and Ozin (14) and later by the much more detailed quantitative work of Oldani and Bor (15).

$Rh_4(CO)_{12}$ has been used for many years as a catalyst precursor for reactions involving the addition of hydrogen to organic substrates. However, definitive evidence for the second species, $HRh(CO)_4$, or its coordinatively unsaturated derivative, $HRh(CO)_3$, is virtually nonexistent. In spite of intensive worldwide research efforts, there is only a single report of the detection of $HRh(CO)_4$ (16) under extreme reaction conditions (at 1542 atm pressure). The very high pressure requirement is somewhat surprising in view of the known catalytic activity of $Rh_4(CO)_{12}$ under reaction conditions that are not far removed from ambient. It occurred to us that the apparent nonobservation of $HRh(CO)_4$ under milder reaction conditions might simply be a consequence of coincident absorption bands.

In our original work, using a dispersive grating spectrometer, a detailed study of this system was hampered by strong absorptions caused by dissolved carbon monoxide. The situation has been considerably improved with access to Fourier transform instrumentation, but problems still remain. First, the subtraction of infinite absorbance from infinite absorbance gives meaningless information. Second, the subtraction of the spectrum of $Rh_4(CO)_{12}$ from a composite $Rh_4(CO)_{12}$–$Rh_2(CO)_8$ spectrum is not trivial because very slight pressure-dependent shifts in the band maxima positions result in the appearance of differential peaks in the subtracted spectra.

Nevertheless we decided to investigate this system again by initially generating the $Rh_4(CO)_{12}$–$Rh_2(CO)_8$ equilibrium mixture at 600 atm of carbon monoxide pressure and room temperature. Dihydrogen was then introduced and spectral changes carefully monitored. Inspection of the resultant spectra (Figure 1) reveals that the absorbances of the 2041- and 1884-cm^{-1} bands characteristic of $Rh_4(CO)_{12}$ do not remain constant with respect to each other upon the addition of dihydrogen. The relative absorbance of the 2041-cm^{-1} band increases by ca. 20–25%. In addition, there is a parallel increase in the half-height bandwidth of this peak (Table III). A similar trend,
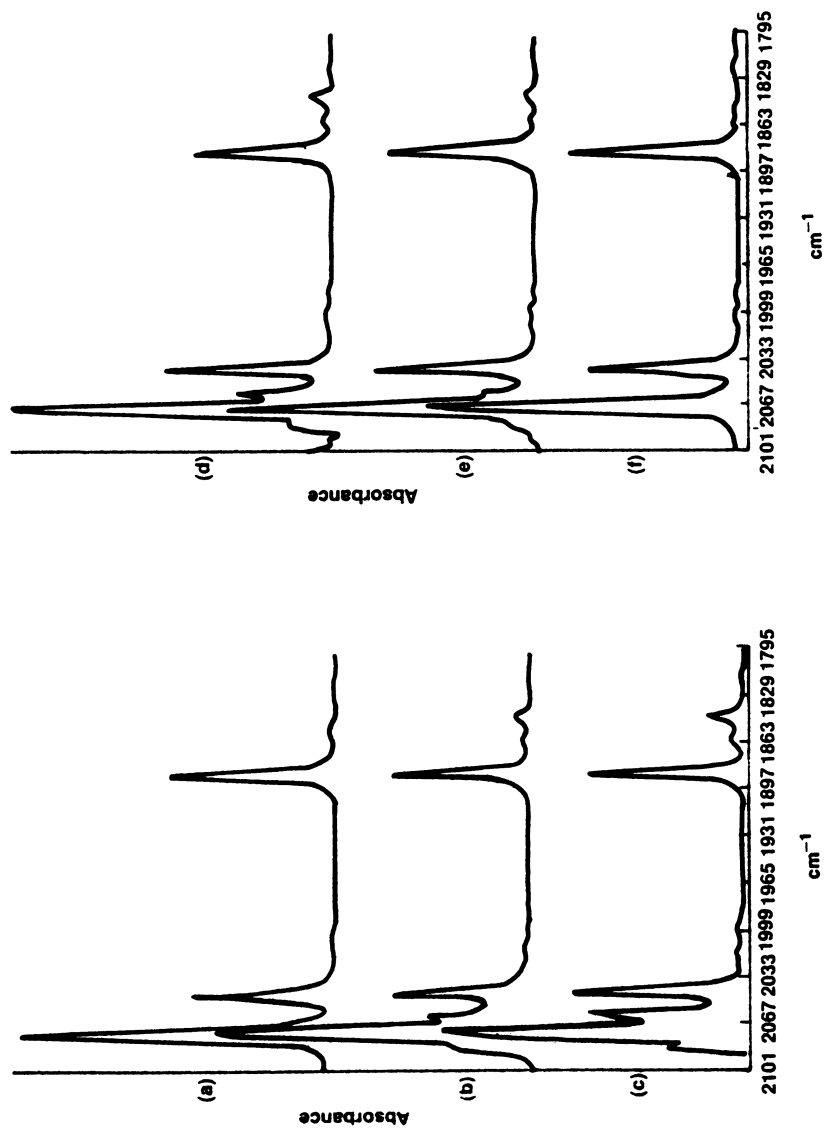
Figure 1. Reactions of $Rh_4(CO)_{12}$ with CO and H_2 in n-heptane at various pressures.

Table III. Addition of H_2 to $Rh_4(CO)_{12}$–$Rh_2(CO)_8$–CO System in *n*-Heptane

Reaction Conditions	Absorbance Ratios[a]	Half-Height Bandwidth[b]
250 atm CO	0.83	1.00
400 atm CO	0.78	1.00
600 atm CO	0.83	1.04
600 atm CO–H_2 (1:1)	0.98	1.18
600 atm CO–H_2 (1:2)	1.10	1.18
600 atm CO–H_2 (1:3)	1.01	1.15
130 atm H_2	0.84	1.04

[a]2041 cm^{-1}/1883 cm^{-1} maxima.
[b]2041-cm^{-1} band.

although much less marked (ca. 5–10% increase), is noted in the absorbance of the 2068-cm^{-1} band.

Furthermore, when the CO–H_2 pressure is slowly released and replaced by H_2 alone, the absorbance ratios and half-height bandwidths return, within experimental error, to their initial values. During this operation, as expected from previous work (*13*), the spectrum reverts to that of $Rh_4(CO)_{12}$ alone. The addition of dihydrogen to the $Rh_4(CO)_{12}$–$Rh_2(CO)_8$ equilibrium mixture thus appears to result in the generation of a transient species that is characterized by absorption bands at ca. 2041 and 2068 cm^{-1}. Of these values, the former peak is significantly more intense.

Carbonyl stretching frequencies for $Rh_4(CO)_{12}$, $Rh_2(CO)_8$, and their cobalt analogs, including $HCo(CO)_4$, are collected in Chart I. Comparison

Chart I. Metal Carbonyl Stretching Frequencies

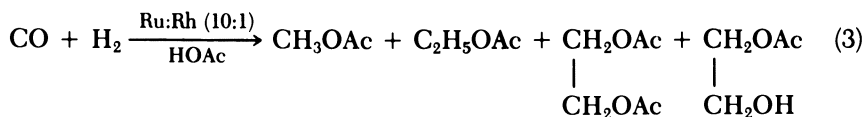| | | | $Co_2(CO)_8$ | | |
| | | | Bridged Isomer | Nonbridged Isomer | |
$Rh_4(CO)_{12}$	$Co_4(CO)_{12}$	$Rh_2(CO)_8$			$HCo(CO)_4$
					2118 vw
		2084 s			
2075 vs					
2070 vs			2071 vs	2069 vs	
	2063 vs	2060 s			
	2055 vs				2052 m
2044 vs			2044 vs		
	2038 m		2042 vs		
	2028 m			2031 ms	2029 s
				2022 vs	
					1996 vw
1884 s	1867 s	1861 mw	1866 sh		
		1845 s	1857 s		

NOTE: Spectra measured in paraffin hydrocarbon solvents. Frequencies measured in wavenumbers (reciprocal centimeters).
ABBREVIATIONS: s, strong; m, medium; w, weak; v, very; sh, shoulder.

between the terminal carbonyl stretching frequencies of the various complexes leads to an estimate of the position of the absorption maxima for the purported $HRh(CO)_4$ to occur at ca. 2043 (s) and 2067 (m) cm^{-1}. The analysis of the high-pressure spectroscopic data presented here is therefore consistent with the transient presence, at room temperature, of $HRh(CO)_4$ upon addition of dihydrogen to the $Rh_4(CO)_{12}$–$Rh_2(CO)_8$ equilibrium mixtures generated under carbon monoxide.

Synthesis Gas Chemistry Under Extreme Reaction Conditions

During our work on synthesis gas chemistry, we discovered a range of composite homogeneous catalysts for the selective production of C_2–oxygenate esters, particularly ethylene glycol diacetate, directly from synthesis gas (17).

$$CO + H_2 \xrightarrow[\text{HOAc}]{\text{Ru:Rh (10:1)}} CH_3OAc + C_2H_5OAc + \underset{\displaystyle CH_2OAc}{\overset{\displaystyle |}{CH_2OAc}} + \underset{\displaystyle CH_2OH}{\overset{\displaystyle |}{CH_2OAc}} \quad (3)$$

In glacial acetic acid as solvent (eq 3), these complex catalyst combinations (which contain mixtures of ruthenium and rhodium as major and minor components, respectively) are promoted by both nitrogen-containing bases and alkali metal cations. Genuine synergistic effects on both catalytic activity and selectivity to C_2 products were observed (Table IV). This behavior is unusual in the light of the commonly observed inverse relationship between catalytic activity and selectivity. Severe reactions conditions (1000 atm CO–H$_2$, 230 °C) were required for optimum selectivities to C_2 products.

To gain some insight into the nature of the species present in solution, we decided to make IR spectroscopic measurements on the various catalyst

Table IV. Activity–Selectivity Behavior of Ru–Rh–Et₃N–HOAc Catalyst Combinations

Catalyst Combination	Catalyst Component (mmol)			Activity[a]	Selectivity[b]
	Ru	Rh	Et₃N		
1	2.0	–	–	0.23	0.09
2	2.0	–	2.0	0.20	0.06
3	–	0.2	–	0.22	0.06
4	–	0.2	2.0	0.44	1.38
5	2.0	0.2	2.0	0.89	1.31

NOTE: Reaction conditions were as follows: 50 mL of glacial acetic acid solvent; 1000 atm of pressure; CO–H$_2$ (1:1); 230 °C; and 2 h.
[a] CO consumed, moles per liter per hour.
[b] Moles of $\overset{\displaystyle |}{\underset{\displaystyle CH_2OAc(H)}{CH_2OAc}}$ per mole of CH_3OAc.
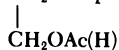
components at pressures and temperatures approaching those under which the catalytic reactions were investigated. These experiments were difficult, partly because the effective spectral range imposed by the strongly absorbing background spectrum of glacial acetic acid, even at extremely narrow path lengths of ca. 20–30 μm between the cell windows, is only 2200–1900 cm^{-1} and partly because of the corrosive nature of acetic acid toward O-rings and ancillary equipment.

Some interesting correlations between the spectroscopic data and the catalytic activities–selectivities have been identified. For the ruthenium catalyst alone the addition of Et_3N has, within experimental error, no influence on either catalytic activity or product selectivity. Infrared spectra of both systems measured at 750 atm and 200 °C are essentially identical and are consistent with the presence of predominantly $[Ru(CO)_3OAc]_2$ together with much smaller concentrations of $Ru(CO)_5$ and $Ru_3(CO)_{12}$.

The addition of Et_3N to the rhodium catalyst doubles the activity and dramatically increases the selectivity to C_2 oxygenate esters. The IR spectra of the two systems show distinct differences. Whereas $Rh_6(CO)_{16}$ is the only detectable species with rhodium alone, the effect of the addition of Et_3N is reflected in the additional formation of $[Rh_6(CO)_{15}X]^-$ (X is either H or OAc). In the composite Ru–Rh–Et_3N (Ru:Rh = 10:1) catalyst, the spectrum (Figure 2) is dominated by an absorption at 2040 cm^{-1}. The most likely assignment of this peak is to a species $HRu(CO)_nOAc$ (n is 3 or 4) formed by a homolytic cleavage reaction between $[Ru(CO)_3OAc]_2$ and H_2, presumably mediated by the presence of the rhodium complex in solution. In addition, minor amounts of $[Rh_6(CO)_{15}X]^-$ may be present.

Although it is not precisely clear how the spectroscopic data relate to the catalytically active species in these complex systems, direct correlations between the spectroscopic data and the catalytic performance are readily apparent.

Conclusion

In this overview of in situ spectroscopic studies, with emphasis on high-pressure IR measurements, examples of applications have illustrated the following points:

- the ease with which, under favorable circumstances, unstable intermediates can be identified,

- the level of information that can be extracted from the spectra of relatively complex mixtures by using advanced instrumentation techniques, and

- the correlations between spectroscopic data and catalytic performance that can be obtained even with multicomponent cat-
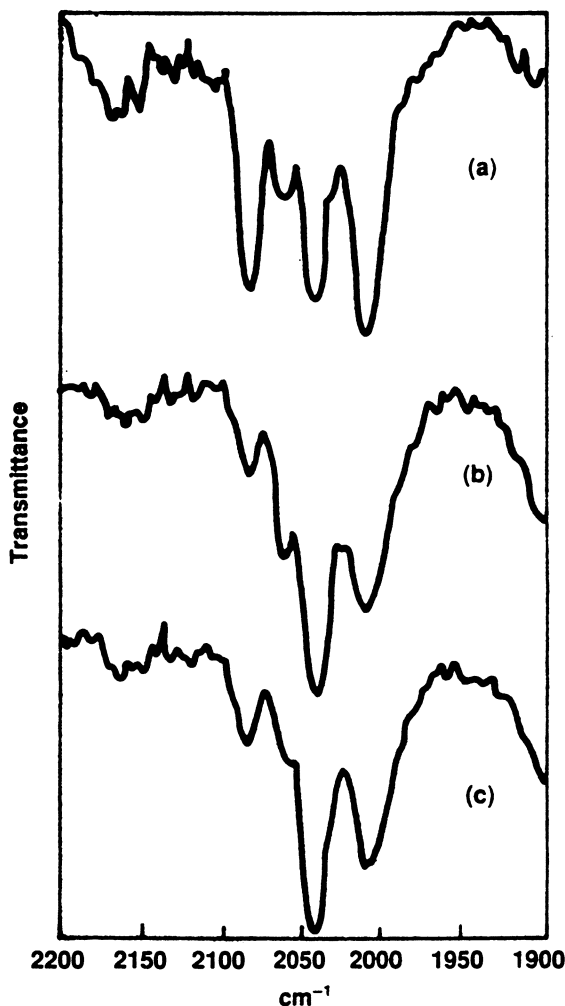
Figure 2. Reactions of synthesis gas with a Ru–Rh–Et₃N (10:1:10) composite catalyst in glacial acetic acid. Reaction conditions: a, 750 atm, 100 °C; b, 850 atm, 175 °C; c, 880 atm, 200 °C.

alyst systems, harsh and highly IR-absorbing reaction media, and extreme conditions of pressure and temperature.

Acknowledgment

References

1. Rooney, J. J. *J. Mol. Catal.* **1985**, *31*, 147.
2. Whyman, R. In *Laboratory Methods in Vibrational Spectroscopy*; Willis, H. A.; van der Maas, J. H.; Miller, R. G. J., Eds.; Wiley: Chichester, England, 1987; p 281.
3. Jonas, J.; Hasha, D. L.; Lamb, W. J.; Hoffman, G. A.; Eguchi, T. *J. Magn. Reson.* **1981**, *42*, 169.
4. Heaton, B. T.; Strona, L.; Jonas, J.; Eguchi, T.; Hoffman, G. A. *J. Chem. Soc., Dalton Trans.* **1982**, 1159.
5. Roe, D. C. *J. Magn. Reson.* **1985**, *63*, 388.
6. Hunt, K. A.; Page, R. W.; Rigby, S.; Whyman, R. *J. Phys. E* **1984**, *17*, 559.
7. Moser, W. R.; Cnossen, J. E.; Wang, A. W.; Krouse, S. A. *J. Catal.* **1985**, *95*, 21.
8. Morris, D. E.; Tinker, H. B. *Rev. Sci. Instrum.* **1972**, *43*, 1024.
9. Penninger, J. M. L. *J. Catal.* **1979**, *56*, 287; *High Pressure Sci. Technol., Proc. Int. AIRAPT Conf., 7th* **1980**, *2*, 842.
10. Walker, W. E.; Cosby, L. A.; Martin, S. T. U.S. Patent 3 886 364, 1975.
11. Whyman, R. *J. Organomet. Chem.* **1973**, *56*, 339.
12. Upmacis, R. K. Ph.D. Thesis, University of Nottingham, 1986.
13. Whyman, R. *J. Chem. Soc., Chem. Commun.* **1970**, 1194.
14. Hanlan, L. A.; Ozin, G. A. *J. Am. Chem. Soc.* **1974**, *96*, 6324.
15. Oldani, F.; Bor, G. *J. Organomet. Chem.* **1983**, *246*, 309.
16. Vidal, J. L.; Walker, W. E. *Inorg. Chem.* **1981**, *20*, 249.
17. Whyman, R. *J. Chem. Soc., Chem. Commun.* **1983**, 1439; U.S. Patent 4 665 222, 1987.

NMR Techniques for Studies of Homogeneous Catalysis

D. Christopher Roe

Central Research & Development, Experimental Station, E. I. du Pont de Nemours and Company, Wilmington, DE 19880-0328

Sapphire NMR tubes have proven to be particularly useful for studying catalytic reactions under conditions of moderate pressure (viz, 100–2000 psi). The tubes, which are commercially available, are grown as single crystals in the required shape and used without further machining. A nonmagnetic valve caps the tube and is used both for the introduction of reactant gases and for making the static seal. Inert gases may also be used to pressurize the sample for high-temperature studies in relatively low-boiling solvents. In addition to straightforward kinetic studies, we have frequently found that magnetization-transfer studies of slow exchange are uniquely well suited to unraveling discrete equilibria in catalytic cycles. Examples involving reactions of CO and C_2H_4 are described.

Nmr spectroscopy is one of the most useful techniques for obtaining detailed information about catalytic systems. Typical approaches include monitoring substrate conversion as a function of temperature or component concentrations. It may also be possible to relate ligand dynamics (studied by variable temperature, line shape, or magnetization-transfer methods) to certain aspects of catalytic activity.

One of the most obvious limitations of conventional NMR approaches is the difficulty encountered when working with reactant gases such as CO or H_2, which require substantial pressures in order to obtain reasonable concentrations in solution. In this chapter, applications involving sapphire NMR tubes, which can withstand such pressures, are described along with a variety of approaches that have been found useful for studying catalytic systems.

High-Pressure NMR Spectroscopy

A number of approaches to high-pressure NMR spectroscopy have been reported in the literature. Their design differences reflect a variety of chemical objectives and engineering compromises. Many of these approaches have been reviewed previously (1), but may be briefly restated here along with some current developments.

Commercially available glass NMR tubes provide the most economical and convenient means for working with gases at modest pressures (less than 150 psi). These medium-wall tubes are fitted with a symmetrical poly(tetrafluoroethylene) (Teflon) valve that can be connected either to a high-pressure line from a gas cylinder or to a vacuum line for the introduction of condensable gases. Great care must be exercised when working with glass tubes under pressure because surface scratches may make the glass increasingly unreliable as a function of repeated use. Despite the caveat associated with these pressure tubes and the limited pressure range available, much practical work can still be accomplished. An early example that inspired the development of commercially available tubes involved the reaction of H_2 at 100 psi with $RhClL_3$ (2).

A medium-pressure NMR tube based on a polyimide resin (Vespel) was described by Kinrade and Swaddle (3). The tube features a 16-mm outside diameter and either 9- or 13-mm inside diameter so as to provide a moderately large sample volume (e.g., 4 mL). This device was found suitable for use up to 225 °C. It was sufficiently chemically inert to strong alkali that it permitted high-temperature studies of alkaline silicate solutions at pressures around 250 psi.

A pressure probe specifically designed for studies of homogeneous catalysts has also been reported (4). This interesting design involves a stainless steel alloy pressure vessel attached to an external stirred reactor. The Teflon-lined sample compartment contains a toroidal-shaped detector coil to increase the proximity of the coil to the sample and thereby improve sensitivity. Although B_1 homogeneity was not particularly good, the reported performance in terms of sensitivity and line shape were very promising. (^{13}C sensitivity was greater than that obtained with a conventional 10-mm broadband probe.) Initial pressure testing at 8500 psi was successful.

More traditional high-pressure NMR probes are generally associated with physical studies at extremes of pressure, 2000 atm or more. NMR studies at these pressures have provided, for example, descriptions for the dynamic structure of liquids (5) and the conformational isomerization of cyclohexane (6). Of greater relevance for catalytic studies is the possibility of using such pressures to obtain (for individual reaction steps) volumes of activation, which may at times be more mechanistically meaningful than the corresponding entropy of activation.

Much early work in this area (e.g., reference 7) involved exchange of relatively hard ligands (e.g., $[Ln(DMF)_8]^{3+}$, where Ln is Ce–Nd and Tb–Yb),

for which the volume of activation is expected to be a relatively sensitive indicator of mechanism. However, when a reaction is clearly associative or dissociative in nature, even soft ligands can be associated with substantial activation volumes. Results of this sort were described (*8*) for the carbonylation of $H_3Ru_3(\mu_3\text{-}COMe)(CO)_9$ and the hydrogenation of $HRu_3(\mu\text{-}COMe)(CO)_{10}$; both reaction steps follow a dissociative mechanism. It is presumed that future applications of this approach may give rise to unique mechanistic information for catalytic systems.

Development of Sapphire NMR Tubes.   The remainder of this chapter will focus on a more limited pressure region (100 psi to ~2000 psi) in which the effect of pressure is simply to control the concentration of reactant gas in solution. With these pressure limits in mind, it is possible to take advantage of the great tensile strength of sapphire (*1*). This material is commercially available (from Saphikon, Milford, NH) as tubular single crystals that are literally grown in the shape of an NMR tube. After the tubes have been annealed, there is no machining or stressing of the crystal. Therefore, the tubes should retain their tensile strength properties with a high degree of reliability. In addition, sapphire is relatively chemically inert and has a small thermal expansion coefficient.

The open end of the sapphire tube is sealed by means of a nonmagnetic Ti-alloy valve, the details of which have been published (*1*). Subsequent refinement of that design reduced the outer diameter of the valve from 36 to 25 mm to accommodate conventional-bore superconducting magnets. This change brought about a corresponding reduction in weight (from 110 to 74 g) that makes the tubes easier to spin. The epoxy that was originally used to attach the Ti-alloy flange to the tube is no longer available. Its replacement (Aremco-Bond 630) appears to be entirely suitable, at least within its specified operating temperature range of –65 to + 155 °C. Methods for the direct attachment of the sapphire tube to the Ti-alloy flange, and for even more convenient valve designs, are being developed (*9*). The present design remains reasonably convenient to manipulate inside a dry box. Once the samples are syringed into the tube, the valve top is bolted in place and the tube–valve assembly is removed from the dry box for subsequent pressurization.

The tube and valve are sufficiently lightweight and symmetrical that they spin and achieve a typical resolution of about 1 Hz. The exterior surface of the tube is not perfectly concentric. Instead, it consists of a large number of parallel ridges that run the length of the tube. These surface imperfections undoubtedly limit the resolution and the line shape. However, spinning side bands do not appear to be a problem, and line separations of 0.25 Hz have been observed without recourse to resolution enhancement. In hydrostatic pressure testing, the burst pressure of one tube was found to be approximately 14,500 psi. It is therefore possible to carry out operations up to

2000 psi (or more) with a reasonable margin of safety. In our hands, the tubes have been operated without incident over a period of years, from −150 to + 150 °C at nominal pressures up to 1200 psi, and at lower pressures up to + 250 °C.

Operation of the Sapphire NMR Tube.   As with any technique involving samples under pressure, safety considerations are of paramount importance when working with sapphire tubes. Sample pressurization and transportation to the spectrometer are carried out with the tube and spinner resting inside a cylindrical poly(methyl methacrylate) safety shield that has a wall thickness of approximately 1/4 inch. It is important to protect the tube from scratches or from any sort of mechanical stress that might come about from even a short drop (e.g., while a tube is being cleaned, the flange end may drop to the bench top). Because the tubes are single crystalline, vibration sources such as ultrasonic baths can shatter them. Given the possibility of damaging the crystal by inadvertent or routine wear and tear, it is important to routinely test the tubes hydrostatically at pressures several times that of intended use, but still well below the burst limit. As a matter of routine, we pressure-check our tubes at 5000–6000 psi initially and then again after four or five experiments.

When the sample tube is ready for pressurization, the bottom of the flange is made to rest on top of the spinner, and the assembly is transported inside the safety shield to the appropriate gas cylinder. The gas is introduced through 1/16-inch stainless steel tubing fitted with a standard Valco 1/16-inch ferrule and male nut that screws into the side of the valve. Rotation of the valve stem handle effects the opening and closing of the valve. Once the sample is sealed under pressure, it may be detached from the line and gently rocked on its side (while still inside its safety shield) to mix the gas with the solution.

The pressurized sample can be placed in the probe while avoiding direct operator exposure to the tube. The base plate of the safety shield is removed, and the remaining safety shield and tube are made to rest on top of the upper probe stack. If spinning the sample is critical, the tube is restrained by means of a removable string or lasso while the supports at the bottom of the spinner are removed. The tube can then be lowered to the top of the probe stack, where it can be supported by the eject air system, and lowered into the probe once the string has been removed. More conveniently, if spinning the sample is not an important goal, the tube can be lowered all the way into the probe with the string still attached for later sample retrieval.

Pressure Stabilization of Reactive Species

Many catalysts (or their precursors) are susceptible to decomposition via dissociative loss of a ligand such as CO, but can be effectively stabilized by

operating under pressure. Perhaps the most obvious such example involves species like $Co_2(CO)_8$ or $CH_3CO–Co(CO)_4$. These compounds are, from a synthetic point of view, relatively unstable above 0 °C because they tend to lose CO and form carbonylcobalt clusters. However, these same materials can provide useful entries into the catalytic hydroformylation cycle that typically operates around 100–140 °C and 3000 psi.

Although the instability and volatility of $Co_2(CO)_8$ and $HCo(CO)_4$ present problems for product purification and catalyst recycle, it is clear that a reasonable trade-off can be found between catalyst stability at elevated temperature and the requirement for open coordination sites for subsequent reactions. It should therefore be possible to directly quantitate the exchange of free (dissolved) CO with $Co_2(CO)_8$ by ^{13}C NMR spectroscopy under conditions closely analogous to those employed in catalytic hydroformylation.

The expectations just stated were borne out in a limited study of CO exchange with $Co_2(CO)_8$ and $CH_3CO–Co(CO)_4$ for CO pressures from 100 to 1100 psi and temperatures from 40 to 80 °C (*10*). Cyclohexane-d_{12} and methylcyclohexane-d_{14} were used as solvents to minimize any effects of solvent coordination. The highest CO pressures were limited by available cylinder pressure. ^{13}C-enriched CO was used to overcome the low signal-to-noise ratio, particularly in the case of $CH_3CO–Co(CO)_4$, where the ^{13}C CO spin-lattice relaxation times (T_1) are around 30 and 13 s, respectively. CO scrambling ensures that the degree of enrichment is uniform. Therefore, no kinetic complications are introduced by the fact that the net enrichment may be 50% in one case and 70% in another.

In the case of $Co_2(CO)_8$, ^{13}C NMR spectra reveal peaks for the cobalt complex around 200.6 ppm and free CO at 184.6 ppm. At 80 °C and above, exchange broadening of the two resonances is evident. However, the quadrupolar cobalt nucleus contributes substantially to the line width of the complex in a temperature-dependent way. A partial line-shape analysis (of the free CO alone) could have been pursued over a limited range of temperatures, but it was decided to avoid these limitations by using magnetization-transfer techniques to study the exchange.

The variant of this approach that appears to offer the most reliable exchange rates is inversion transfer. Selective inversion of one resonance by a soft 180° pulse, followed by a variable time delay and signal acquisition, provides a series of spectra in which a transient decrease in intensity at the noninverted site characterizes the exchange. Whenever possible, the complementary experiment involving selective inversion of the other resonance is also performed. The combined data sets are analyzed to provide a single consistent rate constant, along with estimates for the individual site T_1s.

Rate constants thus obtained for CO exchange with $Co_2(CO)_8$ from 40 to 80 °C showed no dependence on CO concentration from 0.08 to 1.43 M; the averaged results are 40 °C, 0.8 s^{-1}; 50 °C, 3.1 s^{-1}; 60 °C, 11.4 s^{-1}; 70 °C, 32.5 s^{-1}; and 80 °C, 93.6 s^{-1}. The independence of the observed exchange

rate and CO concentration is consistent with the small value of the equilibrium dissociation constant, which is estimated to be $10^{-4} M^{-1}$ (11, 12). The observed rates therefore correspond directly to the forward rate constant k_1 in eq 1.
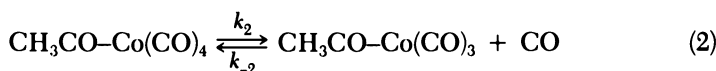
$$Co_2(CO)_8 \underset{k_{-1}}{\overset{k_1}{\rightleftharpoons}} Co_2(CO)_7 + CO \qquad (1)$$
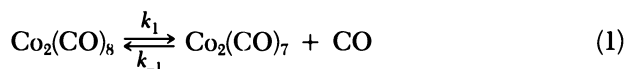
The cited rate constants provide the activation enthalpy $\Delta H^\ddagger = 25.5 \ (\pm 1.5)$ kcal mol^{-1} along with the activation entropy $\Delta S^\ddagger = 22 \ (\pm 4)$ eu. The corresponding free energy of activation is $\Delta G^\ddagger (300 \ K) = 18.8 \ (\pm 0.2)$ kcal mol^{-1}.

An alternative interpretation of the exchange process involves rate-limiting cobalt–cobalt bond breaking followed by very rapid exchange of CO with $\cdot Co(CO)_4$. The observed invariance of exchange rate constants to changes in the accessible CO and cobalt concentrations is in fact consistent with a radical mechanism. However, the process described by eq 1 is preferred for this discussion because it allows for a direct analogy with CO exchange in the monomeric tetracarbonylcobalt complex.

Exchange Involving CH_3CO–$Co(CO)_4$.   Results entirely similar to those just described were obtained with solutions of CH_3CO–$Co(CO)_4$ (10). In view of the greater instability of this complex [compared to $Co_2(CO)_8$], it is interesting that under 1000-psi nominal CO pressure samples appeared to be stable for many hours at 100 °C. Additionally, at 100 psi one sample remained unchanged after 2 months at room temperature.

Exchange of free CO with the $Co(CO)_4$ moiety was studied in the same manner from 50 to 80 °C and was found to be independent of CO concentration from 0.4 to 1.4 M. The dissociation rate constants k_2 (eq 2) appear to be inherently severalfold slower than those observed for $Co_2(CO)_8$. These rate constants lead to the activation parameters $\Delta H^\ddagger = 22.0 \ (\pm 0.2)$ kcal mol^{-1} and $\Delta S^\ddagger = 8 \ (\pm 0.5)$ eu; at 300 K, $\Delta G^\ddagger = 19.5 \ (\pm 0.02)$ kcal mol^{-1}.

$$CH_3CO\text{–}Co(CO)_4 \underset{k_{-2}}{\overset{k_2}{\rightleftharpoons}} CH_3CO\text{–}Co(CO)_3 + CO \qquad (2)$$

The smaller entropy of activation observed in this case is consistent with the idea that the coordinately unsaturated $Co_2(CO)_7$ remains unbridging, although formation of CH_3CO–$Co(CO)_3$ is accompanied by an increase in structure in the transition state. Presumably, this increase in structure corresponds to coordination of the acyl oxygen to give an η^2-bound acyl, as observed in matrix isolation Fourier transform infrared (FTIR) studies (13) and supported by theoretical studies (14).

$$CH_3CO\text{–}Co(CO)_3 \underset{k_{-3}}{\overset{k_3}{\rightleftharpoons}} CH_3\text{–}Co(CO)_4 \qquad (3)$$
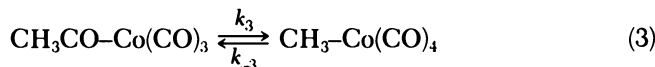
In addition to the dissociation process, a slower scrambling of the acyl and terminal COs can be observed. This exchange process (eq 3) is markedly inhibited by increasing CO concentrations, as expected for the reverse of eq 2. Unfortunately, it is not possible to identify the observed exchange rate k_{acyl} with individual rate constants indicated by eqs 2 and 3. However, if k_{-3} << k_3, the steady-state condition yields eq 4 and a plot of $1/k_{acyl}$ versus CO concentration should yield a straight line.

$$k_{acyl} = \frac{k_2 k_3}{k_{-2}[CO] + k_3} \qquad (4)$$

Such a plot does appear to be linear. From the slope one can estimate the ratio of the rates of reassociation to deinsertion. For $[CO] = 1.0$ M at 70 °C, this ratio is approximately 21. The notion that k_{-3} is small compared to k_3 may seem to be rather nonintuitive, although it is fully consistent with the density-functional MO calculations of Versluis et al. (*14*).

Additional High-Pressure Studies.   It would also be of interest to follow CO dissociation from $HCo(CO)_4$. However, it appears that the ^{13}C chemical shift of this species is coincident with that of free CO. Under this circumstance, little dynamic information can be gathered from ^{13}C NMR studies. Nevertheless, in a preliminary series of experiments, the formation of $HCo(CO)_4$ from $Co_2(CO)_8$ and H_2 (derived from a 1:1 CO–H_2 mixture) could be followed by ^1H NMR spectroscopy over a period of several hours at 70 °C. By enriching the gas mixture with either CO or H_2, the anticipated CO inhibition of the reaction was observed (Figure 1). Further quantitative details were not pursued.

A point of caution is that the titanium alloy valve is potentially subject to hydrogen embrittlement at high temperature. No adverse effects were noted following the present study, presumably because of the relatively low H_2 pressure and the fact that, in the spectrometer, the valve remains close to ambient temperature even though the bottom of the tube is being heated in the probe.

Intermolecular hydroacylation, specifically the reaction of ethylene and benzaldehyde to give propiophenone, is catalyzed by the indenyl complex $(\eta^5\text{-}C_9H_7)Rh(\eta^2\text{-}C_2H_4)_2$ (*15*). The reaction is rather slow at 80 °C and 80 psi C_2H_4. Although no organic side products were observed, substantial catalyst decomposition occurred. Under a nominal pressure of 1000 psi C_2H_4, the sample consists of approximately 70% liquid ethylene. When heated to 100 °C in the sapphire NMR tube, this sample yields smooth NMR kinetics overnight. Additional ^2H and ^{13}C labeling studies led to the suggestion that the reaction proceeds via dissociative loss of one ethylene, oxidative addition of the aldehyde C–H, and subsequent insertion of ethylene into the Rh–H bond, followed by reductive elimination of the alkyl–acyl.
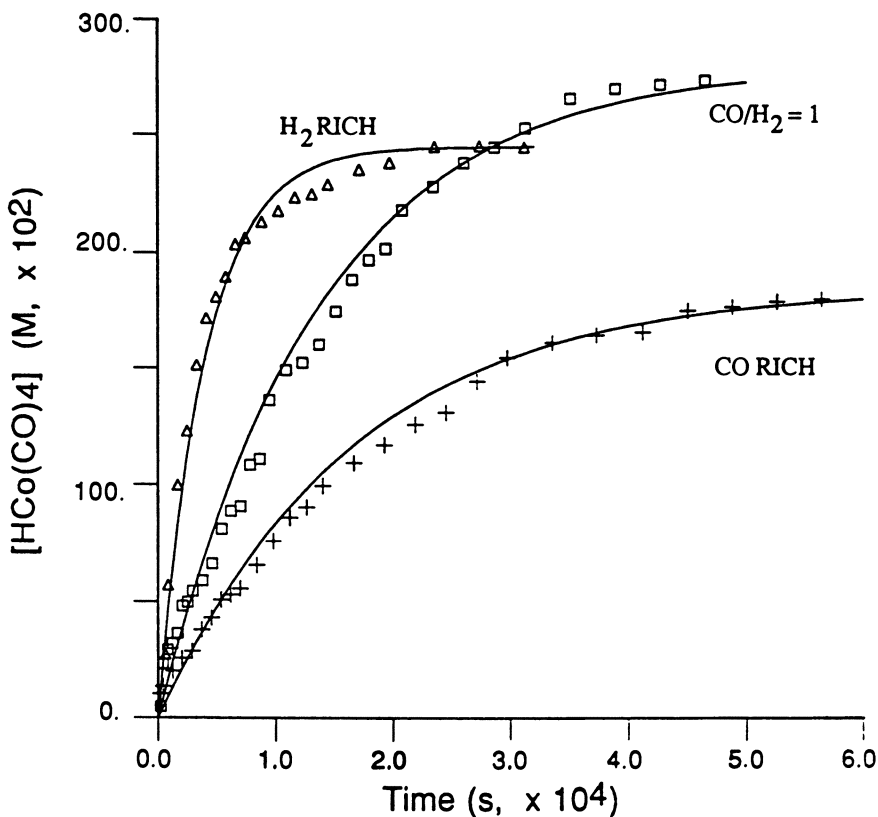
*Figure 1. Rate of HCo(CO)₄ formation as followed by the integrated intensity
of the hydride resonance (δ –11.6 ppm).*

The same sort of sapphire NMR tubes were used to study reversible
ring slippage in a coordinately saturated Cr complex (*16*). This process is of
general interest in the context of providing a possible pathway for accom-
modating reactive ligands in catalytic cycles. Reaction of $(\eta^5\text{-}C_5H_5)_2Cr$ with
1.5 atm of CO resulted in the formation of $(\eta^5\text{-}C_5H_5)_2Cr\text{-}CO$. Increasing
the pressure to 130 atm of CO brought about the formation of $(\eta^5\text{-}C_5H_5)(\eta^3\text{-}C_5H_5)Cr(CO)_2$.

Although rapid ring rotation of the C_5H_5 ligands makes the ring carbons
equivalent even at –140 °C, two different C_5H_5 ligands are evident at
–70 °C. Simulations of the variable-temperature ^{13}C NMR line shapes led
to an estimate of 13.5 kcal mol^{-1} as the activation energy for this process. It
was estimated that the exchange rate of the two C_5H_5 ligands at room
temperature was 76,000 s^{-1}. At the same time, saturation-transfer experi-
ments failed to detect any exchange between the coordinated CO ligands
and free CO. Interconversion of the bent η^3 and the flat η^5 rings therefore
appeared to occur by a simultaneous straightening and bending of the two
rings.

Magnetization Transfer

Magnetization-transfer techniques are frequently useful for studying slow exchange in discrete equilibria in catalytic cycles or model complexes. This methodology is suitable for systems that can basically be described by modified Bloch equations (first-order spectra), where the exchange rate is slow enough to give resolved spectral lines but fast enough to be comparable to the spin-lattice relaxation rate. The most general benefit of this approach is extension of the temperature range of conventional line-shape analysis to improve the quality of the estimate of the activation parameters. It is generally found that once a static line shape has been reached, magnetization transfer can still provide rate information at 40 or perhaps 50 °C lower.

A number of additional advantages may contribute to the utility of magnetization-transfer experiments in a given application. It may be difficult to study thermally labile complexes at temperatures high enough to approach coalescence (where line-shape studies provide their most accurate information). Such thermal lability may be anticipated for model compounds or reactive intermediates related to catalytic processes. Compared to line-shape analysis, magnetization-transfer studies may be more practical to implement for large spin systems and for situations where multisite exchange occurs by a variety of pathways. In connection with this latter point, qualitative interpretation of magnetization-transfer results can sometimes lead to mechanistic insights that would be extremely difficult to deduce from line-shape changes occurring at higher temperatures. Almost any system (nucleus) that gives well-resolved resonances is a candidate for this sort of study, and even partial overlap can be tolerated (*10*, *17*). Finally, the range of rate constants that can be measured in this way is relatively unique (typically 0.05 to 50 s^{-1}).

Of course, such a technique is not without its disadvantages. It is unlikely to find use in highly second-order systems, although such studies are at least possible (*18*). For cases involving exchange of proton sites that are spatially close, nuclear Overhauser effects may compete with (and counteract) the exchange effects. In this instance, however, it may still be possible to obtain the competing cross relaxation rate at lower temperatures and thereby correct the observed exchange rate (*19*, *20*).

The range of temperatures for which magnetization-transfer results can be obtained is seldom more than 50 °C, which is barely enough to provide reasonably accurate activation parameters. Within this temperature range, the most accurate rate information is gathered from a series of selective inversion recovery experiments, which may be relatively time-consuming to complete if each exchanging site is selectively irradiated in turn. Nevertheless, given the importance of kinetic information to an understanding of catalytic processes, it is little wonder that magnetization-transfer techniques play an important role in such studies.

Techniques. The site intensity or population perturbation that is required to initiate these experiments can involve either selective saturation

or inversion of a particular resonance. In the former case, exchange rates can be estimated either from the equilibrium degree of saturation at the exchanging sites or from the transient changes in intensity when the saturating field is turned on or off (21). Because selective inversion provides a larger perturbation than does saturation, the inversion-transfer approach [as described for CO exchange with $Co_2(CO)_8$] is the one that we prefer. Early reports that exemplify the inversion-transfer technique include references 22 and 23.

The selective pulse is most easily derived from the low-power transmitter (available on some older spectrometers) or by direct attenuation of the transmitter on those newer spectrometers that permit fast switching among a number of power levels. The time-scaling property of Fourier transforms is such that time-scale expansion corresponds to frequency-scale compression (24). Because the power spectrum of excitation provided by a rectangular pulse of length t has the shape $[(\sin \omega t)/\omega t]^2$, the excitation bandwidth is roughly $1/t$ and is centered at the spectrometer frequency ω (placed on resonance).

To invert a region of the spectrum encompassed by 10 Hz, a 0.1-s pulse would be reasonably appropriate. The attenuation of the transmitter would then be adjusted so that this "soft pulse" length corresponded to a tip angle of 180°. This calibration is most accurately done by estimating the power level required and searching for a null signal corresponding to a 360° pulse (i.e., twice as long as the pulse used for selective inversion) by making minor adjustments to the pulse length. This calibration can be performed quickly because relaxation effects are unimportant for 360° pulses.

A related technique for obtaining selective excitation is the so-called DANTE pulse sequence, which involves the application of a large number (e.g., 20–40) of small flip-angle pulses separated by an appropriate delay (25). The acronym is meant to remind us of the pulse sequence, namely "delays alternated with nutations for tailored excitation". In turn, nutation refers to the action of the pulse on the magnetization.

The frequency domain profile of this excitation sequence consists of discrete side bands separated by the pulse repetition frequency. Because it is typically desirable to have these side bands fall outside the spectral region of interest (e.g., 2 kHz or more), the interpulse delay should be no longer than 0.5 ms. The small flip-angle pulse length is chosen such that the total pulse time corresponds to a normal 180° pulse. The selectivity is determined by the overall length of the excitation sequence (pulse plus delay repeated n times).

The principal advantage of this approach is that there is no need for switching between power levels. As a matter of practice, 10–15 dB of attenuation would be placed in the transmitter line so that the short pulses could still be made significantly longer than the transmitter turn-on time. Additional possibilities exist for generating slow-exchange spectra by using only nonselective transmitter pulses (26, 27).

Quantitative analysis of inversion-transfer data hinges on the construction of the appropriate exchange and relaxation matrix. Usually the chemical mechanisms underlying the exchange process permit the exchange matrix to be written in terms of a rate constant for a given process times a statistical matrix of exchange coefficients (17). The off-diagonal elements (i,j) specify the probability that transfer from site j terminates in site i, and the diagonal elements are then written to maintain detailed balancing (28). Johnson and Moreland (29) gave a useful prescription for constructing exchange matrices for multisite systems. However, for the line-shape calculations they consider, the elements (i,j) refer to transfers from i to j.

Examples of Magnetization Transfer. Olefin hydride complexes of the sort $HRh(ol)(P\text{-}i\text{-}Pr_3)_2$ are of interest in the context of providing models for olefin insertion and subsequent product distribution in Rh(I)-catalyzed hydroformylation. Although these complexes are obviously somewhat removed from the "real" catalytic system, they are sufficiently simple that rate constants for insertion may be obtained (30). The ethylene hydride undergoes insertion as outlined in eq 5 [L = $P(i\text{-}Pr)_3$].

$$\underset{trans}{HRh(C_2H_4)L_2} \underset{k_{-4}}{\overset{k_4}{\rightleftharpoons}} \underset{cis}{HRh(C_2H_4)L_2} \underset{k_{-5}}{\overset{k_5}{\rightleftharpoons}} [CH_3CH_2\text{-}RhL_2] \tag{5}$$
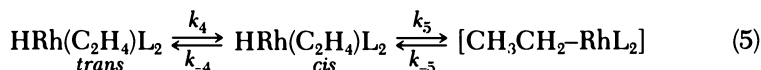
The equilibrium between *cis* and *trans* complexes involves exchange rates that are greater than 10^5 s^{-1} (as judged by ^{31}P dynamic line-shape analysis) at temperatures for which olefin insertion can be observed. Selective inversion of the coordinated ethylene resonance brings about a significant decrease in the hydride intensity from –40 to 0 °C. The observed exchange rates can be related to the specific rate constant for insertion from the *cis* complex by means of eq 6 (31).

$$k_5 = \frac{3}{2} \frac{(K+1)}{K} k_{obs} \tag{6}$$

The equilibrium constant $K = k_4/k_{-4}$ can be approximated by extrapolation of the low-temperature ^{31}P NMR results ($K = 1$ at –130 °C) and room-temperature FTIR results ($K = 0.3$). By using the value $K = 0.4$, estimates for the insertion rate k_5 were obtained (Table I). The rate constant for β-hydride elimination (k_{-5}) must be considerably faster because no direct evidence for the alkyl species is observed.

Analogous results were obtained for the corresponding propylene hydride, although in this case the low-temperature ^{31}P NMR results are not so readily assigned to simple *cis* and *trans* species. Less confidence can be placed in mechanistic interpretations for this system. Nevertheless, the ligand isomerization kinetics are similarly rapid and so do not affect the results

Table I. Exchange Rates for HRh(C_2H_4)(P-i-Pr$_3$)$_2$

T (°C)	k_{obs}	k_5
-40	0.29	1.5
-30	0.78	4.1
-20	2.62	13.8
-10	8.01	42.0
0	18.60	97.6

NOTE: Exchange rates are given in reciprocal seconds.

in a markedly different way compared to the ethylene hydride. Pertinent ^{1}H NMR assignments are presented in Figure 2.

Linear insertion scrambles the hydride H$_5$ with vinylic proton H$_1$ at an exchange rate that is comparable to that for ethylene insertion. At -10 °C the branched insertion pathway brings about observable scrambling of H$_5$ with the other vinylic protons H$_2$ and H$_3$ and, by symmetry, with the methyl protons H$_4$. This latter result indicates that the isopropyl–rhodium intermediate has a lifetime substantially longer than the time required for rotation about the metal–carbon bond. At this temperature, it is estimated that the exchange rate constant for linear insertion is 5.7 s^{-1}; that for branched insertion is 3.0 s^{-1}.
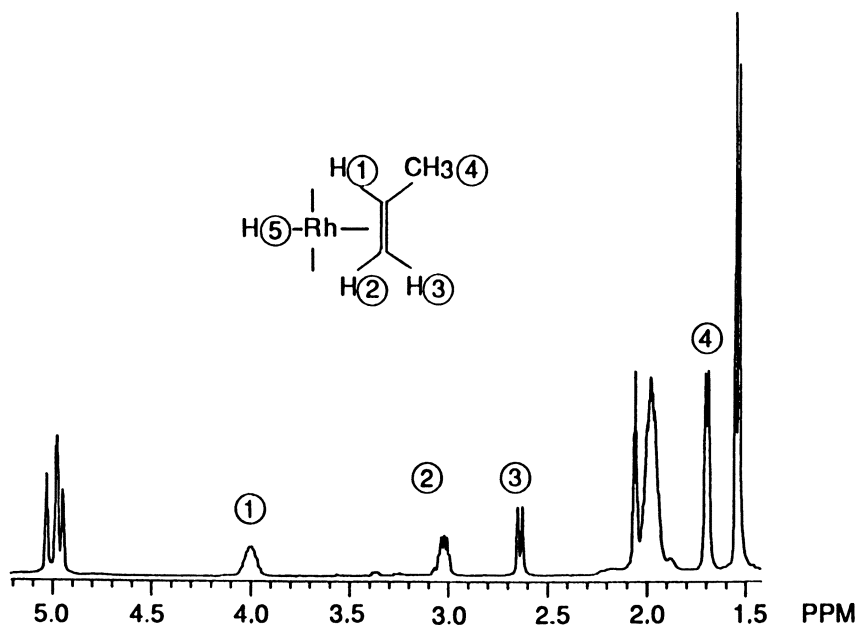
Figure 2. Partial ^{1}H NMR spectrum of HRh(C$_3$H$_6$)(P-i-Pr$_3$)$_2$ in toluene-d$_8$ at -40 °C. Coordinated propylene sites are labeled. Free propylene accounts for the peaks at the extremities of the spectrum. Peaks around 2.0 ppm arise from toluene-d$_7$ and the isopropyl methine resonances of the phosphine ligands.

A different study involving nickel-catalyzed hydrocyanation of ethylene (32) determined the kinetics of ligand dissociation from $H-Ni(CN)L_3$ [L is $P(O-o\text{-tolyl})_3$]. The thermal instability of this complex again precluded rate measurements by line-shape analysis at temperatures above 10 °C. ^{31}P magnetization-transfer experiments permitted an analysis of exchange rates from −40 to 0 °C. In this range, the rates were found to vary from 0.1 to 22.2 s^{-1}, and from this data the activation parameters for this step could be estimated. Ligand exchange kinetics for the key intermediate $(C_2H_5)Ni(C_2H_4)L(CN)$ could also be studied by ^{31}P magnetization transfer from −90 to −60 °C.

It is hoped that the examples presented here give an indication of the general utility of magnetization-transfer techniques in studies of homogeneous catalysis. Efforts are underway to make the data analysis more robust and to codify the generation of the appropriate exchange and relaxation matrix.

References

1. Roe, D. C. *J. Magn. Reson.* **1985**, *63*, 388.
2. Tolman, C. A.; Meakin, P. Z.; Lindner, D. L.; Jesson, J. P. *J. Am. Chem. Soc.* **1974**, *96*, 2762.
3. Kinrade, S. D.; Swaddle, T. W. *J. Magn. Reson.* **1988**, *77*, 569.
4. Rathke, J. W. *J. Magn. Reson.* **1989**, *85*, 150.
5. Jonas, J. *Science (Washington, D.C.)* **1982**, *216*, 1179.
6. Hasha, D. L.; Eguchi, T.; Jonas, J. *J. Am. Chem. Soc.* **1982**, *104*, 2290.
7. Pisaniello, D. L.; Helm, L.; Meier, P.; Merbach, A. E. *J. Am. Chem. Soc.* **1983**, *105*, 4528.
8. Anhaus, J.; Bajaj, H. C.; van Eldik, R.; Nevinger, L. R.; Keister, J. B. *Organometallics* **1989**, *8*, 2903.
9. Horvath, I., Exxon Research and Engineering Company, personal communication, 1991.
10. Roe, D. C. *Organometallics* **1987**, *6*, 942.
11. Ungvary, F. *J. Organomet. Chem.* **1972**, *36*, 363.
12. Ungvary, F.; Marko, L. *J. Organomet. Chem.* **1974**, *71*, 283.
13. Sweany, R. L. *Organometallics* **1989**, *8*, 175.
14. Versluis, L.; Ziegler, T.; Baerends, E. J.; Ravenek, W. *J. Am. Chem. Soc.* **1989**, *111*, 2018.
15. Marder, T. B.; Roe, D. C.; Milstein, D. *Organometallics* **1988**, *7*, 1451.
16. Millar, J. M.; Kastrup, R. V.; Harris, S.; Horvath, I. T. *Angew. Chem., Int. Ed. Engl.* **1990**, *29*, 194.
17. Muhandiram, D. R.; McClung, R. E. D. *J. Magn. Reson.* **1987**, *71*, 187.
18. Wille, E. E.; Stephenson, D. S.; Capriel, P.; Binsch, G. *J. Am. Chem. Soc.* **1982**, *104*, 405.
19. Campbell, I. D.; Dobson, C. M.; Ratcliffe, R. G.; Williams, R. J. P. *J. Magn. Reson.* **1978**, *29*, 397.
20. VanderVelde, D. G.; Holmgren, J. S.; Shapley, J. R. *Inorg. Chem.* **1987**, *26*, 3077.
21. Sandstrom, J. *Dynamic NMR Spectroscopy*; Academic: New York, 1982; pp 54–58.
22. Brown, T. R.; Ogawa, S. *Proc. Natl. Acad. Sci. U. S. A.* **1977**, *74*, 3627.

23. Alger, J. R.; Prestegard, J. H. *J. Magn. Reson.* **1977**, *27*, 137.
24. Brigham, E. O. *The Fast Fourier Transform*; Prentice-Hall: Englewood Cliffs, NJ, 1974; pp 34–37.
25. Morris, G. A.; Freeman, R. *J. Magn. Reson.* **1978**, *29*, 433.
26. Engler, R. E.; Johnston, E. R.; Wade, C. G. *J. Magn. Reson.* **1988**, *77*, 377.
27. Bulliman, B. T.; Kuchel, P. W.; Chapman, B. E. *J. Magn. Reson.* **1989**, *82*, 131.
28. *See* appendix in Roe, D. C. *Organometallics* **1987**, *6*, 942.
29. Johnson, C. S., Jr.; Moreland, C. G. *J. Chem. Educ.* **1973**, *50*, 477.
30. Roe, D. C. *J. Am. Chem. Soc.* **1983**, *105*, 7770. *See* correction in ref. 31.
31. Roe, D. C. *J. Am. Chem. Soc.* **1984**, *106*, 6876.
32. McKinney, R. J.; Roe, D. C. *J. Am. Chem. Soc.* **1986**, *108*, 5167.

4

Parahydrogen-Induced Polarization and Polarization Transfer in Hydrogenation and Oxidative Addition Reactions

A Mechanistic Probe

Richard Eisenberg, Thomas C. Eisenschmid, Mitchell S. Chinn, and Rein U. Kirss

Department of Chemistry, University of Rochester, Rochester, NY 14627

Parahydrogen-induced polarization (PHIP), its occurrence and mechanistic implications in homogeneous hydrogenation chemistry, and its appearance in the oxidative addition of H_2 to transition metal centers are described and analyzed. The PHIP phenomenon, which is characterized by unusual NMR absorptions and emissions in product spectra, arises when para-enriched H_2 is employed in hydrogenation of unsaturated organic substrates with a homogeneous metal catalyst or when para-enriched H_2 is added to a metal complex to form a stable metal dihydride. Both multiplet and net types of polarization are seen. The nature of the polarization is determined by the rate of reaction relative to the rate at which the sample is placed in the magnetic field. Examples of PHIP are found in ruthenium phosphine-catalyzed hydrogenations, catalysis by binuclear rhodium complexes, and in H_2 oxidative addition to Ir(I) complexes. Finally, polarization transfer using parahydrogen results in signal enhancement of other NMR nuclei such as ^{31}P and ^{13}C in the product compounds.

ANOMALOUS EMISSIONS AND ENHANCED ABSORPTIONS in NMR spectra of reaction samples have been interpreted during the past 20 years as evidence of chemically induced dynamic nuclear polarization (CIDNP) and a reaction mechanism involving a radical pair (1–9). Examples of CIDNP involving

transition metal hydrides in hydrogenation and hydrogen-transfer reactions have been reported (10–17). These cases are exemplified by Halpern and Sweany's study (10) of the hydrogenation of α-methylstyrene by HMn(CO)$_5$, which proceeds as shown in Scheme I.
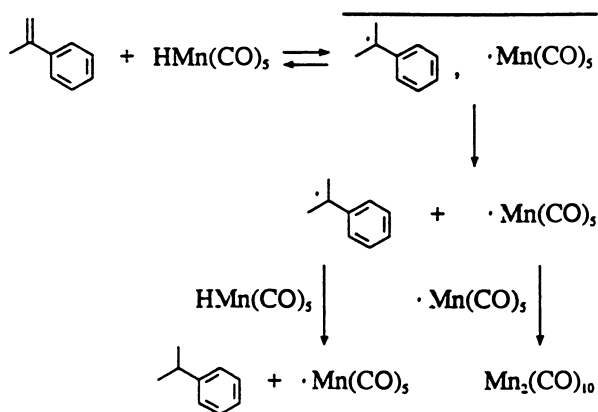
Scheme I.

In 1986 a fundamentally different way of achieving polarization was described by Bowers and Weitekamp (18, 19), in which parahydrogen is transferred pairwise to substrate without loss of spin correlation during the reaction. In this chapter, we focus on this phenomenon, its observation, and its significance.

Our own studies with parahydrogen-induced polarization (PHIP) commenced in 1986 when we witnessed unusual NMR absorptions and emissions in the reaction of the binuclear complex Rh$_2$H$_2$(CO)$_2$(dppm)$_2$ [dppm is bis(diphenylphosphino)methane] with alkynes as in eq 1 (20).

$$2 \quad R-C\equiv C-H \quad + \quad Rh_2H_2(CO)_2(dppm)_2 \longrightarrow$$

$$+ \quad Rh_2(\mu\text{-CCHR})(CO)_2(dppm)_2 \quad (1)$$
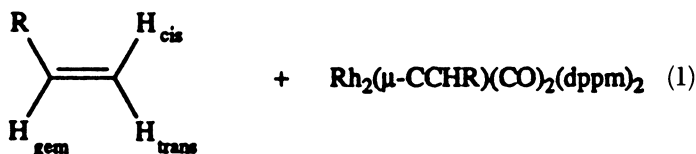
Figure 1 shows one of the earliest of these observations, in which polarization is seen in the resonances of styrene formed by hydrogenating phenylacetylene. The major polarizations occur in the *trans* and *gem* proton
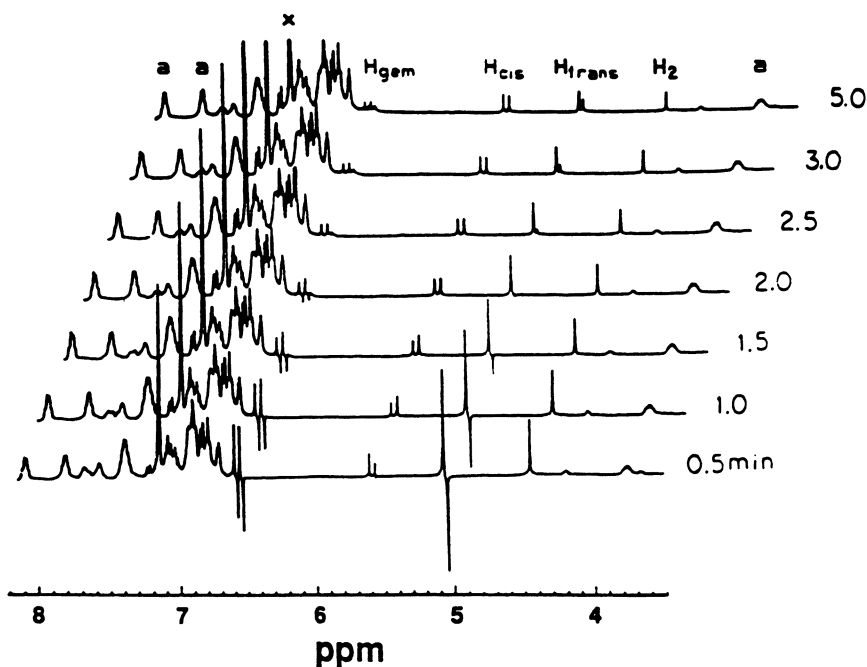
Figure 1. ^1H NMR spectra at 400 MHz for the reaction of $Rh_2H_2(CO)_2(dppm)_2$ with $PhC≡CH$ in C_6D_6 under parahydrogen during the first 5 min of reaction. The resonances labeled a are due to the vinylidene product, $Rh_2(\mu$-$CCHPh)(CO)_2(dppm)_2$. Peak x, which is truncated in later spectra, is due to benzene-d_5. (Reproduced from reference 20. Copyright 1986 American Chemical Society.)

resonances and are of an antiphase type. That is, the *trans* proton, which is normally a doublet through coupling to H_{gem}, exhibits an absorption–emission or A–E pattern. H_{gem}, which is coupled to both *trans* and *cis* protons, shows an A–E–A–E pattern. The antiphase polarization has been referred to in the CIDNP literature as a multiplet effect, and we will use that terminology here. The stacked plot of Figure 1 also shows that the phenomenon rapidly diminishes with time.

We investigated these early observations in the context of CIDNP and showed through labeling studies that this phenomenon did not originate from a mechanism involving organic radicals (20). However, inconsistencies in the magnitude of enhancement and an inability to explain the type of polarization seen in specially designed experiments led to a reassessment of the basis of our observations. When the Weitekamp manner of achieving polarization became known, our results were reexamined in this context. Experiments rapidly established that we were indeed seeing parahydrogen-induced polarization.

The Weitekamp Proposal

At ambient temperatures, normal hydrogen is composed of an approximately 3:1 mixture of ortho- and parahydrogen, reflecting the threefold degeneracy of the nuclear spin functions of the former ($\alpha\alpha$, $\beta\beta$, and $\alpha\beta + \beta\alpha$) and the nondegeneracy of the latter ($\alpha\beta-\beta\alpha$; the nuclear "singlet"). The ratio of ortho- to parahydrogen at 298 K is virtually statistical (3:1), but an energy difference between these two forms makes parahydrogen increasingly favorable as the temperature is lowered. At 80 K, the equilibrium Boltzmann distribution is 51.61% ortho and 48.39% para; at 20 K, it is 0.18% ortho and 99.82% para. Despite the small energy difference between ortho- and parahydrogen, interconversion requires a catalyst and does not occur readily in its absence (21). Paramagnetic solids are the most effective catalysts, but other materials and compounds work as well, including systems that have quadrupolar nuclei and nuclei with large spin-orbit coupling constants.

For PHIP to occur, hydrogen enriched in the para form is required. According to Weitekamp and co-workers (18, 19, 22), polarization can arise if parahydrogen is transferred pairwise to a substrate to yield a product in which the two transferred protons are magnetically distinct. If the reaction occurs fast relative to proton relaxation, then the transferred protons will initially reflect the nuclear spin populations of the starting dihydrogen. This condition is shown in Scheme II for hydrogenation of an internal alkyne with parahydrogen. Because only the $\alpha\beta$ and $\beta\alpha$ states of the product olefin correlate with the nuclear spin function of the reactant parahydrogen, these states will be overpopulated relative to a normal Boltzmann distribution and give rise to polarized A–E or E–A transitions similar to a multiplet effect.
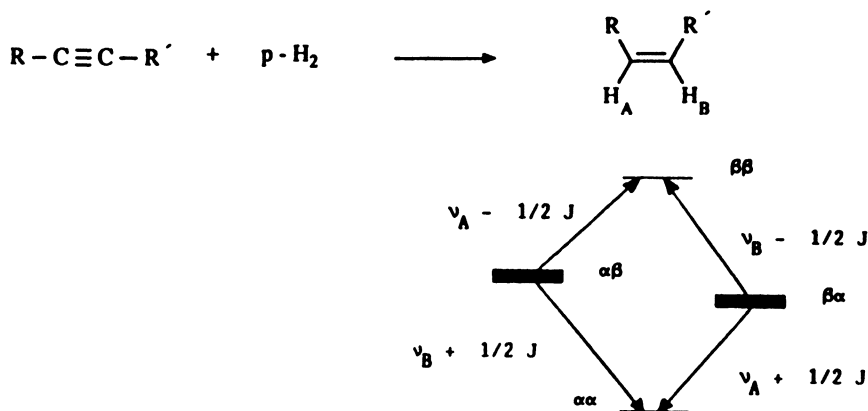
Scheme II.

Experimental Observations

In retrospect, the occurrence of PHIP in our studies (23–25) arose from storing sample tubes at 77 K for several hours prior to thawing and performing the

reaction in the NMR probe. During this period, the platinum group complex in the frozen solution served to catalyze conversion of the hydrogen atmosphere from its normal room-temperature composition to a nearly 1:1 mixture of the two isomers. Thus when the sample tube was thawed and shaken, the reaction commenced using para-enriched H_2.

This effect was demonstrated in a series of experiments shown in Figure 2. The trinuclear complex $[Rh_3Cl_2H_2(CO)_2((Ph_2PCH_2)_2PPh)_2]^+$ (23) serves as a hydrogenation catalyst, with PhC≡CH as the substrate in $CDCl_3$. For trace a the reaction sample was stored under H_2 for several hours at 77 K prior to reaction; for trace b an identical sample was stored under vacuum at 77 K prior to addition of "normal" H_2 and immediate reaction; and for trace c the same procedure as for trace b was followed, except that para-enriched H_2, prepared independently, was added just prior to reaction. Normal H_2 was enriched in the para form by pressurizing a 250-mL bulb to 1 atm of H_2 at −196 °C over activated charcoal and iron oxide (rust) and allowing it to stand for 24 h at −196 °C. Only traces a and c exhibit PHIP. Product resonances are seen in trace b, but without polarization because of the absence of para-enriched H_2.
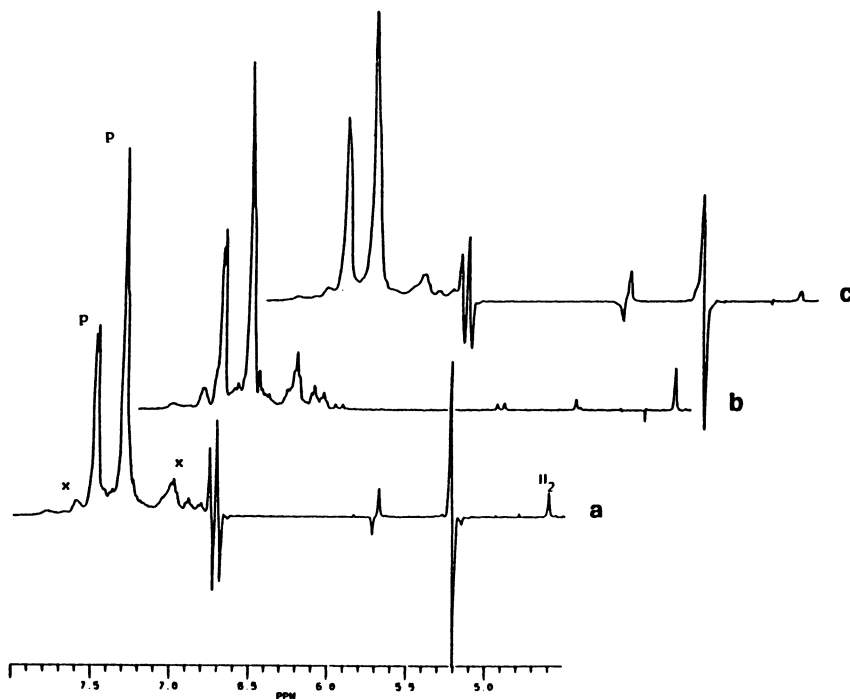
Figure 2. ^1H NMR spectra at 400 MHz showing parahydrogen-induced polarization in the resonances of styrene from the reaction of $[Rh_3Cl_2H_2(CO)_2((Ph_2PCH_2)_2PPh)_2]^+$ with PhC≡CH in $CDCl_3$ under H_2. Key: a, after storage at −196 °C under H_2; b, after storage at −196 °C under vacuum followed by addition of tank H_2; c, after storage at −196 °C under vacuum followed by addition of para-enriched H_2. The resonances marked x are due to the catalyst complex and those marked p are due to excess PhC≡CH. (Reproduced from reference 23. Copyright 1987 American Chemical Society.)

Another feature of the PHIP spectra of Figure 2 is the weaker E–A polarization of the *cis* proton signal of styrene at δ 5.59 ppm. This result contrasts with the H_{cis} signal in Figure 1, which possesses only slight and irregular enhancement. The E–A polarization of H_{cis}, which was never part of the original parahydrogen molecule, results from cross relaxation by dipolar coupling.

The decay of polarization in Figure 1 is representative. Enhancements result from PHIP decay over periods of minutes. The dominant factor is dipolar relaxation, as measured by T_1, the spin-lattice relaxation time. To increase the magnitude and duration of PHIP, we reasoned that deuterated substrates would function better by virtue of longer relaxation times of the transferred protons in the products. This strategy worked as projected, especially with olefinic substrates, for which PHIP was difficult to observe.

Hydrogenations of styrene-d_8, propylene-d_6, and ethylene-d_4 with para-enriched H_2 and a variety of metal complexes as catalysts have led to impressive PHIP of the diproteo alkane products. For example, Figure 3 shows the effect in the hydrogenation of styrene-d_8 catalyzed by $RuH_4(PPh_3)_3$ (24). Figure 4 illustrates PHIP in the hydrogenation of ethylene-d_4 with $[Rh_3Cl_2H_2(CO)_2((Ph_2PCH_2)_2PPh)_2]^+$ as the catalyst (23). The parahydrogen-induced polarization for CHD_2CHD_2 in Figure 4 arises, despite the equivalence of the two protons, because it is a complex $AA'X_2X'_2$ spin system due to H–D coupling.

Recently Bargon et al. (26) demonstrated that similar enhanced absorption–emission patterns can be observed when hydrogenations are performed using orthohydrogen, which must be separated by low-temperature chromatog-
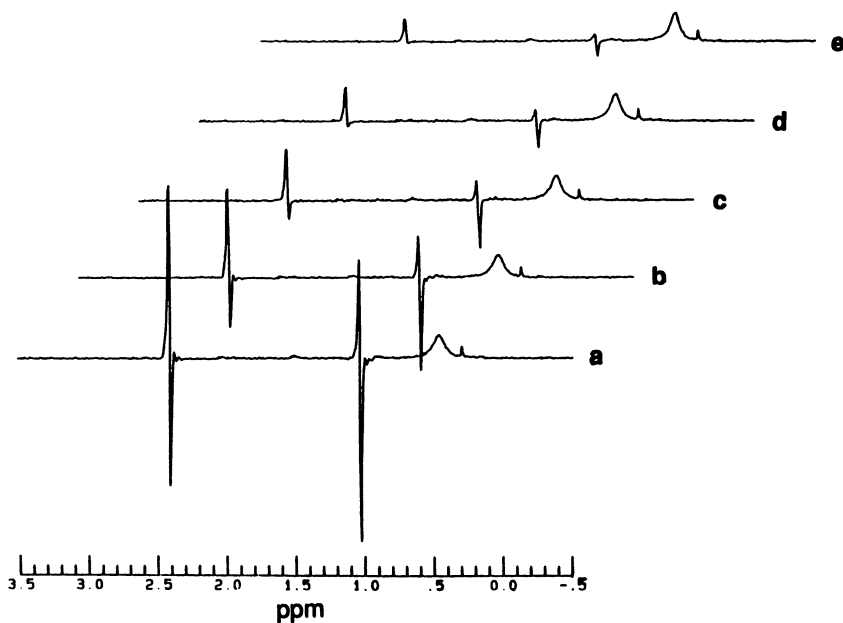
Figure 3. *^1H NMR spectrum of the reaction of styrene-d_8 with para-enriched H_2 catalyzed by $RuH_4(PPh_3)_3$ in C_6D_6 at ~23 °C. Key: a, spectrum taken ~30 s after thawing from –196 °C; b–e, sequential spectra recorded at 15-s intervals.*
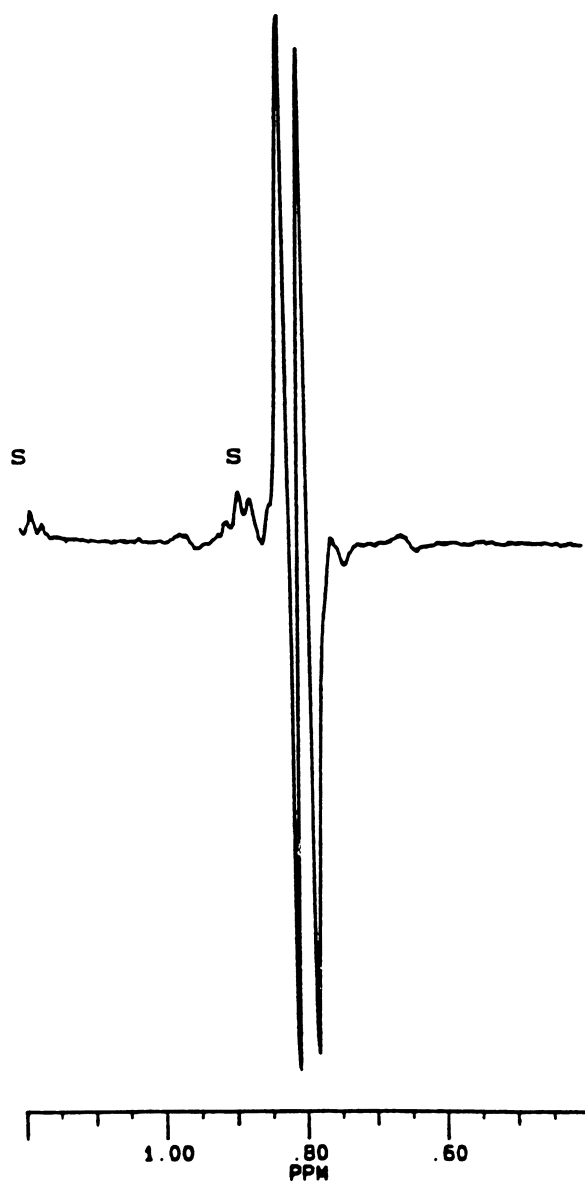
Figure 4. Parahydrogen-induced polarization in the ethane resonances of CHD₂CHD₂. Resonances marked s are due to impurities in the solvent. (Reproduced from reference 23. Copyright 1987 American Chemical Society.)

raphy from the para isomer. As expected from the foregoing analysis, the sense of polarization is reversed when comparing hydrogenations using ortho- rather than parahydrogen (i.e., E–A rather than A–E).

From a reaction mechanism standpoint, the observation of PHIP means that the two H atoms added during the hydrogenation reaction must have originated as part of the same H_2 molecule. Mechanisms such as those invoked for the monohydride catalysts $RhH(CO)(PPh_3)_3$ (27) and $RuHCl(PPh_3)_3$ (28–30) have the two added hydrogens originating in different H_2 molecules. Consequently, they cannot have spins of the added H atoms correlated. The observation of PHIP rules definitively against this type of mechanism. A cautionary note must be added because NMR spectroscopy is an extremely sensitive technique and the magnitudes of polarization are highly variable. Simply put, the occurrence of PHIP does not a priori rule out other parallel paths of reaction. Although quantification of the magnitudes of PHIP may be a way of tackling this problem, further work is needed, both experimentally and theoretically.

Net Polarization and Magnetic Field Effects

Early in the course of our studies, polarizations that were observed differed greatly from those shown in Figures 1 and 2. Specifically, the resonances of product multiplets showed either emission or enhanced absorption (net polarization) rather than antiphase character (multiplet polarization). An example occurred in the hydrogenation of propylene-d_6 catalyzed by $Rh_2H_2(CO)_2(dppm)_2$ (20). In C_6D_6 the hydrogenation proceeded with net polarization, whereas in CD_2Cl_2 multiplet polarization was seen.

In Figure 5, trace a corresponds to the reaction in CD_2Cl_2 with the methylene resonance (δ 1.32 ppm) and the methyl resonance (δ 0.89 ppm) of the product propane-d_6 in A–E polarization. In trace b for the reaction in C_6D_6, the methylene resonance appears as a single enhanced absorption; the methyl resonance is seen as a single emission. The spectrum in trace b thus exhibits not only net polarization but also missing lines (each product resonance is only a single line rather than a doublet). Interestingly, the net polarization appeared more intense and decayed more quickly than the corresponding multiplet polarization.

The basis of net polarization, presented in 1988 by Pravica and Weitekamp (22), derives directly from zero-field polarization and the notion put forth by Glarum (4) of $(n - 1)$ multiplets in field-dependent CIDNP. This explanation proposes that parahydrogen adds to the substrate prior to placement of the sample into the magnetic field of the NMR spectrometer. If the hydrogenation takes place without loss of spin correlation while outside the magnetic field, the product protons are characterized by the $(\alpha\beta-\beta\alpha)$ spin state even though the symmetry of the H_2 molecule no longer holds. As the sample is lowered into the spectrometer, the correlation diagram of Figure 6 is obtained. The transport of the sample into the field occurs adiabatically so that the overpopulation of the $(\alpha\beta-\beta\alpha)$ state is transferred solely to the lower of the $\alpha\beta$ and $\beta\alpha$ product states. Thus only one of the spins can undergo enhanced absorption; the other is restricted to emission.
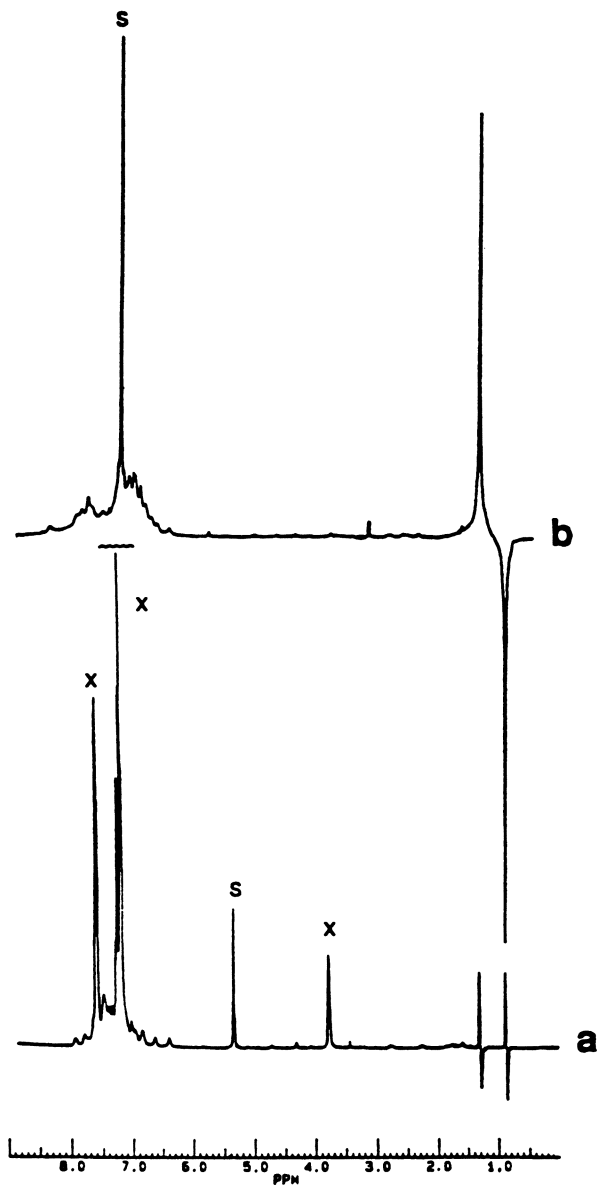
Figure 5. ^{1}H NMR of the hydrogenation of C_3D_6 by $Rh_2H_2(CO)_2(dppm)_2$ under ~3 atm of para-enriched H_2 at 48 °C. Key: a, reaction run using CD_2Cl_2 as the solvent; b, reaction run using C_6D_6 as the solvent. Resonances marked x are from $Rh_2H_2(CO)_2(dppm)_2$ catalyst; resonances marked s are solvent peaks.
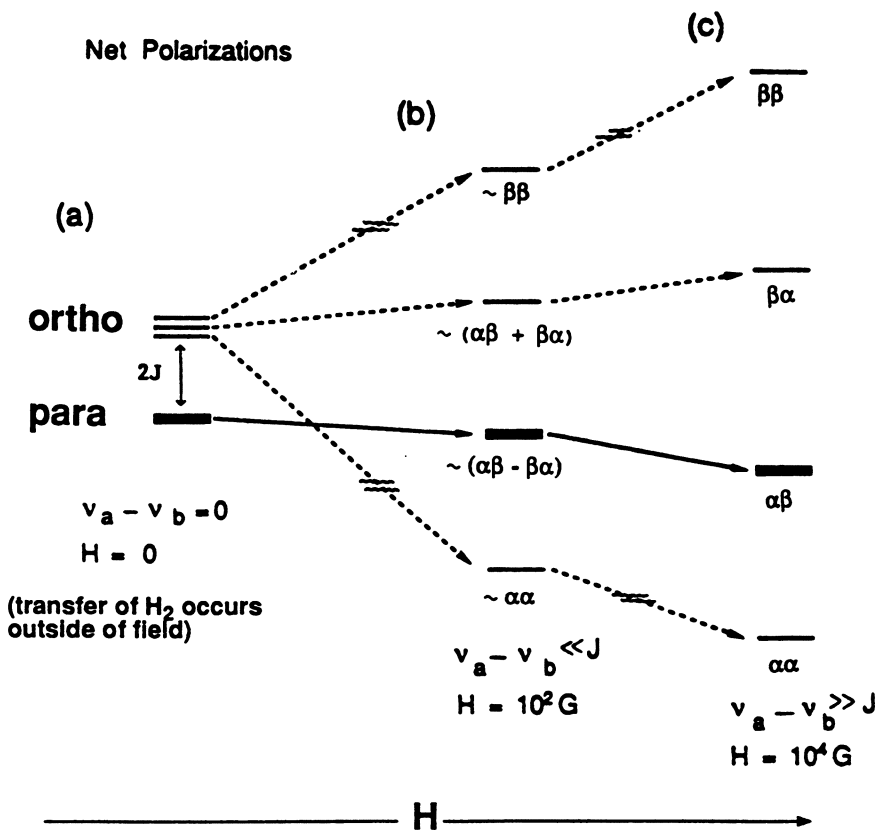
*Figure 6. Correlation diagram leading to net effect polarization in an HH'
spin system. Key: a, energy levels for the protons transferred from para-
enriched H_2 to substrate in the absence of a magnetic field (the labels "ortho"
and "para" indicate the origin of the spin wave functions); b, energy levels in
the fringe of the magnetic field of the spectrometer with $\nu_a - \nu_b \ll J$; c, energy
levels within the high field of the spectrometer with only the $\alpha\beta$ product spin
state overpopulated by correlation with the low-field ($\alpha\beta - \beta\alpha$) spin state.
Here the difference in frequency of the two protons becomes much greater
than the coupling constant J.*

    The influence of magnetic field on polarization type is illustrated by the
hydrogenation of styrene-d_8 in C_6D_6 using $Rh_2H_2(CO)_2(dppm)_2$ as the cat-
alyst (24), as shown in Figure 7. When the sample is lowered into the probe
of the spectrometer immediately after thawing, multiplet polarization occurs
in the ethylbenzene-d_8 product, as seen in trace a, in which the first of 16
scans is collected within 30 s of the sample's removal from liquid nitrogen.
This spectrum, characteristic of multiplet PHIP, exhibits both methylene (δ
2.48 ppm) and methyl (δ 1.05 ppm) protons as absorption–emission (A–E)
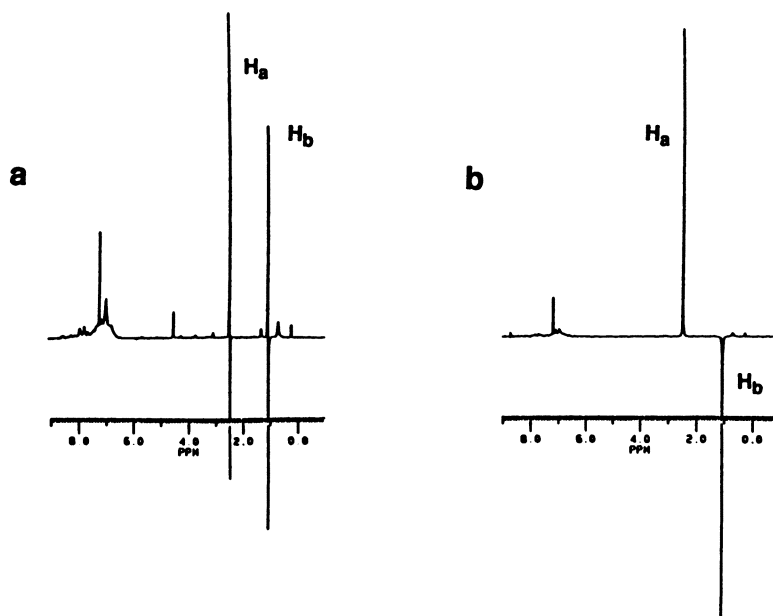
Figure 7. ^1H NMR spectra of the hydrogenation of styrene-d_8 by $Rh_2H_2(CO)_2(dppm)_2$ under ~3 atm of para-enriched H_2 in benzene-d_6 solvent. H_a and H_b are the methylene and methyl resonances, respectively, of ethylbenzene-d_8. Key: a, first scan of the 16-scan spectrum recorded ~30 s after removing the sample from a liquid N_2 bath; b, first scan of a 16-scan spectrum recorded starting ~140 s after thawing from –196 °C, with the sample remaining outside of the spectrometer for ~60 s at 23 °C.

doublets. The difference $\Delta\nu$ between the absorption and emission of each resonance is equal to the coupling between the two protons ($^3J_{HH} = 13$ Hz). In the unpolarized spectrum of ethylbenzene-d_8, J_{HH} coupling is unresolved, partly because of additional coupling to deuterium. With multiplet PHIP it is readily observed.

On the other hand, when the sample is allowed to react away from the high field of the spectrometer, net polarization is observed. Trace b of Figure 7 shows the spectrum of the same sample after it was allowed to react away from high field for 60 s, with a total of 140 s elapsing from the time of its removal from liquid N_2 to the first scan of the 16-scan spectrum. In this polarization, the methylene (–CDH–) proton is solely in enhanced absorption and the methyl (–CD$_2H$) proton shows only emission. The observed positions of these resonances correspond to the downfield absorption and upfield emission of the corresponding doublets of trace a. This positioning of lines is what would be expected if the ethylbenzene-d_8 spin system were simplified to two coupled protons with no additional coupling to deuterium. The en-

ergy-level diagram for this system is that shown in Figure 6, with only the $\alpha\beta$ level overpopulated through adiabatic transport into the field. The observed PHIP transitions are thus at $\nu_A - \frac{1}{2}J$ and $\nu_B + \frac{1}{2}J$.

The proposal of reaction outside the field followed by adiabatic transport into the magnet yields an immediate interpretation of the results of Figure 5. The sample in CD_2Cl_2 (Figure 5a) was introduced into the probe at ca. −50 °C, leading solely to reaction in the probe and multiplet polarization. In contrast, the sample in C_6D_6 (Figure 5b) was warmed outside the probe until thawing at 5 °C. This procedure yielded immediate hydrogenation prior to placement in the spectrometer and consequent net polarization.

Because net polarization results from reaction outside the magnetic field of the spectrometer, its decay was anticipated to relate to the spin-lattice relaxation time (T_1) of the hydrogenated product. The decay of net polarization was found to show simple first-order behavior in a plot of ln (signal intensity) versus time, from which $t_{1/2}$ of 46 s was obtained for the ethylbenzene-d_8 product. This result compares favorably with T_1 of ~80 s for the protons of ethylbenzene-d_8 measured by progressive saturation (31).

One important feature of net polarization is the very large signal enhancements seen relative to multiplet polarization for the same reaction. To date we have achieved 200-fold enhancement in the hydrogenation of styrene-d_8 by using $Rh_2H_2(CO)_2(dppm)_2$ as the catalyst. This value, however, is still well below the 10^3–10^4 enhancement predicted to be possible by using a 1:1 mixture of ortho- and parahydrogen. Theoretical signal enhancements based on the fraction of parahydrogen to total hydrogen can be calculated with eq 2 (18).

$$\frac{S_{\text{maximum}}}{S_{\text{equilibrium}}} = \frac{(1/3)\,(4x_p - 1)\,kT}{3h\nu_0} \tag{2}$$

where S is signal enhancement; x_p is mole fraction of parahydrogen; k is Boltzmann's constant (1.381×10^{-23} J $\cdot$ K^{-1}); T is temperature in kelvins; h is Plank's constant (6.626×10^{-34} J $\cdot$ s); and ν_0 is frequency of the applied field.

Because net polarization results when hydrogenation takes place prior to sample placement in the field, this phenomenon can serve as a qualitative indicator of relative rate. For example, $RuH_4(PPh_3)_3$-promoted hydrogenation of $PhC\equiv CH$ in C_6D_6 yields only net polarization, whereas the same reaction promoted by $Rh_2H_2(CO)_2(dppm)_2$ leads to multiplet alignment. This difference suggests that hydrogenation proceeds more rapidly under the reaction conditions using $RuH_4(PPh_3)_3$. The relative reactivity of substrates can be assessed analogously. For $RuH_4(PPh_3)_3$ in C_6D_6, both phenylacetylene and methyl acrylate yield net polarization, whereas styrene-d_8 shows only multiplet alignment from a similarly handled sample (24).

Competition Experiments

These results led (*31*) to the notion of PHIP as a means of investigating competition reactions of different substrates. This notion was explored by using styrene-d_8 and ethylene-d_4 in C_6D_6 with $Rh_2H_2(CO)_2(dppm)_2$ as the catalyst. These deuterated substrates were chosen over their proteo analogs to minimize relaxation effects. In a series of experiments, the initial pressure of C_2D_4 was kept constant while the quantity of styrene-d_8 was varied. The ethylbenzene-d_8 product in these runs exhibited net polarization; ethane-d_4 appeared as an antiphase multiplet similar to that in Figure 4. The ethane-d_4 polarization was expected to be solely of the antiphase or multiplet type because the αβ and βα proton spin states of the CHD_2CHD_2 product are of the same energy. The similarity obviates selective overpopulation of one of them on transport of the sample into the field.

For a series of runs of the same sample under "fresh" para-enriched hydrogen, the ratio of ethylbenzene-d_8 to ethane-d_4 increased. Figure 8 shows the first spectrum of three successive runs. In this series the ratio of polarization of ethylbenzene-d_8 to ethane-d_4 increased from 0.15 to 0.46 to 1.06. This result is rationalized by the assumption that the hydrogenation of ethylene is more rapid than that of styrene. Therefore, as ethylene is consumed more quickly, the ratio of [styrene]:[ethylene] increases. As a result, polarization in the ethylbenzene product increases with successive runs.

a **b** **c**
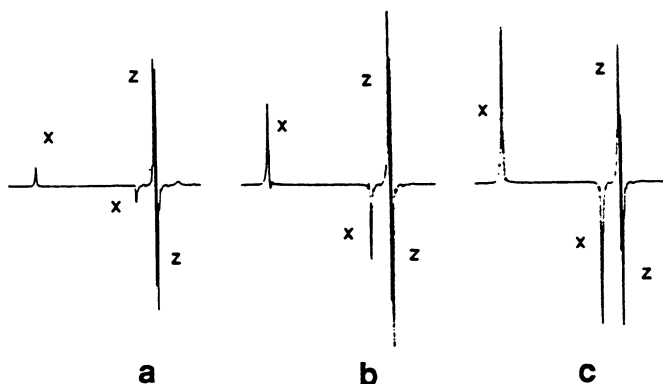
Figure 8. ^1H NMR spectra of the competitive hydrogenation of styrene-d_8 and ethylene-d_4 under ~3 atm of para-enriched H_2 in C_6D_6 at ~23 °C. Resonances marked x are from ethylbenzene-d_8, and those marked z are from ethane-d_4. Key: a, spectrum after 60 s from thawing, which exhibits an enhancement ratio (ethylbenzene-d_8:ethane-d_4) of 0.15; b, spectrum after 300 s under fresh para-enriched H_2, showing an enhancement ratio of 0.46; c, spectrum after 600 s under fresh para-enriched H_2, showing an enhancement ratio of 1.06.

Plots of polarization decay were made for both products in each run. Surprisingly, the decay rate for the two products appeared to be the same in each run. Moreover, the values obtained were similar to those determined from analogous runs involving only single substrates. Although the feasibility of competition experiments based on PHIP has been demonstrated at least in concept, practical application appears limited because of an inability to quantify the magnitude of parahydrogen-induced polarization.

Hydrogenations by Ruthenium Complexes

The occurrence of PHIP means that the two H atoms added to substrate during hydrogenation originate from the same H_2 molecule and maintain correlation during the hydrogenation process. Two well-known homogeneous hydrogenation catalysts of ruthenium that have been examined from a mechanistic standpoint using PHIP are $RuH_4(PPh_3)_3$ and $RuHCl(PPh_3)_3$.

The tetrahydride species readily exchanges H_2 and has recently been shown to be a dihydrogen complex (32–36). The hydrogenation of styrene-d_8 catalyzed by $RuH_4(PPh_3)_3$ in benzene-d_6 under 2–3 atm of para-enriched hydrogen yields strong multiplet polarization, as shown in Figure 3. The polarization, observable for up to 2 min, decays exponentially with a first-order rate constant of 0.044 s^{-1}. During this period the broad hydride resonance of $RuH_4(PPh_3)_3$ at $\delta -7.52$ ppm is observable and remains unchanged. When methyl acrylate and the alkynes $PhC\equiv CH$, t-$BuC\equiv CH$, and Me-$OCH_2C\equiv CH$ are employed as substrates, the polarization changes dramatically to a net effect indicative of a faster reaction for these substrates relative to styrene-d_8 (24). In these experiments, the sample tubes are treated identically, with immediate insertion into the probe of the spectrometer upon sample thawing.

$RuHCl(PPh_3)_3$ is another active catalyst for olefin hydrogenation. Although its mechanism for catalysis has not been established definitively, it is thought to function via phosphine loss, olefin coordination, insertion into the Ru–H bond followed by hydrogenolysis (H_2 addition and alkane elimination) (28–30). Hence, the two hydrogen atoms transferred to the substrate are thought to originate from different H_2 molecules, and catalysis by $RuHCl(PPh_3)_3$ would not be expected to produce PHIP. However, when $RuHCl(PPh_3)_3$ is used to catalyze hydrogenation of styrene-d_8 in $CDCl_3$ or CD_2Cl_2 under para-enriched H_2, A–E polarization of the methylene and methyl resonances of ethylbenzene-d_8 is observed, albeit of much smaller magnitude than that obtained from $RuH_4(PPh_3)_3$ (24). The polarization decays within 90 s, but it can be regenerated by evacuation and addition of more parahydrogen. PHIP thus establishes that for at least some fraction of the product, hydrogenation takes place with pairwise transfer of H_2 to substrate.

That RuHCl(PPh$_3$)$_3$ is not the primary active catalyst in this reaction is suggested by ^{1}H NMR observations of the upfield hydride region. At room temperature, a solution of RuHCl(PPh$_3$)$_3$ under N$_2$ exhibits a hydride resonance as a sharp quartet in either CD$_2$Cl$_2$ (δ –18.22 ppm; J_{PH} = 26 Hz) or CDCl$_3$ (δ –17.85 ppm; J_{PH} = 26 Hz). The complex is fluxional, as has been confirmed by low-temperature ^{1}H NMR studies (24). In contrast with the behavior under N$_2$, when RuHCl(PPh$_3$)$_3$ is placed under H$_2$ at 298 K, the hydride resonance appears broad and without coupling. Under D$_2$ (~3 atm) it disappears within seconds, indicative of facile exchange.

When examined under catalytic hydrogenation conditions, the hydride resonance shows strikingly different behavior. In the presence of styrene in CD$_2$Cl$_2$ under ~3 atm of either H$_2$ or D$_2$, a quartet similar to that for the complex under N$_2$ is observed. Moreover, in experiments using D$_2$ there is no reduction in hydride intensity for up to 2 h, during which several turnovers of ethylbenzene-d_2 are noted. Only after styrene has been consumed is loss of hydride intensity observed.

Although it appears that olefin substrate suppresses hydride–H$_2$ (or D$_2$) exchange, no olefin complex [i.e., RuHCl(PPh$_3$)(olefin)] is observed when RuHCl(PPh$_3$)$_3$ and substrate (styrene-d_8, methyl acrylate, or 1-hexene) are combined in CD$_2$Cl$_2$ at –66 °C. Because the same hydride resonance as seen in the absence of substrate under N$_2$ is observed, rapid exchange of significant amounts of free and complexed olefin can be excluded. Although these results might at first appear contradictory, they do indicate that RuHCl(PPh$_3$) is not the active hydrogenation catalyst nor is it connected to the active catalyst by an equilibrium rapid on the NMR time scale.

Observations suggestive of an active catalyst capable of PHIP are noted when hydrogenations catalyzed by RuH$_4$(PPh$_3$)$_3$ are carried out in halogenated solvents (CDCl$_3$ or CH$_2$Cl$_2$). The color of these reaction solutions changes from colorless to purple-red, and the same hydride resonance seen in RuHCl(PPh$_3$)$_3$-catalyzed systems is noted. In concordance with this color change, the intensity of PHIP is greatly diminished. Thus in halogenated solvents, the nature of the RuH$_4$(PPh$_3$)$_3$ catalyst system changes to that of RuHCl(PPh$_3$)$_3$ systems (24).

A species capable of hydrogenation by pairwise hydrogen transfer and therefore of yielding PHIP is RuH$_2$(PPh$_3$)$_3$, which forms readily from RuH$_4$(PPh$_3$)$_3$ and can be generated by dehydrohalogenation from RuHCl(PPh$_3$)$_3$. This latter pathway has in fact been proposed previously (37, 38), and the species RuH$_2$(PPh$_3$)$_3$ has been invoked as an intermediate in RuH$_4$(PPh$_3$)$_3$-catalyzed hydrogenations (39, 40). We therefore suggest that even in halogenated solvents, if PHIP is observed, a small amount of RuH$_2$(PPh$_3$)$_3$ is present as an active catalyst. The qualitative differences in the magnitudes of PHIP, large for RuH$_4$(PPh$_3$)$_3$ catalysis in C$_6$D$_6$ and weak for RuHCl(PPh$_3$)$_3$ in halogenated solvents, support this notion.

Hydrogenation using the asymmetric hydrogenation catalyst Ru-(binap)(OAc)$_2$, which was synthesized and studied by Noyori et al. (*41, 42*), was also examined by using PHIP.

(*S*)-BINAP
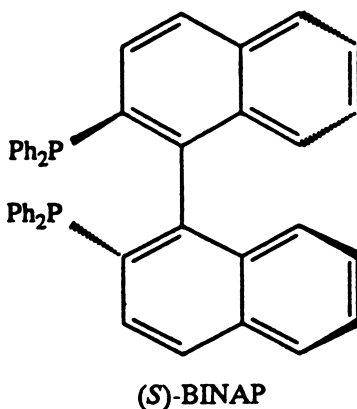
Because most of the reported reaction chemistry using this catalyst employed protic solvents, the intermediacy of a monohydride species formed via protonation was possible. Although the hydrogenation of prochiral substrates proved to be too slow under mild conditions to show any NMR polarization in the products, a number of simpler olefins and alkynes were found to react faster and yielded PHIP. For example, Figure 9 shows the multiplet polarization observed in the hydrogenation of methyl acrylate using Ru(binap)(OAc)$_2$ under para-enriched H$_2$. This result contrasts with the net polarization seen for RuH$_4$(PPh$_3$)$_3$ with the same substrate. The duration of the PHIP in Figure 9 is short (<1 min), as would be expected because of the short relaxation times of the product protons. Similar results were achieved by using allyl alcohol as the substrate, although the PHIP was significantly less pronounced. At this point, it is uncertain if all of the H$_2$ transfers in these Ru(binap)(OAc)$_2$-catalyzed hydrogenations take place pairwise or if the polarizations result from only a small percentage of reaction via pairwise transfer.

The hydrogenation of PhC≡CH catalyzed by Ru(binap)(OAc)$_2$ in CD$_2$Cl$_2$ or CD$_3$OD under ~3 atm of para-enriched H$_2$ provided a significant contrast to other hydrogenations of this substrate using binuclear and trinuclear complexes as catalysts. Figure 10 shows the spectrum observed ~36 s after thawing from −196 °C and insertion into the spectrometer probe at 53 °C. The striking features of the PHIP in this hydrogenation are

1. the approximately equal A–E polarizations of the *trans* and *cis* proton resonances of the styrene product,
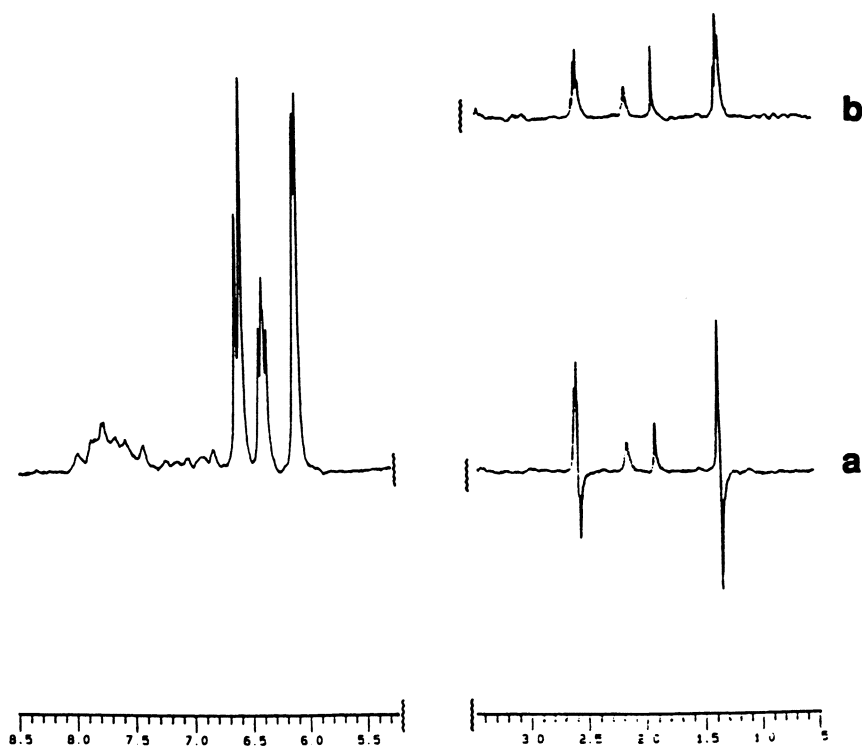
Figure 9. ¹H NMR spectrum of the reaction of methyl acrylate with para-enriched H_2 catalyzed by Ru(binap)(OAc)$_2$ in CD$_3$OD. Key: a, spectrum taken ~37 s after thawing from –196 °C and insertion into the spectrometer probe at 53 °C; b, spectrum taken after ~150 s of reaction in probe. Resonances between δ 6.0 and 6.7 ppm are due to excess methyl acrylate and between δ 6.8 and 8.1 ppm are due to Ru(binap) catalyst.

2. a simple A–E pattern for the *gem* proton,

3. a long-lasting polarization with a distinctly non-first-order decay, and

4. significant PHIP in the secondary hydrogenation product ethylbenzene.

Points 1 and 2 are illustrated by comparing Figure 10 with Figures 1 and 2.

The differences in PHIP for PhC≡CH hydrogenation must be supported by differences in the mechanism of hydrogenation for the various catalyst systems examined. For the binuclear and trinuclear complexes, the *cis* proton polarization was variable and weak, and the *gem* proton appeared as an
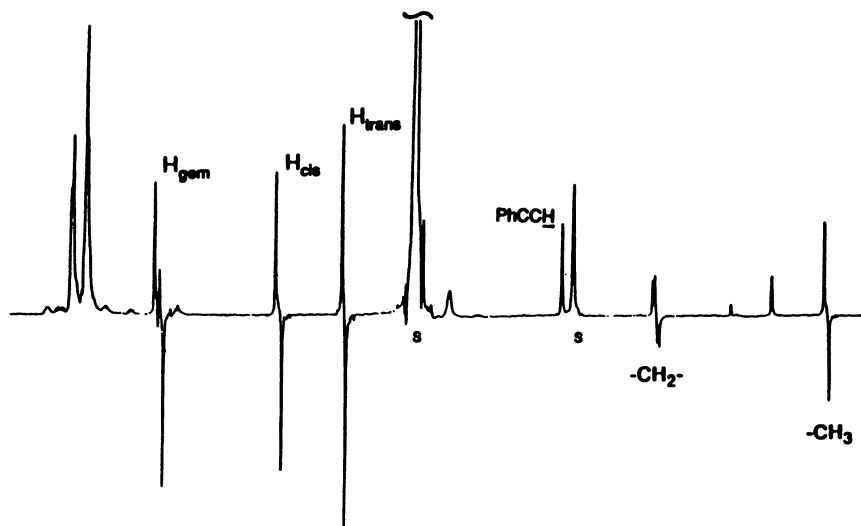
Figure 10. ¹H NMR spectra of the reaction of PhC≡CH with para-enriched H₂ catalyzed by Ru(binap)(OAc)₂ in CD₃OD at 53 °C. Peaks marked s are from orthohydrogen or methanol-d₃.

A–E–A–E pattern. This observation and additional experiments with labeled substrate show that hydrogenation catalyzed by the bi- and trinuclear complexes takes place by *cis* addition across the triple bond. The weak polarization in the *cis* proton resonance of the product styrene thus arises from cross relaxation.

In contrast, the results from using Ru(binap)(OAc)₂ as the catalyst support the notion that for phenylacetylene hydrogenation, the catalysis proceeds in a nonstereoselective manner. One of the protons originating on the parahydrogen molecule adds to the *gem* position; the other ends up in either the *cis* or *trans* position of the product styrene with approximately equal probability. Thus, the catalysis does not proceed by simple *cis* addition.

Also of note in the hydrogenation of PhC≡CH by Ru(binap)(OAc)₂ is the pronounced polarization in the resonances of the secondary product ethylbenzene. This feature contrasts with observations in the hydrogenation of styrene-d_8 catalyzed by Ru(binap)(OAc)₂, in which only weak PHIP occurs in the ethylbenzene-d_8 resonances. The difference between these results is rationalized by the notion that in PhC≡CH hydrogenation, the substrate remains coordinated throughout the double hydrogenation, but with styrene as the substrate the initial binding of substrate is unfavorable. An overall slower rate is manifested by a lower PHIP intensity.

Oxidative Addition Reactions

In the hydrogenation reactions described, the polarization was observed only in the organic product; the role of the metal catalyst was not considered.

The process of H_2 oxidative addition is of central importance in homogeneous catalysis. Therefore, several complexes with well-understood H_2 addition chemistry were examined to focus on the interactions of para-enriched H_2 with the metal center. The reaction chemistry essential to understanding these interactions, shown in eq 3, corresponds to the oxidative addition of H_2 to iridium(I) complexes of the type IrX(CO)(p–p), where p–p is $Ph_2PCH_2CH_2PPh_2$ (dppe) (*43*), *cis*-$Ph_2PCH=CHPPh_2$ (dppv) (*44*), and *o*-$(Ph_2P)_2C_6H_4$ (dppb) (*44*).

$$
O\equiv C\!-\!\overset{\displaystyle }{\underset{\displaystyle X}{Ir}}\!\!\overset{\cdots P}{\underset{\displaystyle P}{}} \; + \; H_2 \;\longrightarrow\; \overset{\displaystyle H}{\underset{\displaystyle \underset{\displaystyle O}{\overset{\|}{C}}}{H\!-\!\overset{}{\underset{X}{Ir}}}}\!\!\overset{\cdots P}{\underset{P}{}} \qquad (3)
$$
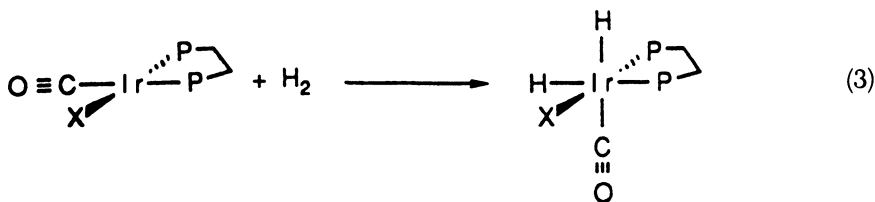
The Ir(III) *cis*-dihydride product of eq 3 forms stereoselectively and under kinetic control. At longer reaction times, conversion to a thermodynamically preferred isomer takes place (*39*). However, in the context of PHIP only the *cis*-dihydride is important. The thermodynamically preferred isomer forms slowly relative to both proton relaxation and orthohydrogen–parahydrogen equilibration in solution, obviating the possibility of PHIP in its hydride resonances.

The reaction of a CD_2Cl_2 solution of IrBr(CO)(dppb) under 3 atm of para-enriched H_2 yields the ^1H NMR spectrum shown in Figure 11. This spectrum, taken after 1 min of reaction, shows polarized resonances at δ –8.73 and –9.32 ppm corresponding, respectively, to the hydride *trans* to P and the hydride *trans* to CO of the kinetic isomer. In this spectrum, each of the ^{31}P coupled lines exists as an E–A doublet with a splitting between the emission minimum and absorption maximum of 3.7 Hz corresponding to J_{HH} coupling, which is not resolved in the unpolarized spectrum. From the phase of the doublets as E–A rather than A–E, the sign of J_{HH} can be assigned as negative. At 23 °C, PHIP due to these hydrides has been observed to last for up to 5 min.

Only multiplet polarizations are seen; reaction within the magnetic field of the spectrometer yields the observable polarization. Because the kinetic dihydride product of eq 3 forms immediately upon shaking the sample outside the spectrometer, any net polarization must decay too quickly to be seen. This conclusion was supported by independent T_1 measurements of the hydrides, which were found through the inversion-recovery method to be 1.49 s for H *trans* to P and 0.73 s for H *trans* to CO. The observed multiplet polarization thus results from the reversibility of H_2 oxidative addition, which continues in the probe.

The process of oxidative addition–reductive elimination has also been established to equilibrate ortho- and parahydrogen (*18, 19, 22, 45*). Despite

Figure 11. ^1H NMR spectrum at 400 MHz of $IrH_2Br(CO)(dppb)$ formed in the reaction of $IrBr(CO)(dppb)$ with ~3 atm of para-enriched H_2 in CD_2Cl_2 at 48 °C, 40 s after thawing from −196 °C. (Reproduced from reference 46. Copyright 1989 American Chemical Society.)

generating newly polarized product, this process would ultimately remove parahydrogen enrichment and eliminate PHIP. This prediction is supported by the fact that raising the reaction temperature to 48 °C increases the rate of H_2 oxidative addition–reductive elimination, thus hastening equilibration of the orthohydrogen–parahydrogen mixture in solution. If the rate of equilibration is increased, the duration over which PHIP is seen is shortened to less than 3 min. However, gas–solution mixing in an NMR tube and hence the relative enrichment of parahydrogen over the solution are little affected on this time scale. As an illustration, after shaking the sample tube and reinserting it into the spectrometer, nearly identical PHIP is reestablished. At room temperature, the orthohydrogen–parahydrogen mixture of the entire closed system is equilibrated on standing over a period of hours. These observations indicate that the rate of PHIP decay is due to a combination of proton relaxation, reaction to generate newly polarized product, and depletion of the parahydrogen enrichment in solution.

The magnitude of enhancement of polarization has been estimated semi-quantitatively in two ways. The first method involves measurement of the relative peak heights of the polarized hydride resonances compared to those when the PHIP has decayed. This method resulted in enhancements of up to 23-fold by comparing the peak difference between the absorption maximum and the emission minimum. As peak height is commonly used in the measurement of relaxation times, this procedure has some merit. However,

line-shape variations and signal-to-noise ratios introduce errors. Alternatively, integration of peak areas of polarized versus unpolarized resonances gives an estimate of enhancement. By using this method, 12-fold enhancements were measured for the same spectrum.

Dipolar Relaxation and Polarization Transfer to Other Nuclei

The notion of dipolar relaxation together with the establishment of non-equilibrium proton spin populations through chemical means using parahydrogen suggested the possibility that these spin populations could be transferred to other nuclei, resulting in polarization and signal enhancement in their resonances. These studies commenced by using the chemistry of eq 3 and ^{31}P NMR spectroscopy to determine if the oxidative addition of parahydrogen would lead to polarization in the ^{31}P resonances of the phosphine donors of the product dihydride complex (46).

As seen in trace a of Figure 12 for the dppb system, polarization transfer does indeed occur. The two ^{31}P resonances show antiphase polarization with a signal enhancement of ~7.4 estimated from integration relative to the normal spectrum of $IrH_2Br(CO)(dppb)$, trace b, taken several minutes later. The ^{31}P polarization decays over a period of ~3 min, similar to the decay of ^1H polarization in the hydride resonances already discussed.

For P *trans* to one hydride and *cis* to the other, phosphorus–proton coupling yields a doublet of doublets or, if $J_{PH}cis$ is unresolved, a doublet of broad resonances. Trace a of Figure 12 shows that this resonance at δ 21.3 ppm exhibits strong E–A polarization with a peak separation corresponding to the sum of $^2J_{PH}trans$ + $^2J_{PH}cis$ (148.0 and 14.8 Hz). The two inner lines of this doublet of doublets are not observed; an explanation for their absence and the observed polarization is offered later. The other ^{31}P resonance at δ 34.2 ppm for the phosphorus *cis* to both hydrides exists as a weaker E–A pattern with a separation of 34 Hz or approximately twice $^2J_{PH}cis$. In this multiplet polarization, only the outer lines of the expected triplet are seen, with the central line absent. The polarization of the resonance at δ 34.2 ppm is temperature-dependent, with the E–A pattern stronger and better defined at 48 °C than at 23 °C. Its duration is very short-lived, however. It is observed only during the first minute after thawing from 77 K, possibly because the phosphorus *cis* to both hydrides experiences dipolar relaxation by each one, which leads to more rapid loss of any nonequilibrium spin population.

For the other $IrH_2Br(CO)(P-P)$ complexes formed by oxidative addition of parahydrogen, polarization transfer to ^{31}P yielded similar results. The more pronounced effect was observed in the resonance of the phosphorus *trans* to one of the hydrides. All examples show an E–A phase, a peak separation of $^2J_{PH}trans$ + $^2J_{PH}cis$, and an estimated signal enhancement of 6–10-fold. Experimentally, the spectrum generated by using parahydrogen
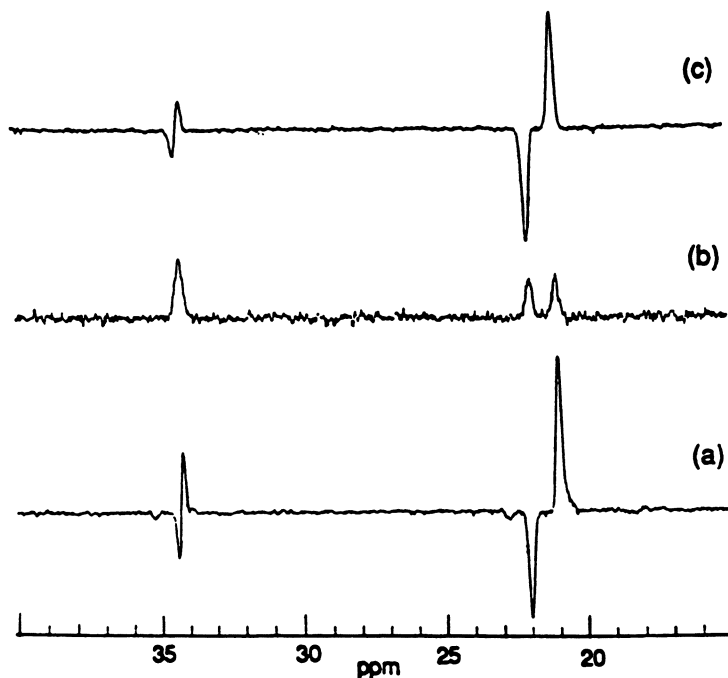
Figure 12. ³¹P NMR spectra at 162 MHz of IrH₂Br(CO)(dppb) formed in the reaction of IrBr(CO)(dppb) with ~3 atm of para-enriched H₂ in CD₂Cl₂ at 48 °C. Key: a, 42 s after thawing from −196 °C, 16 scans; b, 2 min later, 16 scans; c, INEPT spectrum of the same sample with room-temperature equilibrium of ortho- and parahydrogen, 64 scans with J = 148 Hz for ¼J delay in pulse sequence. (Reproduced from reference 46. Copyright 1989 American Chemical Society.)

(Figure 12, trace a) can be duplicated by using the INEPT pulse sequence (46). This spectrum is shown as trace c in Figure 12. In INEPT, the hydride nuclear spin populations are selectively inverted through a pulse sequence to give antiphase character in the ¹H resonances. These population differences are transferred onto the ³¹P transitions. With PHIP, the ¹H populations are perturbed chemically, with the population differences transferred to ³¹P by dipolar relaxation.

The observed polarization in the resonance of P *trans* to H can be understood in terms of the energy-level diagrams of Figure 13 for the HH′P (ABX) spin system, with individual level spin functions designated in the order H$_{trans}$H$_{cis}$P. In Figure 13a, only the ¹H αβ and βα levels are over-populated as a result of the oxidative addition reaction using parahydrogen. Upon introduction of coupling with $J_{PH}trans > 0$ and $J_{PH}cis < 0$, the level ordering is modified to that of Figure 13b. Dipolar relaxation via two-quantum transitions is distance dependent. Therefore, it occurs preferentially
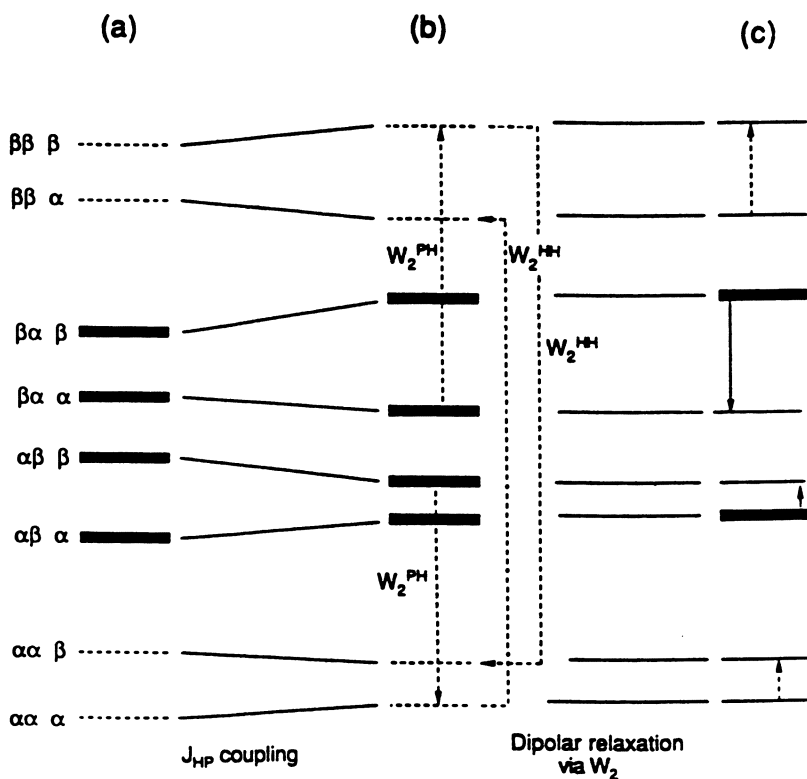
Figure 13. Energy-level diagrams for the HH'P (ABX) spin system with individual spin designations in the order of $H_{trans}H_{cis}P$. Key: a, no $^{31}P-^1H$ coupling. Only the ^1H $\alpha\beta$ and $\beta\alpha$ levels are overpopulated from addition of para-enriched H_2; b, the same diagram after introduction of couplings with $J_{PH}trans > 0$ and $J_{PH}cis < 0$ with dipolar relaxation between levels connected by dotted lines; c, ordering after dipole–dipole relaxation, with enhanced transitions shown as solid arrows. (Reproduced from reference 46. Copyright 1989 American Chemical Society.)

through *cis* partners, as shown by the dotted lines on Figure 13b for H_{cis}–P and H–H, and leads to the energy-level diagram given as Figure 13c. Only two levels, $\alpha\beta$ α and $\beta\alpha$ β, remain unaffected and, by virtue of parahydrogen addition, overpopulated. The ^{31}P NMR transitions in enhancement are shown in Figure 13c by the solid arrows; those that are absent are indicated by dotted arrows. This analysis requires $J_{PH}trans$ to be positive and $J_{PH}cis$ to be negative in order to get the separation between the emission and the enhanced absorption to equal $J_{PH}trans + |J_{PH}cis|$.

These experiments with iridium–phosphine complexes show that PHIP can be used to polarize and enhance NMR signals of less sensitive nuclei. The conditions necessary for this enhancement are that the less sensitive

nucleus has a positive nuclear Overhauser effect (NOE) with a proton that was originally part of a parahydrogen molecule, and the parahydrogen molecule undergoes pairwise addition without loss of spin correlation. This approach can be applied to ^{13}C nuclei in the hydrogenation reactions described earlier. Herein a preliminary observation is presented in support of this notion, in which polarization is found in the ^{13}C NMR spectrum of a hydrogenation product (31).

The reaction leading to this result involves the hydrogenation of styrene-d_8 that has been selectively labeled in the α position with ^{13}C. The catalyst for this reaction is $Rh_2H_2(CO)_2(dppm)_2$ in C_6D_6. The PHIP obtained in the ^1H NMR spectrum shows a ^{13}C coupling of 125 Hz to the polarized methylene proton of the ethylbenzene-d_8 product. When the reaction was performed and monitored by ^{13}C NMR spectroscopy, the results of Figure 14 were obtained. Specifically, trace a shows a 32-scan spectrum of the reaction, with the first acquisition occurring approximately 2 min 40 s from the time when the sample was thawed and shaken to commence reaction. The second trace, b, is a 32-scan spectrum taken approximately 1 min later, in which all polarization is gone. Trace a shows the viability of polarization transfer to ^{13}C
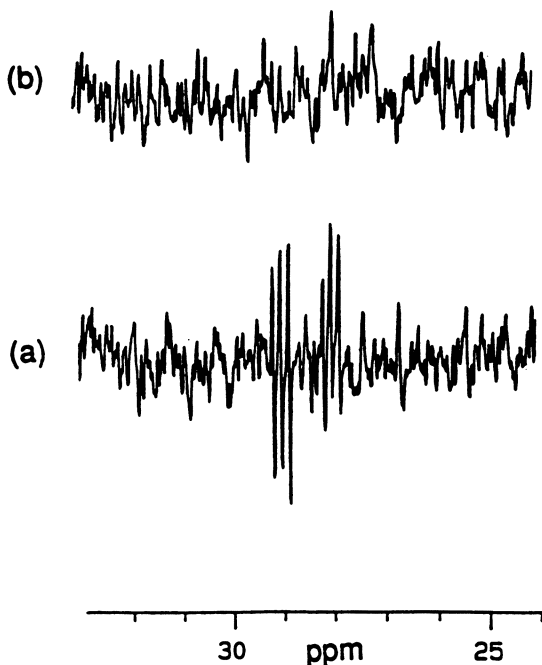
Figure 14. ^{13}C NMR spectra at 125 MHz of the hydrogenation of α-^{13}C–styrene-d_8 by $Rh_2H_2(CO)_2(dppm)_2$ under ~3 atm of para-enriched H_2 in benzene-d_6 solvent. Key: a and b are sequential 32-scan spectra recorded at reaction times of 160 and 200 s, respectively.

and clearly reveals both the deuterium–carbon and proton–proton couplings. With shorter delays from the time of commencing reaction to the beginning of data acquisition, we anticipate more greatly enhanced effects.

The polarization transfer in the spectrum of α-^{13}C–ethylbenzene-d_8 can be analyzed using a cross relaxation mechanism via NOE similar to that done for ^{31}P. If the effects of deuterium coupling are ignored, α-^{13}C–ethylbenzene-d_8 can be reduced to an ABX spin system. In Figure 15a, the nuclear spin energy levels for this system are shown with the spin designators in the order H_aH_bC. The initial overpopulation of the proton $\alpha\beta$ and $\beta\alpha$ levels is due to formation of α-^{13}C–ethylbenzene-d_8 with parahydrogen. Adjustment
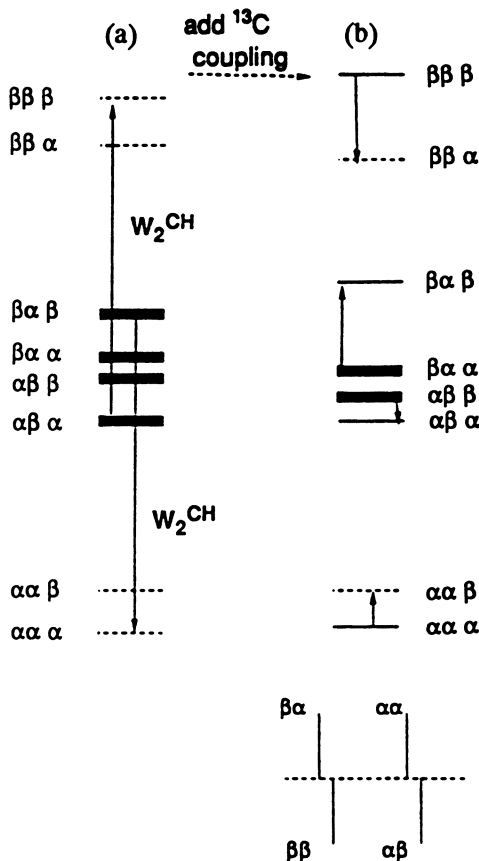
Figure 15. Energy-level diagram and expected transitions for α-^{13}C–ethylbenzene-d$_8$, showing only the spin designations for the ^{13}C-labeled carbon and the two protons. Deuterium coupling is omitted. Key: a, energy levels for the H$_a$H$_b$C spin system with individual spin designations in the order of H$_a$H$_b$C; energies are not to scale and arrows indicate dipolar relaxation; b, energy levels after introduction of couplings with $^1J_{CH_a} > {}^2J_{CH_b}$ and with enhanced ^{13}C NMR transitions shown as solid arrows.

of the level energies to account for proton–carbon coupling with $^1J_{CH} > {}^2J_{CH}$ and adjustment of level populations for dipolar relaxation (between $\alpha\alpha\alpha$ and $\beta\alpha\beta$, and between $\alpha\beta\alpha$ and $\beta\beta\beta$) yield the diagram shown as Figure 15b. The four ^{13}C transitions are thus predicted to be two doublets, each in A–E phase. The addition of deuterium coupling leads to the spectrum shown in Figure 14.

Summary and Conclusions

The relatively new phenomenon of parahydrogen-induced polarization was examined in hydrogenation and H_2 oxidative addition reactions. From a mechanistic standpoint, the occurrence of PHIP means that the reaction proceeds with pairwise addition of two atoms of H_2 into magnetically distinct sites and that, in the course of the addition, the two atoms maintain spin correlation and coupling. For PHIP to occur, a para-enriched H_2 atmosphere must be employed. This atmosphere can be generated independently or by storage of a sealed reaction sample under H_2 for several hours at 77 K prior to reaction.

Two types of polarization were found. The first corresponds to a multiplet effect in which the lines of a multiplet resonance show both absorption and emission. The second, which is termed a net effect, shows individual resonances in emission or enhanced absorption, but with lines missing in the spectrum. The net effect is closely related to the $(n - 1)$ multiplet effect in CIDNP. The difference in polarization relates to the rate of reaction relative to placement of the sample into the magnetic field of the spectrometer. Sizable signal enhancements are possible with PHIP and may allow observation of previously undetected species.

Several homogeneous catalysts of Ru were examined by using PHIP. For $RuH_4(PPh_3)_3$ large polarizations are obtained; for $RuHCl(PPh_3)_3$ the polarization is significantly weaker. In halogenated solvents, the $RuH_4(PPh_3)_3$ catalyst system changes to that of the $RuHCl(PPh_3)_3$ system. One species proposed to be active for both catalyst systems and capable of generating PHIP is $RuH_2(PPh_3)_3$. The asymmetric hydrogenation catalyst Ru(binap)-$(OAc)_2$ was also examined and found to produce PHIP in the hydrogenation of model substrates such as methyl acrylate and allyl alcohol.

The oxidative addition of H_2 to the complexes IrBr(CO)(p–p) proceeds in a concerted way, and when para-enriched hydrogen is employed, impressive polarization is observed in the hydride resonances of the product.

The notion of dipolar relaxation together with chemical perturbation of proton spin populations by para-enriched H_2 led to the observation of polarization transfer to other nuclei. Specifically, enhancement in ^{31}P and ^{13}C resonances is found in systems exhibiting PHIP when dipolar relaxation pathways connect a proton originally on a parahydrogen molecule and the less sensitive nucleus of interest. This may have application for signal enhancement in homogeneously catalyzed reactions involving H_2.

Acknowledgments

References

1. Kaptein, R.; Oosterhoff, L. J. *Chem. Phys. Lett.* **1969**, *4*, 195.
2. Kaptein, R.; Oosterhoff, L. J. *Chem. Phys. Lett.* **1969**, *4*, 214.
3. Closs, G. L. *J. Am. Chem. Soc.* **1969**, *91*, 4552.
4. Glarum, S. H. In *Chemically Induced Magnetic Polarization*; Lepley, A. R.; Closs, G. L., Eds.; Wiley: New York, 1973; Chapter 1.
5. Salikhov, K. M.; Molin, Yu. N.; Sagdeev, R. Z. *Spin Polarization and Magnetic Effects in Radical Reactions*; Elsevier: New York, 1984.
6. Ward, H. R. *Acc. Chem. Res.* **1972**, *5*, 18–24.
7. Lawler, R. G. *Acc. Chem. Res.* **1972**, *5*, 25–31.
8. Kaptein, R. *Adv. Free-Radical Chem.* **1975**, *5*, 319.
9. Closs, G. L. *Adv. Magn. Reson.* **1974**, *7*, 157.
10. Halpern, J.; Sweany, R. L. *J. Am. Chem. Soc.* **1977**, *99*, 8335.
11. Nalesnik, T. E.; Orchin, M. *Organometallics* **1982**, *1*, 222–223.
12. Nalesnik, T. E.; Orchin, M. *J. Organomet. Chem.* **1981**, *222*, C5.
13. Connolly, J. W. *Organometallics* **1984**, *3*, 1333.
14. Thomas, M. J.; Shackleton, T. A.; Wright, S. C.; Gillis, D. J.; Colpa, J. P.; Baird, M. C. *J. Chem. Soc., Chem. Commun.* **1986**, 312.
15. Wassink, B.; Thomas, M. J.; Wright, S. C.; Gillis, D. J.; Baird, M. C. *J. Am. Chem. Soc.* **1987**, *109*, 1995.
16. Bockman, T. M.; Garst, J. F.; King, R. B.; Marko, L.; Ungvary, F. *J. Organomet. Chem.* **1985**, *279*, 165.
17. Garst, J. F.; Bockman, T. M.; Batlaw, R. *J. Am. Chem. Soc.* **1986**, *108*, 1689.
18. Bowers, C. R.; Weitekamp, D. P. *Phys. Rev. Lett.* **1986**, *57*, 2645.
19. Bowers, C. R.; Weitekamp, D. P. *J. Am. Chem. Soc.* **1987**, *109*, 5541.
20. Hommeltoft, S. I.; Berry, D. H.; Eisenberg, R. *J. Am. Chem. Soc.* **1986**, *108*, 5345.
21. *Comprehensive Inorganic Chemistry*; Bailar, J. C.; Emeleus, H. J.; Nyholm, R.; Trotman-Dickenson, A. F., Eds.; Pergamon: Oxford, 1973; pp 11–16.
22. Pravica, M. G.; Weitekamp, D. P. *Chem. Phys. Lett.* **1988**, *145*, 255.
23. Eisenschmid, T. C.; Kirss, R. U.; Deutsch, P. P.; Hommeltoft, S. I.; Eisenberg, R.; Bargon, J.; Lawler, R. G.; Balch, A. L. *J. Am. Chem. Soc.* **1987**, *109*, 8089.
24. Kirss, R. U.; Eisenschmid, T. C.; Eisenberg, R. *J. Am. Chem. Soc.* **1988**, *110*, 8564.
25. Kirss, R. U.; Eisenberg, R. *J. Organomet. Chem.* **1988**, *110*, 8564.
26. Bargon, J.; Kandels, J.; Woelk, K. *Angew. Chem., Int. Ed. Engl.* **1990**, *29*, 58.
27. Collman, J. P.; Hegedus, L. S.; Norton, J. R.; Finke, R. G. *Principles and Applications of Organotransition Metal Chemistry*; University Science Books: Mill Valley, CA, 1987; pp 527–529.
28. James, B. R. *Homogeneous Hydrogenation*; Wiley: New York, 1973, and references therein.
29. James, B. R. *Adv. Organomet. Chem.* **1979**, *17*, 319, and references therein.

30. James, B. R.; Markham, L. D.; Wang, D. K. W. *J. Chem. Soc., Chem. Commun.* **1974**, 439.
31. Eisenschmid, T. C. Ph.D. dissertation, Univerity of Rochester, 1989.
32. Komiya, A.; Yamamoto, A. *Bull. Chem. Soc. Jpn.* **1976**, *49*, 2553.
33. Cole-Hamilton, D. J.; Wilkinson, G. *Nouv. J. Chim.* **1977**, *1*, 141.
34. Sanchez-Delgado, R. A.; Bradley, J. S.; Wilkinson, G. *J. Chem. Soc., Dalton Trans.* **1976**, 399.
35. Crabtree, R. H.; Hamilton, D. G. *J. Am. Chem. Soc.* **1986**, *108*, 3124.
36. Linn, D. E.; Halpern, J. *J. Am. Chem. Soc.* **1987**, *109*, 2969.
37. Strathdee, G.; Given, R. *Can. J. Chem.* **1975**, *53*, 106.
38. Hampton, C.; Dekleva, T. W.; James, B. R.; Cullen, W. R. *Inorg. Chim. Acta* **1988**, *145*, 165.
39. Parshall, G. W. *Acc. Chem. Res.* **1970**, *3*, 139.
40. Keim, W. *J. Organomet. Chem.* **1967**, *19*, 161.
41. Noyori, R.; Ohta, M.; Hsiao, Y.; Kitamura, M.; Ohta, T.; Takaya, H. *J. Am. Chem. Soc.* **1986**, *108*, 7117.
42. Ohta, T.; Takaya, H.; Noyori, R. *Inorg. Chem.* **1988**, *27*, 566.
43. Johnson, C. E.; Eisenberg, R. *J. Am. Chem. Soc.* **1985**, *107*, 3148.
44. Johnson, C. E.; Fisher, B. J.; Eisenberg, R. *J. Am. Chem. Soc.* **1983**, *105*, 7772.
45. Brown, J. M.; Canning, L. R.; Downs, A. J.; Forster, A. M. *J. Organomet. Chem.* **1983**, *255*, 103.
46. Eisenschmid, T. C.; McDonald, J.; Eisenberg, R.; Lawler, R. G. *J. Am. Chem. Soc.* **1989**, *111*, 7267.

The Tricarbonylhydridocobalt-Based Hydroformylation Reaction

A Theoretical Study

Tom Ziegler and Louis Versluis

Department of Chemistry, University of Calgary, Calgary, Alberta T2N 1N4, Canada

Density functional calculations have been carried out on the mechanism proposed by Heck and Breslow for the hydroformylation process based on tricarbonylhydridocobalt [HCo(CO)₃]. Geometries and relative energies were determined for intermediates involved in each elementary step. Reaction profiles were further traced by an approximate linear transit procedure.

$\mathbf{T}$HE OXO OR HYDROFORMYLATION REACTION, discovered in 1938 by Roelen, is used on a large industrial scale (1–3) to convert olefins and synthesis gas into aldehydes. The process employs homogeneous catalysts based on cobalt (1–3) or rhodium (4). The most commonly used precatalyst is $HCo(CO)_4$, which is generated in situ from the hydrogenation of $Co_2(CO)_8$ by H_2.

A mechanism for the cobalt-based hydroformylation process was first proposed by Heck and Breslow (5) in 1961 (Scheme I). The catalytic cycle in Scheme I consists of a number of elementary reaction steps (a–e) that we will discuss. The emphasis of the investigation lies on the identification of the equilibrium geometries and the relative energies of stable intermediates in Scheme I. The energy profile of the reaction paths connecting the intermediates will be modeled by an approximate linear transit procedure (6, 7).
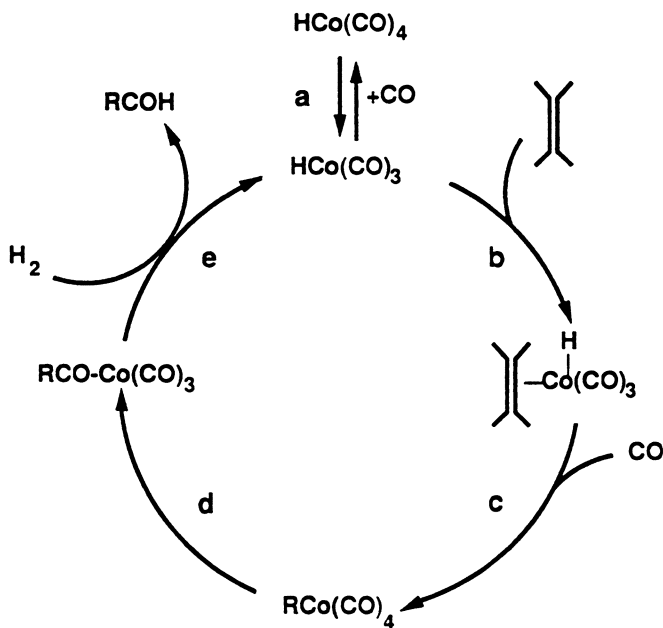
Scheme I.

Computational Details

The calculations were all based on the Hartree–Fock–Slater (HFS) model
as implemented by Baerends and co-workers (*8, 9*). With it we used the
latest version of the fully vectorized HFS–LCAO–STO program developed
by Ravenek (*10*). The bonding energies were calculated by the generalized
transition-state method (*11, 12*) in conjunction with Becke's (*13*) nonlocal
exchange corrections, as well as corrections to allow for correlations between
electrons of different spins (*14*). The numerical integration scheme employed
in this work was formulated by Becke (*15*).

An uncontracted triple-ζ Slater-type orbitals (STO) basis set (*16*) was
used for the 3s, 3p, 3d, 4s, and 4p shells of cobalt. The 2s and 2p shells of
C and O and the 1s shell of H were described by a double-ζ STO basis set
(*16, 17*), which was extended with one polarization function (2p on H and
3d on C and O). The electrons in the lower energy shells on Co, C, and O
were considered as core electrons and treated by the frozen-core approxi-
mation method according to Baerends and co-workers (*8, 9*). All molecular
structures were optimized within the C_s symmetry group. The geometry
optimizations were carried out according to the algorithm developed by
Versluis and Ziegler (*18*).

Application of Density Functional Methods to Organometallic Substances

Calculations on metal carbonyls (*19*), binuclear metal complexes (*20*), alkyl and hydride complexes (*21–23*), and complexes containing metal–ligand bonds for a number of different ligands (*24*) have shown that the approximate density functional method employed here affords metal–ligand and metal–metal bond energies of nearly chemical accuracy (± 5 kcal mol^{-1}). Approximate density functional methods have also been tested in connection with vibrational frequencies (*25*), conformational energies (*6, 7*), triplet–singlet separations (*26*), and transition-state structures (*27*). More than 50 molecular structures optimized by approximate density functional theory have been compared with experiment (*18*). The agreement between experiment and approximate density functional theory is excellent in most cases. The present method has also been applied to a study of C–H activation by late transition metals (*28*), as well as organosilane polymerization (*29*) and halogen abstraction by metal carbonyls (*30*).

Dissociation of CO from HCo(CO)₄ To Form the Catalyst HCo(CO)₃

The initial key step (a of Scheme I) in the hydroformylation process is represented by the dissociation of a CO ligand from HCo(CO)$_4$. The dissociation process results in the formation of the catalytically active species tricarbonylhydridocobalt [HCo(CO)$_3$] (eq 1).

$$HCo(CO)_4 \rightarrow HCo(CO)_3 + CO \qquad (1)$$
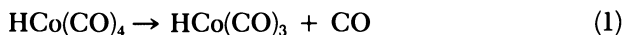
The dissociation is assumed to take place prior to, or in concert with, the complexation of an olefin leading to the olefinic π complex HCo(CO)$_3$ (η^2 olefin) (step b of Scheme I). The coordinatively unsaturated 16-electron species, HCo(CO)$_3$, has been identified by matrix isolation techniques (*31*), but its structure is unknown. We explored (*6, 7*) possible structures for HCo(CO)$_3$. Our investigation was confined to singlet states of HCo(CO)$_3$ because the carbonyl dissociation process of eq 1 probably takes place on the singlet surface.

The precatalyst HCo(CO)$_4$ has (*6, 7*) a trigonal bipyramidal (TBP) ground-state conformation with the hydride in an axial position. Dissociation of either an equatorial or axial CO ligand from HCo(CO)$_4$ will thus give rise to **1a** and **1b**, respectively.

In our calculations both **1a** and **1b** constitute local minima on the singlet surface of HCo(CO)$_3$. We calculate HCo(CO)$_3$ with the butterfly shape (**1a**)
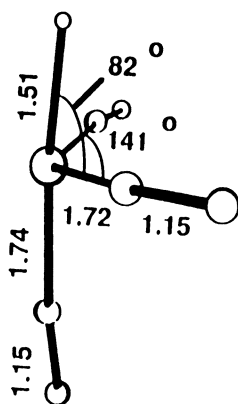
1a
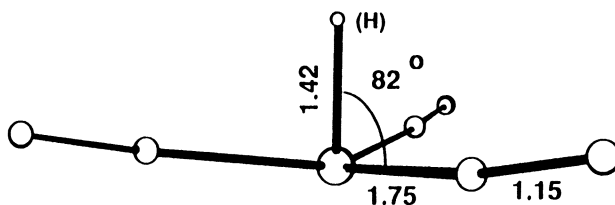
1b

to be 38 kJ mol^{-1} lower in energy than the trigonal-shaped HCo(CO)$_3$ species, **1b**. The equatorial (HCo(CO)$_4$ → **1a**) and axial [HCo(CO)$_4$ → **1b**] CO dissociation energies were found to be 186 and 224 kJ mol^{-1}, respectively. The CO dissociation energies for the d^8 complex HCo(CO)$_4$ are not known experimentally. However, our calculated values compare well with an experimental (32) (singlet) dissociation energy of 183 kJ mol^{-1} in the d^8 complex Fe(CO)$_5$. The energy required to convert the precatalyst HCo(CO)$_4$ into the active coordinatively unsaturated 16-electron species HCo(CO)$_3$ of structure **1a** (186 kJ mol^{-1}) is substantial. We shall show that step a is the most energetically demanding of the steps in Scheme I.

Some experimental evidence for the existence of HCo(CO)$_3$ in different configurations was given by Sweany and Russell (33, 34), who inferred on the basis of results from the photolysis of HCo(CO)$_4$ in an argon matrix that HCo(CO)$_3$ forms two isomers consistent with structures **1a** and **1b**.

Olefin Insertion into the Co–H Bond

The active catalyst HCo(CO)$_3$ of conformation **1a** combines in step b of Scheme I with olefin to generate a π-olefin complex where C$_2$H$_4$ is coordinated to the vacant equatorial site and the C–C bond is placed either in the equatorial plane (**2a**) or parallel to the Co–H bond (**2b**). Conformation **2a** was, as one might expect (35), calculated (7, 36) to be more stable than **2b**. However, the difference is only 20 kJ mol^{-1}, and the Co–C$_2$H$_4$ bond energy in **2a** was estimated to be 70 kJ mol^{-1}.

2a   **2b**
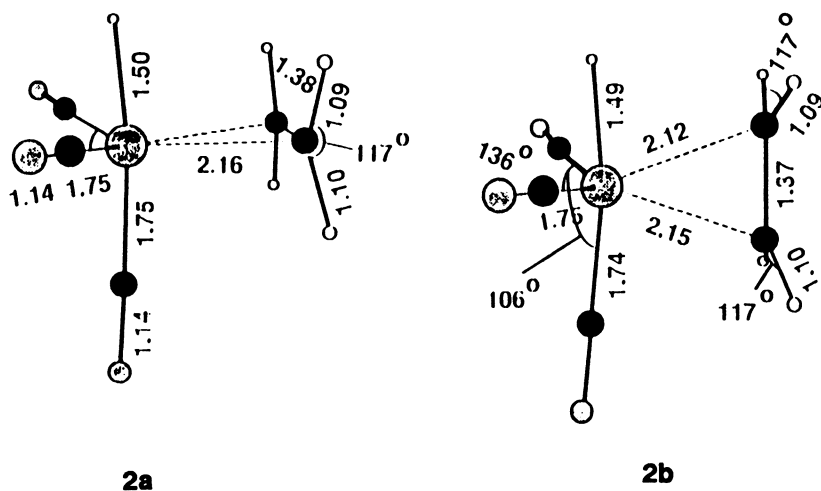
According to step c of Scheme I, the olefin will undergo a migratory insertion into the Co–H bond after its complexation, and thus form an ethyl complex.

$$HCo(CO)_3(\eta^2-C_2H_4) \rightarrow Co(CO)_3C_2H_5 \qquad (2)$$

Only **2b** has the proper relative orientation of ethylene and the hydride for the insertion. Conformation **2a** must, as a consequence, rearrange to **2b** before the process in eq 2 can take place. The reaction profile for the insertion is shown in Figure 1. The insertion process **2b** → **3a** is exothermic by 8 kJ mol^{-1} and has a small activation barrier of 5 kJ mol^{-1}. The calculated exothermicity and modest activation for the process is in agreement with the experimental observation. Thus, the migration of a hydride to a coordinated olefin group is observed experimentally to be very facile (37). In fact, the hydride–olefin insertion reaction has, with a few exceptions (38), rarely been directly observed. As a consequence, metal complexes containing both hydride and olefin are scarce.
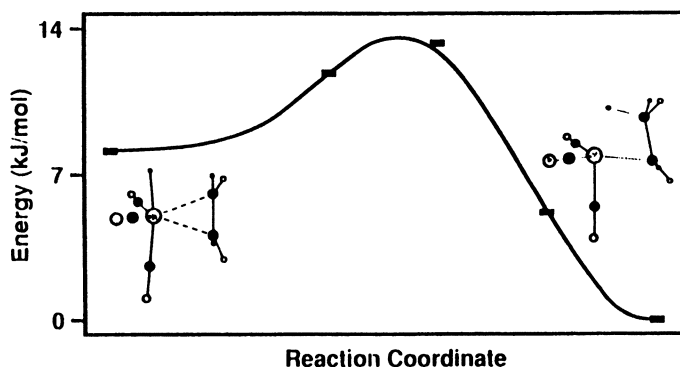
Figure 1. Energy profile of the hydride migration to the ethylene group in HCo(CO)₃(η²–C₂H₄). The energy zero refers to structure 3a.
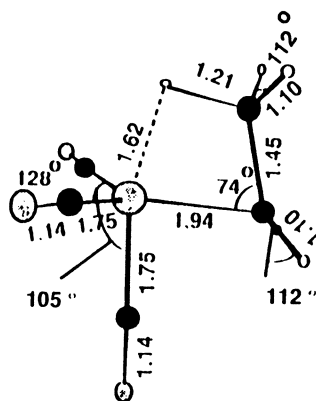
3a

    A hydrogen atom bound to carbon can interact weakly with a metal center. We shall in the following refer to such an interaction as agostic. The optimized structure, **3a**, for the resulting ethyl complex exhibits a clear agostic interaction between a β-hydrogen and the vacant metal center.

    However, under catalytic conditions, with P_{CO} = 200–300 atm, the coordinatively unsaturated complex **3a** will coordinate a CO ligand to form the saturated complex, $C_2H_5Co(CO)_4$, with the ethyl group in the equatorial position (**3b**). The coordinatively saturated ethyl complex of conformation **3b** can subsequently rearrange to the more stable (6) conformation **3c**, in which the ethyl group is in the axial position, by a Berry pseudorotation for which the activation energy is predicted (39) to be low.

3b   **3c**
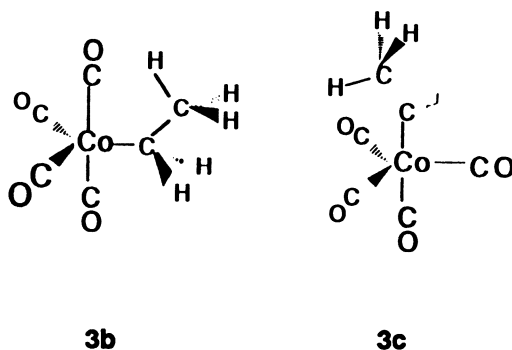
We might conclude that the olefin insertion into the Co–H bond (steps b and c of Scheme I) is very facile. Thus the olefin insertion should not constitute a bottleneck in the hydroformylation process.

Migratory Insertion of Alkyl into the Co–CO Bond

We modeled (6, 7) the migratory insertion process (step d of Scheme I) with $CH_3Co(CO)_4$ (4) rather than $C_2H_5Co(CO)_4$.

$$RCo(CO)_4 \rightarrow RC(O)Co(CO)_3 \tag{3}$$
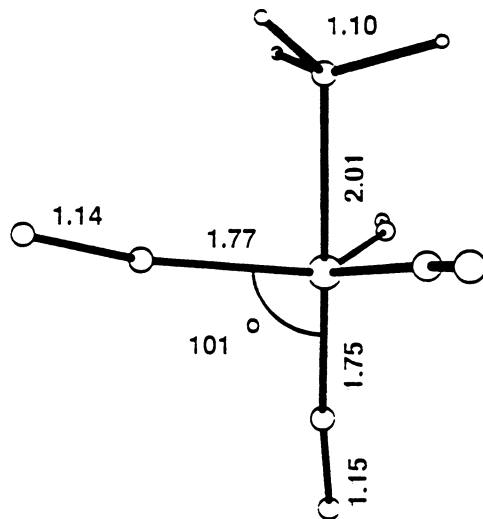
4

The process in eq 3 could in principle proceed by an insertion of a *cis*-CO into the Co–CH$_3$ bond. This insertion would produce the coordinatively unsaturated complex, **5a**, with the acyl group in an axial position. Alternatively, the methyl group might migrate to a *cis*-carbonyl and thus form complex **5b** with the acyl group in an equatorial position. Perhaps not surprisingly, we find that the energy profile for the CO insertion, **4** → **5a**, into
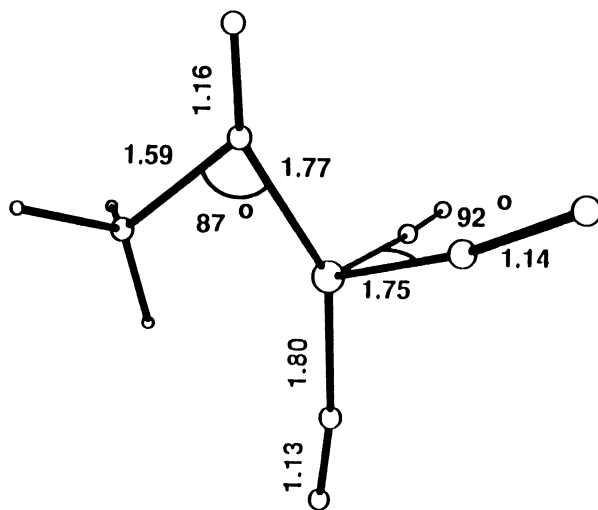
5a
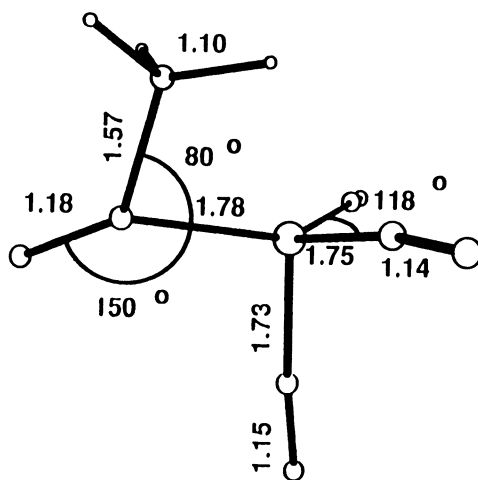
5b

the Co–CH$_3$ bond (Figure 2a) has a prohibitively high activation barrier of 200 kJ mol^{-1}. CO insertion, as a consequence, cannot be a viable mechanism for the process in eq 3.

The migration of CH$_3$ to the *cis*-CO ligand, **4** → **5b**, was calculated (Figure 2b) to have an endothermicity, ΔH, of 71 kJ mol^{-1} and a very modest activation barrier, $\Delta E^{\ddagger}$, of only 9 kJ mol^{-1}. Thus the CH$_3$ migration, **4** → **5b**, seems to be favored as the mechanism for the process in eq 3. The calculated reaction enthalpy and activation barrier for **4** → **5b** compare well with an earlier study (*40*) on the CH$_3$ → CO migration in CH$_3$Mn(CO)$_5$. In that study we found ΔH to be 75 kJ mol^{-1} and $\Delta E^{\ddagger}$ to be 11 kJ mol^{-1}. Our findings are also in agreement with a recent kinetic study by Roe (*41*), who found the rate constant of the methyl back migration of CH$_3$C(O)Co(CO)$_3$ to be considerably larger than the rate constant for the corresponding forward reaction. The structures in Figure 2a illustrate how the methyl group can slide almost parallel along the *cis* C–Co bond onto the *cis* carbonyl carbon while the remaining Co(CO)$_3$ framework stays almost unchanged. The 9 kJ mol^{-1} calculated for $\Delta E^{\ddagger}$ in the present study is an upper bound (*6, 7*) to the actual value. We can thus conclude that the methyl migration, **4** → **5b**, should proceed with a rather modest activation barrier.

The 1,2 shift reaction of an alkyl group in which a metal–alkyl system is converted into a metal–acyl complex, **4** → **5b**, is well documented for a variety of alkyl complexes. The corresponding 1,2 shift reaction, **6a** → **6b**, involving H rather than alkyl, has proven to be rather elusive. The 1,2 hydride shift reaction was inferred in earlier work (*42–44*) as an elementary reaction step. In spite of considerable efforts it has been detected with certainty only in a few cases (*45–47*). It is now widely accepted that the hydride migration, in contrast to the alkyl migration, is thermodynamically unfavorable, at least for middle to late transition metals.

We studied (*6, 7*) the 1,2 shift reaction **6a** → **6b**, which represents a 1,2 shift of a hydride in HCo(CO)$_4$ with C$_{3v}$ symmetry. The formyl structures **6b** do not represent a local energy minima on the HFS energy surface. Thus, any attempt to optimize **6b** resulted in a back migration of the formyl hydrogen to the parent hydrido metal complexes **6a**. Our findings indicate that the formyl complex **6b** is kinetically unstable with respect to the parent hydrido complex **6a**. That is, the decarbonylation reaction (**6b** → **6a**) should have at most a minimal activation barrier. Our findings can be reconciled with the experimental observation that most neutral metal formyl complexes decarbonylate readily to the corresponding hydrido complexes (*48–51*). The decomposition is believed to occur by a back migration of the formyl hydrogen to the metal center under loss of a ligand of the coordinatively saturated formyl complex. We calculate (*6, 7*) the process in eq 4 to have an exothermicity of $\Delta H = -69$ kJ mol^{-1}.

$$HC(O)Co(CO)_4 \rightarrow H\text{--}Co(CO)_4 + CO \qquad (4)$$
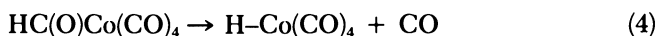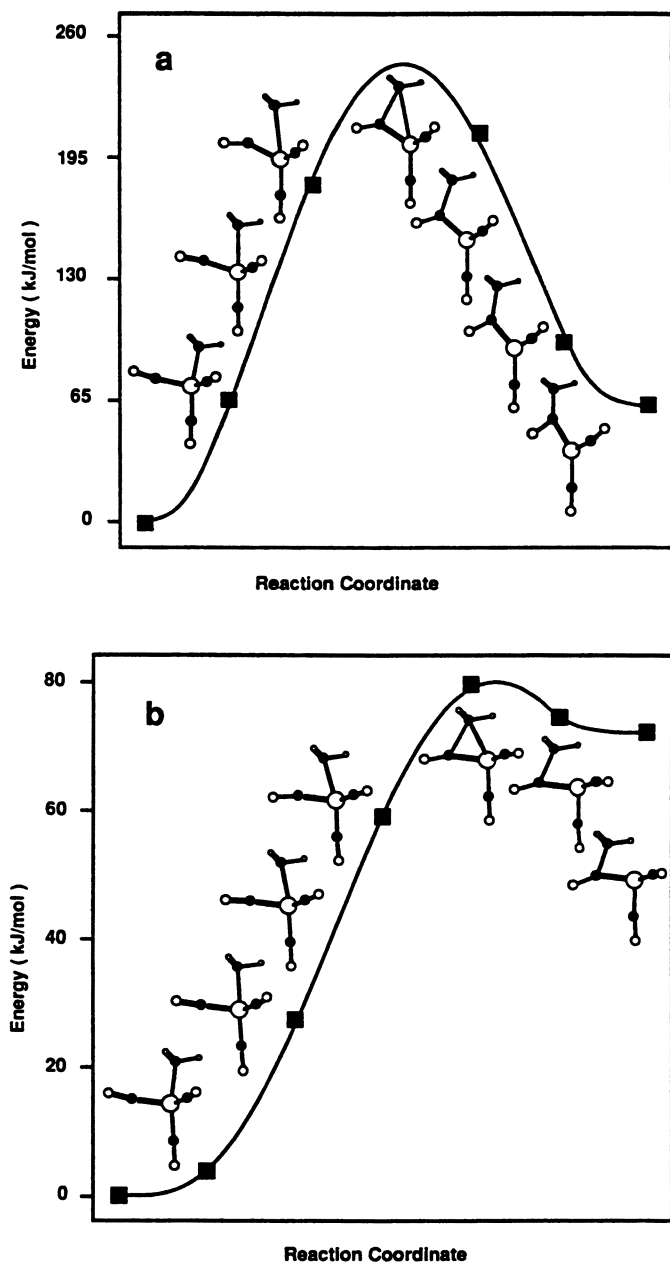
Figure 2. *a: Energy profile for the insertion of CO into the Co–CH₃ bond,* $4 \rightarrow 5a$. *b: Energy profile for the migration of* CH_3 *to CO,* $4 \rightarrow 5b$. *The zero point refers to 4 in both plots.*

6a   **6b**
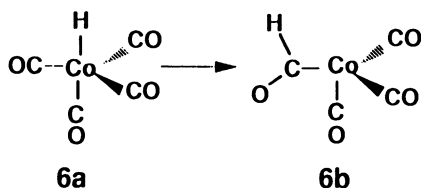
Acyl complexes are, in contrast to their formyl counterparts, well-known molecules. We calculate the corresponding decarbonylation process of $CH_3C(O)Co(CO)_4$ to be endothermic with $\Delta H \sim 20$ kJ mol^{-1}. Thus the acyl complex is thermodynamically stable, although the formyl analog is unstable and decomposes to $HCo(CO)_4$ according to eq 4. The higher exothermicity of the decarbonylation process for the formyl compared to the acyl can largely be ascribed to the higher bond strength (*21, 22, 52*) of Co–H compared to Co–CH$_3$. For middle to late transition metals D(M–H) is ~240 kJ mol^{-1} whereas the corresponding D(M–CH$_3$) bond strength is only ~160 kJ mol^{-1}. The isoelectronic d^8 formyl complex $HC(O)Fe(CO)_4^-$ has been found (*53*) to decompose slowly to $HFe(CO)_4^-$. The kinetic stability can probably be ascribed to the stabilization of the M–CO bond through increased back-bonding interactions of the carbonyl ligands in the charged species. However, the overall reaction is thermodynamically favorable with a reported exothermicity of $\Delta H = -43 \pm 30$ kJ mol^{-1} (*54*).

H₂-Induced Aldehyde Elimination

The last step in the catalytic cycle of the hydroformylation process, e of Scheme I, is the reaction of the acyl intermediate with H$_2$. This reaction results in the formation of the desired aldehyde molecule and the regeneration of the catalyst $HCo(CO)_3$.

The aldehyde product can be formed from the acyl intermediate by several possible routes. Heck and Breslow (*5*) proposed a mechanism in which the coordinatively unsaturated acyl complex undergoes first an oxidative addition of H$_2$ to afford a dihydro acyl compound (eq 5a) followed by an irreversible reductive elimination of an aldehyde molecule (eq 5b).

$$R(O)CCo(CO)_3 + H_2 \rightarrow R(O)CCo(CO)_3(H)_2 \tag{5a}$$

$$R(O)CCo(CO)_3(H)_2 \rightarrow RCHO + HCo(CO)_3 \tag{5b}$$

This type of process has been inferred for numerous catalytic and stoichiometric systems (*37*). As a consequence, these reactions have been studied

extensively by both experimental (55–65) and theoretical (66–75) techniques. However, in the cobalt-based hydroformylation process it has not been established that the product formation proceeds in fact via the oxidative addition–reductive elimination mechanism. Some experimental observations indicate (76–79) that the acyl complex might react with $HCo(CO)_4$, and thereby form an aldehyde molecule and a binuclear cobalt compound (eq 6a).

$$R(O)CCo(CO)_3 + HCo(CO)_4 \xrightarrow{CO} RCHO + Co_2(CO)_8 \qquad (6a)$$

$$Co_2(CO)_8 + H_2 \longrightarrow 2HCo(CO)_4 \qquad (6b)$$
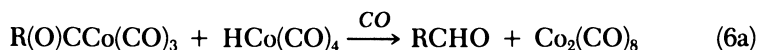
In a subsequent reaction $Co_2(CO)_8$ is then (according to eq 6b) transformed back to the mononuclear hydrido–cobalt complex. Experimental studies (5) of the stoichiometric reactions (eqs 6a and 6b) revealed that the process is very facile. However, under catalytic conditions the overall concentration of cobalt species is low in comparison to the reactants. That is, the probability for reaction between two cobalt complexes is small (77).

For electron-poor systems such as early transition metal complexes (80–83), the hydrogenolysis of the M–C bond proceeds via a mechanism in which an incoming H_2 molecule initially forms a η^2 adduct with the metal complex. This reaction is followed by the concerted cleavage of the hydrogen bond and the formation of H–M and H–C bonds by way of a four-center intermediary structure such as that illustrated by structure 7.
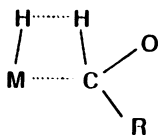
7

This reaction mode thus omits the oxidative addition–reductive elimination mechanism. Such a process could also be envisioned for the cobalt system studied here and was speculated upon by earlier workers (2, 48). In this section we will concentrate our efforts on the study of those cobalt complexes that can result from an interaction of the acyl intermediates with an incoming H_2 molecule. Furthermore, attention will be given to the oxidative addition process of H_2 to the metal fragment as well as to the hydrogenolysis reaction through a four-center intermediary structure.

The two most stable products from the interaction between an acyl complex and H_2 are the dihydrogen complexes **8a** and **8b** with H_2 in the equatorial position. Both represent energy minima on the HFS energy surface; **8b** is about 19 kJ mol^{-1} above **8a** in energy.

8a   **8b**
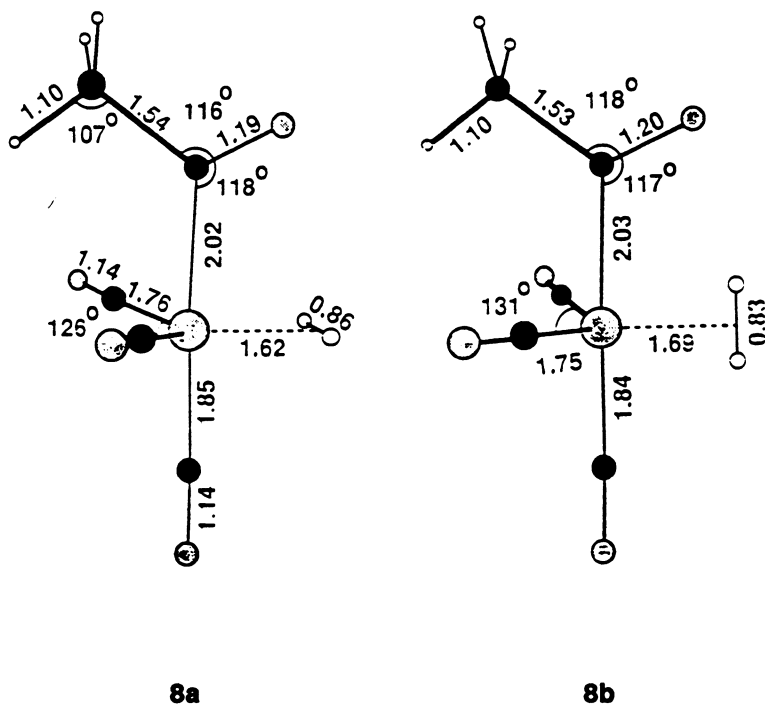
The mechanism by Heck and Breslow (5) suggests that H_2 adds oxidatively to the unsaturated acyl complex to form a dihydride, **8c**. The dihydride complex of configuration **8c** was found to be 25 kJ mol^{-1} higher in energy than the η^2 adduct **8a**. Thus the H_2 complex is more stable than the product of the oxidative addition. Complex **8c** is also 6 kJ mol^{-1} higher in energy than the η^2 compound **8b**. This result is somewhat surprising because a number of d^8 complexes containing phosphine ligands are known to add H_2 readily; this addition results in the formation of dihydrides (66–74). Thermodynamically stable η^2-H_2 complexes have been prepared (85–91). The first of these complexes was the d^6 compound $W[P(i\text{-}Pr)_3]_2(CO)_3(H_2)$ (85), for which the H–H distance was found to be 0.75 ± 0.16 Å.

A theoretical study (92) on the related model systems $W(PH_3)_2(CO)_3(H_2)$ and $W(PH_3)_5(H_2)$ revealed that the η^2-H_2 complex is stabilized by the π-acceptor CO ligands, which lower the energy levels of the metal d orbitals
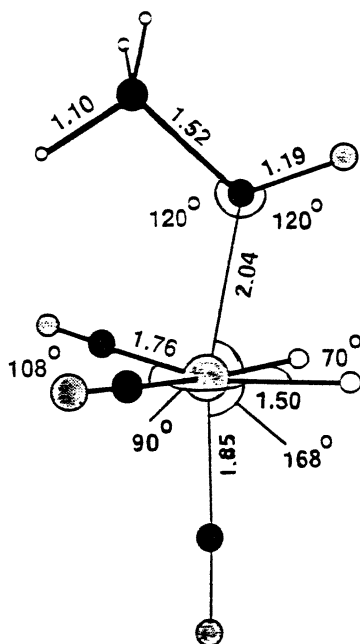
8c

with respect to the corresponding orbitals in $W(PH_3)_5(H_2)$. As a consequence, the capability of the metal fragment to donate electrons into the antibonding σ^* orbital of the H_2 molecule has diminished. In turn, this restriction prevents the system from undergoing oxidative addition. It has also been found in experimental studies involving d^8 and d^{10} complexes that the oxidative addition of H_2 is facilitated by electron-releasing ligands such as phosphines and retarded by π acceptors such as carbon monoxide (37).

Figure 3 displays the energy profile for the oxidative addition reaction **8a** $\rightarrow$ **8c**. We calculated an activation energy ΔE^* of 77 kJ mol^{-1}. This value is markedly larger than the activation energies that have been determined theoretically for the oxidative addition of H_2 to transition metal complexes containing phosphine ligands (49). This difference can be attributed to the stabilization of the η^2–H_2 adduct by the π-acceptor CO ligands. The energy curve modeled in Figure 3 ascends steeply during the early stages of the reaction. The slope indicates that the activation energy arises largely from the initial elongation of the H–H bond distance.

The fact that the oxidative addition process, **8a** $\rightarrow$ **8c**, exhibits a sizable activation barrier led us to consider an alternative mechanism for the last product-forming step (e of Scheme I) in the hydroformylation cycle. The
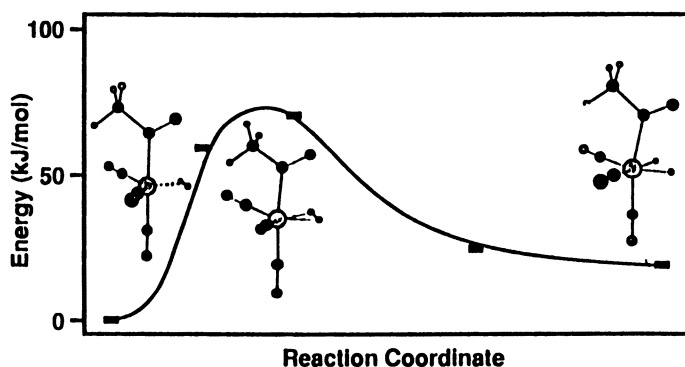
Figure 3. Energy profile for the oxidative addition of H_2 to $CH_3C(O)Co(CO)_3$.

alternative mechanism assumes that one hydrogen atom of the η^2–H_2 complex shifts directly toward the acyl group and thereby forms an aldehyde molecule and regenerates the catalyst $HCo(CO)_3$. This type of reaction mechanism, in which a direct oxidative addition of H_2 is avoided, has, to our knowledge, never been investigated theoretically for the cobalt-based hydroformylation process.

The approximate profile for the reaction 9a → 9b → 9c is given in Figure 4. The first part of the profile connecting 9a and 9b was obtained by changing the internal coordinates of 9a into those of 9b in a linear and stepwise fashion. A total of six steps was used in the transit. We find the reaction proceeds with a minimal activation barrier (Figure 4). The activation energy for the first part, 9a → 9b, is therefore essentially equivalent to the reaction enthalpy ΔE for the reaction 9a → 9b, which was calculated to be 83 kJ mol^{-1}. We have also traced the energy surface for the reaction 9b → 9c by using a similar five-step linear transit procedure. The step 9b → 9c, which is exothermic with a reaction enthalpy of $\Delta E = -26$ kJ mol^{-1}, has a negligible activation energy. Finally, the system, 9c, is lowered in energy by 69 kJ mol^{-1} as the adduct 9c breaks up into acetaldehyde and $HCo(CO)_3$ in its ground-state conformation 1a.

9a   9b   9c

Reaction Coordinate
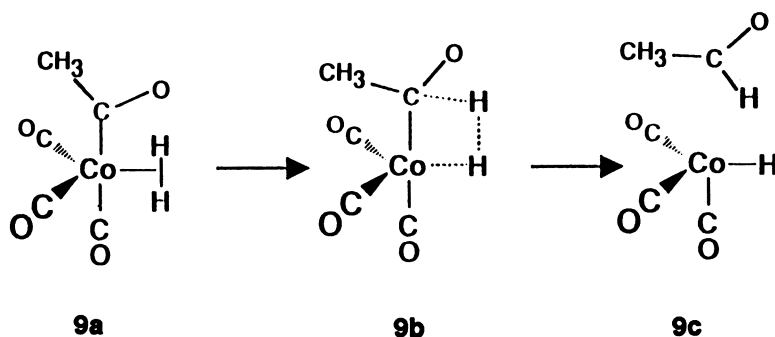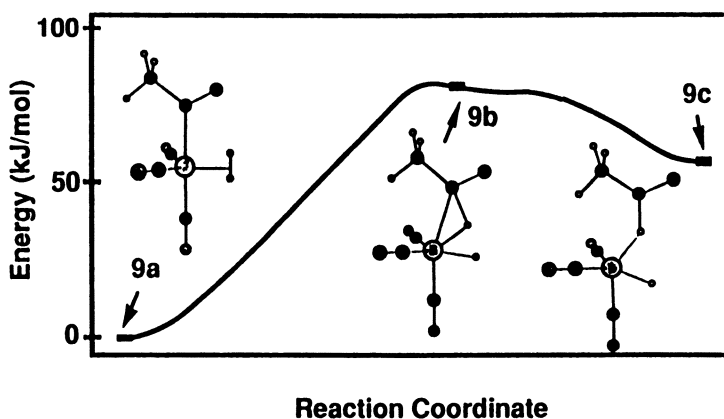
Figure 4. Energy profile for the reaction 9a → 9b → 9c.

Concluding Remarks

We carried out calculations on the elementary steps of the hydroformylation process. Our calculations indicate that the last product-forming step (e of Scheme I, in which aldehyde elimination is induced) has the highest activation energy with $\Delta H^{\ddagger} \sim 80\text{–}90$ kJ mol^{-1}. Step d was calculated to have a similar activation energy ($\Delta H^{\ddagger} \sim 70\text{–}80$ kJ mol^{-1}). The insertion of olefin into the Co–H bond (steps b–c) was, on the other hand, estimated to have a negligible activation energy of $\Delta H^{\ddagger} \sim 10\text{–}20$ kJ mol^{-1}. We finally found that the formation of the active catalyst HCo(CO)$_3$ from HCo(CO)$_4$ by CO dissociation (step a) requires 185 kJ mol^{-1}. More detailed studies of steps a (6), b (93), c (6), d (94), and e (94) of Scheme I can be found elsewhere.

Acknowledgment

References

1. Heck, R. F. *Adv. Organomet. Chem.* **1966**, *4*, 243.
2. Orchin, M.; Rupilius, W. *Catal. Rev.* **1972**, *6*, 85.
3. Orchin, M. *Acc. Chem. Res.* **1981**, *14*, 25.

4. Pino, P.; Piacenti, F.; Bianchi, M. In *Organic Synthesis via Metal Carbonyls,* Vol. II; Wender, I.; Pino, P., Eds.; Wiley: New York, 1977; pp 43–135.
5. Heck, R. F.; Breslow, D. S. *J. Am. Chem. Soc.* **1961**, *83*, 4023.
6. Versluis, L.; Ziegler, T.; Baerends, E. J.; Ravenek, W. *J. Am. Chem. Soc.* **1989**, *111*, 2018.
7. Versluis, L. Ph.D. Thesis, University of Calgary, 1989.
8. Baerends, E. J.; Ellis, D. E.; Ros, P. *Chem. Phys.* **1973**, *2*, 41.
9. Baerends, E. J., Ph.D. Thesis, Vrije Universiteit, Amsterdam, 1975.
10. Ravenek, W. In *Algorithms and Applications on Vector and Parallel Computers*; te Riele, H. J. J.; Dekker, Th. J.; van de Vorst, H. A., Eds.; Elsevier: Amsterdam, 1987.
11. Ziegler, T.; Rauk, A. *Theor. Chim. Acta* **1977**, *46*, 1.
12. Ziegler, T., Ph.D. Thesis, University of Calgary, 1978.
13. Becke, A. D. *J. Chem. Phys.* **1986**, *84*, 4524.
14. Stoll, H.; Golka, E.; Preuss, H. *Theor. Chim. Acta* **1980**, *55*, 29.
15. Becke, A. D. *J. Chem. Phys.* **1988**, *88*, 2547.
16. Snijders, G. J.; Baerends, E. J.; Vernooijs, P. *At. Nucl. Data Tables* **1982**, *26*, 483.
17. Vernooijs, P.; Snijders, G. J.; Baerends, E. J. "Slater Type Basis Functions for the Whole Periodic System"; internal report, Free University of Amsterdam: Netherlands, 1981.
18. Versluis, L.; Ziegler, T. *J. Chem. Phys.* **1988**, *88*, 322.
19. Ziegler, T.; Tschinke, V.; Ursenbach, C. *J. Am. Chem. Soc.* **1987**, *109*, 4825.
20. Ziegler, T.; Tschinke, V.; Becke, A. D. *Polyhedron* **1987**, *6*, 685.
21. Ziegler, T.; Tschinke, V.; Becke, A. D. *J. Am. Chem. Soc.* **1987**, *109*, 1351.
22. Ziegler, T.; Cheng, W.; Baerends, E. J.; Ravenek, W. *Inorg. Chem.* **1988**, *27*, 3458.
23. Ziegler, T.; Tschinke, V.; Baerends, E. J.; Snijders, J. G.; Ravenek, W. *J. Phys. Chem.* **1989**, *93*, 3050.
24. Ziegler, T.; Tschinke, V.; Versluis, L.; Baerends, E. J.; Ravenek, W. *Polyhedron* **1988**, *7*, 1625.
25. Fan, L.; Versluis, L.; Ziegler, T.; Baerends, E. J.; Ravenek, W. *Int. J. Quantum Chem.* **1988**, *S22*, 173.
26. Ziegler, T.; Rauk, A.; Baerends, E. J. *Theor. Chim. Acta* **1977**, *43*, 261.
27. Fan, L.; Ziegler, T. *J. Chem. Phys.* **1990**, *92*, 897.
28. Ziegler, T.; Tschinke, V.; Fan, L.; Becke, A. D. *J. Am. Chem. Soc.* **1989**, *111*, 9177.
29. Harrod, J. F.; Ziegler, T.; Tschinke, V. *Organometallics* **1990**, *9*, 897.
30. Master, A. P.; Soerensen, T. S.; Ziegler, T. *Organometallics* **1989**, *8*, 1088.
31. Wermer, P.; Ault, B. S.; Orchin, M. *J. Organomet. Chem.* **1978**, *162*, 189.
32. Lewis, K. E.; Golden, D. M.; Smith, G. P. *J. Am. Chem. Soc.* **1984**, *106*, 3906.
33. Sweany, R. L.; Russell, F. N. *Organometallics* **1988**, *7*, 719.
34. Sweany, R. L. *Organometallics* **1989**, *8*, 175.
35. Rossi, A. R.; Hoffmann, R. *Inorg. Chem.* **1975**, *14*, 365.
36. Versluis, L.; Ziegler, T. *J. Am. Chem. Soc.* **1990**, *112*, 6763.
37. Collman, J. P.; Hegedus, L. S. In *Principles and Applications of Organotransition Metal Chemistry*; Kelly, A., Ed.; University Science Books: Mill Valley, CA, 1980.
38. Werner, H.; Feser, R. *Angew. Chem., Int. Ed. Engl.* **1979**, *18*, 157.
39. Koga, N.; Jin, S. Q.; Morokuma, K. *J. Am. Chem. Soc.* **1988**, *110*, 3417.
40. Ziegler, T.; Versluis, L.; Tschinke, V. *J. Am. Chem. Soc.* **1986**, *108*, 612.
41. Roe, D. C. *Organometallics* **1987**, *6*, 942.
42. Dombek, B. D. *Ann. N. Y. Acad. Sci.* **1983**, *415*, 176.

43. Dombek, B. D. In *Adv. Catal.* **1983**, *32*, 325.
44. Byers, B. H.; Brown, T. L. *J. Am. Chem. Soc.* **1977**, *99*, 2527.
45. Wayland, B. B.; Duttahmed, A.; Woods, B. A.; Pierce, R. *J. Chem. Soc., Chem. Commun.* **1983**, 143–144.
46. Fagan, P. J.; Manriquers, J. M.; Marks, T. J.; Vollmer, S. H.; Day, C. S.; Day, V. W. *J. Am. Chem. Soc.* **1981**, *103*, 2206.
47. Moloy, K. G.; Marks, T. J. *J. Am. Chem. Soc.* **1984**, *106*, 7051.
48. Tam, W.; Wong, W. K.; Gladysz, J. A. *J. Am. Chem. Soc.* **1979**, *101*, 1589.
49. Collins, T. J.; Roper, W. R. *J. Chem. Soc., Chem. Commun.* **1976**, 1044.
50. Brown, K. L.; Clark, G. R.; Headford, C. E. L.; Marsden, K.; Roper, W. R. *J. Am. Chem. Soc.* **1979**, *101*, 503.
51. Chaudret, B. N.; Cole-Hamilton, D. J.; Nohr, R. S.; Wilinnson, G. *J. Chem. Soc., Dalton Trans.* **1977**, 1546.
52. Martinho Simoes, J. A.; Beauchamp, J. L. *Chem. Rev.* **1990**, *90*, 629.
53. Collman, J. P.; Winter, S. R. *J. Am. Chem. Soc.* **1973**, *95*, 4089.
54. Lane, K. R.; Sallans, L.; Squires, R. R. *Organometallics* **1985**, *4*, 408.
55. Collman, J. P.; Roper, W. R. *Adv. Organomet. Chem.* **1968**, *7*, 53.
56. James, B. R. In *Homogeneous Hydrogenation*; Wiley: New York, 1973.
57. Chock, P. B.; Halpern, J. *J. Am. Chem. Soc.* **1966**, *88*, 3511.
58. Halpern, J. *Acc. Chem. Res.* **1970**, *3*, 386.
59. Lappert, M. F.; Lednor, P. W. *Adv. Organomet. Chem.* **1976**, *14*, 345.
60. Crabtree, R. H.; Morehouse, S. M. *Adv. Organomet. Chem.* **1982**, *21*, 4210.
61. Harrod, J. F.; Yorke, W. J. *J. Inorg. Chem. (USSR)* **1981**, *20*, 1156.
62. Norton, J. *Acc. Chem. Res.* **1979**, *12*, 139.
63. Kemmitt, R. D. W.; Smith, M. A. R. *Inorg. React. Mech.* **1976**, *4*, 3119.
64. Abis, L.; Sen, A.; Halpern, J. *J. Am. Chem. Soc.* **1978**, *100*, 2915.
65. Halpern, J. *Acc. Chem. Res.* **1982**, *15*, 332.
66. Low, J. J.; Goddard, W. A., III *Organometallics* **1986**, *5*, 609.
67. Low, J. J.; Goddard, W. A., III *J. Am. Chem. Soc.* **1984**, *106*, 6228.
68. Noell, J. O.; Hay, P. J. *J. Am. Chem. Soc.* **1982**, *104*, 4578.
69. Obara, S.; Kitaura, K.; Morokuma, K. *J. Am. Chem. Soc.* **1984**, *106*, 7482.
70. Dedieu, A.; Strich, A. *Inorg. Chem.* **1979**, *18*, 2940.
71. Sevin, A. *Nouv. J. Chim.* **1981**, *5*, 233.
72. Balazs, A. C.; Johnson, K. H.; Whitesides, G. M. *Inorg. Chem.* **1982**, *21*, 2162.
73. Lauher, J. W.; Hoffmann, R. *J. Am. Chem. Soc.* **1976**, *98*, 1729.
74. Tatsumi, K.; Hoffmann, R.; Yamamoto, A.; Stille, J. K. *Bull. Chem. Soc. Jpn.* **1981**, *54*, 1857.
75. Rabaâ, H.; Saillard, J.-Y.; Hoffmann, R. *J. Am. Chem. Soc.* **1986**, *108*, 4327.
76. Alemdarogly, N. H.; Penninger, J. L. M.; Oltay, E. *Monatsh. Chem.* **1976**, *107*, 1153.
77. Kovás, I.; Ungváry, F.; Markó, L. *Organometallics* **1986**, *5*, 209.
78. Ungváry, F.; Markó, L. *Organometallics* **1983**, *2*, 1608.
79. Hoff, C. D.; Ungváry, F.; King, R. B.; Markó, L. *J. Am. Chem. Soc.* **1985**, *107*, 666.
80. Lin, Z.; Marks, J. *J. Am. Chem. Soc.* **1987**, *109*, 7979.
81. Steigerwald, M. L.; Goddard, W. A., III *J. Am. Chem. Soc.* **1984**, *106*, 308.
82. Jeske, G.; Lauke, H.; Mauermann, H.; Schumann, H.; Marks, T. J. *J. Am. Chem. Soc.* **1985**, *107*, 8111.
83. Watson, P. J.; Parshall, G. W. *Acc. Chem. Res.* **1985**, *18*, 51.
84. Brintzinger, H. H. *J. Organomet. Chem.* **1979**, *171*, 337.
85. Kubas, G. J.; Ryan, R. R.; Swanson, B. I.; Vergamini, P. J.; Wasserman, H. *J. Am. Chem. Soc.* **1984**, *106*, 451.

86. Kubas, G. J.; Unkefer, G. J.; Swanson, B.; Fukishima, E. *J. Am. Chem. Soc.* **1986**, *108*, 7000.
87. Wasserman, H. J.; Kubas, G. J.; Ryan, R. R. *J. Am. Chem. Soc.* **1986**, *108*, 2294.
88. Upmacis, R. K.; Gadd, G. E.; Poliakoff, M.; Simpson, M. B.; Turner, J. J.; Whyman, R.; Simpson, A. F. *J. Chem. Soc., Chem. Commun.* **1985**, 27.
89. Sweany, R. L. *J. Am. Chem. Soc.* **1985**, *107*, 2374.
90. Church, S. P.; Grevels, F. W.; Hermann, H.; Schaffner, K. *J. Chem. Soc., Chem. Commun.* **1985**, 30.
91. Crabtree, R. H.; Lavin, M. *J. Chem. Soc., Chem. Commun.* **1985**, 794.
92. Hay, P. J. *J. Am. Chem. Soc.* **1987**, *109*, 705.
93. Versluis, L.; Ziegler, T.; Fan, L. *Inorg. Chem.* **1990**, *29*, 5340.
94. Versluis, L.; Ziegler, T. *Organometallics* **1990**, *9*, 2985.

6

Oscillations and Chaos in Some O$_2$ Oxidations

J. D. Druliner[1], L. D. Greller[2], M. G. Roelofs[1], and E. Wasserman[1]

[1]Central Research and Development, E. I. du Pont de Nemours and Company, Experimental Station, P.O. Box 80328, Wilmington, DE 19880–0328
[2]SmithKline Beecham, P.O. Box 1539, King of Prussia, PA 19406–0939

Oscillatory or chaotic dynamics were found for the metal-catalyzed air oxidations of benzaldehyde, cyclohexanone, toluene, and p-xylene. Hydrocarbon autoxidations are suggested as an appropriate area in which to look for new examples of oscillatory behavior.

W ELL-DOCUMENTED OSCILLATIONS of chemical species in homogeneous reactions were reported in 1921. Bray observed the unusual behavior in the reaction of H$_2$O$_2$ with I$_2$ (1). Since then a variety of dynamic behavior has been reported for numerous chemical systems, particularly in the oxidation and reduction of halogens and oxyhalogens. Reactions that are sufficiently far from equilibrium can give rise to a range of dynamic phenomena, including multiple stationary states and simple, two-period, and aperiodic (chaotic) oscillations (2–5).

In this chapter, we summarize chemical observations and dynamics calculations involving our own studies of several organic–O$_2$ oxidations. These oxidations include the catalyzed reaction of O$_2$ with benzaldehyde, cyclohexanone, toluene, and p-xylene. Given the highly exothermic nature of these reactions and the explosive potential of organic vapor–oxygen gas mixtures, appropriate safety precautions must be taken. Thus, all experiments described here were performed with proper barricades.

Some rather general broad-ranging features associated with hydrocarbon autoxidations in solution suggested that this was an appropriate area in which to look for new examples of oscillating behavior. These autoxidations have

features that are generally associated with oscillating behavior. Such a system should

- be far from equilibrium;
- have sufficient mechanistic complexity; and
- exhibit autocatalytic behavior.

When far from equilibrium, a reaction may be highly exothermic and exhibit nonlinear kinetics. The mechanistic complexity of a system can be expressed in terms of independent first-order differential equations. At least two such equations, for two intermediates, are required for periodic oscillations; at least three are required for aperiodic, chaotic behavior.

Finally, feedback is necessary; that is, the product of a reaction step influences the rate of formation or destruction of that product. Autoxidation reactions involve feedback in the autocatalytic buildup of alkyl radicals. These intermediates arise from alkyl hydroperoxides and their hydroxyl and alkoxyl radical homolysis products.

$$R^{\bullet} \xrightarrow{O_2} ROO^{\bullet} \xrightarrow{RH} ROOH + R^{\bullet}$$
$$\downarrow$$
$$RO^{\bullet} \xrightarrow{RH} R^{\bullet} + ROH$$
$$+ HO^{\bullet} \xrightarrow{RH} R^{\bullet} + HOH$$
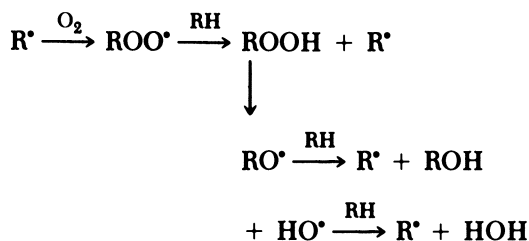
O_2 Oxidation of Benzaldehyde

While searching for examples of oscillating oxidations at Du Pont, we learned of the seminal discovery by J. R. Jensen (6). He examined an often-studied O_2 oxidation reaction, the Co–Br-catalyzed air oxidation of benzaldehyde to benzoic acid in acetic acid–water solutions. His experimental setup differed from those usually used by incorporating an electrode, a detector with a short response time. Sustained oscillations can be observed with it (Figure 1). The period varies with conditions between about 15 s and 7 min.

At the lowest potentials, these solutions are the characteristic pink of Co^{2+}. Near the maxima they are the dark green of Co^{3+} in acetic acid. Simultaneous measurement of the redox potential and the visible absorbance maximum of Co^{3+} at 610 nm (Figure 2) reveals that these quantities exhibit parallel behavior (7, 8).

Although Br^- was present in the reaction, measurements taken with a Br^- ion-selective electrode showed that its concentration varies only slightly
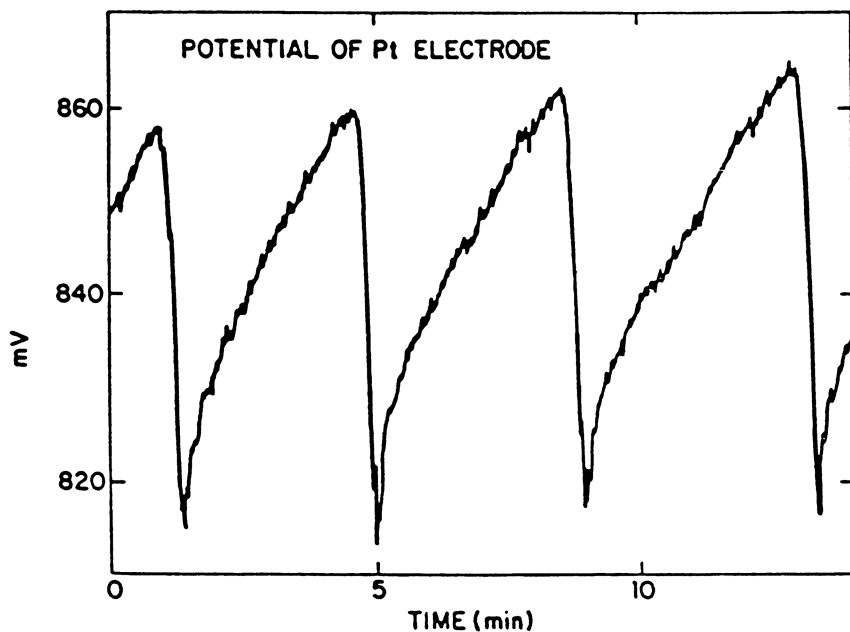
Figure 1. Oscillations in redox potential accompanying O₂ oxidation of benzaldehyde at 70 °C in acetic acid–water (90:10).
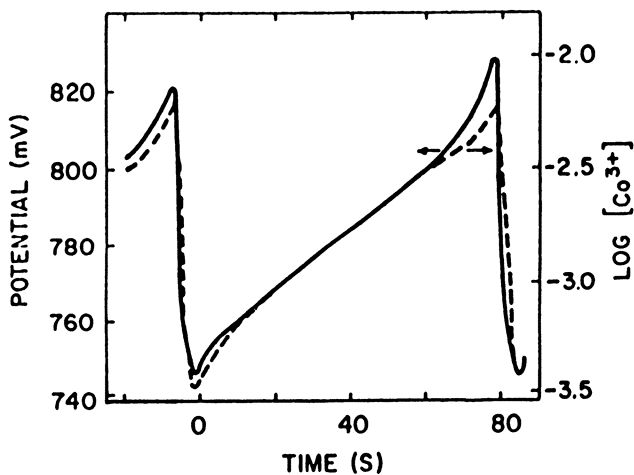
Figure 2. Oscillations in redox potential and visible absorbance accompanying O₂ oxidation of benzaldehyde at 70 °C in acetic acid–water (90:10). (Reproduced from reference 7. Copyright 1983 American Chemical Society.)

within a period. This lack of variation in [Br⁻] is in marked contrast to that of the Belousov–Zhabotinskii and Briggs–Rauscher reactions, both of which are characterized by orders of magnitude changes in concentrations of Br⁻ (or I⁻) and oxyhalogen intermediates, such as $HBrO_2$ (1, 2, 9).

Two different reaction stages, I and II, can be distinguished in the benzaldehyde system (Figure 3). During stage I the concentration of dissolved O_2 increases to a maximum of ~25% of saturation and then decreases to near zero. During stage II the dissolved O_2 remains undetectable, while the redox potential quickly drops from its highest to its lowest values.

The results of ¹⁸O labeling were compatible with two different contributions to the generation of benzoic acid, the final oxidation product. During stage I benzoyl radicals react primarily with dissolved O_2, forming benzoyl-oxy radicals. During stage II, with its absence of dissolved O_2, oxygen from H_2O combines with benzoyl radicals as they are oxidized by Co^{3+}. Increased concentrations of radicals during step II could be detected by electron paramagnetic resonance (EPR) spectroscopy (10). This evidence of two different stages in the oxygen incorporation indicates how the richness of oscillating
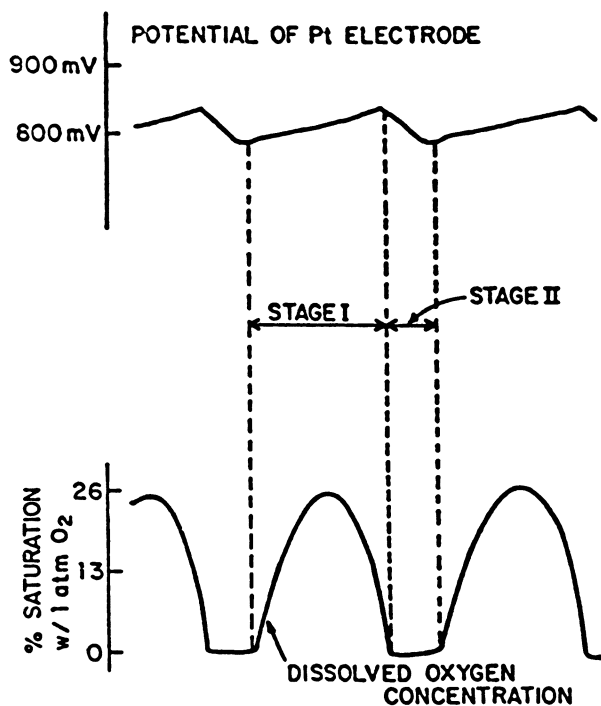
Figure 3. Comparison of potential of the Pt electrode with dissolved O_2 concentration in the oxidation of benzaldehyde at 70 °C in acetic acid–water (90:10). (Reproduced from reference 7. Copyright 1983 American Chemical Society.)

behavior, encountered in a reaction often studied under steady-state conditions, may yield additional mechanistic insight.

Other groups working with this system have described oscillations during oxidations of acetaldehyde or propionaldehyde (*11*), an alternative detailed mechanism (*12, 13*), and a simplified mechanism for the oscillations (*13*). Despite some differences, both proposed detailed mechanisms (*8, 13*) are fundamentally the same and possess some unusual mechanistic features. Both involve reactions whereby benzoyl radicals are autocatalytically produced via reactions in which two radicals are the products of one step. Both assign a key role to the oxidation of benzoyl radicals in a reaction involving a complex containing Co^{3+} and Br^-.

O_2 Oxidation of Cyclohexanone

The O_2 oxidation of cyclohexanone was examined for oscillating behavior in an otherwise well-established aliphatic reaction (*14*). Unlike the high yield (>98%) obtained in the oxidation of benzaldehyde to benzoic acid, the reaction of O_2 with cyclohexanone to form adipic acid is accompanied by at least 100 other products detectable by capillary gas chromatographic (GC) analysis. The same concentrations of $Co(OAc)_2$ and NaBr in acetic acid–water were used for the cyclohexanone system as previously employed with benzaldehyde. Modestly higher concentrations of O_2 were used with temperatures of about 100 °C versus 70 °C with benzaldehyde.

In a comparison of the two systems, the cyclohexanone system exhibits greater changes in both redox potentials and dissolved O_2 concentrations (Figure 4). The qualitative behavior of both variables also differed for the two systems. With cyclohexanone the redox potential rises slowly during the greater part of each cycle, followed by a rapid rise to a maximum value
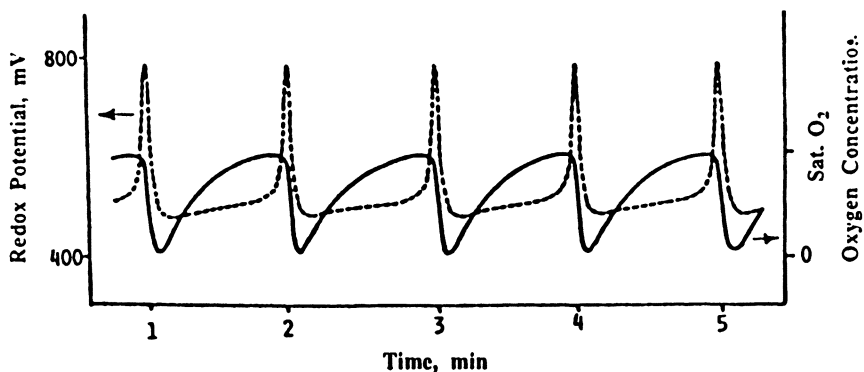
Figure 4. Comparison of potential of the Pt electrode with dissolved O_2 concentration in the oxidation of cyclohexanone at 105 °C in acetic acid–water (90:10). (Reproduced from reference 14. Copyright 1988 American Chemical Society.)

and a very rapid drop to a minimum. The dissolved O_2 concentration rises slowly to near saturation and then decreases very quickly as the redox potential reaches a maximum.

Whereas two distinct stages of behavior were discernible with benzaldehyde (Figure 3), three stages can be assigned in the cyclohexanone system (Figure 5). During stage A the concentration of Co^{3+} remains relatively constant and the redox potential rises very slowly to a knee marking the beginning of stage B. During B both redox potential and $[Co^{3+}]$ rise quickly to maximum values. During stage C both redox potential and $[Co^{3+}]$ rapidly drop to their minimum values. The long period of relatively flat potential in stage A, corresponding to slow autoxidation of cyclohexanone, is absent in the benzaldehyde system.
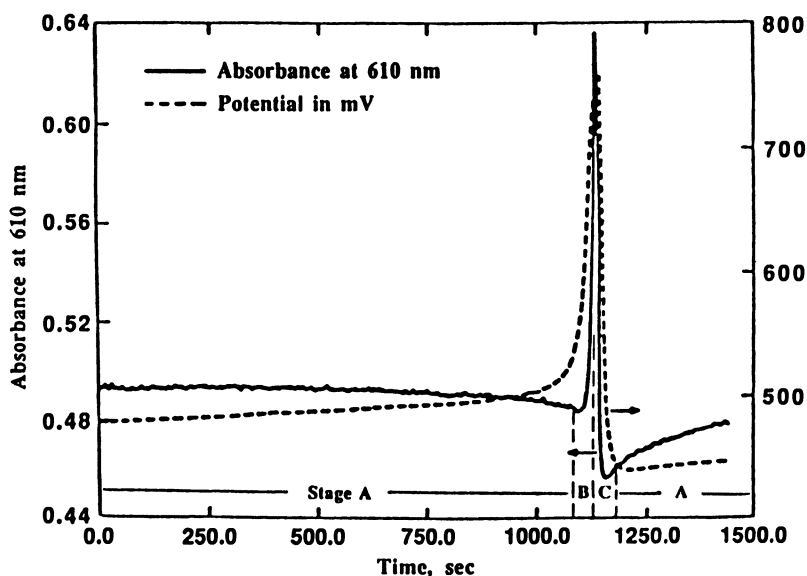
Figure 5. Comparison of redox potential and visible absorbance during one oscillation cycle accompanying O_2 oxidation of cyclohexanone at 99 °C in acetic acid–water (90:10). (Reproduced from reference 14. Copyright 1988 American Chemical Society.)

The primary role of cobalt during stage A is to facilitate the gradual increase in the concentrations of 2-hydroperoxycyclohexanone and 2-hydroxycyclohexanone, with little increase in the concentration of Co^{3+}. Stage B begins when the concentration of 2-hydroxycyclohexanone builds to moderate concentrations. Its facile oxidation by Co^{3+} gives intermediate RCO· (radical X), and stage B begins with the steps outlined in Scheme I. Rapid
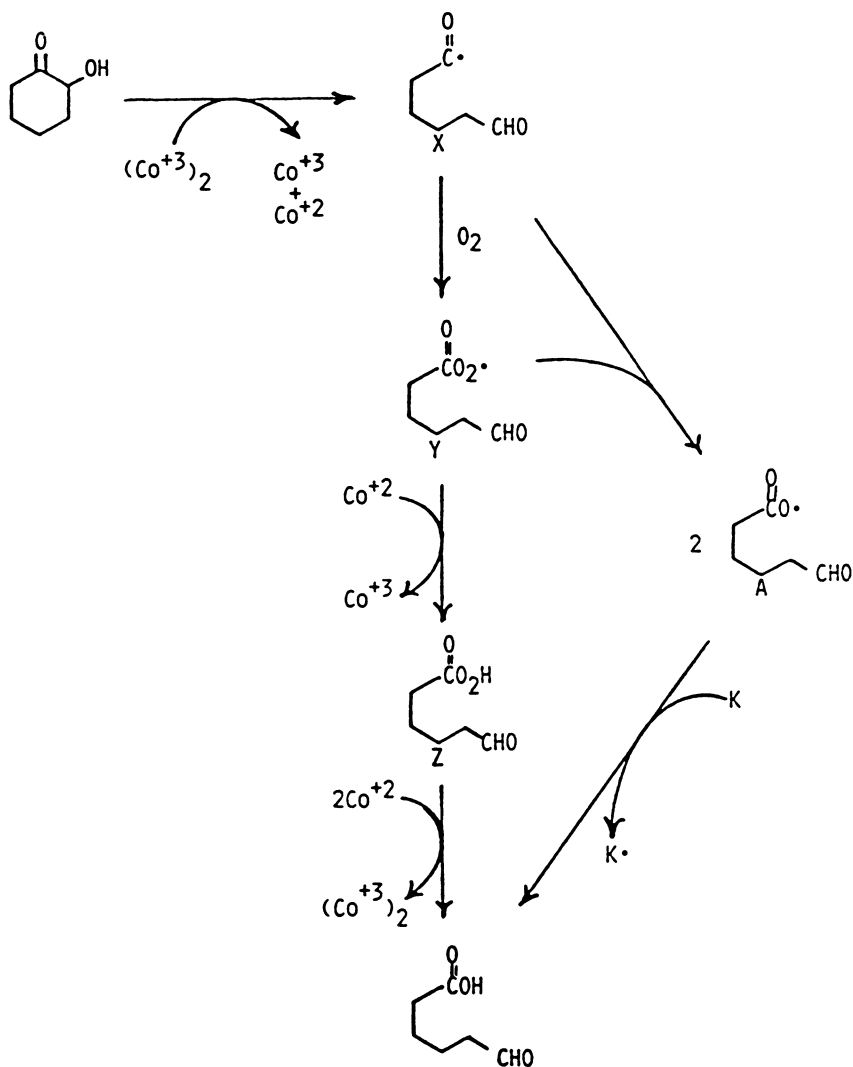
Scheme I. Ring-opening reactions of 2-hydroxycyclohexanone.

generation of RCO_3H (species Z, Scheme I) results and effects conversion of Co^{2+} to Co^{3+}. Co^{3+}, in turn, oxidizes 2-hydroxycyclohexanone even more rapidly.

When the rather constant rate of transfer of O_2 from gas to the liquid phase is finally unable to match its increasing rate of consumption, stage C begins, and Co^{3+} is converted to Co^{2+}. The major reaction pathways for conversion of Co^{3+} to Co^{2+} at low dissolved O_2 concentrations may well involve reactions of the 2-cyclohexanonyl radical with solvent or Br^- ion to
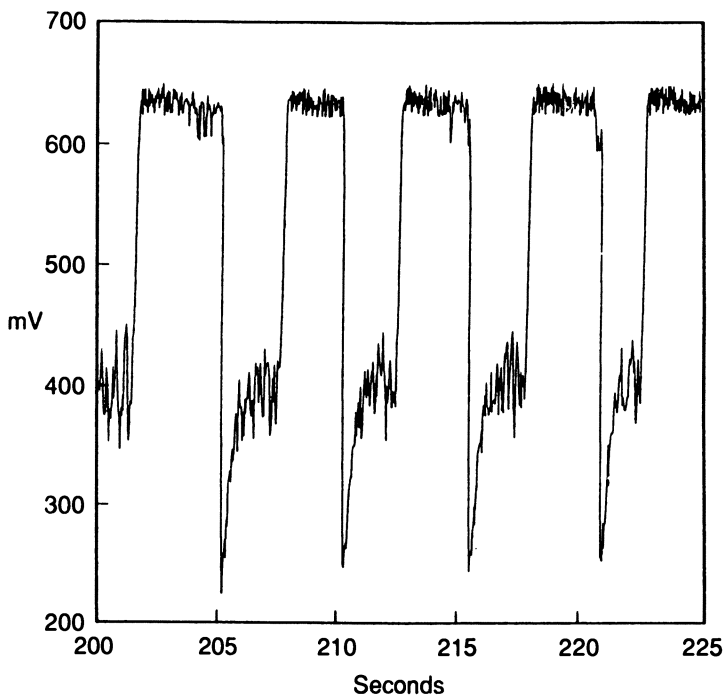
Figure 6. Electrochemical potential measured at a platinum electrode during oxidation of 13 wt % p-xylene in 90:10 wt/wt acetic acid–water solvent in a 7-L continuously fed stirred tank reactor containing Co(OAc)₂, Mn(OAc)₂, and HBr catalysts at 100, 220, and 210 ppm wt basis metal atom and Br, respectively. Twenty-five seconds of a typical 300-s digitized trace sampled at 30 Hz is shown. The average fundamental period of the aperiodic oscillation is about 4.5 s, as determined from power spectral analysis of a full 300-s trace.

yield the intermediates 2-hydroxycyclohexanone, 2-acetoxycyclohexanone, and 2-bromocyclohexanone.

It would be impractical to try to incorporate the many reactions required to account for formation of the 100 or more byproducts into a kinetic model. However, a 29-step kinetic model that was developed describes the main features of the O_2 oxidation of cyclohexanone to adipic acid (*14*). The model simulates the observed oscillating behavior of Co^{3+}, Co^{2+}, dissolved O_2, and the many organic intermediates most likely to be on the pathway between cyclohexanone and acids such as adipic acid.

In contrast to the benzaldehyde system, the cyclohexanone system undergoes sustained oscillations in the absence of Br^- ion (*15*). Although the rates of individual reaction steps involving Co^{3+} are undoubtedly decreased somewhat in the absence of Br^-, the system as a whole still contains sufficient complexity and robustness to exhibit oscillating behavior. The Br^--free cy-

clohexanone system represents one of the few known examples of liquid-phase halogen-free autoxidation oscillators.

O₂ Oxidation of Toluene

Studies of the O_2 oxidation of toluene (*16*), a prototypical organic oxidation, were carried out under conditions more vigorous than those used for cyclohexanone. In this case, $Mn(OAc)_2$ was used with $Co(OAc)_2$ and NaBr, again in acetic acid solution but at 140 °C and 140 psig of air, a substantial increase over the previous examples. As reaction conditions become more stressful, oscillations may evolve from simple to complex to perhaps aperiodic. In the toluene studies, aperiodic temporal oscillations were observed in both light absorption and electrochemical potential between platinum and silver electrodes. A complex time behavior is observed with significant noise and variations in periodic potentials. Several different analyses demonstrate that the dynamics are chaotic. The arguments are somewhat complex, and the details will be published elsewhere.

As a further example of an oscillating O_2 oxidation system, the oxidation of p-xylene was studied (*17*). The reaction conditions included concentrations of $Co(OAc)_2$, $Mn(OAc)_2$, and HBr decreased about threefold from those used for the oxidation of toluene. Also, a temperature of 200 °C was used, versus 140–150 °C for toluene. Aperiodic temporal oscillations in electrochemical potential at platinum and silver electrodes were again observed (Figure 6). In comparison with the corresponding oscillating behavior in the toluene system, the p-xylene electrochemical oscillations were more complex and covered a somewhat larger range of potential. For both toluene and p-xylene oxidations, the detailed analysis of the time behavior exhibited features characteristics of chaos, as distinct from simple or quasiperiodicity.

In the examples of O_2 oxidation discussed, an increase in the driving force for reaction can cause the system to progress from the usual steady-state conditions to periodic oscillations and to aperiodic or chaotic behavior. Although oscillations involve considerably more complexity than steady-state behavior, they may yield insights that might not otherwise be available.

References

1. Bray, W. C. *J. Am. Chem. Soc.* **1921**, *43*, 1262.
2. (a) Field, R. J.; Noyes, R. M. *Acc. Chem. Res.* **1977**, *10*, 214. (b) Field, R. J.; Noyes, R. M. *Acc. Chem. Res.* **1977**, *10*, 273.
3. Nicolis, G.; Prigogene, I. *Self-Organization in Nonequilibrium Systems*; Wiley: New York, 1977.
4. Berge, P.; Pomeau, Y.; Vidal, C. *Order Within Chaos*; Wiley: New York, 1984.
5. Argoul, F.; Arneodo, A.; Richetti, P.; Roux, J. C. *Acc. Chem. Res.* **1987**, *20*, 436–442.
6. Jensen, J. H. *J. Am. Chem. Soc.* **1983**, *105*, 2639.

7. Roelofs, M. G.; Wasserman, E.; Jensen, J. H.; Nader, A. E. *J. Am. Chem. Soc.* **1983**, *105*, 6329.
8. Roelofs, M. G.; Wasserman, E.; Jensen, J. H. *J. Am. Chem. Soc.* **1987**, *109*, 4207.
9. Field, R. J.; Burger, M. *Oscillations and Traveling Waves in Chemical Systems*; Wiley: New York, 1985.
10. Roelofs, M. G.; Jensen, J. H. *J. Phys. Chem.* **1987**, *91*, 3380.
11. Rastogi, R. P.; Das, I.; Mishra, S. B. S.; Jaiswal, K. *Indian J. Chem., Sect. A* **1991**, *30A*, 1.
12. Colussi, A. J.; Ghibaudi, E.; Yuan, Z.; Noyes, R. M. *J. Am. Chem. Soc.* **1990**, *112*, 8660.
13. Guslander, J.; Noyes, R. M.; Colussi, A. J. *J. Phys. Chem.* **1991**, *95*, 4387.
14. Druliner, J. D.; Wasserman, E. *J. Am. Chem. Soc.* **1988**, *110*, 5270.
15. Druliner, J. D.; Greller, L. D.; Wasserman, E. *J. Phys. Chem.* **1991**, *95*, 1519.
16. Greller, L. D.; Roelofs, M. G.; Wasserman, E. to be published.
17. Greller, L. D.; Kegelman, M. R.; Lawson, J. R.; Markham, G. P.; Roelofs, M. G.; Wasserman, E. *J. Am. Chem. Soc.*, submitted for publication.

Flash Photolysis Studies of Reactive Organometallic Intermediates Relevant to Homogeneous Catalysis

Peter C. Ford and Simon T. Belt

Department of Chemistry, University of California, Santa Barbara, CA 93106

The application of flash photolysis with time-resolved optical and infrared detection techniques to the study of reactive organometallic intermediates is described. Examples of these studies are given for several systems. These include tricoordinate rhodium(I) phosphine complexes proposed to be key intermediates in the homogeneous catalytic activation of dihydrogen and the photocatalytic activation of C–H bonds, the coordinatively unsaturated metal carbonyl cluster $Ru_3(CO)_{11}$, plus manganese(I) intermediates relevant to the carbonylation of metal–carbon bonds via migratory insertion.

T HE NATURE AND DYNAMICS of key reactive intermediates must be characterized for a thorough understanding of homogeneous catalysis mechanisms. Such species are generally formed only in (very) low steady-state concentrations. Thus they are difficult to observe by direct methods during a catalytic cycle, and their presence usually can only be inferred from such methods as kinetics studies and stereochemical results. However, by using the flash photolysis technique, it is possible to generate relatively high nonequilibrium concentrations of organometallic intermediates that can be interrogated kinetically and spectroscopically (*see* e.g., refs. 1–19).

In this context, one might anticipate using flash photolysis to probe a wide variety of other reactive species including electronic excited states (ES), coordinatively unsaturated complexes formed by ligand dissociation or reductive elimination, redox partners of ES electron-transfer reactions, radical products of homolytic bond cleavages, and unstable isomers produced by

ES isomerizations. Under favorable circumstances the characterizations are aided by comparison with data from low-temperature matrix experiments. Under these conditions, intermediates, which would have high reactivity at ambient temperature, may be trapped indefinitely and studied by using a full range of spectroscopic methods (20).

This chapter describes several studies in which flash lamp and laser flash photolysis with time-resolved optical and IR detection were used to probe the structure and dynamics of reactive organometallic intermediates of the type routinely proposed in thermal catalytic cycles. This overview will focus on three systems:

1. intermediates in catalysis and photocatalysis by rhodium(I) phosphine complexes,

2. coordinatively unsaturated carbonyltriruthenium clusters, and

3. intermediates relevant to the mechanism of migratory CO insertion into metal–alkyl bonds.

In all three examples, the intermediates studied were coordinatively unsaturated species generated by the photodissociation of carbon monoxide.

Rhodium(I) Phosphine Intermediates

In a study carried out several years ago by our group (21), flash lamp photolysis with optical detection revealed that irradiation of $RhCl(CO)(PPh_3)_2$ in benzene solution results in CO labilization to give the 14-electron tricoordinate complex $RhCl(PPh_3)_2$ (A). This intermediate is often proposed as the active species involved in the catalytic hydrogenation of alkenes by Wilkinson's complex $RhCl(PPh_3)_3$ (22). The reaction dynamics of this intermediate are summarized in Scheme I. Consistent with the previous proposals, A displayed a reactivity ($k_1 = 1 \times 10^5$ M^{-1} s^{-1}) toward H_2 more than 4 orders of magnitude greater than that of the 16-electron trisphosphine complex $RhCl(PPh_3)_3$.

$$RhCl(PPh_3)_2 + H_2 \overset{k_1}{\rightleftharpoons} H_2RhCl(PPh_3)_2 \qquad (1)$$

Another important result of the flash experiments was the opportunity to interrogate the reaction of A with PPh_3, which gave the rate constant $k_L = 3 \times 10^6$ M^{-1} s^{-1} in benzene (L is PPh_3). From this and the previously determined rate constant for dissociation of PPh_3 from $RhCl(PPh_3)_3$ ($k_2 = 0.7$ s^{-1}) (22), the equilibrium constant $K_L = k_2/k_L = 2 \times 10^{-7}$ M was calculated (5) for the phosphine dissociation depicted in eq 2, the first step in dihydrogen activation by Wilkinson's catalyst.

$$RhCl(PPh_3)_3 \overset{K_L}{\rightleftharpoons} RhCl(PPh_3)_2 + PPh_3 \qquad (2)$$

$$RhCl(CO)L_2$$

$$h\nu \quad | \quad -CO$$

$$RhClL_3 \quad \underset{-L,\, 0.68\, s^{-1}}{\overset{+L,\, 3\times10^6\, M^{-1}s^{-1}}{\rightleftharpoons}} \quad "RhClL_2" \quad \underset{}{\overset{2.6\times10^7\, M^{-1}s^{-1}}{\rightleftharpoons}} \quad [RhClL_2]_2$$

$$+CO \qquad 7\times10^7\, M^{-1}s^{-1}$$

$$+H_2 \qquad\qquad +.C_2H_4$$

$$1.0\times10^5\, M^{-1}s^{-1} \qquad >4\times10^7\, M^{-1}s^{-1}$$

$$H_2RhClL_2 \qquad\qquad RhClL_2(H_2C=CH_2)$$

$$2.6\, s^{-1} \qquad\qquad 1\times10^8\, M^{-1}s^{-1}$$

$$+CO \qquad\qquad +CO$$

$$+CO \qquad\qquad RhCl(CO)L_2 \qquad\qquad +CO$$

$$2\times10^5\, M^{-1}s^{-1} \qquad\qquad 1.8\, s^{-1}$$
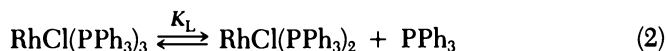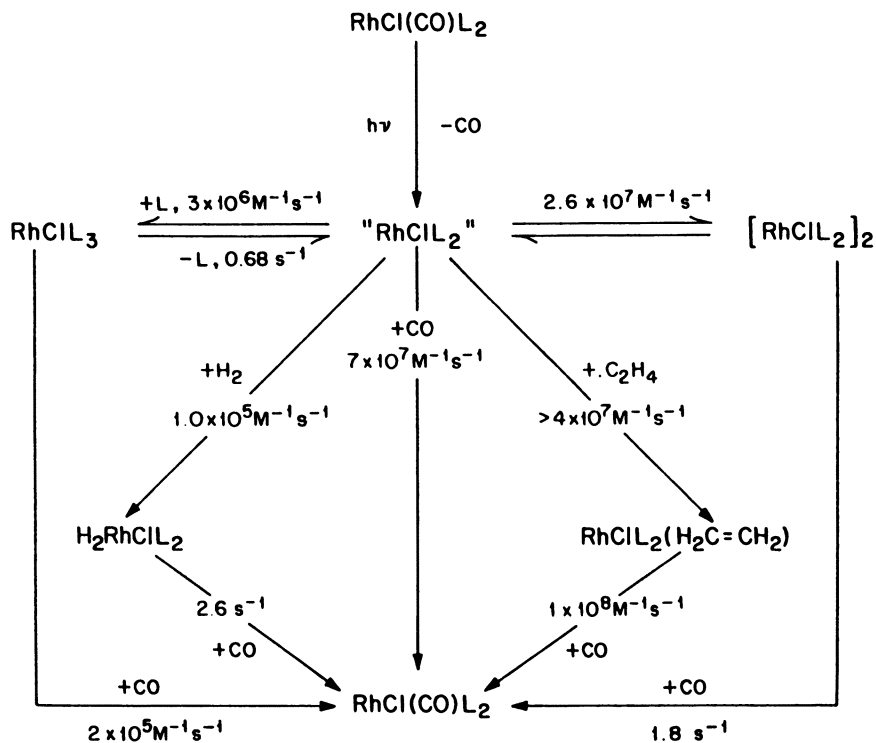
Scheme I. Reaction dynamics of intermediates resulting from the flash photolysis of RhCl(CO)(PPh₃)₂ in benzene solution (25 °C).

In a parallel development, Kunin and Eisenberg (23) found that related Ir(I) and Rh(I) phosphine complexes are photocatalysts for benzene carbonylation under conditions of continuous irradiation.

$$C_6H_6 + CO \xrightarrow{h\nu,\, RhCl(CO)(PPh_3)_2} C_6H_5CHO \qquad (3)$$
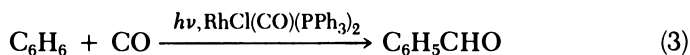
Their work was followed by extensive exploratory studies by Tanaka and co-workers (24–28), who demonstrated that the trimethylphosphine complex *trans*-RhCl(CO)(PMe₃)₂ was especially effective at activating hydrocarbon C–H bonds, not only of arenes but also of alkanes, toward carbonylation and other functionalizations. Sakakura and co-workers (24–28), Normura and Saito (29), and Maguire et al. (30) independently demonstrated that this complex also serves as a photocatalyst for the dehydrogenation of organic substrates such as alkanes (to give alkenes) and 2-propanol (to give acetone). Although related to the cyclopentadienyl complexes of Rh(I), Ir(I), and other metals demonstrated (31–40) to be effective in activating carbon–hydrogen bonds in alkanes, alkenes, and arenes, the PMe₃ complex and analogous phosphine complexes are especially promising because of their ability to

participate in a broad scope of catalytic hydrocarbon functionalizations (23–30).

Ongoing studies (21, 41–43) in this laboratory and in collaboration with Netzel demonstrated that flash photolysis of trans-RhCl(CO)L$_2$ leads principally to CO dissociation for each L studied.

$$trans\text{-RhCl(CO)L}_2 \xrightarrow{h\nu} \underset{\mathbf{A}}{\text{RhClL}_2} + CO \qquad (4)$$

However, subsequent reactions of the resulting tricoordinate intermediates **A** are markedly dependent upon the nature of L. When L = PPh$_3$ (Scheme I), **A** undergoes competitive trapping by the labilized CO and dimerization to the known species [RhCl(PPh$_3$)$_2$]$_2$. The flash photolysis experiment gave no direct evidence of the C–H activation chemistry described by eq 3. However, for L = PMe$_3$, C–H activation appears to be the predominant pathway for species **A** in all hydrocarbon solvents (17).

Flash lamp photolysis (wavelength of irradiation $\lambda_{irr} > 330$ nm) of RhCl(CO)(PMe$_3$)$_2$ in C$_6$H$_6$ under Ar results in the formation of the tricoordinate intermediate RhCl(PMe$_3$)$_2$, which is more strongly absorbing in the region 390–450 nm ($\lambda_{max} = 415$ nm). This species decays via first-order kinetics ($k = 2.8 \times 10^3$ s^{-1}) to give a bleached species **B**, which has a diminished absorbance relative to RhCl(CO)(PMe$_3$)$_2$ over this spectral range. By comparison of these spectral properties with those of the H$_2$RhCl(PPh$_3$)$_2$ intermediate, together with the known carbonylation chemistry, **B** was assigned to RhCl(PMe$_3$)$_2$(Ph)H, the product of RhCl(PMe$_3$)$_2$ insertion into solvent C–H bonds (41).

$$\underset{\mathbf{A}}{\text{RhClL}_2} + PhH \rightarrow \underset{H}{\overset{Ph}{\diagdown}}\underset{\mathbf{B}}{\text{RhClL}_2} \qquad (5)$$
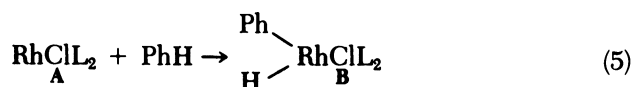
This species decays slowly via first-order kinetics with regeneration of RhCl(CO)(PMe$_3$)$_2$. For L = Ptol$_3$ (tol is 4-tolyl), the spectroscopic and kinetic observations are again consistent with a similar sequence of reactions in benzene solution, although the rate of formation of **B** is an order of magnitude slower than for the PMe$_3$ analog. In both cases, addition of excess CO to the solution (1% CO in Ar) results in acceleration of the rates of decay of the tricoordinate species together with a reduction in the yield of the oxidative addition products because of competition between CO and solvent for the RhClL$_2$ intermediate.

When cyclohexane is used as the solvent, a marked contrast appears between the reactivities of RhCl(PMe$_3$)$_2$ and RhCl(Ptol$_3$)$_2$. Under argon, RhCl(PMe$_3$)$_2$ inserts into the C–H bonds of cyclohexane at a rate comparable to that seen for benzene. The RhCl(Ptol$_3$)$_2$ analog under argon undergoes a dimerization reaction analogous to that observed for RhCl(PPh$_3$)$_2$ in both

benzene and cyclohexane. Thus, the C–H activation pathways of these re-active intermediates demonstrate remarkable sensitivity to the nature of L.

In all cases, the transients **B** formed eventually react with the CO pro-duced in the initial flash photolysis step to regenerate the starting complex $RhCl(CO)L_2$. The lifetimes found for these transients are also dependent on the nature of L, the longest lifetimes being found for the more basic PMe_3. Overall, C–H oxidative addition occurs most readily and gives the most stable intermediates when L is PMe_3.

Flash photolysis studies using picosecond techniques (*43, 44*) have dem-onstrated additional transient species that are generated prior to the for-mation of **A**. In each case, picosecond laser excitation ($\lambda_{irr} = 355$ nm) led to formation of a strongly absorbing transient that decayed in less than a nanosecond to a new absorbing species (in the 400–450-nm range). The spectra of these transients are consistent with that attributed to the tricoor-dinated (or solvated) species $RhClL_2$, which is seen as the first intermediate in conventional flash photolysis experiments. For L = PPh_3 or $Ptol_3$, the decay to **A** proved to be exponential with lifetimes of several hundred pi-coseconds; however, for L = PMe_3 this decay was clearly bimodal, with a fast (~50 ps) step followed by a slower (~1 ns) decay to the **A**-type species. The picosecond laser flash photolyses were largely carried out in tetrahy-drofuran because of solubility and multiphoton absorption problems with other solvents under the experimental conditions.

At this stage, we believe it likely that this first species observed in the picosecond flash experiment is an electronic excited state. However, such an assignment is in need of corroboration by the observation of an emission spectrum from this excited state and the demonstration that this emission has a lifetime comparable to that seen in the transient absorption experiment. The various flash photolysis observations with various *trans*-$RhCl(CO)L_2$ are summarized in Scheme II.

Reactivities of Unsaturated Carbonyltriruthenium Clusters

The continuous and flash photolysis of $Ru_3(CO)_{12}$ serves as a model for understanding the photoreactivity of carbonylmetal clusters with respect to ligand substitutions (*45, 46*), cluster fragmentation (*47–50*), and photoin-duced transformations of organic ligands and substrates (*51–54*). Under con-tinuous photolysis, $Ru_3(CO)_{12}$ undergoes both CO substitution and frag-mentation pathways that have been shown to result from two chemically independent primary photoproducts arising from different excited states of $Ru_3(CO)_{12}$ (*45, 46*).

Fragmentation (eq 6), the major route at lower energy excitation ($\lambda_{irr} > 400$ nm), is proposed to occur via formation of a high-energy isomer of $Ru_3(CO)_{12}$. At short wavelengths, substitution by donor ligands (eq 7) is the dominant pathway. Substitution has been proposed to occur via formation of the coordinatively unsaturated triruthenium cluster $Ru_3(CO)_{11}$, the type
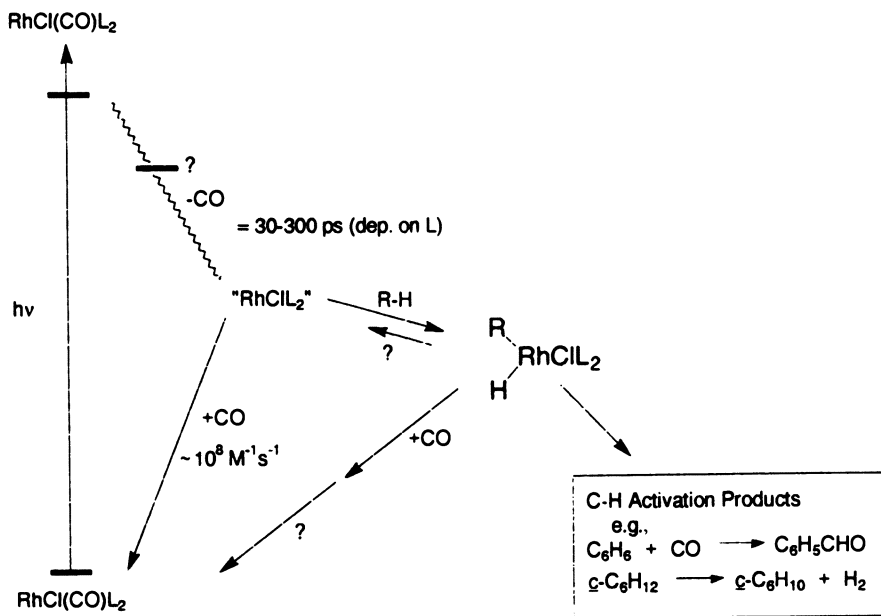
Scheme II. C–H activation by Rh(I) photocatalysts.

of intermediate proposed for photoassisted hydrogenation of alkenes by clusters.

$$Ru_3(CO)_{12} + 3L \xrightarrow{h\nu(\lambda>400\ nm)} 3Ru(CO)_4L \qquad (6)$$

$$Ru_3(CO)_{12} + L \xrightarrow{h\nu(\lambda<400\ nm)} Ru_3(CO)_{11}L + CO \qquad (7)$$
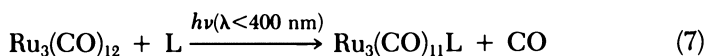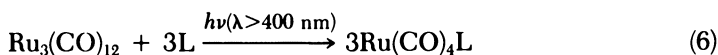
In accord with these observations, short-wavelength flash lamp photolysis ($\lambda_{irr} > 315$ nm, using optical detection techniques) of $Ru_3(CO)_{12}$ in tetrahydrofuran (THF) solution demonstrated the formation of an intermediate proposed to be $Ru_3(CO)_{11}(THF)$, which reacts with donor ligands via rate-limiting dissociation of THF. When the reaction was carried out in cyclohexane, the $Ru_3(CO)_{11}S$ adduct proved too short-lived to allow direct observation (S is solvent). The substitution products $Ru_3(CO)_{11}L$ were formed within the duration of the 30-μs flash.

We extended these studies of the kinetic behavior of the transients characteristic of the photosubstitution pathways by using XeCl excimer laser as the 20-ns excitation source with an IR diode laser as the probe source and a Hg–Cd–Te fast IR detector system (55). This system allows the determination of time-resolved infrared (TRIR) spectra.

Laser flash photolysis (308 nm) of $Ru_3(CO)_{12}$ in isooctane under Ar results in formation of a transient IR spectrum (200 ns). Figure 1 shows depletion of the carbonyl stretching (ν_{CO}) bands at 2061, 2031, 2017, and 2011 cm^{-1}
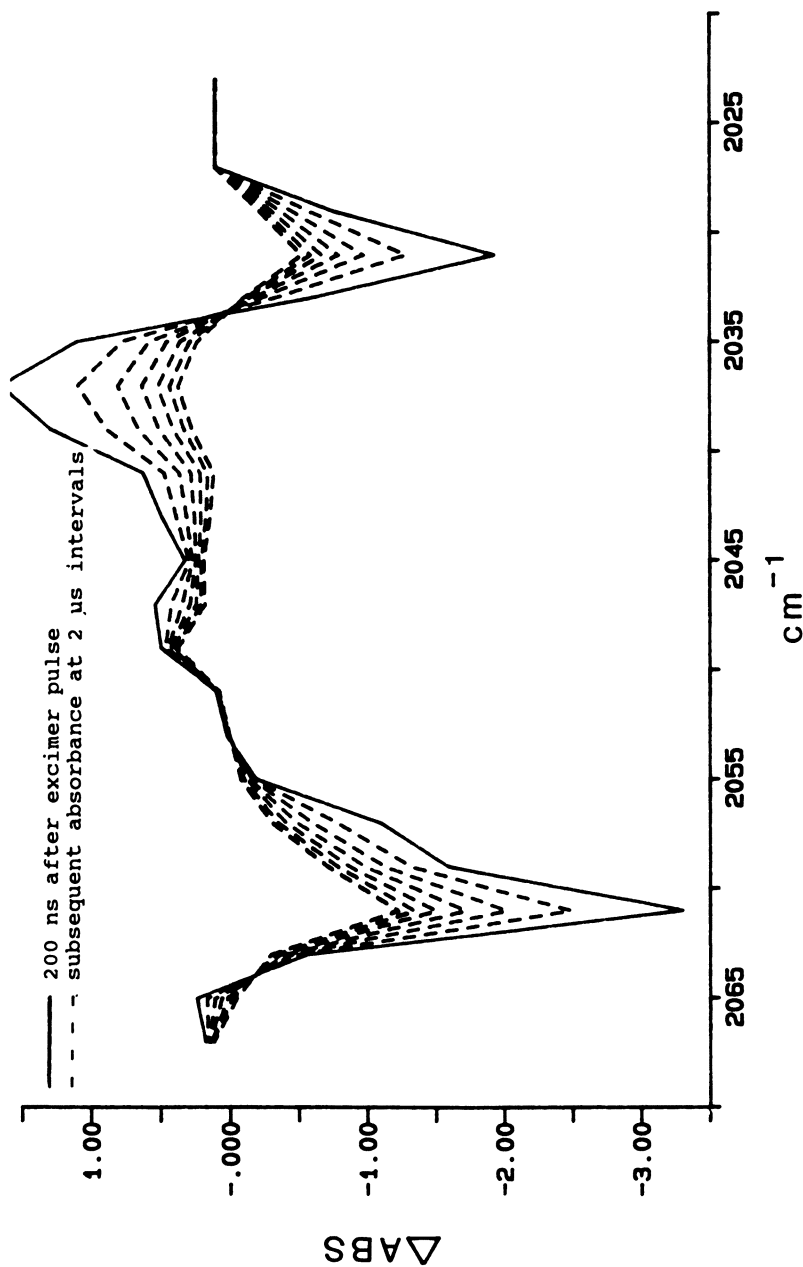
Figure 1. Infrared difference spectrum of the transients formed by 308-nm flash photolysis of Ru₃(CO)₁₂ in ambient-temperature isooctane solution 200 ns after flash. Subsequent curves are recorded at regular intervals of 2.0 μs.

characteristic of this cluster and the appearance of several new bands assigned to an isomer of $Ru_3(CO)_{11}$ (**C**). This intermediate was previously reported as one short-wavelength photolysis product in low-temperature hydrocarbon glasses (56). In THF or in mixed cyclohexane–THF solutions, the relatively stable solvent complex $Ru_3(CO)_{11}THF$ (**D**) was observed and identified on the basis of its ν_{CO} band at 2049 cm^{-1} [cf. $Ru_3(CO)_{11} \cdot 2MeTHF$ at 2049 cm^{-1} in hydrocarbon glasses (56)].

In the absence of added CO, **C** decays via second-order kinetics to regenerate $Ru_3(CO)_{12}$. The second-order rate constant ($k_2 = 2.4 \times 10^9$ M^{-1} s^{-1}, determined from the first-order rate plots at various excess CO concentrations) for reaction with CO proved to be within an order of magnitude of the diffusion-controlled limit (1.3×10^{10} M^{-1} s^{-1}) in isooctane (55) and 3 orders of magnitude larger than those found for the intermediates $Cr(CO)_5$ or $Mn_2(CO)_9$ in alkane solutions (1, 5, 7, 10). Thus, we conclude that there must be negligible stabilization of **C** either by the isooctane solvent or from the bridging CO reported (56) to be a feature of its structure. In alkane solutions containing THF, trapping by CO to give $Ru_3(CO)_{12}$ and by the donor ligand THF to form **D** are competitive. However, **D** itself is labile and reacts with CO to re-form the starting cluster. The reactivity of this transient as a function of [THF] and [CO] proved to be consistent with a limiting dissociative substitution mechanism. These observations are summarized in Scheme III.

Unsaturated Mononuclear Carbonylmanganese Compounds

Carbon–carbon bond formation is a key step in catalytic CO activation in homogeneously catalyzed processes such as hydroformylations of alkenes, carbonylations of alcohols, homologations of carboxylic acids, and reductive CO polymerization (57). One fundamental organometallic reaction commonly invoked in proposed schemes for such catalytic cycles is the reversible migratory insertion of CO into an alkyl–metal bond (58), for which eq 8 serves as a prototype.

$$\tag{8}$$
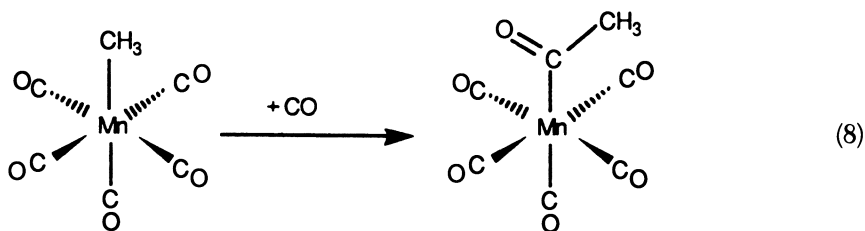
Our third example of using flash photolysis techniques to probe the structures and dynamics of reactive organometallic intermediates involves a study of coordinatively unsaturated mononuclear Mn(I) carbonyls. This study

$$Ru_3(CO)_{12} \xrightarrow{h\upsilon, -CO} Ru_3(CO)_{11}$$

C
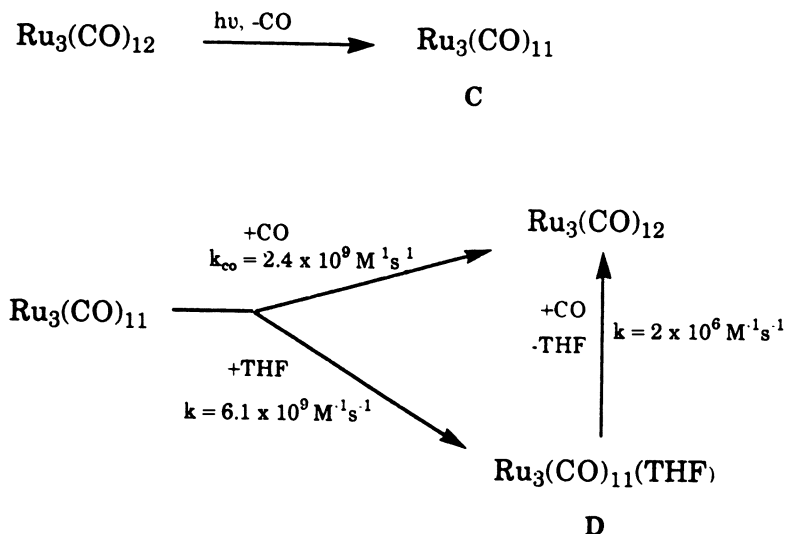
Scheme III. Reactions of the coordinatively unsaturated cluster Ru₃(CO)₁₁.

was initiated with the aim of obtaining a deeper understanding of such C–C bond formation mechanisms.

Investigations focusing on eq 8 (59–62) concluded that this reaction proceeds via methyl migration (as opposed to CO insertion) with rate-limiting formation of an unsaturated acyl intermediate, $(CH_3CO)Mn(CO)_4$ (**E**). Donor solvents and other nucleophiles have marked effects on the reaction dynamics (63–65). Despite the extensive kinetic and stereochemical studies carried out to elucidate the overall reaction mechanism, there has been no direct observation of the 16-e⁻ acyl intermediate **E**.

In this context, our preliminary studies have shown that laser flash photolysis of $(CH_3CO)Mn(CO)_5$ causes CO photodissociation. A transient forms and undergoes solvent-dependent rearrangement to the alkyl complex competitive with trapping by CO to regenerate the starting complex (66). Preliminary data suggest that the reactive intermediate formed in hydrocarbon solutions may be the η^2 bound acyl species **F**, consistent with theoretical predictions (67, 68). In THF this intermediate is the η^1 acyl species **G** with a solvent molecule in the *cis* coordination site. Such results offer one possible reason for the marked solvent effects on migratory insertion rates.

F   **G**
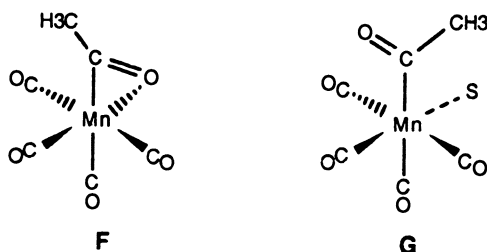
The behavior of the acyl complex has also led us to investigate with time-resolved optical and infrared techniques the transient intermediates resulting from the flash photolysis of $CH_3Mn(CO)_5$ (**H**). Our goal was to provide a model for the pertinent spectroscopic and kinetic data relevant to unsaturated Mn(I) intermediates (69). Laser flash photolysis (λ_{irr} = 308 nm) of **H** in cyclohexane or isooctane solutions results in the 100-μs TRIR spectrum shown in Figure 2.

The depletion of **H** is evident with the negative absorbance changes (Δ_{Abs}) values noted for ν_{CO} modes at 2014 and 1991 cm^{-1}. Accompanying these changes, a transient species is formed that has three ν_{CO} bands at 1986, 1974, and 1940 cm^{-1} in the TRIR spectrum and a λ_{max} at 410 nm in the optical spectrum. These properties are close to those attributed to *cis*-$CH_3Mn(CO)_4 \cdot CH_4$, which is formed by CO photodissociation from **H** in a methane matrix (70). These spectroscopic observations are consistent with the photolabilization of CO followed by solvation to give *cis*-$CH_3Mn(CO)_4S$ (**I**).

$$CH_3\underset{\textbf{H}}{Mn}(CO)_5 + S \xrightarrow{h\nu} \textit{cis-}CH_3\underset{\textbf{I}}{Mn}(CO)_4S + CO \qquad (9)$$
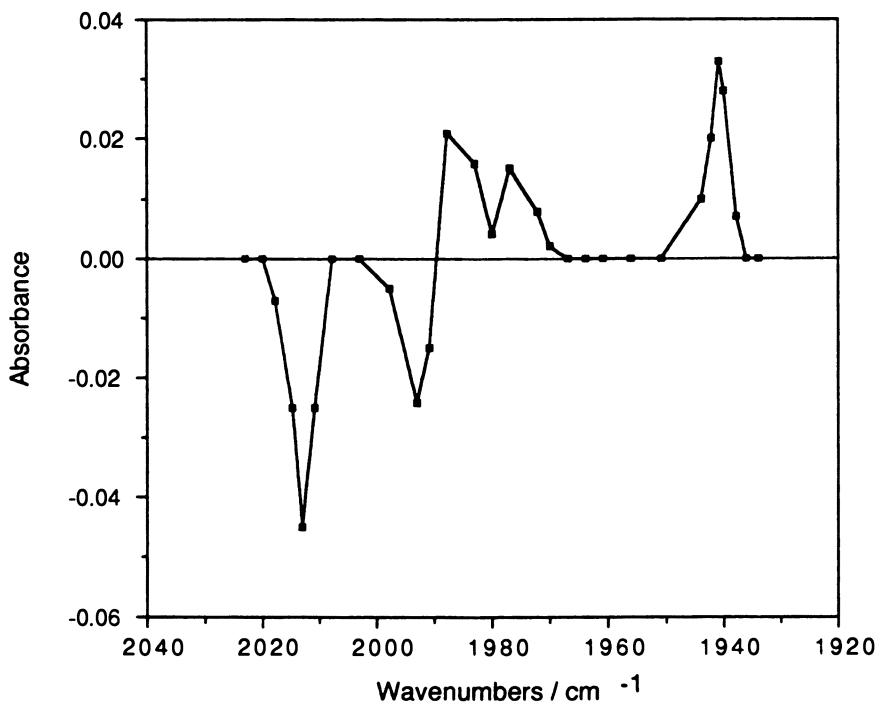
Figure 2. Time-resolved IR spectrum obtained 100 μs after laser flash photolysis of CH₃Mn(CO)₅ in isooctane under Ar. The negative bands correspond to the depletion of CH₃Mn(CO)₅; the positive bands correspond to cis-CH₃Mn(CO)₄S.

We have not observed transients resulting from either *trans*-CO labilization or homolytic metal–alkyl bond cleavage. However, prolonged irradiation leads to the appearance of visible and IR absorbances that indicate the production of $Mn_2(CO)_{10}$.

The decay kinetics of **I** are consistent with the reaction with CO. Under argon the decay of **I** follows second-order kinetics. In contrast, under CO both the rates of decay of **I** and the re-formation of $CH_3Mn(CO)_5$ are accelerated and follow pseudo-first-order kinetics (Figure 3). The second-order rate constant for the reaction of *cis*-$CH_3Mn(CO)_4S$ with CO ($2.1 \pm 0.1 \times 10^6$ M^{-1} s^{-1}) shows excellent agreement between the IR and optical detection methods. It lies in the same range as other weakly bound solvent–carbonylmetal intermediates, such as $Cr(CO)_5S$, measured by flash photolysis techniques (*1, 6, 10*).

Significantly, when THF is used as the solvent, the reaction of **I** with CO (as studied by optical detection) is 4 orders of magnitude slower ($k_2 = 1.4 \times 10^2$ M^{-1} s^{-1}). This change is consistent with the increased donor strength of THF. Thus, the combined spectroscopic and kinetic data show that photolysis of $CH_3Mn(CO)_5$ in hydrocarbon or THF solutions results in
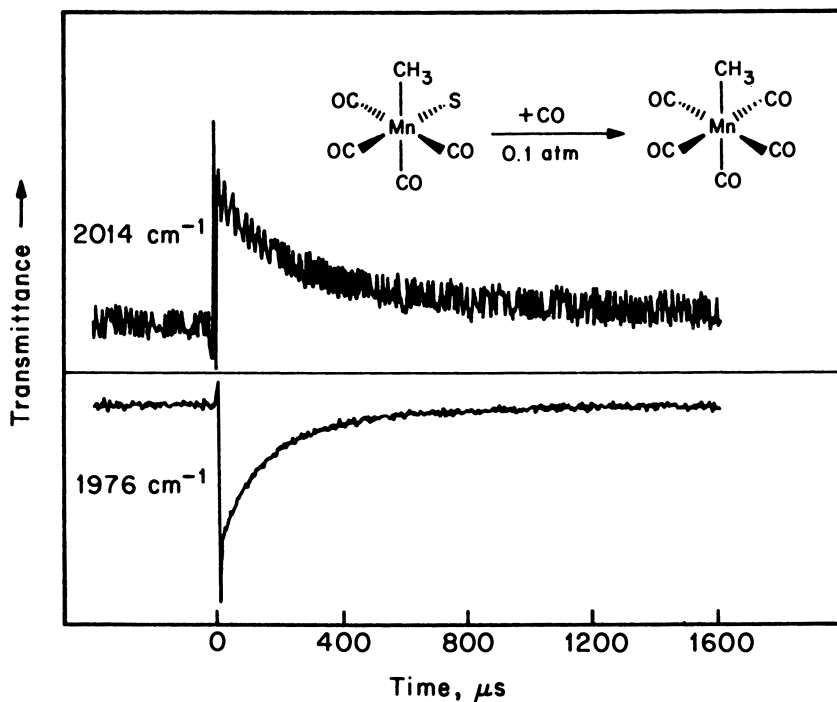
Figure 3. Kinetic traces showing the decay of cis-CH₃Mn(CO)₄S *(S is cyclohexane) at 1976 cm⁻¹ and the reformation of* CH₃Mn(CO)₅ *at 2014 cm⁻¹ following laser flash photolysis of* CH₃Mn(CO)₅ *in cyclohexane under 0.1 atm of CO. IR spectral changes are shown in transmittance mode.*

the formation of *cis*-CH$_3$Mn(CO)$_4$S (S is solvent), which reacts with CO at rates comparable to those found for analogous solvent complexes of d^6 carbonylmetals.

Although *cis*-CH$_3$Mn(CO)$_4$S is the first transient species observable in these experiments, competition experiments suggest that the primary photoproduct CH$_3$Mn(CO)$_4$ shows a remarkable selectivity toward reaction with CO over alkane solvation. In cyclohexane the yield of **I** from the photolysis of **H** is a factor of 5 higher under argon than under CO, with otherwise identical conditions. This feature, which has been observed by both TRIR and optical detection methods, is unprecedented for simple carbonylmetals of this type. It suggests that CH$_3$Mn(CO)$_4$ is sufficiently long-lived to be trapped selectively by CO relative to the solvent alkane (Scheme IV).

In contrast, we observed no [CO] dependence on transient yields following irradiation of **H** in THF or of Cr(CO)$_6$ in cyclohexane. Thus, CH$_3$Mn(CO)$_4$ must be trapped much more effectively by the stronger donor, THF. In the case of Cr(CO)$_6$, our observations are in accord with the extremely rapid solvation of the singlet state Cr(CO)$_5$ fragment as measured by other workers (*12–17*). Apparently the lifetime of this species is too short to allow for selectivity between CO (10^{-2} M) and solvent.

One possible explanation for the apparent selectivity of the CH$_3$Mn(CO)$_4$ fragment would be that this species is formed in a triplet ground state having either a trigonal bipyramidal C_{3v} geometry with an axial CH$_3$ ligand or a
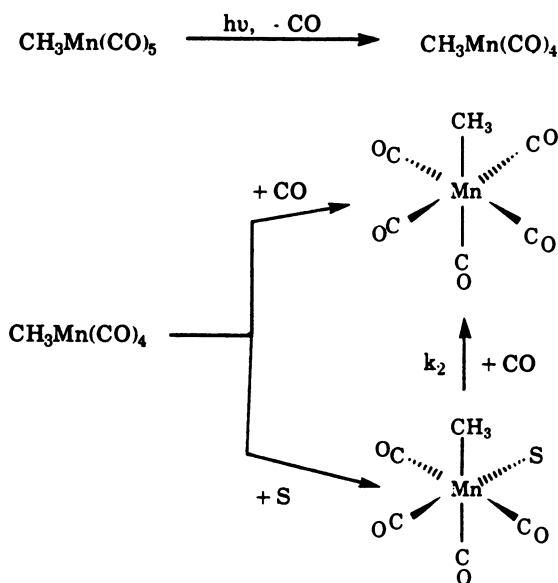
Scheme IV. Competitive trapping of the unsaturated intermediate CH$_3$Mn(CO)$_4$ (**E**).

square pyramidal geometry with a basal CH_3 ligand (*71*). Either geometric or electronic constraints may give this species sufficient lifetime to demonstrate selectivity in coordinating a sixth ligand.

Acknowledgments

References

1. Kelly, J. M.; Bent, D. V.; Herman, H.; Schulte-Frohlinde, H.; Koerner von Gustorf, E. *J. Organomet. Chem.* **1974**, *69*, 259–269.
2. Kelly, J. M.; Bonneau, R. *J. Am. Chem. Soc.* **1980**, *102*, 1220–1221.
3. Perutz, R. N.; Scaiano, J. C. *J. Chem. Soc., Chem. Commun.* **1984**, 457–458.
4. Creaven, B. S.; Dixon, A. J.; Kelly, J. M.; Long, C.; Poliakoff, M. *Organometallics* **1987**, *6*, 2600–2605.
5. Kobayashi, T.; Ohtani, H.; Noda, H.; Teratani, S.; Yamazaki, H.; Yasufuku, K. *Organometallics* **1986**, *5*, 110–113.
6. Poliakoff, M.; Weitz, E. *Adv. Organomet. Chem.* **1986**, *25*, 277–316.
7. Church, S. P.; Herman, H.; Grevels, F.-W.; Schaffner, K. *Inorg. Chem.* **1985**, *24*, 418–422.
8. Dixon, A. J.; Healy, M. A.; Hodges, P. M.; Moore, B. D.; Poliakoff, M.; Simpson, M. B.; Turner, J. J.; West, M. A. *J. Chem. Soc., Faraday Trans. 2* **1986**, *82*, 2083–2092.
9. Dobson, G. R.; Hodges, P. M.; Healy, M. A.; Poliakoff, M.; Turner, J. J.; Firth, S.; Asali, K. J. *J. Am. Chem. Soc.* **1987**, *109*, 4218–4224.
10. Church, S. P.; Herman, H.; Grevels, F.-W.; Schaffner, K. *J. Chem. Soc., Chem. Commun.* **1984**, 785–786.
11. Weiller, B. H.; Wasserman, E. P.; Bergman, R. G.; Moore, C. B.; Pimentel, G. C. *J. Am. Chem. Soc.* **1989**, *111*, 8288–8289.
12. Simon, J. D.; Peters, K. S. *Chem. Phys. Lett.* **1983**, *98*, 53–56.
13. Simon, J. D.; Xie, X. *J. Phys. Chem.* **1986**, *90*, 6751–6753.
14. Rothberg, L. J.; Cooper, N. J.; Peters, K. S.; Vaida, V. *J. Am. Chem. Soc.* **1982**, *104*, 3536–3537.
15. Joly, A. G.; Nelson, K. A. *J. Phys. Chem.* **1989**, *93*, 2876–2878.
16. Wang, L.; Zhu, X.; Spears, K. G. *J. Phys. Chem.* **1989**, *93*, 2–4.
17. Yu, S.-C.; Xu, X.; Lingle, R.; Hopkins, J. B. *J. Am. Chem. Soc.* **1990**, *112*, 3668–3669.

18. Moore, J. N.; Hansen, P. A.; Hochstrasser, R. M. *Chem. Phys. Lett.* **1987**, *138*, 110–114.
19. Moore, J. N.; Hansen, P. A.; Hochstrasser, R. M. *J. Am. Chem. Soc.* **1989**, *111*, 4563–4566.
20. Perutz, R. N. *Annu. Rep. Prog. Chem.*, *Sect. C* **1985**, 157.
21. Wink, D. A.; Ford, P. C. *J. Am. Chem. Soc.* **1987**, *109*, 436–442.
22. Halpern, J. *Inorg. Chim. Acta* **1981**, *50*, 11–19.
23. (a) Kunin, A. J.; Eisenberg, R. S. *J. Am. Chem. Soc.* **1986**, *108*, 535-536; (b) Kunin, A. J.; Eisenberg, R. S. *Organometallics* **1988**, *7*, 2124–2129.
24. Sakakura, T.; Sodeyama, T.; Tokunaga, Y.; Tanaka, M. *Chem. Lett.* **1987**, 2211–2214.
25. Sakakura, T.; Tanaka, M. *J. Chem. Soc., Chem. Commun.* **1987**, 758–759.
26. Sakakura, T.; Sodeyama, T.; Tokunaga, Y.; Tanaka, M. *Chem. Lett.* **1988**, 263–264.
27. Sakakura, T.; Susaki, K.; Tokunaga, Y.; Wada, K.; Tanaka, M. *Chem. Lett.* **1988**, 155–158.
28. Sakakura, T.; Tanaka, M. *Nouv. J. Chim.* **1989**, *13*, 737–745.
29. Normura, K.; Saito, Y. *J. Chem. Soc., Chem. Commun.* **1988**, 161.
30. (a) Maguire, J. A.; Boese, W. T.; Goldman, A. S. *J. Am. Chem. Soc.* **1989**, *111*, 7088; (b) Maguire, J. A.; Boese, W. T.; Goldman, M. E.; Goldman, A. S. *Coord. Chem. Rev.* **1990**, *97*, 179–192.
31. Janowicz, A. H.; Bergman, R. G. *J. Am. Chem. Soc.* **1982**, *104*, 352.
32. Bergman, R. G. *Science (Washington, D.C.)* **1984**, *223*, 902, and references therein.
33. Hoyama, J. K.; Graham, W. A. G. *J. Am. Chem. Soc.* **1982**, *104*, 3723–3725.
34. Ghosh, C. K.; Graham, W. A. G. *J. Am. Chem. Soc.* **1987**, *109*, 4726–4727.
35. (a) Crabtree, R. H. *Chem. Rev.* **1985**, *85*, 245; (b) Crabtree, R. H. *J. Am. Chem. Soc.* **1987**, *109*, 5047.
36. Jones, W. D.; Feher, F. J. *Acc. Chem. Res.* **1989**, *22*, 91.
37. Belt, S. T.; Haddleton, D. M.; Perutz, R. N.; Smith, B. P. H.; Dixon, A. J. *J. Chem. Soc., Chem. Commun.* **1987**, 1347–1349.
38. Belt, S. T.; Grevels, F.-W.; Klotzbucher, W. E.; McCamley, A.; Perutz, R. N. *J. Am. Chem. Soc.* **1989**, *111*, 8373–8382.
39. Belt, S. T.; Duckett, S. B.; Haddleton, D. M.; Perutz, R. N. *Organometallics* **1989**, *8*, 748–759.
40. Ford, P. C.; Friedman, A. In *Photocatalysis: Fundamentals and Applications*; Serpone, N., Ed.; Wiley: New York, 1989; Chapter 16, pp 541–564.
41. Spillett, C. T.; Ford, P. C. *J. Am. Chem. Soc.* **1989**, *111*, 1932–1933.
42. Spillett, C. T. Ph.D. Dissertation, University of California—Santa Barbara, 1989.
43. Ford, P. C.; Netzel, T. L.; Spillett, C. T.; Pourreau, D. B. *Pure Appl. Chem.* **1990**, *62*, 1091–1094.
44. Netzel, T. L., Amoco Technology Company, personal communication, 1989.
45. Desrosiers, M. F.; Wink, D. A.; Trautman, R.; Friedman, A. E.; Ford, P. C. *J. Am. Chem. Soc.* **1986**, *108*, 1917–1927.
46. Ford, P. C. *J. Organomet. Chem.* **1990**, *383*, 339–356.
47. Johnson, B. F. G.; Lewis, J.; Twigg, M. V. *J. Organomet. Chem.* **1974**, *67*, C75–C76.
48. Johnson, B. F. G.; Lewis, J.; Twigg, M. V. *J. Chem. Soc., Dalton Trans.* **1975**, 1876–1879.
49. Grevels, F.-W.; Reuvers, J. G. A.; Takats, J. *Angew. Chem., Int. Ed. Engl.* **1981**, *20*, 452–460.
50. Grevels, F.-W.; Reuvers, J. G. A.; Takats, J. *J. Am. Chem. Soc.* **1981**, *103*, 4069–4073.

51. Bamford, C. H.; Mahmud, M. V. *J. Chem. Soc., Chem. Commun.* **1972**, 762–763.
52. Austin, R. G.; Paonessa, R. S.; Giordano, P. J.; Wrighton, M. S. In *Inorganic and Organometallic Photochemistry*; Wrighton, M. S., Ed.; Advances in Chemistry 168; American Chemical Society: Washington, DC, 1978; pp 189–214.
53. Graff, J. L.; Sanner, R. D.; Wrighton, M. S. *Organometallics* **1982**, *1*, 837–842.
54. Doi, Y.; Tamura, S.; Koshizuki, K. *J. Mol. Catal.* **1983**, *19*, 213–222.
55. DiBenedetto, J. A.; Ryba, D. W.; Ford, P. C. *Inorg. Chem.* **1989**, *28*, 3503–3507.
56. Bentsen, J. G.; Wrighton, M. W. *J. Am. Chem. Soc.* **1987**, *109*, 4530–4544.
57. Henríci-Olivé, G.; Olivé, S. *Catalyzed Hydrogenation of Carbon Monoxide*; Springer-Verlag: Berlin, 1984.
58. Collman, J. P.; Hegedus, J. P.; Norton, J. R.; Finke, R. G. *Principles and Applications of Organotransition Metal Chemistry*; University Science Books: Mill Valley, CA, 1987; Chapter 6, pp 355–400.
59. Wojcicki, A. *Adv. Organomet. Chem.* **1973**, *11*, 87.
60. Calderazzo, F. *Angew. Chem., Int. Ed. Engl.* **1977**, *16*, 299.
61. Flood, T. C. *Top. Stereochem.* **1980**, *12*, 37.
62. Flood, T. C.; Jensen, J. E.; Statler, J. A. *J. Am. Chem. Soc.* **1981**, *103*, 4410.
63. Butler, I.; Basolo, F.; Pearson, R. G. *Inorg. Chem.* **1967**, *6*, 2074.
64. Cawse, J. N.; Fiato, R. A.; Pruett, R. *J. Organomet. Chem.* **1979**, *172*, 405.
65. Webb, S.; Giandomenico, C.; Halpern, J. *J. Am. Chem. Soc.* **1986**, *108*, 345.
66. Belt, S. T.; Ford, P. C.; Ryba, D. W. *Abstracts of Papers*, 199th National Meeting of the American Chemical Society, Boston, MA; American Chemical Society: Washington, DC, 1990; INOR 460.
67. Ziegler, T.; Versluis, L.; Tschinke, V. *J. Am. Chem. Soc.* **1986**, *108*, 612.
68. Axe, F. U.; Marynick, D. S. *J. Am. Chem. Soc.* **1988**, *110*, 3728–3734.
69. Belt, S. T.; Ryba, D. W.; Ford, P. C. *Inorg. Chem.* **1990**, *29*, 3633–3634.
70. Horton-Mastin, A.; Poliakoff, M.; Turner, J. J. *Organometallics* **1986**, *5*, 405–408.
71. Daniel, C. *Coord. Chem. Rev.* **1990**, *97*, 141–154.

New 2,2'-Bis(diphenylphosphino)-1,1'-binaphthyl–Ru(II) Complexes for Asymmetric Catalytic Hydrogenation

Hidemasa Takaya, Tetsuo Ohta, and Kazushi Mashima

Department of Industrial Chemistry, Faculty of Engineering, Kyoto University, Kyoto 606, Japan

2,2'-Bis(diphenylphosphino)-1,1'-binaphthyl–Ru(II) complexes were prepared in high yields and their molecular structures were determined through spectroscopic methods and single-crystal X-ray analysis. These complexes were used as catalysts for the asymmetric hydrogenation of enamides, allylic and homoallylic alcohols, α,β-unsaturated carboxylic acids, and various functionalized ketones in exceptionally high enantiomeric excesses. Stereoselectivity of asymmetric hydrogenation of racemic 2-substituted β-keto esters, which proceeds by dynamic kinetic resolution, was extensively studied. Diastereoselectivity of the hydrogenation depends largely on the solvent and the halide anion, as well as on the substituents of the four phenyl rings of the 2,2'-bis(diphenylphosphino)-1,1'-binaphthyl ligands. The optical purities of the products are less sensitive to these factors. Highly stereoselective hydrogenation of methyl 2-benzamidomethyl-3-oxobutanoate and an efficient synthesis of new chiral bis-(triarylphosphine) ligands were accomplished.

Many biologically active organic compounds (such as pharmaceuticals, vitamins, harvest-protecting chemicals, and perfumes) are optically active. Usually one of the optical isomers produces the desired effects; the others are inert or even poisonous. Careful control of chirality should produce only the optical isomer that has the desired effects. Nature uses enzymes for this purpose.

Recent developments in homogeneous asymmetric catalysis using synthetic catalysts are remarkable. Several breakthroughs were made in the early 1970s in the field of asymmetric hydrogenation promoted by homogeneous transition metal catalysts. Especially noteworthy is the work done by the research groups headed by Kagan (*1, 2*) (Universite de Paris-Sud) and Knowles (*3–5*) (Monsanto Co.). These groups showed the high efficiency of chiral diphosphine ligands in the asymmetric hydrogenation of α-acylaminoacrylic acids.

In 1975, in cooperation with Noyori (Nagoya University), we started to prepare a new chiral diphosphine ligand, 2,2′-bis(diphenylphosphino)-1,1′-binaphthyl (**1**), which we named binap (*6–13*). This bis(triarylphosphine) characterized by C_2 chirality has structural flexibility based on rotation around C(1)–C(1′) axis and yet forms conformationally clear-cut, rigid, seven-membered chelate rings. All of these features are considered responsible for the high efficiency of its Rh and Ru complexes as catalysts for asymmetric hydrogenation (*11–14*) and 1,3-hydrogen migration (*15–17*). The following discussion is a brief summary of our achievements with binap–Ru(II) complexes and some recent results.

$$(R)\text{-}(+)\text{-}1$$
$$[(R)\text{-BINAP}]$$

$$(S)\text{-}(-)\text{-}1$$
$$[(S)\text{-BINAP}]$$
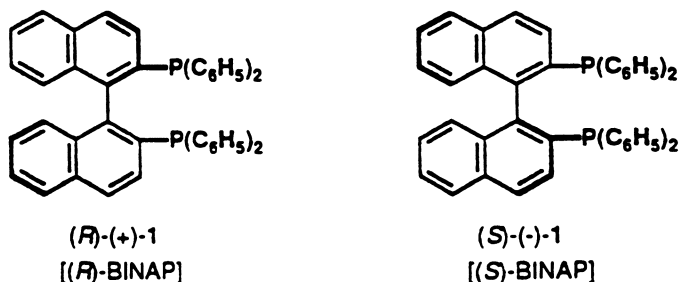
Synthesis and Structures of Mononuclear Binap–Ru(II) Complexes

Ru(OCOR)₂(binap).   The first binap–Ru(II) complex, **2**, was synthesized by the Tokyo University group according to eq 1 (*18*).

$$[RuCl_2(cod)]_n \ + \ (S)\text{-BINAP} \ \xrightarrow[\text{toluene}]{(C_2H_5)_3N}$$

$$Ru_2Cl_4[(S)\text{-binap}]_2 \cdot N(C_2H_5)_3 \quad\quad (1)$$
$$(S)\text{-}2$$
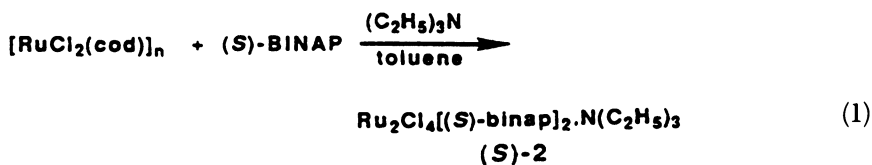
We prepared the mononuclear dicarboxylate complexes **3** in 71–87% yields by treating **2** (or its derivatives) with sodium carboxylate in *t*-butyl alcohol

at 80 °C (eq 2) (*19*). The anion-exchange reaction can also be performed in two phases, with $[(C_6H_5CH_2)(C_2H_5)_3N]Br$ as the phase-transfer catalyst.

(**S**)-**2** ⟶

RCOONa, $(CH_3)_3COH$

or

RCOONa,H_2O—CH_2Cl_2, $(C_6H_5CH_2)(C_2H_5)_3NBr$

(2)

Λ-(**S**)-**3**

a: R = CH_3; Ar = C_6H_5 d: R = CH_3; Ar = p-ClC_6H_4
b: R = CH_3; Ar = p-$CH_3C_6H_4$ e: R = CH_3; Ar = p-FC_6H_4
c: R = CH_3; Ar = p-$CH_3OC_6H_4$ f: R = $C(CH_3)_3$; Ar = C_6H_5
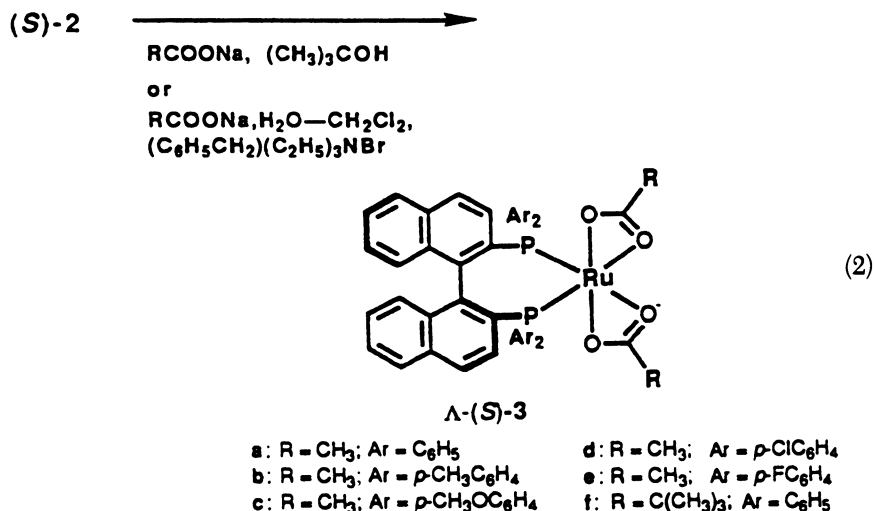
As illustrated in Figures 1 and 2, X-ray crystallography of Λ-(S)-**3f** revealed characteristic features of these complexes. To our knowledge, this finding provides the first X-ray structural data for *cis*-chelating diphos-
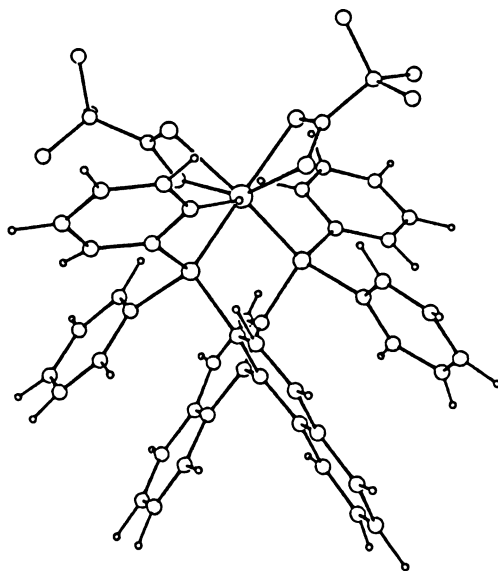
Figure 1. A perspective drawing of Λ-(S)-3f (data collected at –60 °C). Hydrogen atoms of the t-butyl groups were omitted for simplicity.
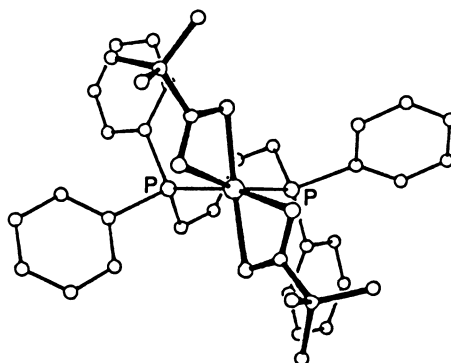
Figure 2. A view of the structure of Λ-(S)-3f along the pseudotwofold axis bisecting the P–Ru–P angle. All hydrogen atoms and carbon atoms of naphthyl groups were omitted for simplicity.

phine–Ru(II) dicarboxylate complexes. Selected bond distances and angles are listed in Table I. The central Ru(II) atom has a distorted octahedron coordination geometry, and the whole structure approximates C_2 chirality.

The dissymmetry of the (S)-binap ligand fixes the seven-membered chelate ring to the δ-conformation. In turn, this position determines the chiral dispositions of the four phenyl rings on the phosphorus atoms. Because of the dissymmetry around the Ru atom endowed by these four phenyl rings, the bidentate ligation of the two carboxylate moieties to Ru occurs stereoselectively to form Λ diastereomer. This conformation avoids nonbonded interactions between the sterically demanding equatorial phenyl rings and the carboxylate ligands.

[RuX(binap)(arene)]Y.   We also synthesized several new cationic binap–Ru(II) complexes in which arene is benzene or p-cymene (20). Treat-

Table I. Selected Structural Parameters of Several Binap–Ru(II) and Binap–Rh(I) Complexes as Determined by X-ray Analyses

Complex	M–P (Å)	P_1–M–P_2 (°)	$θ^a$ (°)
Λ-(S)-**3f**	2.241	90.6	65.6
	2.239		
(S)-**6d**	2.379	91.4	75.7
	2.334		
(R)-**10**[b]	2.305	91.8	74.4
	2.321		
(R)-**11**[c]	2.368	86.3	71.0
	2.388		

[a]Dihedral angle between two naphthyl rings.
[b](R)-**10**: [Rh((R)-binap)(norbornadiene)]ClO$_4$.
[c](R)-**11**: [Rh((R)-binap)$_2$]ClO$_4$.

ment of **5a** or **5b** with one equivalent of (*S*)-binap afforded (*S*)-**6a** or (*S*)-**6b**, respectively (eq 3). A similar reaction of the iodide complex **5c** with (*S*)-binap afforded the rather unstable (*S*)-**6c**, which is prone to lose benzene ligand in solution. The chloride ion of (*S*)-**6a** was easily replaced by BF_4^- and $B(C_6H_5)_4^-$ when the compound was treated with $AgBF_4$ in dichloromethane or with $NaB(C_6H_5)_4$ in methanol to give (*S*)-**6d** or (*S*)-**6e** (eq 3).

The *p*-cymene complexes, (*S*)-**9a** and (*S*)-**9b**, are prepared from **8a** or **8b** and (*S*)-binap (eq 4). They are more stable than the corresponding benzene complexes **6**. Even the iodide complex (*S*)-**9c** could be isolated in pure form in 94% yield by the reaction of **8c** with (*S*)-binap.

The starting complexes **8a–8c** can be conveniently prepared from the natural and easily accessible *p*-mentha-1,5-diene instead of the 1,3-cyclohexadiene used to obtain complexes **5**. Similarly, [RuCl((*S*)-*p*-tolbinap)(C_6H_6)]Cl and [RuCl((*S*)-*p*-tolbinap)(*p*-cymene)]Cl were obtained in 95 and 96% yields, respectively, from **5a** or **8a** and (*S*)-*p*-tolbinap (*p*-tolbinap is 2,2'-bis(di-*p*-tolylphosphino)-1,1'-binaphthyl).

The molecular structure of (*S*)-**6d** was determined by X-ray crystallography (Figure 3). The ruthenium atom has a pseudo-octahedral geometry defined by chloride, two phosphorus atoms of binap, and a tridentate benzene ligand. Selected bond distances and angles are listed in Table I, together with those of [Rh((*R*)-binap)(norbornadiene)]ClO_4 [(*R*)-**10**], and [Rh((*R*)-binap)$_2$]ClO_4 [(*R*)-**11**]. Atomic distances of two Ru–P bonds in (*S*)-**6d** are nonequivalent. This fact agrees with observations of other binap metal complexes, (*S*)-**3f**, (*R*)-**10**, and (*R*)-**11**.
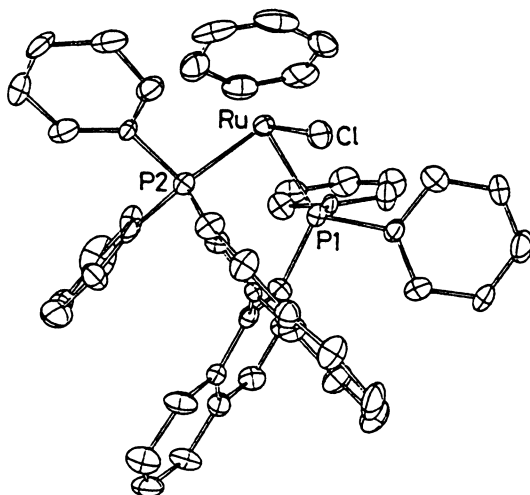
Figure 3. ORTEP view of (S)-**6d**. *(Reproduced with permission from ref. 14. Copyright 1990 Blackwell Scientific.)*

(3)

(S)-6
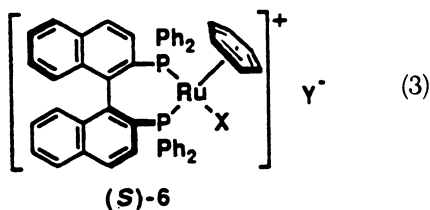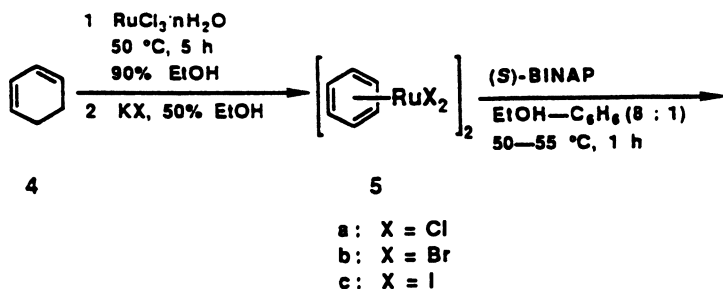
a: X = Y = Cl   90%   yield
b: X = Y = Br   94%
c: X = Y = I   52%
d: X = Cl, Y = BF$_4$
e: X = Cl, Y = BPh$_4$

(4)

(S)-9
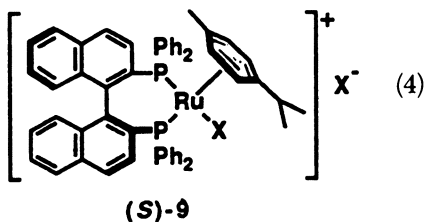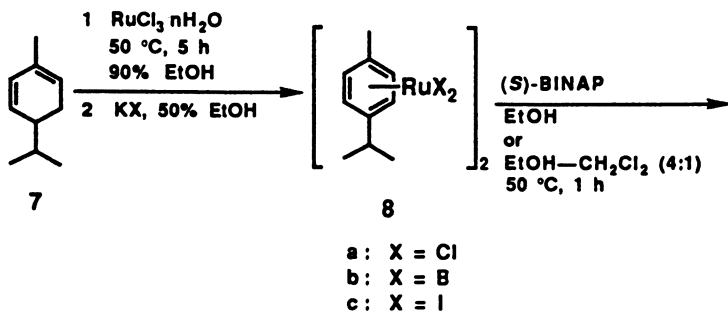
a: X = Cl   94%   yield
b: X = Br   97%
c: X = I   94%

Another characteristic feature of (S)-**6d** is the dihedral angle between two naphthyl planes. The value for (S)-**6d**, 75.7°, is comparable to that of 74.4° for (R)-**10** (8), but larger than the values of 65.6° and 71.0° found for (S)-**3f** (19) and (R)-**11** (16), respectively. These comparisons demonstrate that the binap ligands flexibly change their dihedral angles to form stable chelate complexes with transition metals. The size of the angle depends on the nature of the central metal atom and other coordinated ligands.

Asymmetric Hydrogenation of Olefinic Substrates Catalyzed by Binap–Ru(OCOR)₂ Complexes 3

Complexes **3** are highly efficient catalysts for asymmetric hydrogenation of olefinic substrates such as enamides, α,β- and β,γ-unsaturated carboxylic acids, and allylic and homoallylic alcohols. Highly enantioselective hydrogenations of substrates with only amido, carboxylic, or alcoholic functionality have rarely been attained with other conventional chiral catalysts.

Asymmetric Hydrogenation of Enamides Catalyzed by Complexes 3. 1-Substituted tetrahydroisoquinolines (type **13**) are an important class of compounds. These physiologically active materials also serve as key intermediates for the preparation of a variety of isoquinoline alkaloids. The hydrogenation of Z-enamide substrates **12** in the presence of 0.5–1.0 mol % of (R)-**3** in a mixture of ethanol and dichloromethane afforded **13** (eq 5) with 1R configuration in 95–100% enantiomeric excess (ee) (21). The E-isomers of **12** are inert under such catalytic conditions.
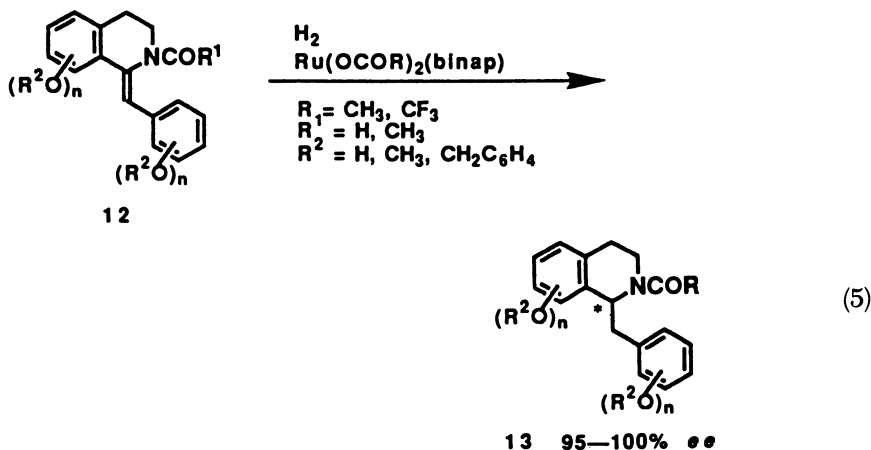
This enantioselective reaction, followed by removal or modification of the N-acyl group, leads easily to tetrahydropapaveline, laudanosine, (R)- and

(S)-trimethoquinol, and norreticurine in high optical purities. A simple 1-methylene analog of **12** gives salsolidine after deacylation.

Extension of this method to the enantioselective hydrogenation of substrate **14** (eq 6) established a general route to benzomorphans and morphinans based on asymmetric catalysis (*22*).

$$
\begin{array}{c}
\text{H}_2 \\
\text{Ru(OCOR)}_2(p\text{-tolbinap}) \\
\hline
\text{R} = \text{CF}_3 \\
\text{R' = CH}_3 \\
\text{R'—R' = —(CH}_2)_4\text{—}
\end{array}
$$

14

(6)

15   **> 97% ee**
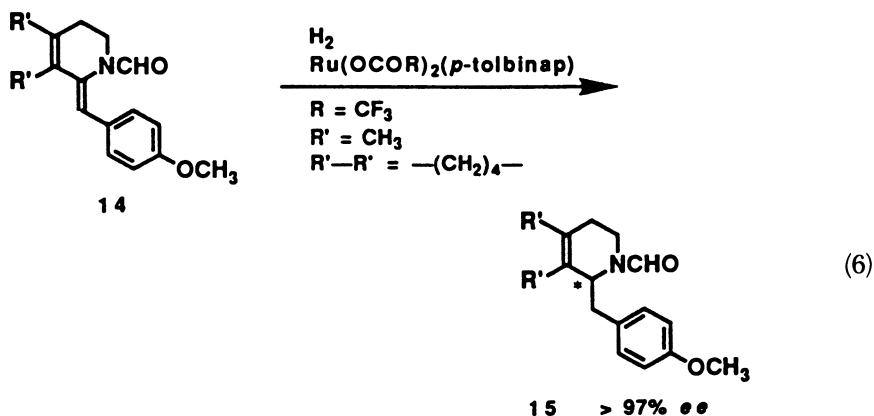
Asymmetric Hydrogenation of Unsaturated Carboxylic Acids Catalyzed by Complexes 3.

All of the catalyst systems designed so far were unable to give high enantiomeric excesses without the amide or related groups. However, very high enantioselectivity (up to 98.4% ee) was reported recently in the asymmetric hydrogenation of trisubstituted acrylic acids catalyzed by a cationic chiral (aminoalkyl)ferrocenyldiphosphine–rhodium complex (*23*). Type 3 complexes are excellent catalysts for asymmetric hydrogenation of disubstituted acrylic acids **16**, which have only carboxylic acid functionality (eq 7) (*24*).

$$
\begin{array}{c}
\text{H}_2 \; 4\text{—135 atm} \\
(R)\text{-BINAP—Ru(II)} \\
\hline
\text{CH}_3\text{OH, room temp.}
\end{array}
$$

16   **17**

(7)

R, 91% ee   *S*, 87% ee   *S*, 85% ee   *R*, 92% ee

R, 93% ee   *R*, 95% ee   *S*, 93% ee   95% ee
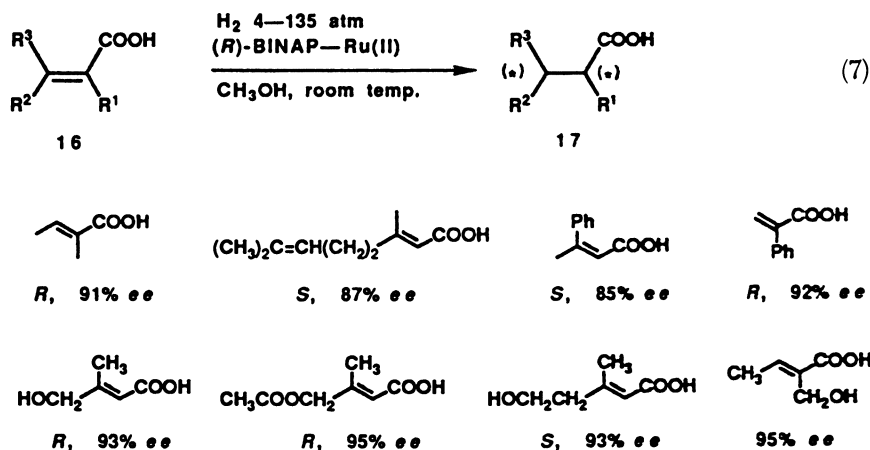
The optimum reaction conditions are highly dependent on the structures of the olefinic substrates and on reaction conditions such as initial pressures of hydrogen. Various oxygen-functionalized unsaturated carboxylic acids can also be used as substrates. Hydrogenation of 18 with (*S*)-3a as catalyst afforded (*S*)-naproxen (19), a useful antiinflammatory agent, in 92% yield and in 97% ee (eq 8). Certain β,γ-unsaturated carboxylic acids were also hydrogenated in 81–88% ee.

$$\text{H}_2 \text{ (135 atm)}$$
$$\text{Ru(OCOCH}_3\text{)}_2\text{((S)-binap)}$$
$$\text{CH}_3\text{OH, -20 °C}$$

18

19, (*S*)-Naproxen 97% *ee*

(8)
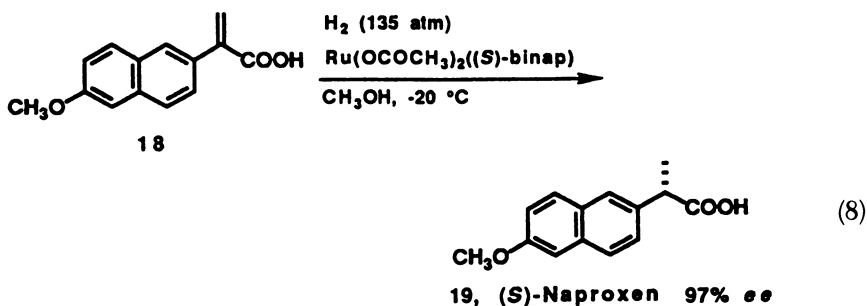
Although the mechanism of these hydrogenations is still unclear, some relevant information has been obtained. For example, the deuterium incorporation experiments for the hydrogenation of acrylic acid derivatives showed that α-hydrogen usually comes from gaseous hydrogen, while most β-hydrogen (50–100%) comes from protic solvents or substrates. In spite of these rather complicated facts, deuteration experiments of tiglic acid and cinnamic acid (25) indicate that the overall stereochemistry of hydrogen addition is *cis*.

Asymmetric Hydrogenation of Allylic and Homoallylic Alcohols Catalyzed by Complexes 3.

Some cationic Rh– and Ir–phosphine complexes are known to catalyze diastereoselective hydrogenation of chiral allylic and homoallylic alcohols. However, highly enantioselective hydrogenation of prochiral substrates has been difficult. The binap–Ru(II) dicarboxylate complexes 3 effectively catalyze enantioselective hydrogenation of prochiral allylic and homoallylic alcohols (26). Geraniol and nerol are hydrogenated in methanol under the initial hydrogen pressure of 90–100 atm at room temperature to give citronellol in nearly quantitative yield and with 96–99% ee (Table II and eqs 9 and 10). The substrate-to-catalyst mole ratio approaches 50,000. The allylic and nonallylic double bonds in the starting olefinic alcohols can be differentiated clearly. Hydrogenation of homogeraniol gave 4,8-dimethyl-7-nonenol in 92% ee.

As shown in Scheme I, this method has been applied successfully to the synthesis of (3*R*,7*R*)-3,7,11-trimethyldodecanol (23), a versatile intermediate for synthesis of α-tocopherol (vitamin E) (20). The synthesis of 23 was started from citronellol (21), for which asymmetric synthesis had already been established for the industrial production of (–)-menthol (15, 16). Conversion

Table II. Asymmetric Hydrogenation of Geraniol and Nerol

Substrate	Catalyst	S/C[a]	op[b] (%)	ee[c] (%)
Geraniol	(S)-3a	530	98	(96)
	(S)-3f	500		(98)
	(S)-3b	10,000	99	(96)
	Ru(OCOCF$_3$)$_2$((S)-binap)	50,000	96	
	(S)-9c	1,900		(96)
Nerol	(R)-3a	540		(98)

NOTE: All products were of (R)-configuration.
[a]Substrate-to-catalyst mole ratio.
[b]Determined on the basis of the value of optical rotation.
[c]Determined by HPLC analysis of the diastereomeric amides prepared by condensation of citronellic acid and (R)-1-(1-naphthyl)ethylamine.

$$\text{Geraniol} \xrightarrow{\text{(S)-BINAP—Ru(II)}} \text{(R)-Citronellol} \quad (9)$$

$$\text{Nerol} \xrightarrow{\text{(S)-BINAP—Ru(II)}} \text{(S)-Citronellol} \quad (10)$$
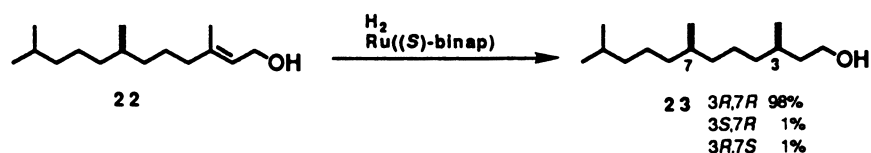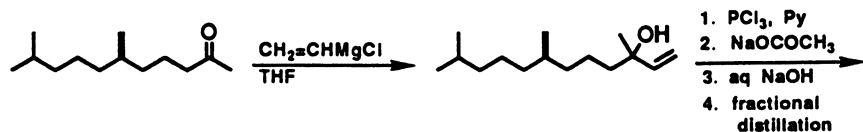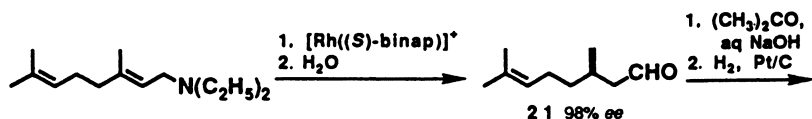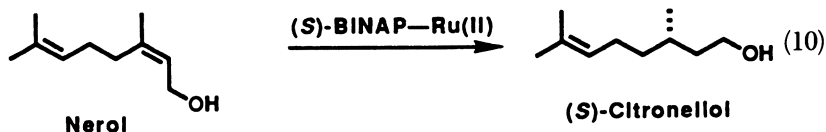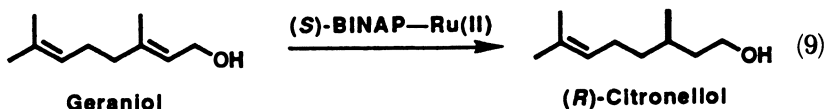
Scheme I.

of **21** to **22** followed by asymmetric hydrogenation catalyzed by the binap–Ru complex afforded the desired alcohol **23** in 99% diastereoselectivity. Chiral allylic secondary alcohols can be kinetically resolved by hydrogenation with (*R*)- or (*S*)-**3** (*27*).

20   2*R*,4'*R*,8'*R*
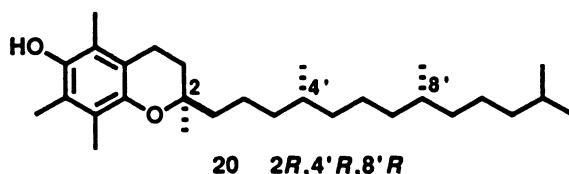
Asymmetric Hydrogenation of Functionalized Ketones Catalyzed by Binap–Ru(II) Complexes

Optically active secondary alcohols with functional groups at neighboring positions are extremely useful starting materials for the synthesis of various biologically active compounds. The binap–Ru(II) dicarboxylate complexes **3** can catalyze the hydrogenation of α-amino ketones **24** to give amino alcohols **25** (eq 11) in high enantioselectivity (*28*).

a : R = CH₃	Ru(OCOCH₃)₂((*S*)-binap)	**96% *ee***
b : R = CH(CH₃)₂	Ru(OCOCH₃)₂((*S*)-binap)	**95% *ee***
c : R = C₆H₅	Ru(OCOCH₃)₂((*S*)-tolbinap)	**93% *ee***
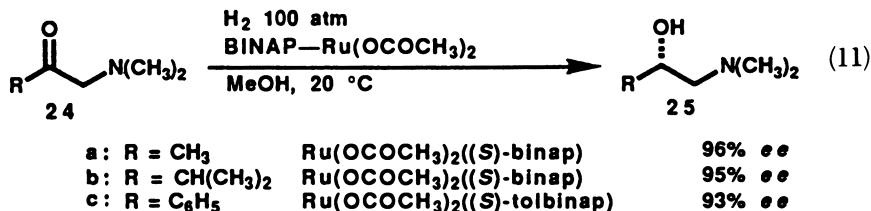
However, other functionalized ketones such as β-keto ester **26** cannot be reduced by using **3**. Fortunately, the binap–Ru(II) complexes derived from **3a** and two equivalents of HX (X is Cl, Br, or I) (*28, 29*), as well as with complex **2** (*28–30*), can catalyze the hydrogenation of ketones bearing various functionalities (including dialkylamino, hydroxyl, alkoxyl, siloxyl, keto, alkoxycarbonyl, alkylthiocarbonyl, dialkylaminocarbonyl, and carboxyl) exceptionally in high enantioselectivities (~100% ee) (eq 12).

$$X = Y, C–Y, C–C–Y$$
$$Y = O, N, Br, etc.$$
$$C = sp^2 \text{ or nonstereogenic } sp^3 \text{ carbon}$$
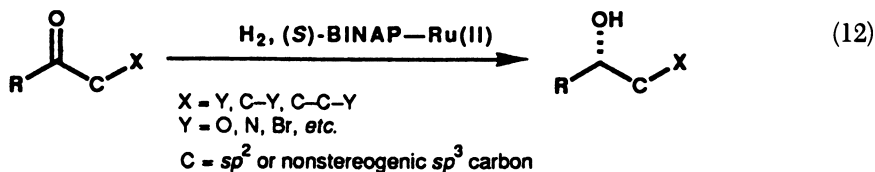
The hydrogenation proceeds smoothly in methanol at room temperature, with initial hydrogen pressure of 70–100 atm. Hydrogenation of prochiral symmetrical α- and β-diketones afforded a mixture of *meso*- and *dl*-diols. The enantioselectivities of the *dl*-diols were very high (99–100% ee) (*28, 30*).

The stereochemistry of the hydrogenation suggests that the key factor in the enantioface differentiation is a simultaneous coordination of the carbonyl oxygen and heteroatom Y to the Ru atom (eq 12).
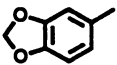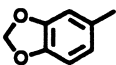
The arene ligands of complexes 6 and 9 are easily liberated under catalytic conditions to afford coordinatively unsaturated species that exhibit sufficient catalytic activity and selectivity in the hydrogenation of a number of unsaturated substrates. Some representative results are given in Table III. α-Amino ketones and β-keto esters were hydrogenated in very high enantioselectivity. Above all, smooth reduction of β-keto esters is important because dicarboxylate complexes 3 cannot reduce substrates of this type.

When methanol was used as a solvent, the reduction of 26 (eq 13) proceeded very quickly, though a small percentage of dimethyl acetal was formed as a byproduct. The formation of such a byproduct can be avoided if dichloromethane or aqueous methanol is used. The hydrogenation can be operated even at 3 atm of hydrogen pressure at room temperature, though a prolonged reaction time (90 h) is necessary.

$$\text{(13)}$$
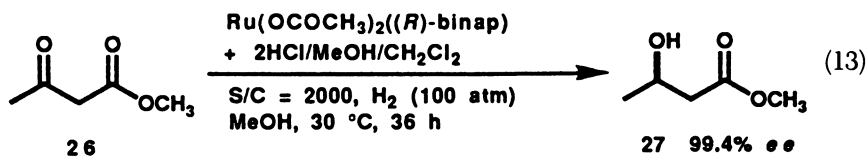
Type 28 β-keto ester with a substituent at the 2-position is a chiral compound, but racemization occurs very rapidly. If stereoselective hydrogenation occurs, only one product forms via the so-called dynamic kinetic resolution of chirally labile racemate. Binap–Ru catalysts can realize this type of hydrogenation (*31*). Very high *syn* selectivities have been obtained when reactions were carried out in dichloromethane (eq 14).

$$\text{(14)}$$
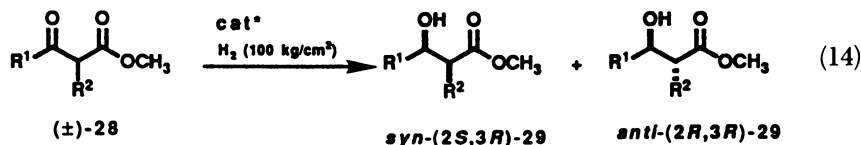
R^1	R^2	solvent	syn % *de* (% *ee*)
CH_3	CH_3	CH_3OH	2 (96)
CH_3	$NHCOCH_3$	CH_2Cl_2	98 (98)
		CH_3OH	42 (90)
methylenedioxyphenyl	$NHCOCH_3$	CH_2Cl_2	98 (94)
methylenedioxyphenyl	$NHCOC_6H_5$	CH_2Cl_2	98 (92)

cat* = $Ru(OCOCH_3)_2((R)$-binap$) + 2$ HBr
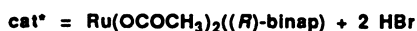
Table III. Asymmetric Hydrogenations Catalyzed by Cationic Complexes 6 and 9

Substrate	Catalyst	S/C^[a]	Solvent	H_2 (atm)	Temperature (°C)	Time (h)	ee (%)	Configuration
26	(S)-6a	2000	CH_3OH	95	17	44	98	S[b]
	(S)-6c	2100	CH_2Cl_2	100	50	35	97	S
	(S)-9c	2500	CH_3OH	100	30	35	99	S[b]
	(S)-9c	2200	$CH_3OH–H_2O^c$	100	30	35	98	S
24a	(S)-9c	1100	$C_2H_5OH–CH_2Cl_2^d$	105	30	40	99	S
(E)-2-Methyl-2-butenoic acid	(S)-6d	1000	CH_3OH	4	20	92	89	S
	(S)-9c	1300	CH_3OH	4	65	17	86	S
18	(S)-9c	200	CH_3OH	116	–20	17	96	S
Geraniol	(S)-9c	1900	$CH_3OH–H_2O$	100	20	8	96	R[e]
	(S)-9c	5000	CH_3OH	112	60	10	95	R[f]

NOTE: Hydrogenations were carried out in 0.2–8.7 M solution of the substrate (2.3–13.9 mmol). Conversions were complete unless otherwise described.

[a] Substrate-to-catalyst mole ratio.

[b] The dimethyl acetal of methyl 3-oxobutanoate was formed in 1.1–3.4% yield. The formation was avoided by use of 95–99% aqueous methanol as solvent.

[c] Methanol:H₂O = 95:5.

[d] Ethanol:CH₂Cl₂ = 5:2.

[e] The conversion was 91%. Dihydrocitronellol (0.3%) was detected by GLC.

[f] Dihydrocitronellol (0.6%) was formed.

A similar asymmetric hydrogenation of (±)-**30** with (R)-binap–Ru(II) produces mostly the *syn* alcohol **31** (eq 15) (*31*). The compound *syn*-(2S,3R)-**31** is an important intermediate for the synthesis of β-lactam antibiotics because it is easily converted to the chiral acetate **33** via **32** (eq 16).

H_2 (50—100 kg/cm^2)

(R)-BINAP—Ru(II)

S/C = 100—1000
50 °C

(±)-**30**

OH O

OCH$_3$

NHCOC$_6$H$_5$

syn-(2S,3R)-**31**   +   *anti*-(2R,3R)-**31**   (15)

OSiMe$_2$Bu^t

RuCl$_3$, CH$_3$CO$_3$H

CH$_3$COOH

OSiMe$_2$Bu^t

OCOCH$_3$

(16)

32   **33**
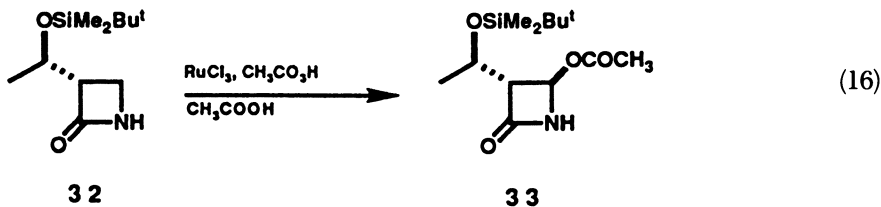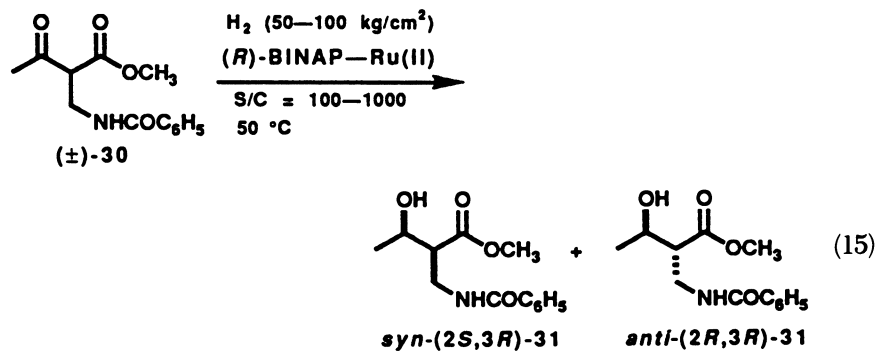
We investigated suitable catalytic conditions that give *syn*-(2S,3R)-**31** selectively by using various binap–Ru(II) complexes (*32*). The diastereoselectivities are highly dependent on the kinds of solvents and halide anions in the binap–Ru(II) complexes, as well as on substituents of the four phenyl rings of the binap ligands. Among the halide complexes, those bearing iodide anions such as **6c** and **9c** gave the highest diastereoselectivity. Some representative results are shown in Table IV.

Much lower diastereoselectivity has usually been obtained in methanol than in dichloromethane, though the hydrogenation proceeds much faster in methanol than in dichloromethane. Introduction of alkyl substituents at the 3- and 5-positions of phenyl rings in binap results in higher diastereoselectivity. In contrast, a substituent at the 4-position (such as CH_3, t-C_4H_9, CH_3O, F, Cl, or CF_3) does not exert a remarkable effect on diastereoselectivity. Replacement of binap phenyl rings by cyclohexyl or cyclopentyl groups resulted in total loss of catalytic activity. The highest diastereoselectivity (98% diastereomeric excess, de) was obtained with a catalytic system derived from [RuI$_2$(p-cymene)]$_2$ and 3,5-t-Bu$_2$-binap. The effect of iodide ion on stereoselectivity has also been observed in the hydrogenation of racemic **34** and **36** (eqs 17 and 18) (*33, 34*).

Table IV. Stereoselectivities of the Asymmetric Hydrogenation of Complex 30 Catalyzed by Binap–Ru(II) Complexes

Catalyst	Solvent	S/C^a	Conversion (%)	de^b (%)	ee^c (%) of syn-31
[RuCl((R)-binap)(p-cymene)]Cl	$CH_2Cl_2^d$	100	91	74	90
[RuBr((R)-binap)(p-cymene)]Br	$CH_2Cl_2^d$	100	91	79	98
[RuI((S)-binap)(p-cymene)]I	$CH_2Cl_2^d$	100	98	88	97
[RuI((S)-binap)(p-cymene)]I	MeOH	100	100^e	51	97
[RuI((R)-binap)(p-cymene)]I	$CH_2Cl_2.MeOH^f$	1000	91	84	99
[RuI((S)-m-tolbinap)(p-cymene)]I^g	MeOH	1000	94	67	91
[RuI((S)-m-xylylbinap)(p-cymene)]I^g	$CH_2Cl_2^d$	100	68	95	99
[RuI$_2$(p-cymene)]$_2$ + (R)-3,5-Bu$^t_2$-binap^{g,h}	CH_2Cl_2–MeOH^f	1000	55	98	99
[RuI$_2$(p-cymene)]$_2$ + (R)-3,5-Bu$^t_2$-binap^{g,h}	MeOH	500	91	92	92

NOTE: Hydrogenation was carried out in an autoclave (50–60 °C) for 20–40 h under an initial hydrogen pressure of 50 kg cm^{-2} unless otherwise stated. The ratio of solvent to substrate was 4 (v/w).

^{a}Substrate-to-catalyst mole ratio.

^{b}Diastereomeric excess was determined by HPLC analysis [Cosmosil 5SL, with hexane–2-propanol (9:1) as eluent].

^{c}Enantiomeric excess of syn-31 was determined by HPLC analysis of the (+)-methoxy(trifluoromethyl)phenylacetyl ester of 31[Nucleosil 100–3, with hexane–tetrahydrofuran–MeOH (400:100:1) as eluent].

^{d}The solvent was saturated with water at –20 °C by addition of 0.5% (v/v) water to stirred dichloromethane (distilled from phosphorus pentoxide).

^{e}Initial pressure of hydrogen was 100 kg cm^{-2}.

^{f}The ratio of dichloromethane to methanol was 7:1.

^{g}Key:

m-tol: *m*-xylyl: 3,5-Bu$^t_2$:
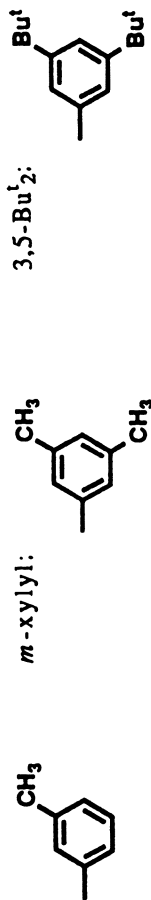
^{h}The catalyst was prepared by heating a 2:1 mixture of the ligand and [RuI$_2$(p-cymene)]$_2$ in ethanol–dichloromethane (1:1) at 80 °C for 18 h.

$$(17)$$
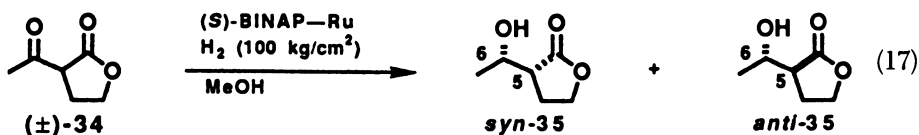
	config.	% de	(% ee)
[RuCl((*R*)-binap)(benzene)]Cl	syn (5*S*,6*R*)	95	(93)[21]
[RuI((*S*)-binap)(benzene)]I	syn (5*R*,6*S*)	98	(97)

$$(18)$$
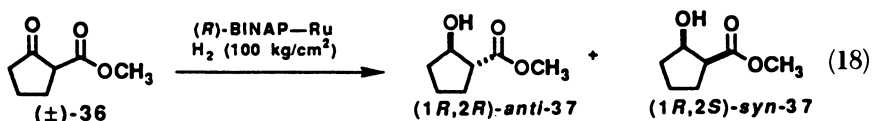
cat	S/C	solvent	config.	% de	(% ee)
[RuCl((*R*)-binap)(benzene)]Cl	1170	MeOH	anti (1*R*,2*R*)	63	(88)[21]
		CH$_2$Cl$_2$	anti (1*R*,2*R*)	98	(92)[21]
[RuI((*S*)-binap)(benzene)]I	2500	MeOH	anti (1*S*,2*S*)	92	(99)

Synthesis of New Chiral Bis(triarylphosphine) Ligands via Asymmetric Hydrogenation of Cyclopentanones

The diphosphines **38** and **39** are chiral, fully aryl-substituted phosphines that have not been synthesized in optically pure forms. *cis*-Chelation is expected for **38** (abbreviated to o-bitap). The *meta*-substituted phosphine **39** (abbreviated to m-bitap) will coordinate to metals in the *trans* manner. Because the structures of such complexes are unique, one may expect new catalytic activity and selectivity. Thus, we prepared these ligands through asymmetric hydrogenation (35).

38 (o-BITAP)   **39 (*m*-BITAP)**
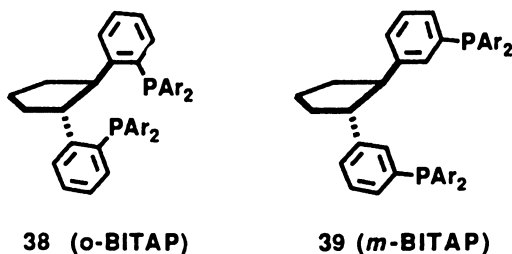
When the racemic 3,4-diaryl-substituted cyclopentanone **40** was hydrogenated under the described conditions, a diastereomeric mixture of **41** and **42** was obtained in 1.6:1.0 ratio (eq 19). This mixture can easily be separated with silica gel column chromatography.

$$
\text{(±)-40 all }trans \quad\xrightarrow[\substack{\text{CH}_2\text{Cl}_2-\text{MeOH}}]{\substack{\text{H}_2\ (90-95\ \text{kg/cm}^2) \\ [\text{RuI}((S)\text{-binap})\text{-} \\ (p\text{-cymene})]\text{I}}}\quad \text{(+)-41} \ + \ \text{(-)-42} \tag{19}
$$
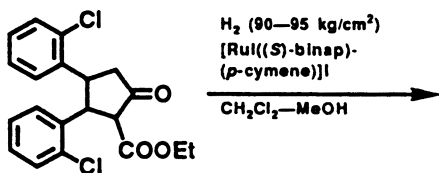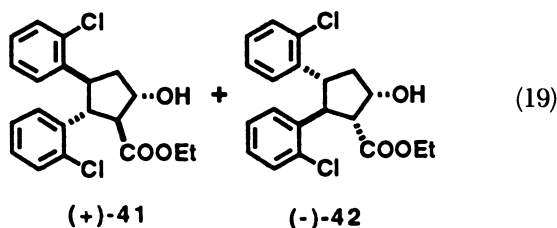
The all-*trans* structure of **41** was established with the aid of X-ray crystallography. The compound (+)-**41** was converted to (+)-**40** (61% ee) by CrO_3 oxidation. Simple recrystallization from methanol gave optically pure (+)-**40** $[[\alpha]_D^{26} +68.0°\ (c\ 0.50,\ CHCl_3)]$. The structure of **42** was assigned on the basis of NMR data and the fact that (–)-**42** can be converted to (–)-**40** (eq 20). No loss of optical activity has been observed for (+)- and (–)-**40**. Thus, hydrogenation does not belong to dynamic kinetic resolution.

$$
\text{(-)-42}\quad\xrightarrow{\ \text{CrO}_3\ }\quad \text{(-)-40} \tag{20}
$$
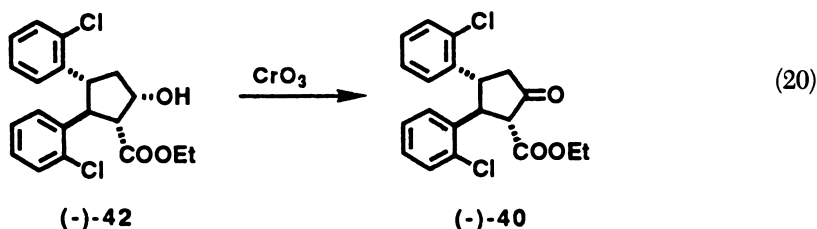
The stereochemistry of the hydrogenation is shown in Scheme II. For both enantiomers, the single-handed catalyst bearing the (S)-binap ligand approaches from the rectus face.

Conversion of the keto ester (–)-**40** $[[\alpha]_D^{24} -66.3°\ (c\ 1.49,\ CHCl_3)]$ to the diphosphine (+)-**38** $[[\alpha]_D^{20} +29.6°\ (c\ 1.02,\ CHCl_3)]$ was carried out by the procedures shown in Scheme III. The 100% optical purity of (–)-**44** was confirmed by HPLC analysis using a chiral column, Chiralcel OD (hexane:isopropyl alcohol = 60:1). The absolute configuration was determined by reduction of (–)-**44** to (1R,2R)-1,2-diphenylcyclopentane.

Thus, the present method provides us with a convenient route to a new class of chiral bis(triarylphosphine) with C_2 chirality. A similar procedure with the *m*-chloro derivative of **40** afforded the chiral *trans*-chelating diphosphines **39**.

Scheme II.

Ar = o-ClC$_6$H$_4$, m-ClC$_6$H$_4$
R = C$_2$H$_5$, CH$_3$
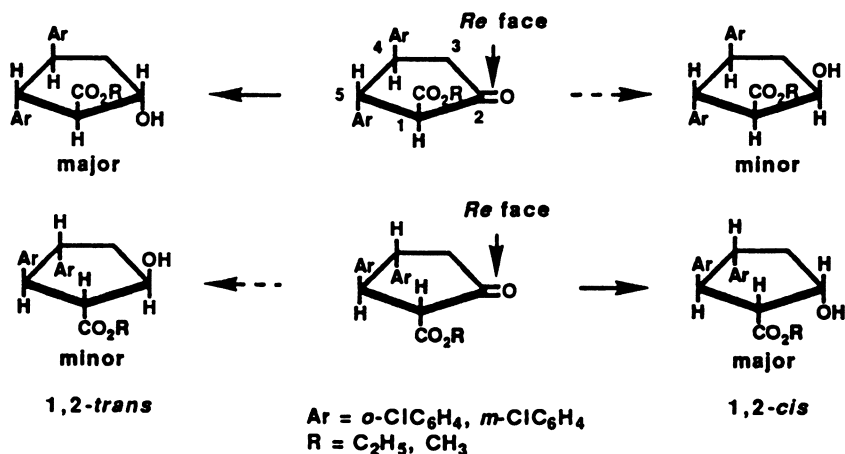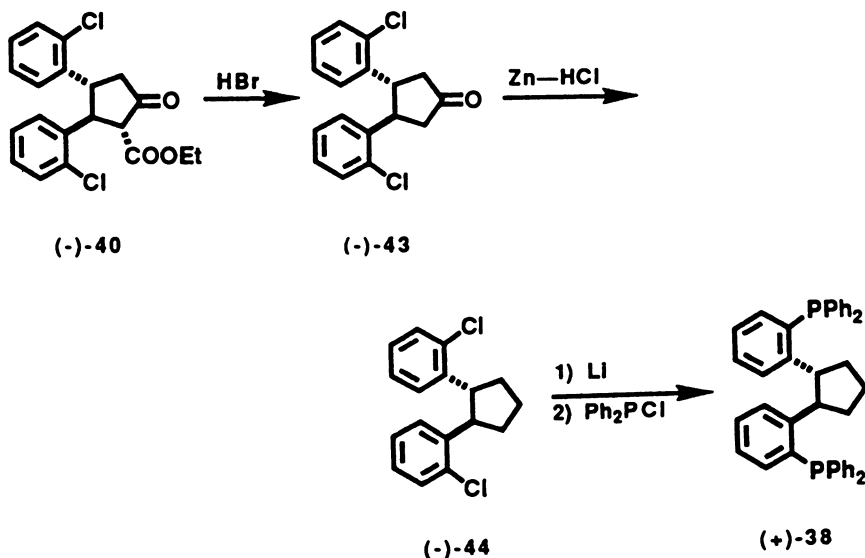
Scheme III.

Conclusion

We developed several binap-based catalysts that are highly efficient for asymmetric hydrogenations of both olefinic and ketonic substrates. In view of their efficiency, the high synthetic applicability is obvious. Some of the compounds described here have so far been prepared only by biological or

biochemical transformations. The present catalytic systems sometimes generate products with optical purity higher than those of natural origin. Moreover, *R* and *S* enantiomers are accessible with equal ease by either variation of the substrate geometry or choice of handedness of the catalysts. The chemical processes are operationally simple and suitable for large-scale production. Thus, asymmetric synthesis by use of manufactured catalysts is expected to become more and more important in both synthetic and industrial chemistry. It will be used cooperatively with biological and biochemical processes.

Acknowledgment

References

1. Dang, T. P.; Kagan, H. B. *J. Chem. Soc., Chem. Commun.* **1971,** 481.
2. Kagan, H. B. In *Asymmetric Synthesis*; Morrison, J. D., Ed.: Academic: Orlando, FL, 1985; Vol. 5, p 1.
3. Knowles, W. S.; Sabacky, M. J.; Vineyard, B. D. *J. Chem. Soc., Chem. Commun.* **1972,** 10.
4. Knowles, W. S.; Christopfel, W. C.; Koenig, K. E.; Hobbs, C. F. In *Catalytic Aspects of Metal Phosphine Complexes*; Alyea, E. C.; Meek, D. W., Eds.; Advances in Chemistry 196; American Chemical Society: Washington, DC, 1982; p 325.
5. Knowles, W. S. *Acc. Chem. Res.* **1983,** *16*, 106.
6. Miyashita, A.; Yasuda, A.; Takaya, H.; Toriumi, K.; Ito, T.; Souchi, T.; Noyori, R. *J. Am. Chem. Soc.* **1980,** *102*, 7932.
7. Miyashita, A.; Takaya, H.; Souchi, T.; Noyori, R. *Tetrahedron* **1984,** *40*, 1245.
8. Toriumi, K.; Ito, T.; Takaya, H.; Souchi, T.; Noyori, R. *Acta Crystallogr.* **1982,** *B38*, 807.
9. Takaya, H.; Mashima, K.; Koyano, K.; Yagi, M.; Kumobayashi, H.; Taketomi, T.; Akutagawa, S.; Noyori, R. *J. Org. Chem.* **1986,** *51*, 629.
10. Takaya, H.; Akutagawa, S.; Noyori, R. *Org. Synth.* **1988,** *67*, 20.
11. Noyori, R.; Takaya, H. *Chem. Scr.* **1985,** *25*, 83.
12. Takaya, H.; Ohta, T.; Mashima, K.; Kitamura, M.; Noyori, R. In *Future Opportunities in Catalytic and Separation Technology*; Misono, M.; Moro-oka, Y.; Kimura, S., Eds.; Elsevier: Amsterdam, 1990; p 332.
13. Noyori, R.; Takaya, H. *Acc. Chem. Res.* **1990,** *23*, 345.
14. Takaya, H.; Ohta, T.; Mashima, K.; Noyori, R. *Pure Appl. Chem.* **1990,** *62*, 1135.
15. Tani, K.; Yamagata, T.; Akutagawa, S.; Kumobayashi, H.; Taketomi, T.; Takaya, H.; Miyashita, A.; Noyori, R.; Otsuka, S. *J. Am. Chem. Soc.* **1984,** *106*, 5208.
16. Tani, K.; Yamagata, T.; Yamagata, Y.; Tomita, K.; Akutagawa, S.; Kumobayashi, H.; Otsuka, S. *Angew. Chem., Int. Ed. Engl.* **1985,** *24*, 217.
17. Inoue, S.; Takaya, H.; Tani, K.; Yamagata, T.; Otsuka, S.; Sato, T.; Noyori, R. *J. Am. Chem. Soc.* **1990,** *112*, 4897.

18. Ikariya, T.; Ishii, Y.; Kawano, H.; Arai, T.; Saburi, M.; Yoshikawa, S.; Akutagawa, S. *J. Chem. Soc., Chem. Commun.* **1985**, 922.
19. Ohta, T.; Takaya, H.; Noyori, R. *Inorg. Chem.* **1988**, *27*, 566.
20. Mashima, K.; Kusano, K.; Ohta, T.; Noyori, R.; Takaya, H. *J. Chem. Soc., Chem. Commun.* **1989**, 1208.
21. Noyori, R.; Ohta, M.; Hsiao, Y.; Kitamura, M.; Ohta, T.; Takaya, H. *J. Am. Chem. Soc.* **1986**, *108*, 7117.
22. Kitamura, M.; Hsiao, Y.; Noyori, R.; Takaya, H. *Tetrahedron Lett.* **1987**, *28*, 4829.
23. Hayashi, T.; Kawamura, N.; Ito, Y. *J. Am. Chem. Soc.* **1987**, *109*, 7876.
24. Ohta, T.; Takaya, H.; Kitamura, M.; Nagai, K.; Noyori, R. *J. Org. Chem.* **1987**, *52*, 3174.
25. Ohta, T.; Takaya, H.; Noyori, R. *Tetrahedron Lett.* **1990**, *31*, 7189.
26. Takaya, H.; Ohta, T.; Sayo, N.; Kumobayashi, H.; Akutagawa, S.; Inoue, S.; Kasahara, I.; Noyori, R. *J. Am. Chem. Soc.* **1987**, *109*, 1596, 4129.
27. Kitamura, M.; Kasahara, I.; Manabe, K.; Noyori, R.; Takaya, H. *J. Org. Chem.* **1988**, *53*, 708.
28. Kitamura, M.; Ohkuma, T.; Inoue, S.; Sayo, N.; Kumobayashi, H.; Akutagawa, S.; Ohta, T.; Takaya, H.; Noyori, R. *J. Am. Chem. Soc.* **1988**, *110*, 629.
29. Noyori, R.; Ohkuma, T.; Kitamura, M.; Takaya, H.; Sayo, N.; Kumobayashi, H.; Akutagawa, S. *J. Am. Chem. Soc.* **1987**, *109*, 5856.
30. Kawano, H.; Ishii, Y.; Saburi, M.; Uchida, Y. *J. Chem. Soc., Chem. Commun.* **1988**, 97.
31. Noyori, R.; Ikeda, T.; Ohkuma, T.; Widhelm, M.; Kitamura, M.; Takaya, H.; Akutagawa, S.; Sayo, N.; Saito, T.; Taketomi, T.; Kumobayashi, H. *J. Am. Chem. Soc.* **1989**, *111*, 9134.
32. Mashima, K.; Matsumura, Y.; Kusano, K.; Kumobayashi, H.; Sayo, N.; Hori, Y.; Ishizaki, T.; Akutagawa, S.; Takaya, H. *J. Chem. Soc., Chem. Commun.* **1991**, 609.
33. Kitamura, M.; Ohkuma, T.; Tokunaga, M.; Noyori, R. *Tetrahedron Asymmetry* **1990**, *1*, 1.
34. Takaya, H.; Mashima, K.; Kusano, K., unpublished results.
35. Fukuda, N.; Mashima, K.; Matsumura, Y.; Takaya, H. *Tetrahedron Lett.* **1990**, *31*, 7185.

Enantioselective Catalysis with Transition Metal Compounds

Right or Left—This Is the Question

Henri Brunner

Institut für Anorganische Chemie, Universität Regensburg, Universitätsstrasse 31, D–8400 Regensburg, Germany

Extension of the scope of enantioselective catalysis with transition metal complexes from well-established reaction types, such as the hydrogenation of dehydroamino acids and the hydrosilylation of ketones, to new reaction types is a challenging goal. The extension to (i) the transfer hydrogenation of itaconic acid with formic acid, (ii) the hydrophenylation of norbornene, and (iii) the homo-Diels–Alder reaction of norbornadiene with acetylenes is described. In reactions i and iii, there is virtually complete optical induction.

OPTICALLY PURE SUBSTANCES are increasingly in demand for human food additives, animal food supplements, pharmaceuticals, and agrochemicals. Enantioselective catalysis with transition metal compounds is a promising approach to meet this demand.

An optically active catalyst is required in only small quantities, an economically important point. It reenters each catalytic cycle with its chiral information. Therefore, large amounts of optically active compounds can be prepared by using only small amounts of an optically active catalyst. Preferably, the enantioselective cocatalyst is applied as an in situ catalyst. Such an in situ catalyst consists of a metal compound (the procatalyst) and an optically active ligand (the cocatalyst), both of which (in favorable cases) are stable and commercially available. Use of in situ catalysts does not require the synthesis of the actual catalyst prior to the catalytic reaction.

Hydrogenation and Hydrosilylation

Well-established reaction types for enantioselective catalysis with transition metal complexes are the hydrogenation of dehydroamino acids (Scheme I) and the hydrosilylation of ketones (Scheme II).

Hydrogenation of (Z)-α-N-acetamidocinnamic acid to give N-acetyl-phenylalanine (Scheme I) is a frequently used standard reaction. A variety of Rh complexes catalyze this reaction under mild conditions (room temperature, no hydrogen pressure), with optical inductions close to 100%. An example of an in situ catalyst is [Rh(cod)Cl]$_2$–Norphos (*see* Abbreviations list) (*1*, *2*). [Rh(cod)Cl]$_2$ is the procatalyst, and the optically active chelate phosphine, Norphos, is the cocatalyst. Both are shown in Scheme I.

In the hydrosilylation of acetophenone with diphenylsilane, first a catalytic addition of a Si–H bond to the C=O bond occurs. This addition gives rise to a silyl ether, which is subsequently hydrolyzed at the O–Si bond.
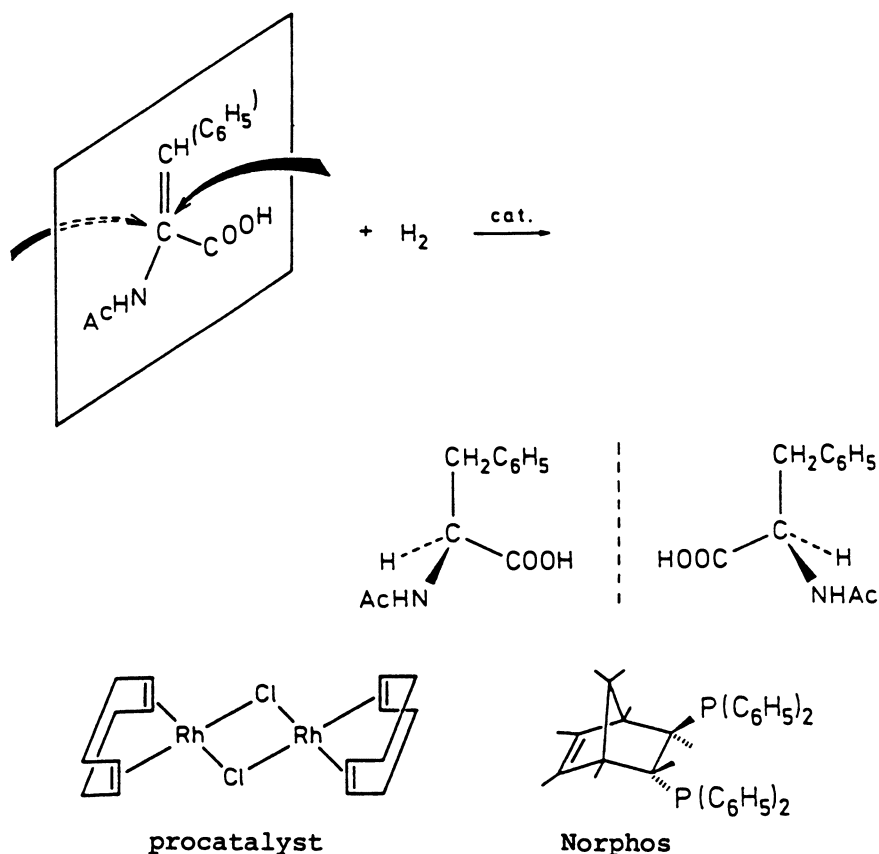
Scheme I.
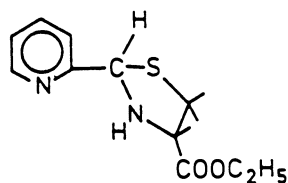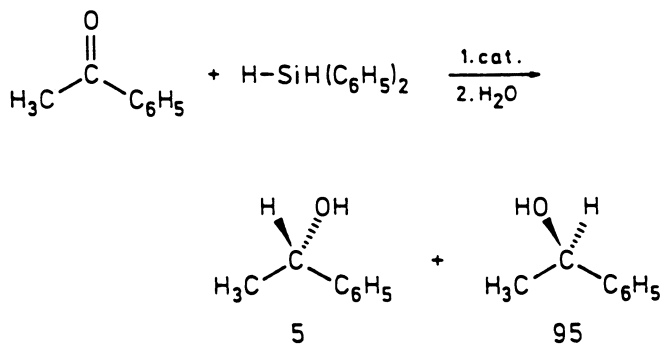
Scheme II.

1-Phenylethanol is the ultimate product (Scheme II). In this reaction, the celebrated optically active chelate phosphines are inefficient cocatalysts as far as enantioselectivity is concerned. Therefore new types of nitrogen ligands have been introduced as optically active cocatalysts, such as the pyridinethiazolidines. In situ catalysts consisting of $[Rh(cod)Cl]_2$ and the pyridinethiazolidine shown in Scheme II give optical inductions close to 100% in the hydrosilylation of acetophenone with diphenylsilane (3, 4).

To extend the scope of enantioselective catalysis with transition metal complexes from the established reaction types (hydrogenation and hydrosilylation, exemplified in Schemes I and II) to new reaction types is a challenging goal. This extension is the topic of the following paragraphs.

Enantioselective Hydrogenation with Formic Acid

Itaconic acid is a frequently used substrate in enantioselective hydrogenation. The best results have been obtained with rhodium catalysts of the ligand BPPM (*see* Abbreviations list) and BPPM derivatives. Molecular hydrogen can be replaced by formic acid as the transfer hydrogenation agent (5, 6). The most convenient choice is the azeotrope HCOOH–NEt_3 (5:2), which is commercially available. This transfer hydrogenation takes place in DMSO (dimethyl sulfoxide) at room temperature. It avoids the inconvenience and risks of molecular hydrogen and pressure.

The in situ catalyst [Rh(cod)Cl]$_2$–BPPM (Scheme III) gives methylsuccinic acid of 85% ee (enantiomeric excess), similar to the enantioselectivity of the hydrogenation with molecular hydrogen (7). In the transfer hydrogenation, chelate phosphines giving seven-membered rings are superior to chelate phosphines giving six- or five-membered rings. In addition to Rh(I) compounds such as [Rh(cod)Cl]$_2$, Rh(II) compounds such as Rh$_2$(OAc)$_4$ or Rh(III) compounds such as RhCl$_3$ are suitable procatalysts (6).

Triethylamine can be replaced by other amines. The use of (R)-1-phenylethylamine decreases the enantioselectivity of all the in situ catalysts, whereas (S)-1-phenylethylamine increases the enantioselectivity of all the systems, and thus gives virtually complete optical induction (Scheme III).

Another type of reaction with HCOOH–NEt$_3$ as the reducing agent is the hydroarylation of norbornene with iodobenzene. This reaction is catalyzed by phosphine palladium acetate complexes (8, 9). The product is *exo*-

cocat.:
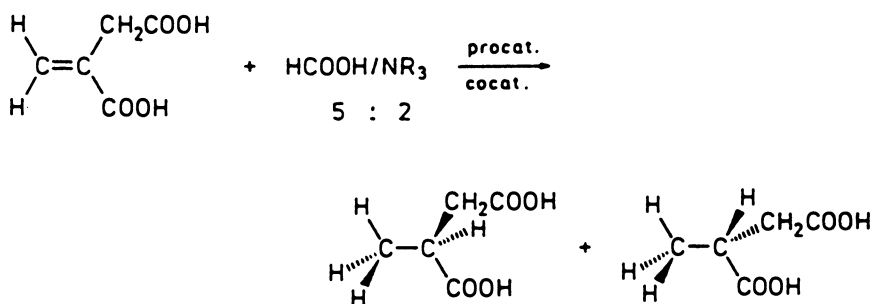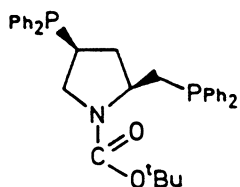
procat.:

NR$_3$	[Rh(cod)Cl]$_2$	Rh$_2$(OAc)$_4$	RhCl$_3$
NEt$_3$	84.9	92.2	82.2 % ee
(R)–PhMeCHNH$_2$	74.6	87.0	80.1 % ee
(S)–PhMeCHNH$_2$	90.5	98.7	99.5 % ee

Scheme III.

phenylnorbornane, a chiral molecule. With an in situ catalyst consisting of Pd(OAc)$_2$ and Norphos (Scheme IV) we obtain phenylnorbornane in 60% chemical yield and 45% ee (*10*). The optical purity of the hydrocarbon phenylnorbornane can be determined by gas chromatography using a permethylated β-cyclodextrin column (*11*).
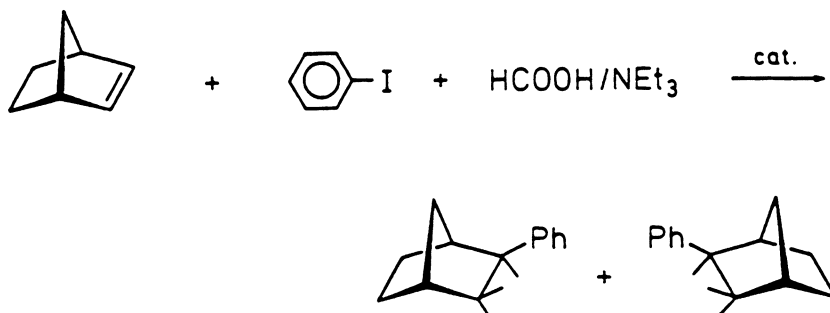
cat.:
Pd(OAc)$_2$/Norphos
1 Mol %
DMF, 60°C, 16h

45% ee (60% yield)

Scheme IV.

Other new reaction types have been opened up to enantioselective catalysis with transition metal compounds, such as the Michael addition of methyl 1-indanone-2-carboxylate to methyl vinyl ketone (*12, 13*), the monophenylation of *meso*-diols with Ph$_3$Bi(OAc)$_2$ (*14, 15*), and the hydrosilylation of oximes with diphenylsilane (*16, 17*). Because the results have been published previously, they will not be repeated here.

Homo-Diels–Alder Reactions of Norbornadiene

The reaction of norbornadiene with olefins and acetylenes will be described in the final paragraphs. Reaction with acetylenes gives rise to extremely high optical inductions.

The reaction of norbornadiene with acrylonitrile is catalyzed by phosphine nickel cyano complexes (*18*). It produces the deltacyclanes shown in Scheme V, which form diastereomers that differ in the orientation of the CN group with respect to the deltacyclane skeleton. Each diastereomer consists of a pair of enantiomers. To render the reaction enantioselective, PPh$_3$ is replaced by the optically active phosphines Diop (*see* Abbreviations list) and Norphos (*19*). With Diop the chemical yield is 100% (diastereomer

ratio 60:40), but the optical induction is only 4 and 3% (Scheme V). With a Ni(CN)$_2$–Norphos catalyst a poor (10%) chemical yield is obtained (diastereomer ratio 55:45), and the optical inductions of 12 and 15% are only slightly higher (*19*).
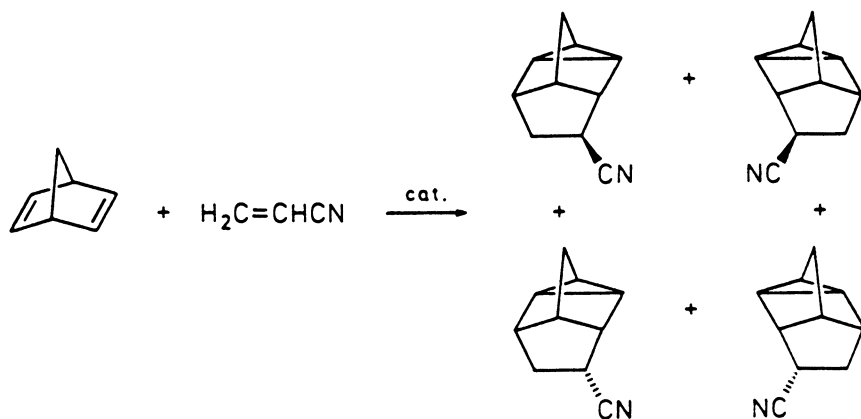
cat.:	yield	ratio diastereomers	optical induction
Ni(CN)$_2$/Diop	100%	60 : 40	4 and 3% ee
Ni(CN)$_2$/Norphos	10%	55 : 45	12 and 15% ee

Scheme V.

A much more favorable situation is the reaction of norbornadiene with phenylacetylene, in which phenyldeltacyclenes are formed (Scheme VI). In this reaction there are no diastereomers, only a pair of enantiomers being the possible product. In situ catalysts for this reaction are cobalt(III) compounds such as Co(acac)$_3$ (*see* Abbreviations list) in combination with phosphine ligands and diethylaluminum chloride (*20, 21*). With Norphos as the optically active phosphine, a catalyst quantity of 0.2 mol % is sufficient for a quantitative formation of the phenyldeltacyclene in tetrahydrofuran (THF) at 35 °C during 4 h (Scheme VI). According to a gas chromatographic (GC) analysis with a chiral cyclodextrin column (*22*), the optical purity is 99.2:0.8 (*19*).

Scheme VII shows the reaction of norbornadiene with 1-hexyne. This reaction is quantitative, giving 99% ee with a catalyst Co(acac)$_3$–Norphos–Et$_2$AlCl. The GC traces are shown at the bottom of Scheme VII for the racemic mixture, for the Diop-containing catalyst (ca. 20% ee), and for the Norphos-containing catalyst (99% ee).

Five-membered chelate rings containing compounds such as Prophos, Chiraphos, and Norphos (*see* Abbreviations list) are puckered (*23–27*). A ring

cat.:
Co(acac)₃ / Norphos / Et₂AlCl
0.2 Mol %
THF, 35°C, 4 h

99.2 : 0.8 (98.4% ee)

(yield quantitative)

Scheme VI.

cat.:
Co(acac)₃ / Norphos / Et₂AlCl

99 : 1 (98% ee)

(yield quantitative)
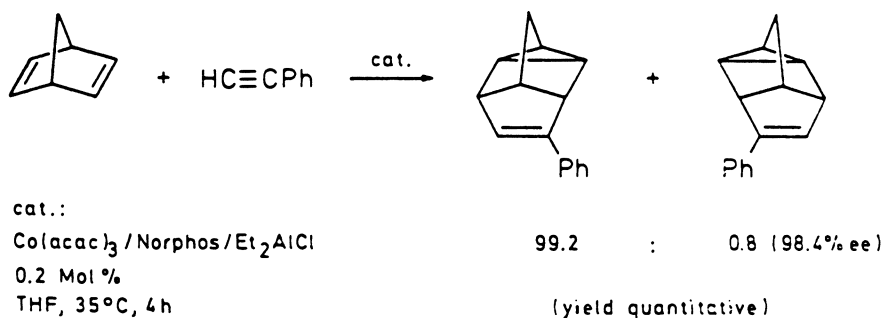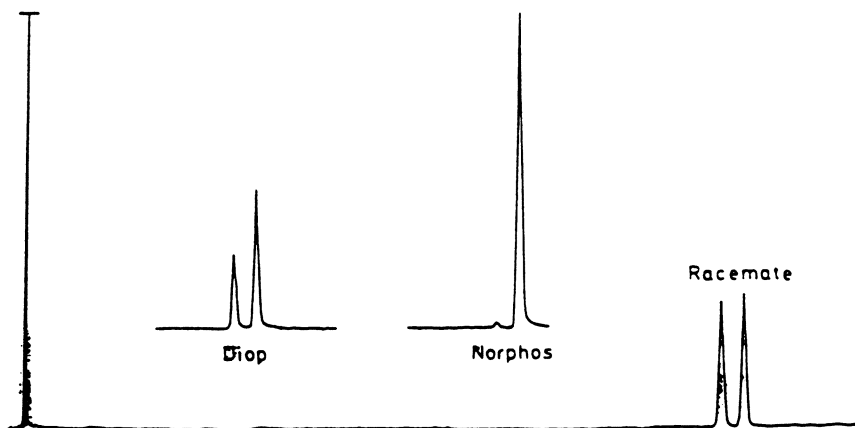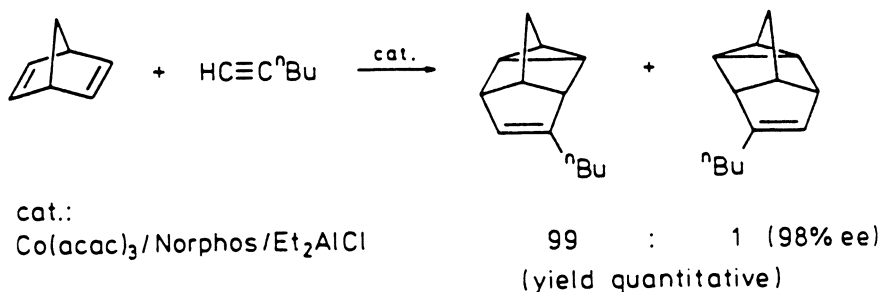
Scheme VII.

conformation that places the large substituents in an equatorial position is favored, as shown in structure A, which is also a suitable cocatalyst for the homo-Diels–Alder reaction of norbornadiene and acetylenes. The puckering of the chelate ring results in an equatorial–axial differentiation of the phenyl substituents at the phosphorus atoms. This puckering allows the phenylacetylene to bind in the preferred orientation shown in structure B, in which the phenyl substituent of the acetylene is in the neighborhood of the equa-

A

B
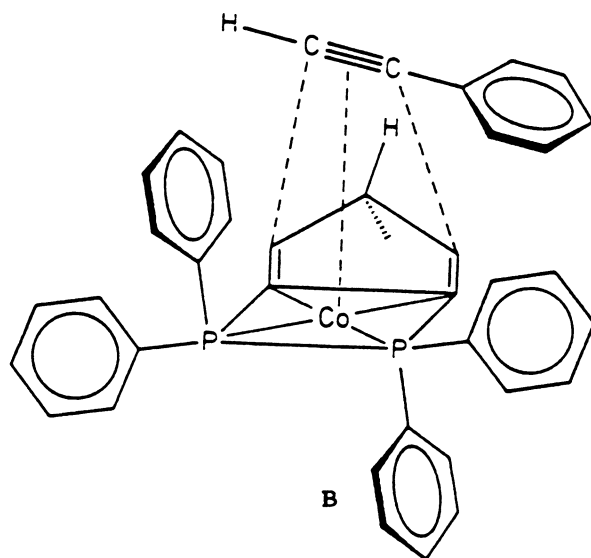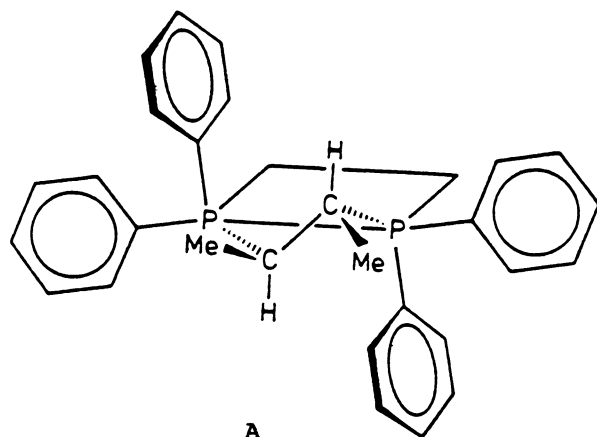
torial phenyl substituent at phosphorus. The formation of the two dashed carbon–carbon bonds completes the deltacyclene skeleton in an almost enantiospecific way.

Abbreviations and Chemical Names

acac acetylacetonate
BPPM 1,1-dimethylethyl ester of (2R-4R)-4-(diphenylphosphino)-2-[(diphenylphosphino)methyl]-1-pyrrolidinecarboxylic acid; *see* cocat. in Scheme III

Chiraphos   (S,S)-(1,2-dimethyl-1,2-ethanediyl)bis[diphenylphosphine]; *see* structures A and B
cod   1,5-cyclooctadiene
Diop   (S,S)-[(2,2-dimethyl-1,3-dioxolane-4,5-diyl)bis(methylene)]bis-[diphenylphosphine]
Norphos   (S,S)-bicyclo[2.2.1]hept-5-ene-2,3-diylbis[diphenylphosphine]
Prophos   (R)-(1-methyl-1,2-ethanediyl)bis[diphenylphosphine]

Acknowledgment

References

1. Brunner, H.; Pieronczyk, W. *Angew. Chem., Int. Ed. Engl.* **1979**, *18*, 620.
2. Brunner, H.; Pieronczyk, W.; Schönhammer, B.; Streng, K.; Bernal, I.; Korp, J. *Chem. Ber.* **1981**, *114*, 1137.
3. Brunner, H.; Riepl, G.; Weitzer, H. *Angew. Chem., Int. Ed. Engl.* **1983**, *22*, 331; *Angew. Chem. Suppl.* **1983**, 445.
4. Brunner, H.; Becker, R.; Riepl, G. *Organometallics* **1984**, *3*, 1354.
5. Brunner, H.; Leitner, W. *Angew. Chem., Int. Ed. Engl.* **1988**, *27*, 1180.
6. Brunner, H.; Graf, E.; Leitner, W.; Wutz, K. *Synthesis* **1989**, 743.
7. Ojima, I.; Kogure, T.; Yoda, N. *J. Org. Chem.* **1980**, *45*, 4728.
8. Arcadi, A.; Marinelli, F.; Bernocchi, E.; Cacchi, S.; Ortar, G. *J. Organomet. Chem.* **1989**, *368*, 249.
9. Larock, R. C.; Johnson, P. L. *J. Chem. Soc., Chem. Commun.* **1989**, 1368.
10. Brunner, H.; Kramler, K. *Synthesis* in press.
11. Schurig, V.; Nowotny, H.-P.; Schmalzing, D. *Angew. Chem., Int. Ed. Engl.* **1989**, *28*, 736.
12. Brunner, H.; Hammer, B. *Angew. Chem., Int. Ed. Engl.* **1984**, *23*, 312.
13. Brunner, H.; Kraus, J. *J. Mol. Catal.* **1989**, *49*, 133.
14. Brunner, H.; Obermann, U.; Wimmer, P. *J. Organomet. Chem.* **1986**, *316*, C1.
15. Brunner, H.; Obermann, U.; Wimmer, P. *Organometallics* **1989**, *8*, 812.
16. Brunner, H.; Becker, R. *Angew. Chem., Int. Ed. Engl.* **1984**, *23*, 222.
17. Brunner, H.; Becker, R.; Gauder, S. *Organometallics* **1986**, *5*, 739.
18. Schrauzer, G. N.; Glockner, P. *Chem. Ber.* **1964**, *97*, 2451.
19. Brunner, H.; Muschiol, M.; Prester, F. *Angew. Chem., Int. Ed. Engl.* **1990**, *29*, 653.
20. Lyons, J. E.; Myers, J. E.; Schneider, A. *Ann. N. Y. Acad. Sci.* **1980**, *333*, 273.
21. Lautens, M.; Crudden, C. M. *Organometallics* **1989**, *8*, 2733.
22. Ehlers, J.; König, W. A.; Lutz, S.; Wenz, G.; tom Dieck, H. *Angew. Chem., Int. Ed. Engl.* **1988**, *27*, 1556.
23. Vineyard, B. D.; Knowles, W. S.; Sabacky, M. J.; Bachman, G. L.; Weinkauff, D. J. *J. Am. Chem. Soc.* **1977**, *99*, 5946.
24. Fryzuk, M. D.; Bosnich, B. *J. Am. Chem. Soc.* **1977**, *99*, 6262.

25. Knowles, W. S.; Vineyard, B. D.; Sabacky, M. J.; Stults, B. R. In *Fundamental Research in Homogeneous Catalysis*; Ishii, Y.; Tsutsui, M., Eds.; Plenum: New York, 1979; Vol. 3, p 537.
26. Slack, D. A.; Greveling, I.; Baird, M. C. *Inorg. Chem.* **1979**, *18*, 3125.
27. Koenig, K. E.; Sabacky, M. J.; Bachman, G. L.; Christopfel, W. C.; Barnstorff, H. D.; Friedman, R. B.; Knowles, W. S.; Stults, B. R.; Vineyard, B. D.; Weinkauff, D. J. *Ann. N. Y. Acad. Sci.* **1980**, *333*, 16.

Shape-Selective Olefin Epoxidation Catalyzed by Metallo "Picnic-Basket" Porphyrins

James P. Collman[1], Xumu Zhang[1], Virgil Lee[1], Robert T. Hembre[2], and John I. Brauman[1]

[1]Department of Chemistry, Stanford University, Stanford, CA 94305
[2]Department of Chemistry, University of Nebraska, Lincoln, NE 68588

Dramatic selectivities are observed in the epoxidation of several olefin pairs with a series of manganese "picnic basket" porphyrin catalysts, which have a rigid cavity of variable dimensions on one side of the porphyrin ring and a bulky anionic ligand (3,5-di-t-butyl phenoxide) on the other side. The pronounced selectivities are in contrast to those obtained with flat porphyrins such as tetraphenylporphyrin (TPP) and sterically hindered porphyrins such as tetramesitylporphyrin (TMP). When substrates of varying shapes and sizes are used, the selectivities obtained from the picnic-basket porphyrins with a synthetic cavity mimic the substrate specificity of enzymes with a protein cavity.

SHAPE SELECTIVITY is an important characteristic of enzymatic reactions. The substrate specificity of an enzyme generally results from the interaction of the three-dimensional protein structure and the unique shape of the substrate. In the past, much attention has been devoted to understanding binding between a substrate and an enzyme. Host–guest chemistry and molecular recognition are terms used to describe these and related studies. Many host–guest systems such as crown ethers, cyclodextrins, cyclophanes, and molecular clefts have been synthesized to elucidate the nature of substrate–enzyme interactions (1–6). Although these systems successfully mimic substrate binding in enzymes, few of the systems incorporate catalytic cen-

ters in the host cavities. Therefore, these systems have failed to address the problem of substrate selectivities in catalytic processes.

In contrast, zeolites, a type of heterogeneous shape-selective catalyst, have been applied successfully as important catalysts in the petroleum industry. Zeolites can have acid–base or metallic catalytic centers in an extended pore structure. The framework of zeolites controls the shape selectivity of substrates and influences the product distribution in the catalysis. Xylene isomerization and the methanol-to-gasoline process (MTG) are two such examples (7). The development of homogeneous shape-selective catalysts is important and remains a challenging problem in homogeneous catalysis.

"Picnic-Basket" Porphyrins

An effective strategy in the development of shape-selective homogeneous catalysts is to mimic enzymes. In the past, we have been involved in modeling the chemistry of cytochrome P-450. Cytochrome P-450, a family of enzymes, is crucial in oxidative metabolism. The active site contains an iron protoporphyrin moiety (structure 1) with an axial cysteine thiolate ligand. These enzymes catalyze the reaction of hydrocarbons with molecular oxygen, incorporating one oxygen atom into the substrate and reducing the other oxygen atom to water. The hydroxylation of alkanes and the epoxidation of olefins are well-studied reactions catalyzed by these enzymes. As do many other enzymatic systems, cytochrome P-450 controls its substrate selectivity exclusively by its surrounding protein cavity (8–9). The catalytic cycle of cytochrome P-450 is shown in Scheme I (10).

Iron Protoporphyrin IX

1
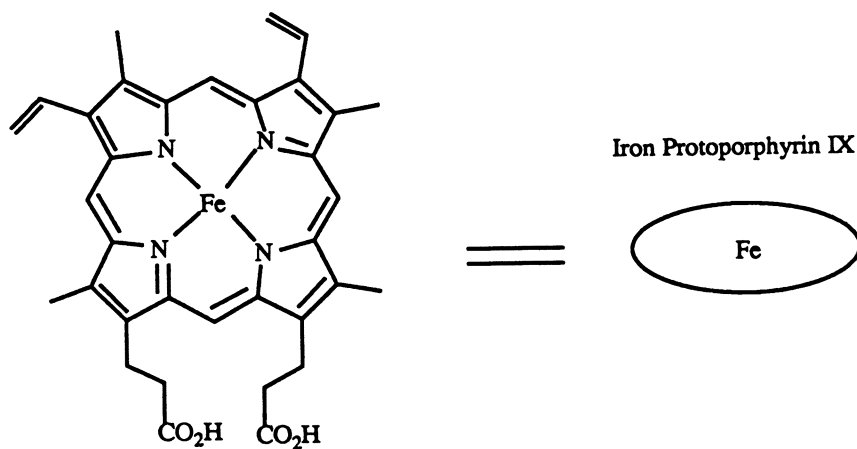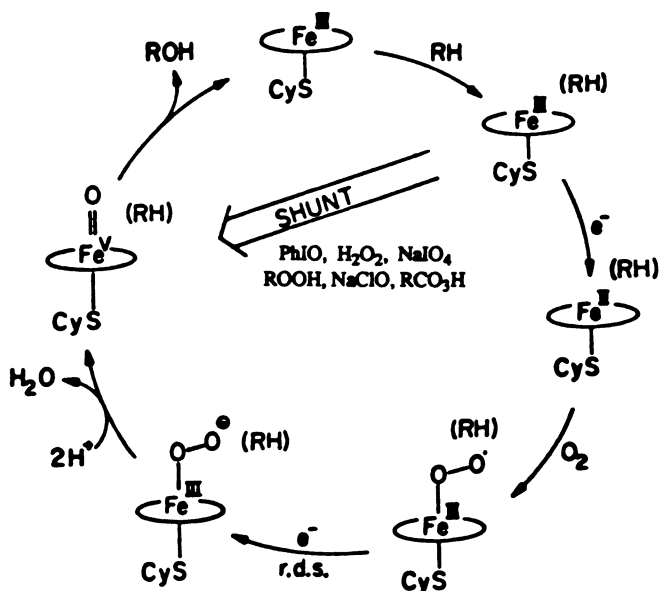
Scheme 1. Catalytic cycle of cytochrome P-450.

Although nature uses oxygen as the oxygen-atom source, it is possible to use other oxygen-transfer agents in what is called the shunt pathway. Synthetic metalloporphyrins have similar activities in alkane hydroxylation and in olefin epoxidation when such oxygen-transfer reagents are employed (Scheme II) (*11*).

On the basis of these findings, shape-selective oxygenation catalysts were developed. The shape-selective catalysts employ diverse strategies, including sterically hindered porphyrins (*12–17*), membrane-spanning porphyrins (*18*), and zeolite-encapsulated macrocyclic complexes (*19*) and metal ions (*20*). To mimic the substrate selectivity found with cytochrome P-450, we developed a new porphyrin system, the "picnic-basket" porphyrins (PBP) (Chart I) (*21–23*).

The PBP complexes have a rigid cavity of variable dimensions on one face of the porphyrin ring. A bulky axial ligand is used to block the open face of the porphyrin. This conformation allows for the formation of the active oxygenating species inside the porphyrin superstructure. The interaction between this superstructure and the olefin leads to shape-selective epoxidation. For example, some cyclic olefins like cyclooctene have a larger size than comparable acyclic olefins like *cis*-2-octene. The difference results in the latter being epoxidized at a faster rate in certain PBP cavities (Scheme III).

tetraphenylporphyrin (TPP)

tetramesitylporphyrin (TMP)
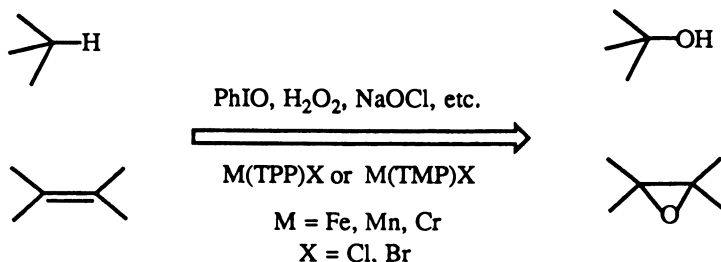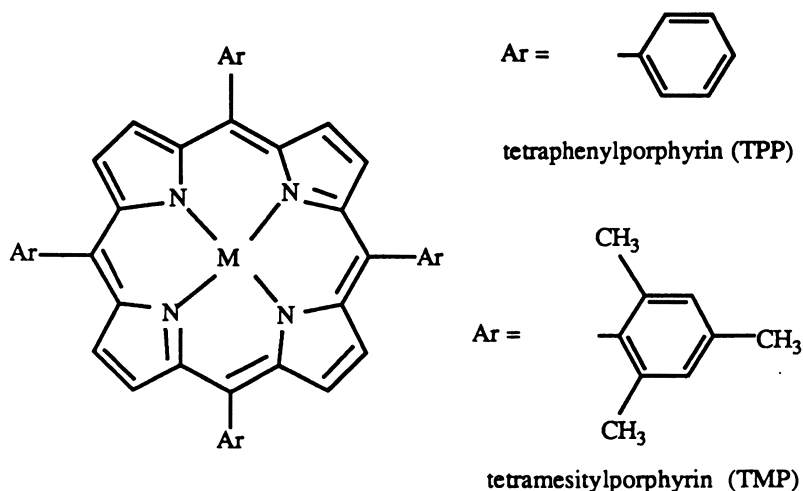
Scheme II. Metalloporphyrin models for cytochrome P-450.

Results

We failed to achieve shape selectivity in olefin epoxidation by using Mn(PBP)Br and bulky neutral axial ligands such as 1,5-diphenylimidazole to block the open face of the porphyrin (8). The reason for this failure seems to be as follows.

Suppose the bulky imidazole ligand coordinates to the open face of the porphyrin and bromide coordinates inside the basket cavity. For epoxidation to occur inside the cavity, the bromide must be displaced from manganese by coordination of an oxygen-transfer agent such as PhIO. This process might be thermodynamically unfavorable, as suggested in a related system (24). In contrast, the displacement of a neutral imidazole by PhIO could be a more favorable pathway, and this reaction is likely to take place on the more accessible open face of the porphyrin. To solve this problem a bulky anionic axial ligand, 3,5-di-*t*-butyl phenoxide, was used to block the open face of PBP (Scheme IV).

R

-(CH₂)ₙ-

n = 2	C2PBP
4	C4PBP
6	C6PBP
8	C8PBP
10	C10PBP

-CH₂-⟨⟩-CH₂-   PXYLPBP

R-BINAPPBP
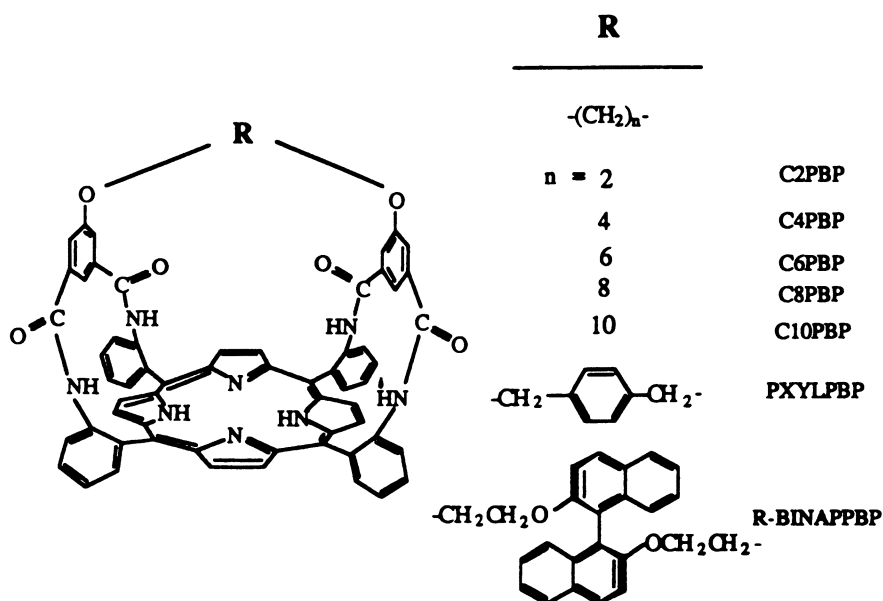
Chart 1. "Picnic-basket" porphyrins.

Four olefin pairs were studied in competitive epoxidations. A 1:1 ratio of two olefins was used as a substrate mixture; manganese complexes of tetraphenylporphyrin (TPP), tetramesitylporphyrin (TMP), or PBP were used as the catalyst. The oxidations were carried out in dry acetonitrile with PhIO as the oxygen-atom source. The results are summarized in Table I. A catalytic asymmetric epoxidation of styrene was also studied with (R)-binapPBP at 0 °C; S(+)-styrene oxide is formed in 13% enantiomeric excess (ee), as determined with an NMR chiral shift reagent.

Discussion

Very slow epoxidation is observed with the Mn(C₂PBP)(OAr) or Mn(C₄PBP)(OAr) as catalyst. The competitive epoxidation ratios of four olefin pairs with either Mn(C₂PBP)(OAr) or Mn(C₄PBP)(OAr) are close to those obtained with Mn(TPP)(OAr) (Table I). The only exception is the ratio of the third olefin pair with Mn(C₄PBP)(OAr). The slow rate and low selectivity may be a manifestation of reaction "leaking", in which the oxidation occurs on the open unhindered face of the porphyrin.

Dramatic selectivity is found in the epoxidation of *cis*-2-octene and *trans*-β-methylstyrene (the first olefin pair in Table I). When Mn(C₆PBP)(OAr) or Mn(PXYLPBP)(OAr) is used as the catalyst, the competitive epoxidation
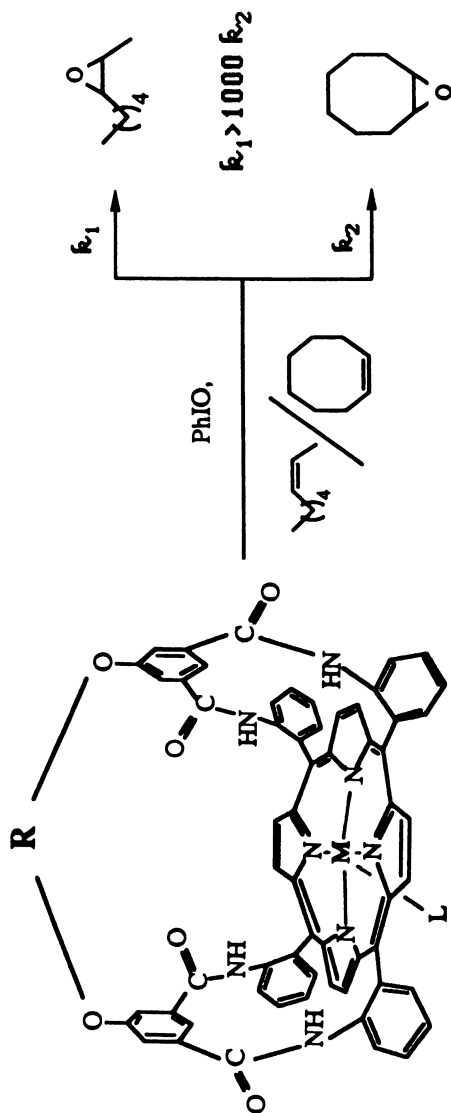
Scheme III. Competitive epoxidation with the PBP.

What is the problem ?
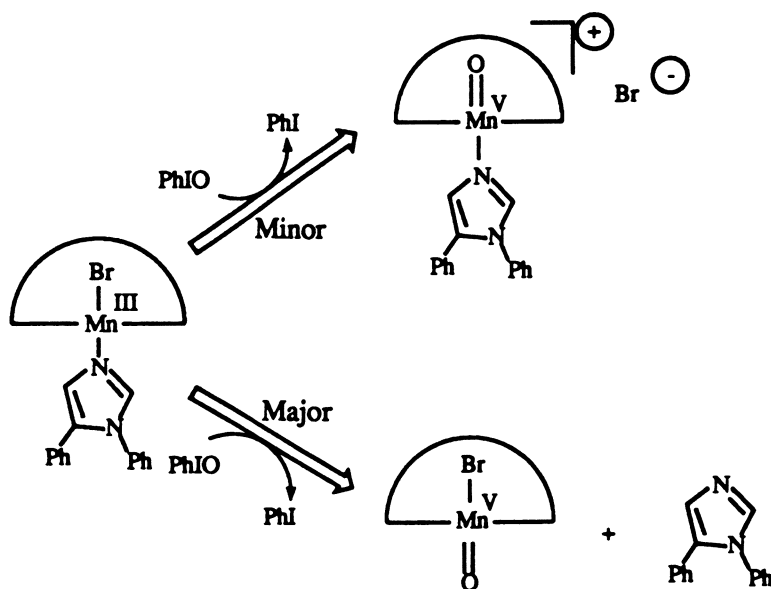
Solution: Bulky anionic ligand ?
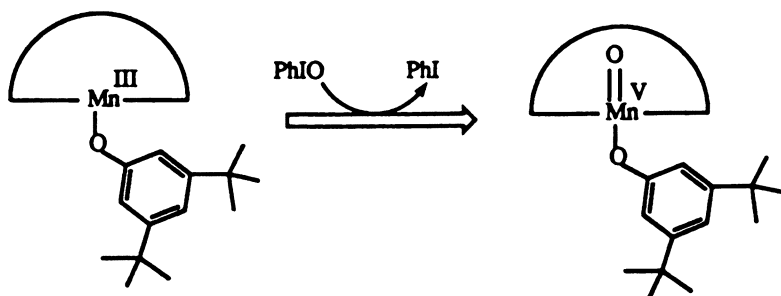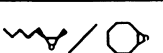
Scheme IV. Problems with the PBP strategy.

ratios are 70 and 29, respectively. These ratios are larger than those obtained with the sterically hindered porphyrin catalyst, Mn(TMP)(OAr), and much larger than that obtained with the flat porphyrin catalyst, Mn(TPP)(OAr). The latter ratios are 14.4 and 1.2, respectively.

Selectivity decreases as the size of PBP increases to C_8PBP and $C_{10}PBP$ with competitive ratios of 12.7 and 8.8, respectively. This selectivity can be

Table I. Competitive Olefin Epoxidation Results

Catalyst[a]	(Ratio)	(Ratio)	(Ratio)	(Ratio)
Mn(TPP)(OAr)	1.2	1.1	0.03	0.9
Mn(TMP)(OAr)	14.4	0.7	0.04	2.5
Mn(C_2PBP)(OAr)	0.4[b]	1.1[b]	0.05[b]	1.3[b]
Mn(C_4PBP)(OAr)	1.0[b]	2.1[b]	0.4[b]	1.8[b]
Mn(C_6PBP)(OAr)	70	67	1.7	>1000
Mn((PXYLPBP)(OAr)	29	>1000	7.0	>1000
Mn(C_8PBP)(OAr)	12.7	1.6	0.06	21.1
Mn(C_{10}PBP)(OAr)	8.8	0.2	0.04	17.9

[a]OAr is 3,5-di-t-butyl phenoxide.
[b]These reactions are very slow.

attributed to a combination of steric effects, the ability of a particular olefin to attain a favorable geometry for epoxidation, and size effects, which determine whether the olefin can approach the active site of the cavity. Compared to *cis*-2-octene, *trans*-β-methylstyrene is less reactive toward sterically hindered porphyrins. Presumably, its larger size makes it difficult for it to react inside the porphyrin cavity.

The second olefin pair, *cis*-2-octene and cyclooctene, are both *cis*-olefins. They have a similar reactivity toward the flat porphyrin catalyst Mn(TPP)(OAr) and the sterically hindered porphyrin catalyst Mn(TMP)-(OAr). The competitive epoxidation ratios are 1.1 with Mn(TPP)(OAr) and 0.7 with Mn(TMP)(OAr). However, with Mn(C_6PBP)(OAr) or Mn-(PXYLPBP)(OAr) these ratios are 67 or >1000, respectively. The ratios drop dramatically to 1.6 with Mn(C_8PBP)(OAr) and 0.2 with Mn-(C_{10}PBP)(OAr). These results indicate that the cavities of both Mn-(C_6PBP)(OAr) and Mn(PXYLPBP)(OAr) tend to exclude cyclooctene from the catalytic centers, presumably because of the greater steric bulk of this cyclic olefin relative to the linear *cis*-2-octene.

The third olefin pair is 1-octene and cyclooctene. As terminal olefins are generally more electron-deficient than internal olefins, 1-octene is less reactive than cyclooctene toward electrophilic attack by M=O. With Mn(TPP)(OAr) or Mn(TMP)(OAr), the competitive ratios for this olefin pair are 0.03 or 0.04, respectively. However, with Mn(C_6PBP)(OAr) or Mn(PXYLPBP)(OAr), the respective ratios are 1.7 or 7.0. This contrast indicates that cyclooctene is excluded from the cavities of Mn(C_6PBP)(OAr) and Mn(PXYLPBP)(OAr). With the larger Mn(C_8PBP)(OAr) or Mn(C_{10}PBP)(OAr) the selectivity in the competitive epoxidation of *cis*-2-octene and cyclooctene decreases to 0.06 or 0.04, respectively. Both olefins are now able to get inside the cavity. This result is consistent with our earlier argument.

The final olefin pair is *cis*-2-octene and 2-methyl-2-pentene. This pair allows us to compare the shape selectivity of a disubstituted versus a tri-

substituted olefin. With Mn(TPP)(OAr) or Mn(TMP)(OAr) the competitive epoxidation ratios are 0.9 or 2.5, respectively. However, with Mn(C_6PBP)(OAr) or Mn(PXYLPBP)(OAr), the ratios are >1000 in each case. These values demonstrate that the disubstituted *cis*-2-octene is much more reactive than the trisubstituted 2-methyl-2-pentene.

The ratios using Mn(C_8PBP)(OAr) or Mn(C_{10}PBP)(OAr) are also larger than those with Mn(TPP)(OAr) or Mn(TMP)(OAr). This reactivity pattern reflects the required orientation of the Mn=O group with the olefin axis. Perhaps the alkene approaches the Mn=O bond from the side and is parallel to the porphyrin plane, as has been suggested by Groves and Nemo (*12*) in related Fe=O systems and further discussed by Ostovic and Bruice (*25, 26*). The oxidation of trisubstituted olefins is allowed with the hindered Mn(TMP)(OAr), probably because the substituents on the olefin face can orient themselves between the methyl groups of TMP. However, the steric interactions between the walls of the PBP and the trisubstituted olefins disfavor the oxidation of these trisubstituted systems.

Styrene was oxidized to (*S*)-styrene oxide in 13% ee with the Mn(*R*)-binapPBP(OAr) catalyst. Because the chiral site is far above the reaction locus, the low ee value is not surprising (*27–30*). However, this geometry demonstrates that some, perhaps all, of the reaction occurs within the cavity. This result suggests that we may be able to develop synthetically useful and efficient chiral catalysts on the basis of these systems.

Conclusions

These studies have led to dramatic shape-selective catalytic epoxidation of several olefin pairs and chiral epoxidation of a prochiral olefin, albeit in modest yield. These selectivities depend upon the dimensions of the cavity and are different from those achieved with simple porphyrin catalysts derived from TPP or TMP. We seem to be on the verge of predictable, shape-selective, catalytic oxygenation with a readily available, variable series of synthetic catalysts. For example, highly regioselective epoxidation of polyenes such as steroids and terpenoids may be possible. By applying variable chiral groups on the porphyrins, we hope to develop efficient asymmetric epoxidation catalysts for unsubstituted olefins.

Acknowledgments

References

1. Lehn, J. M. *Science (Washington, D.C.)* **1985**, *227*, 849.
2. Rebek, J., Jr. *Science (Washington, D.C.)* **1987**, *235*, 1478.
3. Cram, D. J. *Science (Washington, D.C.)* **1988**, *240*, 760.
4. Gutsche, C. D. *Acc. Chem. Res.* **1983**, *16*, 161.
5. D'Souza, V. T.; Bender, M. L. *Acc. Chem. Res.* **1987**, *20*, 146.
6. Sutherland, I. O. *Chem. Soc. Rev.* **1986**, *15*, 63.
7. Newsman, J. M. *Science (Washington, D.C.)* **1986**, *231*, 1093.
8. Jefcoate, C. R. In *Cytochrome P-450: Reactions, Mechanism, and Biochemistry*; Ortiz de Montellano, P. R., Ed.; Plenum: New York, 1986; p 387.
9. Sligar, S. G.; Murry, R. I. In *Cytochrome P-450: Reactions, Mechanism, and Biochemistry*; Ortiz de Montellano, P. R., Ed.; Plenum: New York, 1986; p 429.
10. *Cytochrome P-450: Reactions, Mechanism, and Biochemistry*; Ortiz de Montellano, P. R., Ed.; Plenum: New York, 1986.
11. McMurry, T. J.; Groves, J. T. In *Cytochrome P-450: Reactions, Mechanism, and Biochemistry*; Ortiz de Montellano, P. R., Ed.; Plenum: New York, 1986; p 1.
12. Groves, J. T.; Nemo, T. E. *J. Am. Chem. Soc.* **1983**, *105*, 5786.
13. Suslick, K. S.; Cook, B. R.; Fox, M. M. *J. Chem. Soc., Chem. Commun.* **1985**, 580.
14. Suslick, K. S.; Cook, B. R. *J. Chem. Soc., Chem. Commun.* **1987**, 200.
15. Cook, B. R.; Reinert, T. J.; Suslick, K. S. *J. Am. Chem. Soc.* **1986**, *108*, 7281.
16. Collman, J. P.; Brauman, J. T.; Meunier, B.; Hayashi, T.; Kodadek, T.; Raybuck, S. A. *J. Am. Chem. Soc.* **1985**, *107*, 2000.
17. Nappa, M. J.; Tolman, C. A. *Inorg. Chem.* **1985**, *24*, 4711.
18. Groves, J. T.; Newmann, R. *J. Am. Chem. Soc.* **1987**, *109*, 5045.
19. Herron, N.; Stucky, G. D.; Tolman, C. A. *J. Chem. Soc., Chem. Commun.* **1986**, 1521.
20. Herron, N.; Tolman, C. A. *J. Am. Chem. Soc.* **1987**, *109*, 2837.
21. Collman, J. P.; Brauman, J. I.; Fitzgerald, J. P.; Hampton, P. D.; Naruta, Y.; Michina, T. *Bull. Chem. Soc. Jpn.* **1988**, *61*, 47.
22. Collman, J. P.; Brauman, J. I.; Fitzgerald, J. P.; Hampton, P. D.; Naruta, Y.; Sparapany, J. W.; Ibers, J. A. *J. Am. Chem. Soc.* **1988**, *110*, 3411.
23. Collman, J. P.; Brauman, J. I.; Fitzgerald, J. P.; Sparapany, J. W.; Ibers, J. A. *J. Am. Chem. Soc.* **1988**, *110*, 3486.
24. Powell, M. F.; Pai, E. F.; Bruice, T. C. *J. Am. Chem. Soc.* **1984**, *106*, 3277.
25. Ostovic, D.; Bruice, T. C. *J. Am. Chem. Soc.* **1988**, *110*, 6906.
26. Ostovic, D.; Bruice, T. C. *J. Am. Chem. Soc.* **1989**, *111*, 6511.
27. Groves, J. T.; Myers, R. S. *J. Am. Chem. Soc.* **1983**, *105*, 5791.
28. Mansuy, D.; Battioni, P.; Renaud, J. P.; Guerin, P. *J. Chem. Soc., Chem. Commun.* **1985**, 155.
29. Naruta, Y.; Tani, F.; Maruyama, K. *Chem. Lett.* **1989**, 1269.
30. O'Malley, S.; Kodadek, T. *J. Am. Chem. Soc.* **1989**, *111*, 9116.

Stereocontrol in Catalyzed and Uncatalyzed Hydroborations

Kevin Burgess and Michael J. Ohlmeyer

Chemistry Department, Rice University, Houston, TX 77251

Catalyzed hydroborations are potentially valuable in organic syntheses. This value is illustrated with examples of enantioselective hydroboration of prochiral alkenes with catecholborane in the presence of optically active rhodium complexes, and with stereocomplementarity in catalyzed and uncatalyzed hydroborations of chiral alkenes. Stereocomplementarity is rationalized in terms of secondary orbital effects that perturb incipient Dewar–Chatt bonding. This theory may have repercussions in other areas besides hydroboration chemistry.

MANY BORON HYDRIDE COMPOUNDS ADD TO ALKENES under mild conditions without intervention of catalysts; others do not. For instance, hydroboration of alkenes and alkynes by boron hydride cluster molecules (1–7) and by borazine (8) occurs at convenient rates only in the presence of various transition metal complexes. Reactions of boron hydride clusters and borazine are of little consequence to practical organic chemists, but Noth's discovery (9) that hydroborations involving catecholborane could be catalyzed exposed a range of possibilities.

Hydroboration of alkenes and alkynes with unreactive boranes via transition-metal-mediated reactions are potentially valuable when one is restricted by the chemo-, regio-, or stereoselectivity of conventional hydroborations. Consequently, we (10–14) and others (15–18) became interested in exploiting catalyzed transition metal reactions in organic synthesis. This chapter describes efforts to control absolute and relative stereochemistry via catalyzed hydroborations. It focuses on features that complement conventional methodology.

Enantioselective Hydroborations

Previously, all methods for hydroboration of prochiral alkenes with control of absolute stereochemistry relied upon reagent-controlled diastereoselectivity (*19–26*) (i.e., reactions of optically active boron hydrides) to give diastereomers in unequal amounts (Scheme I).
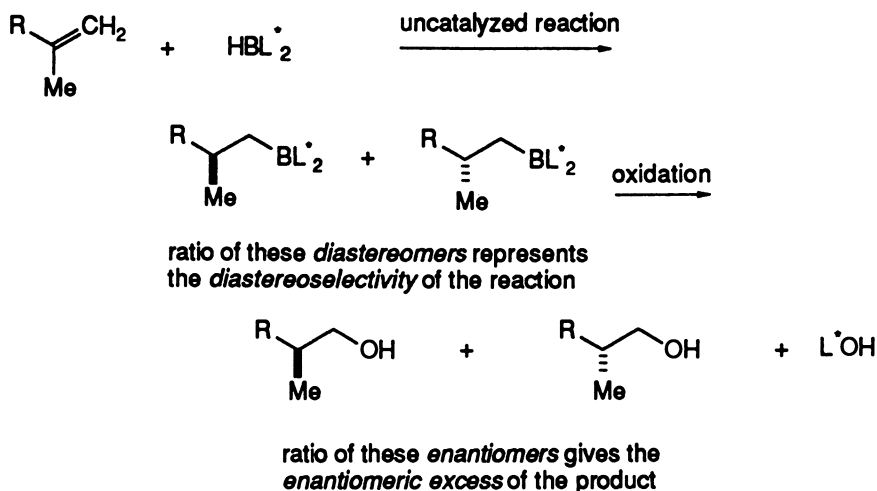
Scheme I. Uncatalyzed hydroboration of prochiral alkenes.

Several disadvantages are associated with such processes:

- optically active boranes are air- and water-sensitive; they must be prepared and isolated before use;

- optically active boranes also tend to be high-molecular-mass compounds, so relatively large quantities must be synthesized to hydroborate alkenes of low molecular mass;

- diastereoselectivities are variable; and

- separation of products from chiral auxiliary residues is problematic.

A conceptually superior approach to this problem is the use of optically active transition metal catalysts to accelerate hydroborations of relatively unreactive boranes (Scheme II). This approach may give one enantiomer preferentially, and hence the processes are *enantioselective* (i.e., diastereoselective interactions within a catalytic cycle).
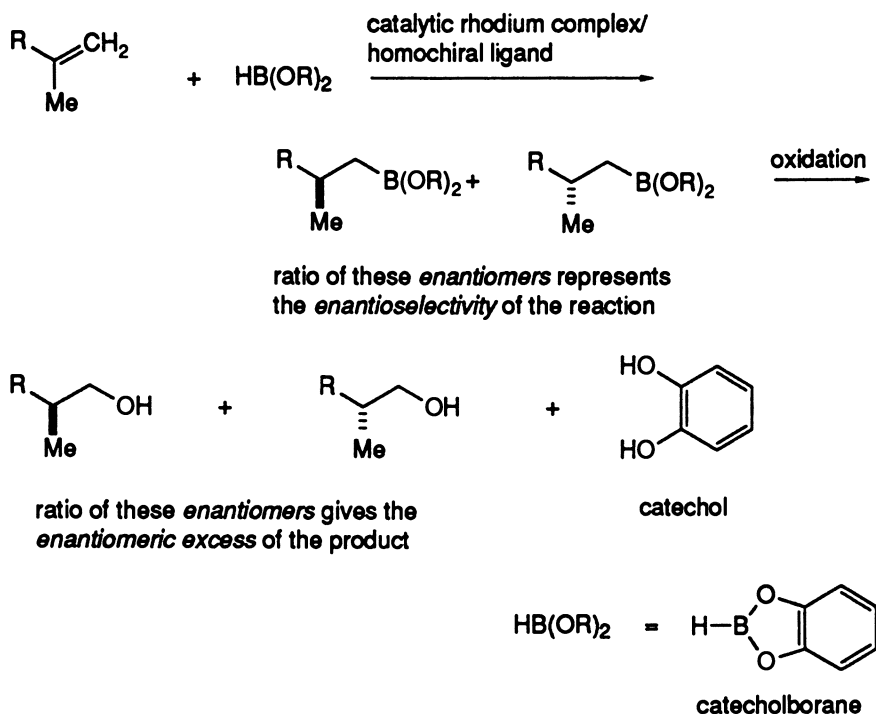
Scheme II. Hydroboration of unreactive boranes catalyzed by optically active transition metal catalysts.

Our preliminary work (*10*) proved that enantioselective hydroborations of substrates 1–5 are possible (Chart I and Table I). The ligand 2,3-*O*-isopropylidene-2,3-dihydroxy-1,4-bis(diphenylphosphino)butane (DIOP) was used simply because it can be prepared cheaply and easily. It is usually not the best ligand for asymmetric induction, but enantiomeric excesses of up to 76% were obtained nevertheless. Hydroborations of substrates 4 and 5 with appreciable enantioselectivity are particularly significant because 1,1-disubstituted alkenes are notoriously difficult to hydroborate with any control of absolute stereochemistry (*25*).

Enantioselection must be increased if these processes are to be of practical value. Fortunately, it seems likely that better optical yields can be obtained by using other catalyst systems. Table I indicates slight improvement when the ligand 2,2′-bis(diphenylphosphino)-1,1′-binaphthyl (binap) is used (entries 3 and 6), and other ligands remain to be tested. Recently Hayashi et al. (*16*) found that catalyzed hydroborations of styrenes can occur in a Markovnikoff sense with good control of absolute stereochemistry. Another group (*18*) reproduced many of the results presented in Table I.

substrates:

(1)   (2)   (3)   (4)   (5)

products:

(6)   (7)   (8)   (9)   (10)

ligands:

(R,R)-DIOP   (R)-BINAP
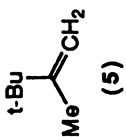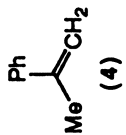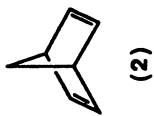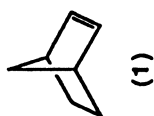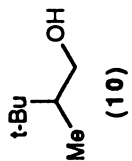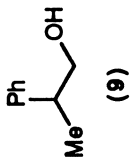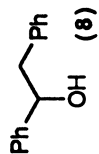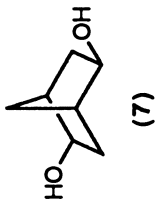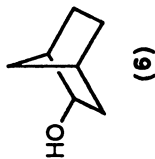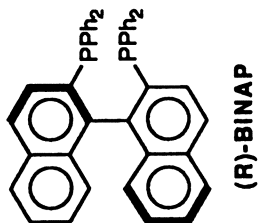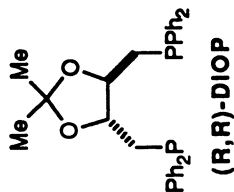
Chart 1.

Table I. Enantioselective Hydroborations

Entry[a]	Substrate	Temperature (° C)	Catalyst[b]/ Solvent	Product	Enantiomeric Excess (%)	Absolute Configuration[c]
1	1	40	A/C$_6$H$_6$	6[d]	23	1R, 2R
2	1	5	A/C$_6$H$_6$	6	31	1R, 2R
3	1	5	B/C$_6$H$_6$	6	43	1R, 2R
4	1	–5	A/THF	6	46	1R, 2R
5	1	–25	A/THF	6	57	1R, 2R
6	1	–25	B/THF	6	64	1R, 2R
7	1	–40	A/THF	6	55	1R, 2R
8	2	–25	A/THF	7	76	1R, 2R[d]
9	E-3	20	A/C$_6$H$_6$	8	7	S
10	E-3	5	A/C$_6$H$_6$	8	~0	—[e]
11	Z-3	5	A/C$_6$H$_6$	8	17	S
12	Z-3	–25	A/THF	8	19	S
13	4	–5	A/THF	9	27	—[e]
14	5	–5	A/THF	10	69	R

[a]Reaction times were 48–72 h.
[b]**A:** in situ [Rh(COD)Cl]$_2$ · 2(R,R)-DIOP. **B:** in situ [Rh(COD)Cl] · 2(R)-binap.
[c]Determined by ^{1}H NMR analysis of Mosher's ester derivatives and ^{1}H NMR experiments with Eu(heptafluorobutyrylcamphorate)$_3$, to within ±5%.
[d]By inference from previous entries.
[e]Not determined.

Substrate-Controlled Diastereoselectivity

Hydroboration of chiral allylic alcohol derivatives can give *syn* or *anti* diastereomers, as shown in the scheme in Table II. Still and Barrish (27) proved that conventional hydroborations of these substrates are *anti*-selective. We (*11, 13*) and Evans et al. (*15*) independently decided to explore catalyzed hydroborations of such substrates. Table II shows the data obtained. Variation of the protecting group X effectively "tunes" steric and electronic characteristics of the OX substituent. For instance, replacing the acetate group (entry 2) with a trifluoroacetate (entry 3) increases the electron-withdrawing capacity of the OX and causes a three-fold increase in *syn* selectivity. Conversely, substitution of pivolate (entry 5) or trityl (entry 6) for acetate (entry 2) primarily increases steric demands of the OX substituent; *syn* selectivity also increases. One might conclude that *syn* selectivity is largest when the OX substituent is a large σ-acceptor. Evans et al.'s results (*15*) with silyl-protected ethers (entries 7 and 8) support this inference.

Table III gives Still and Barrish's results (*27*), augmented with two of our own. For uncatalyzed hydroborations of the same substrates, they are all *anti*-selective. Thus the transition-metal-mediated reactions are stereo-complementary insofar as they give the *syn* isomer preferentially. Such behavior underlines the potential of catalyzed hydroborations as a synthetic method.

It is necessary to speculate about the mechanism of transition-metal-mediated hydroborations to explain differences between conventional and

Table II. Catalyzed Hydroborations of Allylic Alcohol Derivatives
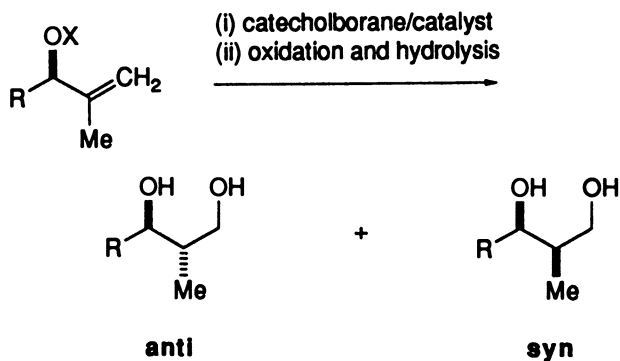
Entry	X	Syn:Anti[a]
1	H	2.2:1
2	Ac	2.7:1
3	$COCF_3$	7.5:1
4	CO-t-Bu	6.5:1
5	THP	8.4:1
6	CPh_3	18:1
7[b]	t-BuMe$_2$Si	24:1
8[b]	t-BuPh$_2$Si	24:1
9	$CONMe_2$	2.4:1

NOTE: Reaction took place in tetrahydrofuran (THF), 48 h, with 1 mol % of [Rh(COD)Cl]$_2$–PPh$_3$ in a 1:4 ratio; workup with hydrogen peroxide–aqueous base gave near-quantitative yields of the diols, contaminated only with trace amounts of triphenylphosphine oxide derived from the catalyst (^{1}H NMR spectrum). The samples were derivatized without further purification.

[a]Stereochemistries were assigned by comparison with authentic samples or by ^{1}H NMR analysis of acetonide derivatives; diastereomeric ratios were determined by capillary gas chromatographic analysis of acetonide derivatives.

[b]Evans and co-workers (15); reaction took place in catecholborane (3 equiv), 3 mol % RhCl(PPh$_3$)$_3$, 25 °C.

catalyzed reactions of chiral allylic alcohol derivatives. Several oxidative additions of B–H compounds to low-valent transition metal complexes are known (28–33). Significantly, Wilkinson's catalyst and catecholborane combine to give [RhClH(BO$_2$C$_6$H$_4$)(PPh$_3$)$_2$] (34). This product reacts with alkenes to give hydroboration products (9). Consequently, the generalized mechanism shown in Scheme III seems reasonable; pathways that deviate from this are less plausible. Recently we proved that the catalyzed hydroboration of 1-methylcyclohexene is at least highly *cis*-selective and perhaps stereospecifically *cis* (35). This fact provides further evidence in support of the mechanism shown in Scheme III.

Table III. Uncatalyzed Hydroborations of Allylic Alcohol Derivatives

Entry	X	Syn:Anti[a]
1[b]	H	1:11
2[b]	Ac	1:7.5
3[b]	$COCF_3$	1:14
4	CO-t-Bu	1:15.4
5	THP	1:3.7
6[b]	CPh_3	1:5.5
7[b]	t-BuMe$_2$Si	1:9
8[b]	t-BuPh$_2$Si	1:6
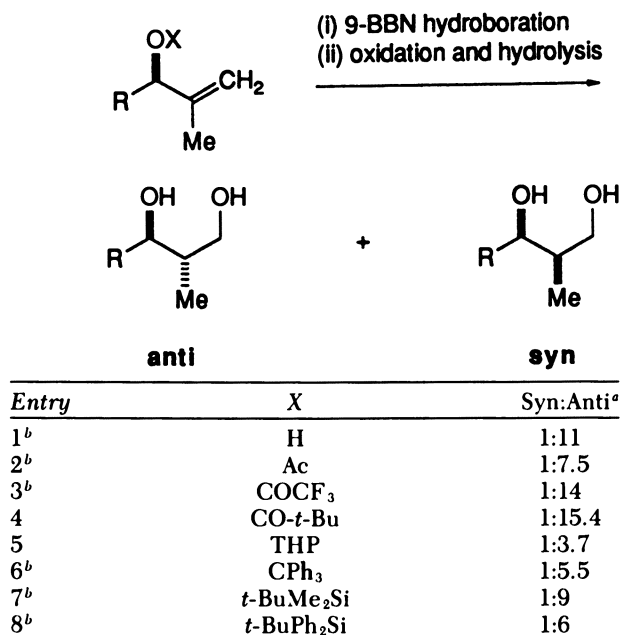
NOTE: Reaction took place in 9-BBN, THF, −78 to 25 °C; workup with hydrogen peroxide–aqueous base and purification via flash chromatography.
[a]Stereochemistries were assigned by comparison with authentic samples or by ^{1}H NMR analysis of acetonide derivatives; diastereomeric ratios were determined by capillary gas chromatographic analysis of acetonide derivatives.
[b]Still and Barrish (27).

Formation of complex **A** could be the stereodeterminant step in these reactions. If this is true, the diastereoselectivities in the overall process can be rationalized on the basis of orbital arguments, by considering electronic and steric effects separately. Electronic factors are governed by frontier orbitals involved in the bonding process. The weakest bond in complexation is back donation of d-electron density from the metal to the π* orbital of the alkene, as represented in Chart II (13).

Orientations of the adjacent chiral center, which preferentially cause the orbital mixing that stabilizes this interaction, lead to stereoselectivity. Such stabilization will arise by mixing a σ* orbital with the alkene π*, thus producing a lower energy lowest unoccupied molecular orbital (LUMO) for interaction with the highest occupied molecular orbital (HOMO) (Chart III).

Rh——L   +   H—B (catecholborane)   oxidative addition ⟶

**Coordinatively unsaturated
rhodium complex; L = ligand.**

(H)(L)Rh—B (catechol)   ligand exchange
(L for alkene) ⟶   alkene complex A

alkene complex A

migratory insertion ⟶   reductive elimination ⟶

Rh——L   +   R*—CH₂CH₂—B (catechol)
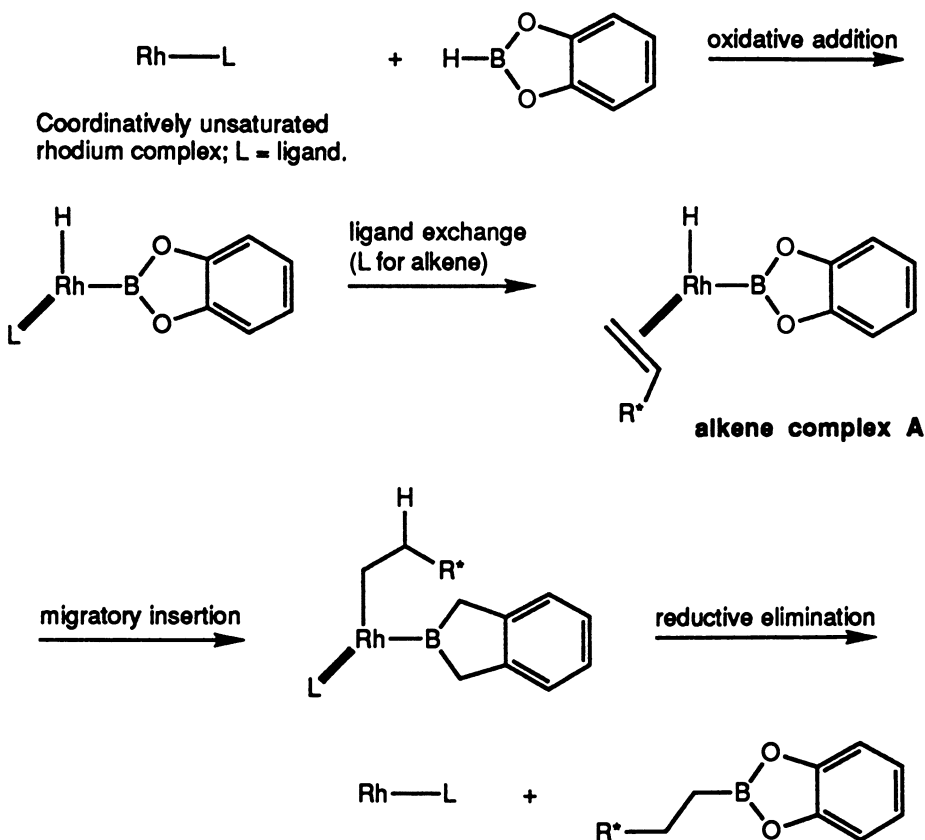
Scheme III. Generalized mechanism for catalyzed hydroborations.

π* **LUMO**

d HOMO
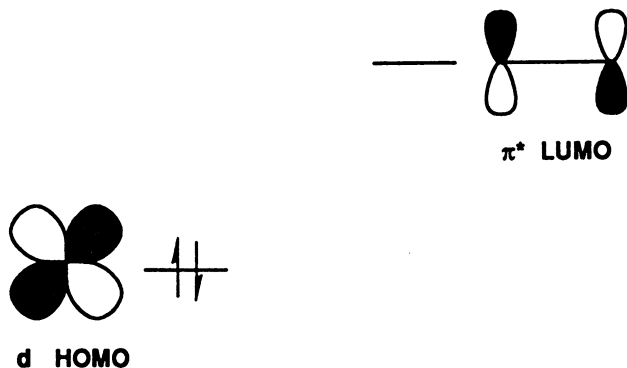
Chart II. Back-bonding in coordination of an alkene to a transition metal.

d **HOMO**
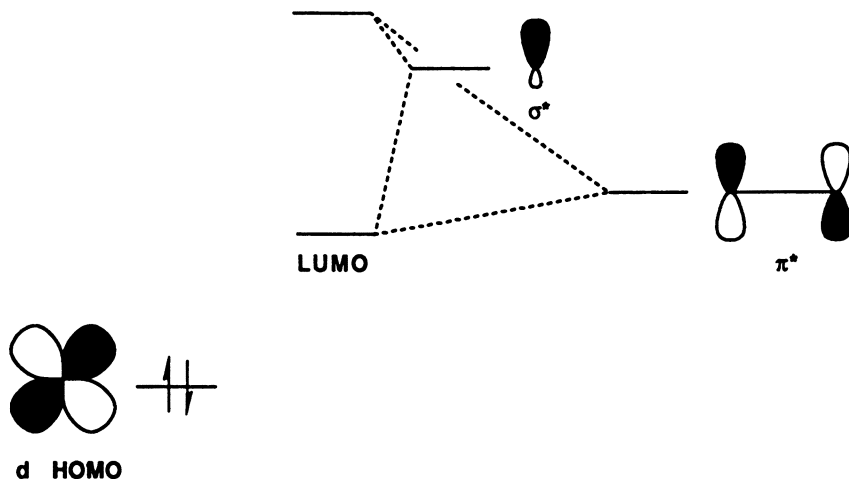
Chart III. "Secondary interactions" involving a σ* orbital of the adjacent chiral center enhance the primary interaction.

To establish a strong secondary interaction, one group on the asymmetric center must be oriented *anti* to the approaching metal so that the corresponding σ* orbital can mix with the π system of the alkene (*36*). If a σ-acceptor group and a σ-donating group compete for this position then, in terms of electronic factors, the σ-acceptor group will adopt the *anti* position because it has a low-energy σ* orbital available to interact with the π* of the alkene. The σ* orbital associated with the electron-donating group is of relatively high energy and would overlap less. Consequently, if one of the substituents is hydrogen and an "inside crowded model" (*37*) applies (as would be expected for formation of a π complex), then the reactive conformer shown in structure 1 (Chart IV) would be used to account for the stereoselectivity (based on electronic factors). For the specific case of allylic alcohols this translates to the projection shown in structure 2 (Chart IV), which indicates that catalyzed hydroborations should be *syn*-selective.

Steric effects are operative in addition to the electronic effects already discussed. Consider a situation in which the chiral center bears large (L), medium (M), and small (S) substituents that are electronically equivalent. The L group will orient *anti* to the approaching metal complex; the M substituent will preferentially adopt the outside position (*37*), which is less encumbered than the inside site, a space best occupied by the smallest group, S (structure 3). Structures 2 and 3 imply that *syn* diastereoselectivity in catalyzed hydroborations will be highest when the OX substituent is a large σ acceptor group; this is so (*see* Table I).

Houk et al. (*38*) analyzed stereoselectivity in conventional hydroborations. We conclude that steric considerations for conventional hydroborations
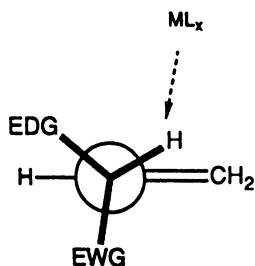
Structure 1. Electronic bias for orientation of an electron withdrawing group (EWG) and an electron donating group (EDG) in complexation of a chiral alkene.
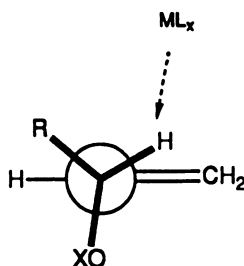
Structure 2. Interpretation for a chiral allylic alcohol (R = alkyl, X = a protecting group)..
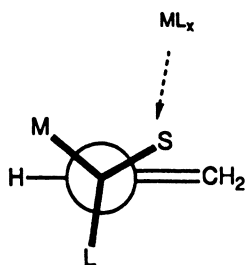
Structure 3. Preferential orientation in π-complexation based upon steric demands of the substituents.
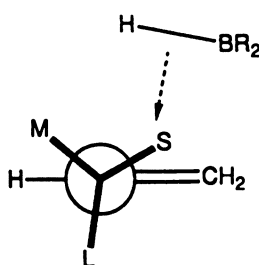
Structure 4. Preferential orientation in conventional hydroboration based upon steric demands of the substituents.
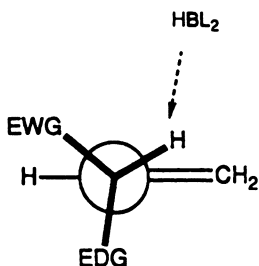
Structure 5. Preferential orientation in conventional hydroborations based on electronic demands of the substituents.
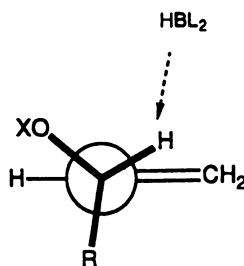
Structure 6. Preferred reactive conformation in uncatalyzed hydroborations of allylic alcohol derivatives

Chart IV.

p LUMO

π HOMO
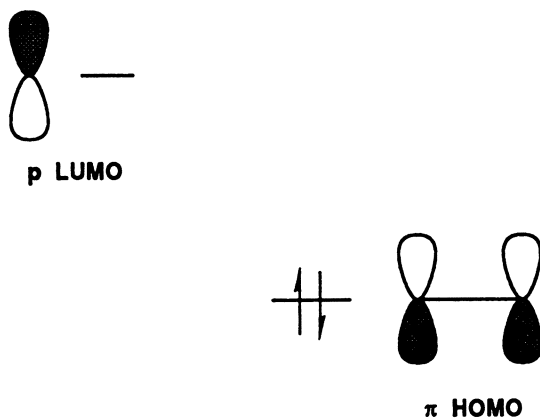
Chart V. Primary interaction in uncatalyzed hydroborations of chiral allylic alkenes.

of chiral allylic alcohols (structure 4) are similar to those for the corresponding catalyzed processes but that opposite diastereofacial selectivities in catalyzed and uncatalyzed hydroborations originate from frontier orbital differences for the transformations. Chart V shows the primary interaction involved in a conventional hydroboration. Chart VI illustrates how mixing of a σ orbital of the α chiral center can enhance this interaction by destabilizing the π system of the alkene.

Electron-donating substituents orient *anti* to the approaching borane in uncatalyzed hydroborations (structure 5) because this places a high-energy σ orbital in the correct position to mix with the alkene π system. (Relatively

p LUMO

HOMO

σ

π
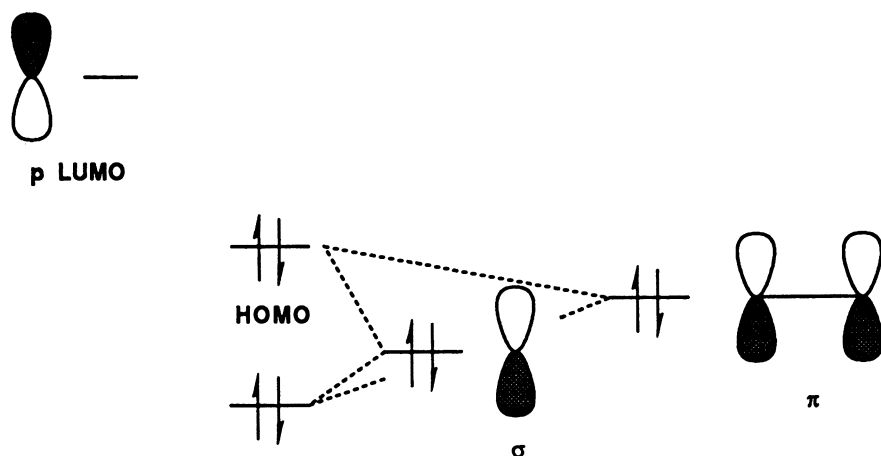
Chart VI. Secondary interactions in uncatalyzed hydroborations of chiral allylic alkenes enhance incipient bonding by destabilizing the HOMO.

low-energy σ orbitals are associated with electron-withdrawing groups.) Structure **6** applies this model to the specific case of chiral allylic alcohols, a model that rationalizes *anti* selectivity.

The foregoing reasoning accounts for stereocomplementary behavior in catalyzed and uncatalyzed hydroborations of the allylic alcohol substrates shown in Table I. However, Table IV shows data for hydroborations of phenyl-substituted allylic alcohols. At first glance, these data appear to contradict the theory given here because the catalyzed processes are *anti*-selective (*11*). These are special cases because aryl groups are good σ-acceptors and are quite large. They tend to orient *anti* to the approaching rhodium complex in reactive conformations, apparently in preference to OAc groups (entry 1). Phenyl and OCOCF$_3$ functionalities seem to be comparable in terms of combined electronic and steric features. Consequently, *anti* selectivity in entry 2 is less than in entry 1.

To confirm these ideas we prepared analogous fluorinated substrates and tested them. Replacement of phenyl with pentafluorophenyl greatly increases the aromatic group's σ-acceptor abilities and makes it slightly bigger. These factors enhance *anti* selectivity (entry 4). Conversely, *anti* selection in uncatalyzed hydroborations of these substrates decreases, as expected (entries 3 and 5).

Table IV. Hydroborations of Phenyl-Substituted Allylic Alcohols
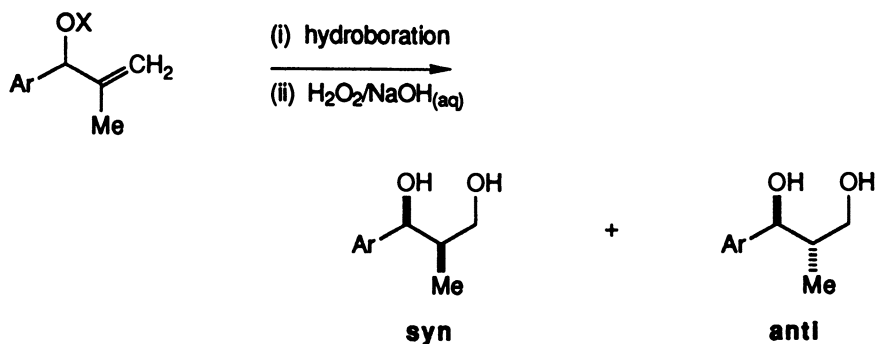
Entry	Ar	X	Method[a]	Syn:Anti
1	Ph	Ac	catalyzed	1.0:3.5
2	Ph	COCF$_3$	catalyzed	1.0:1.5
3	Ph	Ac	uncatalyzed	1.0:4.5
4	C$_6$F$_5$	Ac	catalyzed	1.0:6.9
5	C$_6$F$_5$	Ac	uncatalyzed	1.0:3.0

[a]Catalyzed hydroborations were performed in THF solutions of 2 mol % of [Rh(COD)Cl]$_2$ · 4PPh$_3$ and 3 equiv of catecholborane at 25 °C. Uncatalyzed hydroborations were performed in THF solutions of 4 equiv of 9-BBN at −78 to 25 °C. Oxidation was with NaOH–H$_2$O$_2$ in both cases. Stereochemistries were assigned by formation of acetonides, and analysis was done by gas chromatography.

Experiments with allyl amine-derived substrates (Table V) prove that the hypotheses presented here have predictive value. *N*-Tosyl allylic amines were prepared (in optically pure form from amino acids) and hydroborated under catalyzed and uncatalyzed conditions (*12*). Entries 1, 3, 5, and 7 show that diastereoselectivities in the catalyzed reactions are *syn*, consistent with a model similar to that given in structure 2 but with tosylamide functionality replacing the OX groups. The uncatalyzed processes, however, are nonselective (entries 2 and 8) or *anti*-selective (entry 6). Catalyzed and uncatalyzed hydroborations of these substrates are, therefore, stereocomplementary, but *syn* selectivities in the rhodium-mediated processes are moderate.

We predicted on the basis of the theories presented here that increasing the electron-withdrawing ability or the size of the NHTs group should lead to enhanced *syn* selection. Entries 9 and 10 show that catalyzed hydroborations of the corresponding *N*-benzylated substrates are indeed appreciably *syn*-selective. Hence, we were able to use steric effects to rationally bias product distribution.

Table V. Hydroborations of Allylic Amine Derivatives
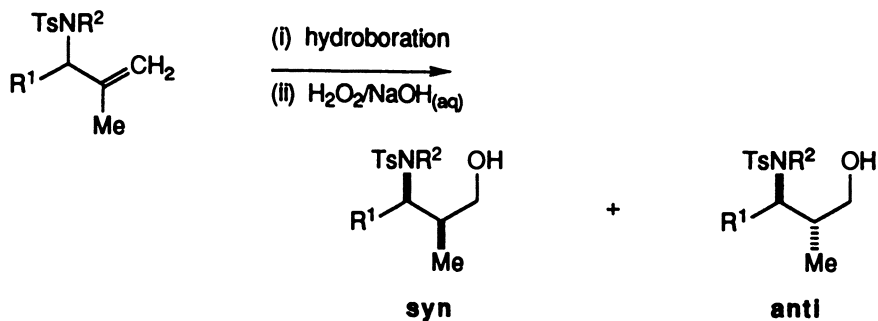
Entry	R^1	R^2	Method[a]	Syn:Anti
1	$PhCH_2$	H	catalyzed	7.0:1.0
2	$PhCH_2$	H	uncatalyzed	1.0:1.0
3	i-PrCH$_2$	H	catalyzed	4.0:1.0
4[b]	i-PrCH$_2$	H	uncatalyzed	2.5:1.0
5	i-Pr	H	catalyzed	6.7:1.0
6	i-Pr	H	uncatalyzed	1.0:7.4
7	$BnOCH_2$	H	catalyzed	4.0:1.0
8	$BnOCH_2$	H	uncatalyzed	1.0:1.0
9	$PhCH_2$	Bn	catalyzed	16.0:1.0
10	i-PrCH$_2$	Bn	catalyzed	10.0:1.0

[a]Catalyzed hydroborations were performed in THF solutions of 2 mol % of [Rh(COD)Cl]$_2$ · 4PPh$_3$ and 3 equiv of catecholborane at 25 °C. Uncatalyzed hydroborations were performed in THF solutions of 4 equiv of 9-BBN at –78 to 25 °C. Oxidation was with NaOH–H$_2$O$_2$ in both cases.

[b]Entry 4 shows an anomalous *syn* selectivity for an uncatalyzed process. This experiment was repeated several times to check the result. We cannot account for this small *syn* selectivity at present.

Conclusions

Catalyzed hydroborations may be of considerable value in organic synthesis. Refinements of methodologies presented here may supersede reagent-controlled diastereoselectivity for dictating absolute stereochemistry in hydroborations of some prochiral alkenes. Catalyzed hydroborations of chiral 1,1-disubstituted alkenes complement conventional methods for adding B–H to alkenes insofar as the former are *syn*-selective.

The theory proposed to account for stereocomplementarity in catalyzed and uncatalyzed hydroborations may be applicable to other processes involving metal π complexation. Many reactions of cuprates, for instance, involve transient formation of π complexes that collapse to give products (*39, 40*). Others (*41*) have mentioned possible involvement of d orbitals in S_N2' reactions of cuprates, but this is a question of orienting a complexing metal relative to a leaving group. Stereoselectivity of cuprate additions to γ-chiral-α,β-unsaturated carbonyl compounds is more relevant (*42, 43*). We suspect that several reaction types can be explained in terms of secondary orbital interactions that perturb incipient Dewar–Chatt bonding. We are actively investigating this area.

Acknowledgments

References

1. Wilczynski, R.; Sneddon, L. G. *J. Am. Chem. Soc.* **1980**, *102*, 2857.
2. Wilczynski, R.; Sneddon, L. G. *Inorg. Chem.* **1981**, *20*, 3955.
3. Wilczynski, R.; Sneddon, L. G. *Inorg. Chem.* **1982**, *21*, 506.
4. Davan, T.; Corcoran, E. W.; Sneddon, L. G. *Organometallics* **1983**, *2*, 1693.
5. Mirabelli, M. G. L. *Organometallics* **1986**, *5*, 1510.
6. Hewes, J. D.; Kreimendahl, C. W.; Marder, T. B.; Hawthorne, M. F. *J. Am. Chem. Soc.* **1984**, *106*, 5757.
7. Mirabelli, M. G. L.; Sneddon, L. G. *J. Am. Chem. Soc.* **1988**, *110*, 449.
8. Lynch, A. T.; Sneddon, L. G. *J. Am. Chem. Soc.* **1987**, *109*, 5867.
9. Mannig, D.; Noth, H. *Angew. Chem., Int. Ed. Engl.* **1985**, *24*, 878.
10. Burgess, K.; Ohlmeyer, M. J. *J. Org. Chem.* **1988**, *53*, 5178.
11. Burgess, K.; Ohlmeyer, M. J. *Tetrahedron Lett.* **1989**, *30*, 395.
12. Burgess, K.; Ohlmeyer, M. J. *Tetrahedron Lett.* **1989**, *30*, 5857.
13. Burgess, K.; Ohlmeyer, M. J. *Tetrahedron Lett.* **1989**, *30*, 5861.
14. Burgess, K.; Ohlmeyer, M. J.; Whitmire, K. H. *J. Org. Chem.* **1990**, *55*, 1359.
15. Evans, D. A.; Fu, G. C.; Hoveyda, A. H. *J. Am. Chem. Soc.* **1988**, *110*, 6917.
16. Hayashi, T.; Matsumoto, Y.; Ito, Y. *J. Am. Chem. Soc.* **1989**, *111*, 3426.
17. Satoh, M.; Nomoto, Y.; Miyaura, N.; Suzuki, A. *Tetrahedron Lett.* **1989**, *30*, 3789.
18. Sato, M.; Miyaura, N.; Suzuki, A. *Tetrahedron Lett.* **1990**, *31*, 231.
19. Brown, H. C.; Desai, M. C.; Jadhav, P. K. *J. Org. Chem.* **1982**, *47*, 5065.

20. Brown, H. C.; Mandal, A. K.; Yoon, N. M.; Singaram, B.; Schwier, J. R.; Jadhav, P. K. *J. Org. Chem.* **1982**, *47*, 5069.
21. Brown, H. C.; Jadhav, P. K.; Mandal, A. K. *J. Org. Chem.* **1982**, *47*, 5074.
22. Brown, H. C.; Singaram, B. *J. Org. Chem.* **1984**, *49*, 945.
23. Brown, H. C.; Prasad, J. V. N. V.; Zaidlewicz, M. *J. Org. Chem.* **1988**, *53*, 2911.
24. Brown, H. C.; Randad, R. S.; Bhat, K. S.; Zaidlewicz, M.; Weissman, S. A.; Jadhav, P. K.; Perumal, P. T. *J. Org. Chem.* **1988**, *53*, 5513.
25. Brown, H. C.; Jadhav, P. K. In *Asymmetric Synthesis*; Academic: New York, 1983; Vol. 2.
26. Masamune, S.; Kim, B. M.; Pedersen, J. S.; Sato, T.; Veenstra, S. J. *J. Am. Chem. Soc.* **1985**, *107*, 4549.
27. Still, W. C.; Barrish, J. C. *J. Am. Chem. Soc.* **1983**, *105*, 2487.
28. Hoel, E. L.; Hawthorne, M. F. *J. Am. Chem. Soc.* **1975**, *97*, 6388.
29. Corcoran, E. W.; Sneddon, L. G. *Inorg. Chem.* **1983**, *22*, 182.
30. Corcoran, E. W.; Sneddon, L. G. *J. Am. Chem. Soc.* **1984**, *106*, 7793.
31. Corcoran, E. W.; Sneddon, L. G. *J. Am. Chem. Soc.* **1985**, *107*, 7446.
32. Gilbert, K. B.; Boocock, S. K.; Shore, S. G. In *Comprehensive Organometallic Chemistry*; Pergamon: New York, 1982; p 879.
33. Marks, T. J.; Kolb, J. R. *Chem. Rev.* **1977**, *77*, 263.
34. Kono, H.; Ito, K. *Chem. Lett.* **1975**, 1095.
35. Burgess, K.; Linsell, M. S., Rice University, unpublished results.
36. For a discussion of orbital distortion, *see* Burgess, E. M.; Liotta, C. L. *J. Org. Chem.* **1981**, *46*, 1703.
37. Houk, K. N.; Paddon-Row, M. N.; Rondan, N. G.; Wu, Y.; Brown, F. K.; Spellmeyer, D. C.; Metz, J. T.; Li, Y.; Loncharich, R. J. *Science (Washington, D.C.)* **1986**, *231*, 1108.
38. Houk, K. N.; Rondan, N. G.; Wu, Y.; Metz, J. T.; Paddon-Row, M. N. *Tetrahedron* **1984**, *40*, 2257.
39. Hallnemo, G.; Olsson, T.; Ullenius, C. *J. Organomet. Chem.* **1985**, *282*, 133.
40. Dorigo, A. E.; Morokuma, K. *J. Chem. Soc., Chem. Commun.* **1989**, 1884.
41. Corey, E. J.; Boaz, N. W. *Tetrahedron Lett.* **1984**, *25*, 3063.
42. *See*, for instance Corey, E. J.; Boaz, N. W. *Tetrahedron Lett.* **1985**, *26*, 6015.
43. Marshall, J. A. *Chem. Rev.* **1989**, *89*, 1503.

Functionalization of Hydrocarbons by Homogeneous Catalysis

Masato Tanaka and Toshiyasu Sakakura

National Chemical Laboratory for Industry, Tsukuba, Ibaraki 305, Japan

*Various catalytic functionalizations of hydrocarbons, including al-
kanes, have been achieved by using the Vaska-type rhodium complex
ligated by trimethylphosphine under irradiation. The functionali-
zations are divided into two categories: insertion of unsaturated com-
pounds to and dehydrogenation from C–H bonds. A possible common
intermediate involved in these reactions is a hydridoalkyl complex
formed via alkane oxidative addition to $RhCl(PMe_3)_2$. The catalytic
system exhibits unique regioselectivities: terminal selectivity for n-
alkanes and meta selectivity for substituted benzenes. The use of inert
solvents enables us to achieve more than 90% conversion in dehy-
drogenation of alkanes.*

ALKANES ARE UNREACTIVE ENOUGH to be safely used as "inert" solvents,
according to most organic chemistry textbooks. Hence, quite a high tem-
perature (500–1000 °C) is required for today's organic chemical industry to
use petroleum products (mainly alkanes) as raw materials.

In 1982 and 1983, Bergman, Graham, Jones, and co-workers successively
reported (*1–3*) that some coordinatively unsaturated iridium and rhodium
complexes can activate even alkane C–H bonds below room temperature
(eqs 1–3; Cp* is a pentamethylcyclopentadienyl ligand).

$$Cp^*IrH_2(PMe_3) + RH \xrightarrow{\ h\nu\ } \underset{\underset{H}{\overset{\displaystyle Cp^*}{\underset{|}{R\diagdown\overset{|}{\underset{|}{Ir}}\diagup PMe_3}}}}{} \tag{1}$$

$$Cp^*Ir(CO)_2 \ + \ RH \ \xrightarrow{h\nu} \ \underset{\underset{H}{|}}{\overset{\overset{Cp^*}{|}}{R-Ir-CO}} \qquad (2)$$

$$Cp^*RhH_2(PMe_3) \ + \ RH \ \xrightarrow{h\nu} \ \underset{\underset{H}{|}}{\overset{\overset{Cp^*}{|}}{R-Rh-PMe_3}} \qquad (3)$$
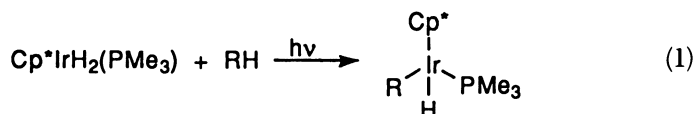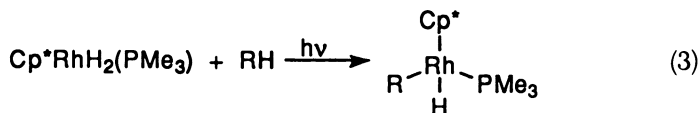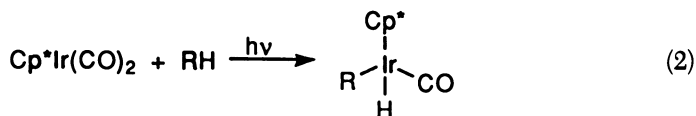
Although the oxidative addition of arene C–H bonds with transition metal complexes was described by Chatt, Green, Tolman, and co-workers (4–6), clear examples of alkane oxidative addition had been lacking. Moreover, Bergman (7) reported a very high regioselectivity for a terminal methyl group in the reaction of n-alkane with Cp*Rh(PMe₃). This selectivity cannot be attained by conventional methods for alkane activation with radicals or strong acids (8). Since then, alkane oxidative addition has been intensively and extensively studied. The resulting complexes have a carbon–metal bond and seem to be quite promising intermediates in various catalytic organic syntheses. Influenced by these papers, in 1985 we started to investigate selective functionalizations of alkanes triggered by C–H oxidative addition as an elemental step in homogeneous catalysis.

When we started the project, some pioneering groups (9–16) had already studied functionalization of C–H bonds catalyzed by metal complexes, as depicted in eqs 4–10. However, most of them deal with sp² C–H bonds of aromatic rings.

$$2 \quad \underset{}{\bigcirc} \quad \xrightarrow[O_2, \ 150°C, \ 4 \ h]{Pd(OAc)_2 \ + \ acetylacetone}$$

$$\underset{}{\bigcirc}-\underset{}{\bigcirc} \qquad \text{turnover 31} \qquad (4)$$

$$\underset{}{\bigcirc} \ + \ \underset{}{\bigcirc}\diagup^{\diagdown} \quad \xrightarrow[O_2, \ AcOH, \ reflux, \ 8 \ h]{Pd(OAc)_2\text{-}Cu(OAc)_2}$$

$$\underset{}{\bigcirc}\diagdown\diagup\diagdown\underset{}{\bigcirc} \qquad (5)$$

$$\text{turnover } 4.5$$

$$\underset{}{\bigcirc} \ + \ CO \ + \ t\text{-BuOOH} \quad \xrightarrow[\substack{\diagup\diagdown^{Cl} \ , \ AcOH \\ 75°C, \ 24\text{-}72 \ h}]{Pd(OAc)_2}$$

(other reagents: CO₂, O₂)

$$\underset{}{\bigcirc}-CO_2H \qquad (6)$$

$$\text{turnover } 12$$

$$\text{C}_6\text{H}_6 + \text{CH}_2\text{=CH}_2 \xrightarrow[\text{CO, 250°C, 7 h}]{\text{Rh}_4(\text{CO})_{12}} \text{PhCH=CH}_2 \quad (7)$$

turnover 118

(other reagents: $CH_2=CHCO_2Me$, $PhC\equiv CPh$, $Ph_2C=C=O$, $Ph-N=C=O$, $Ph-NO_2$)

$$\text{C}_6\text{H}_6 + \underset{R}{\overset{R}{Si}}\text{-O-}\underset{R}{\overset{H}{Si}}\text{-O-} \xrightarrow[\text{100°C, 49 days}]{\text{IrCl(CO)(PPh}_3)_2}$$

$$\underset{R}{\overset{R}{Si}}\text{-O-}\underset{R}{\overset{Ph}{Si}}\text{-O-} \quad (8)$$

turnover 13

$$\text{C}_6\text{H}_6 + \text{CO} \xrightarrow[\text{r.t.}]{\text{hv, IrH}_3(\text{CO})(\text{Ph}_2\text{PCH}_2\text{CH}_2\text{PPh}_2)}$$

$$\text{C}_6\text{H}_5\text{-CHO} \quad (9)$$

turnover < 2

(various other complexes of Ir, Rh, or Ru show activity)

$$\text{(cyclooctane)} + \text{t-BuCH=CH}_2 \xrightarrow[\text{150°C, 5 days}]{\text{IrH}_5[\text{P(i-Pr)}_3]_2}$$

$$\text{(cyclooctene)} + \text{t-BuCH}_2\text{CH}_3 \quad (10)$$

turnover 70

Although transfer hydrogenation of *t*-butylethylene with alkanes proceeds effectively (eq 10), the reaction is not attractive from a practical viewpoint because it consumes one molecule of *t*-butylethylene to make one molecule of alkenes. Other systems have also been reported since 1985 (*17–21*), as shown in eqs 11–15. However, "productive" functionalization of alkanes is still very rare and has been a challenging subject for organic chemists.

$$\text{CN-}(\text{dimethylbenzene}) \xrightarrow[\text{140°C, 94 h}]{\text{Ru(Me}_2\text{PCH}_2\text{CH}_2\text{PMe}_2)_2} \text{HN-(indole)} \quad (11)$$

turnover 3.5

$$\text{(cyclooctane)} \xrightarrow[\text{r.t., 7 days}]{\text{hv, IrH}_2(\text{OCOCF}_3)(\text{PAr}_3)_2} \text{(cyclooctene)} + \text{H}_2 \quad (12)$$

turnover 8

$$\text{benzene} + \text{t-BuCH}_2\text{NC} \xrightarrow[\text{r.t.}]{h\nu,\ \text{Fe}(\text{PMe}_3)_2(\text{t-BuCH}_2\text{NC})_3} \quad (13)$$

turnover 7

$$\text{MeO-CH}_2\text{CH}_2\text{-OMe} + \text{t-BuCH=CH}_2 \xrightarrow[\text{50°C, 24 h}]{\text{IrH}_5[\text{P(i-Pr)}_3]_2} \quad (14)$$

turnover 12

$$\text{2-methylpyridine} + \text{propene} \xrightarrow[\text{r.t., 25 h}]{\text{Cp}_2\text{ZrR}} \quad (15)$$

turnover 23
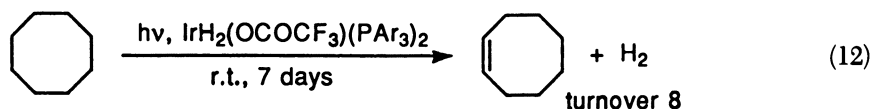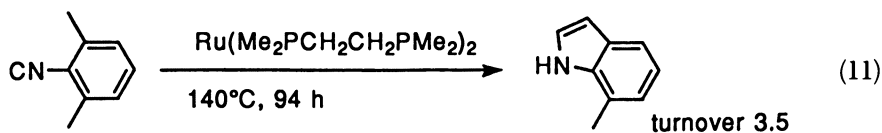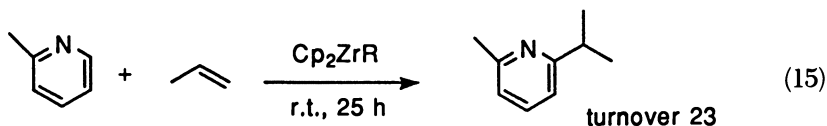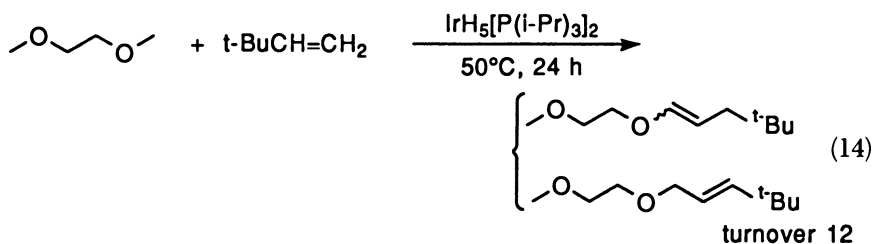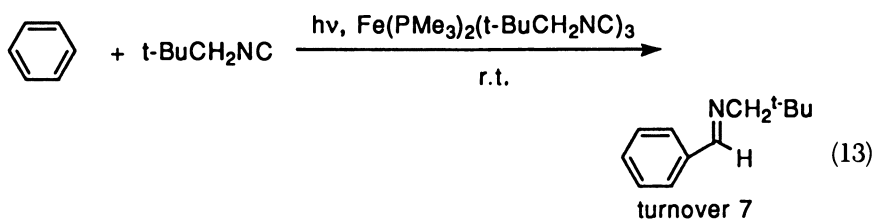
Recently we developed a catalytic system that can transform hydrocarbons, including alkanes, to various useful compounds under mild conditions. The system comprises $\text{RhCl(CO)(PMe}_3)_2$ and irradiation of near-UV light (Scheme I). This chapter summarizes the progress of our research.

$$[\text{M}]\text{-CO} \xrightarrow{h\nu} [\text{M}] \xrightarrow{\text{RH}} \text{R-[M]-H}$$

Insertion

C≡O	R-C(=O)-H
R'N≡C	R-C(=N-R')-H
R'C≡CH	R,R'C=CH$_2$

Dehydrogenation

-H$_2$	Olefin (R = alkyl)
-H$_2$	R-R (R = aryl)
R'CH=CH$_2$, -H$_2$	R-C(H)=C(H)-R'
R'$_3$SiH, -H$_2$	R-SiR'$_3$
R'CHO	R'CH$_2$OH + Olefin
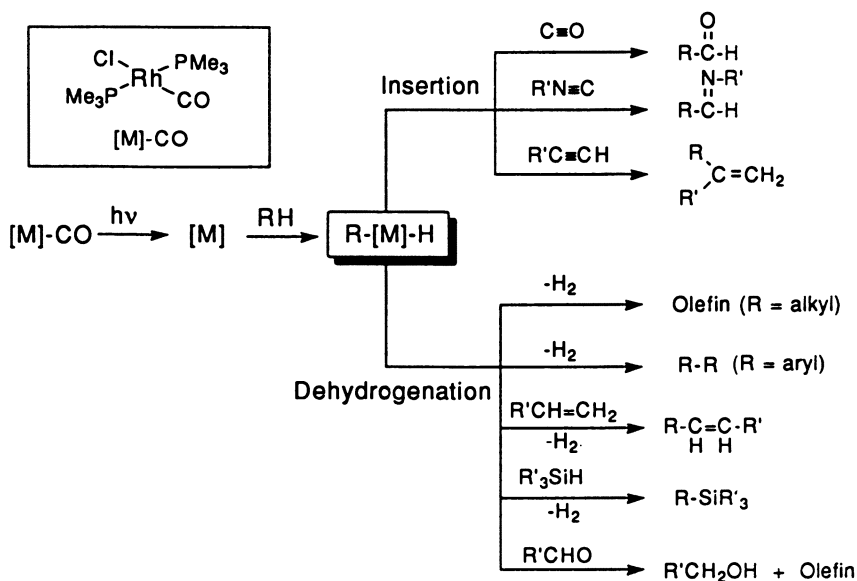
Scheme I.

Experimental Details

Synthesis of the Catalyst. $RhCl(CO)(PMe_3)_2$ was prepared by the reaction of $[RhCl(CO)_2]_2$ with trimethylphosphine in benzene and recrystallized from MeOH at 0 °C. Most of the other Vaska-type rhodium complexes were synthesized similarly.

General Procedure.   A solution of $RhCl(CO)(PMe_3)_2$ and a reagent (carbon monoxide, isonitrile, acetylene, olefin, hydrosilane, etc.) in a hydrocarbon was irradiated with a high-pressure mercury lamp. Dehydrogenation of alkanes and dehydrogenative coupling of arenes were conducted without any additional reagents under an inert atmosphere. The reactions were carried out in a Pyrex flask with an immersion-type lamp unless otherwise stated. Wavelength-regulated reactions were conducted with a lamp-housed high-pressure mercury lamp through glass filters.

The products were identified by comparison of gas chromatographic (GC) retention times in capillary columns and fragmentation patterns of GC–mass spectroscopy (MS) with authentic samples. When authentic samples were not available, products were isolated and characterized by NMR, IR, and mass spectroscopy and elemental analyses. Yields were generally evaluated by using capillary GC with an internal standard.

Results and Discussion

Carbonylation.   Our group, which has been investigating utilization of carbon monoxide (22), first examined insertion of CO to a C–H bond of hydrocarbons (aldehyde synthesis). Several attempts (23–25) have been made to obtain carbonylated products from hydridoalkyl (or aryl) complexes formed via oxidative addition of hydrocarbons (eqs 16–18).

$$Cp^*Ir(R)H(PMe_3) + CO \longrightarrow Cp^*Ir(CO)(PMe_3) + RH \qquad (16)$$

$$IrCl(Ph)H[P(i\text{-}Pr)_3]_2 + CO \longrightarrow IrCl(Ph)H(CO)[P(i\text{-}Pr)_3]_2 \qquad (17)$$

$$Ir(Ph)H(RCO_2)(PAr_3)_2 + CO \longrightarrow Ir(Ph)H(CO)(RCO_2)(PAr_3)_2 \qquad (18)$$
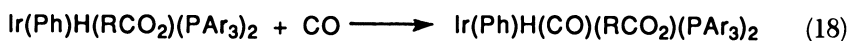
Because $Cp^*IrR(H)(PMe_3)$ is an 18-electron complex, the reaction with carbon monoxide resulted in dissociation of RH. Although $IrCl(Ph)(H)(PR_3)_2$ and $Ir(RCO_2)(Ph)(H)(PAr_3)_2$ could react with carbon monoxide, the resulting carbonyl iridium complexes were rather stable and did not produce aldehyde.

We investigated the carbonylation of benzene on the following three working hypotheses.

- As a central metal, rhodium would be promising because rhodium complexes are very active for both carbonylation and C–H activation.

- It is desirable that hydridoalkyl complexes formed through oxidative addition of a C–H bond remain coordinatively unsaturated to react further. Hence, the preferred active species before C–H oxidative addition is a 14-electron complex (Scheme II). The same idea is discussed by Felkin, Crabtree, and co-workers in their studies (25, 26) of dehydrogenation of alkanes.

- Promotion of oxidative addition would lead to higher catalytic activity. In other words, ligands should be strong electron donors that are resistant to intramolecular C–H oxidative addition.
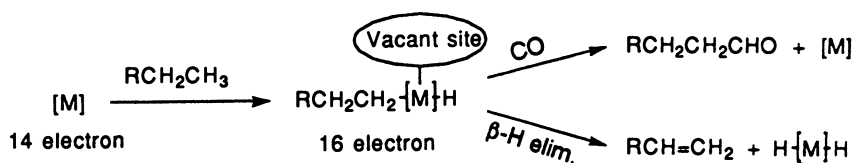
Scheme II.
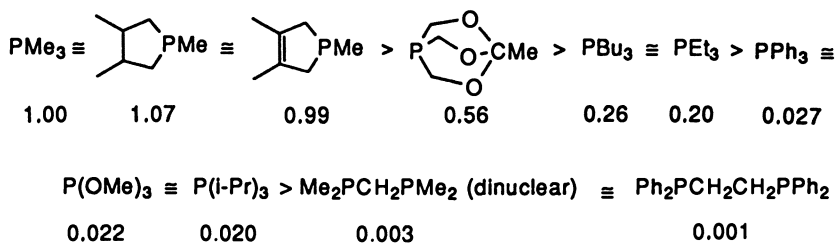
Chart I. Effect of phosphine ligands on the carbonylation of benzene by RhCl(CO)(PR₃)₂; relative catalytic activity (room temperature, 16.5 h).

After extensive studies (27, 28), we discovered that $RhCl(CO)(PMe_3)_2$ under irradiation is the most effective catalyst (Chart I). The effect of the phosphine ligand is remarkable; $RhCl(CO)(PMe_3)_2$ was 30–40 times more active than $RhCl(CO)(PPh_3)_2$. Highly electron-donating and sterically small phosphines like 1,3,4-trimethylphospholane and 1,3,4-trimethylphospholene were as effective as trimethylphosphine. The results of our mechanistic investigations indicate that the favorable effect of these phosphines results not from the promotion of C–H oxidative addition but from suppression of reductive elimination of hydrocarbons from a hydridoalkylcarbonyl intermediate (eq 19).

(19)

In the carbonylation of benzene, benzyl alcohol and benzophenone were formed as secondary products from benzaldehyde (eq 20). To clarify the secondary reactions of aldehydes formed, the carbonylation reactions were carried out in the presence of an additional aldehyde (Table I). The formation of alcohols and ketones was clearly demonstrated. Although there was little decarbonylation of aromatic aldehyde, decarbonylation was the main secondary reaction of cyclohexanecarbaldehyde.

3 h	13.7	0.08	0.00	0.75
18 h	73.7	10.9	6.50	3.72
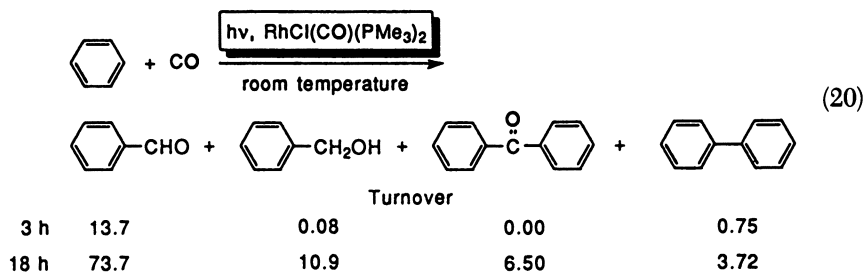
The most fascinating feature of carbonylation of the C–H bond lies in its regioselectivity. In the carbonylation of pentane or 2-methylpentane, the methyl group was distinguished from the methylenes in nearly 100% selectivity (29, 30). On the other hand, substituted benzenes like toluene or anisole were carbonylated mainly at the meta position (31). These selectivities, which are entirely different from the selectivity observed in radical or electrophilic reactions, must be a characteristic of C–H oxidative addition to low-valent transition metals. The regioselectivity of this carbonylation can be controlled by the wavelength of irradiation (32). When short wavelength (below 325 nm) was cut off, the weakest C–H bonds were carbonylated: methylene in alkane and benzylic methyl in toluene (eqs 21 and 22).

Regioselectivity in the carbonylation of alkanes (> 295 nm)
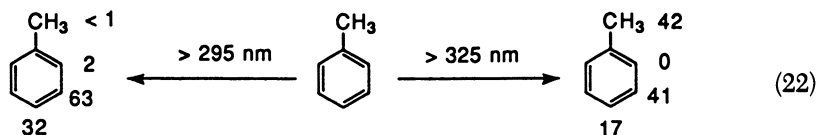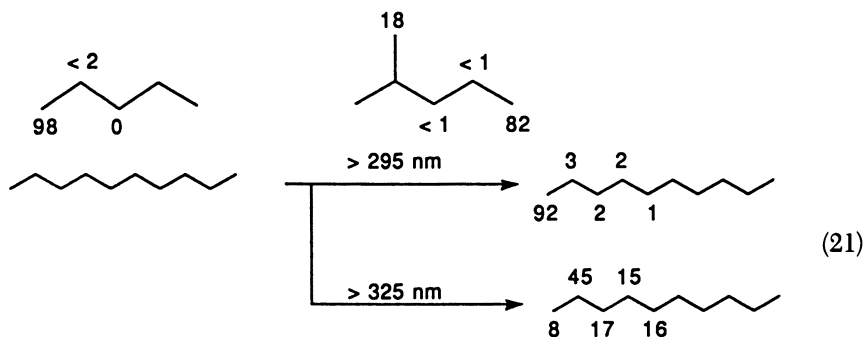
Table I. Yields of Secondary Reactions of Aldehydes in the Carbonylation Reaction by the RhCl(CO)(PMe₃)₂–hν System

$$R^1H + CO + R^2CHO \rightarrow R^1CHO + R^1CH_2OH + R^1COR^1 +$$
$$R^2CH_2OH + R^2COR^1 + R^2H + R^2\text{–}R^1 + \cdots$$
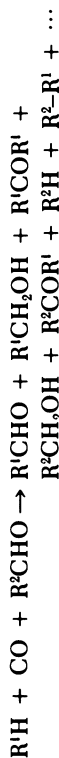
Case	R¹H	R²CHO	R²CH₂OH	R²COR¹ [or R²CH(OH)R¹]	R²H	R²–R¹
1	toluene	benzaldehyde	61	26	2	0
2	benzene	p-tolualdehyde	5	20	4	0
3	benzene	cyclohexanecarbaldehyde	trace	32	43	5

NOTE: Reaction conditions were as follows: Rh, 0.7 mM; arene, 30 mL; aldehyde, 0.80 mmol; CO, 1 atm; room temperature; and 16.5 h. All yields are based on the amount of R²CHO used.

The following observations may also be concerned with wavelength effect.

- Cyclohexane was carbonylated efficiently in a mixture with benzene (eq 23), although cyclohexanecarbaldehyde was barely obtained when cyclohexane was used alone. This carbonylation may have occurred because decarbonylation of the cyclohexanecarbaldehyde formed was suppressed by the presence of benzene that absorbs short-wavelength light.

- Methyl selectivity for alkanes was lost when they were carbonylated as a mixture with benzene (eq 24).

$$\text{[benzene]} \Big/ \text{[cyclohexane]} + CO \xrightarrow[\text{r.t., 2 h}]{hv, \ RhCl(CO)(PMe_3)_2}$$

1 : 1 (mol / mol)

$$\text{Ph—CHO} + \text{Ph—CH}_2\text{OH} + \text{Cy—CHO} + \text{Cy—C(O)—Ph}$$ (23)

Turnover   10.7   5.6   14.2   4.3

$$\text{[pentane]} \Big/ \text{[benzene]} + CO \xrightarrow[\text{r.t., 2 h}]{hv, \ RhCl(CO)(PMe_3)_2}$$

1 : 1 (mol / mol) (24)

branched-CHO + branched(CHO)(CHO) + linear-CHO + PhCHO + PhCH$_2$OH

Turnover   2.6   1.4   0.94   12.3   3.0
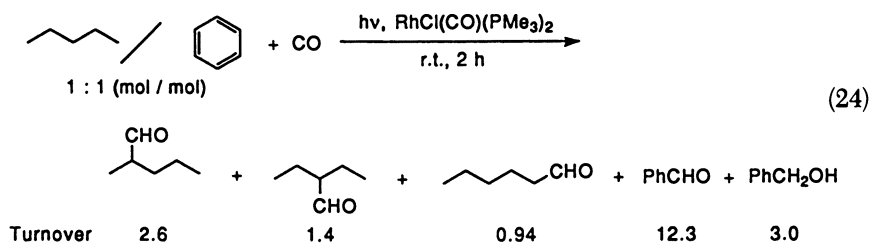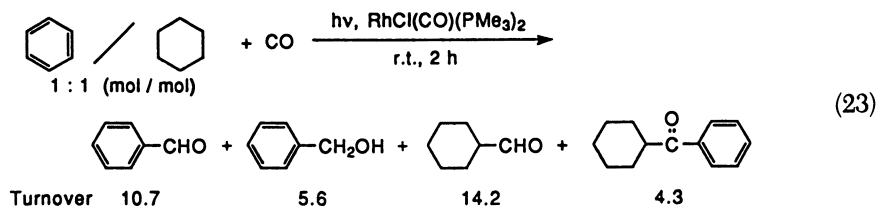
In addition to carbon monoxide, other unsaturated compounds like isonitriles and acetylenes can also insert into C–H bonds to give aldimines (eq 25) and substituted alkenes (eq 26), respectively (*33, 34*).

$$\text{[benzene]} + \text{Cy—NC} \xrightarrow{hv, \ [Rh]} \text{aldimine}$$ (25)

$$\text{[benzene]} + \text{Ph—C}\equiv\text{CH} \xrightarrow{hv, \ [Rh]} \text{1,1-diphenylethylene}$$ (26)
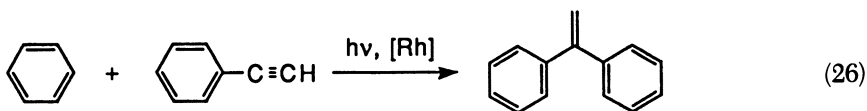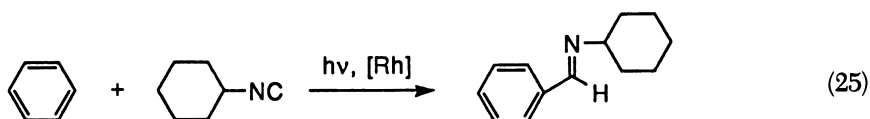
Dehydrogenation of Alkanes. Hydridoalkyl complexes formed through oxidative addition of the C–H bond are expected to be a good intermediate for alkene synthesis as well as aldehyde formation, because alkyl complexes of transition metals readily produce alkenes via β-hydride elimination (Scheme II). As a matter of fact, when alkanes were irradiated in the presence of $RhCl(CO)(PMe_3)_2$ under an inert atmosphere, alkenes and hydrogen were produced quite efficiently (eq 27, Chart II) (35, 36).

$$\text{(27)}$$

Turnover 667
(Conversion 6.7%)

PMe_3 > (structure) > PPh_3 > $Ph_2PCH_2PPh_2{}^*$ > $P(OMe)_3$

1.00   0.71   0.19   0.17   0.085

> PBu_3 > $Me_2PCH_2PMe_2{}^*$ > $P(i\text{-}Pr)_3$ > $Ph_2PCH_2CH_2PPh_2$

0.049   0.016   0.009   ≅ 0
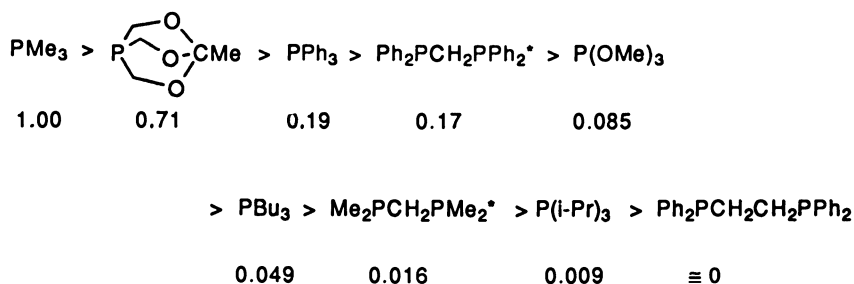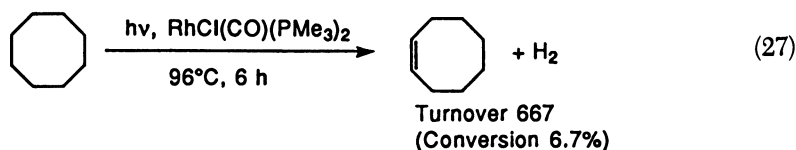
*Chart II. Effect of phosphine ligands on the dehydrogenation of cyclooctane by RhCl(CO)(PR₃)₂; relative activity (96 °C, 6 h, * indicates dinuclear complex).*

The reaction proceeds well even under H_2 atmosphere. Irradiation must be a driving force to promote the thermodynamically unfavorable reaction. Turnover rate of the dehydrogenation of cyclooctane at room temperature is about 10 times faster than that of the carbonylation of benzene. The dehydrogenation can be further accelerated by heating.

Catalytic activity significantly depends on the nature of the phosphine ligands of the catalyst; trimethylphosphine is the best ligand, as in the case of carbonylation. The complexes of triphenylphosphine and trimethylphosphite exhibited much higher catalytic activity than expected from the result of the carbonylation. However, because the deactivation of these complexes occurred rather fast, total turnovers achieved in the use of these ligands, especially $P(OMe)_3$, were much lower than in the case of PMe_3.

When acyclic alkanes were dehydrogenated, internal alkenes were obtained as major isomers. This product resulted partly from the isomerization of a terminal alkene to thermodynamically more stable internal alkenes. Terminal alkenes could be obtained in the presence of additional phosphine ligand at the expense of the reaction rate (eq 28) (37).

$$hv, RhCl(CO)(PMe_3)_2 + PMe_3$$
room temp.

(28)

P/Rh	Time(h)						Total turnover
2	1	7	:	77	:	15	5.4
5	3	70	:	24	:	6	4.0
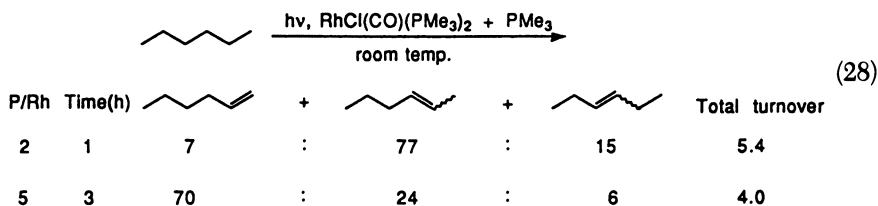
A principal problem in the hydrocarbon transformation catalyzed by the $RhCl(CO)(PMe_3)_2–hv$ system is the lack of solvents that are stable in these reactions. Hence, we must use a substrate itself as a solvent. This requirement has strongly restricted the achievement of high conversions and application of the reactions to expensive or high-melting substrates. We recently developed inert solvents for the dehydrogenation of alkanes (*38*). In 2,2,5,5-tetramethylhexane, more than 90% conversion was achieved in 3 h for the dehydrogenation of cyclooctane (eq 29).

(2 vol.%)

$$hv, RhCl(CO)(PMe_3)_2$$

t-Bu ⌢ t-Bu

100°C, 3 h

Conv. 92%

Yield 59%   27%

0.65%   0.18%   + dimers
5.5%

(29)
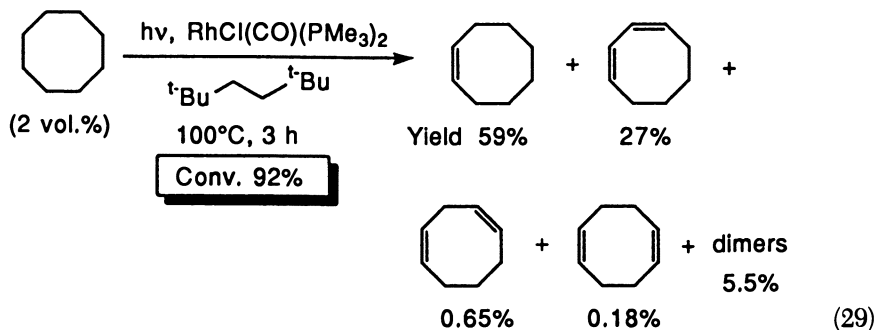
As the conversion increased, the initially formed cyclooctene further reacted to give 1,3-cyclooctadiene. Regioselective formation of the 1,3-diene is probably a result of the high reactivity of the allylic C–H bond, although very rapid isomerization of primarily formed unconjugated dienes to the 1,3-diene cannot be excluded. The dehydrogenated product of the solvent, 2,2,5,5-tetramethyl-3-hexene, was not detected at all. A quite bulky aromatic hydrocarbon like 1,3,5-tri-*t*-butylbenzene also works as an inert solvent in the dehydrogenation (Table II). Dilution of cyclooctane with 2,2,5,5-tetramethylhexane did not significantly reduce the initial turnover rate as compared with the reaction of neat cyclooctane. This comparison strongly suggests that oxidative addition of a C–H bond to the rhodium complex is not the rate-determining step in this dehydrogenation.

Because hydridorhodium species are suspected as intermediates in the dehydrogenation of alkanes, hydrogenation of unsaturated compounds using alkanes as hydrogen donors is expected to occur. As a matter of fact, addition

Table II. Dehydrogenation of Alkanes in Solvents

Substrate	Solvent	Time (h)	Conversion (%)	Yield[a] (%) (Turnover)		
				COE	1,3-COD	Dimers
Cyclooctane	(t-BuCH$_2$)$_2$	1	60	52 (38)	7	1
Cyclooctane	cyclooctane	3	92	59	27	6
Cyclooctane[b]	(t-BuCH$_2$)$_2$	1	1.9	1.9 (72)	0	0
Cyclooctane[b]	1,3,5-tri-t-butylbenzene	3	90	60 (156)	21	9
Cyclooctane		7	92	62	25	4
				Decenes[c]		
				t-2-	c-2-	others
Decane[b]	1,3,5-tri-t-butylbenzene	48	42	16	5	19
				Pentadecenolides[c]		
Pentadecanolide[b]	(t-BuCH$_2$)$_2$	1	34		32 (54)	
Pentadecanolide[b]		3	53		50 (84)	

NOTE: Reaction conditions were as follows: substrate, 0.050 cm^3; solvent, 2.5 cm^3; RhCl(CO)(PMe$_3$)$_2$, 5.04 μmol; 100 °C; and irradiation by a high-pressure mercury lamp through a Pyrex filter.
[a] Based on the charged amount of the substrate. COE and COD are cyclooctene and cyclooctadiene, respectively.
[b] In these cases, 1.26 μmol of Rh was used.
[c] Regioisomeric mixtures; t-2- and c-2- are trans-2- and cis-2-decene, respectively.

of cyclohexene to the dehydrogenation reaction of cyclooctane by the $RhCl(CO)(PMe_3)_2$–hv system resulted in the formation of cyclohexane. Aldehydes were also reduced to the corresponding alcohols under similar conditions (eq 30, Table III) (39).

$$R^1\text{CHO} + R^2\text{---}R^3 \xrightarrow{\ hv,\ [Rh]\ } R^1\text{---}CH_2OH + R^2\text{==}R^3 \qquad (30)$$
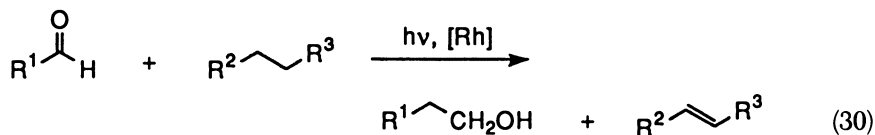
Table III. Reduction of Carbonyl Compounds Using Cyclooctane as a Hydrogen Donor

| Substrate | Time (h) | Conversion (%) | Yield (%)[a] | | Efficiency of H₂ Transfer[c] |
			Alcohol	Decarbonylated[b]	
Cyclohexanecarbaldehyde	24	73	69	1	46
	48	94	87	1	36
Phenylpropanal	24	56	45	2	59
	48	78	67	3	50
Octanal	24	72	70	1	47
	48	93	89	1	31
2-Octanone	24	1	1	0	1

NOTE: Reaction conditions were as follows: substrate, $0.1\ cm^3$; cyclooctane, $2.0\ cm^3$; $RhCl(CO)(PMe_3)_2$, 0.0020 mmol; and irradiation by a high-pressure mercury lamp through UV-35 filter at room temperature.
[a]Yields are evaluated by GC analysis and based on the charged amount of substrates.
[b]Decarbonylated products (mainly alkane).
[c]$100 \times$ alcohol/cyclooctene.

Although the photoreduction of aldehydes has been extensively studied, simple reduction to the corresponding alcohols is still rare. Ketones were barely reduced under the same conditions. Thus, the chemoselective reduction of aldehyde in the presence of ketone is possible. Furthermore, Wilkinson-type rhodium complexes, $RhCl(PR_3)_3$, are known to be inactive for the hydrogenation of aldehydes because they are easily deactivated through the formation of Vaska-type complexes, $RhCl(CO)(PR_3)_2$. Actually, $RhCl(CO)(PMe_3)_2$ was inactive even under irradiation for the hydrogenation of aldehydes with dihydrogen in benzene.

Besides alkene formation from alkane, the $RhCl(CO)(PMe_3)_2$–hv system can catalyze various dehydrogenative reactions of hydrocarbons (eqs 31–35) (40–44).

$$\text{(cyclohexane)} + \text{(cyclohexane)} \xrightarrow[-H_2]{\ hv,\ [Rh]\ } \text{(biphenyl)} \qquad (31)$$

$$\text{(cyclohexane)} + R_3SiH \xrightarrow[-H_2]{\ hv,\ [Rh]\ } \text{(phenyl)}\text{---}SiR_3 \qquad (32)$$

$$\text{(33)}$$

$$\text{(34)}$$

$$\text{(35)}$$
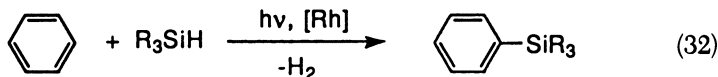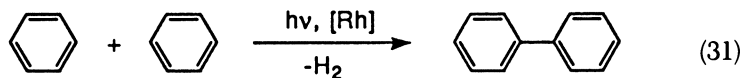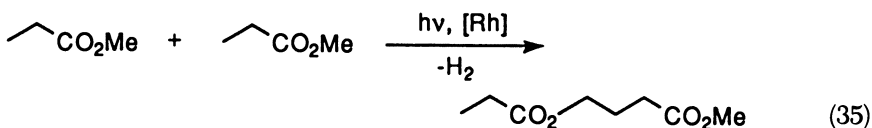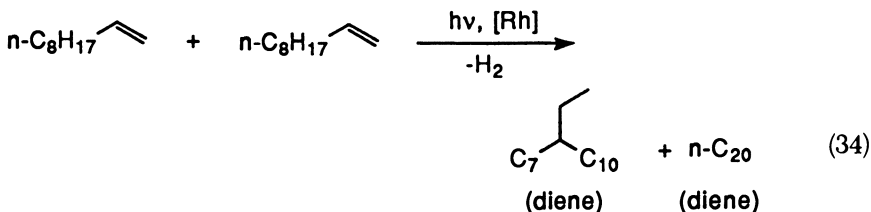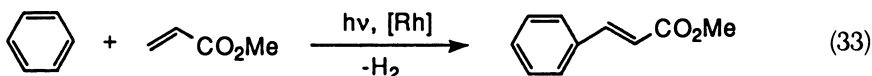
In the dehydrogenative silylation and vinylation of toluene, almost the same regioselectivity was observed as in the carbonylation ($o:m:p = 0:2:1$). The formation of an ethyl-branched diene in the dehydrogenative dimerization of 1-decene (eq 34) is associated with the activation of the allylic C–H bond, which was also pointed out for the formation of 1,3-cyclooctadiene (eq 29). The head-to-tail dimerization of methyl propionate possibly proceeds via methyl acrylate generated as an intermediate.

Conclusions

We have shown that it is possible to functionalize hydrocarbons under mild conditions by homogeneous catalysis. Further application of C–H oxidative addition to catalysis will probably lead to development of versatile organic synthetic reactions with alkanes. We hope that our research has provided a clue to creation of an entirely new high-efficiency chemical industry. We have found that the use of $RhCl(CH_2=CH_2)(PMe_3)_2$ in place of $RhCl(CO)(PMe_3)_2$ allows dehydrogenation either by visible light irradiation or thermally (45).

Acknowledgments

References

1. Janowicz, A. H.; Bergman, R. G. *J. Am. Chem. Soc.* **1982**, *104*, 352–354.
2. Hoyano, J. K.; Graham, W. A. G. *J. Am. Chem. Soc.* **1982**, *104*, 3723–3725.

3. Jones, W. D.; Feher, F. J. *Organometallics* **1983**, *2*, 562–563.
4. Chatt, J.; Davidson, J. M. *J. Chem. Soc.* **1965**, 843–855.
5. Berry, M.; Elmitt, K.; Green, M. L. H. *J. Chem. Soc., Dalton Trans.* **1979**, 1950–1958.
6. Tolman, C. A.; Ittel, S. D.; English, A. D.; Jesson, J. P. *J. Am. Chem. Soc.* **1979**, *101*, 1742–1751.
7. Periana, P. A.; Bergman, R. G. *J. Am. Chem. Soc.* **1986**, *108*, 7332–7346.
8a. Pines, H. *The Chemistry of Catalytic Hydrocarbon Conversions*; Academic Press: New York, 1981.
8b. Pryor, W. A. *Free Radicals*; McGraw–Hill: New York, 1966.
9. Itatani, H.; Yoshimoto, H. *J. Org. Chem.* **1973**, *38*, 76–79.
10. Fujiwara, Y.; Moritani, I.; Danno, S.; Asano, S.; Teranishi, S. *J. Am. Chem. Soc.* **1969**, *91*, 7166–7169.
11. Fujiwara, Y.; Kawata, I.; Sugimoto, H.; Taniguchi, H. *J. Organomet. Chem.* **1983**, *256*, C35–C36.
12. Hong, P.; Yamazaki, H. *J. Mol. Catal.* **1984**, *26*, 297–311.
13. Gustavson, W. A.; Epstein, P. S.; Curtis, M. D. *Organometallics* **1982**, *2*, 884–885.
14. Fisher, B. J.; Eisenberg, R. *Organometallics* **1983**, *2*, 764–767.
15. Kunin, A. J.; Eisenberg, R. *Organometallics* **1988**, *7*, 2124–2129.
16. Crabtree, R. H. *Chem. Rev.* **1985**, *85*, 245–269.
17. Jones, W. D.; Kosar, W. P. *J. Am. Chem. Soc.* **1986**, *108*, 5640–5641.
18. Burk, M. J.; Crabtree, R. H.; McGrath, D. V. *J. Chem. Soc., Chem. Commun.* **1985**, 1829–1830.
19. Jones, W. D.; Foster, G. P.; Putinas, J. M. *J. Am. Chem. Soc.* **1987**, *109*, 5047–5048.
20. Lin, Y.; Ma, D.; Lu, X. *Tetrahedron Lett.* **1987**, *28*, 3249–3252.
21. Jordan, R. F.; Taylor, D. F. *J. Am. Chem. Soc.* **1989**, *111*, 778–779.
22. Tanaka, M. *Yuki Gosei Kagaku Kyokaishi* **1987**, *45*, 716–728.
23. Janowicz, A. H.; Bergman, R. G. *J. Am. Chem. Soc.* **1983**, *105*, 3929–3939.
24. Werner, H.; Hohn, A.; Dizallas, M. *Angew. Chem., Int. Ed. Engl.* **1986**, *25*, 1090–1092.
25. Burk, M. J.; Crabtree, R. H. *J. Am. Chem. Soc.* **1987**, *109*, 8025–8032.
26. Felkin, H.; Fillebeen-Khan, T.; Gault, Y.; Holmes-Smith, R.; Zakrzewski, J. *Tetrahedron Lett.* **1984**, *25*, 1279–1282.
27. Sakakura, T.; Tanaka, M. *Chem. Lett.* **1987**, 249–252.
28. Sakakura, T.; Sodeyama, T.; Sasaki, K.; Wada, K.; Tanaka, M. *J. Am. Chem. Soc.* **1990**, *112*, 7221–7229.
29. Sakakura, T.; Tanaka, M. *J. Chem. Soc., Chem. Commun.* **1987**, 758–759.
30. Sakakura, T.; Hayashi, T.; Tanaka, M. *Chem. Lett.* **1987**, 859–862.
31. Sakakura, T.; Tanaka, M. *Chem. Lett.* **1987**, 1113–1116.
32. Sakakura, T.; Sasaki, K.; Tokunaga, Y.; Wada, K.; Tanaka, M. *Chem. Lett.* **1988**, 155–158.
33. Tanaka, M.; Sakakura, T.; Tokunaga, Y.; Sodeyama, T. *Chem. Lett.* **1987**, 2373–2374.
34. Tokunaga, Y.; Sakakura, T.; Tanaka, M. *J. Mol. Catal.* **1989**, *56*, 305–314.
35. Sakakura, T.; Sodeyama, T.; Tanaka, M. *New J. Chem.* **1989**, *13*, 737–745.
36. Sakakura, T.; Sodeyama, T.; Tokunaga, Y.; Tanaka, M. *Chem. Lett.* **1988**, 263–264.
37. Sakakura, T.; Sodeyama, T.; Tanaka, M. *Chem. Ind. (London)* **1988**, 530–531.
38. Sakakura, T.; Ishida, K.; Tanaka, M. *Chem. Lett.* **1990**, 585–588.
39. Sakakura, T.; Abe, F.; Tanaka, M. *Chem. Lett.* **1990**, 583–584.

40. Sakakura, T.; Sodeyama, T.; Tokunaga, Y.; Tanaka, M. *Chem. Lett.* **1987,** 2211–2214.
41. Sakakura, T.; Tokunaga, Y.; Sodeyama, T.; Tanaka, M. *Chem. Lett.* **1987,** 2375–2378.
42. Sakakura, T.; Sasaki, K.; Tokunaga, Y.; Wada, K.; Tanaka, M. *Chem. Lett.* **1988,** 685–688.
43. Sakakura, T.; Tokunaga, Y.; Sodeyama, T.; Tanaka, M. *Chem. Lett.* **1988,** 885–888.
44. Sakakura, T.; Sodeyama, T.; Tanaka, M. *Chem. Lett.* **1988,** 683–684.
45. Sakakura, T.; Abe, F.; Tanaka, M. *Chem. Lett.* **1991,** 297–298.

13

Mercury-Photosensitized C–H Bond Functionalization

Robert H. Crabtree, Steven H. Brown, Cesar A. Muedas, Paul Krajnik, and Richard R. Ferguson

Chemistry Department, Yale University, New Haven, CT 06511

A variety of organic compounds such as alkanes, alcohols, ethers, and silanes can be dimerized by mercury photosensitization on a preparative scale at room temperature and pressure. Alkane functionalization can be effected by cross-dimerizing an alkane with any of these substrates. The presence of H_2 leads to the efficient formation of H atoms. In turn, this reaction allows alkenes (including unsaturated acids, esters, nitriles, and epoxides) to be hydrodimerized. It also allows a much wider range of saturated substrates (such as saturated esters, carboxylic acids, and amides) to be dehydrodimerized. Quantitative studies allow prediction of product ratios and relative reactivities. Recent advances in chemical physics and theoretical chemistry throw light on the role of exciplex formation in the mechanism. Alkanes can be converted to sulfonic acids, aldehydes, ketones, and hydroperoxides by mercury photosensitization in the presence of SO_2, CO, and O_2.

OUR WORK ON MERCURY-PHOTOSENSITIZED REACTIONS (*1*) grew from our interest in thermal and photochemical homogeneous catalysis of alkane dehydrogenation with iridium phosphine complexes (*2–8*). These complexes were tested for catalyst homogeneity with metallic Hg, which poisons heterogeneous Ir catalysts. With the photochemical iridium system (*2, 3*), the alkane-derived products coming from the Hg photosensitization pathway far exceeded those from the iridium catalyst. This result attracted our attention and we looked at the system in detail. We have now found several ways in which alkanes and organic compounds with unactivated C–H bonds can be converted to a variety of functionalized materials on a preparative scale at

room temperature and pressure. A much greater variety of products is available in this way than by the iridium chemistry, separation is easier because no solvent is used, and moles rather than millimoles of product are formed.

Mercury Photosensitization

An involatile residue, formed along with the expected products from cyclooctane in the presence of the iridium catalyst and a drop of Hg, resulted from vapor-phase mercury-photosensitized dehydrodimerization of cyclooctane to bicyclooctyl. No iridium was required, and none of the reactions described here require Ir. Photosensitization is not always thought of as an aspect of catalysis. Thermal catalysts use the free energy of the reagents to drive a reaction in a desired way. Photosensitizers channel the energy of a photon into pathways that would otherwise be inaccessible to the system. Thus the overall chemical reaction can be substantially endoergonic and yet proceed (e.g., photosynthesis). Because many alkane reactions are endoergonic, this form of catalysis is particularly suited to alkane conversion.

Hg photosensitization dates from the early part of the century (9). Although several thousand papers have been published in the area, little work has been done since about 1974. The focus of the early work was almost exclusively physicochemical, with kinetics and mechanism receiving the greatest attention. Preparative applications were not usually intended, although occasional examples can be found (10–14). The obstacles to such applications were the paucity of studies on organic compounds of any complexity and the lack of detailed product studies. In addition, relatively few organic preparative reactions are carried out in the vapor phase, and so the appropriate apparatus was not obvious.

Mechanism. The earlier work provides a detailed mechanistic insight. The $^3P_1$ excited state of mercury (Hg*), formed by irradiation at 254 nm, leads to homolytic cleavage of a C–H bond in the vapor phase. Abstraction and recombination of the resulting C-based radicals then takes place. The energy of the Hg* is efficiently channeled into C–H bond cleavage even in large alkanes because the intermediate exciplex probably has the structure {R–H–Hg}*, as suggested by experimental and theoretical work (15–20).

The exciplex then breaks down to R• and {H–Hg}*. In the case of H_2, the exciplex is thought to undergo a rearrangement to {H–Hg–H}* before breaking down to give H atoms and Hg. This reaction is equivalent to an oxidative addition in organometallic chemistry. It illustrates an interesting parallel between the chemistry of Hg* and that of low-valent main group and transition metal ions. It is not known whether a similar rearrangement occurs for {R–H–Hg}*.

$$Hg + h\nu \rightarrow Hg* \tag{1}$$

$$Hg^* + RH \rightarrow \{R{-}H{-}Hg\}^* \rightarrow R\cdot + H\cdot + Hg \qquad (2)$$

$$H\cdot + RH \rightarrow R\cdot + H_2 \qquad (3)$$

$$2R\cdot \rightarrow R_2 \qquad (4)$$
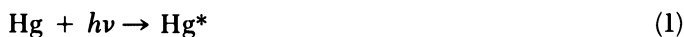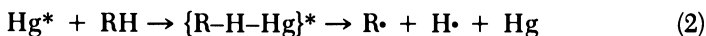
Vapor-Phase Selectivity.   A key feature of the reaction, which differentiates it from a solution-phase radical reaction, is that oligomers tend not to be formed even at high conversions. Normally, the initial product R_2 is intrinsically more reactive than the starting material, RH, and is preferentially attacked by the H-abstracting reagent. In our system, the dimer has so low a vapor pressure that essentially only the original substrate, cyclooctane, is present in the vapor phase, and reaction takes place only in the vapor.

$$\text{(octane ring)} \xrightarrow{Hg^*} \text{(octane ring–octane ring)} + H_2 \qquad (5)$$
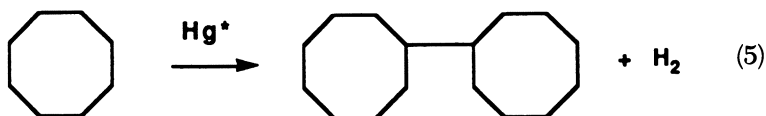
This vapor-phase selectivity effect is very useful (*21, 22*). Instead of the 5–20% conversions usually needed to produce good yields of products from alkanes in solution work, we find excellent selectivity even at 90% conversion. Any product of an alkane functionalization will be less volatile than the starting alkane. Therefore, if the reaction takes place only in the vapor phase, as happens here, then the product condenses and is protected from further conversion. We are now also applying this principle to thermal alkane functionalization.

The reaction only goes in the vapor phase because the photon emitter is a Hg* atom in a low-pressure Hg lamp, which ensures a very narrow emission line. Hg atoms in the vapor phase of the reactor have narrow absorption spectra, and so emitter and receiver are matched. In contrast, Hg atoms in the solution phase suffer continual collisions with the solvent. Their absorption spectrum is strongly broadened and shifted, and therefore mismatched with the emitter. The absorption of light is very inefficient in solution, so the reaction rate is no more than 10^{-3} of the rate of the vapor-phase reaction.

An unexceptional preparative photochemical setup (*21, 22*) can take advantage of this vapor-selectivity effect. The substrate and a drop of mercury are refluxed in a quartz vessel and irradiated at 254 nm with low-pressure Hg lamps. Much poorer rate and selectivity are obtained with medium-pressure lamps. The product dimers quickly return to the liquid phase, and the vapor phase is constantly replenished with substrate. The volume of hydrogen evolved shows the progress of the reaction.

All of the light is absorbed within a millimeter or so of the wall, as shown by running the reaction in two concentric test tubes as reactor. De-

pending on the temperature, if the gap between the tubes is more than a few millimeters, no reaction takes place within the inner reactor because the light has not penetrated sufficiently. The reaction rate goes up with the surface area of the reactor and not with its volume, as expected if all the light is absorbed near the surface. The rate is proportional to the intensity of irradiation if the reactor geometry is held constant.

3° 3° Isomer
35%

+

3° 2° Isomers
65%

(6)
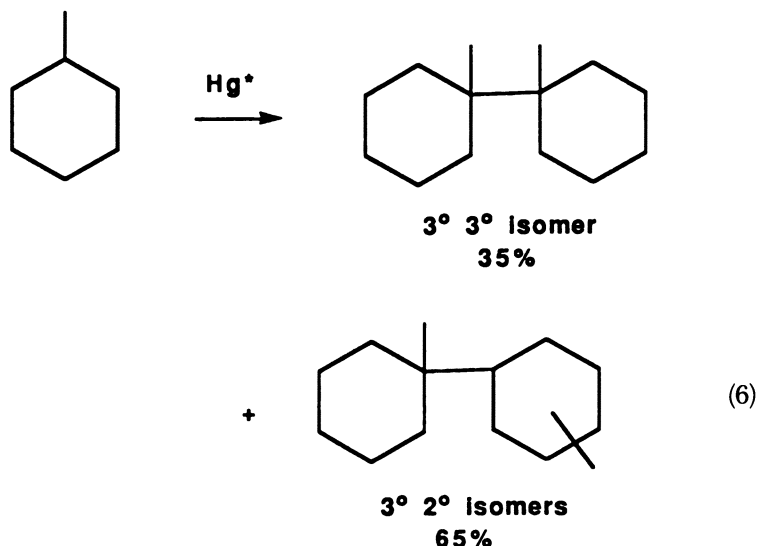
C–H bonds react in the order: tertiary (3°) > secondary (2°) > primary (1°) with a rate ratio of ca. 360:60:1. Thus, the Hg* seeks out the weakest C–H bond in the molecule. The k_h/k_d (ratio of rate constants for protio- and deuterocompounds) of 11 for cyclohexane-d_{12}–cyclohexane at 60 °C is consistent with a homolytic pathway. The 3°–3° dimers are formed very efficiently by reaction of a precursor containing a 3° C–H bond. (We name the dimers after the bond broken, not the bond formed in the process.) Some 3°–2° product is also formed. The product ratio can be altered by diluting the alkane with such gases as N_2 and running the reaction below the boiling point. This procedure leads to increased selectivity for the 3°–3° product by a process to be described in a later section.

Heteroatom-Substituted Species. Of the main classes of organic compounds, alkanes were the chief substrates studied in prior work, although a few previous reports (23–26) dealt with alcohols, ethers, amines, and silanes. We find that reactions involving these and other saturated but heteroatom-substituted species are preparatively useful, especially when carried

out under our conditions. The system is selective for C–H bonds alpha to the heteroatom and for Si–H bonds. For example, Et_3SiH gives $Et_3SiSiEt_3$.

$$CH_3OH \rightarrow HOCH_2CH_2OH \tag{7}$$

$$t\text{-BuOCH}_3 \rightarrow t\text{-BuOCH}_2CH_2O\text{-}t\text{-Bu} \tag{8}$$

50:50 dl:meso
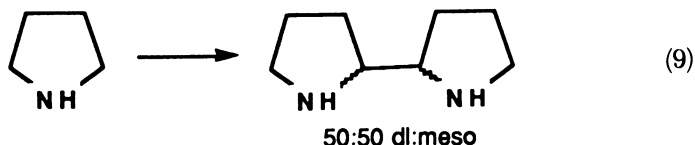
Some other heteroatom-substituted systems are less effective substrates (e.g., some amines). This difference may exist because the Hg* preferentially binds to the more basic lone pairs of the heteroatom and not to the C–H bonds of the molecule. Exciplex formation between the Hg* and the substrate has been demonstrated (*15–18*). This process explains how the energy of the Hg* can be efficiently channeled into one bond of a large substrate. The order of binding energy is roughly what would be expected for a relatively soft transition metal ion. For example, the binding energy of Hg* with NH_3 (17 kcal mol^{-1}) greatly exceeds that for Hg* with CH_4 (2 kcal mol^{-1}) (*15–18*).

Functionalized Product. Alkanes can be functionalized by cross-dimerization with other species. Equation 10 shows the results from the reaction of cyclohexane and methanol. The three products are formed in close to statistical amounts after the relative vapor pressures and reactivities of the two species have been taken into account. The polarities of the three products in eq 10 are so different that separation is easy; the glycol can be removed by solvent extraction with water, and the bicyclo-hexyl–cyclohexylmethanol mixture can be separated by column chromatography.

(10)
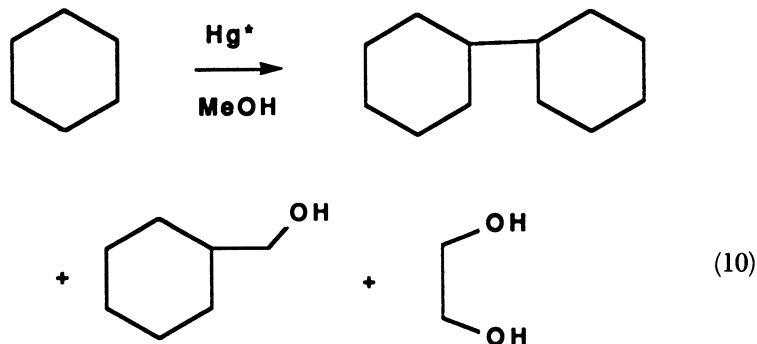
If the cyclohexane:methanol ratio in the vapor phase is adjusted to favor methanol, then the product mix is skewed in favor of glycol and cross-product. Under these conditions of "vapor-pressure biasing" we obtain a product mixture that can be purified by simple water wash, because the bicyclohexyl formation is minimal. This arrangement also gives the largest yield of functionalized alkane, based on alkane.

Cyclohexane and trioxane, the formaldehyde trimer, give an acetal on cross-dimerization. In turn, the acetal yields cyclohexanecarboxyaldehyde on hydrolysis (eq 11). Similarly, a protected form of prolinal is formed from trioxan and pyrrolidine. These aldehydes are the same products that might be formed by hydroformylation. However, we start from the alkane (not the alkene) and we see a wider functional group tolerance than for hydroformylation.

(+ homo-dimers)

$$ \xrightarrow{\text{H}^+} \qquad (11) $$
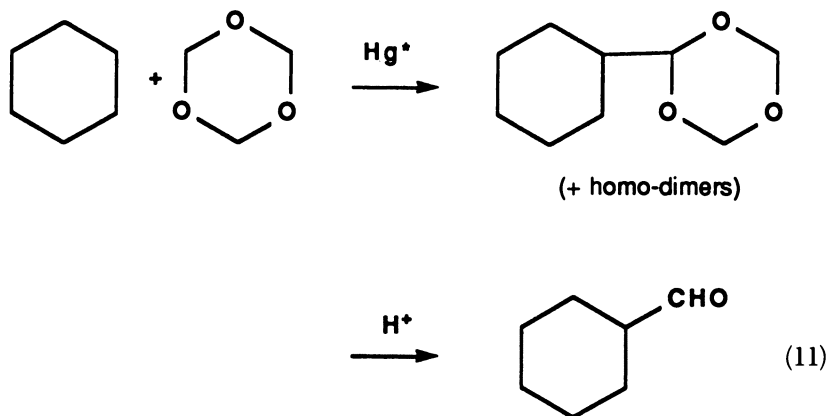
$R_3SiCH(CH_3)OH$ is obtained from the silane R_3Si-H and ethanol in spite of the much greater strength of Si–O over Si–C bonds. This difference favors the formation of an ethoxysilane (R_3SiOEt) in all other reactions of silanes with alcohols. Hydroxymethyl ethers are formed from alcohols and ethers (eq 12).

(+ homo dimers)   (12)
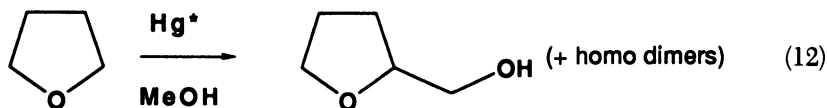
Tens of grams of functionalized product can be obtained over 24 h, and there does not seem to be any upper limit to the number of catalytic cycles possible. Under certain conditions, up to 10^4 turnovers can be observed per Hg atom without a measurable decrease in reaction rate. The buildup of colored impurities tends to stop photochemical reactions in reactors with solid walls. In our reactor the walls consist of a film of falling liquid (the refluxing substrate), and no buildup takes place.

The system may therefore have advantages over the more complicated metal phosphine catalysts such as $[IrH_2(O_2CCF_3)(PR_3)_2]$, which have many more deactivation pathways open to them. None of the published examples, reported by us (*2, 3*), by Felkin and co-workers (*27–31*), or by Sakakura and Tanaka (*32*), had very stable catalysts. On the other hand, metal phosphine catalysts do have the very useful property of selectively attacking the least hindered C–H bond in the alkane, in contrast to the selectivity pattern observed in the Hg system and in all the "classical" alkane functionalization reactions based on radicals and carbonium ions.

The reason for the different selectivities of the two systems is believed to be the steric bulk of a catalyst such as $RhCl(CO)L_2$, compared with the smaller Hg atom; the sterically demanding side-on transition state probably operates in both cases (*1, 5*). This picture may be oversimplified, however, because of the uncertainty in the structure of the transition state for Hg* reactions.

$$M \begin{array}{c} H \\ | \\ C \end{array}$$
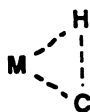
Methane has relatively strong C–H bonds and normally does not react readily with Hg*, but we have recently found conditions under which even this substrate can be activated. In the presence of N_2O, the Hg* attacks the N_2O to release an O atom. This atom abstracts H largely from methanol, also present in the vapor, to give $\cdot CH_2OH$ and $\cdot OH$. The hydroxyl radical formed in this step is sufficiently reactive to attack methane. Some of the resulting methyl radicals cross-dimerize with CH_2OH to give ethanol, which is still volatile under our conditions and so tends to cross-dimerize with methanol to give propylene glycol (*33*).

Alkane Dimerization.   An important feature of the Hg*–alkane reaction is that only a trace of alkene is formed in alkane dimerization. Yet, especially for tertiary radicals, disproportionation to give alkene is known to be rapid. Alkene does not build up because hydrogen atoms, also present as a result of eq 5, react very rapidly with alkenes to form the most substituted radical, as shown in eq 13.

$$RCH=CH_2 \xrightarrow{H\cdot} RCH\cdot-CH_3 \qquad (13)$$

This process recycles the alkene back into the radical pool and prevents it from building up. We were able to verify that this was happening by running an alkane dimerization under D_2. In this case, selective D incorporation was observed at positions beta to the newly formed C–C bond in the dimer, as expected on the basis of eq 16.

Disproportionation also occurs in dimerizations of light alcohols. Once again, we do not observe a substantial buildup of the expected ketone or aldehyde product. The reason this time is not that H atoms attack the carbonyl, but rather that the disproportionation product is more volatile than the alcohol and selectively distills out of the reactor in the H_2 stream under the reaction conditions. Using a trap at -80 °C allows the expected quantity of carbonyl compound to be collected. For heavier alcohols, RCH_2OH, the aldehyde disproportionation product is not as volatile and aldehyde-derived products such as $RCH(OCH_2R)_2$ are found in the products.

Reactions Involving H Atoms

H atoms have not been used widely in preparative work, perhaps because some of the methods (34) often used for their synthesis (e.g., radiolysis of water, passing H_2 over a hot tungsten wire, and microwave discharge) are not convenient for synthetic application. A few such studies have been reported, however (35–37). Mercury photosensitization of H_2 is a very efficient way of forming useful amounts of H atoms under ambient conditions.

The reactions of H atoms shown in eqs 3 and 13 suggested that this chemistry might be useful for the sorts of reactions we studied, with the advantage of working even for substrates that would not react under the Hg* conditions. The reaction of Hg* with H_2 to give H atoms is exceptionally efficient, and, if eq 3 is correct, these H atoms should be efficient H abstractors. When we tried to dehydrodimerize unsaturated organic compounds (such as alkenes, ketones, or carboxylic acids) under the Hg* conditions described, we obtained other products, often as mixtures. We thought that this might be the result of the soft Hg* attacking the double bond or the heteroatom lone pairs directly and not the C–H bonds.

H atoms do indeed become the abstracting reagents if the usual Hg* reaction is run not at reflux, but instead at 20–50 °C below the boiling point of the reagent in an atmosphere of H_2 gas. H_2 and not the substrate quenches the Hg*. The resulting H atoms carry out the desired chemistry, and essentially no Hg*-derived products are seen (38). Hg* itself does not photosensitize the substrate directly because it always reacts with H_2 first. H_2, present in excess and with a high quenching cross-section, also has a very high average molecular speed in the vapor, which increases its frequency of collisions. The result of the quenching is that H• replaces Hg* as the principal high-energy reagent in the system.

Alkene as Substrate. For one class of substrate we see a different reactivity pattern. If the substrate is an alkene, then the sequence of events shown in eqs 14–17 seems to occur.

$$Hg + h\nu \rightarrow Hg^* \tag{14}$$

$$Hg^* + H_2 \rightarrow 2H + Hg \qquad (15)$$

$$H + RCH=CH_2 \rightarrow RCH–CH_3 \qquad (16)$$

$$2RCH–CH_3 \rightarrow R(CH_3)CH–CH(CH_3)R \qquad (17)$$
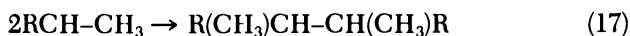
The result is that the hydrodimer is formed from the 1-alkene. The selectivity for H atom attack on alkenes has been determined (*39*). The attack is largely (ca. 95% for a 1-alkene) at the terminal position to give the stabler 2° alkyl radical. The product of hydrodimerization is therefore largely the 2,2′-isomer, but some 1,2-dimer is also seen. The position of the double bond in the starting material therefore governs the position at which the new C–C bond is formed. For example, 1-hexene gives 85% of 2,2′-bihexyl, and 3-hexene gives essentially only 3,3′-bihexyl.

This specificity has been very useful to us in identifying products from dehydrodimerization of the saturated species. For example 2,2′-, 2,3′-, and 3,3′-bihexyl are all formed from hexane but can be identified by comparison with the hydrodimerization products of 1-, 2-, and 3-hexene.

Functional Groups.   The H atom reaction tolerates functionality not tolerated by Hg* itself. For example, compounds with double bonds (such as acids, esters, or amides) or with strained rings (such as epoxides) do not react cleanly with Hg*. If a substrate containing this functionality also has a C=C double bond, then the H atom selectively attacks the C=C double bond and the functionalized dimer forms normally. Chart I shows some of the compounds that can be made from alkenes in this way. We were very pleased to see that unsaturated esters and acids are dimerized, but the fact that unsaturated epoxides can be used was a great surprise. The case of fluoroalkenes is significant, because there are no other ways of making the fluorinated hydrodimers.

The fact that the H atom method tolerates so many functional groups in the case of substituted alkenes led us to try the reaction of H atoms on saturated functionalized substrates. We were very glad to see that these too react to produce dehydrodimer (*40*). Ketones are attacked in the α-position. Carboxylic acids and esters are also dimerized. In the case of the ester RCO_2R', abstraction takes place at R or R′, according to the usual reactivity order: 3° > 2° > 1°. If R and R′ are the same, attack tends to take place at the position adjacent to C rather than O. The use of *t*-Bu or Me as R or R′ protects that R group from attack.

Even in cases where the dehydrodimer can be made with Hg* as abstractor, the H atom variant is still sometimes useful because it is more selective. For example, the α,α-dimer is only 40% of the product from Et_2NH with Hg*, but 90% with H atoms. Once again, cross-dimerization is possible, although we have not studied very many examples to date. Chart II shows some of the compounds that can be made via H atom reactions with saturated substrates.
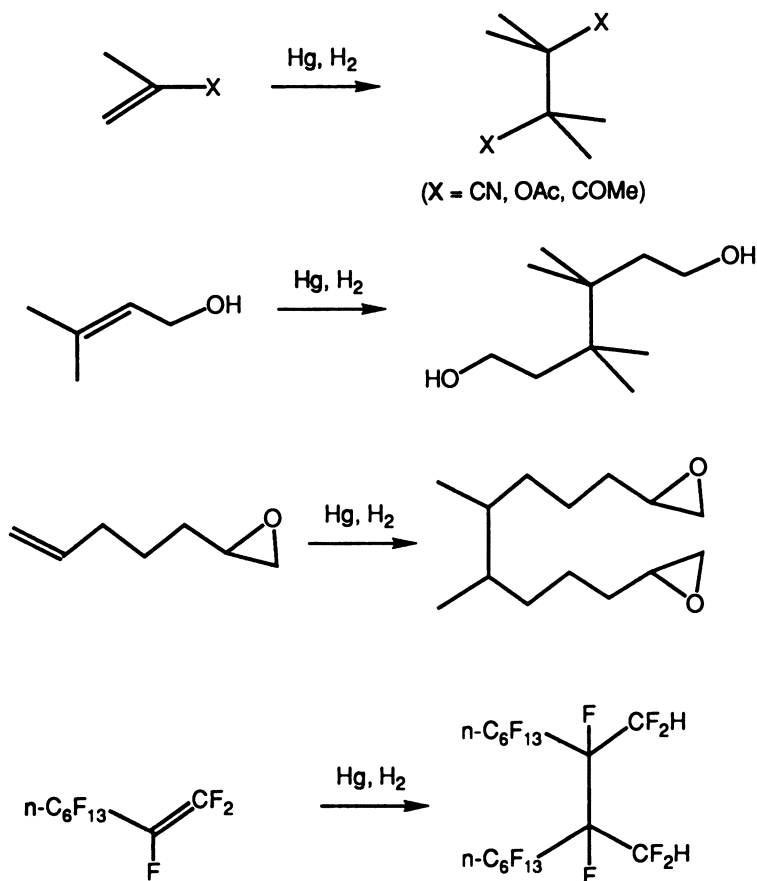
Chart I. Some compounds that can be made from alkenes by H atom chemistry.

Quantitative Studies

In the Hg* work, the reaction rate is linear with irradiation time and is limited by the number of photons produced by the lamps. Quantum yields for good substrates vary between 0.14 (isobutane) and 0.8 (Et_3SiH); they are low when considerable disproportionation takes place. 1°:2°:3° selectivity for alkanes is ca. 1:50:350. Linear alkanes give a mixture of all possible 2°–2° dimers. Singly branched alkanes give all possible 2°–3° and 3°–3° dimers. For doubly or multiply branched alkanes, the product ratio can be affected by steric effects. When multiple 1,3-*syn* diaxial repulsions of alkyl groups are created in a dimerization, that dimerization is disfavored. If more than four such interactions are present, the dimer in question is never seen.

If mixing within the reactor is good, for example under reflux conditions, then a statistical ratio of homo- and cross-dimers will be seen. From R^1–H
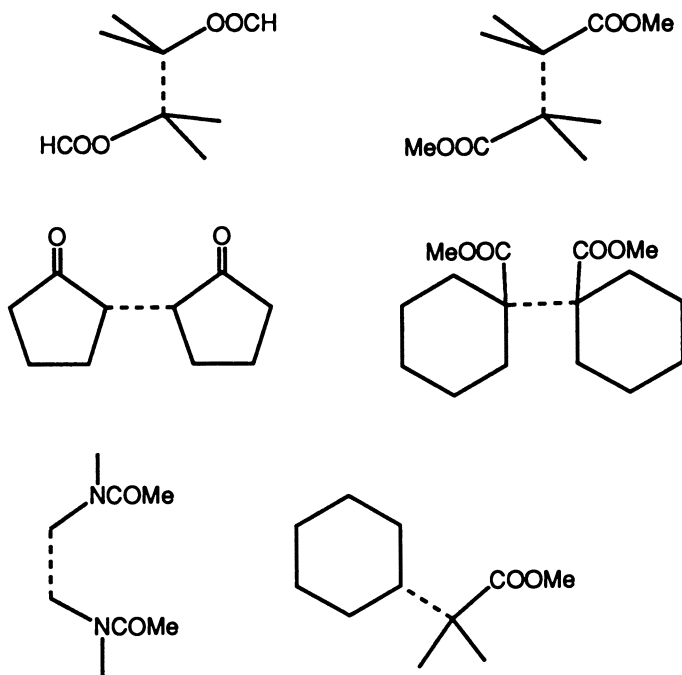
Chart II. Some compounds that can be made from saturated substrates by H atom chemistry. The dotted line shows the new C–C bond formed.

and R^2–H, the ratios of R^1–R^1:R^1–R^2:R^2–R^2 will be x^2:$2xy$:y^2, where x and y reflect the ratio of radicals formed in the gas phase. As noted in a series of patents by Cier (*41*), an empirical relationship exists between the relative reactivity of different alkane substrates and the strength of the weakest C–H bonds in the molecule. Equation 18, which can be deduced from the Evans–Polanyi and Arrhenius relationships, fits the observations rather well and allows the relative reactivities of different substrates to be estimated. Because of exciplex formation, this relationship breaks down for substrates with heteroatoms. Moving to H atoms as abstractors restores the validity of eq 18 for organic compounds with functional groups. In several cases we have been able to obtain bond strengths for compounds for which no previous measurement is available.

$$\frac{r_1}{r_2} = \left(\frac{b_2}{b_1}\right)\left[\exp\left\{\frac{E_1 - E_2}{RT}\right\}\right] \tag{18}$$

where r_1/r_2 is the ratio of radicals in the products, b_n is the number of the weakest C–H bonds in each substrate, E_n is the bond energy of the weakest bonds, R is the gas constant, and T is absolute temperature.

Knowing this ratio and the vapor pressures of the two substrates gives the relative reactivity of each substrate, which we call ρ. We base the scale on MeOH as unity, in which case reactivities for common substrates are cyclohexane, 12; ethanol, 20; isobutane or THF, 70; and Et_3SiH, 700. Similar studies on the hydrogen atom system are still in progress.

Trapping the Radicals

In more recent work (42), we find that SO_2 can trap the radicals formed from the reaction of alkanes with Hg*. In this case, a rather complex product mixture is found, but subsequent oxidation with performic acid leads in large part to the formation of the sulfonic acid RSO_3H. CO is a less efficient trap, but some ketone from cyclohexane is observed. The case of Hg–O_2–RH, in which the hydroperoxide ROOH is the main product, is somewhat different. Here even methane is attacked (43). The Hg* attack on methane is inefficient because of the high C–H bond strength. This explanation implies that the Hg* attacks the O_2 to give a highly reactive oxygen-containing intermediate, which then attacks the alkane. The details remain to be worked out.

Conclusions

The Hg and H atom systems are capable of rapidly assembling relatively complex molecules from simple starting materials, and doing so on a preparatively useful scale. The principle that selectivity for the partial oxidation product may be achieved by physical separation of reactants and products may also be applicable to thermal alkane conversion. The selective oxidation of methane to methanol may be an example.

The outcome of the any particular reaction can usually be predicted by consulting the quantitative data we obtained and using the appropriate equations. No organomercury compounds have ever been detected in these reactions, either because they are never formed or because they are photolyzed under the reaction conditions. The small amount of elemental Hg in the product and in the exit gases can be effectively removed with Zn dust if desired.

Acknowledgments

References

1. Crabtree, R. H. *Chem. Rev.* **1985**, *85*, 245.
2. Burk, M. J.; Crabtree, R. H.; McGrath, D. V. *J. Chem. Soc. D* **1985**, 1829.

3. Burk, M. J.; Crabtree, R. H. *J. Am. Chem. Soc.* **1987**, *109*, 8025.
4. Crabtree, R. H.; Mihelcic, J. M.; Quirk, J. M. *J. Am. Chem. Soc.* **1979**, *101*, 7738.
5. Crabtree, R. H.; Mellea, M. F.; Mihelcic, J. M.; Quirk, J. M. *J. Am. Chem. Soc.* **1982**, *104*, 107.
6. Burk, M. J.; Crabtree, R. H.; Parnell, C. P.; Uriarte, R. J. *Organometallics* **1984**, *3*, 816.
7. Crabtree, R. H.; Dion, R. P.; Gibboni, D. J.; McGrath, D. V.; Holt, E. M. *J. Am. Chem. Soc.* **1986**, *108*, 7222.
8. Anton, D. R.; Crabtree, R. H. *Organometallics* **1983**, *2*, 855.
9. Cvetanovic, R. J. *Prog. React. Kinet.* **1964**, *2*, 77.
10. Dalton, J. C. *Org. Photochem.* **1985**, *7*, 149.
11. Inoue, Y.; Takamuku, S.; Sakurai, H. *Can. J Chem.* **1976**, *54*, 3117.
12. Lemal, D. M.; Shim, K. S. *J. Am. Chem. Soc.* **1964**, *86*, 1550.
13. Niki, H.; Mains, G. J. *J. Phys. Chem.* **1964**, *68*, 304.
14. Plotkin, J. S.; Sneddon, L. G. *J. Am. Chem. Soc.* **1979**, *101*, 4155.
15. Breckenridge, W. H.; Jouvet, C.; Soep, B. *J. Chem. Phys.* **1986**, *84*, 1443.
16. Duval-Ete, M. C. Thesis, University of Paris, Orsay, France, 1988.
17. Duval, M. C.; Soep, B. *Chem. Phys. Lett.* **1987**, 141.
18. Duval, M. C.; Soep, B.; van Zee, R. D.; Bosma, W. B.; Zwier, T. S. *J. Chem. Phys.* **1988**, *88*, 2148.
19. Bernier, A.; Millie, P. *J. Chem. Phys.* **1988**, *88*, 4843.
20. Bernier, A.; Millie, P.; Pelissier, M. *J. Chem. Phys.* **1986**, *106*, 195.
21. Brown, S. H.; Crabtree, R. H. *J. Chem. Soc. D* **1987**, 970.
22. Brown, S. H.; Crabtree, R. H. *J. Am. Chem. Soc.* **1989**, *111*, 2935, 2946.
23. Porter, R. F. *Inorg. Chem.* **1980**, *19*, 447.
24. Plotkin, J. S.; Sneddon, L. G. *J. Am. Chem. Soc.* **1979**, *101*, 4155.
25. Nay, M. A.; Woodall, G. N. C.; Strausz, O. P.; Gunning, H. E. *J. Am. Chem. Soc.* **1965**, *87*, 179.
26. Mains, G. J. *Inorg. Chem.* **1966**, *5*, 114.
27. (a) Baudry, D.; Ephritikine, M.; Felkin, H. *J. Chem. Soc. D* **1982**, 606; (b) Baudry, D.; Ephritikine, M.; Felkin, H. *J. Chem. Soc. D* **1983**, 788.
28. (a) Baudry, D.; Ephritikine, M.; Felkin, H.; Zakrzewski, J. *J. Chem. Soc. D* **1982**, 1235; (b) Baudry, D.; Ephritikine, M.; Felkin, H.; Zakrzewski, J. *Tetrahedron Lett.* **1984**, 1283.
29. Felkin, H.; Fillebeen-Khan, T.; Gault, Y.; Holmes-Smith, R.; Zakrzewski, J. *Tetrahedron Lett.* **1984**, 1279.
30. Cameron, C. J.; Felkin, H.; Fillebeen-Khan, T.; Forrow, N. J.; Guittet, E. *J. Chem. Soc. D* **1986**, 801.
31. Felkin, H.; Fillebeen-Khan, T.; Holmes-Smith, R.; Lin, Y. *Tetrahedron Lett.* **1985**, *26*, 1999.
32. Sakakura, T.; Tanaka, M. *J. Chem. Soc. D* **1987**, 758.
33. Ferguson, R. R.; Crabtree, R. H. *Nouv. J. Chem.* **1989**, *13*, 647.
34. Neta, P. *Chem. Rev.* **1972**, *72*, 533.
35. Vaughan, W. E.; Rust, F. F. *J. Org. Chem.* **1942**, *7*, 472.
36. Baum, A. A.; Karnischky, L. A.; McLeod, D., Jr.; Kasai, P. H. *J. Am. Chem. Soc.* **1973**, *95*, 617.
37. Beeri, A.; Berman, E.; Vishkautsan, R.; Mazur, Y. *J. Am. Chem. Soc.* **1986**, *108*, 6413.
38. Muedas, C. A.; Ferguson, R. R.; Crabtree, R. H. *Tetrahedron Lett.* **1989**, *30*, 3389.
39. Falconer, W. E.; Sunder, W. A. *Int. J. Chem. Kinet.* **1971**, *3*, 395.

40. Boojamra, C. G.; Crabtree, R. H.; Ferguson, R. R.; Muedas, C. A. *Tetrahedron Lett.* **1989,** *30,* 5583.
41. Cier, H. U.S. Patent 2 640 023, 1953; 2 655 474, 1953; 2 762 768, 1956.
42. Ferguson, R. R.; Crabtree, R. H. *J. Org. Chem.* **1991,** *56,* 5503.
43. Gray, J. A. *J. Chem. Soc.* **1952,** 3150.

14

Activation of Carbon–Hydrogen Bonds in Alkanes and Other Organic Molecules Using Organotransition Metal Complexes

Robert G. Bergman

Department of Chemistry, University of California, Berkeley, and Materials and Chemical Sciences Division, Lawrence Berkeley Laboratory, Berkeley, CA 94720

The scope, selectivity, and mechanism of reactions in which low-valent iridium and rhodium complexes undergo intermolecular C–H oxidative addition reactions were investigated. Progress was made on the development of stoichiometric methods for converting the metal complexes formed by C–H activation into functionalized organic molecules. In an effort to locate an inert solvent for the reaction, C–H activation reactions were carried out in liquefied noble gases such as liquid xenon and liquid krypton. This approach allowed us to directly examine the C–H activation reactivity of gaseous and solid substrates. It also provided a means for carrying out flash kinetic studies designed to generate transient coordinatively unsaturated metal complexes and directly measure the rates of their reactions with C–H bonds.

$\mathbf{A}$LKANES ARE AMONG THE MOST CHEMICALLY INERT organic molecules. The potential for using alkanes as feedstocks in chemical synthesis has stimulated a search for metal complexes capable of undergoing the C–H oxidative addition process shown in eq 1, so that alkane chemistry more selective than that available using free radical reagents might be developed (*1–3*).

$$M + R\text{–}H \rightarrow R\text{–}M\text{–}H \tag{1}$$

Intramolecular C–H oxidative addition to metal centers has been known for some time. However, despite many efforts the corresponding intermolecular C–H oxidative addition process illustrated in eq 1 was not observed directly until 1982. At that time our group (*4, 5*) and Graham's (*6*) independently found that irradiation of complexes such as Cp*(L)IrH$_2$ [1, Cp* is (η^5-C$_5$Me$_5$), L is PMe$_3$)] and Cp*Ir(CO)$_2$ causes successful insertion of the Cp*IrL fragment into C–H bonds in alkanes. This procedure leads to stable alkyliridium hydride complexes Cp*(L)Ir(R)(H) (**2**). This reaction is exceedingly general. So far no organic liquid in which Cp*(L)IrH$_2$ has been irradiated has failed to react with the intermediate generated in the reaction. Some of the solvents that have been observed to give intermolecular C–H insertion products upon irradiation of **1** are illustrated in Scheme I.
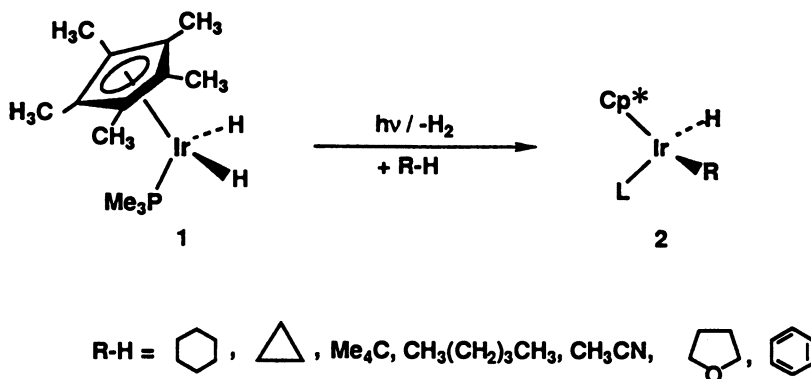
Scheme I.

Characteristics of Oxidative Addition Reactions

Much has been learned about the scope and mechanism of this reaction (*7–9*). Following our initial studies with iridium, alkane C–H oxidative addition was observed at several other second- and third-row transition metal centers (where M–H and M–R bonds are expected to be relatively strong) such as rhodium, rhenium, platinum, and osmium, and even at one first-row metal, iron (*10–14*).

The selectivity of the iridium and rhodium C–H oxidative addition reaction was investigated by carrying out competition studies with various hydrocarbon substrates. The results are summarized in Scheme II. Although the absolute magnitudes of the selectivities are different for Ir and Rh, their trends are parallel. This observation indicates that C–H oxidative additions proceed by similar mechanisms at these two metal centers, but that the Rh reactions are less exothermic than their Ir counterparts. The selectivity experiments also suggest that steric effects and C–H acidities, rather than

	$\hexagon$	$\pentagon$	$\triangle$	$\heptagon$	$\octagon$		$\curlywedge$	$\hexagon$
$k_{rel}(Ir)$	1.0	1.6	2.63	-	0.09	0.23	-	4.0
$k_{rel}(Rh)$	1.0	1.8	10.4	0.14	0.06	-	3.6	19.5
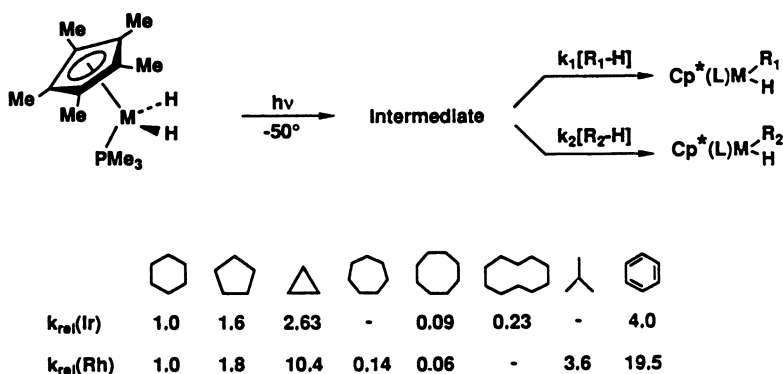
Scheme II.

bond energies, control the rate of attack of the metal center on particular C–H bonds.

The oxidative addition reaction is reversible. In the rhodium series most Cp*(L)Rh(R)(H) complexes, which are much less stable than their iridium analogs, eliminate R–H at temperatures below 0 °C. A similar reaction takes place on heating the more stable iridium alkyl hydrides, Cp*(L)Ir(R)(H), to temperatures above 100 °C. This procedure provides a thermal, rather than photochemical, method for carrying out the C–H insertion reaction. Kinetic studies are consistent with a rate-determining step in which R–H is eliminated from the starting coordinatively saturated (18-electron) alkyl hydride. This elimination yields a very reactive intermediate that can then be trapped by other hydrocarbons.

Strong evidence (8, 9) has been obtained that the reactive species responsible for the C–H insertion reaction in benzene and other aromatic solvents are π- (or "η^2-arene") complexes. More recently, evidence (10, 11) has been obtained that analogous, but more weakly bound, alkane "σ-complex" intermediates intervene in the saturated hydrocarbon oxidative addition process before full C–H bond cleavage occurs.

In combination with conventional and photoacoustic calorimetric investigations, the thermal reactions have also provided information about absolute iridium–carbon and iridium–hydrogen bond energies. These in turn have given us a quantitative idea of the thermodynamic driving force for the C–H oxidative addition reaction (15). The energetics of the processes that occur when an alkyl and phenyl C–H bond are exchanged at iridium (from our work) and rhodium (from the work of Jones and Feher (16)) demonstrate that the overall conversion of alkyl hydride to phenyl hydride is exothermic in both systems. However, each alkyl hydride must surmount a significant energy barrier to reach the intermediates that are capable of reacting with C–H bonds in another molecule of alkane or arene.

Unanswered Questions

The studies just summarized raise a number of important questions about the C–H oxidative addition process. Some of these questions are being addressed in current work, and preliminary results are illustrated in Scheme III. Unlike many C–H oxidative addition systems studied earlier, intramolecular cyclometallation products such as 3 and 4 are never observed in our system; the reactions are exclusively intermolecular. We would like to know the physical basis for this unusual selectivity.

Another question concerns whether the photochemical and thermal reactions proceed by analogous mechanisms. As shown in Scheme III, if thermal decomposition of hydrido(alkyl) complex 2 and photochemical decomposition of dihydride 1 both pass through coordinatively unsaturated species Cp*IrL, then when mixtures of alkane solvents are used, similar selectivities should be observed in the two reactions. However, it is possible that in the thermal reaction, one alkane complex (e.g., 5) might be converted to another (6) by a direct process that avoids Cp*IrL. Similarly, irradiation of 1 (which presumably gives initially the electronically excited state 1*) might be attacked directly by a hydrocarbon substrate R–H. This attack could lead to intermediate 7, which would subsequently lose H_2 in a second step. In this case, it is possible that the thermal and photochemical reactions would give different selectivities. We are attempting to distinguish these possibilities
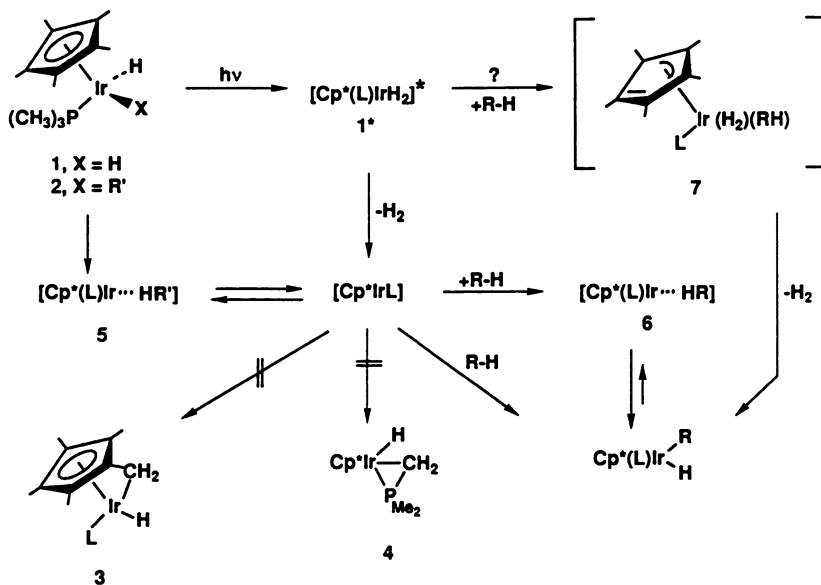
Scheme III.

by developing methods to carefully examine the selectivity exhibited by the photochemical and thermal iridium reactions in mixtures of alkane solvents under precisely identical conditions.

Conversion to Functionalized Organic Molecules

We are also working on the development of methods for the conversion of alkane oxidative addition products to functionalized organic molecules. We have found it possible to convert alkylmetal hydrides to organic halides by using the sequences outlined in Scheme IV (*4, 5, 10, 11*). However, it would be substantially more useful to generate functionalized molecules by a combination of C–H oxidative addition and migratory insertion reactions with a second molecule, such as CO or CO_2. Unfortunately, it is very difficult to generate an open coordination site in the Cp*(L)M(R)(H) oxidative addition products. As a result, these materials have resisted attempts to induce them to undergo migratory insertion.
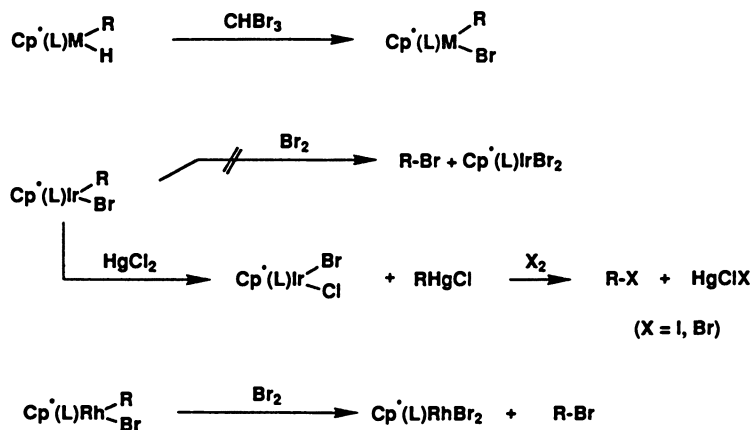
Scheme IV.

We have made some progress on this problem by replacing the Cp* ligand with an indenyl (Ind) ligand. This ligand undergoes much easier interconversion between its η^5 and η^3 configurations. Thus it provides a means of opening up a coordination site at the metal center to which it is complexed. Synthetic routes to (Ind)(L)IrR$_1$R$_2$ (R$_1$ and R$_2$ are alkyl and H) complexes have been worked out. As expected, migratory insertion of CO and other ligands occurs much more rapidly than in the corresponding Cp* complexes. Combined C–H oxidative addition–migratory insertion processes are now being developed that use these indenyl systems (Scheme V) (*17*).
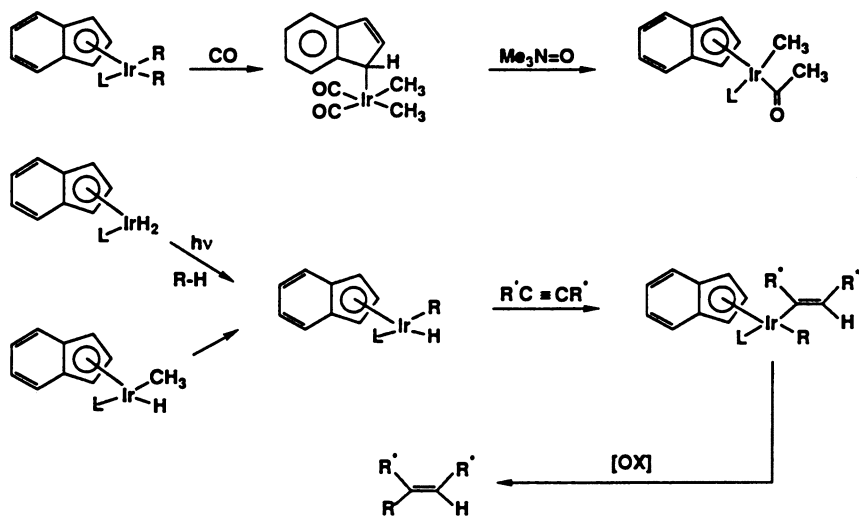
Scheme V.

Effect of Functional Groups

Most of our initial studies were directed toward the investigation of C–H oxidative addition in alkanes. We have recently begun to investigate the interaction of C–H activating iridium and rhodium complexes with functionalized organic molecules to determine the effect of functional groups on the process as well as to investigate the propensity of Ir and Rh to insert into C–H versus other types of X–H bonds.

Scheme VI illustrates some of our initial results. Reaction with ethylene gives both a π-complex and a C–H insertion product. The π-complex is stable to the reaction conditions (in fact, it is the thermodynamic product of the reaction), and so it cannot be an intermediate in the C–H insertion (*18, 19*). When the reaction is carried out in alcohol or amine solvents C–H insertion appears to occur in preference to O–H insertion (*20*), although with methanol and ethanol surprising products are produced by subsequent transformation of the proposed initially formed insertion products (*21*).

Studies in Liquefied Noble Gas Solvents

As mentioned earlier, we have not yet found an organic liquid that is unreactive toward iridium, so that it might be used as an inert solvent in these reactions. While such ubiquitous reactivity is useful for carrying out chemical transformations on normally recalcitrant substrates, it presents a problem in another sense. It has prevented us from investigating the C–H insertion propensity of substrates that are difficult to liquefy under easily accessible
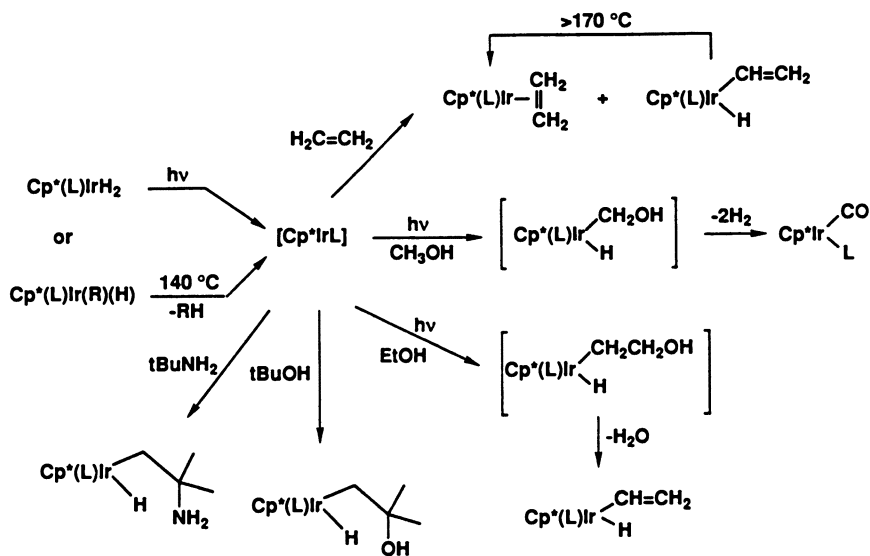
Scheme VI.

conditions (e.g., solids or gases with very low boiling points). Even fluorocarbons, we have found, react with the intermediates generated on irradiation of Cp*(L)IrH$_2$, probably by electron-transfer pathways (22).

To solve this problem we investigated the use of liquid xenon as a potential inert solvent for iridium C–H oxidative addition reactions. Hydrocarbons are known to have reasonable solubility in xenon, and we have found that Cp*(L)IrH$_2$ exhibits this property as well. Xenon (liquefied at –70 °C and 10 atm of pressure), serves as an inert solvent for the C–H oxidative addition reaction (22). The C–H oxidative addition chemistry that we observed in this medium is summarized in Scheme VII.

We prepared and isolated, for the first time, C–H oxidative addition products formed from high-melting solid substrates such as naphthalene, adamantane, and even cubane. The cubane reaction represents the first observation of C–H oxidative addition at a tertiary C–H bond. Liquid xenon also enabled us to carry out more conveniently the C–H oxidative addition reactions of low-boiling gases that are difficult to liquefy, such as methane. Finally, methanol and ethanol give O–H oxidative addition products in liquid xenon. This reaction contrasts with their behavior at higher temperatures in neat alcohol solvents, in which products believed to be derived from initial C–H activation are observed. The reasons for this unusual change in behavior are not yet understood.

In addition to these preparative studies, we also used liquefied noble gases as inert solvents for carrying out time-resolved flash kinetic studies with infrared detection. These experiments, designed to generate transient

([Ir] = Cp*IrPMe₃)
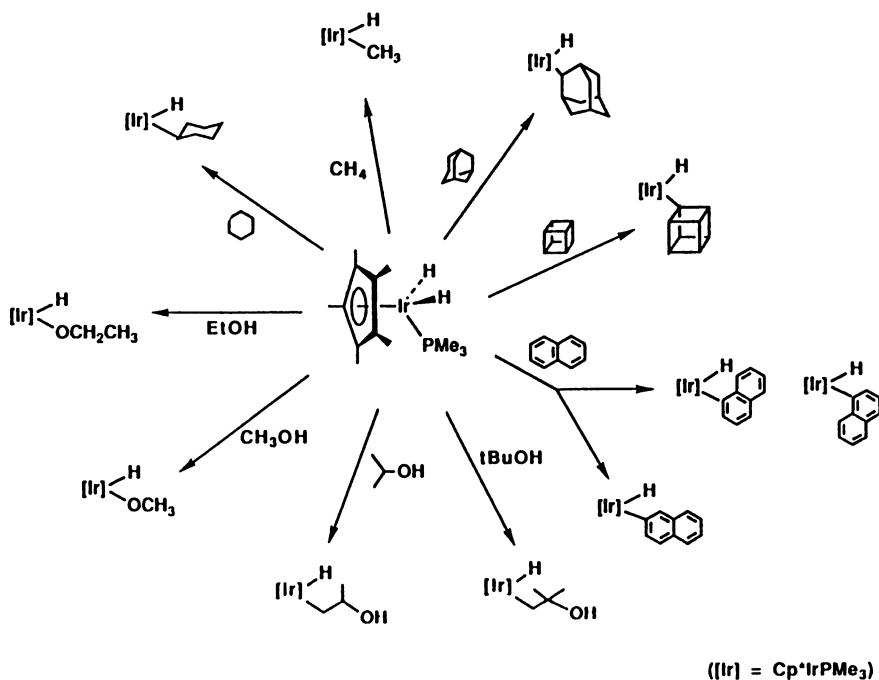
*Scheme VII. Products formed on irradiation of solutions of 1 and the indicated
organic molecules in liquid xenon at –60 to –75 °C.*

coordinatively unsaturated C–H activating intermediates, directly measure
the rates of their reactions with C–H bonds (23). In this case, Cp*Rh(CO)₂
was used to take advantage of the higher quantum yields in the rhodium
system and the large IR extinction coefficients observed in metal carbonyl
complexes. Irradiation of the rhodium dicarbonyl complex in liquid krypton
between –90 and –120 °C gave rise to a transient metal–CO absorption at
1947 cm⁻¹, which decayed rapidly in the presence of cyclohexane and led
to Cp*(CO)Rh(H)(C₆H₁₁).

By examining the dependence of the decay rates on the concentration
of cyclohexane (Figure 1) and cyclohexane-d_{12}, we concluded that the tran-
sient IR absorption results from a rapidly equilibrating mixture of the
krypton complex Cp*Rh(CO)(Kr) and the cyclohexane σ-complex
Cp*Rh(CO)(C₆H₁₂). The latter predominates at high cyclohexane concen-
trations. Under these conditions the rate of direct conversion of the cy-
clohexane complex to the C–H oxidative addition product
Cp*(CO)Rh(H)(C₆H₁₁) can be measured. From the temperature dependence
of this rate constant, we determined that the activation energy associated
with this process is 4.8 kcal/mol.

Recently we carried out analogous studies in the gas phase. Under these
conditions "naked" rather than solvated Cp*Rh(CO) is formed, and this
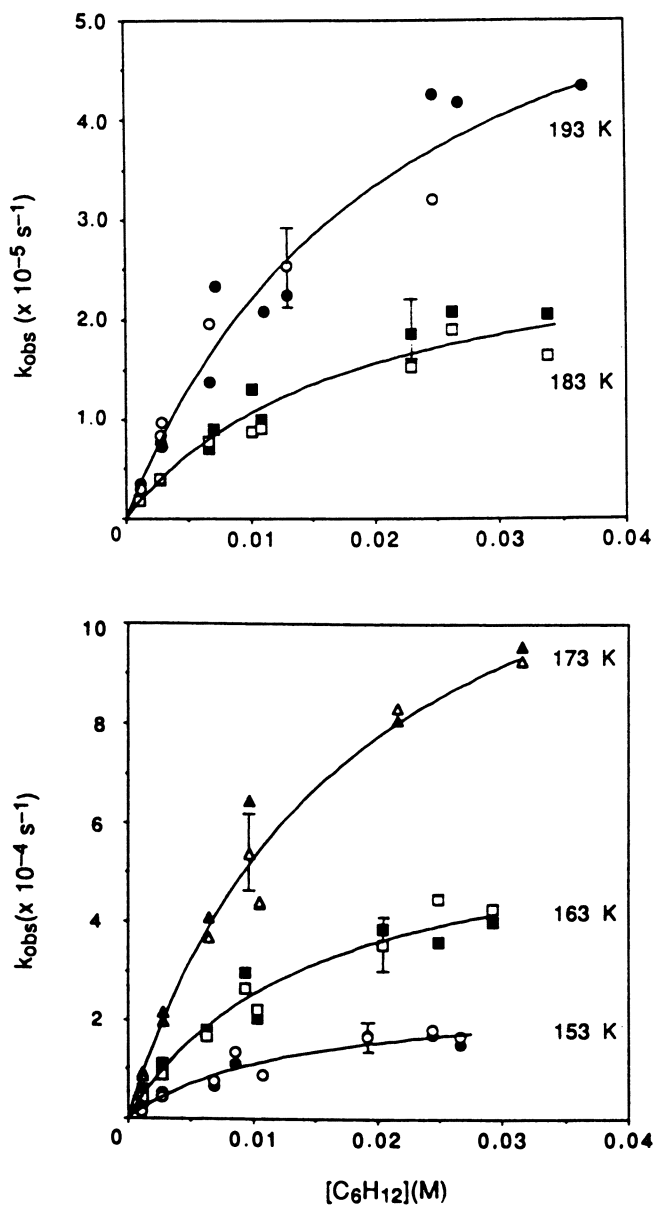
Figure 1. The observed rate constants (k_{obs}) for the decay of the transient at 1947 cm^{-1} (filled symbols) and for the formation of the product at 2003 cm^{-1} (open symbols) as a function of cyclohexane concentration and temperature. For clarity, only representative error bars are indicated explicitly.

species reacts with cyclohexane at nearly gas-kinetic rates (24). Collision between Cp*Rh(CO) and cyclohexane is the slowest step in the overall C–H activation process. In contrast, association of solvent with free Cp*Rh(CO) in solution is so rapid that the step involving C–H bond cleavage in the coordinated alkane complex becomes rate-determining.

Acknowledgments

References

1. Shilov, A. E. *Activation of Saturated Hydrocarbons by Transition Metal Complexes*; Reidel: Dordrecht, 1984.
2. Crabtree, R. H. *Chem. Rev.* 1985, *85*, 245.
3. Bergman, R. G. *Science (Washington, D.C.)* 1984, *223*, 902.
4. Janowicz, A. H.; Bergman, R. G. *J. Am. Chem. Soc.* 1982, *104*, 352.
5. Janowicz, A. H.; Bergman, R. G. *J. Am. Chem. Soc.* 1983, *105*, 3929.
6. Hoyano, J. K.; Graham, W. A. G. *J. Am. Chem. Soc.* 1982, *104*, 3723.
7. *See*, for example, Buchanan, J. M.; Stryker, J. M.; Bergman, R. G. *J. Am. Chem. Soc.* 1986, *108*, 1537.
8. Jones, W. D.; Feher, F. J. *J. Am. Chem. Soc.* 1986, *108*, 4814.
9. Jones, W. D.; Feher, F. J. *J. Am. Chem. Soc.* 1983, *2*, 562.
10. Periana, R. A.; Bergman, R. G. *Organometallics* 1984, *3*, 508.
11. Periana, R. A.; Bergman, R. G. *J. Am. Chem. Soc.* 1986, *108*, 7332.
12. Hackett, M.; Whitesides, G. M. *J. Am. Chem. Soc.* 1988, *110*, 1449.
13. Bergman, R. G.; Seidler, P. F.; Wenzel, T. T. *J. Am. Chem. Soc.* 1985, *107*, 4358.
14. Baker, M. V.; Field, L. D. *J. Am. Chem. Soc.* 1987, *109*, 2825.
15. Nolan, S. P.; Hoff, C. D.; Stoutland, P. O.; Newman, L. J.; Buchanan, J. M.; Bergman, R. G.; Yang, G. K.; Peters, K. S. *J. Am. Chem. Soc.* 1987, *109*, 3143.
16. Jones, W. D.; Feher, F. J. *J. Am. Chem. Soc.* 1984, *106*, 1650.
17. Foo, T.; Bergman, R. G. *Organometallics*, in press.
18. Stoutland, P. O.; Bergman, R. G. *J. Am. Chem. Soc.* 1985, *107*, 4581.
19. Stoutland, P. O.; Bergman, R. G. *J. Am. Chem. Soc.* 1988, *110*, 5732.
20. Klein, D. P.; Hayes, J. C.; Bergman, R. G. *J. Am. Chem. Soc.* 1988, *110*, 3704.
21. Sponsler, M. B.; Weiller, B. H.; Stoutland, P. O.; Bergman, R. G. *J. Am. Chem. Soc.* 1989, *111*, 6841.
22. Sponsler, M. B.; Bergman, R. G., unpublished results.
23. Weiller, B.; Wasserman, E. P.; Bergman, R. G.; Moore, C. B.; Pimentel, G. C. *J. Am. Chem. Soc.* 1989, *111*, 8288.
24. Wasserman, E. P.; Bergman, R. G.; Moore, C. B. *Science (Washington, D.C.)*, in press.

Selective Hydroxylation of Hydrocarbons by Platinum Salts in Aqueous Media

Direct Conversion of Ethanol to Ethylene Glycol

Jay A. Labinger, Andrew M. Herring, and John E. Bercaw

Division of Chemistry and Chemical Engineering, California Institute of Technology, Pasadena, CA 91125

Water-soluble organic compounds are hydroxylated by aqueous solutions of chloroplatinum(II) and chloroplatinum(IV) salts. p-Toluenesulfonic acid is converted stepwise to the corresponding alcohol and aldehyde, the first step being somewhat faster than the second. No further conversion to the carboxylic acid is observed. Ethanol shows substantial selectivity for attack at a C–H bond of the methyl group, affording ethylene glycol and 2-chloroethanol, as well as more expected products such as acetaldehyde and acetic acid. The origin of the unusual selectivity patterns is discussed in terms of the mechanism of activation of C–H bonds by Pt(II) species.

T HE ACTIVATION OF C–H BONDS IN ALKANES by transition metal complexes, not long ago thought to be among the most difficult challenges facing organometallic chemists, is now almost commonplace. Many intriguing examples, often under remarkably mild conditions, have appeared in the past few years (*1–3*). However, the elaboration of these fundamental transformations into a practical alkane conversion process remains elusive. Why is this so?

A primary reason is the incompatibility of most, if not all, potentially useful functionalization reactions with either thermodynamics or catalyst stability. Consider eqs 1–4: The first two appear compatible with known

reactions of organotransition metal complexes, but both are thermodynamically uphill at near-ambient temperatures. Both reactions have been achieved, but only by shifting the equilibrium by providing a hydrogen acceptor such as another olefin (4, 5) or by driving the reaction photochemically (6–8). Either approach almost certainly becomes impractical for economic reasons. The last two are thermodynamically favored, but most systems known to activate alkanes are incompatible with O_2 and could not be the basis of a catalytic reaction.

$$RCH_2CH_3 \rightarrow RCH{=}CH_2 + H_2 \tag{1}$$

$$RCH_2CH_3 + CO \rightarrow RCH_2CH_2CHO \tag{2}$$

$$RCH_2CH_3 + \frac{1}{2} O_2 \rightarrow RCH{=}CH_2 + H_2O \tag{3}$$

$$RCH_2CH_3 + \frac{1}{2} O_2 \rightarrow RCH_2CH_2OH \tag{4}$$
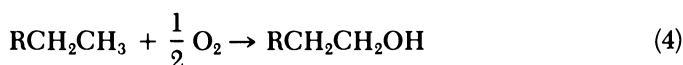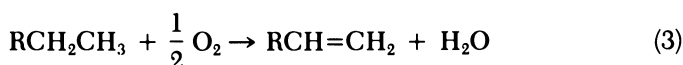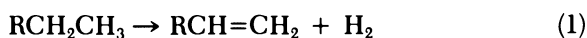
A secondary issue is selectivity. Regioselectivity is an obvious problem, as in eq 4, if terminal alcohols are the preferred isomeric products. More important, though, the products (alcohols, alkenes, etc.) tend to be considerably more reactive than the starting alkanes. This reactivity would place a ceiling on achievable yields. As with heterogeneously catalyzed selective oxidation, there is always a tradeoff between selectivity and conversion (9). This tradeoff may be especially problematical when a hydrogen-atom abstraction route is involved, as with cytochrome P-450 and models thereof (10). That organometallic alkane activations may proceed by quite different mechanisms, and thus exhibit different patterns of selectivity, is clearly of key importance.

Most of the relatively facile alkane activations can be placed in one of three categories: oxidative addition (eq 5), σ-bond metathesis (eq 6), or electrophilic substitution (eq 7) (1–3). The first has been found for low-valent, electron-rich, coordinatively unsaturated metal centers toward the right end of the transition series (Groups 6–10). The second category is observed for d^0 complexes of Groups 3 (including lanthanides and actinides) and 4 (there are also intramolecular examples with Group 5). Both lead to stable organometallic products, but only very limited examples of functionalization have been achieved, for reasons cited. All of the species involved are highly sensitive to O_2 or the oxygenated products that would be produced.

$$L_nM + R{-}H \rightarrow L_nM(H)(R) \tag{5}$$

$$L_nM{-}X + R{-}H \rightarrow L_nM{-}R + H{-}X \tag{6}$$

$$L_nM^{y+} + R{-}H \rightarrow L_nM{-}R^{(y-1)+} + H^+ \tag{7}$$
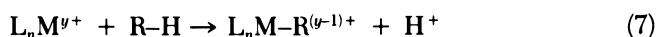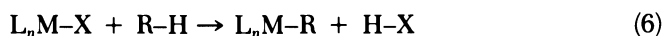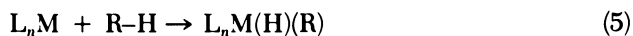
In contrast, the third class (eq 7) has been observed with the "classic" coordination complexes, $PtCl_x(H_2O)_{4-x}^{(x-2)-}$ (*11, 12*), and, more recently, with related Pd(II) complexes (*13*). Here a stable organometallic species is not obtained, but net functionalization of alkane is. An NMR signal attributed to a methyl–Pt(IV) complex was reported (*14*) in a study of methane oxidation by the Pt(II)–Pt(IV) system.

These systems, furthermore, appear attractive in that the species involved [Pd(II), Pt(II)] will tolerate O_2. This characteristic allows in principle for the closing of a catalytic cycle. On the other hand, catalytic oxidation has not yet been achieved, nor is much known about detailed mechanism or selectivity, and lack of reproducibility has sometimes been a problem. During an attempt to further delineate the mechanism we observed unexpected selectivity patterns.

Experimental Procedure

General Specifications. Except as noted, all reagents were obtained commercially and used without further purification. NMR spectra were recorded on Bruker AM500, JEOL GX 400Q, or JEOL FX 90Q spectrometers at 500, 400, or 90 MHz (^{1}H), 22.5 MHz (^{13}C), and 107.5 MHz (^{195}Pt). IR spectra were recorded on a Perkin-Elmer 1600 Fourier transform (FT) IR spectrometer, with a 10-cm gas cell. Gas chromatograms were recorded on a Perkin-Elmer 8410 gas chromatograph, with a Carbowax column.

Oxidation of *p*-Toluenesulfonic Acid (1). Solutions containing 1 (0.2–0.5 M), Na_2PtCl_6 (0.2–0.5 M), and Na_2PtCl_4 (0.02–0.05 M) in D_2O were sealed in NMR tubes. The sealed tubes were heated in thermostatted oil baths in an inverted position, so that any Pt particles or mirrors formed would not interfere with the recording of NMR spectra. Stepwise conversion to 2 and 3 was monitored by growth of the corresponding NMR signals. Both 2 (*15*) and 3 (*16*) are known, but their ^{1}H NMR spectra have not previously been reported. Their parameters (chemical shift, δ, parts per million) along with those of the carboxylic acid 4 (*17*) are

2: 4.44 (s), $ArCH_2OH$; 7.26 (d), 7.56 (d) (J = 8.3 Hz), $HO_3SC_6H_4CH_2OH$

3: 9.72 (s), ArCHO; 7.73 (d), 7.78 (d) (J = 8.3 Hz), $HO_3SC_6H_4CHO$

4: 7.64 (d), 7.73 (d) (J = 8.4 Hz), $HO_3SC_6H_4CO_2H$

For determination of absolute product yields, reactions were run in H_2O (to eliminate perturbation from H–D exchange). After completion, solvent was removed in vacuo and the residue redissolved in D_2O to which a weighed amount of an NMR reference was added. Oxidations of 2 and 5 (*p*-ethylsulfonic acid) were performed similarly.

Oxidation of Ethanol. Reactions were performed under the described conditions, except that it was necessary to add ∼1 equiv of acid–Pt(IV); otherwise

deposition of Pt metal began shortly after reaching reaction temperature. Either HCl or the sulfonic–carboxylic diacid 4 can be used. The latter is convenient in that it provides an internal NMR reference signal.

Two-carbon products were identified by ^{1}H and ^{13}C NMR signals, by using ordinary as well as mono- and di-^{13}C-labeled ethanol. All shifts, J_{CH}, and J_{CC} values agree with literature data for the products shown in eq 10 [including acetaldehyde, which in aqueous solution exhibits ^{13}C signals characteristic of the hydrate (18)]. The presence and amount of ethylene glycol was further verified by gas chromatography. CO_2 was quantified by Toepler pump transfer to a volumetric bulb and thence to a cell for infrared spectroscopic identification. The expected frequency shift was found when ^{13}C-labeled ethanol was oxidized, confirming the origin of the CO_2. About 65% of the consumed ethanol is accounted for in eq 10. A number of signals in the ^{1}H and ^{13}C NMR spectra (mostly weak) remain to be assigned. Several products show evidence of a partial H–D exchange. The small isotope shift separates the signals of the exchanged species from the main signal, so that it can be seen clearly that the extent of exchange is quite small. The higher water-soluble alcohols were examined similarly.

Results and Discussion

Oxidation of p-Toluenesulfonic Acid and Related Compounds.
To facilitate mechanistic studies we sought a simple water-soluble model substrate. Thus, the reaction medium would be homogeneous and NMR spectroscopy could be used to monitor reaction progress. p-Toluenesulfonic acid (1) proved a suitable choice. Standard experimental conditions, here and elsewhere, involve heating D_2O solutions of substrate, Na_2PtCl_6, and Na_2PtCl_4 (typical ratios ~ 1:1:0.1) in NMR tubes. The extent of reaction after any given time is determined by ^{1}H NMR spectroscopy.

1 is oxidized by the Pt(II)–Pt(IV) system according to eq 8. ^{1}H NMR spectra (Figure 1) show clearly that only two products are formed to any significant degree: alcohol 2 and aldehyde 3. In particular, no products resulting from oxidation at aromatic ring positions could be detected.

Slow H–D exchange at both methyl and ring positions competes with oxidation. H–D exchange can be observed in all reactions run in D_2O. In general, it is relatively slow compared to oxidation and occurs at comparable rates at the various sites, so that determination of product yields by NMR spectroscopy is not significantly perturbed. More accurate yields were obtained by carrying out reactions in H_2O, removing solvent in vacuo, and redissolving in D_2O before running the NMR spectrum.

No further oxidation of 3 to the carboxylic acid 4 is detected. Conversion of 3 is inferred from the appearance of additional weak NMR signals in the aromatic region toward the end of reaction 8. These signals have not been assigned, but they do not correspond to 4, which was independently synthesized.

Solutions remain visibly homogeneous during the first few hours of the reaction, although eventual deposition of platinum metal was observed in
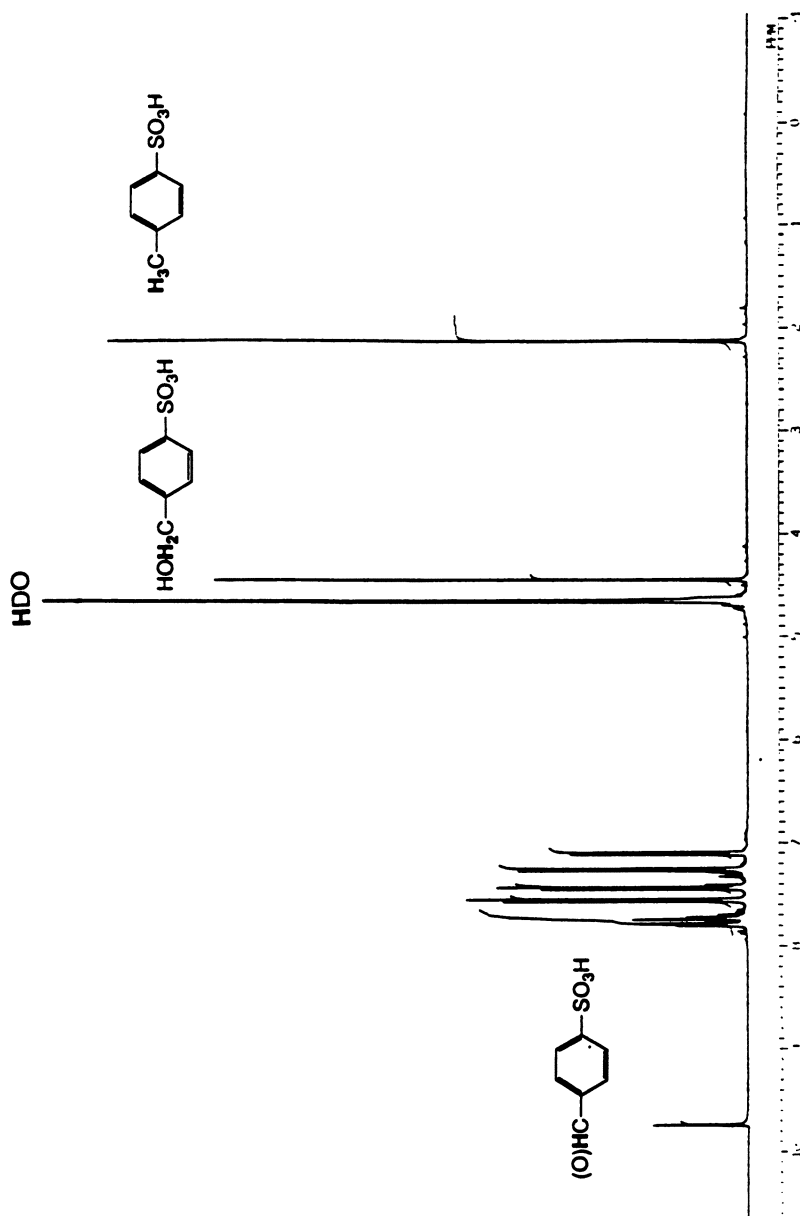
Figure 1. ¹H NMR spectra of reaction mixture PtCl₄²⁻–PtCl₆²⁻–1 after 2 h at 122 °C.

all cases. Shilov (*1*) reports that Pt deposition may be suppressed by addition of excess acid or chloride. However, we have never been able to achieve this result except by adding enough chloride to suppress the reaction completely. This observation raises the question of possible heterogeneous activation. Addition of metallic mercury (*19*) does not completely suppress oxidation. There is some decrease in rate, which is attributable to the fact that Hg(0) reduces both Pt(II) and Pt(IV). Other observations also support a homogeneous mechanism.

$$p\text{-}HO_3SC_6H_4\text{-}CH_3 \xrightarrow[\text{H}_2\text{O, 80-120 °C, 6 h}]{\text{Pt(IV)/Pt(II), Cl}^-} Ar\text{-}CH_2OH$$
$$\underset{1}{} \qquad\qquad\qquad\qquad\qquad\qquad\qquad \underset{2}{}$$

$$\rightarrow Ar\text{-}\underset{3}{CHO} \rightarrow Ar\text{-}\underset{4}{CO_2H} \qquad\qquad (8)$$
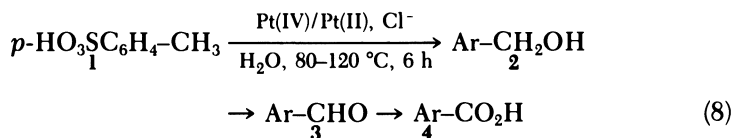
The progress of the reaction over time (Figure 2) clearly shows that **2** and **3** are formed sequentially. Furthermore, though the kinetics cannot be fit to any simple rate law, it is possible to estimate the relative rate constants for **1** → **2** vs. **2** → **3**, either from the data in Figure 2 or from a separate experiment in which **2** is used as substrate. Both procedures yield the same result: The first step is faster than the second by a factor of around 1.5. Thus the selectivity for attack at C–H bonds in this system follows the unexpected order: $-CH_3 > -CH_2OH >$ aryl-H $>> -CHO$.

The possibility that selectivity for attack at the methyl position in **1** is related to its benzylic character can be tested by examining the ethyl analog **5**. Substantial oxidation takes place at the β-position (eq 9), which indicates that benzylic activation is not essential. The reason for the appearance of substantial ring-oxidation products here, in contrast to eq 8, is not clear. However, the fact that **5** was examined as the sulfonate salt may be important. Oxidation of **5** in the conjugate acid form gives a product whose NMR spectrum suggests a coordinated styrene derivative, presumably resulting from acid-catalyzed dehydration of the alcohol products of eq 9. Sodium *p*-toluate similarly gives a mixture of methyl and ring oxidation.

$$-O_3SC_6H_4\text{-}CH_2CH_3 \rightarrow Ar\text{-}CH_2CH_2OH + Ar\text{-}CH(OH)CH_3$$
$$\underset{5}{} \qquad\qquad\qquad \underset{25\%}{} \qquad\qquad\quad \underset{35\%}{}$$

$$+ \text{ ring oxidation} \qquad (9)$$
$$\underset{30\%}{}$$
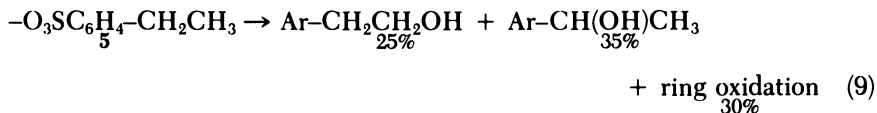
Oxidation of Ethanol.   Normally the reaction of alcohols with reducible metal species (*20*), including Pt(II) (*21*), leads readily to aldehydes. On the contrary, the fact that $-CH_3$ can be more reactive than $-CH_2OH$ suggests that glycol could be a possible product. Indeed, ethylene glycol is produced when ethanol is substituted for **1** in eq 8, as shown in eq 10. The additional products include acetaldehyde (as the hydrate) and acetic acid,
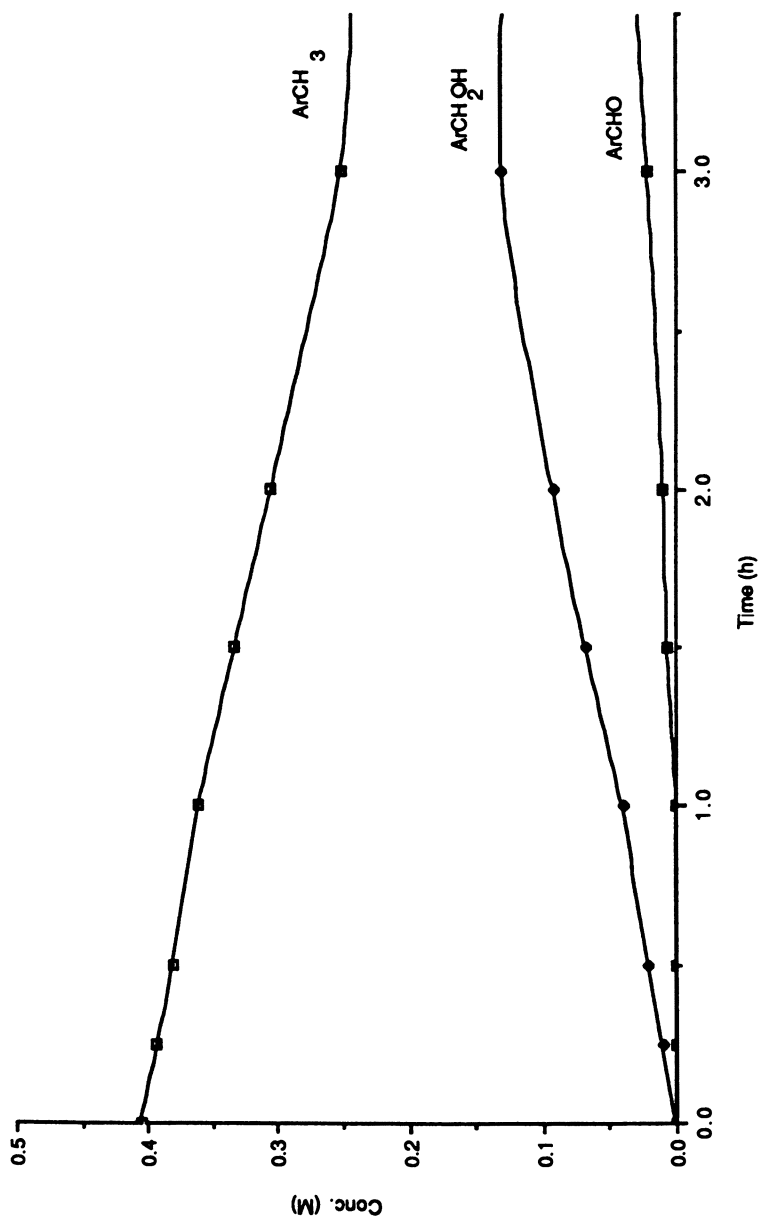
Figure 2. Concentrations of 1, 2, and 3 vs. time. They are formed in reaction mixture $PtCl_4^{2-}$–$PtCl_6^{2-}$–1 at 122 °C.

both of which clearly arise from initial oxidation at the $-CH_2OH$ position; glycolic acid, which could form either via hydroxylation of acetic acid or oxidation of ethylene glycol; and CO_2.

$$CH_3CH_2OH \xrightarrow[120\ °C,\ 3\ h]{Pt(II)/PT(IV),\ Cl^-} HOCH_2CH_2OH + HOCH_2CH_2Cl +$$
$$\text{50\% converted} \qquad\qquad\qquad\quad \text{5\%} \qquad\qquad \text{2\%}$$

$$CH_3CH(OH)_2 + CH_3CO_2H + HOCH_2CO_2H + CO_2 \quad (10)$$
$$\text{5\%} \qquad\qquad \text{7\%} \qquad\qquad \text{5\%} \qquad\qquad \text{8\%}$$
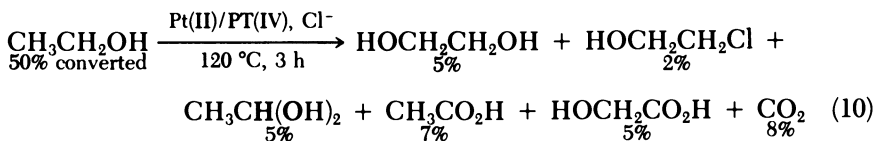
Overall partitioning of products between the two sites for initial attack can be estimated by labeling one carbon of ethanol. When $^{12}CH_3{}^{13}CH_2OH$ is used as substrate, the glycolic acid produced is labeled nearly equally in the two positions (eq 11). Thus, it arises mostly (>90%) via oxidation of ethylene glycol rather than hydroxylation of acetic acid. The CO_2 shows an excess of ^{13}C, suggesting that around 40% comes from oxidative decarboxylation of acetic acid and 60% from ethylene glycol, presumably via oxalic acid. Oxalic acid should be readily oxidized by either Pt(II) or Pt(IV) to CO_2, according to standard reduction potentials.

$$CH_3{}^*CH_2OH \rightarrow HOCH_2{}^*CO_2H + HO^*CH_2CO_2H + CO_2 +$$
$$\text{54\%} \qquad\qquad \text{46\%} \qquad\qquad \text{37\%}$$

$$^*CO_2 \text{ inter alia} \quad (11)$$
$$\text{63\%}$$
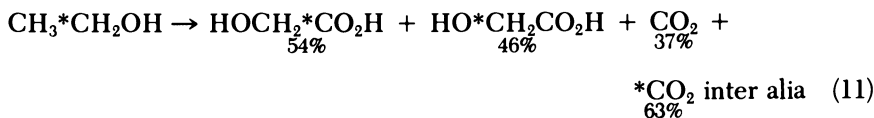
From these labeling studies and the overall product distribution, relative rates for the various steps may be estimated. These rates are shown in Scheme I. Attack at the methyl and hydroxymethyl groups of ethanol are approximately equally facile. This result is striking; any direct conversion of ethanol to ethylene glycol appears to be unprecedented in the literature.

The higher water-soluble alcohols were briefly examined as well. With 1-propanol, selectivity for attack at the $-CH_3$ group is particularly high; 1,3-propanediol and 3-chloro-1-propanol account for 80% of the product. 2-Propanol and 1-butanol give complex mixtures that have not yet been fully assigned.

Mechanisms. *Nature of Active Pt Complex.* Shilov's original proposal (*1*) involved formation of an alkyl–Pt(II) complex, transfer of the alkyl group to Pt(IV), and nucleophilic cleavage of the Pt–C bond, as shown in Scheme II. This cleavage would mean Pt(IV) is an obligatory oxidant. However, we find that the oxidation of 1 to 2 plus 3 proceeds at comparable rates even when Pt(IV) is omitted from the reaction mixture; in this case precipitation of Pt metal begins immediately. This result is clearly incompatible with Scheme II (the known disproportionation of 2Pt(II) → Pt(IV) + Pt(0) is much slower than substrate oxidation under these conditions). It suggests that, at least for this hydrocarbon, oxidation proceeds by Scheme III.

$$CH_3CH_2OH \xrightarrow{1} HOCH_2CH_2OH \xrightarrow{.2} ClCH_2CH_2OH$$

$$\downarrow .95 \qquad\qquad \downarrow 10$$

$$CH_3CHO \qquad\qquad HOCH_2CHO$$

$$\downarrow 8 \qquad\qquad \downarrow 16$$

$$CH_3COOH \xrightarrow{.7} HOCH_2COOH$$

$$\downarrow 10$$

$$[HOOCCOOH]$$

$$5 \qquad \downarrow fast$$

$$X \qquad\qquad CO_2$$
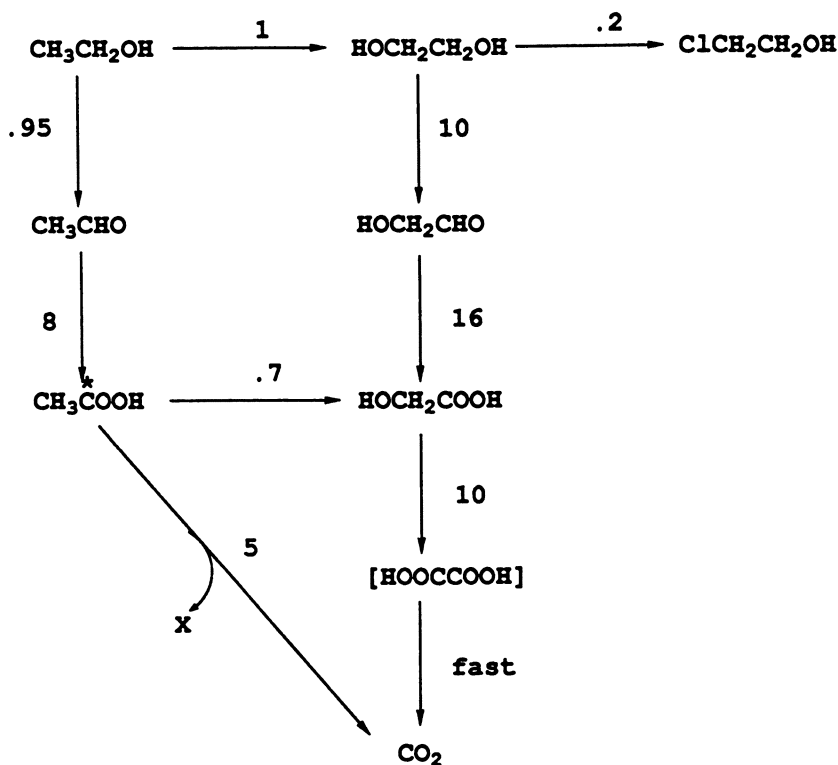
Scheme I. Reaction sequence and estimated relative rates.

$$Cl_3Pt^- + R-H \longrightarrow Cl_3Pt-R^{2-} + H^+$$

$$Cl_3Pt-R^{2-} + Cl_5Pt^- \longrightarrow Cl_5Pt-R^{2-} + Cl_3Pt^-$$

$$Cl_5Pt-R^{2-} + H_2O \longrightarrow ROH + Cl_3Pt^- + HCl + Cl^-$$
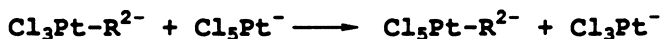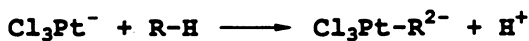
Scheme II. Originally proposed mechanism (reference 1).

$$Pt^{2+} + R-H \rightleftharpoons Pt \cdots \begin{array}{c} R \\ | \\ H \end{array}^{2+} \longrightarrow Pt-R^+ + H^+$$

$$Pt^{2+} \qquad\qquad \downarrow H_2O$$

$$Pt^{4+} \qquad Pt^\circ + ROH + H^+$$
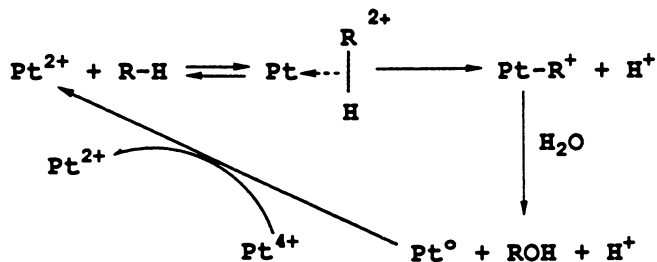
Scheme III. Proposed mechanism for C–H activation and oxidation.

It is not possible to confirm this mechanism from kinetics, as neither the progress of the reaction over time nor the dependence on [Pt(II)] or [Pt(IV)] follow any simple rate law. This disparity is almost certainly a consequence of the fact that each oxidation state of Pt actually consists of a mixture of species [$PtCl_n(H_2O)_{4-n}^{(2-n)+}$ and $PtCl_n(H_2O)_{6-n}^{(4-n)+}$].

The reactivity of each of these species will be different. As reaction proceeds and Pt(IV) is reduced to Pt(II), additional Cl$^-$ is liberated, shifting the distribution of these species. Speciation can be followed by means of ^{195}Pt NMR spectroscopy. In the early stages, when the reaction is proceeding, signals due to both $PtCl_4^{2-}$ and $PtCl_3(H_2O)^-$ are detected (22, 23). After several hours, when reaction has ceased (even though none of the reagents has been fully consumed), only the former signal is present. It appears therefore that only species with at least one Cl$^-$ replaced by H_2O are able to activate C–H bonds.

Approximate reaction rates may be estimated from the initial rate of product appearance and correlate much more strongly with [Pt(II)] than [Pt(IV)]. An Eyring plot of initial rate data collected from 80–122 °C gives an enthalpy of activation, $\Delta H^{\ddagger}$, of 26 kcal mol^{-1} and an entropy of activation, $\Delta S^{\ddagger}$, of 11 eu. Without a rate law, the significance of these parameters is unclear.

Origin of Selectivity in C–H Attack.   The selectivity patterns are clearly incompatible with a radical mechanism. They are similar to patterns observed for the other modes of alkane activation (eqs 5 and 6), both in the preference for sterically least-hindered sites (1–3) and in the rather remarkable selectivity for attack at C–H instead of O–H or C–O (24).

We propose that selectivity is determined by an initial M–H–C interaction in all modes of alkane activation. The three types diverge after formation of the metal–alkane complex, which may undergo oxidative addition, σ-bond metathesis, or electrophilic displacement, according to the nature of the complex. In the present case, conversion to alkyl–Pt(II) most likely proceeds via deprotonation (Scheme III), which is consistent with the known enhanced acidity of related η^2–H_2 complexes (25).

Future Prospects

Although the oxidations demonstrated here are not catalytic, the selectivity is not outstanding, and the rates are too low for practical application, the specificity for methyl group hydroxylation coupled with the stability toward oxidizing conditions suggests considerable potential for further development.

In principle, it appears possible to replace Pt(IV) with a cheaper oxidant, perhaps even O_2, by means of a Wacker-like regeneration scheme. However, any oxidant used must be capable of reoxidizing Pt(0) to Pt(II) without oxidizing Pt(II) to Pt(IV). Unfortunately, the potentials for these two couples

are very close. Our current efforts are focused on finding more stable and characterizable Pt(II) complexes that can activate alkanes, in order to eliminate the Cl^--H_2O exchange problem that both complicates mechanistic studies and shuts the reaction down before completion, and in hopes of constructing a system that can be catalytically cycled.

Acknowledgments

References

1. Shilov, A. E. *Activation of Saturated Hydrocarbons by Transition Metal Complexes*; D. Reidel: Dordrecht, 1984.
2. Crabtree, R. H. *Chem. Rev.* **1985**, *85*, 245.
3. *Activation and Functionalization of Alkanes*; Hill, C. L., Ed.; Wiley-Interscience: New York, 1989.
4. Burk, M. J.; Crabtree, R. H. *J. Am. Chem. Soc.* **1987**, *109*, 8025.
5. Cameron, C. J.; Felkin, H.; Fillebeen-Khan, T.; Forrow, N. J.; Gutittet, E. *J. Chem. Soc., Chem. Commun.* **1986**, 801.
6. Kunin, A. J.; Eisenberg, R. E. *J. Am. Chem. Soc.* **1986**, *108*, 535.
7. Sakakura, T.; Tanaka, M. *J. Chem. Soc., Chem. Commun.* **1987**, 758.
8. Maguire, J. A.; Boese, W. T.; Goldman, A. S. *J. Am. Chem. Soc.* **1989**, *111*, 7088.
9. For example, see Labinger, J. A.; Ott, K. C. *Catal. Lett.* **1990**, *4*, 245.
10. *Cytochrome P-450: Structure, Mechanism, and Biochemistry*; Ortiz de Montellano, P. R., Ed.; Plenum: New York, 1989.
11. Shilov, A. E. *Activation of Saturated Hydrocarbons by Transition Metal Complexes*; D. Reidel: Dordrecht, 1984; pp 163–182.
12. *Activation and Functionalization of Alkanes*; Hill, C. L., Ed.; Wiley-Interscience: New York, 1989; pp 3–11.
13. Gretz, E.; Oliver, T. F.; Sen, A. *J. Am. Chem. Soc.* **1987**, *109*, 8109.
14. Kushch, L. A.; Lavrushko, V. V.; Misharin, Yu. S.; Moravsky, A. P.; Shilov, A. E. *Nouv. J. Chim.* **1983**, *7*, 729.
15. Hubbuch, A.; Bindewald, R.; Fohles, J.; Nuithani, V. K.; Zuhn, H. *Angew. Chem., Int. Ed. Engl.* **1980**, *19*, 394.
16. Bollag, W. *Eur. J. Med. Chem.–Chim. Ther.* **1983**, *18*, 425.
17. Smiles, S.; Harrison, D. C. *J. Chem. Soc.* **1922**, *21*, 2023.
18. Chastrette, F.; Bracoud, C.; Chastrette, M.; Mattioda, G.; Christidis, Y. *Bull. Soc. Chim. Fr.* **1985**, 66.
19. Anton, D. R.; Crabtree, R. H. *Organometallics* **1983**, *2*, 855.
20. Stern, E. W. In *Transition Metals in Homogeneous Catalysis*; Schrauzer, G. N., Ed.; Dekker: New York, 1971; pp 107–108.

21. Hass, D.; Hauthal, T. *Z. Chem.* **1975**, *15*, 33.
22. Freeman, W.; Pregosin, P. S.; Sze, S. N.; Venanzi, L. M. *J. Magn. Reson.* **1976,** *22*, 473.
23. Pregosin, P. S. *Coord. Chem. Rev.* **1982,** *44*, 247.
24. For example, *see* Wu, J.; Bergman, R. G. *J. Am. Chem. Soc.* **1989,** *111*, 7628.
25. Chinn, M. S.; Heinekey, D. M. *J. Am. Chem. Soc.* **1987,** *109*, 5865.

16

Amidocarbonylation

Catalyst, Reaction Scope, and Industrial Application

J. J. Lin[1] and J. F. Knifton

Texaco Chemical Company, P.O. Box 15730, Austin, TX 78761

Amidocarbonylation, first discovered by Wakamatsu in 1971, is an underrated and underused technology in synthesis gas chemistry. In combination with hydroformylation, amidocarbonylation provides a versatile route to the synthesis of α-amidocarboxylic acids from an olefin, acetamide, and CO–H₂. Our research focused on the application and extension of amidocarbonylation technology to the synthesis of a wide range of amidocarboxylic acids, including surface-active agents (C₁₀–C₁₆ amido acids), specialty surfactants (sarcosinates), intermediates for sweeteners, food additives (glutamic acid), and chelating agents. Homogeneous cobalt- and rhodium-based catalysts, modified with sulfoxide and bidentate phosphine ligands, were tailored to the synthesis of each individual class of products. Processing studies (reaction rate, product selectivity, and catalyst stability) and economic assessments are discussed.

AMIDOCARBONYLATION, the synthesis of N-acyl-α-amino acids from aldehyde, carbon monoxide, and amide, was first reported by Wakamatsu et al. in 1971 (1). In 1979 Parnaud et al. (2) investigated the reaction mechanism, and in 1981 Stern (3) patented a process for making amido acids directly from olefins. By 1985, Ojima et al. (4) demonstrated that this technology can be extended to other substrates (including trifluoropropene, oxirane, and allyl alcohols) by the use of binary metal catalysts. Applications of amino acid derivatives in the areas of enhanced oil recovery (5), liquid detergents (6), and gas-scrubbing agents (7) have been reported.

[1]Current address: Shell Development Company, P.O. Box 1380, Houston, TX 77251

Currently, most amino acids are obtained from natural sources or fermentation. Amidocarbonylation can be considered a viable alternative to the conventional Strecker reaction, which uses highly toxic hydrogen cyanide and ammonia to make α-amino acids from aldehydes. Since 1983 we have been interested in amidocarbonylation technology for two reasons: (1) production of specialty chemicals is an extension of our synthesis gas (syngas) research and (2) amidocarbonylation is a unique technique for constructing two functionalities in a single step.

Herein we report the use of amidocarbonylation technology for the synthesis of a wide range of amido acids, including surface-active agents (C_{10}–C_{16} amido acids), specialty surfactants, intermediates for aspartame sweeteners (β-phenylalanine and N-acetylglycine), food additives (sodium monoglutamate), and chelating agents (iminoacetic acid and polyamido acids). Therefore, many products can be made by the same technology.

Amidocarbonylation

N-Acetylglycine. N-Acetylglycine, the simplest amido acid, was synthesized in 60% yield from paraformaldehyde, carbon monoxide, and acetamide by using octacarbonyldicobalt as the catalyst under 2900 psi CO–H_2 (3:1) at 120 °C in ethyl acetate solvent. The effect of ligands on reaction yield and catalyst recovery was studied. The addition of diphenyl sulfoxide or succinonitrile ligands to this catalyst system increased the yield of N-acetylglycine to 78% yield. In addition, catalyst recovery increased from 50% to 85% (on the basis of cobalt used). Similarly, addition of tributylphosphine promoted the reaction at lower pressure (800 psi). By comparison, the chelating tetramethylethylenediamine adversely affected the reaction. The effects of ligands on reaction yield and catalyst recovery are summarized in Table I (8).

L-Phenylalanine.   L-Phenylalanine is a key intermediate for aspartame sweetener, a methyl ester of the L-phenylalanine–L-aspartic acid dipeptide (*see* structure). Currently, L-phenylalanine is produced by tyrosine fermentation (by Genex and Searle). One proposed synthetic route is the oxidative carbonylation of styrene to form cinnamate ester and subsequent
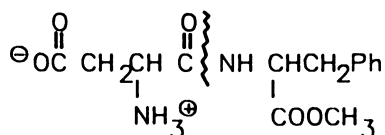
aspartame (L-aspartic acid + L-phenylalanine)

Table I. *N*-Acetylglycine Synthesis and Catalyst Improvement

$$(CH_2O)_x \;+\; CH_3CONH_2 \;\xrightarrow{\;Co_2(CO)_8\;}\; CH_2\!\!\begin{array}{l} COOH \\ NHCOCH_3 \end{array} \;+\; CH_2\!\!\begin{array}{l} NHCOCH_3 \\ NHCOCH_3 \end{array}$$

$$\text{(I)} \qquad\qquad \text{(II)}$$
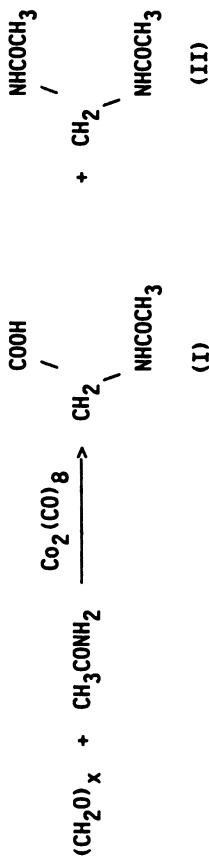
		Conditions[a]			Molar Ratio		Yield of I	Co Recovery
Ligand	CO-H_2	Pressure (psi)	Temperature (°C)	Time (h)	I	II	(%)	(%)
None	3:1	2900	120	2	80	20	60	<50
Ph$_2$SO	3:1	2900	120	2	94	6	68	70
Succinonitrile	3:1	2900	120	2	100	0	78	80
TMEDA[b]	3:1	2900	120	2	0	100	0	—
n-Bu$_3$P	8:1	800	110	5	85	15	70	80
None	8:1	800	110	5	—	—	0	—

[a]Paraformaldehyde (2.0 g), acetamide (5.9 g), Co$_2$(CO)$_8$ (0.34 g), EtOAc (15–20 g).
[b]Tetramethylethylenediamine.

A. VIA CINNAMATE ESTER

$$STYRENE \xrightarrow[Pd]{CO, O_2, ROH}$$

$$PhCH=CH-COOR \xrightarrow[NH_3]{ENZYME} PhCH_2CH \begin{matrix} COOR \\ NH_2 \end{matrix}$$
$$90\%$$

B. VIA GLYCINE

$$H_2NCH_2COOH \longrightarrow CH_3CONHCH_2COOH \xrightarrow{PhCHO}$$

$$PhCH=C \begin{matrix} NHCOCH_3 \\ COOH \end{matrix} \xrightarrow{H_2} PhCH_2CH \begin{matrix} NHCOCH_3 \\ COOH \end{matrix}$$
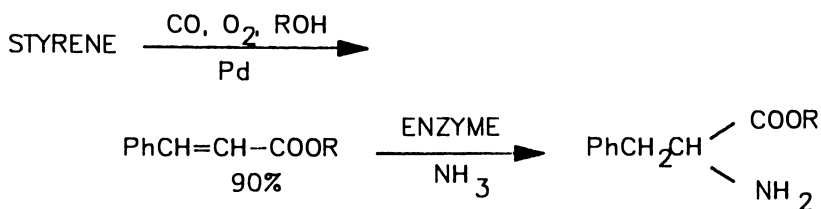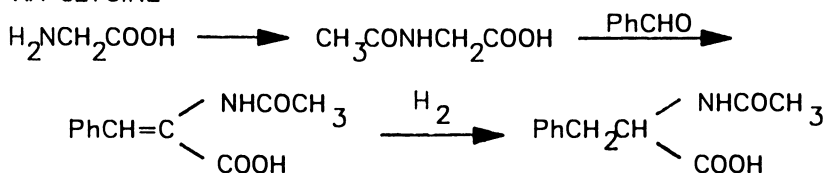
Scheme I. Phenylalanine synthesis via cinnamate ester or glycine.

A

$$Ph\ CH-CH_2 + CH_3CONH_2 \xrightarrow[\substack{CO/H_2=4,\ 110°C \\ 100\ atm}]{CO_2(CO)_8-Ti(O^iPr)_4}$$

$$PhCH_2CH \begin{matrix} COOH \\ NHCOCH_3 \end{matrix}$$

B

$$PhCH_2CHO + CH_3CONH_2 \longrightarrow PhCH_2CH \begin{matrix} COOH \\ NHCOCH_3 \end{matrix}$$

$$\uparrow$$
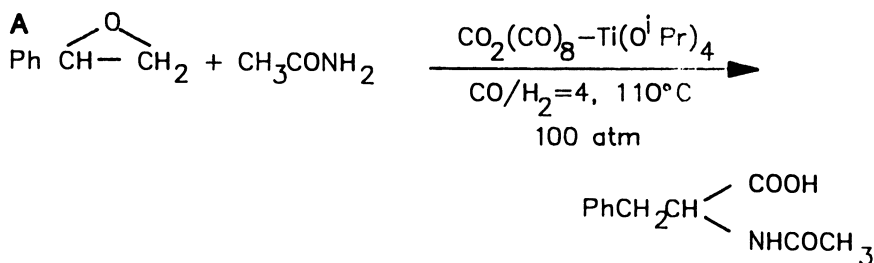
STYRENE OXIDE

$$\uparrow$$

STYRENE

CATALYST: $Co_2(CO)_8 - Ph_2PCH_2CH_2PPh_2$ (4:1 MOLAR

CONDITIONS: $CO/H_2=3$, 2200 psi, 80 °C, 4h

RESULTS: 72 MOLE % YIELD
          >98% COBALT RECOVERY

Scheme II. Phenylalanine synthesis via styrene oxide.

enzymatic amination (9) (Scheme IA). Another route is from *N*-acetylglycine (Scheme IB). The amidocarbonylation of styrene oxide to phenylalanine by bimetallic catalyst was reported by Ojima (10) (Scheme IIA). Amidocarbonylation from phenylacetaldehyde, which can be made from styrene oxide, afforded phenylalanine in 72% yield (Scheme IIB) (11).

Alkyl Sarcosinate. The syntheses of sarcosinate specialty surfactants by the conventional method and by amidocarbonylation are compared in Scheme III. The use of secondary amide for amidocarbonylation was reported to give poor yields of amido acid because the corresponding oxazolone intermediate cannot be formed (2, 12, 13). However, the amidocarbonylation of *N*-methylamide gave excellent yields of alkyl sarcosinates. This reactivity allows the introduction of carboxylic acid and secondary amide moieties in a single step (14).

CONVENTIONAL ROUTE

$$R\text{-}\underset{\text{Cl}}{\overset{\overset{\displaystyle O}{\|}}{C}}\text{-} + \underset{\underset{\displaystyle CH_3}{|}}{HNCH_2COOH} \longrightarrow R\text{-}\underset{\underset{\displaystyle CH_3}{|}}{\overset{\overset{\displaystyle O}{\|}}{C}}NCH_2COOH$$

AMIDOCARBONYLATION

$$C_{11}H_{23}\overset{\overset{\displaystyle O}{\|}}{C}OH + CH_3NH_2 \xrightarrow{230^{\circ}C}$$

$$C_{11}H_{23}\underset{\underset{\displaystyle CH_3}{|}}{\overset{\overset{\displaystyle O}{\|}}{C}}NH \xrightarrow[\substack{Co_2(CO)_8 \\ CO/H_2 = 3 \\ 120^{\circ}C}]{(CH_2O)_x} C_{11}H_{23}\underset{\underset{\displaystyle CH_3}{|}}{\overset{\overset{\displaystyle O}{\|}}{C}}NCH_2COOH$$
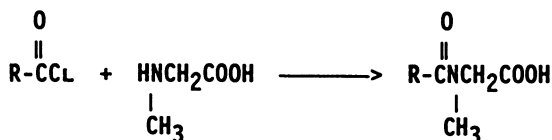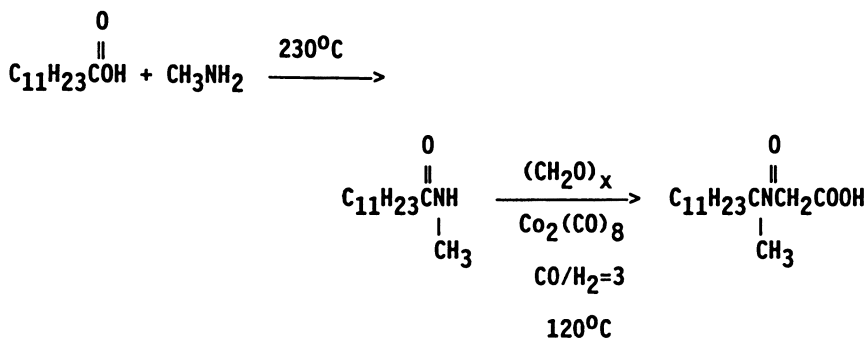
Scheme III. Alkyl sarcosinate synthesis.

Other Amido Acids. Amidocarbonylation of lactams, butyrolactam, and caprolactam to prepare the corresponding amido acids has been demonstrated (Scheme IV) (15).
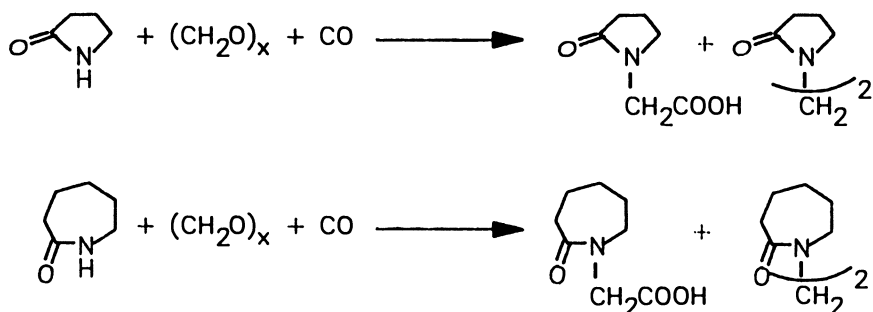
Scheme IV. Amido acids from N-substituted amides.

Hydroformylation and Amidocarbonylation

Simple Olefins.   In 1981 Stern patented a process to make *N*-acetylamino acid from olefin, acetamide, and synthesis gas in the presence of octacarbonyldicobalt (*3*). The hydroformylation and amidocarbonylation occurred in a single step. It was also reported that the one-step reaction afforded an 11.5:1 ratio of linear to branched amido acids, in contrast to the 2.4:1 ratio via the corresponding two-step route. Ojima et al. (*4*) reported that product selectivity was affected by the addition of a rhodium cocatalyst (Scheme V).

Our results showed that amido acid with a 94% linearity was obtained by using $Co_2(CO)_8$, 75% linearity with $Co_2(CO)_8$–$Rh_6(CO)_{16}$, and 95% linearity with $Co_2(CO)_8$–$HRh(CO)(PPh_3)_3$. Furthermore, addition of bidentate phosphines enabled hydroformylation–amidocarbonylation at lower pressures. For example, combination of bis(diphenylphosphino)propane with octacarbonyldicobalt afforded good activity at 2000 psi of synthesis gas pressure (*16*). The process to make C_{16} amido acid from 1-tetradecene was optimized. A recrystallization procedure was designed to purify the amido acid product by removing cobalt and rhodium catalyst contaminants (*17*). The sodium salt of this amido acid has uses in cosmetics (*18*) (Tables II–IV).

Diolefins.   Various amido acids were prepared from diolefins, such as dicyclopentadiene, 4-vinyl-1-cyclohexene, 1,3-butadiene, and 1,7-octadiene. Monoamido acids were selectively made from the unsymmetrical dienes, dicyclopentadiene, and 4-vinyl-1-hexene. However, diamido acids were produced when symmetric diene substrates were used (Table V).

Functionalized Olefins.   When hydroformylation–amidocarbonylation was extended to functionalized olefins, a number of interesting amido acids were obtained. Glutamic acid ester, a precursor for monosodium glutamate, can be synthesized from acrylate, acetamide, and synthesis gas in

$$CF_3CH=CH_2 \longrightarrow \begin{cases} \xrightarrow{Co} CF_3CH_2CH_2CHO \ (93\%) \longrightarrow CF_3CH_2CH_2CH(COOH)(NHCOCH_3) \quad (I) \\ \xrightarrow{Rh} CF_3CHCHO(CH_3) \ (96\%) \longrightarrow CF_3CHCH(COOH)(NHCOCH_3)(CH_3) \quad (II) \end{cases}$$

ONE-STEP PROCESS

CATALYST	LINEAR (I) %	BRANCHED (II) %
$Co_2(CO)_8$ (5 MOLE%)	94	4
$Co_2(CO)_8$ (5%) + $Rh_6(CO)_{16}$ (0.1%)	6	94
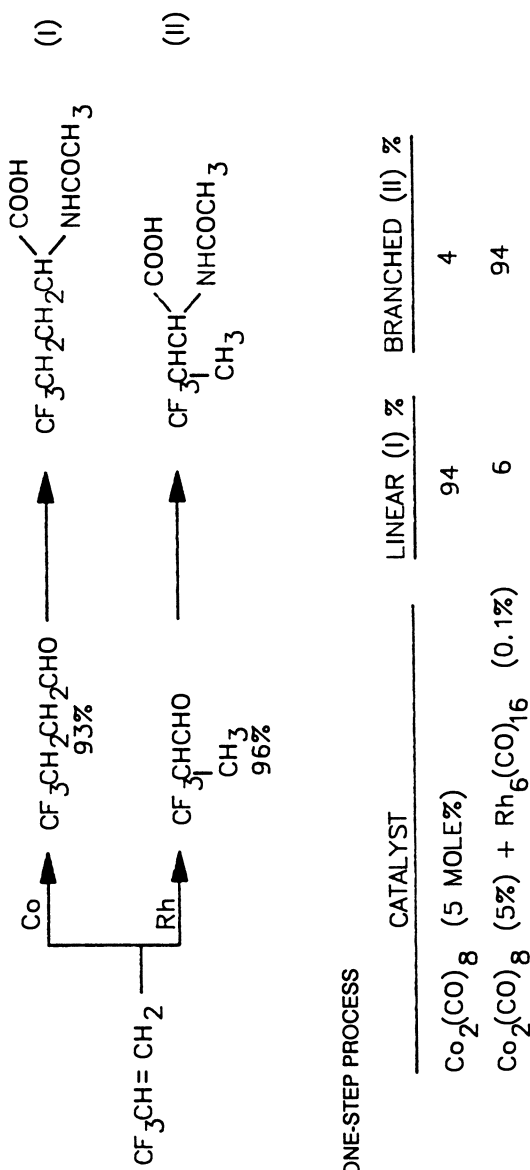
Scheme V. Hydroformylation–amidocarbonylation: product selectivity.

Table II. Hydroformylation–Amidocarbonylation: Cocatalyst Effect

$$RCH=CH_2 \ + \ CH_3CONH_2 \ + \ CO/H_2 \ \longrightarrow \ RCH_2CH_2CH \begin{smallmatrix} COOH \\ / \\ \\ \backslash \\ NHCOCH_3 \end{smallmatrix}$$
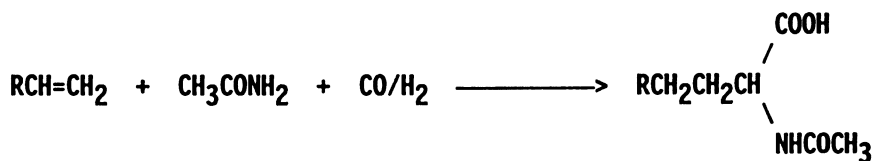
Catalyst–Cocatalyst	Conditions	Yield (%)	Linearity (%)
Co₂(CO)₈	1900 psi, 100–110 °C	70	92
Co₂(CO)₈–Rh₆(CO)₁₆ (35:1)	2000 psi, 100 °C	70	75
Co₂(CO)₈–HRh(CO)(PPh₃)₃ (40:1)	2000 psi, 100 °C	89	95
Co₂(CO)₈–HRh(CO)(PPh₃)₃ (40:1)	800 psi, 100 °C	55	—

85% yield (*19*). This in situ hydroformylation–amidocarbonylation route afforded the linear amido acid as the major product. By comparison, rhodium-catalyzed hydroformylation of acrylate afforded dimethyl 2-formyl-2-methylglutarate at 75% selectivity and 60% conversion (*20*). This product was derived from hydroformylation of acrylate at the alpha position and subsequent Michael addition to a second equivalent of acrylate (*2*) (Scheme VI).

The reactions of allyl acetate, 2-pentenenitrile, and allyl alcohol ethoxylate afforded the corresponding amido acids in good yield. These structures are cited in Table VI.

Conclusion
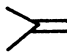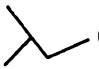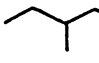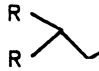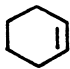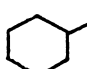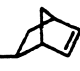
We have used amidocarbonylation technology for many applications. Modifications of homogeneous cobalt catalyst with diphenyl sulfoxide

Table III. Effects of Ligand on Reaction Rate

Ligands	Temperature (°C)	Olefin Conversion (%)	Cobalt Recovery (%)
None	130	68	81
Ph₂P(CH₂)PPh₂	130	40	80
Ph₂P(CH₂)₂PPh₂	130	80	—
Ph₂P(CH₂)₃PPh₂	130	95	85
Ph₂P(CH₂)₄PPh₂	130	60	—
Ph₂P(CH₂)₆PPh₂	130	75	100
n-Bu₃P	130	60	—
Ph₂P(CH₂)₃PPh₂	150	95	80
None	150	0	—
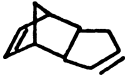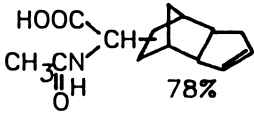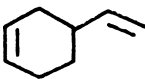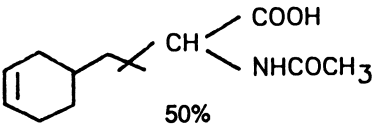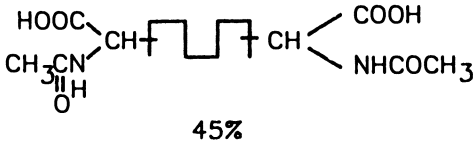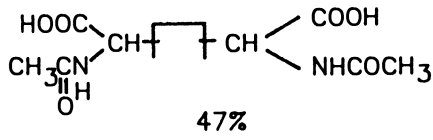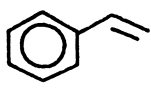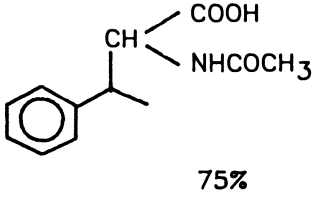
NOTE: Catalyst: Co₂(CO)₈ (2 mmol). Reactants: 1-dodecene (100 mmol), acetamide (100 mmol), and *p*-dioxane (30 g). Conditions: CO–H₂ (1:1), 800 psi, 4 h, ligand (1 mmol).

Table IV. Hydroformylation–Amidocarbonylation: Reaction Scope

Starting Olefins	Major Products	Yield; M.P.
(olefin structure)	$CH_3CH_2CH_2CH$ < COOH / NHCOCH$_3$	70%
(olefin structure)	CH < COOH / NHCOCH$_3$	84%; 128–135 °C
(olefin structure)	CH < COOH / NHCOCH$_3$	34%; 130–135 °C
R, R >= (C14)	R, R CH < COOH / NHCOCH$_3$	66%; 93–98 °C
$1-C_{10}^=$ TO $C_{14}^=$	R–CH < COOH / NHCOCH$_3$	91%; 95 °C
$7-C_{14}^=$ OR $9-C_{18}^=$	R_1 R_2 >– CH < COOH / NHCOCH$_3$	85%; LIQUID
(cyclohexene structure)	CH < COOH / NHCOCH$_3$	85%; 180–186 °C
C_8H_{17} (norbornene structure)	C_8H_{17} –CH < COOH / NHCOCH$_3$	80–90%

and succinonitrile improved catalyst recovery and increased the yield of amidocarbonylation product. In addition, two catalyst systems, $Co_2(CO)_8$–$HRh(CO)(PPh_3)_3$ and $Co_2(CO)_8$–$Ph_2P(CH_2)_3PPh_2$, were found to be effective for olefin hydroformylation–amidocarbonylation. These modified catalysts greatly expand upon the versatility of this technology, which can be used to synthesize N-acetylglycine, phenylalanine, (potential intermediates for the sweetener, aspartame), specialty surfactants from olefins, and glutamic acid.

Table V. Amido Acids from Other Olefins

Starting Materials	Products and Yields

The new amidocarbonylation technology has the following advantages:

- Versatility: The same technology can be used to make a host of amino acids.

- Less hazardous synthetic route: an alternative to the Strecker process.

$$CH_2=CHCOOC_2H_5 + CH_3CONH_2 + CO/H_2 \xrightarrow[130-150°C]{Co_2(CO)_8}$$

$$HOOC-CHCH_2CH_2COOC_2H_5 \xrightarrow{H^+} GLUTAMIC\ ACID$$

$$\overset{|}{NH}$$
$$\overset{|}{C=O}$$
$$\overset{|}{CH_3}$$

(85% YIELD)
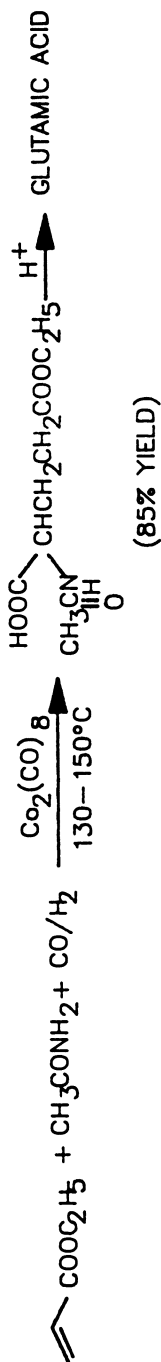
ALDEHYDE INTERMEDIATES

$$CH_2=CHCOOR \xrightarrow{Co_2(CO)_8} OHC \diagdown COOR \quad 91\%\ SELECTIVITY$$

$$\xrightarrow{HRh(CO)(PPh_3)_3} \left[\begin{array}{c} CHO \\ | \\ COOR \end{array} \right]$$

$$ROOC \diagup \overset{CHO}{\diagdown} COOR$$

75% SELECTIVITY
60% CONVERSION
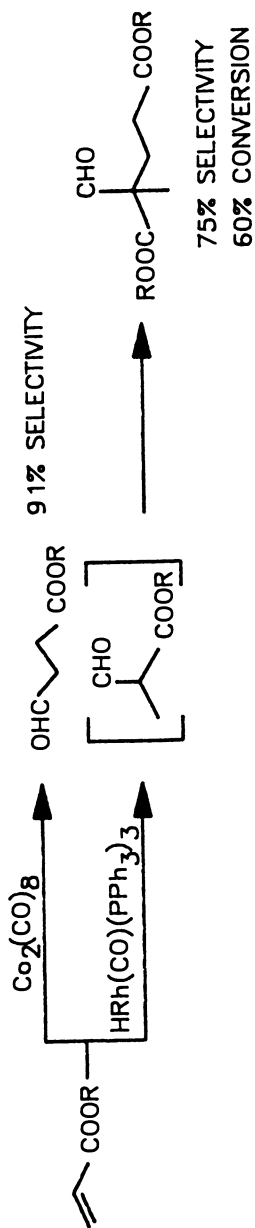
Scheme VI. Glutamic acid synthesis.

Table VI. Amido Acids from Functionalized Olefins

Starting Materials	Products
CH₂=CH−CONH₂	pyrrolidinone-COOH + succinimide
CH₃CH=CH−OAc + CH₃CONH₂	HOOC−CH(NHCOCH₃)−CH₂CH₂−OAc
CH₃CH=CHCH₂−CN + CH₃CONH₂	CH(COOH)(NHCOCH₃)−CH₂CH(CH₃)−CH₂CN
CH₂=CHCH₂−O(CH₂CH₂O)ₓH + CH₃CONH₂	HOOC−CH(NHCOCH₃)−CH₂CH₂−O(CH₂CH₂O)ₓH
R−CH=CH₂ + CH₃C(O)NH−CH₂CH₂−OH	R−CH₂CH₂−CH(COOH)(N(COCH₃)−CH₂CH₂−OH)

- Inexpensive feedstocks: synthesis of specialty chemicals from commercially available aldehydes or olefins.
- Specialty chemicals from synthesis gas: The feasibility of making specialty chemicals from syngas technology has been shown.

It remains a challenge for chemists to develop new synthetic routes, or to use less expensive feedstocks, for the synthesis of high-value chemicals. The versatility of amidocarbonylation is remarkable in this sense.

References

1. Wakamatsu, H.; Uda, J.; Yamakami, N. *J. Chem. Soc., Chem. Commun.* **1971,** 1540.
2. Parnaud, J.-J.; Campari, G.; Pino, P. *J. Mol. Catal.* **1979,** 6, 341.

3. Institut Français du Pétrole, U.S. Patent 4 264 515, 1981.
4. Ojima, I.; Hirai, K.; Fujita, M.; Fuchikami, T. *J. Organomet. Chem.* **1985**, *279*, 203.
5. Société Nationale Elf Aquitaine, U.S. Patent 4 404 109, 1983.
6. Procter & Gamble, U.S. Patent 4 397 776, 1983.
7. Exxon Research and Engineering Company, U.S. Patent 4 405 579, 1983.
8. Texaco Development Corporation, U.S. Patent 4 918 222, 1990.
9. Genex, U.S. Patents 4 434 228, 1984, and 4 504 582, 1985.
10. Sagami Chemical Research Center, U.S. Patent 4 497 964, 1985.
11. Texaco Development Corporation, U.S. Patent 4 891 442, 1990.
12. Magnue, P.; Slater, M. *Tetrahedron Lett.* **1987**, *28*, 2829.
13. Izawa, K.; Nishi, S.; Asada, S. *J. Mol. Catal.* **1987**, *41*, 135.
14. Texaco Development Corporation, U.S. Patent in application.
15. Texaco Development Corporation, U.S. Patent 4 620 949, 1986.
16. Texaco Development Corporation, U.S. Patent 4 892 687, 1990.
17. Texaco Development Corporation, U.S. Patent 4 676 933, 1987.
18. Texaco Development Corporation, U.S. Patent 4 704 226, 1987.
19. Texaco Development Corporation, U.S. Patent 4 720 573, 1988.
20. Texaco Development Corporation, U.S. Patent 4 849 543, 1989.

Activation of Carbon Monoxide by Metalloradicals

Bradford B. Wayland, Alan E. Sherry, and Virginia L. Coffin

Department of Chemistry, University of Pennsylvania, Philadelphia, PA 19104–6323

Rhodium(II) porphyrin derivatives are observed to activate carbon monoxide toward one-electron reactions at the carbonyl carbon. Reductive coupling of carbon monoxide to form dimetal diketone complexes (M–C(O)–C(O)–M) is one prominent example of this type of reactivity. Thermodynamic and kinetic–mechanistic studies for reactions of CO with a series of cobalt, rhodium, and iridium porphyrins provide insights into criteria for obtaining CO coupling. Seventeen-electron monocarbonyl complexes, (porphyrin)Rh–CO, are implicated as reactive intermediates. Electron paramagnetic resonance studies of the tetramesitylporphyrin derivative (TMP)Rh–CO illustrate how this type of complex directs radicallike reactivity to the carbon center.

$\mathbf{A}$CTIVATION OF CO BY ONE-ELECTRON STEPS is illustrated by the reaction of methyl radicals with CO to form a transient intermediate acyl (CH_3CO) radical. This intermediate subsequently takes part in a second one-electron reaction at the carbonyl carbon to produce acetone, $(CH_3)_2CO$, and biacetyl, CH_3–C(O)–C(O)–CH_3 (eqs 1–3) (1–3). Related reactions of alkyl radicals and atomic species like H• and Cl• are also well known (3–5).
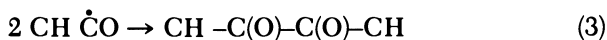
$$CH_3\bullet + CO \rightarrow CH_3\overset{\bullet}{C}O \qquad (1)$$

$$CH_3\overset{\bullet}{C}O + CH_3\bullet \rightarrow (CH_3)_2CO \qquad (2)$$

$$2\ CH\ \overset{\bullet}{C}O \rightarrow CH\ \text{--C(O)--C(O)--CH} \qquad (3)$$

In transition metal chemistry one-electron activation of CO has been accomplished by reduction of 18-electron metal carbonyl complexes to form transient "19-e$^-$" species like $[(CO)_4FeCO]^{\bullet-}$ (6–11). One important reaction of 19-e$^-$ carbonyl complexes like $[(CO)_4FeCO]^{\bullet-}$ is hydrogen atom abstraction from metal hydrides to form transient 18-e$^-$ metalloformyl species, $[Fe(CO)_4CHO]^-$ (eq 4) (6). Reactions 2–4 serve as models for several types of reactions that are characteristic of one-electron activated carbon monoxide.

$$[(CO)_4FeCO]^{\bullet-} + H–M \rightarrow (CO)_4Fe–C(O)H + [M\bullet] \qquad (4)$$
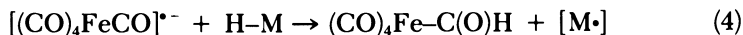
As part of a program to evaluate the reactivity patterns of metalloradicals with small molecules, we have been studying the reactions of Co(II), Rh(II), and Ir(II) porphyrins with CO. One of our objectives was to determine whether metalloradicals (M·) can react with CO to form intermediate complexes, [MCO]·, that exhibit one-electron carbonyl carbon reactions in analogy with the acyl radical $(CH_3\overset{\bullet}{C}O)$ (eqs 1–3). A feature that distinguishes this study from previous work is that the one-electron activating species (M·) is present at thermal equilibrium. This characteristic provides an opportunity to have an equilibrium source of one-electron activated CO, (M$\overset{\bullet}{C}$O).

A series of Group 9 metalloporphyrin complexes [(POR)M(II); M is Co(II), Rh(II), Ir(II)] were selected as sources of metalloradicals. Monomeric d^7 metal ion complexes of porphyrins are expected to be low-spin ($s = \frac{1}{2}$) complexes with the unpaired electron effectively localized in the d_{z^2} orbital normal to the porphyrin plane. Species of this type are often referred to as metalloradicals because there is a single metal-based unpaired electron ($s = \frac{1}{2}$) in an orbital (d_{z^2}) capable of giving one-electron reactions.

Cobalt(II) porphyrins are invariably low-spin monomeric complexes with the expected d_{xy^2}, d_{xz,yz^4}, $d_{z^2 1}$ electron configuration (12). Rhodium(II) and iridium(II) porphyrin complexes are usually diamagnetic M–M bonded dimers, but function as sources of the paramagnetic monomers (13, 14). The large steric requirements of tetramesitylporphyrin (TMP) preclude dimerization through M–M bonding and provide a stable monomeric Rh(II) complex, (TMP)Rh(II) (15). Electron paramagnetic resonance (EPR) spectra for (TMP)Rh(II) in toluene glass (90 K) clearly indicate that this low-spin d^7 ($s = \frac{1}{2}$) complex has a $d_{z^2 1}$ electron configuration (Figure 1a).

Figure 1. EPR spectra for (TMP)Rh(II) and (TMP)Rh–$\overset{\bullet}{C}$O in toluene. Key: a, anisotropic EPR spectrum for (TMP)Rh(II) (90 K) [$g_{1,2}$ = 2.65, g_3 = 1.915; $A^{103}Rh(g_{1,2})$ = 197 MHz, $A^{103}Rh(g_3)$ = 158 MHz]; b, anisotropic EPR spectrum that results from exposing a frozen solution of (TMP)Rh(II) to ^{12}CO (P_{CO} = 200 torr, T = 100 K), warming to 195 K and refreezing to 100 K; c, anisotropic EPR spectrum for (TMP)Rh–$^{13}\overset{\bullet}{C}$O (90 K) [$g_1$ ~ 307 MHz; g_2 = 2.14, $A^{13}C(g_2)$ = 330 MHz; g_3 = 1.995, $A^{103}Rh(g_3)$ = 299 MHz; $A^{13}C(g_3)$ = 67 MHz]; d, isotropic spectrum for (TMP)Rh–$^{13}\overset{\bullet}{C}$O (90 K) [$<g>_{iso}$ = 2.101; $<A^{13}C>$ = 312 MHz].
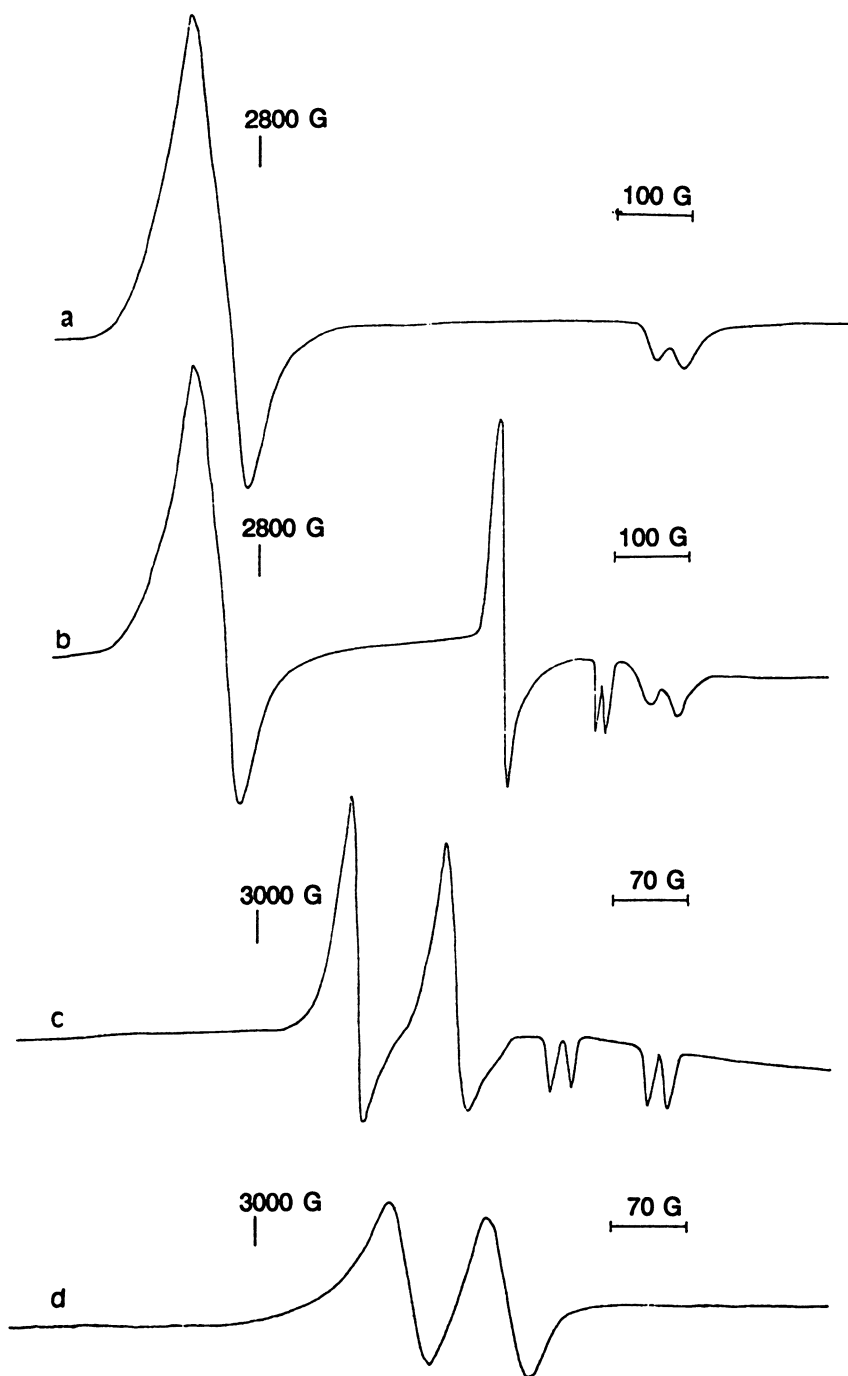
**Table I. Thermochemical Estimates for Generalized Reactions of X–X and X·
with CO To Form Ketone and 1,2-Ethanedionyl Compounds**

Reactions	ΔH^0 (kcal mol^{-1})	ΔG^0 (298 K) (kcal mol^{-1})
X–X + CO $\rightleftarrows$ X–C(O)–X	(X–X) – 2[X–C(O)] + 70	(X–X) – 2[X–C(O)] + 78
2X· + CO $\rightleftarrows$ X–C(O)–X	–2[X–C(O)] + 70	–2[X–C(O)] + 86
X–X + 2CO $\rightleftarrows$ X–C(O)–C(O)–X	(X–X) – 2[X–C(O)] + 70	(X–X) – 2[X–C(O)] + 86
2X· + 2CO $\rightleftarrows$ X–C(O)–C(O)–X	–2[X–C(O)] + 70	–2[X–C(O)] + 94

NOTE: Bond energies from reference 22 were used in deriving the table: (C≡C)–(C=O), 70 kcal mol^{-1}, and C(O)–C(O), 70 kcal mol^{-1}. Bond energies for X–X species were discussed in the chapter: H–H, 104; H$_3$C–CH$_3$, 85; (OEP)Rh–Rh(OEP), 15; (TXP)Rh–Rh(TXP), 12; (OEP)Ir–Ir(OEP), 23; and (TXP)Ir–Ir(TXP), 20 kcal mol^{-1}.

Interaction of a half-occupied metal σ orbital (d$_{z^2}$^{1}) with the CO σ orbitals places spin density at the carbonyl carbon and should also result in a bending of the M–CO unit (*16*). As the M–C covalent bond strength increases, the carbonyl carbon will rehybridize toward sp^2, the C–O bond order will decrease, the M–C–O angle will decrease from 180° toward 120°, and the carbon spin density will increase. The limiting case is approximated by CH$_3$–CO, which is properly depicted as CH$_3$–Ċ=O. Evidence for one-electron metalloradical activation can come from observation of these structural and spin density changes, but further requires the characteristic overall reactivity depicted by eqs 1–4. Guideline thermodynamic criteria for the metal analogs of reactions 2 and 3 are given in Table I.

Reactions of (Porphyrin)M(II) Complexes with CO

Co(II) Porphyrin. Monomeric cobalt(II) complexes of porphyrins have the low-spin d^7 electron configuration, which is frequently associated with metalloradical species, and accomplish one-electron reactions with NO and O$_2$ (eqs 5 and 6) (*16*).

$$(POR)Co + NO \rightleftarrows (POR)Co–NO \quad (s = 0) \quad (5)$$

$$(POR)Co + O_2 \rightleftarrows (POR)Co–O_2 \quad (s = \tfrac{1}{2}) \quad (6)$$
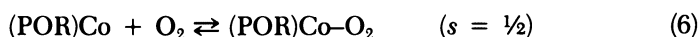
Tetraphenylporphyrincobalt(II), (TPP)Co, binds CO in toluene glass (90 K) to form a monocarbonyl complex [(TPP)CoCO] (eq 7) (*16*).

$$(TPP)Co + CO \rightleftarrows (TPP)CoCO \quad (7)$$

EPR spectra of (TPP)Co^{13}CO were used in probing the properties of this species. An isotropic ^{13}C hyperfine coupling constant of 170 MHz yields a C$_{2s}$ spin density of 0.054. A nonlinear Co–C–O fragment should be a fundamental feature of a half-filled d$_{z^2}$ orbital forming a σ bond with CO. However, the EPR g values and the ^{13}C hyperfine coupling constants are

compatible with axial symmetry (**A**) for (TPP)CoCO ($g_{\parallel} = 2.017$; $g_{\perp} = 2.217$; $A_{\parallel}$ $^{13}C = 179$ MHz; $A_{\perp}$ $^{13}C = 166$ MHz). The anisotropic ^{13}C coupling constants yield a C_{2p} spin density of 0.049 for an axially symmetric complex. They are used to deduce that the carbonyl carbon exhibits near-sp hybridization ($\rho_{C_{2s}}/\rho_{C_{2p}} = 1.1$) and that the total CO spin density is ~0.13. The odd electron in (TPP)CoCO is thus largely based on cobalt. The Co–CO covalent bonding is too weak to produce sufficient carbonyl carbon rehybridization for the associated bending of the Co–CO unit to be detected in the EPR spectrum. The Co–C bond energies determined for cobalt porphyrin alkyls (20–30 kcal mol^{-1}) (*17*) are far too small to produce reactions analogous to reactions 2–4, which result in reduction of the CO bond order to 2.

Rh(II) Porphyrin.   The search for metal complexes capable of one-electron activation of CO was subsequently extended to Rh(II) and Ir(II) porphyrins, which are expected to form stronger M–C bonds than Co(II) complexes. Reactivity studies of CO with octaethylporphyrinrhodium(II) dimer, [(OEP)Rh]$_2$, revealed the formation of dimetal ketone [(OEP)Rh–C(O)–Rh(OEP)] and dimetal α-diketone [(OEP)Rh–C(O)–C(O)–Rh(OEP)] complexes (eqs 8 and 9) (*18, 19*).

$$[(OEP)Rh]_2 + CO \rightleftarrows (OEP)Rh{-}C(O){-}Rh(OEP) \qquad (8)$$

$$[(OEP)Rh]_2 + 2CO \rightleftarrows (OEP)Rh{-}C(O){-}C(O){-}Rh(OEP) \qquad (9)$$
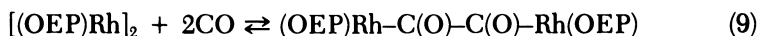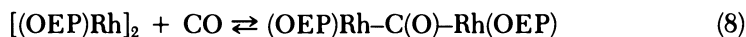
These products have a formal relationship to acetone (CH_3–C(O)–CH_3) and biacetyl (CH_3–C(O)–C(O)–CH_3) that results from the reaction of CH_3· with CO (eqs 2 and 3). The desired type of CO complex, (OEP)Rh–ĊO, could be an intermediate in reactions 8 and 9. The insertion of CO into the Rh–H bond in (OEP)Rh–H to produce a metalloformyl complex (OEP)Rh–C(O)H (eq 10) (*20*) involves a radicallike pathway in benzene.

$$(OEP)Rh{-}H + CO \rightleftarrows (OEP)Rh{-}C(O)H \qquad (10)$$
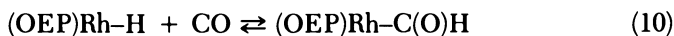
A detailed kinetic study of the [(OEP)Rh]$_2$ catalysis of reaction 10 (*21*) demonstrated a rate law consistent with a radical chain process in which (OEP)Rh–CO functions as an intermediate (eqs 11–13).

$$[(OEP)Rh]_2 \rightleftarrows 2(OEP)Rh· \qquad (11)$$

$$(OEP)Rh· + CO \rightleftarrows (OEP)Rh{-}CO \qquad (12)$$

$$(OEP)Rh{-}CO + (OEP)Rh{-}H \rightleftarrows (OEP)Rh{-}C(O)H + (OEP)Rh· \qquad (13)$$
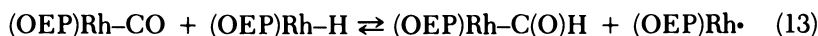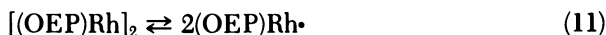
Our efforts to observe the proposed intermediate complex, (OEP)Rh–CO, directly by EPR spectroscopy were not successful. However,

^{13}C NMR spectra of bulk ^{13}CO in solutions of [(OEP)Rh]$_2$ with ^{13}CO manifest large line broadening of the ^{13}CO peak as the temperature increases. This broadening provides qualitative evidence for CO exchange with a paramagnetic complex, (OEP)Rh–CO (22).

Subsequent investigations of the reaction of CO with the monomeric tetramesitylrhodium(II) complex, (TMP)Rh·, have resulted in the direct observation of (TMP)Rh–CO. This observation led to evaluation of some general structural and electronic features of this 17-electron monocarbonyl complex (15).

(TMP)Rh· (1) reacts with CO to form a mono-CO complex, (TMP)Rh–CO (2), and an α-diketone (TMP)Rh–C(O)–C(O)–Rh(TMP) (3) (eqs 14 and 15) (15).

$$(TMP)Rh\cdot \; + \; CO \; \rightleftarrows \; (TMP)Rh\text{–}CO \qquad (14)$$

$$2(TMP)Rh\cdot \; + \; 2CO \; \rightleftarrows \; (TMP)Rh\text{–}C(O)\text{–}C(O)\text{–}Rh(TMP) \qquad (15)$$
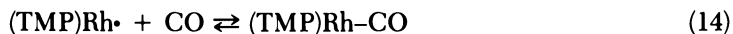
A dimetal ketone [M–C(O)–M] is not observed for the (TMP)Rh system because of the large steric requirements of tetramesitylporphyrin. Similarly, tetramesitylporphyrin was previously shown to block formation of oxo-bridged Fe and Ru complexes (23). EPR spectra for (TMP)Rh–CO are illustrated in Figure 1. The toluene glass (EPR) spectrum of (TMP)Rh–^{13}CO was obtained under nonequilibrium conditions by exposing a solution of (TMP)Rh· near the solvent freezing point and then rapidly freezing to 90 K (Figure 1c). The EPR g values clearly place the unpaired electron in a molecular orbital with d$_{z^2}$ character. The large ^{13}C coupling constants indicate substantial intermixing of d$_{z^2}$ with the CO σ orbitals.

In contrast with (POR)Co–^{13}CO complexes, the anisotropic EPR spectrum of (TMP)Rh–^{13}CO provides evidence for a bent Rh–CO unit. Observation of a smaller ^{13}C coupling on the g_3 (g_z) transition than observed for g_1 or g_2 indicates that the g and A ^{13}C tensors are not coincident. This property is shared with both HCO (24) and [(CO)$_4$FeCO]$^{\cdot-}$ (25). It provides a clear indication of nonaxial symmetry and a bent XCO unit. The isotropic ^{13}C coupling constant of 312 MHz in (TMP)Rh^{13}CO is larger than in [(CO)$_4$FeCO]$^{\cdot-}$ (224 MHz) (25) and approaches the value for the formyl radical (365 MHz) (23). An isotropic ^{13}C coupling constant of 312 MHz corresponds to a C$_{2s}$ spin density of 0.10 electrons (ρ_{2s} = <A^{13}C>/3110 MHz) compared to ρ_{2s} = 0.12 in HCO. Anisotropy of the ^{13}C coupling constants on the g value transitions cannot be used to extract the C$_{2p}$ spin density because the principal values of the A ^{13}C tensor are not observable in the glass spectrum. Presence of a bent Rh–CO unit implies substantial rehybridization at the carbonyl carbon from sp toward sp^2. The carbonyl carbon spin density is thus ~0.2–0.3, which implies that the total CO spin density is ~0.25–0.35. The CO spin density in (TMP)Rh–CO is 2 to 3 times larger than in (TPP)Co–CO but probably substantially less than that in HCO

($\rho_{CO} = 1 - \rho_{H_{1s}} \simeq 0.75$) (*23, 24*). (TMP)Rh–CO thus contains a bent, partially rehybridized Rh–CO unit in which the unpaired electron occupies a σ molecular orbital ($d_{z^2} + CO_\sigma$) that has ~70% d_{z^2} and ~30% CO_σ character. The electronic structure can be depicted as a resonance hybrid of limiting electron structures that localize the odd electron in the rhodium d_{z^2} ($\cdot$Rh–C≡O) or a carbon sp^2 hybrid (Rh–$\overset{\centerdot}{C}$=O). The 17-electron complex, (TMP)Rh–CO, is thus poised for a second one-electron reaction at either the rhodium or carbonyl carbon sites. Reaction with a one-electron species X$\cdot$ at the metal would produce an 18-electron Rh(III) carbon monoxide complex, (TMP)Rh(X)(CO). Correspondingly, reaction at the carbonyl carbon forms a 16-electron Rh(III) complex, (TMP)Rh–C(O)X.

Reversible dimerization of (TMP)Rh–CO (**1**) through C–C bond formation to produce a 1,2-ethanedionyl complex, (TMP)Rh–C(O)–C(O)–Rh(TMP) (**2**), illustrates a carbonyl carbon-centered one-electron reaction that can be viewed as an organometallic analog of formyl radical coupling [2H $\overset{\centerdot}{C}$O → H–C(O)–C(O)–H] (eq 16).

$$2(TMP)Rh–CO \rightleftarrows (TMP)Rh–C(O)–C(O)–Rh(TMP) \qquad (16)$$
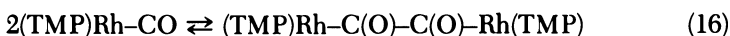
The type of CO reductive coupling depicted by eq 16 is presently known only for reactions of (POR)Rh(II) complexes with CO. Temperature dependence of the isotropic EPR intensity for (TMP)RhCO (**1**) has been analyzed to provide the enthalpy change for reaction 16 ($\Delta H_{16}^0 = -18.3 \pm 0.8$ kcal mol^{-1}) (*15*).

Temperature dependence of the pyrrole ^{1}H line broadening of (TMP)Rh–C(O)–C(O)–Rh(TMP) (**2**) is ascribed to exchange of the diamagnetic dimer (**2**) with the paramagnetic monomer (**1**) and used in deriving the activation energy for the dissociation of **2** into **1** ($\Delta H^\ddagger = 21.3 \pm 0.8$ kcal mol^{-1}) (Figure 2). An energy profile for the reversible dimerization of (TMP)Rh–CO is illustrated in Figure 3. The activation energy for dimerization ($\Delta H_{16}^\ddagger \sim 3 \pm 1$ kcal mol^{-1}) is derived from ΔH_{16}^0 (–18.3 kcal mol^{-1}) and $\Delta H_{-16}^\ddagger$ (+21.3 $\pm$ 0.8 kcal mol^{-1}), which is close to the value calculated for a diffusion-controlled process in benzene (3.1 kcal).

Assuming that the dionyl unit [–C(O)–C(O)–] in **3** is similar to the organic analogs like biformyl, the dissociation of **3** into **2** results in cleavage of a 65–70-kcal C–C bond. The experimental dissociation energy ($\Delta H_{-16}^0 = 18.3 \pm 0.8$ kcal mol^{-1}) is considerably smaller than the expected C–C bond energy in **3** (~65–70 kcal mol^{-1}) (*26*). The energy difference indicates that ~50 kcal of the energy change associated with reduction of the CO bond order in forming the α-diketone complex [2(C≡O)–2(C=O) $\simeq$ 140 kcal mol^{-1}] is regained in forming (TMP)Rh–CO. This observation supports the EPR evidence that (TMP)Rh–CO contains only a partially rehybridized carbonyl unit with a bond order between 2 and 3 (Rh–C$\overset{\cdots}{=}$O).

Thermodynamic studies for reactions of [(OEP)Rh]$_2$ and (OEP)Rh–H with CO have been used in deriving values for the Rh–C(O)X bond energies
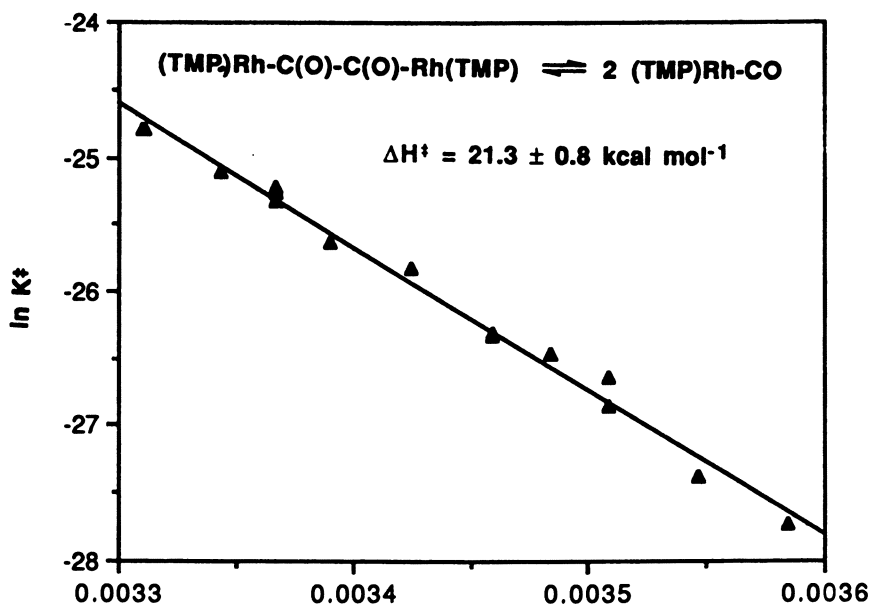
Figure 2. Temperature dependence of the pyrrole ^1H line broadening for (TMP)Rh–C(O)–C(O)–Rh(TMP) in C_6D_6.
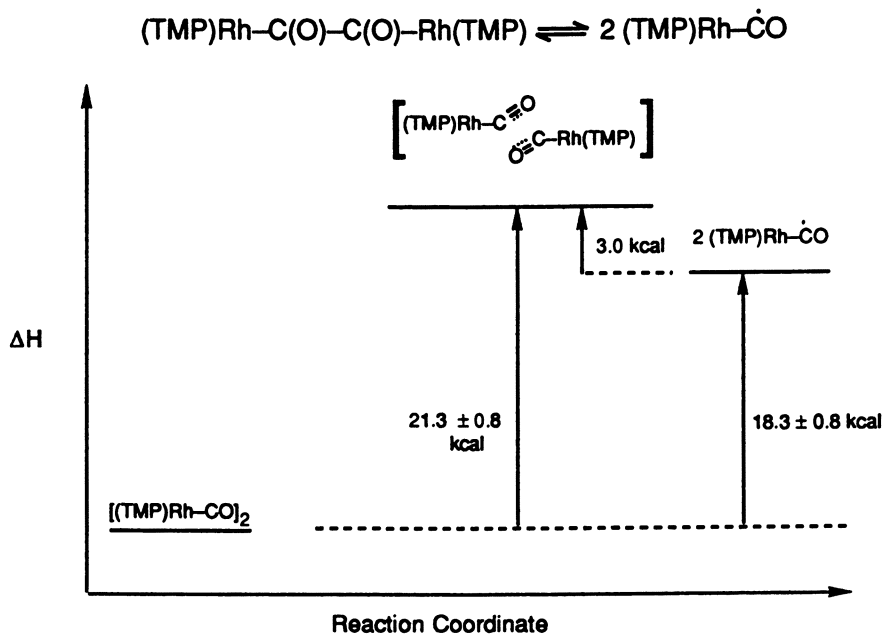
Figure 3. Enthalpy profile for the dissociation of (TMP)Rh–C(O)–C(O)–Rh(TMP) into two (TMP)Rh–CO in C_6D_6.

in (OEP)Rh–C(O)H (58 kcal mol^{-1}) (*13*), (OEP)Rh–C(O)–C(O)–Rh(OEP) (54 kcal mol^{-1}), and (OEP)Rh–C(O)Rh(OEP) (49 kcal mol^{-1}) (*16*). The current maximum Rh–C(O)X bond energy of ~58 kcal mol^{-1} is insufficient to justify full rehybridization of C≡O to a C=O unit [(C≡O)–(C=O) ≃ 70 kcal mol^{-1}].

More complete CO rehybridization occurs in the formyl radical because of the stronger H–C(O) bond. The bond strength and directional character of the CH$_3$–C(O) bond produces virtually complete CO rehybridization in the acyl radical (Table II). In (POR)Rh–CO complexes, reduction of the C–O bond order to 2 (C=O) requires the formation of a second bond at the carbonyl carbon. This bond formation is observed to be effectively accomplished in forming (POR)Rh–C(O)H, (POR)Rh–C(O)–Rh(POR), and (POR)Rh–C(O)–C(O)–Rh(POR) complexes, where the observed CO stretching frequencies for these species fall in the range for C–O double bonds (1700–1770 cm^{-1}) (*18, 21, 29*).

(POR)Rh–CO is the probable central intermediate in reactions of rhodium porphyrins that produce formyl, ketone, and α-diketone complexes. The bent and partially rehybridized Rh–CO fragment provides a relatively low-energy pathway for reversible one-electron reactions at the carbonyl carbon. Thermodynamic and kinetic studies of the dissociation of (TMP)Rh–C(O)–C(O)–Rh(TMP) provide a detailed view of how the nature of (TMP)Rh–CO provides a facile pathway for (O)C–C(O) bond homolysis. The stretching and ultimate cleavage of the C–C bond is synchronized with an increase in the CO bond order such that the activation energy for dissociation ($\Delta H^{\ddagger}$ = 21 kcal mol^{-1}) is ~43–48 kcal mol^{-1} less than the C–C bond energy (~65–70 kcal mol^{-1}) in the α-diketone complex. The Rh–CO units in the transition state are thus similar to that present in the monomer, (TMP)Rh–CO.

Most of the reorganization energy expended for rehybridization of the carbonyl unit in forming the C–C bond is regained in the transition state, in which an increase in the C–O bond order occurs at the expense of breaking

Table II. Reorganization Energies for the XCO Units
in the Homolysis of the (O)C–C(O) Bonded Dimers

XC(O)C(O)X → 2XCO

X	ΔH^0 (kcal mol^{-1})	Reorganization Energy^a/XCO (kcal mol^{-1})
CH$_3$	69.20	0
H	69.9	0
(TMP)Rh	18.3	–25

^{a}The reorganization energy per XCO unit is defined here as one-half of the difference between the enthalpy of dissociation (*24, 27, 28*) and the enthalpy for the bond homolysis without electronic or structural reorganization in the resulting fragments. The (O)C–C(O) bond energies in biformyl and biacetyl are 69–70 kcal mol^{-1} and assumed to be similar in dimetal α-diketone species (*25*).

the C–C bond. Similarly, homolytic dissociation energies and potentially associated activation enthalpies for dissociation of any X· from (POR)Rh–C(O)X should be ~25 kcal mol^{-1} less than the C(O)–X bond energy. This feature of (POR)Rh–C(O)X species can be contrasted with organic analogs CH$_3$–C(O)–X, in which the C(O)–X bond homolysis enthalpies approach the values for the C(O)–X bond energies (Table II) (30).

Ir(II) Porphyrin. [(OEP)Ir]$_2$ and (OEP)Ir–H are in many ways closely related to the corresponding (OEP)Rh complexes. However, their reactions with CO are surprisingly different (eqs 17 and 18).

$$[(OEP)Ir]_2 + CO \rightleftarrows [(OEP)Ir]_2(CO)_n \qquad (n = 1, 2) \qquad (17)$$

$$(OEP)Ir–H + CO \rightleftarrows (OEP)Ir–(H)(CO) \qquad (18)$$
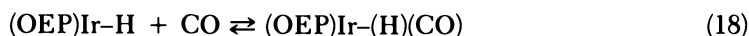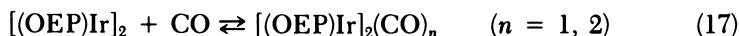
Carbon monoxide reacts with [(OEP)Ir]$_2$ and (OEP)Ir–H (31) to form only terminal CO complexes. Reactions that give overall insertion of CO into Ir–Ir and Ir–H bonds, which are prominent types of reactions for rhodium porphyrins, are not observed for (OEP)Ir derivatives. These observations indicate that increases in the M–M and M–H bond energies in going from Rh to Ir are not compensated by corresponding increases in the Ir–C(O)– bond energies. Weakening of the Ir–Ir bond by increasing the ligand steric requirements should permit formation of dimetal ketone and α-diketone complexes. However, testing of this supposition must await results from studies utilizing tetramesitylporphyriniridium(II).

Summary

Reactions of carbon monoxide with Group 9 M(II) porphyrin complexes (M is Co, Rh, Ir) have been evaluated. At present only rhodium(II) porphyrin complexes have manifested the characteristics of one-electron CO activation. Cobalt–carbon bond energies (~20–30 kcal mol^{-1}) are too small and the Ir–Ir and Ir–H bond energies are too large for the compounds studied to produce observable equilibrium quantities of acyl derivatives. Rhodium(II) porphyrin complexes react with CO to form equilibrium distributions of dimetal ketone and dimetal α-diketone complexes. The porphyrin rhodium hydrides are also known to form metalloformyl complexes.

    Studies of the reaction of (TMP)Rh(II) with CO have provided direct observation of the monocarbonyl species (TMP)RhCO, which contains a nonlinear RhCO unit and substantial carbon spin density. (POR)RhCO species contain one-electron activated carbon monoxide that provides low-energy pathways for a second one-electron reaction to occur at the carbonyl carbon. (POR)RhCO species can thus function as productive intermediates in the sequential two-electron reduction of CO manifested in reactions of CO that produce metalloformyl, dimetal ketone, and dimetal diketone species.

Acknowledgment

References

1. Watkins, K. W.; Word, W. W. *Int. J. Chem. Kinet.* **1974**, *6*, 855–873.
2. Anastasi, C.; Maw, P. L. *J. Chem. Soc., Faraday Trans. 1* **1982**, *78*, 2423.
3. O'Neal, H. E.; Benson, S. W. *Thermochemistry of Free Radicals in Free Radicals*, Vol. 2; Kochi, J. K., Ed.; Wiley: New York, 1973; Chapter 17.
4. Watkins, K. W.; Thompson, W. W. *Int. J. Chem. Kinet.* **1973**, *5*, 791.
5. Ryu, I.; Kusano, K.; Ogawa, A.; Kambe, N.; Sonoda, N. *J. Am. Chem. Soc.* **1990**, *112*, 1295.
6. Narayanan, B. A.; Amatore, C.; Kochi, J. K. *Organometallics* **1986**, *5*, 926.
7. Narayanan, B. A.; Kochi, J. K. *J. Organomet. Chem.* **1984**, *272*, C49.
8. Amatore, C.; Verpeaux, J. N.; Krusic, P. J. *Organometallics* **1988**, *7*, 2426.
9. Crocker, L. S.; Heinekey, D. M.; Schulte, G. L. *J. Am. Chem. Soc.* **1989**, *111*, 405.
10. Pan, Y. H.; Ridge, D. P. *J. Am. Chem. Soc.* **1989**, *111*, 1151.
11. Fairhurst, S. A.; Morton, J. R.; Preston, K. F. *J. Chem. Phys.* **1982**, *76*, 234.
12. La Mar, G. N.; Walker, F. A. *J. Am. Chem. Soc.* **1973**, *95*, 1790.
13. Wayland, B. B.; Coffin, V. L.; Farnos, M. D. *Inorg. Chem.* **1988**, *27*, 2745.
14. Del Rossi, K. J.; Wayland, B. B. *J. Chem. Soc., Chem. Commun.* **1986**, 1653.
15. Sherry, A. E.; Wayland, B. B. *J. Am. Chem. Soc.* **1989**, *111*, 5010.
16. Wayland, B. B.; Minkiewicz, J. V.; Abd-Elmageed, M. E. *J. Am. Chem. Soc.* **1974**, *96*, 2795.
17. Geno, M. K.; Halpern, J. *J. Am. Chem. Soc.* **1987**, *109*, 1238.
18. Wayland, B. B.; Woods, B. A.; Coffin, V. L. *Organometallics* **1986**, *5*, 1059–1062.
19. Coffin, V. L.; Brennen, W.; Wayland, B. B. *J. Am. Chem. Soc.* **1988**, *110*, 6063–6069.
20. Wayland, B. B.; Woods, B. A.; Pierce, R. *J. Am. Chem. Soc.* **1982**, *104*, 302.
21. Paonessa, R. S.; Thomas, N. C.; Halpern, J. *J. Am. Chem. Soc.* **1985**, *107*, 4333.
22. Coffin, V. L. Ph.D. Dissertation, University of Pennsylvania, 1989.
23. Groves, J. T.; Quinn, R. *Inorg. Chem.* **1984**, *23*, 3844.
24. Holmberg, R. W. *J. Chem. Phys.* **1969**, *51*, 3255.
25. Fairhurst, S. A.; Morton, J. R.; Preston, K. F. *J. Chem. Phys.* **1982**, *77*, 5872.
26. Wayland, B. B. *Polyhedron* **1988**, *7*, 1545–1555.
27. Wagman, D. D.; Evans, W. H.; Parker, V. B.; Halow, I.; Bailey, S. M.; Schumm, R. H. NBS Technical Note 270-3, Institute for Basic Standards, National Bureau of Standards: Washington, DC, 1968.
28. Cox, J. D.; Pilcher, G. *Thermochemistry of Organic and Organometallic Compounds*; Academic: New York, 1970.
29. Wayland, B. B.; Sherry, A. E.; Coffin, V. L. *J. Chem. Soc., Chem. Commun.* **1989**, 662.
30. Benson, S. W. *Thermochemical Kinetics*; Wiley: New York, 1968.
31. Farnos, M. D.; Woods, B. A.; Wayland, B. B. *J. Am. Chem. Soc.* **1986**, *108*, 3659.

Electrochemical vs. Chemical Synthesis of Homogeneous Catalysts for Regio- and Enantioselective Olefin Hydroformylation

André Mortreux and Francis Petit[1]

Laboratoire de Chimie Organique Appliqueé de l'ENSC Lille, URA Centre National de la Recherche Scientifique 402, Université des Sciences et Techniques de Lille Flandres Artois, BP 108, 59652 Villeneuve d'Ascq Cedex, France

Electrochemical reduction of organometallic complexes of rhodium and platinum was used for the synthesis of active species useful for regio- and enantioselective olefin hydroformylation. These catalytic species behave differently from conventional catalysts by enhancing the regio- and enantioselectivity. A 98% regioselectivity is obtained for 1-hexene with platinum. Analyses of the catalysts synthesized under these conditions revealed the structural characteristics of the main species obtained in solution. From the structural knowledge of these complexes it was possible to identify other catalytic systems prepared by purely chemical means in which electrochemistry was not needed, and to produce similar species with the same interesting catalytic properties.

Electrochemistry is a useful tool for the synthesis of catalytic moieties because the number of electrons transferred tends to be easily checked. Consequently, by controlling the electrode potential, one can often obtain specifically different oxidation states. Furthermore, because there is no excess of cocatalyst, the side reactions occurring when chemical reducing agents are used can be avoided.

[1]Corresponding author

An organometallic complex $ML_nX_xZ_z$ generates unsaturated species in neutral or acidic medium by electroreduction according to eq 1. A vacant coordination site is available after this electrochemical process. Thus, a catalytic cycle can occur in the presence of an organic substrate, through an organometallic intermediate that decomposes further into products and again generates the catalytic species. All the intermediates are in accordance with the 18-electron Tolman rule.

$$ML_nX_xZ_z + pe^- \underset{\text{(precursor)}}{} \xrightarrow{H^+} [ML_nX_{x-p}Z_zH]^+$$

$$\searrow pX^-$$

$$\to [ML_nX_{x-p}Z_z] \quad \text{substrate}$$
$$\text{(catalyst)}$$

$$[ML_nX_{x-p}Z_zS]$$

$$\text{products} \longleftarrow \begin{bmatrix} \text{organometallic} \\ \text{intermediate} \end{bmatrix} \tag{1}$$
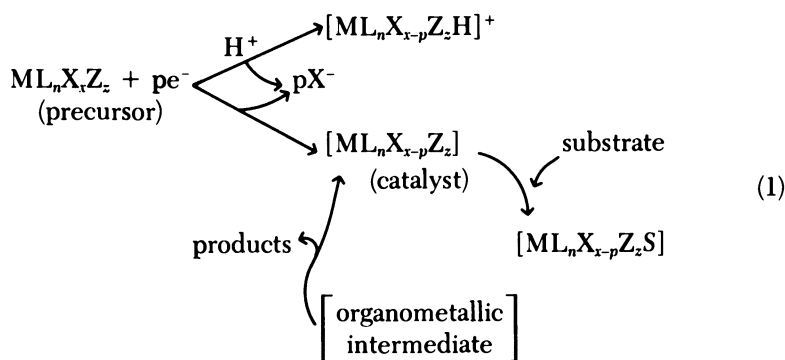
We already used this method to describe the synthesis of several catalytic systems for the reaction of cyclic or linear dimerization (*1*) of mono- or diolefins (*2*) and metathesis (*3*) of alkenes. The olefin hydroformylation reaction has been the subject of numerous studies (*4–6*). However, new hydroformylation catalysts can be electrosynthesized for producing aldehydes or acetals (*7*) by using platinum, rhodium, or cobalt precursors and olefins as substrates.

Catalysis by Electrogenerated Platinum Species

Concerning the bimetallic platinum–tin system (*8*), several species have been isolated from the reaction mixture (*9*). However, the role of the $SnCl_2$ cocatalyst in both activity and selectivity remains an open question (*10*).

This chapter describes the electrochemical synthesis of new platinum species from PtL_2Cl_2, **1**, complexes. After $CO–H_2$ treatment these complexes afford well-defined platinum hydride cationic moieties. These moieties may be responsible for the very high regioselectivity observed during 1-hexene and styrene hydroformylation (eq 2).

$$RCH=CH_2 + CO + H_2 \xrightarrow[P,T]{PtL_2Cl_2/e^-/Sn}$$

$$\underset{\text{b}}{RCH(CHO)CH_3} + \underset{\text{n}}{RCH_2CH_2CHO} \tag{2}$$
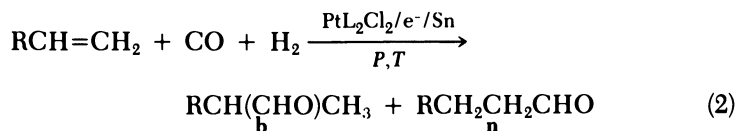
where P is pressure, T is temperature, b is branched, and n is normal (straight-chained). Thus, a preliminary voltamperometric study on the $Pt(DIOP)Cl_2$ (**1a**) complex in a propylene carbonate–benzene mixture (NBu_4PF_6 as supporting electrolyte) shows a reduction wave at −1.6 V vs. Ag–AgCl; DIOP is 2,3-O-isopropylidene-2,3-dihydroxy-1,4-bis(diphenylphosphino)butane.

If a tin anode is used during electrolysis of this complex, Sn^{2+} is generated. In this way a new Pt–Sn couple can be produced electrochemically.

In a typical experiment, 10^{-2} mmol of complex **1a** is introduced in an undivided electrochemical glass cell in a propylene carbonate–benzene mixture (25 mL, 40:60). The electrolysis is then performed under controlled potential (−1.85 V vs. Ag–AgCl) with a cylindrical platinum gauze and a cylindrical tin plate. It is stopped after two electrons per platinum atom have passed, which corresponds to the dissolution of one Sn^{2+} per Pt. The overall mixture is then transferred into an autoclave under nitrogen, and 0.9 g (8.66 mmol) of styrene is added. The hydroformylation test is conducted at 90 °C under $CO–H_2$ (1:1, 100 atm), and the reaction is followed by gas–liquid chromatography. Table I compares the results obtained with the classical $SnCl_2 \cdot 2H_2O$ cocatalyst and also with an iron anode.

Table I. Styrene Hydroformylation over 1a Modified Chemically or Electrochemically

Cocatalyst	Reaction Time (h)	Conversion (mol %)	PhEt (mol %)	n-Aldehyde (mol %)	n/b Ratio[a]
$SnCl_2 \cdot 2H_2O$	5	100	22	53.5	2.2
Sn, e⁻	7	100	8	73.5	4
Fe, e⁻	24	100	3	87.5	9.2
Fe, e⁻	24	46[b]	1	90	10

NOTE: See text for conditions of hydroformylation.
[a]Normal-to-branched ratio.
[b]$CO–H_2 = 4$.

These electrochemically reduced catalysts have been applied to 1-hexene hydroformylation. For a substrate-to-catalyst ratio of 500, a 98% selectivity into 1-heptanal is obtained with the Pt–Sn system. Previous experiments conducted in propylene carbonate mixtures have shown no effect on regioselectivity with PtL_2Cl_2–$SnCl_2$ combinations.

These remarkable regioselectivities prompted us to look at other phosphines in PtL_2Cl_2 precursors that could substitute the ligand DIOP (Table II).

Obviously, a long methylene chain in the ligand is the key factor governing regioselectivity into linear aldehyde. The activity also depends on the rigidity of the four-membered carbon chain. Such behavior agrees with previous studies on 1-pentene hydroformylation (*11*).

Table II. Ligand Effect on Linear Aldehyde Regioselectivity with PtL₂Cl₂–Sn Catalysts

| | | PtL₂Cl₂–SnCl₂ | | | | PtL₂Cl₂–Sn–e⁻ | | | |
Ligand	Complex	Reaction Time (h)	Conversion (%)	PhEt (%)	n-Aldehyde (%)	Reaction Time (h)	Conversion (%)	PhEt (%)	n-Aldehyde (%)
2PPh₃	1b	24	96	4.5	65	24	3	10	58.5
PPh₂CH₂PPh₂	1c	22	30	17.3	48	20	6	18	39.5
PPh₂(CH₂)₂PPh₂	1d	4	95	37	16	17	27	47	7
PPh₂(CH₂)₃PPh₂	1e	1.5	100	27	28	16	30	2	34.5
PPh₂(CH₂)₄PPh₂	1f	1.5	100	17	45.5	24	25	4	72
(cyclohexane-1,2-diyl)bis(CH₂PPh₂)	1g	1	100	14.5	43.5	4	100	7	73
(dioxolane)bis(PPh₂)	1a	1	100	20	49.5	5	100	7	73.5

NOTE: Conditions are the same as in Table I, except that styrene–Pt–Sn = 100:1:2.5. The solvent is benzene (25 mL) for PtL₂Cl₂–SnCl₂ and propylene carbonate–benzene (60:40) for PtL₂Cl₂–Sn–e⁻ catalysts.

As indicated, the reactions were conducted in a benzene–propylene carbonate mixture in each case. The choice of propylene carbonate as cosolvent, previously made to enhance the solution conductivity for the electrolysis, appears to be critical. Indeed, with the electrogenerated $Pt(DIOP)Cl_2$–Sn–e^- catalysts, the selectivities during styrene hydroformylation change drastically with the propylene carbonate:benzene ratio, as shown in Table III.

Table III. Effect of Solvent Concentration During Styrene Hydroformylation over $Pt(DIOP)Cl_2$–Sn–e^- Catalyst

Selectivities	8	20	40	50	60	92
Conversion (%)	60	58	67	61	53	17
PhEt (mol %)	15	10.5	6	6.5	4	0.2
$Ph(CH_2)_2CHO$ (mol %)	53	60	76	76.5	81	89

NOTE: The column headings are the concentrations of propylene carbonate in volume percents. Conditions were as follows: solvent, 25 mL; $Pt(DIOP)Cl_2$–Sn–styrene = 1:2.5:100; P_{CO} = P_{H_2} = 25 atm; T = 80 °C; t = 24 h.

The same behavior is observed with ethylene carbonate but not with other acyclic alkyl carbonates, whose dielectric constant is much lower. Furthermore, as shown in Table II, activity and selectivity are strongly dependent upon ligand structure.

These results indicate that the nature of the solvent and ligand are critical in these reactions. Dissociated platinum complexes are probably responsible for this unexpected regioselectivity. The role of tin or iron is to abstract chloride anions to produce cationic platinum species. The presence of bulky, highly strained chelating ligands is also required, as previously shown in the PtL_2Cl_2–$SnCl_2$ combination.

The high regioselectivity observed with iron prompted us to study $Pt(DIOP)Cl_2$–Fe combinations in which the cocatalyst is in a formal 2+ or 3+ oxidation state. With styrene, the hydrocinnamaldehyde–hydratropaldehyde ratio is enhanced to 12.4 and 13.6 with Fe_2O_3 and Fe_3O_4, respectively, as cocatalysts in a benzene–propylene carbonate mixture (80:20) with the following conditions: styrene–Pt–Fe = 100:1:1; P_{CO} = P_{H_2} = 50 atm; T = 90 °C; conversion = 100% after 18 h.

Finally, spectroscopic studies were performed on the $Pt(DIOP)Cl_2$ electroreduced solution (obtained with a tin anode) after it had been treated with CO–H_2 under 100 atm for 2 h at 90 °C and after the catalytic reaction (12). In both cases, the same spectra with the following characteristics were observed.

The 32.45-MHz $^{31}P\{^1H\}$ NMR spectrum shows the presence of three different phosphorus species. This spectrum can be interpreted as second-order because of the proximity of the P_A and P_B chemical shifts (11.5 and 10 ppm vs. H_3PO_4, respectively, 5 ppm for P_X). The $^1J_{Pt-P}$ coupling constants are 2850 Hz for P_A, 2680 Hz for P_B, and 2050 Hz for P_X.

A 162-MHz $^{31}P\{^1H\}$ NMR spectrum gives an ABX system in which the $^2J_{P-P}$ coupling constants are measured accurately: $^2J_{P_A-P_B} = 315$ Hz; $^2J_{P_A-P_X}$ and $^2J_{P_B-P_X} = 21$ Hz. These values are consistent with a structure in which P_A and P_B are *trans* to each other and P_X is in a *cis* position vs. P_A and P_B.

The 400-MHz ^1H NMR spectrum reveals the presence of a Pt–H bond. It consists of a series of doublets of triplets: δ –5.2 ppm, $^2J_{P-H}$ *trans* = 160 Hz, $^2J_{P-H}$ *cis* = 18 Hz. (The resolution of this spectrum did not allow the measurement of the second $^2J_{P-H}$ *cis* coupling constant.) The satellite signals are due to the ^{195}Pt–H coupling ($^1J_{Pt-H}$ = 825 Hz).

A ν-Pt–H vibration is also observed at 2010 cm^{-1} in the infrared spectrum.

In the 85.88-MHz $^{195}Pt\{^1H\}$ NMR analysis, an octuplet is centered at –5390 ppm vs. H_2PtCl_6 where the values of $^1J_{Pt-P_X}$ coupling constant are equivalent to those observed in the ^{31}P NMR spectrum. This agreement indicates the unicity of the complex, for which the following structure can ᵇe assigned.
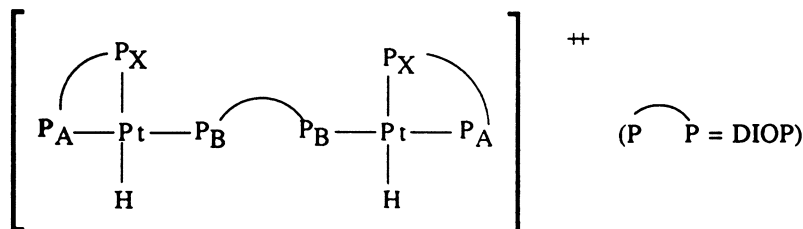
The counteranion was determined by ^{119}Sn NMR spectroscopy, as well as by mass spectrometry, to be the $SnCl_3^-$ structure. In the 149.21-MHz ^{119}Sn NMR, a single peak is observed at –36 ppm, with $SnMe_4$ as reference.

A similar spectroscopic study conducted with the other complexes shows that only complex 1g gives rise to the same dihydrido structure, whereas complex 1f does not give well-defined spectra. Significantly, the same dihydride structure appears when the iron anode is used, in which case the anion formed is $FeCl_3^-$.

Therefore, we suggest that the bridged dimeric structure of the chelated complex, dissociated by the polar solvent, plays a key role in the regioselective step of this reaction, via steric interaction between the substrate and the ligand in this cage-type structure.

Catalysis by Electrogenerated Rhodium Species

Olefin hydroformylation can also be performed on an electrochemically generated rhodium catalyst. The active species are obtained under very mild conditions, as shown in the following reaction.

$$Rh(CO)(PPh_3)_2Cl \ + \ 2e^- \xrightarrow[\quad]{V_c} [Rh(CO)(PPh_3)_2]^- \qquad (3)$$
$$\downarrow$$
$$Cl^-$$
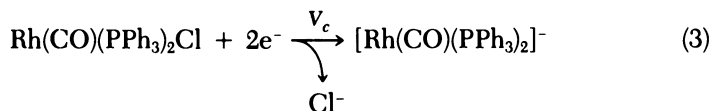
This coulometry is effected in an undivided cell in propylene carbonate, under pressure (10 atm, $CO-H_2 = 1:1$) at a fixed cathodic potential ($V_c = -900$ mV vs. Ag–AgCl), with an iron as anode and a platinum as cathode.

These results (Table IV) suggest that the electrochemically generated catalyst is less isomerizing than the Rh hydride but gives similar n:b ratio. This result is related to that observed on $Pd(CO)(PPh_3)_2$, which is isoelec-

Table IV. Hydroformylation of 1-Hexene on Rhodium Catalysts

Precursor	$Rh(CO)(PPh_3)_2Cl$	$HRh(CO)(PPh_3)_3$	$[Rh(CO)(PPh_3)_2]^-$
Aldehydes (%)	0	31	19
1-Hexene isomerization[a]	0	17	0
Products ratio (n/b)	—	3.1	3.1

NOTE: Conditions were as follows: solvent, CP (20 mL); 1-hexene–Rh = 300; P = 10 atm, $CO-H_2$ = 1:1; T = 25 °C; t = 20 h.
[a] 2-Hexenes and 3-hexenes (mol %).

tronic with $[Rh(CO)(PPh_3)_2]^-$ and can be suggested as the catalytic precursor in reactions where $Pd(PPh_3)_4$ is used as a starting material (eq 4).

$$Pd(PPh_3)_4 \ \rightleftharpoons \ 2PPh_3 \ + \ Pd(PPh_3)_2 \ \underset{\quad}{\overset{CO}{\rightleftharpoons}} \ Pd(CO)(PPh_3)_2 \qquad (4)$$
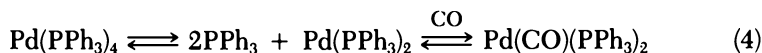
High enantiomeric excesses during hydroformylation of styrene and related compounds were attained with platinum catalysts (*13*). Rhodium catalysts still remain far from these excellent results, although they have been the subject of numerous attempts with several chiral ligands (*14*). Our current interest in asymmetric catalytic synthesis of C–C bonds with aminophosphinephosphinite ligands (*15*) prompted us to use these new ligands in asymmetric hydroformylation of olefins. In particular, we looked at different rhodium catalytic precursor systems to achieve the synthesis of the trigonal $HRh(CO)_2L_2$ catalytic species (*16*). This synthesis can be performed via at least two different routes:

- direct use of chiral $Rh(CO)L_2*Cl$ complexes (catalysts **2**)

- ligand exchange between a chiral one and $HRh(CO)(PPh_3)_3$ (catalysts **3**) (*17*)

We first applied these methods to compare the ligand (–)DIOP (catalysts **2a** and **3a**) with the aminophosphinephosphinite L(+)EPHOS [(1R,2S)-$Ph_2PNMeCHMeCPhOPPh_2$, catalysts **2b** and **3b**] during styrene hydroform-

Table V. Asymmetric Hydroformylation of Styrene with Rhodium Catalysts
2 and 3

Catalyst	L_2^*:Rh	Reaction (h)	Conversion (%)	b/n[a]	ee[b] (%)
2a	1	160	89	13.1	8
2b	1	94	23	19.8	2.4
3a	4	48	44	2.2	18.2
3b	4	90	90	8.1	18.8

NOTE: Conditions were as follows: solvent, benzene (15 mL); [Rh] = 2.86×10^{-3} M; styrene–Rh = 400; P = 12 atm; CO–H_2 = 1:1; T = 40 °C.
[a]Branched-to-linear aldehyde ratio.
[b]Determined according to the method described by Consiglio et al. (18). In all cases, the excesses were (R)-configuration.

ylation (eq 5, Table V). The L(+)EPHOS complex was prepared by CO displacement from $Rh_2(CO)_4Cl_2$ and analyzed by $^{31}P\{^1H\}$ NMR spectroscopy. This complex had a typical pattern consisting of four series of doublets of doublets. Two of them correspond to one complex in which the P–N moiety is *trans* to Cl and the others to the complex in which P–N is *trans* to CO. The two P–N signals are localized at 9.7 ppm (*trans* to CO, $^1J_{Rh-P}$ = 180.2 Hz, $^1J_{P-P}$ = 33.5 Hz), 90.1 ppm (*trans* to Cl, $^1J_{Rh-P}$ = 140.8 Hz, $^2J_{P-P}$ = 33.5 Hz) and two P–O resonances at 128.7 ppm (P–O *trans* to CO, $^1J_{Rh-P}$ = 181.2 Hz, $^2J_{P-P}$ = 33.5 Hz) and 111.6 ppm (P–O *trans* to Cl, $^1J_{Rh-P}$ = 145.7 Hz, $^2J_{P-P}$ = 33.5 Hz).

$$PhCH=CH_2 + CO + H_2 \xrightarrow[L_2^*]{[Rh]}$$

$$PhCH\underset{b}{M}e(CHO) + PhCH_2\underset{n}{CH_2}CHO \qquad (5)$$
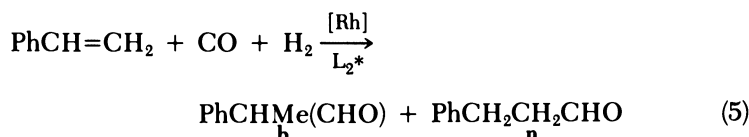
The absence of hydrogen chloride in catalysts 3 seems to be a crucial factor to avoid racemization in the case of the L(+)EPHOS ligand. Therefore, removal of the chloride anion from 2 under mild conditions before catalysis should increase the enantioselectivity. We attempted to synthesize the rhodium hydride via electrochemical reduction of the $Rh(CO)L_2^*Cl$ complex in the presence of an excess of ligand, as already described for $[Rh(CO)(PPh_3)_2]^+$ (19). This process used an iron anode in the undivided cell to provide Fe^{2+} by oxidation and hence avoid H^+ production.

In a typical electrochemical synthesis and use of catalysts 4a and 4b, 0.05 mmol of $Rh(CO)L_2Cl$ complex is solubilized in 50 mL of a benzene–acetonitrile mixture (80:20) in an undivided electrochemical glass cell. The electrolysis was conducted under synthesis gas (syngas) at 40 °C with a cylindrical platinum gauze electrode as the cathode and an inner iron cylindrical plate as the anode. The use of iron as the anode is important because

the electrochemical oxidation process can be depicted as $Fe \rightarrow Fe^{2+} + 2e^-$. This reaction provides the countercation for the chloride anion coming from the cathodic reaction.

The coulometry was conducted under controlled cathodic potential (-1.2 V vs. $Ag-Ag^+$) and stopped after 2 F per mole of rhodium had passed, which took about 1 h. The solution was then removed from the electrochemical cell under $CO-H_2$ and introduced into an autoclave. After evaporation of the solvent, styrene (2.08 g, 20 mmol) was introduced as a solution in benzene (15 mL) and the $CO-H_2$ pressure admitted. The reactor was then heated rapidly by means of a circulation water bath at 40 °C. The gas chromatographic analysis showed that practically no products other than aldehydes were formed. Table VI reports the observed activities and selectivities of catalysts **4a** and **4b**.

Table VI. Asymmetric Hydroformylation of Styrene on Electroreduced Rh(CO)L$_2$*Cl Complexes 4

Catalyst	L$_2$*:Rh	Reaction Time (h)	Conversion (%)	b/n[a]	ee[b] (%)
4a	1	115	83	4.3	12.2
4b	2	138	73	1.8	18.3
4a	1	72	76	9.5	16.3
4b	2	111	63	9.1	30.9

NOTE: Conditions were as follows: solvent, benzene–acetonitrile (80:20, 60 mL), [Rh(CO)L$_2$*Cl] = 2.86 × 10^{-3} M, V_c = −1.2 V vs. Ag–AgCl; P = 1 atm, $CO-H_2$ = 1:1; T = 40 °C; t = 1 h (for 2e/Rh).
[a]Conditions were as follows: solvent, benzene (15 mL); [Rh] = 2.86 × 10^{-3} M; styrene–Rh = 400, P = 12 atm, $CO-H_2$ = 1:1; T = 40 °C.
[b]All excesses were (*R*)-configuration.

^{31}P NMR spectroscopic analysis of the electroreduced solutions clearly indicates the presence of a mixture of monomeric and dimeric complexes (eq 6).

$$[Ru(\mu CO)(CO)L_2^*]_2 + H_2 \rightleftarrows 2HRh(CO)_2L_2^* \qquad (6)$$
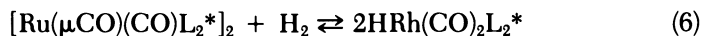
The following data have been observed for catalysts **4a** and **4b**. For **4a**: ^{31}P{^{1}H} NMR (161 MHz, CH_2Cl_2) 3.9 ppm (dm, J_{Rh-P} = 160 Hz) (dimer); 16.9 ppm (d, J_{Rh-P} = 122.6 Hz), 20–30 (m) (hydrides). For **4b**: ^{31}P{^{1}H} NMR (161 MHz, CH_2Cl_2) 93 ppm (dm, J_{Rh-P} = 115 Hz) (dimer, P–N) 113.2 ppm (dm, J_{Rh-P} = 245 Hz (dimer, P–O); 106.4 ppm (dd, J_{Rh-P} = 106.7 Hz, J_{P-P} = 21.3 Hz (hydride, P–N); 127.7 ppm (dd, J_{Rh-P} = 158.9 Hz, J_{P-P} = 21.3 Hz (hydride, P–O). However, after evaporation of the solvent, the spectrum observed after dissolution in C_6D_6 is somewhat different. This result is consistent with similar transformations already mentioned by Evans et al. (*20*) and Moser et al. (*16*), which are believed to correspond to the following equilibrium.

$$[Rh(\mu CO)L_2]_2 \underset{}{\overset{}{\rightleftarrows}} [Rh(S)(CO)L_2]_2 \qquad (7)$$
$$\text{yellow} \qquad\qquad \text{red}$$
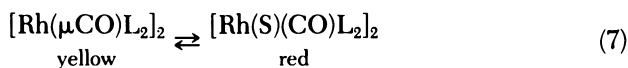
These compounds can be also obtained upon cleavage of the metal–metal bond in the $Rh_4(CO)_{12}$ cluster by hydrogen in the presence of bidentate ligands (21, 22). Then we checked and compared catalysts **5a** and **5b**, prepared from $Rh_4(CO)_{12}$ and ligands (–)DIOP and L(+)EPHOS, respectively, under the same reaction conditions (Table VII).

Table VII. Asymmetric Hydroformylation of Styrene with $Rh_4(CO)_{12}$–L_2* Mixtures (Catalysts 5)

Catalyst	L_2*:Rh	Reaction Time (h)	Conversion (%)	b/n[a]	ee[b] (%)
5a	1	96	64	1.6	17.8
5b	1.5	91	79	2.4	17.9
5a	2	120	59	2.3	17.4
5b	1	60	87	6.2	23.9
5a	1.5	96	86	7.1	30.3
5b	2	88	64	7.5	26.3

NOTE: Conditions were the same as in Table V. Premixing cluster and ligand was done in benzene under nitrogen for 30 min before reaction.
[a]Branched to linear aldehyde ratio.
[b]All excesses were (R)-configuration.

The stereoselectivities obtained either on electrochemical catalysts **4** or on catalysts **5** are very similar, and this result suggests a probable similarity in the catalytic species. Indeed, addition of 4 equiv of ligand L_2* to $Rh_4(CO)_{12}$ under syngas for 2 h at 20 °C affords a mixture of dimers and hydrides in equilibrium. In accordance with previous experiments, the DIOP system gives a hydride mixture (23).

In contrast, the $^{31}P\{^{1}H\}$ NMR spectrum arising from the L(+)EPHOS complex consists mainly of two doublets of doublets corresponding to only one hydride, together with the dimer (Figure 1, signals a and c), whose position and patterns are identical to those observed on the electroreduced catalyst **4b**. In this spectrum, the presence of the Rh–H moiety is confirmed by a proton-decoupling ^{31}P experiment (Figure 1) where splitting of the (P–N) phosphorus at 106.7 ppm (signal b) is only observed. The (P–O) phosphorus at 128 ppm (signal d) seems to be unchanged, indicating that the (P–O) moiety is in a *cis* position vs. the hydrogen.

The $^2J_{P-H}$ *cis* coupling constant is probably too small to be detected in this ^{31}P NMR spectrum. For Ir(CO)(triphos)H (triphos is $MeC(CH_2PPh_2)_3$), coupling constants of 88 ($^2J_{P-H}$ *trans*) and 14 Hz ($^2J_{P-H}$ *cis*) have been reported (24). A rhodium trigonal dihydrido cationic complex has been shown to have large $^2J_{P-H}$ *trans* (ca. 125 Hz) and small $^2J_{P-H}$ *cis* (ca. 16 Hz) (25).
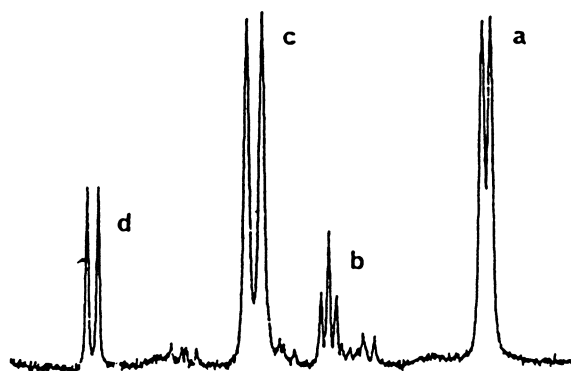
Figure 1. ^{31}P NMR spectrum of $Rh_4(CO)_{12}$ + 4 EPHOS after $CO-H_2$ treatment.

The 400-MHz ^1H NMR spectrum (Figure 2) consists of two series of doublets of doublets centered at –8.6 ppm, in which the $^2J_{P-H}$ *trans* observed as ca. 115 Hz in the ^{31}P NMR spectra can be accurately measured at 115.9 Hz. $^1J_{Rh-H}$ and $^2J_{P-H}$ have either 10.9- or 9.9-Hz values. This confirmation suggests the trigonal structure **6** for this hydride, as previously reported by Moser (*16*) with PPh$_3$ as ligand from Rh$_4$(CO)$_{12}$ under hydroformylation conditions.
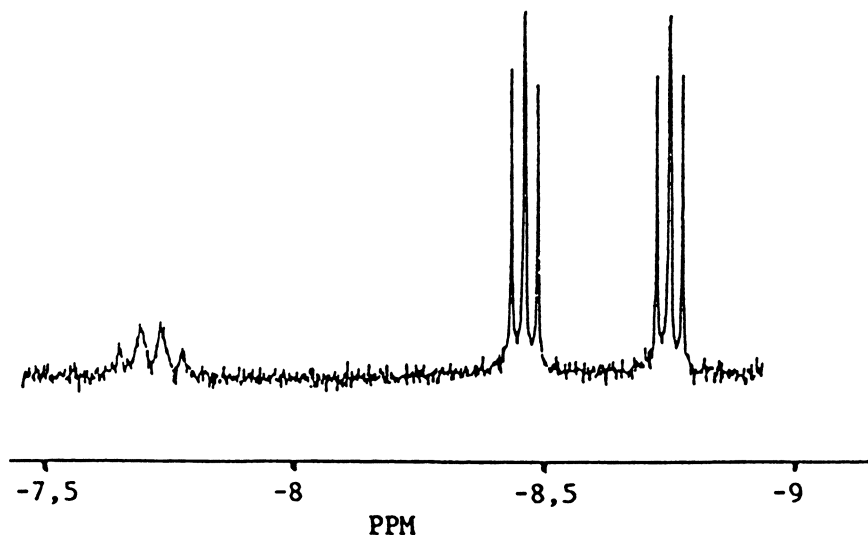
Figure 2. 400-MHz ^1H NMR spectrum of $Rh_4(CO)_{12}$ + 4 EPHOS after $CO-H_2$ treatment.

6
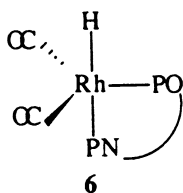
This pentacoordinate complex has the phosphinite group in an equatorial position. This conformation is expected if one considers that a phosphinite is a stronger π acceptor than an aminophosphine ligand. Theoretical studies (as well as several examples in which crystal structure determinations have been done) led to the conclusion that for d^8–d^{10} pentacoordinate complexes a π acceptor will favor an equatorial site (26). A similar rhodium trigonal hydride HRh(CO)(triphos) complex has already been reported (27) and shown to have dynamic behavior at ambient temperature. The absence of such a processing with 6 gives further evidence for the specificity of the EPHOS ligand.

The most interesting feature of these spectroscopic analyses is that the species obtained via electrochemical reduction or from $Rh_4(CO)_{12}$ are the same, as are the enantiomeric excesses (ee) on catalyst 4a and 5a (ca. 18%) and 4b and 5b (ca. 30%).

The presence of three different hydrides in catalysts 4a and 5a is certainly not a favorable factor for asymmetric hydroformylation. The overall optical yield must then result from the average enantioselectivity of several hydrides whose intrinsic hydroformylation activities and stereoselectivities are not identical.

In contrast, it might well be possible that the unexpected selective production of the hydride 6, in which the (P–N) moiety is specifically in a *trans* position vs. hydrogen, is at least partly responsible for the enantioselectivity given by the EPHOS ligand (ee ~ 30%). This enantioselectivity is one of the highest ever reported for this reaction with rhodium catalysts. These results also show that electrochemistry can substitute the use of a cluster as precursor. Extension of this work to other aminophosphinephosphinite (AMPP) ligands such as (S)-Ph₂PNMeCH-*i*-PrCH₂OPPh₂ [(S)-ValNOP] has also shown that the enantioselectivity could be improved (ee ~ 32% with (S)-ValNOP) (28).

Catalysis by Electrogenerated Cobalt Species

The complex $Sn[Co(CO)_4]_4$, 7, was prepared in high yield by controlled cathodic potential electrolysis of $Co_2(CO)_8$ in the presence of a sacrificial tin anode. The quantity of tin consumed from the anode, together with the quantity of charge passed, indicates the production of 7 consistent with eqs 8 and 9.

$$Co_2(CO)_8 + 2e^- \rightarrow 2[Co(CO)_4]^- \qquad \text{cathode} \qquad (8a)$$

$$Sn \rightarrow Sn^{2+} + 2e^- \qquad \text{anode} \qquad (8b)$$
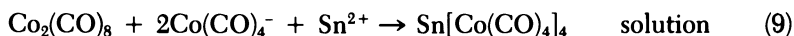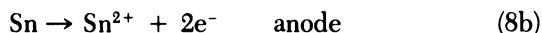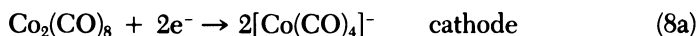
$$Co_2(CO)_8 + 2Co(CO)_4^- + Sn^{2+} \rightarrow Sn[Co(CO)_4]_4 \qquad \text{solution} \qquad (9)$$
$$\mathbf{7}$$

The hypothetical intermediate complex $Sn[Co(CO)_4]_2$ has not been detected by infrared studies. Therefore, reaction 9 appears to be rapid.

The electrochemical synthesis of **7** offers numerous advantages over conventional chemical methods. It produces complex **7** rapidly, without any byproducts (29). X-ray diffraction studies show that **7** has a Td symmetry.

Compound **7** is a good catalyst for the synthesis of aldehydes from olefins in C_6H_6 (eq 10) under higher reaction conditions ($T = 150\,°C$, $P = 60$ atm, $CO-H_2 = 1:1$), as expected with a cobalt-based catalyst.

$$RCH_2CH{=}CH_2 + CO + H_2 \xrightarrow{\textbf{7}\ (1:100)}$$

$$RCH_2CH(CH_3)CHO + R(CH_2)_3CHO \qquad (10)$$
$$\mathbf{b} \qquad\qquad\qquad \mathbf{n}$$
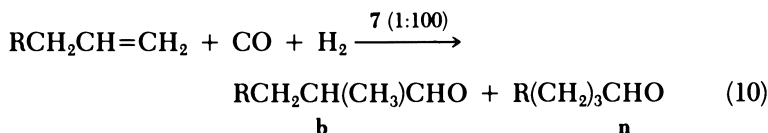
Acetals are also produced from aldehydes and alcohols or organic carbonates (eq 11).

$$C_6H_{13}CHO + CH_3CHCH_2O(CO)O \xrightarrow{[7]} C_6H_{13}CHOCH(CH_3)CH_2O \qquad (11)$$
$$\downarrow$$
$$CO_2$$
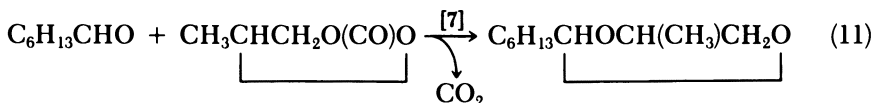
Because of the presence of the tin atom, a direct synthesis of acetals is observed from olefins, syngas, and cyclic carbonates. This synthesis indicates that compound **7** acts as a bifunctional catalyst.

Conclusion

Electrochemistry is a useful tool for the synthesis of active and selective species. In the hydroformylation field, this technique induces particularly selective catalysts. They are generated via electrochemical reduction of either PtL_2Cl_2 complexes in the presence of a tin or iron anode, $Rh(CO)L_2{}^*Cl$ under syngas atmosphere, or electroreduced $Co_2(CO)_8$ with tin as a sacrificial anode.

Spectroscopic analyses of the resulting solutions have shown the production of the cationic dihydride $[Pt_2(L_2)_2(\mu L_2)(H)_2]^{2+}$, $2SnCl_3^-$, the hydride $HRh(CO)L_2{}^*$, and the cluster $Sn[Co(CO)_4]_4$.

The platinum complex was used to selectively hydroformylate α-olefins such as styrene into linear aldehydes (>92%). With a chiral L_2* ligand in rhodium systems, asymmetric hydroformylation of styrene into hydratropaldehyde was observed (95% yield, >30% ee). The synthesis of acetals was also realized with organic carbonates and alkenes in the presence of syngas atmosphere with $Sn[Co(CO)_4]_4$ as catalyst.

Finally, the structural knowledge of the species resulting from electrosynthesis led to the discovery of new selective catalysts that can be prepared by purely chemical processes. This procedure provides interesting synthetic systems.

References

1. Sibille, Y.; Coulombeix, J.; Perichon, J.; Fuchs, J. M.; Mortreux, A.; Petit, F. *J. Mol. Catal.* **1985**, *32*, 239.
2. Huchette, D.; Théry, B.; Petit, F. *J. Mol. Catal.* **1978**, *4*, 433.
3. Gilet, M.; Mortreux, A.; Folest, J. C.; Petit, F. *J. Am. Chem. Soc.* **1983**, *105*, 3876.
4. Roelen, O. *Angew. Chem.* **1948**, *7*, 213.
5. Pruett, R. L. *Adv. Organomet. Chem.* **1979**, *17*, 1.
6. Ojima, I.; Kato, K.; Okabe, M.; Fuchikami, T. *J. Am. Chem. Soc.* **1987**, *109*, 7714.
7. Cabrera, A.; Mortreux, A.; Petit, F. *J. Mol. Catal.* **1988**, *47*, 11.
8. Toniolo, L.; Botteghi, C.; Scrivant, A.; Bertow, A. *J. Organomet. Chem.* **1988**, *344*, 261.
9. Swager, J.; Knifton, J. F. *J. Catal.* **1976**, *45*, 256.
10. Ruegger, H. J.; Pregogin, P. S. *Inorg. Chem.* **1987**, *26*, 2912.
11. Hayashi, T.; Kawabata, Y.; Isoyama, T.; Ogata, I. *Bull. Chem. Soc. Jpn.* **1981**, *54*, 3438.
12. Paumard, E.; Mortreux, A.; Petit, F. *J. Chem. Soc., Chem. Commun.* **1989**, *18*, 1380.
13. Parinello, G.; Stille, J. K. *J. Am. Chem. Soc.* **1987**, *109*, 7122.
14. Consiglio, G.; Pino, P. *Top. Curr. Chem.* **1982**, *105*, 77.
15. Mortreux, A.; Petit, F.; Buono, G.; Peiffer, G. *Bull. Soc. Chim. Fr.* **1987**, *4*, 631.
16. Moser, W. E.; Papille, C. J.; Brannon, D. A.; Duwell, R. A.; Weininger, S. *J. Mol. Catal.* **1987**, *41*, 271.
17. Salomon, C.; Consiglio, G.; Botteghi, C.; Pino, P. *Chimia* **1973**, *27*, 215.
18. Consiglio, G.; Pino, P.; Flowers, L. I.; Pittman, C. V. *J. Chem. Soc., Chem. Commun.* **1983**, *2*, 1452.
19. Zotti, G.; Zecchin, S.; Pilloni, G. *J. Organomet. Chem.* **1983**, *246*, 61.
20. Evans, D.; Osborn, J. A.; Wilkinson, G. *J. Chem. Soc. A* **1968**, 3133.
21. Mutin, R.; Abboud, W.; Basset, J. M.; Sinou, D. *J. Mol. Catal.* **1985**, *33*, 47.
22. James, B. R.; Mahajan, D.; Rettig, S. J.; Williams, G. M. *Organometallics* **1983**, *2*, 1452.
23. Young, O. R.; Young, D. A. *J. Am. Chem. Soc.* **1981**, *103*, 6636.
24. Jansen, P.; Venanzi, L. M.; Bachechi, F. *J. Organomet. Chem.* **1985**, *296*, 229.
25. Yoshida, T.; Okano, T.; Ueda, Y.; Otsuka, S. *J. Am. Chem. Soc.* **1981**, *103*, 3411.

26. Rossi, A. R.; Hoffmann, R. *Inorg. Chem.* **1975**, *2*, 365.
27. Ott, J.; Venanzi, L. M.; Ghilardi, C. A.; Midollini, S.; Orlandini, A. *J. Organomet. Chem.* **1985**, *291*, 89.
28. Pottier, Y.; Mortreux, A.; Petit, F. *J. Organomet. Chem.* **1989**, *370*, 333.
29. Cabrera, A.; Samain, H.; Mortreux, A.; Petit, F. *Organometallics* **1990**, *9*, 959.

New Carbonylations Catalyzed by Transition Metal Complexes

Iwao Ojima, Zhaoda Zhang, Anna Korda, Patrizia Ingallina, and Nuria Clos

Department of Chemistry, State University of New York at Stony Brook, Stony Brook, NY 11794

The Rh-catalyzed hydroformylation of N-allylamides gives isoaldehyde with good regioselectivity through chelation control. The Rh- and $Co_2Rh_2(CO)_{12}$-catalyzed reactions of an N-methallylamide give a novel double carbonylation product and a pyrrolidine, respectively. These reactions are successfully applied to homoallylic systems to generate the corresponding azabicyclo[4.n.0]alkenes and alkanes. Intramolecular amidocarbonylation of 3-butenamide catalyzed by a Rh complex with excess phosphine ligands gives 3,4-dihydro-2-pyridone. The same reaction with excess $P(OPh)_3$ affords a unique heterodimer selectively. The reaction of 4-pentenamide gives 5-methyl-3,4-dihydro-2-pyridone exclusively, regardless of rhodium catalysts used. Reactions of hydrosilanes with 1-hexyne catalyzed by $Co_2Rh_2(CO)_{12}$ and $Rh_4(CO)_{12}$ at 25 °C under CO give (Z)-1-silyl-2-formyl-1-hexenes, which are the products of "silylformylation". Novel Rh–Co complexes, $(R_3Si)_2Rh(CO)_n$–$Co(CO)_4$ and $RhCo(n$-Bu-$C≡CH)$–$(CO)_5$, are found to be important catalyst species for the reaction catalyzed by $Co_2Rh_2(CO)_{12}$. The catalytic cycle of the reaction is proposed.

CHELATION-CONTROLLED REGIOSELECTIVE and stereoselective reactions have been studied extensively in the field of organometallic chemistry for organic synthesis. In the catalysis field, the asymmetric hydrogenation of dehydroamino acids and dehydropeptides (*1–4*), asymmetric epoxidation of allylic alcohols (*5*), and asymmetric isomerization of allylamines (*6, 7*) are

excellent examples of the chelation-controlled methodologies to attain high stereoselectivity. However, to the best of our knowledge, no systematic studies have been performed on the application of chelation control to selective carbonylations. We describe here our recent results on the successful chelation control in hydrocarbonylations of *N*-allylamides and alkenamides catalyzed by rhodium and Co–Rh mixed-metal complexes and other novel carbonylation reactions such as sequential double carbonylation (8).

New Syntheses of Nitrogen Heterocycles Through Amide-Directed Hydrocarbonylations

Intramolecular Amidocarbonylation of *N*-Alkenylamides.   The hydroformylation of *N*-allylacetamide was carried out by using a variety of rhodium catalysts [i.e., $RhCl(PPh_3)_3$, $RhCl(CO)(PPh_3)_2$, $HRh(CO)(PPh_3)_3$, [Rh(dppb)(NBD)]ClO$_4$, $Rh_4(CO)_{12}$, and a Co–Rh mixed-metal complex, $Co_2Rh_2(CO)_{12}$]. Typical results are summarized in Table I.

Table I. Hydrocarbonylation of *N*-Allylacetamide

Entry	Catalyst (mol %)	Yield (%)[a]	Products Ratio[a]			
			1	2	3	4
1	[Rh(dppb)(NBD)]ClO$_4$[b] (1.0)	78	71	—	5	24
2	$RhCl(PPh_3)_3$ (1.0)	80	65	—	7	28
3	$RhCl(CO)(PPh_3)_2$ (1.0)	79	66	—	7	27
4	$HRh(CO)(PPh_3)_3$ (1.0)	76	63	11	13	13
5	$Rh_4(CO)_{12}$ (0.25)	78	79	6	6	9
6	$Co_2Rh_2(CO)_{12}$ (0.5)	80	79	—	21	—
7	$Co_2Rh_2(CO)_{12}$ (1.0)[c]	80	82	—	18	—

NOTE: All reactions were run by using a Pyrex reaction vessel (50 mL) in a stainless steel autoclave (300 mL) with 1.50 mmol of *N*-allylacetamide in THF (3.6 mL) at 80 °C and 1200 psi of carbon monoxide and hydrogen (CO/H$_2$ = 1) for 18 h unless otherwise noted. The products were isolated by column chromatography on silica gel and identified by ^1H and ^{13}C NMR, IR, and mass spectroscopy.
[a]Determined by ^1H NMR and GLC analyses.
[b]dppb is 1,4-bis(diphenylphosphino)butane. NBD is norbornadiene.
[c]60 °C.

As Table I shows, the major product of the reaction is isoaldehyde (2-methyl-3-acetylaminopropanal) (1) and the minor products are *n*-aldehyde (4-acetylaminobutanal) (2), 1-acetylpyrrolidine (3) and/or 1-acetyl-2-formyl-pyrrolidine (4), which is the product of novel sequential double carbonylation (eq 1).

(1)
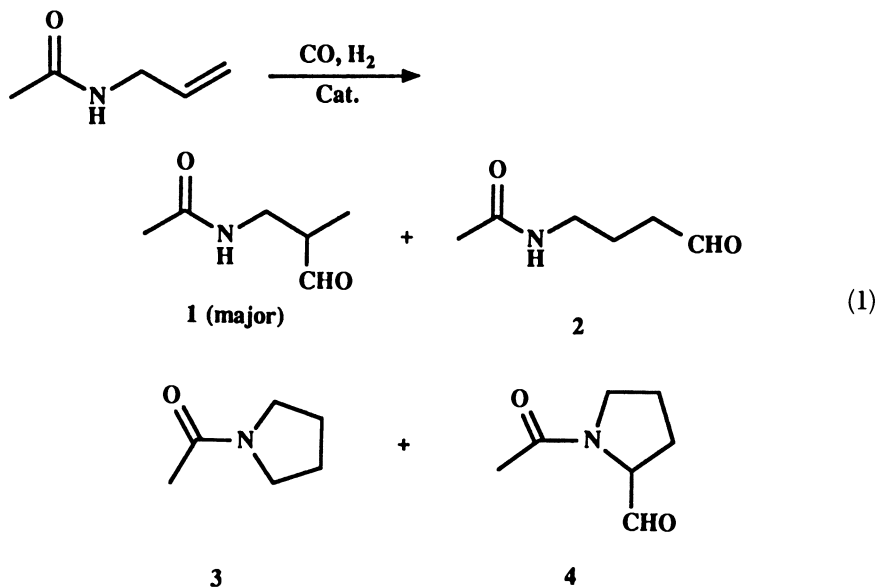
Hydroformylation of 1-alkenes catalyzed by rhodium complexes gives *n*-aldehyde as the predominant product. *n*-Aldehyde selectivity is increased when phosphine ligands are introduced [i.e., the *n*-to-iso ratio is in the range of 5–10 for phosphine–rhodium complexes and 1.1–2 for rhodium carbonyls (9)]. Accordingly, good isoselectivities observed in the present system are opposite to those for the usual 1-alkenes. The Co–Rh mixed-metal catalyst, $Co_2Rh_2(CO)_{12}$, brings about substantially better product selectivity than other rhodium complexes (entries 6 and 7, Table I). This result implies the synergistic effects of the mixed-metal system: The $Co_2(CO)_8$-catalyzed hydrocarbonylation was reported (10, 11) to give a mixture of three amino acids instead of amino aldehydes [i.e., 2-(benzoylamino)butanoic acid (45%), 2-methyl-3-(benzoylamino)propanoic acid (8%), and *N*-benzoylproline (21%) (10)].

The results of the rhodium complex-catalyzed reactions shown in Table I are not as selective as those of the $Co_2Rh_2(CO)_{12}$-catalyzed reaction. Thus, there is a substantial synergistic effect when the two metals are combined. The observed unique isoselectivity is best interpreted by taking into account the amide-directed chelation control of regioselectivity.

1-Acetyl-2-formylpyrrolidine (4), obtained as a minor product in rhodium-catalyzed reactions, is formed through a new type of amidocarbonylation via a hemiamidal (5) arising from *n*-aldehyde (2) followed by the sequential formation of an alkyl–Rh complex (6) and an acyl–Rh complex (7), as shown in Scheme I. In the final reductive elimination step, the acyl–Rh bond is
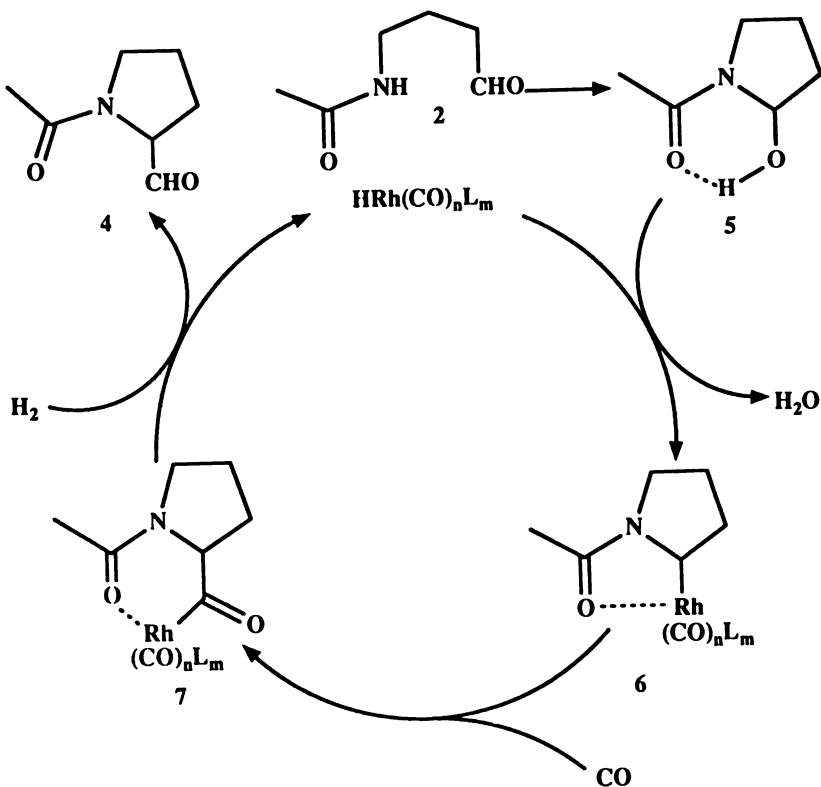
Scheme 1. Proposed mechanism for sequential double carbonylation.

selectively cleaved by hydrogen to yield aldehyde (**4**). This reaction forms
a sharp contrast to the cobalt-catalyzed amidocarbonylation, which gives the
corresponding carboxylic acid exclusively (*10–13*). This new type of amido-
carbonylation reaction provides the first example of rhodium-catalyzed se-
quential double carbonylation. Because this novel reaction has high potential
as a synthetic method, we studied the reaction further to make it more
selective.

We employed *N*-(2-methyl-2-propenyl)benzamide as a substrate (eq 2).
The results are summarized in Table II. Because of the 2-methyl group,
initial hydroformylation became highly regioselective. Thus the reaction gave
an expected 2-formylpyrrolidine (**8**) (1:1 diastereomer mixture) as the pre-
dominant product (almost exclusive in entry 3) together with a pyrrolidine
(**9**) and a hemiamidal (**10**) in rhodium-catalyzed reactions (entries 1–8, Table
II). In contrast to the rhodium-catalyzed reactions, the $Co_2Rh_2(CO)_{12}$-cat-
alyzed reaction gave **9** with ≥98% selectivity (entries 9 and 10, Table II).
This reaction clearly demonstrates the synergistic effects of the mixed-metal
system.

$$(2)$$
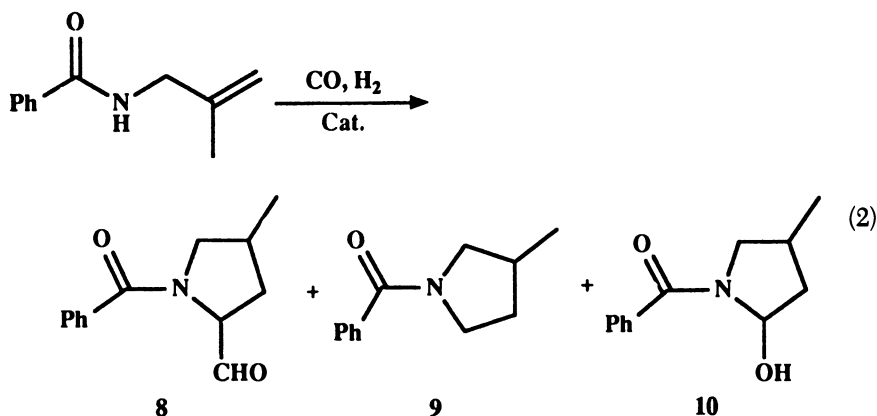
8   **9**   **10**

Table II. Hydrocarbonylation of *N*-(2-Methyl-2-propenyl)benzamide

Entry	Catalyst (mol %)	CO (psi)	H_2 (psi)	Yield[a] (%)	Products Ratio[a]		
					8	9	10
1	[Rh(dppb)(NBD)]ClO$_4$[b] (1.0)	600	600	94	62	27	11
2	[Rh(dppb)(NBD)]ClO$_4$[b] (1.0)	1500	300	90	87	—	13
3[c]	[Rh(dppb)(NBD)]ClO$_4$[b] (1.0)	1700	150	87	>99.5	—	—
4	RhCl(PPh$_3$)$_3$ (1.0)	600	600	85	54	46	—
5	RhCl(PPh$_3$)$_3$ (1.0)	1500	300	91	82	7	11
6	HRh(CO)(PPh$_3$)$_3$ (1.0)	600	600	93	48	13	39[d]
7	Rh$_4$(CO)$_{12}$ (0.25)	600	600	95	46	20	34[e]
8	Rh$_4$(CO)$_{12}$ (0.25)	600	200	87	—	—	100[f]
9	Co$_2$Rh$_2$(CO)$_{12}$ (0.5)	600	600	83	2	98	—
10	Co$_2$Rh$_2$(CO)$_{12}$ (0.5)	300	900	85	0	100	—

NOTE: All reactions were run by using a Pyrex reaction vessel (50 mL) in a stainless steel autoclave (300 mL) with 1.50 mmol of *N*-(2-methyl-2-propenyl)benzamide in THF (3.6 mL) at 100 °C for 18 h unless otherwise noted. The products were isolated by column chromatography on silica gel and identified by ^{1}H and ^{13}C NMR and mass spectroscopy.
[a]Determined by ^{1}H NMR and GLC analyses.
[b]dppb is 1,4-bis(diphenylphosphino)butane. NBD is norbornadiene.
[c]The reaction was run with 2.0 mol % of catalyst for 71 h.
[d]Containing 15% of *n*-aldehyde.
[e]Containing 18% of *n*-aldehyde.
[f]Containing 13% of *n*-aldehyde.

We looked into the mechanisms of these reactions and found that the hemiamidal (**10**) is the common intermediate to **8** and **9**. Controlled experiments using **10** revealed that **10** was actually converted to **8** (95% yield) in the presence of CO (1500 psi), H_2 (300 psi), and RhCl(PPh$_3$)$_3$ (1 mol %) at 100 °C for 18 h and that **10** was transformed to **9** (95% yield) in the presence of Co$_2$Rh$_2$(CO)$_{12}$ (1 mol %) at 100 °C and 1200 psi (CO:H$_2$ = 1) for 18 h. We also found that the hydrocarbonylation of **10** with Co$_2$(CO)$_8$ (10 mol %) at 125 °C and 2000 psi (CO:H$_2$ = 1) for 20 h gives *N*-benzoyl-4-methylproline (**11**) cleanly in 72% yield (Scheme II).
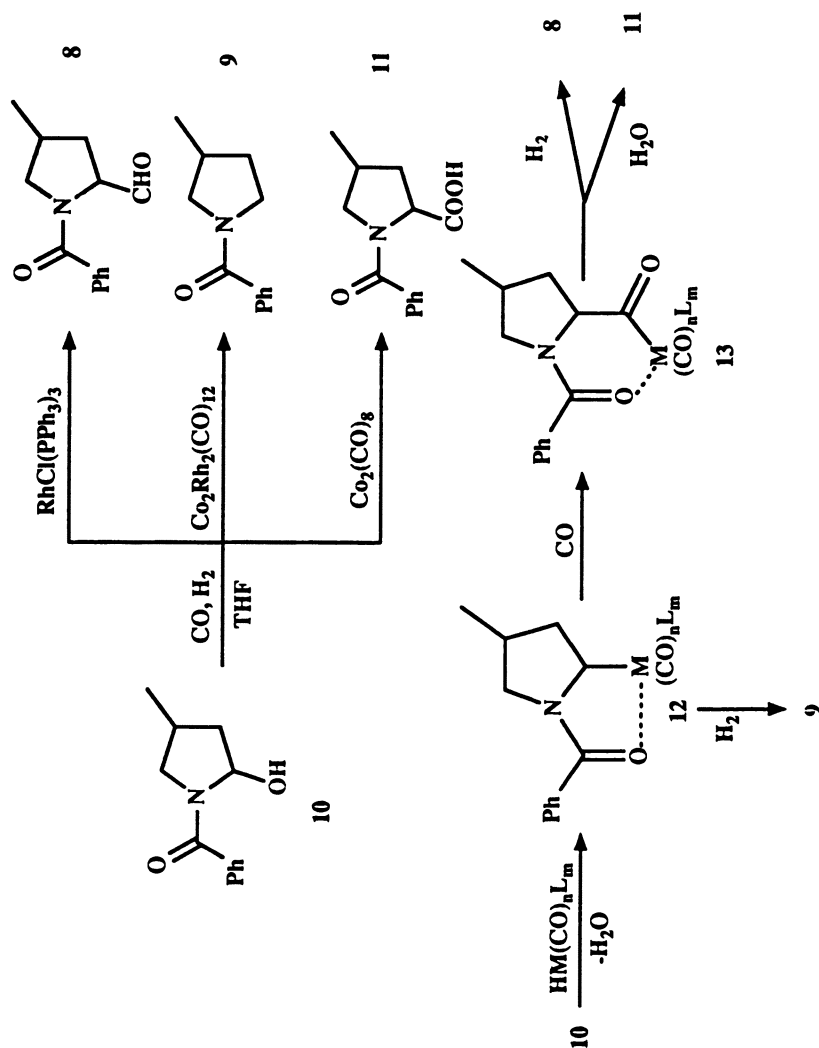
Scheme II. *Hydrocarbonylation of N-benzoyl-2-hydroxy-4-methylpyrrolidine.*

The formations of **8**, **9**, and **11** are rationalized by taking into account the formylation, the hydrogenolysis, and the carboxylation, respectively, of an alkyl–metal complex **12** that is generated from **10** (Scheme II). The three reactions are competing processes. Carbon monoxide insertion is the predominant process for rhodium and cobalt catalysts; hydrogenolysis is almost exclusive for $Co_2Rh_2(CO)_{12}$. The rhodium catalyst gives aldehyde **8** through exclusive hydrogenolysis of an acyl–metal complex **13**, whereas the cobalt catalyst gives carboxylic acid **11** through exclusive hydrolysis of **13**.

Because the intramolecular amidocarbonylation has high potential as a new annulation method in organic synthesis, we applied these amide-directed hydrocarbonylations to 5-(2-methyl-2-propenyl)-2-pyrrolidinone (**14**) and 6-(2-methyl-2-propenyl)piperidinone (**15**) (Scheme III).

The hydrocarbonylation of **14** and **15** with rhodium catalysts (1 mol % Rh) such as $HRh(CO)(PPh_3)_3$, $RhCl(PPh_3)_3$, $RhCl(CO)(PPh_3)_2$, and $Rh_4(CO)_{12}$ at 100 °C and 1800 psi ($CO:H_2 = 1$) for 18 h gave 4-methyl-1-azabicyclo[4.3.0]-2-nonen-9-one (**16**) and 4-methyl-1-azabicyclo[4.4.0]-2-decen-10-one (**17**), respectively, in 60–65% yield. The product included small amounts of the corresponding saturated bicyclic lactams (**18** and **19**; 10–20%). The reactions catalyzed by $Co_2Rh_2(CO)_{12}$ (0.5 mol %) at 125 °C and 1800 psi ($CO:H_2 = 0.5$) for 18 h, gave 4-methyl-1-azabicyclo[4.3.0]-9-nonanone (**18**) and 4-methyl-1-azabicyclo[4.4.0]-10-decanone (**19**), respectively, in 75–80% yield. The $Co_2(CO)_8$-catalyzed reactions at 125 °C and 2000 psi ($CO:H_2 = 1$) with 10 mol % of the catalyst for 24 h gave 2-carbohydroxy-4-methyl-1-azabicyclo[4.3.0]-9-nonanone (**20**) and 2-carbohydroxy-4-methyl-1-azabicyclo[4.4.0]-10-decanone (**21**), respectively, in only moderate yield (25–45%). The Rh-catalyzed hydroformylation of **14** or **15**, carried out in the presence of ethyl orthoformate at 100 °C and 1800 psi ($CO:H_2 = 1$), gave the corresponding homologous O-ethyl hemiamidals (**22** and **23**) in 65–80% yield. This product results through a sequential formation of the diethylacetal followed by cyclization. The subsequent $Co_2(CO)_8$-catalyzed carbethoxylation gave the ethyl ester of **24** or **25** in much better yield (60–75%). Treatment of **22** and **23** with trifluoroacetic acid in chloroform gave **16** and **17**, respectively, in nearly quantitative yields. Construction of 1-azabicyclo[4.n.0] systems through hydrocarbonylation can serve as a new annulation method in organic synthesis, especially for alkaloid syntheses.

Amide-Directed Hydrocarbonylation of Alkenamides.

The dihydro-2-pyridone skeleton is one of the important nitrogen heterocycles for pharmaceutical and agrochemical agents (*14, 15*). Simple dihydro-2-pyridones have been synthesized by the direct reaction of 2,4-pentadienoic acid or sorbic acid with ammonia (*16*) and by the sodium borohydride reduction of glutarimide (*17*). The 2,4-pentadienoic acid reaction gives a mixture of 3,6-dihydro- and 5,6-dihydro-2-pyridones; the reaction yields 3,4-dihydro-2-pyridones selectively. We describe here new and convenient routes to

$Co_2(CO)_8$
CO, H_2

COOH

20 : n = 1
21 : n = 2

COOEt

$Co_2(CO)_8$
CO, H_2

24 : n = 1
25 : n = 2

14 : n = 1
15 : n = 2

OEt

22 : n = 1
23 : n = 2

TFA

16 : n = 1
17 : n = 2

$HRh(CO)(PPh_3)_3$
CO, H_2

$Co_2Rh_2(CO)_{12}$
CO, H_2

$RhCl(PPh_3)_3$
CO, H_2

16 : n = 1
17 : n = 2

18 : n = 1
19 : n = 2

14 : n = 1
15 : n = 2
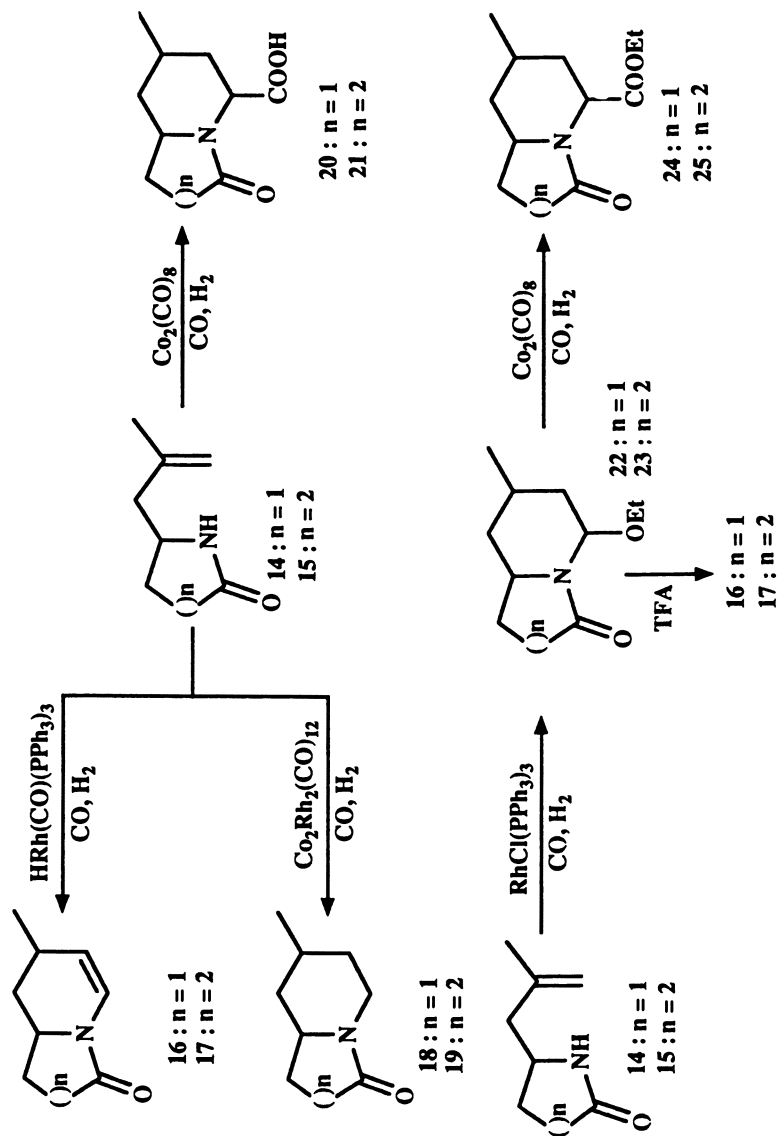
Scheme III. Amide-directed hydrocarbonylations.

3,4-dihydro-2-pyridones through intramolecular amidocarbonylation (*18–20*) of alkenamides, as well as a novel coupling reaction giving 6-(4-methyl-3-pyrrolidin-2-on-1-yl)-2-piperidone (*21, 22*).

First, the intramolecular amidocarbonylation of 3-butenamide was carried out by using typical rhodium catalysts for hydroformylation (i.e., RhCl(PPh$_3$)$_3$, RhCl(CO)(PPh$_3$)$_2$, and Rh$_4$(CO)$_{12}$ at 80–100 °C and 1200 psi (CO:H$_2$ = 3/1 or 1/1) (eq 3). Results are shown in Table III.

$$\text{(3)}$$

26   **27**   **28**
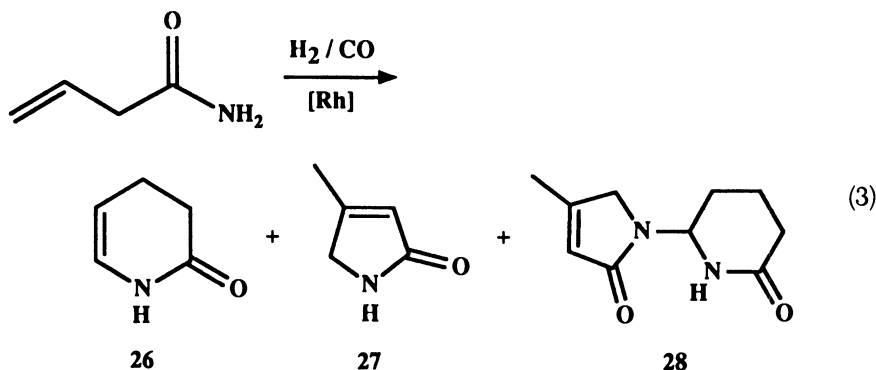
As Table III shows, the reaction under those conditions gave a mixture of 3,4-dihydro-2-pyridone (**26**), 4-methyl-3-pyrrolin-2-one (**27**), and a heterodimer, 6-(4-methyl-3-pyrrolin-2-on-1-yl)-2-piperidone (**28**). As Scheme IV shows, **26** and **27** are formed via 4-formylbutanamide (**30**) and 3-formylbutanamide (**31**), respectively, whereas **28** is yielded via the crossed coupling of **26** (via **34**) and **27** under the reaction conditions. Only the crossed coupling product, heterodimer **28**, was obtained; no homocoupling of **26** or **27** was observed.

To obtain **26–28** selectively, we examined the effects of phosphine ligands on the regioselectivity, as well as monomer–dimer selectivity of the reaction. As Table III shows (entry 3), the addition of 20 equiv of triphenylphosphine to RhCl(PPh$_3$)$_3$ remarkably improved the selectivity for the formation of **26** (92%); no heterodimer **28** was formed. On the other hand, when 10 equiv of triphenylphosphite was employed instead of triphenylphosphine for RhCl(PPh$_3$)$_3$, heterodimer **28** was produced with excellent selectivity (94%) in 90% yield. Heterodimer **28** may serve as a useful intermediate for the synthesis of tricyclic or tetracyclic nitrogen heterocycles. Reaction conditions that afford **27** selectively have not been found so far.

Next we employed *N*-benzyl-3-butenamide as the substrate (eq 4). It was found that the *N*-benzylation of 3-butenamide favors the formation of a 2-pyrrolinone (**27a**) to some extent. The reaction catalyzed by RhCl(PPh$_3$)$_3$ under 1200 psi of carbon monoxide and hydrogen (CO:H$_2$ = 1) gave **27a** as the major product [e.g., **27a**:**26a** = 2 (70% yield) at 100 °C; **27a**:**26a** = 3 (64% yield) at 120 °C.] The results contrast with those for 3-butenamide, in

Table III. Intramolecular Amidocarbonylation of 3-Butenamide

Entry	Catalyst	CO (psi)	H_2 (psi)	Temperature (°C)	Time (h)	Yield[a] (%)	Product Ratio (%)[b]		
							26	27	28
1	RhCl(PPh₃)₃	900	300	80	18	92	13	9	78
2	RhCl(PPh₃)₃–10 PPh₃	900	300	80	40	99	57	17	26
3	RhCl(PPh₃)₃–20 PPh₃	900	300	80	40	100	92	8	—
4	RhCl(CO)(PPh₃)₂	600	600	100	18	96	18	10	72
5	RhCl(CO)(PPh₃)₂–10 PPh₃	600	600	100	40	99	47	6	47
6	RhCl(CO)(PPh₃)₂–20 PPh₃	600	600	100	40	98	74	9	17
7	Rh₄(CO)₁₂	600	600	80	18	98	25	22	53
8	RhCl(PPh₃)₃–10 P(OPh)₃	900	300	80	40	90	3	3	94

NOTE: All reactions were run with 3-butenamide (1.50 mmol) and a rhodium catalyst (0.015 mmol) in THF (3.6 mL) in a stainless steel autoclave (300 mL) using a Pyrex reaction vessel (50 mL) with magnetic stirring. Conversion was 100% for all cases. Products were isolated by column chromatography on neutral alumina and identified by ^1H and ^{13}C NMR, IR, and mass spectroscopy.
[a] Determined by GLC analysis.
[b] Determined by GLC and ^1H NMR analyses.
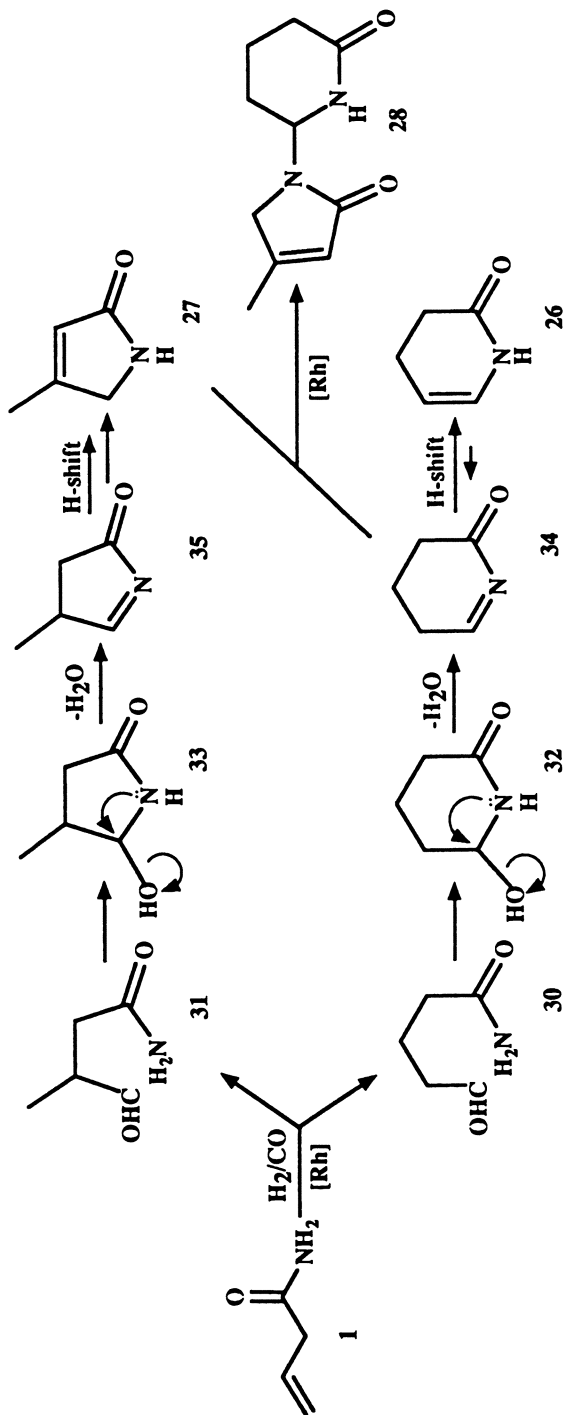
Scheme IV. Proposed mechanism for the formation of dihydropyridone (26), 4-methylpyrrolinone (27), and heterodimer (28).

(4)

26a   27a
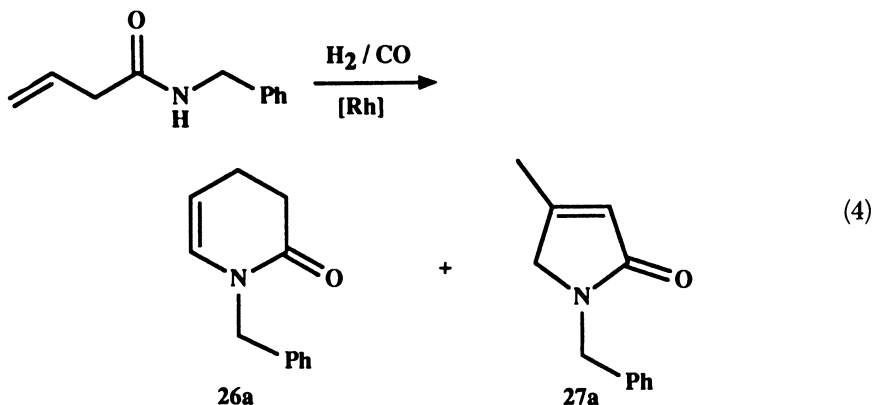
which 2-pyrrolinone (**27**) is the minor product. However, the addition of 20 equiv of triphenylphosphine to RhCl(CO)(PPh$_3$)$_2$ gave **26a** with 91% selectivity in 98% yield, which was similar to the case of 3-butenamide. Because of the N-protection, no dimer formation was observed with this substrate.

Amidocarbonylation of N-benzyl-3-butenamide catalyzed by Co$_2$(CO)$_8$ at 100 °C and 1470 psi (CO:H$_2$ = 1) is reported to give 3-(N-benzylcarbamoyl)-2-methylpropanoic acid in 69% yield; no formation of nitrogen heterocycles was observed (11). Finally, the reaction of 4-pentenamide was examined in a similar manner (eq 5). Results are shown in Table IV.

(5)

29
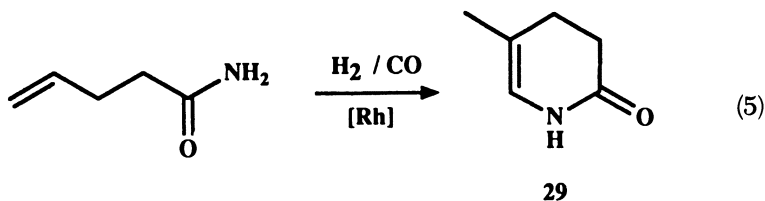
Table IV. Synthesis of 5-Methyl-3,4-dihydro-2-pyridone (29) Through Intramolecular Amidocarbonylation of 4-Pentenamide

Entry	Catalyst	CO (psi)	H$_2$ (psi)	Temperature (°C)	Time (h)	Yield[a] (%)
1	RhCl(PPh$_3$)$_3$	600	600	100	18	91
2	RhCl(CO)(PPh$_3$)$_2$	600	600	100	18	89
3	HRh(CO)(PPh$_3$)$_3$	600	600	100	18	88
4	Rh$_4$(CO)$_{12}$	600	600	100	18	92

NOTE: All reactions were run with 1.50 mmol of 4-pentenamide and 0.015 mmol of a rhodium catalyst in THF (3.6 mL) in an autoclave (300 mL) using a Pyrex reaction vessel (50 mL). The product, **29**, was isolated by column chromatography on silica gel.
[a] Isolated yield.

As Table IV shows, the reaction catalyzed by several rhodium complexes gave 5-methyl-3,4-dihydro-2-pyridone (**29**) as the sole product in excellent yield (88–92%). Although the formation of seven-membered ring lactam is conceptually possible, such a product was not detected at all, even when 20 equiv of triphenylphosphine to RhCl(PPh$_3$)$_3$ was employed as an additive. The result clearly indicates that a "chelation control" is operative in this reaction.

The result also strongly suggests that a similar chelation control is operating in the reactions of 3-butenamide and *N*-benzyl-3-butenamide as well. Thus, the effects of a large excess of triphenylphosphine to the rhodium catalysts cannot be accommodated by the blocking (or disruption) of the amide-directed chelation control, but can be interpreted as the regioselective hydroformylation of 3-butenamide (or *N*-benzyl-3-butenamide) with the amide chelation intact. It is clearly indicated that the coordination of alken-amide to the rhodium catalysts is much stronger than that of triphenylphosphine.

Silylformylation of 1-Alkyne Catalyzed by Rh–Co Mixed-Metal System

The silicon version of hydroformylation of olefins, known as "silylcarbonylation", was discovered by Murai and co-workers (*23*). It is promoted by Co$_2$(CO)$_8$ to give silyl enol ethers of homologous aldehydes. In Murai's silylcarbonylation, the silicon moiety always attaches to oxygen: No silicon migration is observed to the olefinic bond to form a silicon–carbon bond. As a part of our study of the catalysis of Co–Rh mixed-metal complexes such as Co$_2$Rh$_2$(CO)$_{12}$ and CoRh(CO)$_7$ (*20, 24–28*), we investigated the reactions of Co$_2$Rh$_2$(CO)$_{12}$ and CoRh(CO)$_7$ with hydrosilanes in the presence and absence of carbon monoxide, substrates, or both. Our goal was to determine the active sites of these Co–Rh mixed-metal catalyst systems by identifying active catalyst species as well as intermediates for catalytic cycles. To examine possible synergistic effects in the Co–Rh mixed systems, Rh$_4$(CO)$_{12}$ and Co$_2$(CO)$_8$ also were used as references.

We carried out the hydrosilylation of 1-hexyne with triethylsilane catalyzed by Co$_2$Rh$_2$(CO)$_{12}$ at 25 °C in the presence of carbon monoxide (ambient pressure) in toluene. (Z)-1-Triethylsilyl-2-formyl-1-hexene (**36c**) was formed, in addition to usual hydrosilylation product, 1-triethylsilyl-1-hexene (**37c**) (**36c:37c** = 58/42) and some higher molecular weight materials (heavies). Dimethylphenylsilane gave **36a** as the exclusive product under the same reaction conditions, although the formation of heavies was detected as well. This reaction yielding compound **36** from an alkyne is a new type of silylcarbonylation (i.e., silylformylation, which is different from Murai's reaction.

While our study was in progress (29, 30), Matsuda et al. (31) reported the discovery of silylformylation catalyzed by $Rh_4(CO)_{12}$ by using a variety of alkynes and dimethylphenylsilane as the specific hydrosilane at 100 °C and 150–450 psi of carbon monoxide. We describe here our Co–Rh mixed-metal version of silylformylation with mechanistic study. This procedure unveiled the presence of $(R_3Si)_2Rh(CO)_n$–$Co(CO)_4$ (38: n = 2 or 3) as one of the key active catalyst species for the reaction.

$$HSiR_3 = a : HSiPhMe_2; \quad b : HSiMe_2Et; \quad c : HSiEt_3; \quad d : HSi(OMe_3)_3$$
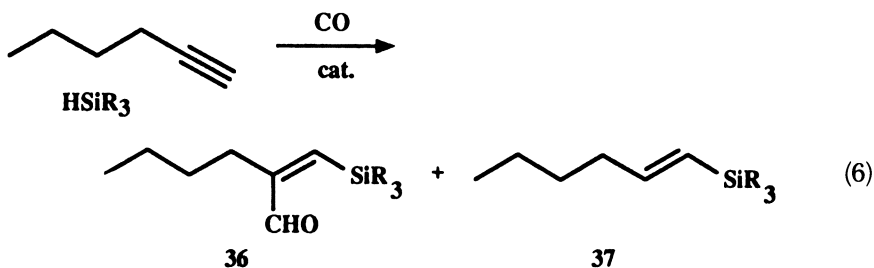
We carried out the reactions of 1-hexyne with a variety of hydrosilanes in toluene at 25 °C and ambient pressure or 150 psi of carbon monoxide in the presence of $Co_2Rh_2(CO)_{12}$ (substrate:catalyst = 1000) for 24 h; $Rh_4(CO)_{12}$ was also employed for comparison purposes. The results are summarized in Table V.

As Table V shows, the structure of hydrosilane exerts a marked influence on the selectivity of the reaction (i.e., silylformylation vs. hydrosilylation). Trimethoxysilane clearly favors hydrosilylation, whereas dimethylphenylsilane gives silylformylation product exclusively and trialkylsilanes give ca. 40:60 mixture of the hydrosilylation and silylformylation products. At 25 °C and ambient pressure of carbon monoxide, the reaction catalyzed by $Rh_4(CO)_{12}$ is substantially faster than that catalyzed by $Co_2Rh_2(CO)_{12}$, although the ratio of the hydrosilylation to silylformylation is very similar. In both cases, considerable amounts of heavies are formed. At 25 °C and 150 psi of carbon monoxide, $Co_2Rh_2(CO)_{12}$ acts as an excellent catalyst, giving the silylformylation product (36) with 93–100% selectivity (entries 2, 4, and 6) except for $HSi(OMe)_3$ (entry 8). Formation of the heavies is also substantially decreased. Under the same conditions, the $Rh_4(CO)_{12}$-catalyzed reactions give a larger amount of heavies compared with the $Co_2Rh_2(CO)_{12}$-catalyzed ones, and $HSi(OMe)_3$ does not give any silylformylation product (36) (entry 16). As $Co_2(CO)_8$ is found to be virtually inactive even under forced conditions, it is apparent that there is a synergistic effect in the Co–Rh mixed-metal system.

The regio- and stereochemistry of both silylformylation and hydrosilylation deserve mention. All silylformylation products (36) have (Z)-1-silyl-2-

Table V. Reactions of Hydrosilanes with 1-Hexyne Catalyzed by $Co_2Rh_2(CO)_{12}$ and $Rh_4(CO)_{12}$ in the Presence of Carbon Monoxide

Entry	Catalyst	Hydrosilane	Condition[a]	Yield[b] (%)	Product Ratio[c]	
					36	37
1	$Co_2Rh_2(CO)_{12}$	$HSiMe_2Ph$	A	72	100	—
2	$Co_2Rh_2(CO)_{12}$		B	92	100	—
3	$Co_2Rh_2(CO)_{12}$	$HSiMe_2Et$	A	48	60	40
4	$Co_2Rh_2(CO)_{12}$		B	84	100	—
5	$Co_2Rh_2(CO)_{12}$	$HSiEt_3$	A	63	58	42
6	$Co_2Rh_2(CO)_{12}$		B	80	93	7
7	$Co_2Rh_2(CO)_{12}$	$HSi(OMe)_3$	A	86	20	80
8	$Co_2Rh_2(CO)_{12}$		B	95	38	62
9	$Rh_4(CO)_{12}$	$HSiMe_2Ph$	A	72	100	—
10	$Rh_4(CO)_{12}$		B	76	100	—
11	$Rh_4(CO)_{12}$	$HSiMe_2Et$	A	61	65	35
12	$Rh_4(CO)_{12}$		B	80	91	9
13	$Rh_4(CO)_{12}$	$HSiEt_3$	A	65	65	35
14	$Rh_4(CO)_{12}$		B	77	86	14
15	$Rh_4(CO)_{12}$	$HSi(OMe)_3$	A	76	—	100
16	$Rh_4(CO)_{12}$		B	80	—	100

NOTE: All reactions were run with 5.0 mmol of 1-hexyne, 5.5 mmol of a hydrosilane, and 5×10^{-3} mmol of a catalyst in toluene (7.5 mL) at 25 °C for 24 h.
[a]Condition A: Reaction was carried out at ambient pressure of carbon monoxide in a Schlenck reactor; Condition B: Reaction was carried out at 150 psi of carbon monoxide in a stainless steel autoclave using a Pyrex reaction vessel (50 mL).
[b]Yield was determined by GLC analysis based on 1-hexyne consumed.
[c]Determined by GLC analysis.

formyl structure (i.e., the reaction is extremely regioselective as well as stereoselective). All hydrosilylation products (37) turn out to be (E)-isomers exclusively. This result makes a sharp contrast to the reported rhodium complex-catalyzed hydrosilylation of 1-alkenes, which gives a mixture of (Z)-isomer (major) and (E)-isomer (minor) (32–35).

As for the mechanism of silylformylation, the following facts should be taken into account. Silylformylation must include

- a silicon shift from catalyst metal to an alkyne to form a 2-silyl-1-alkylethenyl–RhCo complex,
- subsequent formation of 3-silyl-2-alkylacryloyl–RhCo complex,
- formation of 3-silyl-2-alkylacryloyl–RhCo hydride, and
- reductive elimination giving the silylformylation product (36).

To obtain structural information about active catalyst species in the silylformylation, we looked at the reaction of hydrosilanes with $Co_2Rh_2(CO)_{12}$ (30). The tetrametallic cluster (deep reddish brown) was converted to a Co–Rh mixed-bimetallic complex (pale yellow) during the reaction. The

reaction of $Co_2Rh_2(CO)_{12}$ with 1-alkynes in the absence of hydrosilane gave the corresponding purple butterfly cluster complexes, $Co_2Rh_2(CO)_{10}(R-C\equiv CH)$. The structure of a triphenylphosphine complex, $Co_2Rh_2(CO)_9(n\text{-Bu}-C\equiv CH)(PPh_3)$, was determined by X-ray crystallography (36).

When a hydrosilane (4 equiv) was allowed to react with $Co_2Rh_2(CO)_{12}$ under carbon monoxide atmosphere in organic solvent (e.g., chloroform-d and n-hexane) at ambient temperature for an hour, novel $(R_3Si)_2Rh(CO)_n-Co(CO)_4$ complexes ($n = 2$, 38A; $n = 3$, 38B) were quantitatively formed. The structure of 38 is suggested by the following facts:

- the number of silyl groups on the rhodium metal was unambiguously determined to be 2 by titration, with ferrocene as the internal standard,

- the ^1H NMR spectra of 38 [R_3Si = (a) $PhMe_2Si$, or (c) Et_3Si] do not show any Rh–H signals (δ 0 to –20 ppm) and the Fourier transform IR spectrum of 38c prepared from Et_3Si-D and $Co_2Rh_2(CO)_{12}$ does not show any Rh–D stretching band at all in the expected region (1600–1450 cm^{-1}), and

- the silyl groups were replaced by R–NC (R = t-Bu, cyclohexyl, and 2,6-dimethylphenyl) to form $[(R-NC)_4Rh]^+[Co(CO)_4]^-$.

These results clearly indicate that 38 is generated through oxidative addition of two molecules of hydrosilanes to a rhodium, followed by evolution of molecular hydrogen. These disilyl–RhCo complexes (38) are stable in n-hexane under carbon monoxide for more than a week at ambient temperature, but decompose slowly under nitrogen and/or in chloroform.

We carried out the reaction of $(PhMe_2Si)_2Rh(CO)_n-Co(CO)_4$ (38a-A and 38a-B) with 1 equiv of 1-hexyne at 25 °C and ambient pressure of carbon monoxide for 30 min (eq 7) (30).

The ^1H NMR monitoring of the reaction clearly demonstrated the formation of 36a (with 5% E-isomer) accompanied by a small amount of 38a-B (38a-A disappeared) and a mixed-metal butterfly complex, $Rh_2Co_2(n\text{-Bu}-C\equiv C-H)(CO)_{10}$ (39). This reaction strongly suggests that 38a is an active catalyst species or its direct precursor.

Next, we looked at the reaction of $Co_2Rh_2(CO)_{12}$ with 1-hexyne under carbon monoxide. The reaction of $Co_2Rh_2(CO)_{12}$ with 2 equiv of 1-hexyne at 25 °C and 75 psi of carbon monoxide in hexane for 20 h gave a novel Rh–Co mixed-bimetallic alkyne complex bearing semibridging carbonyl (ν_{CO}, 1935 cm^{-1}), $RhCo(n\text{-Bu}-C\equiv C-H)(CO)_5$ (40), as the major product. The complex was isolated through column chromatography on silica gel under carbon monoxide as a reddish-orange solid (30). Complex 40 was then allowed to

$$R_3Si=PhMe_2Si$$

(7)
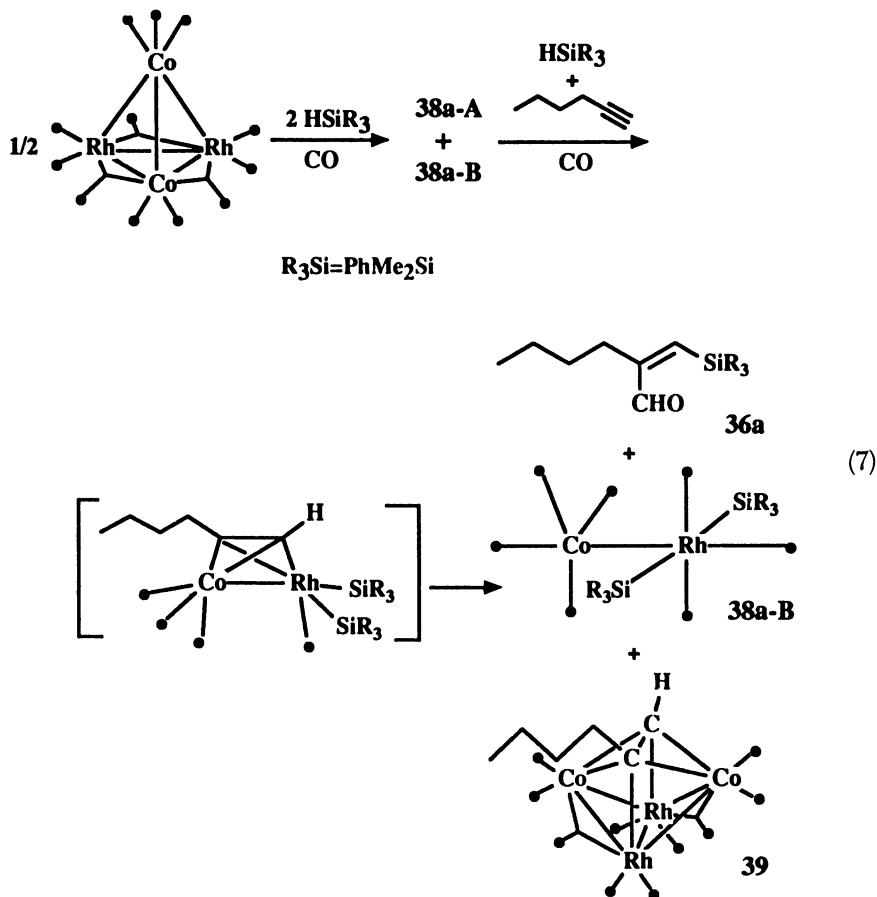
react with 6 equiv of dimethylphenylsilane and 4 equiv of 1-hexyne at 25 °C and ambient pressure of carbon monoxide in chloroform for 1 h to give cleanly the silylformylation product **36a**. The ^{1}H NMR spectrum of the reaction mixture only shows **36a**, **40**, and unreacted hydrosilane (eq 8) (*30*). This result clearly indicates that **40** is an active catalyst species or its direct precursor.

Accordingly, there are two possible catalytic cycles for silylformylation at present. Either one or both catalytic cycles may be operative, depending on the reaction conditions. Mechanisms for the silylformylation of 1-hexyne using $Co_2Rh_2(CO)_{12}$ as the catalyst precursor, which can accommodate all the observations described, are proposed in Scheme V (*30*).

The unique disilyl–RhCo complex (**38**) and alkyne–RhCo complex (**40**) are identified as the key catalytic species for silylformylation of 1-alkyne.

$$(8)$$
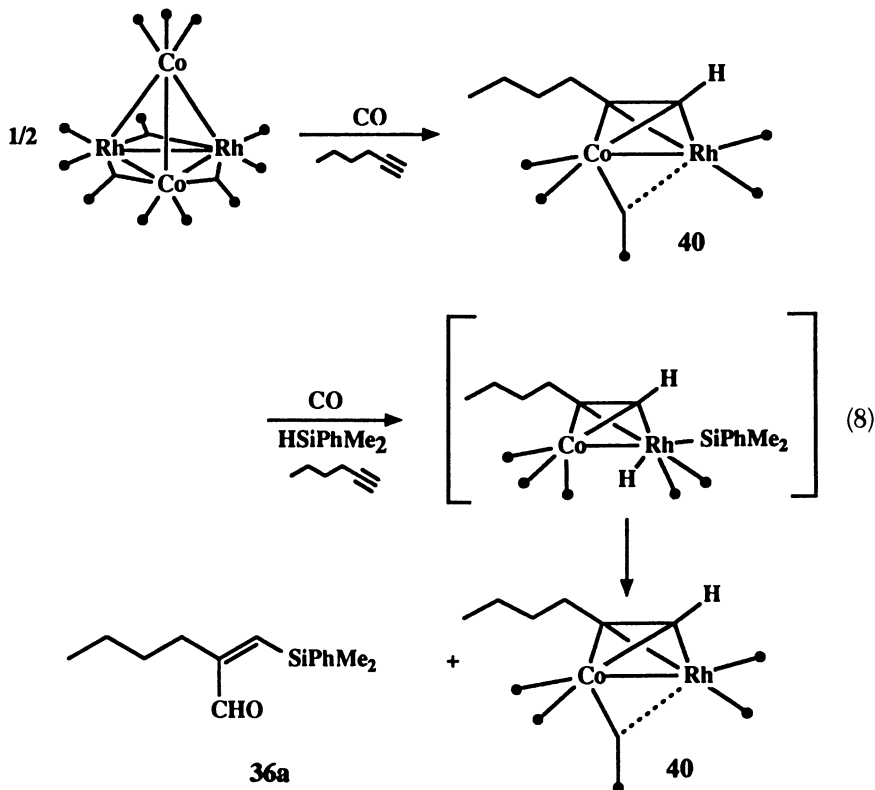
Although the insertion of carbonyl compounds or imines into silicon–transition metal bonds is known in rhodium complex-catalyzed hydrosilylations, that of alkynes and alkenes in catalysis has not been reported under thermal reaction conditions. Recently we found the selective insertion of 1-alkynes to the Rh–Si bond in rhodium complex-catalyzed hydrosilylation (35). Our results present the first examples of such a process in catalysis by taking advantage of the unique properties of the Co–Rh mixed-bimetallic system. Also, the silylformylation of alkynes catalyzed by the Co–Rh mixed-metal system is very likely to involve homogeneous bimetallic catalysis.

Acknowledgment
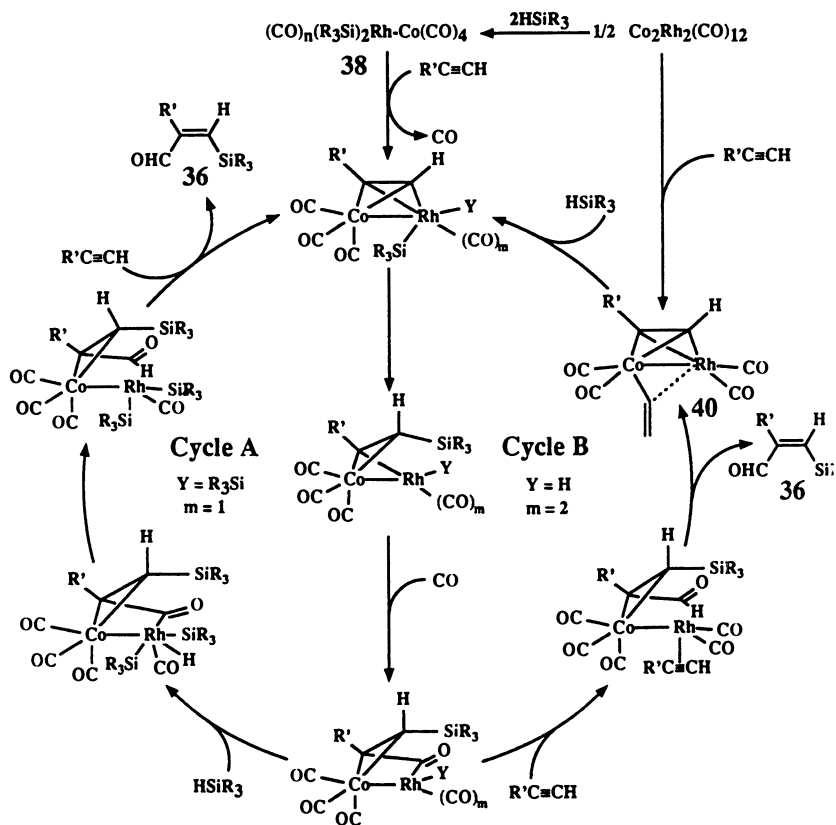
Scheme V. Proposed mechanisms for the $Co_2Rh_2(CO)_{12}$-catalyzed silylform-ylation.

References

1. Halpern, J. In *Asymmetric Synthesis*; Morrison, J. D., Ed.; Academic: New York, 1985; Vol. 5, pp 41–69 and references therein.
2. Ojima, I.; Yoda, N.; Yatabe, M.; Tanaka, M.; Kogure, T. *Tetrahedron* 1984, *40*, 1255 and references therein.
3. Evans, D. A.; Morrissey, M. M. *J. Am. Chem. Soc.* 1984, *106*, 3866.
4. Brown, J. M.; Hall, S. A. *Tetrahedron Lett.* 1984, *25*, 1393.
5. Finn, M. G.; Sharpless, K. B. In *Asymmetric Synthesis*; Morrison, J. D., Ed.; Academic: New York, 1985; Vol. 5, pp 247–308 and references therein.
6. Otsuka, S.; Tani, K. In *Asymmetric Synthesis*; Morrison, J. D., Ed.; Academic: New York, 1985; Vol. 5, pp 171–191 and references therein.
7. Tani, K.; Yamagata, T.; Akutagawa, S.; Kumobayashi, H.; Taketomi, T.; Takaya, H.; Noyori, R.; Otsuka, S. *J. Am. Chem. Soc.* 1984, *106*, 5208.
8. Ojima, I.; Zhang, Z. *J. Org. Chem.* 1988, *53*, 4422.
9. Cornils, B. In *New Synthesis with Carbon Monoxide*; Falbe, J., Ed.; Springer-Verlag: Berlin, 1980; pp 1–225 and references therein.

10. Sato, S. *Nippon Kagaku Zasshi* **1969**, *90*, 404.
11. Nishi, S.; Asada, S.; Izawa, K. Presented at the 31st Symposium on Organo-metallic Chemistry, Japan; Tsukuba, Japan, October 30–31, 1984; Abstract B202.
12. Wakamatsu, H.; Uda, J.; Yamakami, N. *Chem. Commun.* **1971**, 1540.
13. Wakamatsu, H. *Sekiyu Gakkaishi* **1974**, *17*, 105.
14. Jones, R. A.; Bean, G. P. *The Chemistry of Pyrroles*; Academic: London, 1977; pp 209–238.
15. Coutts, R. T.; Casy, A. F. In *Pyridine and Its Derivatives,* Supplement Part Four; Abramovitch, R. A., Ed.; Wiley-Interscience: New York, 1975; pp 445–524.
16. Kheddis, B.; Bahibah, D.; Hamdi, M.; Périé, J.-J. *Bull. Soc. Chim. Fr.* **1981**, 135.
17. Hubert, J. C.; Wijnberg, J. B. P. A.; Nico Speckamp, W. N. *Tetrahedron* **1975**, *31*, 1437.
18. Izawa, K.; Nishi, S.; Asada, S. *J. Mol. Catal.* **1987**, *41*, 135.
19. Izawa, K. *Yuki Gosei Kagaku Kyokaishi* **1988**, *46*, 218.
20. Ojima, I. *Chem. Rev.* **1988**, *88*, 1011 and references therein.
21. Ojima, I.; Korda, A. *Tetrahedron Lett.* **1989**, *30*, 6283.
22. Ojima, I.; Korda, A.; Shay, W. R. *J. Org. Chem.* **1991**, *56*, 2024.
23. Murai, S.; Sonoda, N. *Angew. Chem., Int. Ed. Engl.* **1979**, *18*, 837 and references therein.
24. Ojima, I.; Okabe, M.; Kato, K.; Kwon, H. B.; Horváth, I. T. *J. Am. Chem. Soc.* **1988**, *110*, 150.
25. Horváth, I. T.; Bor, G.; Garland, M.; Pino, P. *Organometallics* **1986**, *5*, 1441.
26. Bor, G. *Pure Appl. Chem.* **1986**, *58*, 543.
27. Spindler, F.; Bor, G.; Dietler, U. K.; Pino, P. *J. Organomet. Chem.* **1981**, *213*, 303.
28. Horváth, I. T. *Organometallics* **1986**, *5*, 2333.
29. Ojima, I. *Abstracts*; XXII Organosilicon Symposium, Philadelphia, PA, April 7–8, 1989; Plenary 7.
30. Ojima, I.; Ingallina, P.; Donovan, R. J. D.; Clos, N. *Organometallics* **1991**, *10*, 39.
31. Matsuda, I.; Ogiso, A.; Sato, S.; Izumi, Y. *J. Am. Chem. Soc.* **1989**, *111*, 2332.
32. Ojima, I.; Kumagai, M.; Nagai, Y. *J. Organomet. Chem.* **1974**, *66*, C14.
33. Dickers, H. M.; Hazeldine, R. N.; Mather, A. P.; Parish, R. V. *J. Organomet. Chem.* **1978**, *161*, 91.
34. Brady, K. A.; Nile, T. A. *J. Organomet. Chem.* **1981**, *206*, 299.
35. Ojima, I.; Clos, N.; Donovan, R. J.; Ingallina, P. *Organometallics* **1990**, *9*, 3127.
36. Ojima, I.; Clos, N.; Donovan, R. J.; Ingallina, P. *Organometallics* **1991**, *10*, 39.

Tetracarbonylalkylcobalts from Tetracarbonylhydridocobalt and Dimethyl Fumarate or Aldehydes

Ferenc Ungváry, Attila Sisak, and László Markó

Institute of Organic Chemistry, University of Veszprém, Veszprém, Hungary 8201

Tetracarbonylalkylcobalts, supposed intermediates in olefin hydro-formylation and aldehyde reduction, were prepared. When tetra-carbonylhydridocobalt reacted with dimethyl fumarate at 10 °C, tet-racarbonyl[1,2-bis(methoxycarbonyl)ethyl]cobalt was formed and isolated in 65% yield. The rate of the accompanying carbon monoxide uptake was found to be 0.5 order with respect to $Co_2(CO)_8$. Tetra-carbonyl-α-hydroxyalkylcobalts were prepared by the reactions of tetracarbonylhydridocobalt with formaldehyde, pivalaldehyde, glyoxal, ethyl glyoxylate, and crotonaldehyde between −40 and −79 °C and characterized partly in the form of their silylated deriv-atives by IR and NMR spectroscopy. An ionic path that accounts for the observed regiochemistry is suggested for the reaction with al-dehydes.

CARBONYLALKYLCOBALTS AND CARBONYLACYLCOBALTS are intermediates in olefin hydroformylation (*1, 2*). The studies of Heck and Breslow (*3*) leave little doubt of this fact. However, only tetracarbonylacylcobalts have been detected under catalytic reaction conditions by high-temperature, high-pressure infrared spectroscopy (*4*). The failure to detect carbonylalkylcobalts can be explained by the assumption that at high pressure the alkyl–acyl equi-librium is far on the side of the acyl complex. Under ambient conditions we can detect and in some cases isolate tetracarbonylalkylcobalts in reaction mixtures of $CoH(CO)_4$ and olefins bearing electron-withdrawing substit-uents.

Intermediate complex formation between aldehydes and $CoH(CO)_4$ was repeatedly postulated in mechanistic suggestions for aldehyde reductions under catalytic (5, 6) and stoichiometric (7) conditions, CO reductions (8), and alcohol homologations (9). We found that complex formation between formaldehyde and $CoH(CO)_4$ takes place at -40 °C (10). Further experiments showed that tetracarbonyl-α-hydroxyalkylcobalts are formed with other aldehydes as well; they can be isolated in form of their silylated and PPh_3-substituted derivatives.

Experimental Details

All manipulations involving air-sensitive compounds were carried out by the usual Schlenk technique (11) using deoxygenated dry solvents and gases and thermostated reaction vessels with magnetic stirring. Kinetic runs were performed in a gasometric apparatus fitted with a mercury-filled gas burette. Infrared spectra were recorded by using a 0.06-mm CaF_2 cuvette on a spectrometer (Specord IR 75; Carl Zeiss, Jena, Germany), which was calibrated with benzene (1959.6 cm^{-1}) and polystyrene (1601.4 cm^{-1}). ^{1}H NMR spectra were obtained on an 80-MHz spectrometer (BS–487; Tesla, Brno, Czechoslovakia), using hexamethyldisiloxane as an internal reference. A ^{13}C NMR spectrum was obtained on a 20-MHz spectrometer (CFT 20, Varian, Palo Alto, California). Solutions of $CoH(CO)_4$ in n-pentane or n-octane, which were prepared from $Co_2(CO)_8$, dimethylformamide (DMF), and concentrated HCl (12), contained 1–3 mol % of $Co_2(CO)_8$ according to IR and Co analyses. Other starting materials were commercial products purified by crystallization or distillation.

Preparation of Tetracarbonyl[1,2-bis(methoxycarbonyl)ethyl]cobalt. A
1.0 M solution of $CoH(CO)_4$ in n-pentane (16 mL, -60 °C) was added through a cannula to a stirred solution of 13.83 g (96 mmol) of dimethyl fumarate in 400 mL of a 2.5:1 (v:v) mixture of dichloromethane and n-pentane under CO atmosphere at 10 °C. The CO pressure was then raised to 150 mm Hg ($\sim$20 $\times$ 10^3 Pa) over atmospheric pressure. After 3 h of continuous stirring, the resulting light brown solution was concentrated in vacuum at -20 °C and placed on dry ice overnight. Cold filtration at dry ice temperature on a P–2 glass frit gave 10.8 g of crystals and a light reddish-yellow filtrate. After the crystals were washed with 5 $\times$ 10 mL of n-pentane at -10 °C, 10.2 g of dimethyl fumarate remained on the frit and 0.5 g of $Co_2(CO)_8$ could be crystallized from the dark brown n-pentane solution at -79 °C. The light reddish-yellow filtrate was further concentrated in vacuum at -20 °C to 70 mL and crystallized on dry ice overnight.
After separation of a light yellow crystalline solid (1.0 g), the filtrate was concentrated to 20 mL in vacuum at -20 °C and stored on dry ice overnight. After separation of ca. 0.2 g of solid and a repetition of the foregoing procedure, the final concentrate (ca. 7 mL) was diluted with 14 mL of n-pentane and crystallized at -79 °C. Cold filtration, washing with 3 $\times$ 4 mL of cold n-pentane, and drying in vacuum at -20 °C gave 3.27 g (65% yield) of the title compound as ivory-colored crystals. For the IR spectrum, see Table I and Figure 1. ^{13}C NMR spectroscopy (CDCl$_3$, -15 °C, tetramethylsilane) revealed chemical shifts downfield (δ) at 194.10 $(CO)_4$, 177.60 ($CHCO_2Me$), 169.91 (CH_2CO_2Me), 50.04–49.77 (CH_3O_2C), 39.59 (CH_2), 19.95 (CH) ppm.

Table I. Infrared Spectroscopic Data of $R^1R^2CHCo(CO)_4$-Type Complexes in the C=O Stretching Region

R^1	R^2	ν (CO) (cm^{-1})	Ref.
H	H	2104, 2035, 2018	15
EtO$_2$C	H	2111, 2046, 2036, 2027, 1720	16
MeO$_2$C	MeO$_2$CCH$_2$	2111, 2046, 2036, 2026, 1744, 1720	this work
EtO$_2$C	EtO$_2$CCH$_2$	2110, 2044, 2036, 2024, 1740, 1714	this work
EtO$_2$C	Me	2107, 2041, 2031, 2021, 1726	17, 18
EtO$_2$C	Et	2106, 2040, 2030, 2020, 1718	18
MeO$_2$C	Ph	2106, 2040, 2031, 2025, 1717	17
CN	Me	2109, 2044, 2029, 2020	19

NOTE: In *n*-hexane solution.
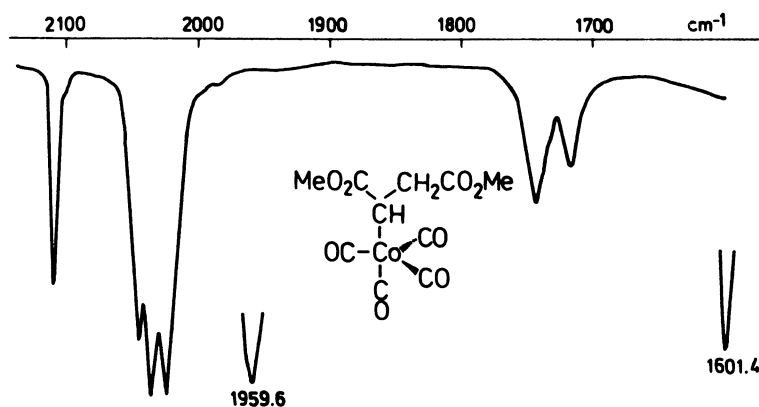
Figure 1. The infrared spectrum of the reaction mixture of dimethyl fumarate and CoH(CO)$_4$ just after CO uptake has stopped and Co$_2$(CO)$_8$ and dimethyl fumarate have been removed at –79 °C.

Preparation of Tetracarbonyl(1-hydroxy,1-formyl)methylcobalt, 1c. To 58 mg (1 mmol) of monomeric glyoxal (*13*) dissolved in 3.8 mL of dichloromethane, 1 mmol of CoH(CO)$_4$ in 1.2 mL of *n*-pentane was added under Ar at –79 °C. Overnight storage on dry ice resulted in a bright yellow precipitate, which was filtered off and dried in an Ar stream. This compound is extraordinarily sensitive to air and heat; it decomposes above –50 °C. Its IR spectrum was recorded at this temperature in dichloromethane solution (Table II).

Preparation of Tetracarbonyl(1-hydroxy,1-ethoxycarbonyl)methylcobalt, 1d. This compound was prepared analogously in toluene–*n*-pentane from ethyl glyoxylate.

Preparation of Tetracarbonyl(2-trimethylsilyloxy)-*trans*-3-pentenoylcobalt, 4e. To 201 μL (2.43 mmol) of crotonaldehyde in 4 mL of *n*-hexane, 0.81 mmol of CoH(CO)$_4$ in 1.0 mL of *n*-pentane was added under CO at –55 °C. After 1 min, 213 μL of bis(trimethylsilyl)trifluoroacetamide (BSTFA) was injected into the reaction mixture. Within 5 min the solution turned lemon yellow. In addition to some Co$_2$(CO)$_8$, tetracarbonylacylcobalt 4e resulted (Table II).

Table II. Spectral Data of Complexes 1–5

Compound	IR: ν (CO) (cm^{-1})	^{1}H NMR^a: δ (ppm)
1a	2100, 2050, 2021[b]	
1c	2109, 2048, 2032, 2024[b]	
1d	2105, 2045, 2027, 2018, 1729, 1712[c]	
2a	2109, 2051, 2028, 2013, 1695[b]	3.30 (s, 1H), 3.93 (s, 2H)
3a	2100, 2032, 2019, 2008[d]	0.07 (s, 9H), 4.97 (s, 2H)
3b	2101, 2035, 2022, 2005[e]	
4a	2107, 2044, 2028, 2010, 1701[d]	
4e	2102, 2042, 2023, 2003, 1695[e]	
5a	2051, 1986, 1964, 1688, 1672[d]	0.03 (s, 9H), 4.45 (s, 2H), 6.6–7.4 (m, 15H)
5b	2041, 1973, 1958, 1647[c]	0.03 (s, 9H), 0.93 (s, 9H), 3.54 (s, 1H), 6.5–6.8 (m, 15H)

[a] In toluene–d_8.
[b] In dichloromethane.
[c] In toluene.
[d] In n-heptane.
[e] In n-hexane–n-pentane mixture.

Preparation of Tetracarbonyl(1-trimethylsilyloxy-2,2-dimethyl)propyl cobalt, 3b, and Tricarbonyltriphenylphosphine(2-trimethylsilyloxy-3,3-dimethyl)butanoylcobalt, 5b. To a solution of 172 µL (162 mmol) of pivalaldehyde in 3 mL of *n*-hexane, 1.62 mmol of CoH(CO)$_4$ in 2.0 mL of *n*-pentane was added under Ar at −55 °C. After 1 min, 472 µL (1.62 mmol) of BSTFA was injected. The IR spectrum recorded after 45 min reaction time showed the complete conversion of CoH(CO)$_4$ and the presence of **3b** together with traces of Co$_2$(CO)$_8$. Addition of PPh$_3$ in 10 mol % excess and stirring at 0 °C for 3 h gave a yellow precipitate, which was filtered and washed with 2 × 1 mL of *n*-pentane and dried in vacuum to produce 480 mg of **5b** (50% yield). For spectral data, *see* Table II.

Results and Discussion

Reaction of Dialkyl Fumarate with CoH(CO)$_4$.   Diethyl fumarate (DEF) reacts readily with CoH(CO)$_4$ at 10 °C under atmospheric pressure of CO. This reaction forms diethyl succinate (DES) as the hydrogenated product (*14*) and diethyl 2-formylsuccinate as hydroformylated product (eqs 1 and 2).

$$\text{DEF} + 2\text{CoH(CO)}_4 \rightarrow \text{DES} + \text{Co}_2(\text{CO})_8 \tag{1}$$

$$\text{DEF} + 2\text{CoH(CO)}_4 + \text{CO} \rightarrow \underset{\overset{|}{\text{CHO}}}{\text{EtO}_2\text{CCHCH}_2\text{CO}_2\text{Et}} + \text{Co}_2(\text{CO})_8 \tag{2}$$
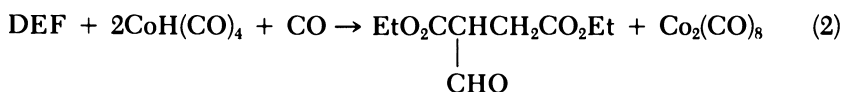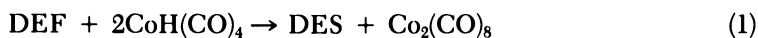
Both reactions were found to be autocatalytic with respect to Co$_2$(CO)$_8$. Thus, when these reactions were started at different Co$_2$(CO)$_8$ concentrations, the induction period decreased with increasing initial Co$_2$(CO)$_8$ concentration (Figure 2), and the initial rates showed a 0.5-order dependence in [Co$_2$(CO)$_8$]$_0$ (Table III).

In experiments with excess diethyl fumarate, a large part (60–70%) of the converted CoH(CO)$_4$ could not be accounted for by the products of reactions 1 and 2. Instead, the formation of tetracarbonyl[1,2-bis(ethoxycarbonyl)ethyl]cobalt could be observed (eq 3).

$$\text{DEF} + \text{CoH(CO)}_4 \rightarrow \underset{\overset{|}{\text{Co(CO)}_4}}{\text{EtO}_2\text{CCHCH}_2\text{CO}_2\text{Et}} \tag{3}$$
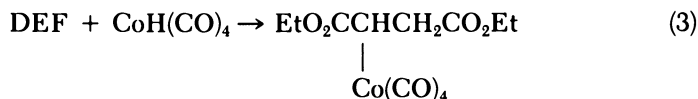
Just after CO uptake stopped, and after Co$_2$(CO)$_8$ was removed by crystallization at −79 °C, the infrared spectrum of the reaction mixture showed carbonyl stretching bands characteristic of a tetracarbonylalkylcobalt (Table I; cf. refs. 15–19), as well as bands for two different ester carbonyls.

With the dimethyl ester of fumaric acid, not only Co$_2$(CO)$_8$ but the surplus dimethyl fumarate as well could be removed by low-temperature
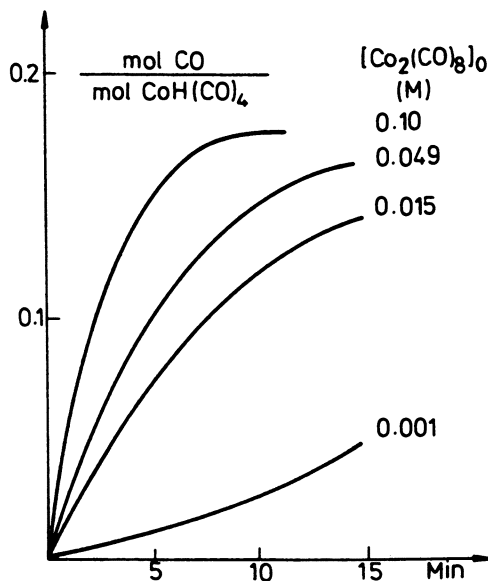
Figure 2. The effect of initial $Co_2(CO)_8$ concentration on the reaction of diethyl fumarate (DEF) with $CoH(CO)_4$ under CO atmosphere at 10 °C in n-octane. $[DEF]_0 = 0.152$ M, $[CoH(CO)_4]_0 = 0.030$ M, $[CO] = 0.00946$ M.

Table III. Effect of Initial $Co_2(CO)_8$ Concentration on the Amount of Absorbed CO and on the Initial Rate of CO Absorption in the Reaction of DEF with $CoH(CO)_4$

$[Co_2(CO)_8]_0$ (M)	CO_{max} [mol CO/mol CoH(CO)$_4$]	$10^6 \, r_{in}$ (M s^{-1})	$10^5 \, r_{in}/[Co_2(CO)_8]_0^{0.5}$ (M$^{0.5}$ s^{-1})
0.001	0.159	1.58	5.0
0.015	0.167	6.22	5.1
0.049	0.176	11.5	5.2
0.10	0.16	16.1	5.1

NOTE: CO_{max} is adsorbed CO; r_{in} is the initial rate of CO absorption; [CO] is 0.00946 M; [DEF]$_0$ is 0.152 M; $[CoH(CO)_4]_0$ is 0.030 M; 10 °C; n-octane solution.

fractional crystallization (Figure 1). From this solution pure tetracarbonyl[1,2-bis(methoxycarbonyl)ethyl]cobalt could be crystallized at −79 °C in 65% yield.

On the basis of the kinetic behavior of reactions 1 and 2, similar to that already observed for 1-heptene, 1-octene (20), and ethyl acrylate (18) under the same conditions, we assume that the role of $Co_2(CO)_8$ is to catalyze the formation of a tricarbonyl(hydridoolefincobalt) intermediate according to Scheme I. This intermediate converts to a tricarbonylalkylcobalt, which then reacts in competing fast reactions to form the products of reactions 1, 2, and
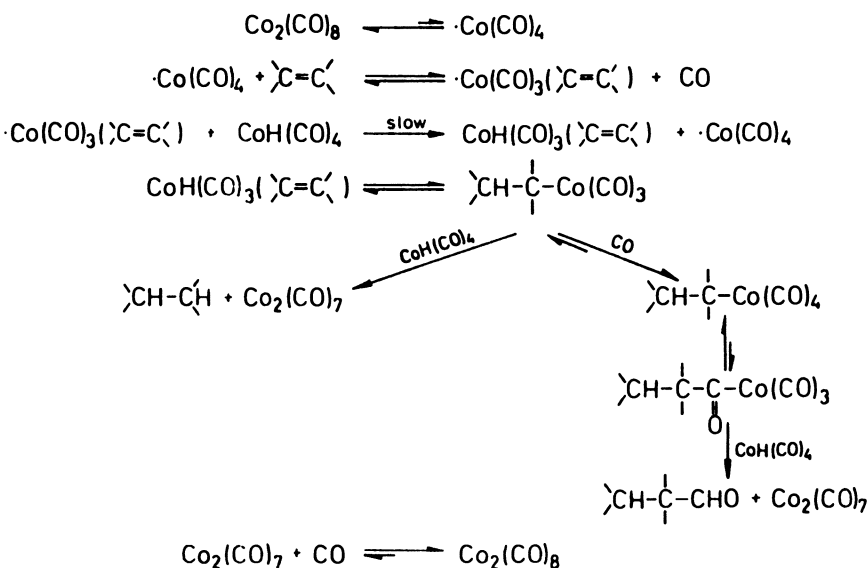
Scheme I.

3. $Co_2(CO)_8$ is one of the products in both reaction 1 and reaction 2. Its increasing concentration during the conversion of $CoH(CO)_4$ accounts for the observed autocatalytic behavior.

Reaction of Aldehydes with $CoH(CO)_4$. Aldehydes react with $CoH(CO)_4$ between −79 and −40 °C under Ar or CO atmosphere to produce tetracarbonyl-α-hydroxyalkylcobalt (**1**) or tetracarbonyl-α-hydroxyacylcobalt (**2**), respectively (eq 4).

$$RCHO + CoH(CO)_4 \rightarrow \underset{\mathbf{1}}{RCH(OH)Co(CO)_4} \underset{-CO}{\overset{+CO}{\rightleftarrows}}$$

$$\underset{\mathbf{2}}{RCH(OH)C(O)Co(CO)_4} \qquad (4)$$
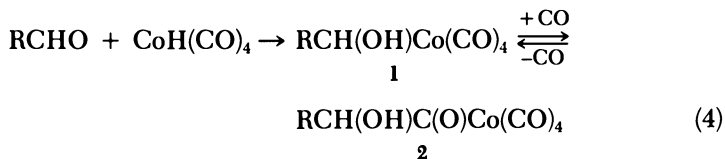
Number	R
1a, 2a	H
1b, 2b	*t*-Bu
1c, 2c	CHO
1d, 2d	CO_2Et
1e, 2e	*trans*-CH=CH–Me

Compounds **1** and **2** were identified by infrared spectroscopy, but they decompose below –20 °C and are too unstable for isolation. More stable *O*-silyl derivatives **3** and **4** could be formed by adding powerful silylating agents, such as BSTFA, to the cold solutions of **1** and **2** (eqs 5 and 6).

$$1 \ + \ BSTFA \rightarrow \underset{\textbf{3}}{RCH(OSiMe_3)Co(CO)_4} \tag{5}$$

$$2 \ + \ BSTFA \rightarrow \underset{\textbf{4}}{RCH(OSiMe_3)C(O)Co(CO)_4} \tag{6}$$
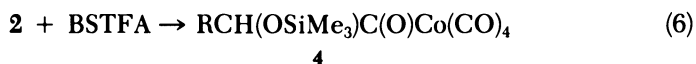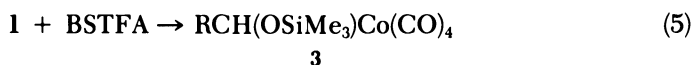
By adding PPh_3 to solutions of compounds **3** and **4**, isolable derivatives **5** were obtained (eq 7). Spectral data of the compounds prepared are listed in Table II.

$$3 \text{ or } 4 \ + \ PPh_3 \rightarrow \underset{\textbf{5}}{RCH(OSiMe_3)C(O)Co(CO)_3PPh_3} \tag{7}$$
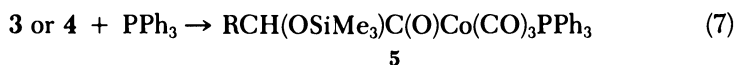
The formation of type **1–5** complexes could not be detected in mixtures of $CoH(CO)_4$ and isobutyraldehyde or methyl isobutyl ketone at –50 °C. Substantial amounts of silyl enol ethers were formed, however, by adding BSTFA to the cold reaction mixtures (eqs 8 and 9). Generation of ethers indicated that an interaction with $CoH(CO)_4$ preceded the silylation. Without $CoH(CO)_4$, isobutyraldehyde and methyl isobutyl ketone do not react with BSTFA at such a low temperature.

$$Me_2CHCHO \ + \ BSTFA \xrightarrow[\text{–50 °C}]{CoH(CO)_4,\ 10\ \text{mol \%}} \underset{35\%}{Me_2C{=}CHOSiMe_3} \tag{8}$$

$$Me_2CHCH_2C(O)Me \ + \ BSTFA \xrightarrow[\text{–50 °C}]{CoH(CO)_4,\ 10\ \text{mol \%}}$$

$$\underset{>90\%}{Me_2CHCH{=}C(OSiMe_3)Me} \ + \ Me_2CHCH_2C(OSiMe_3){=}CH_2 \tag{9}$$
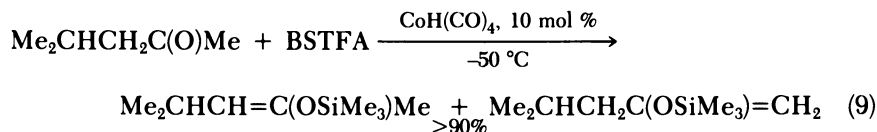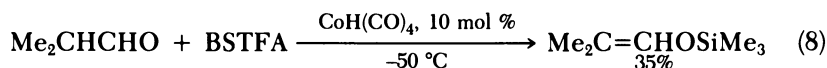
The preparative results obtained with different carbonyl compounds can be explained by Scheme II.

It is conceivable that aldehydes and ketones, similarly to ketenes (*21*) or oxiranes (*22, 23*), behave as hard bases and deprotonate $CoH(CO)_4$ in a fast but unfavorable equilibrium reaction, and that the resulting ion pair collapses rapidly to the α-hydroxyalkylcobalt compound **1**. In consecutive reactions, **1** can insert CO to form a tetracarbonyl-α-hydroxyacylcobalt, **2**, and give the more stable derivative **3** by silylation of the hydroxy group. Addition of PPh_3 to silylated compounds **3** and **4** provides the substitution product **5**. The catalytic effect of $HCo(CO)_4$ on the formation of silyl enol

Scheme II.
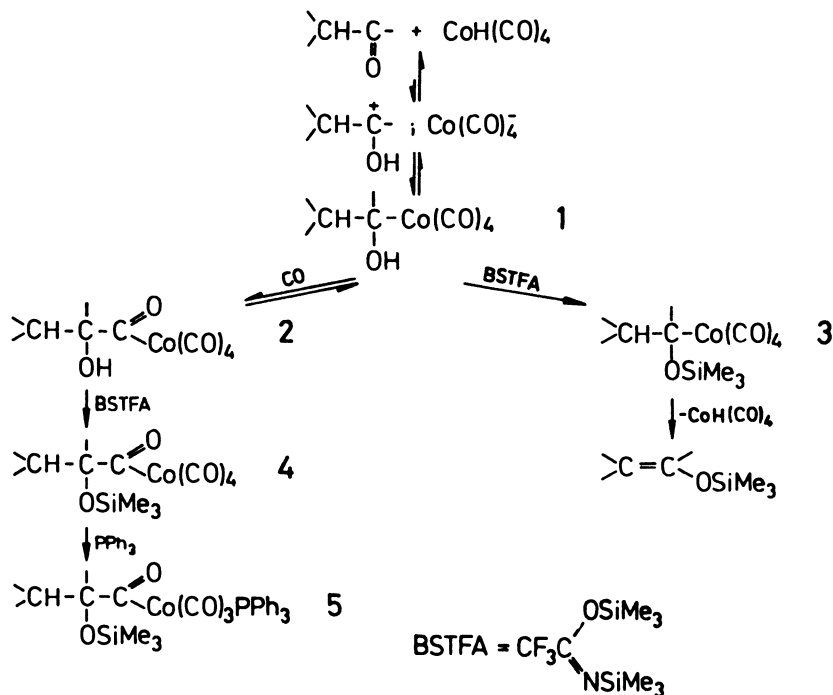
ethers from aldehydes or ketones and BSTFA is explained by intermediates 1 and 3.

The observed regiospecificity of reaction 4 has important mechanistic implications concerning some catalytic processes. In both aldehyde and CO reductions, $CoH(CO)_4$ was postulated to lose CO, resulting in $CoH(CO)_3$, which is able to coordinate aldehyde. Insertion into the Co–H bond could then occur in two ways (5, 6, 8) (eq 10).

$$\begin{array}{c} O \\ \| \\ C \\ / \backslash \\ R \quad H \end{array} \text{-----} CoH(CO)_3 \Big\langle \begin{array}{l} \longrightarrow RCH_2OCo(CO)_3 \\ \\ \longrightarrow RCH(OH)Co(CO)_3 \end{array} \qquad (10)$$
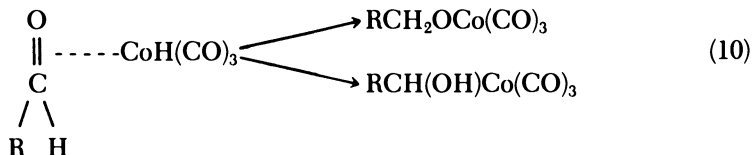
This mechanism is, however, not very probable. According to molecular orbital calculations, the energy of CO dissociation from $CoH(CO)_4$ is presumably high; a dissociation energy of 186 kJ mol^{-1} was estimated (24, 25). The suggestion of a tricarbonyl intermediate is therefore incompatible with

the easy and regiospecific formation of tetracarbonyl-α-hydroxyalkylcobalts in our experiments. We prefer an explanation through a low-energy ionic path, which may start with the protonation of the aldehyde, as depicted in Scheme II. The important role of bases in the hydroformylation of formaldehyde with rhodium catalysts (26) and in the synthesis of ethylene glycol with rhodium (27, 28) or ruthenium (29) also support this view.

Acknowledgments

References

1. Pino, P.; Piacenti, F.; Bianchi, M. In *Organic Syntheses via Metal Carbonyls*; Wender, I.; Pino, P., Eds.; Wiley: New York, 1977; Vol. 2, pp 43–153.
2. Tkatchenko, I. In *Comprehensive Organometallic Chemistry*; Wilkinson, G.; Stone, F. G. A.; Abel, E. W., Eds.; Pergamon: Oxford, 1982; Vol. 8, pp 140–143.
3. Heck, R. F.; Breslow, D. S. *J. Am. Chem. Soc.* **1961**, *83*, 4023.
4. Mirbach, M. F. *J. Organomet. Chem.* **1984**, *265*, 205.
5. Markó, L. *Proc. Chem. Soc., London* **1962**, 67.
6. Aldridge, L.; Jonassen, B. *J. Am. Chem. Soc.* **1963**, *85*, 886.
7. Goetz, R. W.; Orchin, M. *J. Org. Chem.* **1962**, *27*, 3698.
8. Fahey, D. R. *J. Am. Chem. Soc.* **1981**, *103*, 136.
9. Slocum, D. W. *Catal. Org. Synth.* **1980**, *7*, 245.
10. Sisak, A.; Sámpár-Szerencsés, E.; Galamb, V.; Németh, L.; Ungváry, F.; Pályi, G. *Organometallics* **1989**, *8*, 1096.
11. Shriver, D. F. *Manipulation of Air-Sensitive Compounds*; McGraw-Hill: New York, 1969.
12. Kirch, L.; Orchin, M. *J. Am. Chem. Soc.* **1958**, *80*, 4428.
13. Harries, C.; Temme, P. *Ber. Dtsch. Chem. Ges.* **1907**, *40*, 165.
14. Csizmadia, J.; Ungváry, F.; Markó, L. *Transition Met. Chem. (London)* **1976**, *1*, 170.
15. Markó, L.; Bor, G.; Almásy, G.; Szabó, P. *Brennst.-Chem.* **1963**, *44*, 184.
16. Galamb, V.; Pályi, G. *Acta Chim. Acad. Sci. Hung.* **1982**, *111*, 131.
17. Galamb, V.; Pályi, G.; Cser, F.; Furmanova, M. G.; Struchkov, Y. T. *J. Organomet. Chem.* **1981**, *209*, 183.
18. Ungváry, F.; Markó, L. *Organometallics* **1986**, *5*, 2341.
19. Sisak, A.; Ungváry, F.; Markó, L. *J. Org. Chem.* **1990**, *55*, 2508.
20. Ungváry, F.; Markó, L. *J. Organomet. Chem.* **1981**, *219*, 397.
21. Ungváry, F. *J. Organomet. Chem.* **1986**, *303*, 251.
22. Heck, R. F. *J. Am. Chem. Soc.* **1963**, *85*, 1460.
23. Kreisz, J.; Ungváry, F.; Sisak, A.; Markó, L. *J. Organomet. Chem.* **1991**, *417*, 89.
24. Versluis, L., Ph.D. Thesis, University of Calgary, Calgary, Alberta, Canada, 1989.
25. Versluis, L.; Ziegler, T.; Baerends, E. J.; Ravenek, W. *J. Am. Chem. Soc.* **1989**, *111*, 2018.

26. Chan, A. S. C.; Carroll, W. E.; Willis, W. E. *J. Mol. Catal.* **1983**, *19*, 377.
27. Pinett, R. L. *Ann. N. Y. Acad. Sci.* **1977**, *295*, 239.
28. Masuda, T.; Murata, K.; Matsuda, A. *Bull. Chem. Soc. Jpn.* **1988**, *61*, 2865.
29. Kiso, Y.; Saeki, K.; Hayashi, T.; Tanaka, M.; Matsunaga, Y.; Ishino, M.; Tamura, N.; Deguchi, T.; Nakamura, S. *J. Organomet. Chem.* **1987**, *335*, C27.

Oxides as Heterogeneous Promoters for Liquid-Phase Hydrocarbonylation Reactions with Iodocarbonylruthenium Catalysts

Giuseppe Braca[1], Anna Maria Raspolli Galletti[1], Glauco Sbrana[1], and Elizeu Trabuco[2]

[1]Department of Chemistry, University of Pisa, 56126 Pisa, Italy
[2]Instituto de Biocencias, Letras e Ciencias Exatas, Universidade Estadual Paulista, San Jose do Rio Preto, Brazil

Basic or acid oxides, used as heterogeneous promoters of carbonyl-ruthenium catalysts in liquid-phase hydrocarbonylation reactions on oxygenated substrates, strongly affect the activity and selectivity of the catalytic system. Concurrent or successive reactions of simple carbonylation, homologation, hydrogenation to hydrocarbons, and etherification take place to varying extents. Carbonylation and etherification are favored by acid oxides and homologation and hydrogenation by basic oxides. This behavior is related to the formation and stabilization by the oxides of H+ and H- hydridocarbonylruthenium catalytic species, whose relative concentrations in solution depend on the nature of the oxide. Heterogeneous oxides are easily separated and recycled from the reaction mixture. Their use simplifies the catalytic system and allows one to direct the catalytic process toward the target product.

IN HOMOGENEOUS AND HETEROGENEOUS CATALYSIS, promoters or cocatalysts generally operate in the same phase of the catalytically active species. This feature is practically an unvarying rule in heterogeneous gas–solid catalysis, whereas it is not essential in homogeneous liquid-phase systems. Liquid-phase promoters and cocatalysts can interact directly and easily with

the soluble active species. However, chemical interactions at the liquid–solid interface are also important when the two components are in different phases.

In our research on carbonylation and hydrocarbonylation reactions of oxygenated substrates with carbonylruthenium iodide systems, we demonstrated the important role various promoters play in the activity and selectivity of the reaction: iodide derivatives (1), complexing agents, Lewis acids, and protonic acids (2). Moreover, promoters with different acid–base properties can modify the nature or the relative concentration of the different carbonylmetal species present in solution and thus change the total activity and selectivity of the system (3, 4).

Analogous effects related to acid–base interactions are also extensively reported in the literature for carbon monoxide hydrogenation with rhodium and ruthenium heterogeneous catalysts (5–8).

With the aim of establishing a bridge between homogeneous and heterogeneous catalytic phenomena related to the role of promoters, we studied the effect of some heterogeneous oxides, γ-Al_2O_3, MgO, La_2O_3, TiO_2, and Nb_2O_5. These oxides have different Lewis or Brönsted acidity or basicity on hydrocarbonylation reactions of oxygenated substrates catalyzed by homogeneous carbonyl- and iodocarbonylruthenium systems.

Carbonylation–Homologation of Ethanol and 1-Butanol

The test reaction chosen was the carbonylation–homologation of ethanol and 1-butanol with synthesis gas. It was carried out under typical conditions used for the hydrocarbonylation of oxygenated substrates with iodocarbonylruthenium systems (9): ruthenium precursor, $Ru(acac)_3$ (acac is acetyl acetonate, $C_5H_7O_2$) or $Ru(CO)_4I_2$; iodide promoter, CH_3I or HI; T, 200 °C; CO/H_2, 1; P, 14 MPa (Tables I and II).

Under these conditions a number of concurrent and successive reactions (Scheme I), catalyzed either by the protonic cocatalyst or by the ruthenium species, take place. The relative selectivities are greatly affected by the reaction conditions and by the intervention of the added promoters.

Under specific conditions, products coming from the direct activation of CO are also produced. Water produced in various reactions also plays an important role by interacting with the surfaces of the oxides and affecting their acid–base properties (10, 11).

To better distinguish and compare the action of the cocatalysts and of the ruthenium species, the tables indicate both the total conversion and the conversion due only to metal-catalyzed reactions.

Soluble and Insoluble Aluminum Promoters. The role of soluble aluminum halides acting as effective Lewis acids in the activation of CO groups bound to organometallic derivatives has been extensively reviewed

Table I. Hydrocarbonylation of Ethanol with Soluble or Insoluble Aluminum Promoters

Run	Promoter System		Conversion (%)		Types of Reactions (% selectivity)			Metal-Catalyzed Reactions (% selectivity)		
	Iodide Supplier (mmol)	Oxide (g)	A^a	B^b	Etheri-fication	Esteri-fication	Metal-Catalyzed	Homolo-gation	Carbonyl-ation	Hydrogen-ation
1	CH_3I (3.6)		71.2	21.6	64.1	5.6	30.3	27.1	29.3	43.6
2	AlI_3^c (2.1)		77.4	24.0	60.1	8.9	31.0	20.1	40.0	39.9
3	CH_3I (3.6)	Al_2O_3 (2.0)	28.7	12.2	53.6	3.7	42.7	33.0	14.5	52.5
4	CH_3I (3.6)		92.3	49.7	26.6	20.2	53.2	6.2	57.7	36.1
5	AlI_3 (1.2)		85.3	40.0	36.0	16.8	47.2	14.0	47.8	38.2
6	CH_3I (3.6)	Al_2O_3 (2.0)	44.4	18.4	46.7	11.7	41.6	25.8	29.2	45.0

NOTES: Reaction conditions: $Ru(acac)_3$, 0.36 mmol; EtOH, 480 mmol; temperature, 200 °C; time, 8 h; pressure, 14 MPa; CO/H_2, 1; I/Ru, 10. In runs 4–6 the solvent was 14 mL of toluene.

[a] Total conversion.

[b] Conversion to metal-catalyzed reaction products.

[c] I/Ru, 17.

Table II. Hydrocarbonylation of 1-Butanol

Run	Promoter System Iodide Supplier (mmol)	Oxide (g)	Conversion (%) A^a	B^b	Types of Reactions (% selectivity) Etheri-fication	Esteri-fication	Metal-Catalyzed	Metal-Catalyzed Reactions (% selectivity) Homolo-gation	Carbonyl-ation	Hydrogen-ation
7	CH_3I (4.5)		84.2	45.2	31.0	15.3	53.7	16.9	48.6	34.5
8^c	CH_3I (4.4)		88.7	59.4	22.5	10.6	66.9	10.7	73.5	15.8
9	CH_3I (4.5)	Al_2O_3 (1.0)	17.9	6.8	55.9	6.2	37.9	54.0	16.2	29.8
10	CH_3I (4.5)	MgO (1.0)	21.9	8.0	52.9	10.8	36.3	40.8	30.8	28.4
11	CH_3I (4.5)	La_2O_3 (1.0)	72.1	34.7	36.1	15.8	48.1	26.4	51.6	22.0
12	CH_3I (4.5)	TiO_2 (1.0)	90.7	58.5	21.7	13.8	64.5	12.6	47.4	40.0
13	CH_3I (4.5)		94.1	53.3	27.8	15.6	56.6	12.2	48.0	39.8

NOTE: Reaction conditions: $Ru(acac)_3$ = 0.45 mmol; I/Ru = 10; 1-BuOH = 376 mmol; T = 200 °C; time = 8 h; CO/H_2 = 1; P = 14 MPa.
^{a}Total conversion.
^{b}Conversion to metal-catalyzed reaction products.
^{c}Toluene = 17 mL; 1-BuOH = 188 mmol.
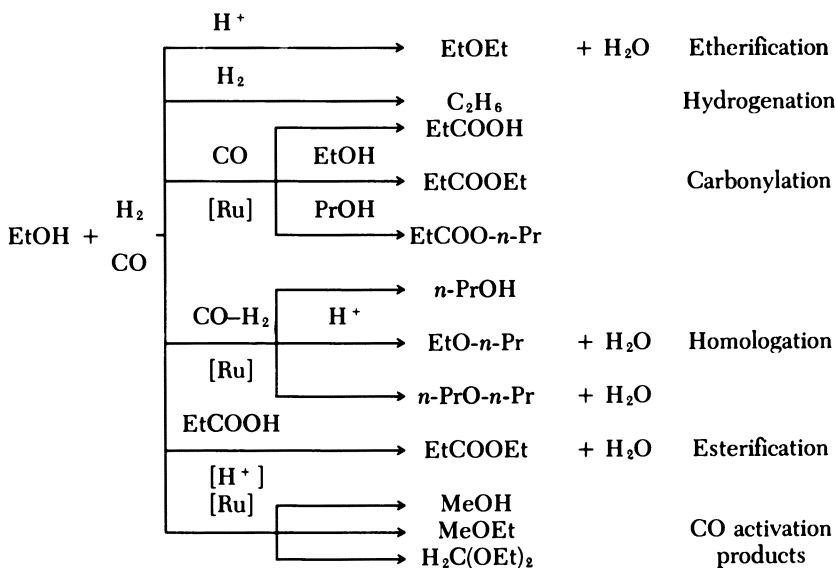
Scheme 1. Products formed in the hydrocarbonylation of ethanol.

(12). We reported their positive effect on activity and selectivity in some hydrocarbonylation reactions of esters *(2)* and alcohols *(3)*.

The results of ethanol hydrocarbonylation runs, without solvent or in toluene, using different aluminum-soluble and -insoluble promoters, are shown in Table I and compared with data obtained by using the usual iodide promoter, CH_3I, alone.

When initially soluble AlI_3 is used as promoter, it undergoes a partial hydrolysis by the water with separation of insoluble aluminum hydroxide. This hydrolysis leads to a change in the acid–base properties of the catalytic system. In addition, selectivity toward hydrogenation and homologation products improves with time (Table III). Accordingly, the ratio of the carbonylation to the hydrogenation reaction rate, 1.9 at the beginning, decreases to about 0.9 when the conversions are higher than 50%.

The interactions of carbonylruthenium clusters with the metal oxide surfaces and particularly with the hydroxylated aluminum oxides are well documented *(7, 13–16)*. A promotion effect of the alumina surface on the kinetics of the alkyl migration–carbonyl insertion reaction in some carbonylmanganese derivatives has also been reported *(12, 17)*. However, experimental data concerning the kinetic and selectivity effects of these interactions in catalytic reactions are almost rare.

In our experiments, when hydroxylated alumina is used as a heterogeneous promoter the basic properties of the –OH groups predominate *(13)*. The Lewis acid character, generated by the presence of surface-exposed

Table III. Dependence of Selectivity on Conversion in the Hydrocarbonylation of Ethanol with Different Promoters

| Promoter System | Period (h) | Conversion[a] (%) | Turnover Number (h^{-1})[b] | | | Ratio[c] |
			Homolo-gation	Carbonyl-ation	Hydrogen-ation	
CH₃I	0–6	22.3	12.3	25.9	11.4	2.27
	18–24	43.5	1.92	1.91	1.71	1.11
AlI₃	0–4	20.9	16.3	35.0	18.2	1.92
	18–24	57.1	1.26	5.86	6.71	0.87
Nb₂O₅	0–8	22.4	9.2	26.2	1.92	13.60
	18–24	49.2	5.81	18.30	2.64	6.93

NOTE: Figure 2 caption gives reaction conditions.
[a]Only metal-catalyzed reactions.
[b]Calculated as (moles of product formed in the indicated reaction) ÷ [(moles of catalyst) (hour)].
[c]Ratio of turnover number carbonylation/turnover number hydrogenation.

Al^{3+} ions, can be exerted only using a high-temperature dehydroxylated γ-alumina in the absence of water (12–18). Thus in the hydrocarbonylation of ethanol with CH_3I and Al_2O_3 (Table I, run 3), the decrease in ethanol conversion can be ascribed to the lowered acidity of the catalytic system due to the neutralization of the acid species by the –OH groups.

Furthermore, the observed increase in selectivity toward hydrogenation and homologation (carbonylation plus hydrogenation) products probably results from the involvement of the anionic carbonylruthenium hydrides $[HRu_3(CO)_{11}]^-$ and $[HRu(CO)_4]^-$, which are particularly active in the hydrogenation of acyl intermediates (19).

IR spectra of the reaction product solution recorded at room temperature and CO atmosphere show the presence of $[HRu_3(CO)_{11}]^-$ (Figure 1, spectrum C) $(\nu_{(CO)} = 2002, 1990 \text{ cm}^{-1})$. This species can be produced on the surface by the reaction of chlorocarbonylruthenium derivatives with hydroxylated aluminum oxide acting as a halide acceptor (13).

However, once formed, this HRu-active species can easily be displaced from the surface by the strong lone-pair donor ethanol and water. Operating in solution can improve the formation of hydrogenation products, while depressing that of simple carbonylation.

When an apolar solvent is used (i.e., toluene) the opposite effect is observed. Hydrogenation decreases and carbonylation product selectivity increases (Table I; compare runs 1–3 with runs 4–6).

Analogous effects are observed in 1-butanol hydrocarbonylation (Table II), in which the maximum selectivity toward carbonylation products is obtained by operating in toluene as solvent. In all cases the use of γ-Al_2O_3 as promoter decreases the activity and favors the hydrogenation and homologation reactions.

Magnesium Oxide. The second promoter tested, magnesium oxide, was almost completely hydroxylated (MgO-25: hydrated MgO dried at
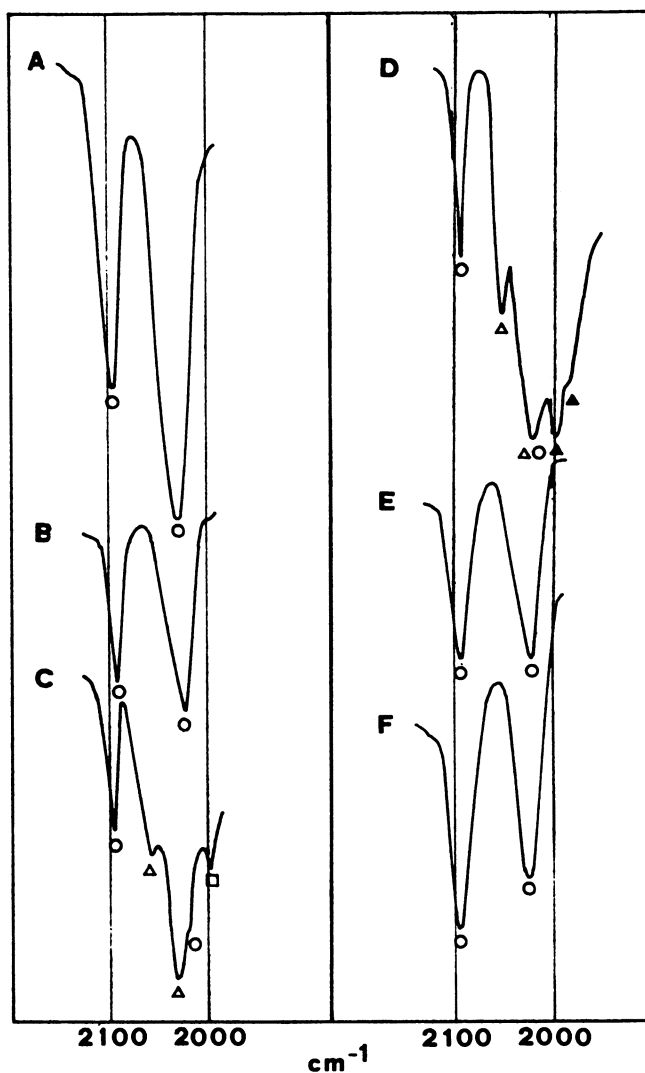
Figure 1. CO stretching frequencies in the carbonylruthenium species present in solution. Promoter system: A, Ch₃I; B, AlI₃; C, γ-Al₂O₃–Ch₃I; D, MgO–Ch₃I; E, La₂O₃–CH₃I; F, Nb₂O₅–CH₃I. Key: ○, [Ru(CO)₃I₃]⁻; △, [Ru₃(CO)₁₂]; ▲, [HRu₃(CO)₁₁]⁻.

25 °C) and only partially hydroxylated (hydrated MgO dried at 200 °C) according to the literature (*20*). The results obtained (Table IV, runs 14 and 15) agree with the following actions displayed by these oxides:

- neutralization of the protonic species HI and $HRu(CO)_3I_3$ by its strong Brönsted basicity (*11*);

Table IV. Hydrocarbonylation of Ethanol with Different Oxides as Promoters

Run	Promoter System Iodide Supplier (mmol)	Oxide (g)	Conversion (%) A^a	Conversion (%) B^b	Types of Reactions (% selectivity) Etheri- fication	Esteri- fication	Metal- Catalyzed	Metal-Catalyzed Reactions (% selectivity) Homolo- gation	Carbonyl- ation	Hydrogen- ation
14[c]	CH₃I (3.6)	MgO₂₅°C (1.0)	13.3	7.1	43.0	4.0	53.0	29.0	4.6	66.4
15[c]	CH₃I (3.6)	MgO₂₀₀°C (1.0)	27.0	13.3	47.0	3.8	49.2	20.4	7.4	72.2
16	CH₃I (3.6)	MgCO₃ (1.0)	16.7	8.1	47.8	3.6	48.6	31.4	12.2	56.4
17	CH₃I (3.6)	La₂O₃ (1.0)	56.3	22.0	58.4	7.5	34.1	25.6	23.8	50.6
18	CH₃I (3.6)	TiO₂ (1.0)	68.4	20.5	62.8	7.3	29.9	25.4	34.2	40.4
19	CH₃I (3.6)	Nb₂O₅ (1.0)	61.3	19.9	59.2	8.4	32.4	34.8	37.1	28.1

NOTE: Reaction conditions are given in Table I.
[a]Total conversion.
[b]Conversion to metal-catalyzed reaction products.
[c]C₁ products formed by CO hydrogenation: run 14 = 8 mmol; run 15 = 7.5 mmol.

- absorption of the I^- ligands (*21*); and
- promotion of the formation in solution of $[HRu_3(CO)_{11}]^-$ species (*20*).

Neutralization negatively affects the activation of the substrate by protonation (*3*). The result is a decrease in conversion. The lowest activity is observed with the more hydroxylated oxide, MgO-25.

The second effect, related to the formation of basic magnesium iodides (*21*), seems to be a reversible process. The equilibrium is displaced to right under CO pressure, with formation of $Ru_3(CO)_{12}$, and to left toward iodo-carbonyl species when CO is removed (reaction 1).

$$Mg\overset{O}{\diagup} + HRu(CO)_3I_3 \underset{-CO}{\overset{+CO}{\rightleftharpoons}} Mg\overset{OH}{\underset{I}{\diagup}} + [Ru(CO)_4]_3 \qquad (1)$$
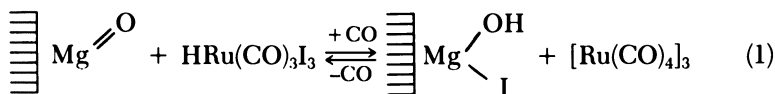
Finally, hydroxylated magnesia promotes the formation of $[HRu_3(CO)_{11}]^-$ on the surface (*20*). This anion is released in solution, as indicated by the presence in the IR spectrum (Figure 1, spectrum D) of its characteristic ν_{CO} bands.

$$Ru_3(CO)_{12} + H-O-Mg \rightarrow$$

$$[HRu_3(CO)_{11}]^- (Mg^{2+})_{1/2} + CO_2 \text{ (adsorbed)} \quad (2)$$
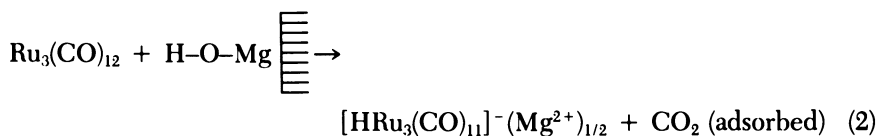
This behavior is in accord with the reactivity on the MgO surface of the halocarbonylruthenium derivatives (*22*).

The formation of the $[HRu_3(CO)_{11}]^-$ species favors hydrogenation to hydrocarbons and the homologation reaction. It also leads to a significant production of C_1 derivatives (methanol, methyl ethyl ether, and formaldehyde diethyl acetal) by CO hydrogenation (Table IV, runs 14 and 15) (*7, 23*).

When a promoter without Brönsted basicity (such as $MgCO_3$) is used, the $[HRu_3(CO)_{11}]^-$ species are not produced. In this case $[Mg]^{2+}[Ru(CO)_3-I_3]_2^-$ is the predominant species, and an increase in simple carbonylation products is observed (Table IV, run 16).

Lanthanum and Titanium Oxide. Lanthanum oxide, La_2O_3, has a lower basic surface sites content (OH^- and O^{2-}) than MgO and hydroxylated Al_2O_3. Its use causes a lower decrease of catalytic activity and favors the formation of carbonylation products by reducing hydrogenation to hydrocarbons. The IR spectra of the solution indicate the prevailing presence of the $[Ru(CO)_3I_3]^-$ on the $[HRu_3(CO)_{11}]^-$ species (Figure 1, spectrum E).

Therefore, the use of the neutral oxide TiO_2 does not affect the process to a great extent. Conversions and selectivities obtained in the presence or
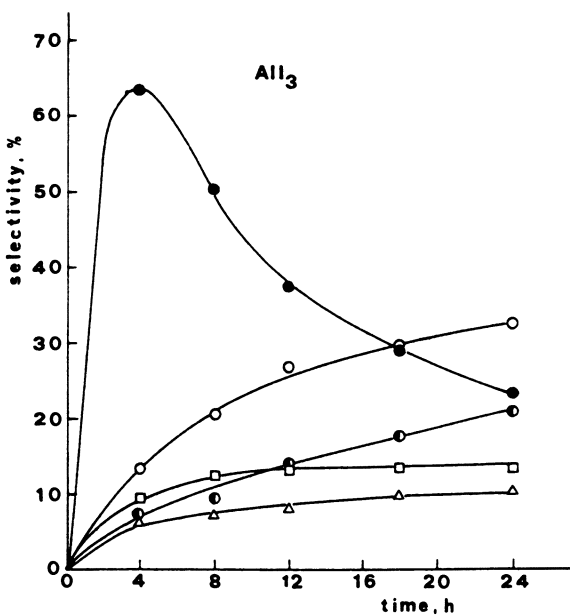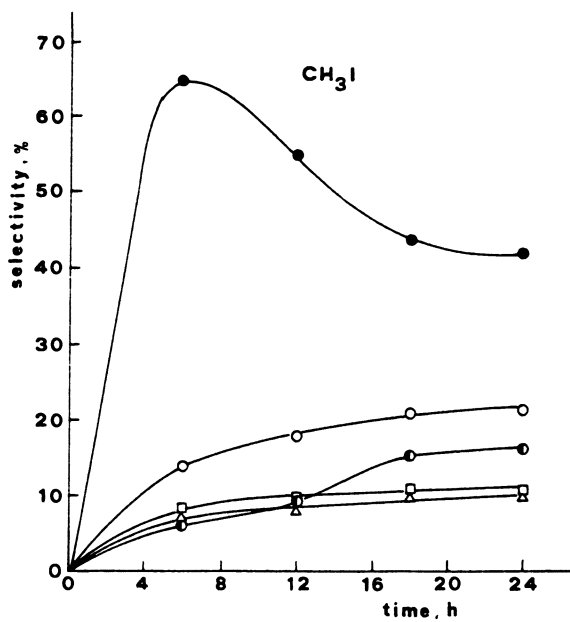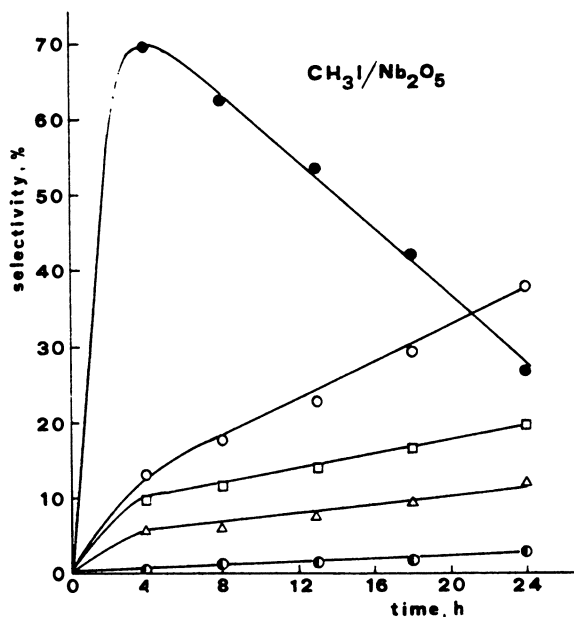
Figure 2. Hydrocarbonylation of ethanol with different promoter systems. Reaction conditions: Ru(acac)₃, 3.6 mmol; I/Ru, 10; EtOH, 4.8 mol; T, 200 °C; P, 14 MPa; CO/H₂, 1; Nb₂O₅, 3 g. Key: Selectivity to ●, etherification products; ○, carbonylation products; □, esterification products; △, homologation products; ○, hydrogenation products; evaluated according to reference 3.

absence of the support are practically the same (compare run 1, Table I, and run 18, Table IV). In this case only $[Ru(CO)_3I_3]^-$ species are evident in the IR spectrum of the reaction solution.

Niobium Pentoxide.   Niobium pentoxide, Nb_2O_5, has the highest Brönsted acidity strength among all the metal oxides dried at 100 °C, coupled with the coexistence of Lewis acid sites on the surface (*24, 25*).

This peculiarity has been well exploited in the hydrocarbonylation of ethanol. The result is a high activity of the catalytic system with a significant decrease in hydrogenation and an improvement of the carbonylation reaction.

The best performances in the production of valuable products (propionates and *n*-propyl derivatives) are obtained by using Nb_2O_5. This advantage is illustrated by the change with time of the selectivities obtained with different catalytic promoters (Figure 2). Nb_2O_5 appears to be particularly effective for the carbonylation and homologation reactions of diethyl ether.

Table V. Hydrocarbonylation of Methyl Acetate in Acetic Acid Solution

Run	Promoter (g)	Conversion (%)		Product Selectivity (%)				
		AcOMe	AcOH	$MeOH+Me_2O+\frac{1}{2}MeOEt$	$EtOH+Et_2O+\frac{1}{2}MeOEt$	AcOEt	AcOH	$CH_4+C_2H_6$
20	—	35.1	19.1	7.3	6.5	65.5	—	19.6
21	HPF_6	1.3	42.7	—	4.9	3.6	64.3	7.9
22	Nb_2O_5	0.5	62.0	—	8.1	6.9	54.1	11.0

NOTE: Reaction conditions: $Ru(acac)_3$, 3.6×10^{-4} mol; CH_3I, 3.6×10^{-3} mol; AcOMe, 0.18 mol; AcOH, 0.18 mol; T, 200 °C; P_{H_2}, 10 MPa; P_{CO}, 5 MPa; time, 10 h; reactor volume, 190 mL.

Under the reaction conditions, diethyl ether is consumed about 10 times more rapidly than in the presence of CH_3I alone.

This behavior is also observed in the methyl acetate homologation to ethyl acetate in acetic acid solution. The Nb_2O_5–$[Ru(CO)_3I_3]^-$ system parallels that of a homogeneous system promoted with an external soluble noncomplexing protonic acid like HPF_6 (2), the activity being higher and the selectivities comparable (Table V).

Conclusions

The action of oxides used as promoters for soluble ruthenium hydrocarbonylation catalysts originates from their acid–base (Brönsted and Lewis) properties. These properties are more or less enhanced by the solvating capacity of the liquid medium. This action is strictly related to the formation and stabilization in solution of different metal species active in the fundamental steps of the catalytic cycle.

Several cluster species are formed and stabilized by interaction of carbonylruthenium derivatives with oxide surfaces (26). However, only three types of derivatives are produced in solution when these species are brought into contact, under hydrocarbonylation conditions, with a liquid polar medium. The detected species are $[Ru(CO)_3I_3]^-$, $[HRu_3(CO)_{11}]^-$ (probably in equilibrium with $[HRu(CO)_4]^-$), and the neutral species $Ru_3(CO)_{12}$. Their relative concentrations are strongly dependent on the type of oxide.

Basic oxides (MgO, hydroxylated Al_2O_3, and La_2O_3), acting as Brönsted bases and iodide acceptors, promote the formation of the carbonyl hydrido species $[HRu_3(CO)_{11}]^-$. They have a pronounced hydrogenating activity (3) and favor the production of homologation products and (unfortunately) of hydrocarbons.

Acid oxides (e.g., Nb_2O_5), acting as Brönsted acids, have a positive effect on the activation of the substrate. They promote the formation of carbonylruthenium iodide species, active in the carbonylation steps of the process (3).

Thus these insoluble oxides may be advantageously used, for instance, in fixed beds contacted with liquid hydrocarbonylation solutions containing the homogeneous catalytic species. Here they would improve the activity and modify the selectivity of the process without introducing complications connected with the use of soluble acid or basic promoters.

Acknowledgments

References

1. Raspolli Galletti, A. M.; Braca, G.; Sbrana, G.; Marchetti, F. *J. Mol. Catal.* **1985**, *32*, 291.
2. Braca, G.; Raspolli Galletti, A. M.; Sbrana, G.; Zanni, F. *J. Mol. Catal.* **1986**, *34*, 183.
3. Braca, G.; Raspolli Galletti, A. M.; Sbrana, G.; Trabuco, E. *J. Mol. Catal.* **1989**, *55*, 184.
4. Dombek, B. D. *Comments Inorg. Chem.* **1985**, *4*(5), 241.
5. Ichikawa, M. *CHEMTECH* **1982**, *12*, 674.
6. Sachtler, W. M. H.; Ichikawa, M. *J. Phys. Chem.* **1986**, *90*, 4753.
7. Uchiyama, S.; Gates, B. C. *J. Catal.* **1988**, *110*, 388.
8. Yoshida, S.; Mori, S.; Kinoshita, H.; Watanabe, Y. *J. Mol. Catal.* **1987**, *42*, 215.
9. Braca, G.; Guainai, G.; Raspolli, A. M.; Sbrana, G.; Valentini, G. *Ind. Eng. Chem. Prod. Res. Dev.* **1984**, *23*, 409.
10. Knoezinger, H.; Stubner, B. *J. Phys. Chem.* **1978**, *82*, 1526.
11. Lamb, H. H.; Gates, B. C. *J. Am. Chem. Soc.* **1986**, *108*, 81.
12. Horwitz, C. P.; Shriver, D. F. *Adv. Organomet. Chem.* **1984**, *23*, 219.
13. Bergmeister, J. J.; Hanson, B. E. *J. Organomet. Chem.* **1988**, *352*, 367.
14. Beck, A.; Dobos, S.; Guczi, L. *Inorg. Chem.* **1988**, *27*, 3220.
15. Darensbourg, D. J.; Ovalles, C. *Inorg. Chem.* **1986**, *25*, 1603.
16. Pierantozzi, R.; Valagene, E.; Nordquist, A. F.; Dyer, P. *J. Mol. Catal.* **1983**, *21*, 189.
17. Correa, F.; Nakamura, R.; Stimson, R. E.; Burwell, R. L.; Shriver, D. F. *J. Am. Chem. Soc.* **1980**, *102*, 5114.
18. Hugues, F.; Smith, A. K.; Ben Taarit, Y.; Basset, J. M.; Commereuc, D.; Chauvin, Y. *J. Chem. Soc., Chem. Commun.* **1980**, 68.
19. Tanaka, M.; Sakakura, T.; Hayashi, T.; Kobayashi, T. *Chem. Lett.* **1986**, 39.
20. D'Ornelas, L.; Theolier, A.; Choplin, A.; Basset, J. M. *Inorg. Chem.* **1988**, *27*, 1261.
21. Leofanti, G.; Solari, M.; Tauszik, G. R.; Garbassi, F.; Galvagno, S.; Schwank, J. *Appl. Catal.* **1982**, *3*, 131.
22. Psaro, R. et al., unpublished results.
23. Kiso, Y.; Tanaka, M.; Nakamura, H.; Yamasaki, T.; Saeki, K. *J. Organomet. Chem.* **1986**, *312*, 357.
24. Iizuka, T.; Ogasawara, K.; Tanabe, K. *Bull. Chem. Soc. Jpn.* **1983**, *56*, 2927.
25. Bernholc, J.; Horsley, J. A.; Murrell, L. L.; Sherman, L. G.; Soled, S. *J. Phys. Chem.* **1987**, *91*, 1526.
26. Zanderighi, G. M.; Dossi, C.; Ugo, R.; Psaro, R.; Theolier, A.; Choplin, A.; D'Ornelas, L.; Basset, J. M. *J. Organomet. Chem.* **1985**, *296*, 127.

Rhodium-Catalyzed Reductive Carbonylation of Methanol

Kenneth G. Moloy and Richard W. Wegman

Union Carbide Corporation, P.O. Box 8361, South Charleston, WV 25303–0361

Rhodium catalyzes the reductive carbonylation of methanol to acet-aldehyde if the appropriate diphosphine ligands are employed. The reductive carbonylation of methanol has been studied for nearly 50 years. Cobalt catalysis has dominated this area from its beginning, and significant improvements were made through the use of various promoters and cocatalysts. However, in all cases the reaction conditions are extreme (4000–8000 psi, 175–220 °C). The new rhodium catalyst gives rates and selectivities comparable to the best cobalt catalysts (100–200 turnovers per hour, 80–90%) but at much lower temperature and pressure (140 °C, 1000 psi). Addition of ruthenium to this catalyst results in the in situ hydrogenation of acetaldehyde and production of ethanol. The catalyst is very robust, and crystalline acetyl complexes Rh(diphosphine)(COCH₃)(I)₂ are isolated quanti-tatively after catalysis. These complexes can be reused as catalysts with no loss in catalyst performance and again be isolated in very high yield. Mechanistic studies suggest that the acetyl complexes are important intermediates in the catalytic reaction.

COBALT-BASED CATALYSTS HAVE DOMINATED research activity in the area of reductive carbonylation of methanol for nearly 50 years (1–8). Although other metals also catalyze these reactions, they are generally inferior to cobalt-based catalysts.

$$CH_3OH \xrightarrow{CO/H_2} CH_3CHO + H_2O \qquad (1)$$
$$\text{(methanol hydroformylation)}$$

$$CH_3OH \xrightarrow{CO/H_2} CH_3CH_2OH + H_2O \qquad (2)$$
$$\text{(methanol homologation)}$$
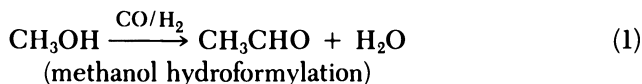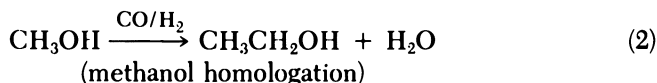
Improvements in cobalt-based catalysts have been made through the use of various cocatalysts and promoters such as iodide, phosphines, and transition metals. Iodide, by far the most important of this group, is almost always employed. In spite of significant advances in catalyst performance, high pressures and temperatures are required. These traditional catalysts are usually operated at pressures of 4000–8000 psi and temperatures of 175–200 °C. The high-pressure requirement poses obvious difficulties. The high temperatures employed often result in the formation of heavy byproducts via aldol condensation reactions of acetaldehyde. A catalyst exhibiting high activity at pressures below 1000 psi and at lower temperature would be of significant practical interest.

We became interested in the homologation of methanol as part of a Department of Energy contract to investigate the synthesis of fuel alcohols from synthesis gas. The drawbacks of the traditional cobalt catalysts prompted us to consider other metals. An obvious choice is rhodium.

Both rhodium and cobalt catalyze a variety of carbonylation reactions, such as olefin hydroformylation and the carbonylation of alcohols to acids (9, 10). Rhodium catalysts are significantly more active than their cobalt counterparts, allowing reactions to be conducted at much lower extremes of temperature and pressure. Previous studies of the use of rhodium in the reductive carbonylation of methanol were not encouraging (11). The reason is quite simple. Iodide is a standard promoter in the cobalt-based catalysts. In the presence of iodide and CO, rhodium is an extremely proficient catalyst for the carbonylation of methanol to acetic acid. Of course, this property forms the basis for the well-known Monsanto acetic acid process (12–15).

To devise a strategy to divert the carbonylation to reductive carbonylation, it is instructive to consider the mechanism of the carbonylation reaction. Fortunately, the mechanism of the Monsanto chemistry has been studied extensively (12–15). It is summarized in Scheme I.

A key step is the reductive elimination of acetyl iodide from $Rh(CO)_2(COCH_3)I_3$. This elimination is facile, occurring rapidly at temperatures as low as 25 °C (oxidative addition of CH_3I to Rh(I) is rate-limiting). If rhodium is to be employed in a reductive carbonylation scheme, it would seem that acyls much more stable with respect to reductive elimination of acid iodides or other nonproductive reactions would be required. In this way interception of the acyl by hydrogen or other reductant might be possible.

Work by Slack et al. (16) and McGuiggan et al. (17) suggests a ligand environment to achieve this interception. They showed that chelating diphosphines [e.g., $Ph_2P(CH_2)_3PPh_2$] impart high stability to rhodium acyl complexes. Thus, the five-coordinate complexes (1) resist reductive elimi-

$$CH_3COI + CH_3OH \longrightarrow CH_3CO_2CH_3 + HI$$

$$CH_3OH + HI \longrightarrow CH_3I + H_2O$$
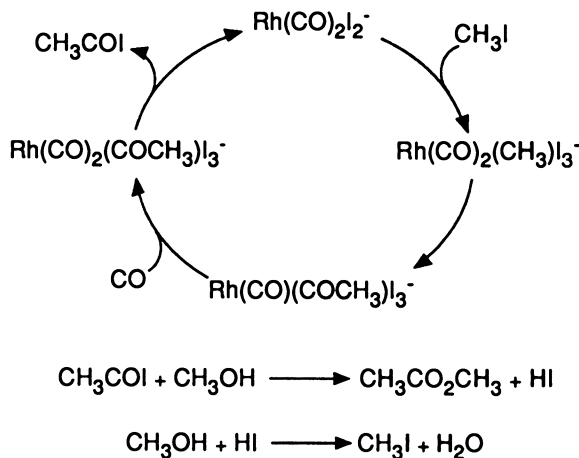
Scheme 1. Mechanism of the carbonylation reaction. (Reproduced from reference 22. Copyright 1989 American Chemical Society.)

nation and decarbonylation even at elevated temperatures. To our knowledge, the reactivity of these acyls with respect to reducing agents has not been investigated, although they have been reported to catalyze methanol carbonylation (18). The stability of these complexes prompted us to attempt the reductive carbonylation of methanol with rhodium, iodide, and diphosphine ligands (19–22).

R = phenyl, alkyl

1
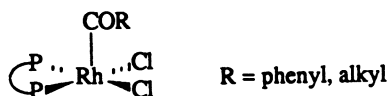
Experimental Procedure

The following is a general procedure for conducting catalysis experiments. In a nitrogen-filled glove box a 100-mL Parr autoclave was charged with Rh(CO)$_2$(acac) (0.26 g, 1 mmol; acac is acetylacetonate) and methanol. Ph$_2$P(CH$_2$)$_3$PPh$_2$ (0.41 g, 1 mmol) was slowly added. When gas evolution ceased, RuCl$_3$(H$_2$O)$_x$ (0.82 g, ~4 mmol) was added; the reactor was sealed and removed from the glove box. Next the reactor was connected to a stirrer and high-pressure gas manifold. The apparatus was flushed with synthesis gas (2:1 H$_2$:CO) by pressurizing to 30 psig and venting three times. CH$_3$I (2.5 mL, 40 mmol) was added via syringe; the reactor was sealed and pressurized to 400 psig. The reactor was heated to 140 °C and then pressurized to 975 psig. The reaction was monitored by gas uptake. After each 50-psig drop, the reactor was repressurized to 975 psig. After 2.5 h the autoclave was cooled to 18 °C and the gas was vented through a trap cooled by dry ice.

Analysis of the liquid products (gas chromatography) showed the presence of CH_3CHO, CH_3CH_2OH, and CH_3CO_2H, in addition to unreacted methanol. The selectivity to reductive carbonylation products was 80%. This calculation takes into account the many ether-, ester-, and acetal-producing equilibria that are established in these reaction mixtures, as is traditional in studies of this chemistry (1–8). Table I shows the composition of a typical product mixture resulting from these reactions.

Table I. Representative Product Distribution

Product	Condition A^a	Condition B^b
CH_3CHO	1.9	12.1
$CH_3CH(OCH_3)_2$	0.3	1.7
$CH_3CH(OCH_3)(OCH_2CH_3)$	0.2	0.4
CH_3CH_2OH	68.9	55.5
$CH_3CH_2OCH_3$	6.1	8.1
$(CH_3CH_2)_2O$	1.2	0.7
$CH_3CO_2CH_2CH_3$	4.5	2.3
CH_3CO_2H	6.2	4.3
$CH_3CO_2CH_3$	10.2	14.5

NOTE: All values are given in mole percents. All experiments were conducted with 40 mL of CH_3OH and 40 mmol of CH_3I, at 100 psi of 2:1 H_2–CO and 140 °C.
^{a}Condition A: catalyst, Rh, $Rh(CO)_2(acac)$ (2.0 mmol); ligand, $Ph_2P(CH_2)_3PPh_2$ (2.0 mmol); Ru, $RuCl_3$ (4.0 mmol); time, 2.5 h.
^{b}Condition B: catalyst: Rh, $Ph_2P(CH_2)_3PPh_2$ (2.0 mmol); no ligand; Ru, $(CH_3)_4NRu(CO)_3I_3$ (4.0 mmol); time, 2.0 h.

The rate of methanol conversion to these products was 3 mol of CH_3OH per liter of catalyst per hour, which corresponds to a turnover frequency of ~120 per hour. Analysis of the gaseous products showed small amounts of CH_4 and trace amounts of CO_2. The autoclave also contained an orange crystalline material, which was shown by NMR and IR spectroscopy and elemental analysis to be $Rh(Ph_2P(CH_2)_3PPh_2)(COCH_3)(I)_2$. IR analysis also showed the presence of $Ru(CO)_3(I)_3^-$ (23–25). This species is formed regardless of the ruthenium source employed and therefore is a thermodynamic sink under these reaction conditions. The most likely counterion is H^+ (23–25).

Further details regarding experimental procedures and characterization of the complexes described here may be found elsewhere (22).

Results and Discussion

Our initial experiments involved the addition of diphosphine ligands to methanol suspensions of $Rh(CO)_2(acac)$. When gas evolution ceases (displacement of CO by diphosphine), the reactor is charged with CH_3I and synthesis gas. The resulting solution contains a very active catalyst for the hydroformylation of methanol to acetaldehyde. More important, the catalysis occurs at much lower temperatures and pressures than those required for cobalt catalysts. Thus, for the diphosphine $Ph_2P(CH_2)_3PPh_2$, acetaldehyde is produced at rates of 4–6 mol L^{-1} h^{-1} and 80+ % selectivity at 1000 psi total pressure and

140 °C. The remaining liquid products are composed entirely of acetic acid (as the free acid and its methyl ester). Small amounts of methane are also produced, but generally no more than 5 mol %. Methanol can be hydrogenated to methane in the presence of rhodium and iodide (26).

Reaction Selectivity. As our initial interest in this topic was the production of higher alcohols via synthesis gas chemistry, we investigated methods to hydrogenate the acetaldehyde produced in the hydroformylation reaction to ethanol. Addition of ruthenium to the rhodium–diphosphine–iodide catalyst results in the homologation of methanol to ethanol (27–31). As shown in Figure 1, the relative amount of CH_3CHO and CH_3CH_2OH is directly related to the amount of ruthenium employed. Moreover, the total selectivity (defined as the sum of CH_3CHO and CH_3CH_2OH) remains constant with changing ruthenium concentration. This result shows that rhodium governs the overall reaction selectivity and ruthenium serves as an in situ reductant.

The reaction selectivity is highly dependent on the diphosphine ligand. Although a wide spectrum of diphosphines has been examined (Table II), to date we have found little correlation between ligand structure and catalyst performance. The best results are obtained with diphosphines related to $Ph_2P(CH_2)_3PPh_2$, where selectivities greater than 80% can be achieved. In contrast, shortening or lengthening the diphosphine bridge or replacing the phenyl groups with alkyls results in significant losses in selectivity. As expected, monodentate phosphines (e.g., PPh_3) give very poor results.
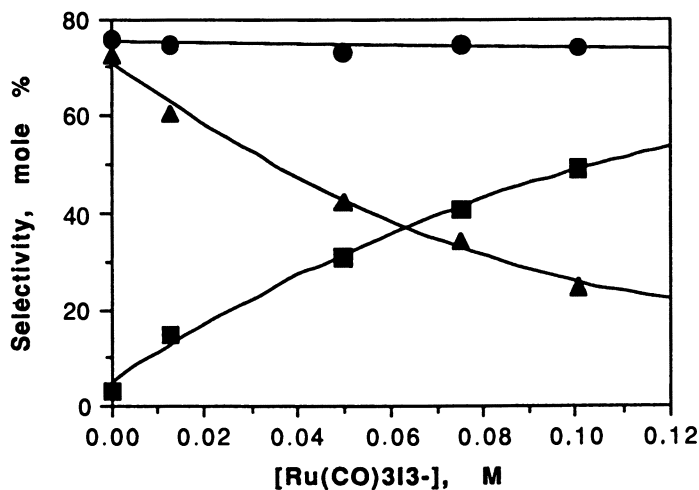
Figure 1. Product distribution as a function of ruthenium concentration. Key: ▲, CH_3CHO; ■, CH_3CH_2OH; ●, CH_3CHO + CH_3CH_2OH. Conditions for all experiments: 1000 psi of 2:1 H_2–CO, 140 °C, 0.0188 M **2a**. (Reproduced from reference 22. Copyright 1989 American Chemical Society.)

**Table II. Selectivity as a Function
of Diphosphine Ligand**

Diphosphine	Selectivity (mmol)[a]
$Ph_2P(CH_2)_3PPh_2$	80
$(CH_3)_2P(CH_2)_3P(CH_3)_2$	35
$(p\text{-tol})_2P(CH_2)_3P(p\text{-tol})_2$	54
$(p\text{-ClC}_6H_5)_2P(CH_2)_3P(p\text{-ClC}_6H_5)_2$	29
$(CH_3)PhP(CH_2)_3PPh(CH_3)$	24
$(c\text{-hex})_2P(CH_2)_3P(c\text{-hex})_2$	34
$(CH_3CH_2)_2P(CH_2)_3PPh_2$	54
$Ph_2P(CH_2)_4PPh_2$	7
$Ph_2P(CH_2)_2PPh_2$	39
$(p\text{-tol})_2P(CH_2)_2P(p\text{-tol})_2$	26
$Ph_2P(CH_2)_2CH(CH_3)PPh_2$	65
$Ph_2P(CH_2)_2C(CH_3)_2PPh_2$	71
$2PPh_3$	6

NOTES: All experiments were conducted at 140 °C, 1000 psig of 2:1
H_2–CO. Ph, phenyl; tol, tolyl; and c-hex, cyclohexyl.
[a]Selectivity to CH_3CHO–CH_3CH_2OH; liquid products only.

Stability.   For most diphosphines, an orange crystalline product is
typically present at the end of these experiments. We have unequivocally
identified a number of these complexes as the acetyl complexes **2a–2f**. These
same complexes led us to investigate the use of diphosphine ligands. The
fact that they are isolated in quantitative yield at the end of these experiments
further demonstrates their stability. The complexes so isolated, or prepared
by alternative synthetic routes, can be employed as catalysts with no change
in rate or selectivity and again be isolated unchanged in essentially quan-
titative yield.

Some phosphine ligands are quaternized by CH_3I under the reaction
conditions, particularly monodentate phosphines such as PPh_3. This situation

$Ph_2P(CH_2)_3PPh_2$	**2a**
$Ph_2P(CH_2)_2PPh_2$	**2b**
$Ph_2PCH_2C(CH_3)_2CH_2PPh_2$	**2c**
$Ph_2P(CH_2)_2CH(CH_3)PPh_2$	**2d**
$(p\text{-tol})_2P(CH_2)_3P(p\text{-tol})_2$	**2e**
$(p\text{-ClC}_6H_5)_2P(CH_2)_3P(p\text{-ClC}_6H_5)_2$	**2f**
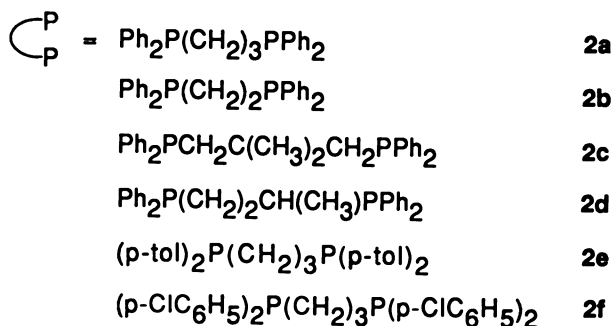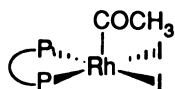
is easily detected by the presence of $Rh(CO)_2I_2^-$ (IR) or $CH_3PR_3^+$ (^{31}P NMR) in the product solutions. Diphosphine complexes 1 are very resistant to this degradation, showing no evidence of quaternization under reaction conditions after the longest times we have investigated to date (11 h).

Reactivity of Complexes 2. The stability and isolation of what may be a key reactive intermediate in the catalysis provided us with a unique opportunity to investigate the mechanism of this chemistry. A reasonable assumption is that the acyls are converted to acetaldehyde. This possibility was tested by investigating the reaction chemistry of complex 2a. We first examined the reaction of 2a directly with H_2 (120 psi, 120 °C); it does indeed yield acetaldehyde. The hydride complex 3 is also produced in this reaction, as shown in eq 3. Spectroscopic data indicate that this complex adopts a square-based pyramidal structure with an apical hydride, analogous to acyl complexes 2. X-ray crystallography, done in collaboration with J. L. Peterson (West Virginia University), shows that the structure of complex 3 is a centrosymmetric dimer with bridging iodides. Both the hydride and acetaldehyde are formed in essentially quantitative yield.

$$2a + H_2 \xrightarrow{CH_3OH} Rh(PPh_2(CH_2)_3PPh_2)(H)I_2 + CH_3CH(OCH_3)_2 \quad (3)$$
$$3$$
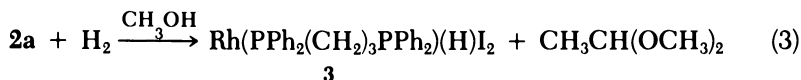
Other pathways to convert the acetyl ligand of 2 to acetaldehyde were also investigated. One likely possibility is via the protonation of 2 (32). Given the acidic nature of these reaction solutions, this possibility seemed reasonable. However, treating 2a with the powerful acids HI or CF_3SO_3H does not produce acetaldehyde. In fact, no reaction at all occurs. IR monitoring of CH_2Cl_2 solutions of 2a in the presence of CF_3SO_3H shows no shift in the acetyl carbonyl vibration at 1701 cm^{-1}. This result is perhaps not surprising in that little backbonding from Rh(III) to the acetyl ligand is expected. Thus the contribution of a resonance form such as 5 is minimized. This result seems to rule out the involvement of acid in the production of acetaldehyde.
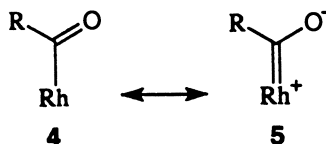
Reaction of 2 with hydride (e.g., Rh–H) is also a potential route to acetaldehyde. However, treatment of 2 with a variety of hydridic (R_3SnH, R_3BHLi) reagents does not lead to liberation of CH_3CHO. Complexes 2 are also unreactive with hydride complex 3. Further, bimolecular reactions of 2 with a rhodium hydride is inconsistent with kinetic results (vide infra).

In addition to the possibility that the acyl complexes are directly re-sponsible for the production of acetaldehyde, the *cis* arrangement of acetyl and iodide ligands in complexes **2** suggests that reductive elimination of acetyl iodide is also possible. In the presence of CH_3OH or H_2O this reaction would immediately result in the formation of acetate and therefore explain the formation of acetic acid. In view of the preceding discussion, however, it was not surprising to find that thermolysis of complex **2a** in CH_3OH (140 °C, N_2, 45 min) leads to only trace amounts of CH_3CO_2H (as the free acid or its methyl ester) and recovery of **2a**.

This rate is far too slow to account for the formation of CH_3CO_2H during catalysis. If the reaction is conducted under a CO atmosphere, however, CH_3CO_2H is produced much more rapidly. In fact, this reaction leads to the catalytic carbonylation of CH_3CO_2H, and complex **2a** is again recovered intact (*18*). No additional CH_3I was added. This result not only confirms the possibility that **2** can be used to generate CH_3CO_2H, but also demonstrates that **2** is a competent catalyst for this transformation. The fact that CH_3CO_2H is observed only upon treatment of **2** with CO suggests that CO coordination is required prior to reductive elimination of CH_3COI.

Kinetic Studies.   These studies suggest a reaction sequence in which complexes **2** are intimately involved in the selectivity-determining step. Thus, conversion of the acetyl ligand to acetaldehyde has been demonstrated by reaction with H_2. Alternatively, the catalytic formation of CH_3CO_2H is possible if **2** is treated with CO in the presence of CH_3OH. The stability of complexes **2** (relative to other reaction intermediates) further indicates that they are thermodynamic sinks. This conclusion predicts that complexes **2** are directly involved in the overall rate-determining step.

The reaction studies discussed suggest that the rate- and selectivity-determining step involves the reaction of **2** with either H_2 or CO. If this is true, then the reaction rate should be first-order in **2**. No other chemistry should appear in the rate law. Thus, the reaction should be zero-order in iodide. A brief kinetic analysis was undertaken to test these predictions.

The rate dependence on **2a** was first investigated. The kinetic analyses were performed by monitoring gas uptake as a function of time. Uptake is typically linear for the first 40–50 min; at longer times significant curvature occurs. This time span corresponds to ~5% CH_3OH conversion and is there-fore suitable for determining reaction orders by the method of initial rates (*33*). Reaction orders were determined by measuring the initial gas uptake rate vs. time at different concentrations of **2a**. Concentrations were varied by 1 order of magnitude.

Figure 2 illustrates the results from these experiments. The data show that the reaction is first-order in **2a** over the concentration range 0–0.03 M. This result is consistent with the reaction scheme discussed. However, the rate law abruptly changes to zero-order in [Rh] at concentrations greater
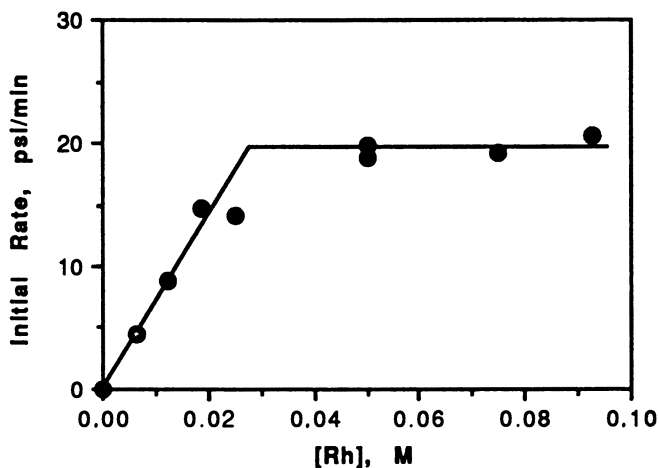
Figure 2. Initial gas uptake rate dependence on rhodium concentration. Conditions for all experiments: 1000 psi of 2:1 H_2–CO, 140 °C, 0.10 M $(CH_3)_4NRu(CO)_3I_3$, 1.0 M CH_3I. (Reproduced from reference 22. Copyright 1989 American Chemical Society.)

than ~0.03 M. The explanation for this observation is straightforward: at concentrations greater than 0.03 M the solubility limit of **2a** is exceeded. We measured the solubility of **2a** at 140 °C in CH_3OH; it corresponds exactly with the change in rate law. This observation is very significant.

Although **2a** was employed as the catalyst charge for these experiments, the experiments in reality only measure the rate as a function of rhodium concentration and do not distinguish among the many possible rhodium species that could be responsible for the observed kinetics. The observation that the rate behavior depends on a distinct physical property of **2** is consistent with a model wherein this species is involved in the rate-determining step. However, the possibility cannot be ruled out that another species with similar solubility properties is actually responsible for the observed rate behavior.

The reaction order with respect to iodide was also measured. Figure 3 shows that over the concentration range 0–1.0 M the rate exhibits a zero-order dependence on iodide. This result is exactly as predicted. In these experiments rhodium and ruthenium are charged as the iodo complexes **2a** and $[(CH_3)_4N][Ru(CO)_3I_3]$, respectively. Thus, there is an ample reservoir of iodide available for catalysis. Gas chromatographic analyses of the final reaction solutions show that experiments employing little or no CH_3I initially have only trace amounts of CH_3I present at the end of the experiment, and the metal–iodo complexes are recovered intact. This analysis further confirms that very little free CH_3I is required for catalysis.

Although this latter result may further suggest that CH_3I is not involved in the reaction chemistry whatsoever, labeling studies indicate otherwise.
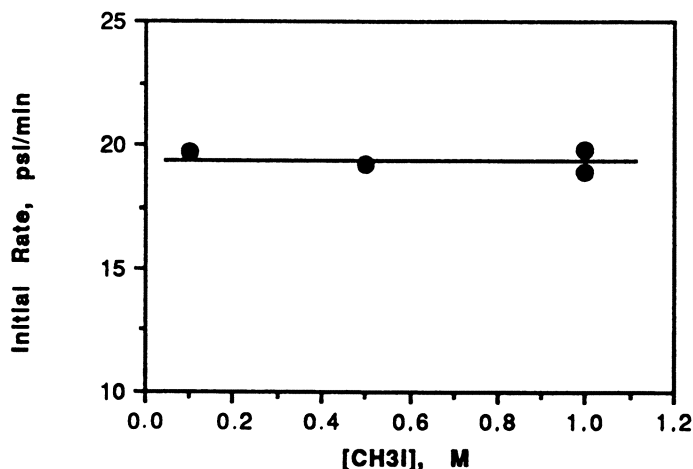
Figure 3. Initial gas uptake rate dependence on iodide concentration. Conditions for all experiments: 1000 psi of 2:1 H_2–CO, 140 °C, 0.0188 M 2a, 0.1 M $(CH_3)_4NRu(CO)_3I_3$. (Reproduced from reference 22. Copyright 1989 American Chemical Society.)

Thus, a typical reductive carbonylation experiment was conducted with $^{13}CH_3I$ as promoter. Analysis of the reaction products showed incorporation of the label in both the CH_3CHO–CH_3CH_2OH and CH_3CO_2H produced. The CH_3I in the final reaction solution was found to be almost entirely ^{12}C. CH_3I is apparently converted to products and regenerated under the reaction conditions. This result is consistent with the involvement of iodide as a promoter in this chemistry, although it has no influence on the reaction rate.

Isotopic Tracer Studies.   An additional pathway to CH_3CHO that must be considered is via hydrogenation of CH_3CO_2H or its esters. The diphosphine catalyst has been shown to catalyze the carbonylation of CH_3OH. The selectivity to reductive carbonylation products may simply reflect the different ability of various catalysts to hydrogenate the acid or ester. To test this possibility a homologation run was spiked with labeled acetic acid ($CH_3{}^{13}CO_2H$). The resulting products, analyzed by gas chromatography–mass spectroscopy, showed no detectable amounts of label in the CH_3CHO or CH_3CH_2OH produced. Diluted label was detected in CH_3CO_2H and its methyl and ethyl esters. Hydrogenation of acetic acid–acetate ester is therefore not a viable pathway to the reductive carbonylation products. This result is not surprising in that hydrogenation of esters and acids is difficult. It requires much more extreme conditions than those employed here (34–37).

The Catalytic Cycle.   The catalytic cycle shown in Scheme II is consistent with the available kinetic, mechanistic, and labeling results. The
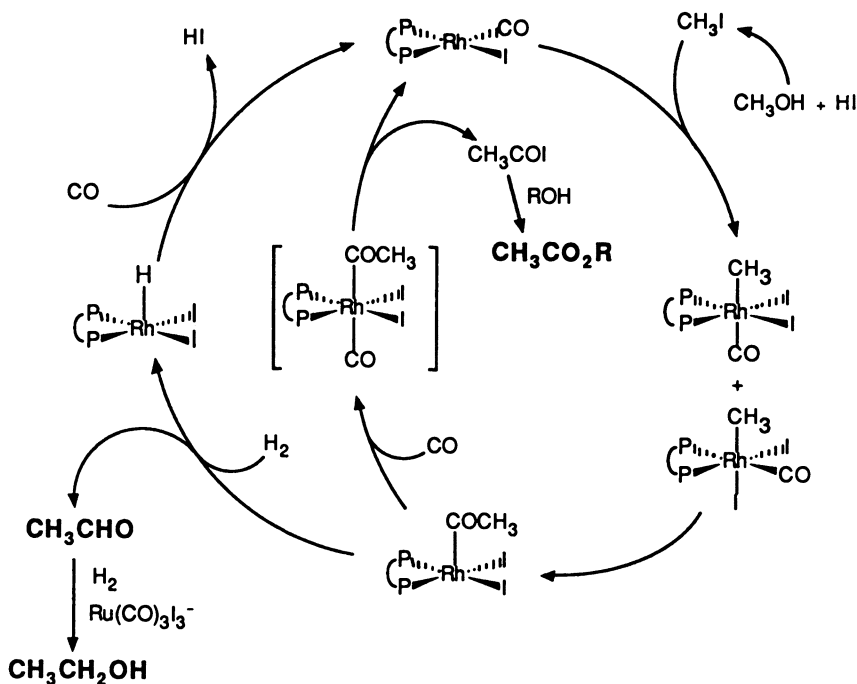
Scheme II. The catalytic cycle.

first step is oxidative addition of CH_3I to Rh(I); a reasonable possibility is Rh(diphosphine)(CO)I. We tested this theory by preparing Rh(PhP$_2$(CH$_2$)$_n$-PPh$_2$)(CO)I (n = 2 or 3) and examining their reactivity with CH$_3$I. Oxidative addition occurs under mild conditions (25 °C, several hours) and produces a mixture of the two isomeric methyl complexes, as shown in eq 4.
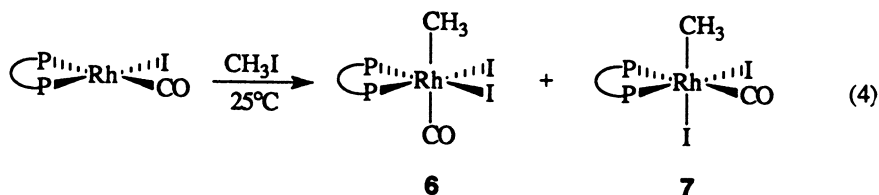
These transient complexes have not been isolated, as they gradually undergo migratory insertion to yield the acyl complexes **2**. Similar behavior has been reported for analogous complexes with monodentate phosphines (*38–41*). Note that only isomer **7** has the required *cis* arrangement of CH_3 and CO

ligands required for migratory insertion. The oxidative addition must therefore be reversible, at least with respect to isomer **6**. At the 130–150 °C temperatures employed for catalysis, this sequence of oxidative addition–migratory insertion is expected to be extremely rapid.

The next step in the reaction is the most critical. Complexes **2** may react with H_2 to give CH_3CHO and hydride or with CO to generate CH_3CO_2H. The evidence available so far is consistent with this step being both rate- and selectivity-determining. Thus, the key to the successful application of diphosphine ligands to effect reductive carbonylation lies in the intrinsic reactivity of complexes **2** with H_2 vs. CO. Reductive elimination of CH_3COI directly from **2** is apparently disfavored, probably because they are already unsaturated with 16 electrons. Thus, prior coordination of CO is required to give the 18-e$^-$ intermediate $Rh(diphosphine)(CO)(COCH_3)I_2$, from which reductive elimination is much more favorable.

The hydrogenolysis of **2** to CH_3CHO, obviously the most critical step of the reaction, is also the most perplexing. Hydrogenolysis of Rh(I)–carbon bonds is well known and is an important step in many catalytic reactions that employ rhodium. These reactions are believed to involve oxidative addition of H_2 to generate a Rh(III)–dihydride. Reductive elimination results in hydrogenolysis of the Rh–carbon bond and formation of a Rh(I)–hydride. The mechanism of the corresponding reaction with the Rh(III)–carbon bond in complexes **2** is not so obvious. Several mechanisms can be envisioned, but to date there is little or no evidence by which to judge them.

The remaining step in this sequence is conversion of the hydride to acyl complexes **2**. Although hydride **3** is thermally robust (it is prepared at 120 °C), heating this complex in the presence of CO (CH_3OH solvent) leads to rapid, quantitative formation of complex **2a** and catalytic production of CH_3CO_2H. Precoordination of CO to produce the carbonyl adduct $Rh(diphosphine)(CO)(H)I_2$, followed by reductive elimination of HI, is a reasonable explanation for this observation. The HI so produced is expected to form CH_3I rapidly in CH_3OH solvent. Oxidative addition of CH_3I to $Rh(diphosphine)(CO)I$ would then rapidly generate acyl complex **2** as the observed product.

Conclusions

We have demonstrated that with the proper choice of ligands, rhodium catalyzes the reductive carbonylation of methanol. The catalyst performs with good rates and selectivities at much lower temperatures and pressures than previously demonstrated for more traditional catalysts. Its robust nature has allowed us to explore in-depth the chemistry of this catalyst.

Although most of the reaction steps appear to be straightforward, the key step, hydrogenolysis of acyl complexes **2**, is not well understood. In particular, the hydrogenolysis of a Rh(III)–carbon bond is unusual and sug-

gests several interesting mechanisms such as heterolytic H_2 activation or four-centered transition states, among other possibilities. The available evidence suggests that this hydrogenolysis is both rate- and selectivity-determining. Thus, a better understanding of this reaction may lead to simultaneous enhancement of both the reaction rate and selectivity.

Acknowledgments

References

1. Roper, M.; Loevenich, H. In *Catalysis in C₁ Chemistry*; Keim, W., Ed.; Reidel: Dordrecht, 1983; p 105.
2. Chen, M. J.; Rathke, J. W. *Organometallics* **1987**, *6*,1833.
3. Wegman, R. W.; Busby, D. C.; Letts, J. B. In *Industrial Chemicals via C₁ Processes*; Fahey, D. R., Ed.; ACS Symposium Series 328; American Chemical Society: Washington, DC, 1987; p 125.
4. Pretzer, W. R.; Kobylinski, T. P. *Ann. N. Y. Acad. Sci.* **1980**, *333*, 58.
5. Keim, W. In *Industrial Chemicals via C₁ Processes*; Fahey, D. R., Ed.; ACS Symposium Series 328; American Chemical Society: Washington, DC, 1987; p 1.
6. Fakley, M. E.; Head, R. A. *Appl. Catal.* **1983**, *5*, 3.
7. Rizkalla, N.; Goliaszewski, A. In *Industrial Chemicals via C₁ Processes*; Fahey, D. R., Ed.; ACS Symposium Series 328; American Chemical Society: Washington, DC, 1987; p 136.
8. Gauthier-Lafaye, J.; Perron, R. *Methanol and Carbonylation*; Editions Technip: Paris, 1987; Chapter 4.
9. Sneeden, R. P. A. In *Comprehensive Organometallic Chemistry*; Wilkinson, G.; Stone, F. G. A.; Abel, E. W., Eds.; Pergamon: Oxford, 1982; Vol. 8, Chapter 50.2.
10. Tkatchenko, I. In *Comprehensive Organometallic Chemistry*; Wilkinson, G.; Stone, F. G. A.; Abel, E. W., Eds.; Pergamon: Oxford, 1982; Vol. 8, Chapter 50.3.
11. Dumas, H.; Levisalles, J.; Rudler, H. *J. Organomet. Chem.* **1979**, *177*, 239.
12. Forster, D. *J. Am. Chem. Soc.* **1976**, *98*, 846.
13. Forster, D. *Adv. Organomet. Chem.* **1979**, *17*, 255.
14. Adamson, G. W.; Daly, J. J.; Forster, D. *J. Organomet. Chem.* **1974**, *71*, C17.
15. Adams, H.; Bailey, N. A.; Mann, B. E.; Manuel, C. P.; Spencer, C. M.; Kent, A. G. *J. Chem. Soc., Dalton Trans.* **1988**, 489.
16. Slack, D. A.; Egglestone, D. L.; Baird, M. C. *J. Organomet. Chem.* **1978**, *146*, 71.
17. McGuiggan, M. F.; Doughty, D. H.; Pignolet, L. H. *J. Organomet. Chem.* **1980**, *185*, 241.
18. Bartish, C. M. U.S. Patent 4 102 920, 1978.
19. Wegman, R. W.; Miller, D. S. U.S. Patent 4 594 463, 1986.
20. Wegman, R. W.; Moloy, K. G. U.S. Patent 4 727 200, 1988.

21. Moloy, K. G.; Wegman, R. W. *J. Chem. Soc., Chem. Commun.* **1988**, 820.
22. Moloy, K. G.; Wegman, R. W. *Organometallics* **1989**, *8*, 2883.
23. Braca, G.; Galletti, A. M. R.; Sbrana, G. In *Industrial Chemicals via C₁ Processes*; Fahey, D. R., Ed.; ACS Symposium Series 328; American Chemical Society: Washington, DC, 1987; p 220.
24. Galletti, A. M. Raspolli; Braca, G.; Sbrana, G.; Marchetti, F. *J. Mol. Catal.* **1986**, *34*, 183.
25. Braca, G.; Galletti, A. M. Raspolli; Sbrana, G.; Zanni, F. *J. Mol. Catal.* **1986**, *34*, 183.
26. Drury, D. J.; Green, M. J.; Ray, D. J. M.; Stevenson, A. J. *J. Organomet. Chem.* **1982**, *236*, C23.
27. Jenner, G.; Andrianary, P. *J. Catal.* **1987**, *103*, 37.
28. Jung, C. W.; Garrou, P. E. *Organometallics* **1982**, *1*, 658.
29. Strohmeier, W.; Weigelt, L. *J. Organomet. Chem.* **1978**, *145*, 189.
30. Sanchez-Delgado, R. A.; Andriollo, A.; De Ochoa, O. L.; Suarez, T.; Valencia, N. *J. Organomet. Chem.* **1981**, *209*, 77.
31. Tsuji, J.; Suzuki, H. *Chem. Lett.* **1977**, 1085.
32. Collman, J. P.; Hegedus, L. S.; Norton, J. R.; Finke, R. G. *Principles and Applications of Organotransition Metal Chemistry*; University Science: Mill Valley, CA, 1987; p 107.
33. Moore, J. W.; Pearson, R. G. *Kinetics and Mechanism*, 3rd ed.; Wiley: New York, 1981; p 65.
34. Grey, R. A.; Pez, G. P.; Wallo, A.; Corsi, J. *J. Chem. Soc., Chem. Commun.* **1980**, 783.
35. Grey, R. A.; Pez, G. P.; Wallo, A. *J. Am. Chem. Soc.* **1980**, *102*, 5948.
36. Wilczynski, R.; Fordyce, W. A.; Halpern, J. *J. Am. Chem. Soc.* **1983**, *105*, 2066.
37. Bianchi, M.; Menchi, G.; Francalanci, F.; Piacenti, F.; Matteoli, U.; Frediani, P.; Botteghi, C. *J. Organomet. Chem.* **1980**, *188*, 109.
38. Douek, I. C.; Wilkinson, G. *J. Chem. Soc. A* **1969**, 2604.
39. Franks, S.; Hartley, F. R.; Chipperfield, J. R. In *Catalytic Aspects of Metal Phosphine Complexes*; Alyea, E. C.; Meek, D. W., Eds.; Advances in Chemistry 196; American Chemical Society: Washington, DC, 1982; p 273.
40. Franks, S.; Hartley, F. R.; Chipperfield, J. R. *Inorg. Chem.* **1981**, *20*, 3238.
41. Doyle, M. J.; Mayanza, A.; Bonnet, J.-J.; Kalck, P.; Poilblanc, R. *J. Organomet. Chem.* **1978**, *146*, 293.

Hydrogen Activation by Soluble Metal Oxide Complexes

R. J. Klingler, T. R. Krause, and J. W. Rathke

Chemical Technology Division, Argonne National Laboratory, Argonne, IL 60439

To better define the chemistry associated with nucleophilic oxide centers, the catalysis of the water–gas shift reaction was investigated in triethylene glycol solution (150–250 °C and 1–300 atm) by employing alkali metal hydroxide catalysts. Under reaction conditions most of the sodium salt is in the form of the formate complex, which is produced through the carbonylation of hydroxide ion. The resultant water–gas shift reaction is first order in sodium formate over a concentration range from 0.01 to 1.0 M. Both formic and acetic acids have a beneficial effect on the rate of dihydrogen evolution within the sodium hydroxide–formate water–gas shift system. Deuterium, D_2, is produced in 93% isotopic purity when the reaction is conducted in D_2O–triethylene glycol-d_2. It exhibits a substantial inverse kinetic isotope effect ($k_H/k_D = 0.5$) compared to the analogous water–gas shift reaction conducted in H_2O–triethylene glycol. The kinetic results indicate that the sodium hydroxide–formate water–gas shift system proceeds through an intermediate (or transition state) with substantial H–H bond order. This activity contrasts with earlier proposals for nucleophilic dihydrogen activation, which focused on a free hydride ion intermediate.

DIHYDROGEN IS HETEROLYTICALLY CLEAVED (*1*) on most metal oxides, with the hydride and the proton residues going to the metal and oxygen centers, respectively. For example, dihydrogen is reversibly chemisorbed onto zinc oxide at –45 °C with the formation of zinc hydride and surface hydroxyl groups (eq 1) (*2, 3*), both of which are observed by IR spectroscopy.

$$\{-Zn-O-Zn-\}_s + H_2 \rightarrow \{-ZnH + HOZn-\} \qquad (1)$$

The heterolytic cleavage of dihydrogen by metal oxides is usually described as a four-centered transition state in which an empty Lewis acid site on the metal center and a Lewis base site on the oxygen center simultaneously interact with opposite ends of the dihydrogen molecule. Furthermore, although the metal-centered Lewis acid and the oxygen-centered Lewis base act in concert in the four-centered transition state, they are not necessarily equal partners in the process. Indeed, the metal is usually considered to be the primary point of interaction for the dihydrogen molecule (4).

However, the role of the nucleophilic oxygen centers may be underestimated in many of these metal oxide systems because the hydrogenation of an organic substrate can be catalyzed with a hydroxide ion catalyst in the complete absence of a metal center (5).

Deuterium exchange has been known to be catalyzed by bases since the 1936 work of Wirtz and Bonhoeffer (6) (eqs 2 and 3).

$$H_2O + D_2 \xrightarrow{OH^-} HOD + HD \qquad (2)$$

$$NH_3 + D_2 \xrightarrow{NH_2^-} NH_2D + HD \qquad (3)$$
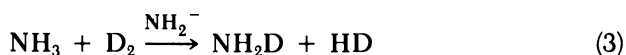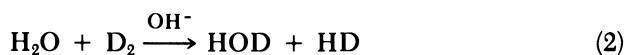
Base-catalyzed deuterium exchange can be quite rapid. The half-life in the liquid ammonia–sodium amide system (7) is less than 1 min at −53 °C. The kinetics of the base-catalyzed deuterium-exchange reaction has been investigated by a number of groups (6–12). The early mechanistic work is described in terms of hydroxide attack on the dihydrogen molecule to displace a free hydride ion intermediate, which subsequently reacts rapidly with the proton source (eqs 4 and 5).

$$D_2 + OH^- \longrightarrow D^- + DOH \qquad (4)$$

$$D^- + H_2O \xrightarrow{fast} HD + OH^- \qquad (5)$$
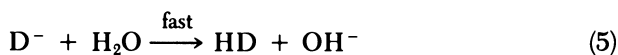
However, more recent gas-phase work (13) is able to rule out a free hydride ion intermediate, at least in the gas phase. The heat of formation of gaseous hydride ion is known, and the observed barrier for deuterium exchange is too small, by a factor of 5, to generate a high-energy hydride ion intermediate. Instead, Grabowski et al. (13) propose an addition adduct between the hydroxide ion and the dihydrogen molecule.

The proposed intermediate, H_3O^- ion, is a long-lived species in ion cyclotron resonance experiments (14–16). The nature of the bonding within this species has been investigated by extended basis set molecular orbital calculations (17, 18). The molecular orbital calculations on the H_3O^- ion

system indicate that hydride ion is stabilized by 26 kcal through coordination to the Lewis acidic end of a water molecule, $[HOH \cdot H]^-$. Stabilization of the hydride ion increases the lifetime of this species and could facilitate hydride transfer to organic substrates.

Indeed, it is possible to hydrogenate organic substrates with base catalysts, as demonstrated by Walling and Bollyky (*19, 20*). These workers observed the hydrogenation of benzophenone and nitrobenzene employing a potassium *t*-butoxide catalyst. Walling (*20*) proposed a mechanism similar to that suggested for the early solution work on deuterium exchange. Thus, Walling's mechanism for base-catalyzed hydrogenation contains a free hydride ion intermediate. Alternatively, the hydride ion might exist as a tight complex with the Lewis acidic end of the alcohol solvent. No kinetic data are available for this system.

We attempted to probe the potential application of nucleophilic dihydrogen activation processes for synthesis gas transformations with metal oxide catalysts. Our recent efforts in this direction have been focused on determining the kinetics for the reduction of carbon dioxide catalyzed by alkali metal hydroxide complexes in triethylene glycol solution (eq 6).

$$H_2 + CO_2 \xrightarrow{\text{OH}^-} H_2O + CO \qquad (6)$$
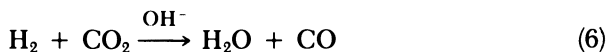
This reaction is commonly referred to as the water–gas shift equilibrium, and standard commercial catalysts are available. The experimentally reversible reaction is usually conducted in the thermodynamically favorable dihydrogen evolution direction. The homogeneous alkali metal system is of fundamental mechanistic interest. Measurements (*5*) have demonstrated that the activation barrier observed for the catalysis of the water–gas shift reaction by solvated hydroxide ion is comparable to the activation barrier exhibited by an industrially used iron oxide catalyst. In this industrial reaction the metal and oxide centers are free to exert synergistic effects.

Results

The reactions were conducted in gold-plated stainless steel autoclaves, as described elsewhere (*5*). Identical results were obtained in a Teflon [poly(tetrafluoroethylene)] block reactor in which no part of the solution or gas phase contacts the stainless steel support walls. These precautions were necessary because formic acid produced through the carbonylation of water (eq 7) rapidly builds up to nearly equilibrium concentration levels under steady-state water–gas shift reaction conditions at 180 °C.

$$H_2O + CO \xrightarrow{\text{OH}^-} H_2CO_2 \qquad (7)$$
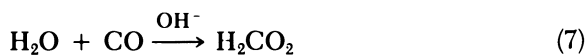
Formic acid is corrosive to stainless steel and pentacarbonyliron is known to be a water–gas shift catalyst in basic solutions (21, 22). Significantly, pentacarbonyliron was not detected in any of the solutions removed from either the gold-plated or the Teflon block reactors. In addition, as a control reaction, pentacarbonyliron was intentionally added to the alkali metal system and no increase in the rate of dihydrogen evolution was observed (5).

This evidence demonstrates that the equilibrium formic acid level produced by reaction 7 would be sufficient to inhibit the pentacarbonyliron mechanistic pathway for water–gas shifting even if pentacarbonyliron was present at concentration levels below the Fourier transform IR detection limit of 50 μM. Furthermore, because of the presence of formic acid from reaction 7, most of the sodium salt exists as the formate complex (5). The steady-state hydroxide ion concentration is correspondingly low.

Cation Reactivity. Catalysis of the water–gas shift reaction was found to proceed cleanly, even in the metal-free system that employed the organic tetrabutylammonium cation. Indeed, of the cations investigated, the metal-free tetrabutylammonium system was the most active (5); $Bu_4N^+ > Cs^+ > Na^+ > Li^+ > H^+ > Ca^{2+}$. This ordering of reactivity indicates that metal coordination or ion pairing is detrimental to the rate of water–gas shifting by soluble alkali and alkaline earth metal hydroxide complexes. Most significantly, it shows that a metal center is not required to stabilize the reaction intermediates.

Furthermore, catalysis of the water–gas shift reaction by solvated hydroxide ion is a low-energy mechanistic pathway. The homogeneous sodium hydroxide system was found (5) to exhibit an activation energy (26 ± 1 kcal) comparable to that reported for a commercially used iron oxide water–gas shift catalyst (27 ± 0.2 kcal). Additional information on the kinetics and the deuterium isotope effect for the homogeneous sodium hydroxide-catalyzed water–gas shift reaction has been obtained and is reported here.

Rate of Dihydrogen Evolution. The initial rate of dihydrogen evolution is linear for an 8-h period and increases monotonically with the sodium formate concentration, as indicated in Figure 1. The inset demonstrates that a plot of the rate of dihydrogen evolution vs. sodium formate concentration extrapolates to the origin, as required if the catalytic species is the sodium formate complex.

The reaction is first order in sodium formate as concentration changes by 2 orders of magnitude. This kinetic order is demonstrated by plotting the log of the rate of dihydrogen evolution vs. the log of the sodium formate concentration in Figure 2. The addition of formic acid at constant sodium formate concentration results in an increase in the rate of dihydrogen production, as demonstrated in Figure 3. This observation provides additional evidence against adventitious cocatalysis by pentacarbonyliron. The penta-
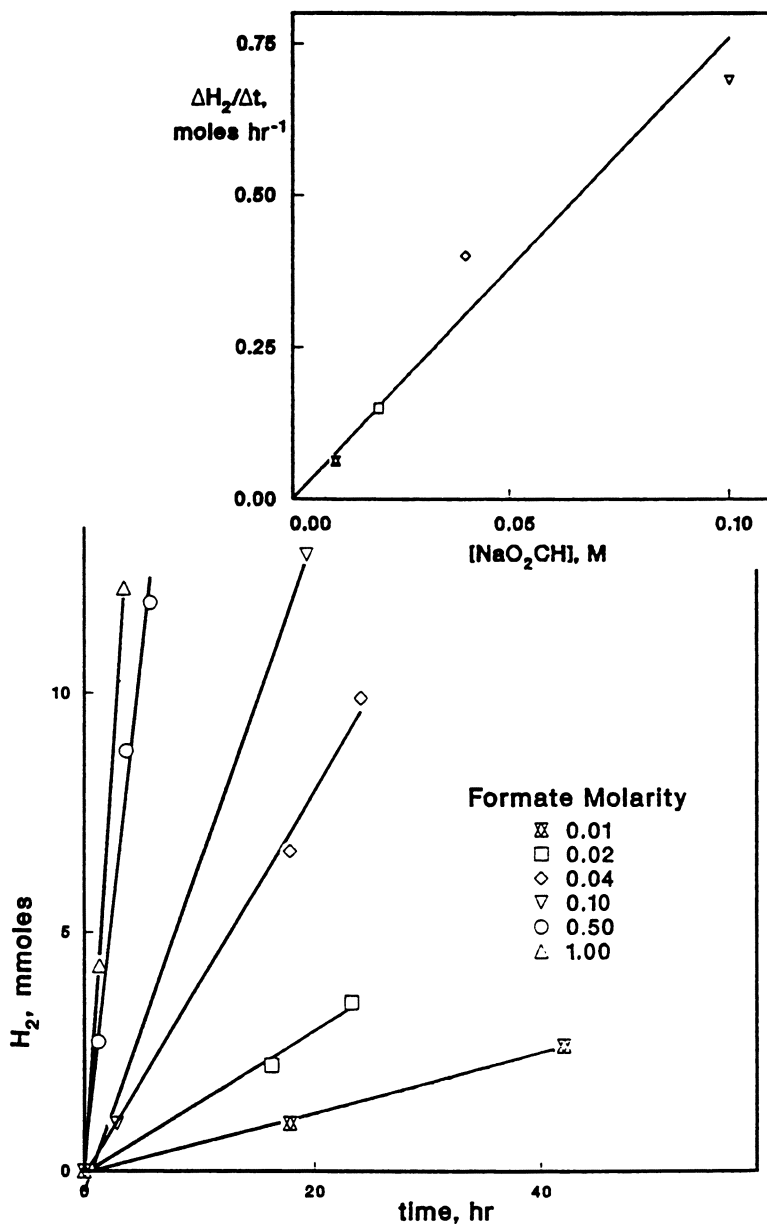
Figure 1. Effect of the sodium formate concentration on the initial rate of dihydrogen evolution in the reaction of carbon monoxide (180 atm) and water (7.8 M) in triethylene glycol at 180 °C.
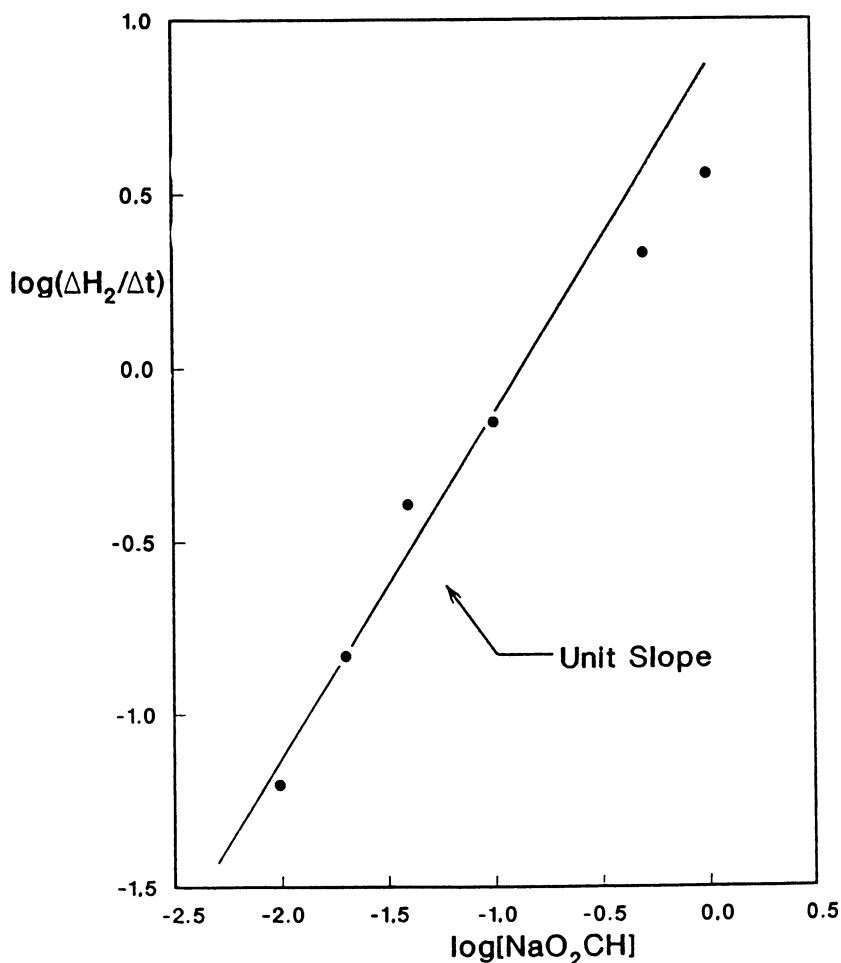
Figure 2. Kinetic order in sodium formate for water–gas shifting; conditions as in Figure 1.

carbonyliron mechanistic pathway exhibits the opposite trend with pH. The pentacarbonyliron water–gas shift system is strongly inhibited by formic acid (*21, 22*).

A large inverse kinetic isotope effect (k_H/k_D = 0.5) was observed in the reaction of deuterated formate with deuterium oxide, compared to that with the analogous reaction in water (Figure 4). It is not possible to independently label the formate ion and the proton source, because ^{2}H NMR measurements indicate that NaO_2CD exchanges with H_2O under these conditions. The results from four different experiments (data plotted as circles and squares, respectively, in Figure 4) demonstrate the reproducibility of the inverse kinetic isotope effect.
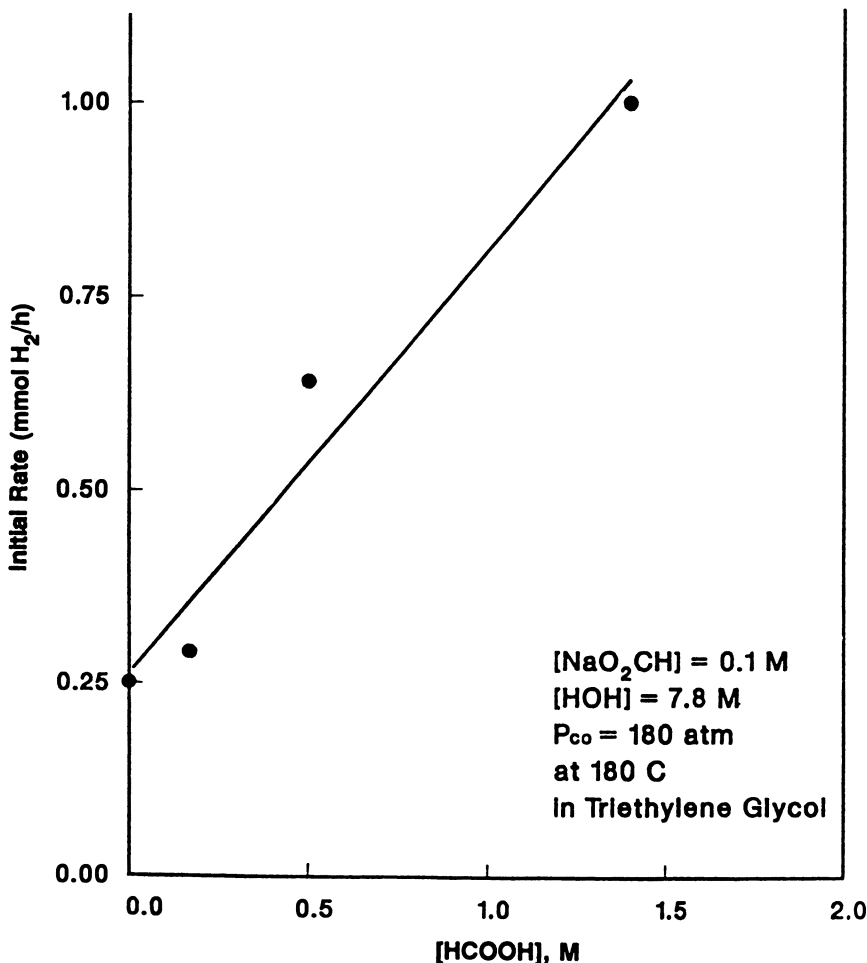
Figure 3. Effect of added formic acid on the initial rate of dihydrogen evolution at constant sodium formate concentration. Formic acid, monitored (FTIR spectroscopy) by measuring the absorbance for the band at 1724 cm^{-1}, was found to be constant during the initial rate measurements.

Discussion

The water–gas shift reaction is experimentally reversible and is first order in sodium formate concentration. The tetrabutylammonium system demonstrates that a metal center is not required to catalytically activate dihydrogen. The cation effect suggests that the active species is the solvated anion. The reaction proceeds by transferring a hydride moiety from solvated formate ion to a proton source, as indicated for water in eq 8.

$$O_2C-H^- + H-OH \rightarrow O_2C + H_2 + OH^- \qquad (8)$$
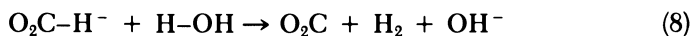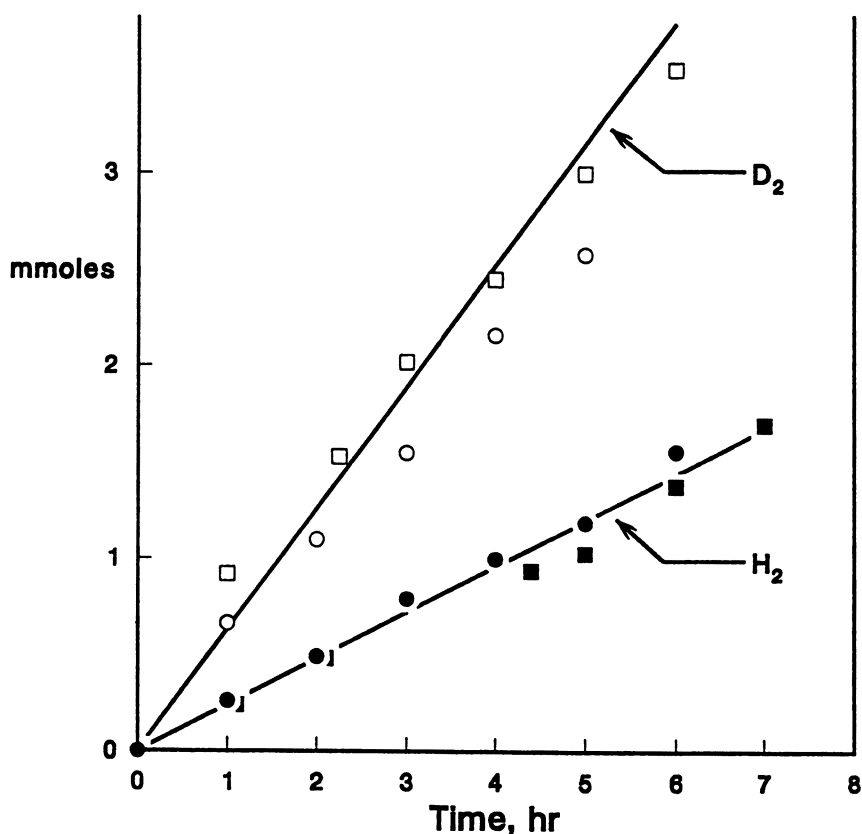
Figure 4. Initial rate of D_2 (○, □) and H_2 (●, ■) evolution from reactions conducted in D_2O–triethylene glycol-d_2 and H_2O–triethylene glycol, respectively, with 0.1 M sodium formate at 180 °C under 180 atm of carbon monoxide. The dihydrogen isotopes were identified by mass spectroscopy and quantitated by gas chromatography against authentic standards of D_2 and H_2. Samples from the reactions conducted with D_2O exhibited isotopic purity in excess of 93% for D_2.

Some recent work (*23*) with a heterogeneous metal oxide system similarly indicates that the combination of surface formate and surface water is necessary to effect water–gas shifting in the heterogeneous MgO system. These workers find that surface hydroxyl is not good enough. The reaction requires adsorbed water in addition to surface formate.

Involvement of Proton Source. The first major mechanistic problem that needs to be addressed for the hydride-transfer process of eq 8 is clarification of the potential involvement of the proton source in the rate-limiting step of the net transformation. The most direct approach to this question would be to determine the kinetic order in the water concentration. However, it was not possible to directly determine the kinetic order in the water

because polar protic solvents are required to dissolve the sodium formate catalysts. Therefore, this question was addressed by investigating the deuterium kinetic isotope effect and the effect of the addition of proton donors more acidic than the water molecule.

Formic acid has a beneficial effect on the rate of dihydrogen evolution and argues for some sort of bimolecular process. Furthermore, formic acid is the only acid that can be added to the system without reducing the free formate ion concentration. Thus, the addition of other acids to the system can lead to more complex kinetic behavior, as the common ion effect will decrease the solvated formate ion concentration. This effect is demonstrated for acetic acid in Figure 5. Small quantities of acetic acid have a beneficial effect on the rate of dihydrogen production. However, at higher acetic acid concentrations the hydride-transfer reaction slows. This general parabolic behavior is what might be expected for a bimolecular reaction between formate anion and a proton source.

Inverse Deuterium Kinetic Isotope Effect.   Additional insight into the nature of the transition state was obtained by the observation of an inverse deuterium kinetic isotope effect. This observation argues against a rate-limiting formate decarboxylation reaction yielding a free hydride ion because in that case a normal isotope effect would be expected. In addition, the formic acid results suggest that the proton source is involved in the rate-limiting step of the reaction.
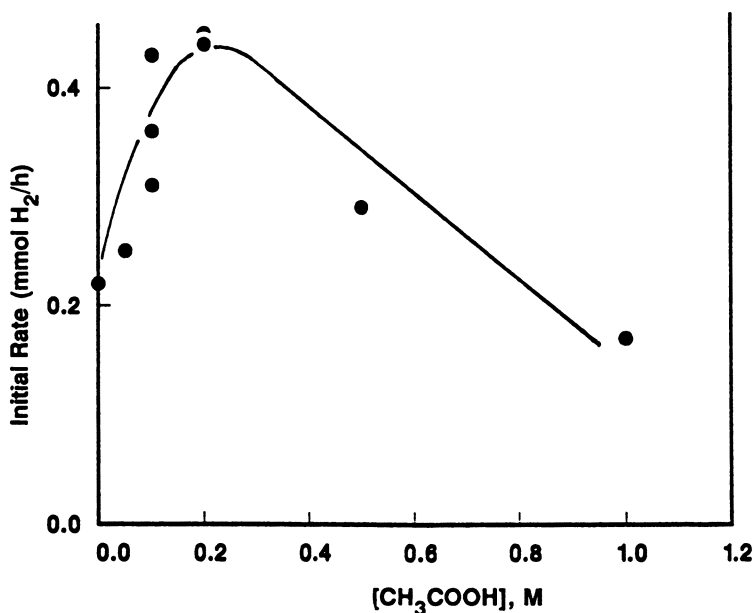
Figure 5. Effect of acetic acid on the initial rate of dihydrogen evolution at constant sodium formate concentration (0.1 M); conditions as in Figure 1.

An inverse deuterium kinetic isotope effect could result if the bonds formed in the transition state are stronger than those broken in the reactants (24, 25). Such a situation could result if the transition state includes a significant degree of H–H bond formation. Two mechanistic possibilities are consistent with these observations. The first possibility is a concerted reaction with a productlike four-centered transition state for the reaction in eq 8. A second possibility involves an intermediate with significant H–H bond order. This mechanistic possibility, suggested on the basis of recent molecular orbital calculations for the gas-phase H_3O^- ion, is summarized by eqs 9–11.

$$O_2CH^- + H_2O \rightarrow O_2C + [H \cdot HOH]^- \qquad (9)$$

$$[HOH \cdot H]^- \rightarrow [HO \cdot H_2]^- \qquad (10)$$

$$[HO \cdot H_2]^- \rightarrow OH^- + H_2 \qquad (11)$$
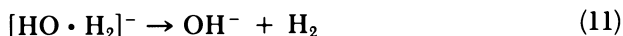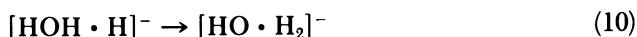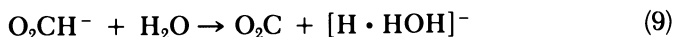
Intermediate Substances. Molecular orbital calculations indicate that the gas-phase H_3O^- system is characterized by two local energy minimums or intermediates. One intermediate is described as a hydride adduct to the Lewis acidic end of the water molecule, $[HOH \cdot H]^-$. The other intermediate is best described as an ion–dipole adduct between hydroxide ion and the dihydrogen molecule, $[HO \cdot H_2]^-$. Both of these species have a characteristic end-on bonded geometry.

The calculations indicate a small barrier, 3–9 kcal, for proton transfer in going from the ion–dipole complex to the hydride adduct. The calculations also suggest that the hydride moiety in the resultant hydride adduct moves between the two protic ends of the water molecule over a shallow potential energy surface, consistent with the small experimental barrier for deuterium exchange (eq 2). Significantly, a free hydride ion does not exist in the system. The protic end of the water molecule bonds with and stabilizes the otherwise high-energy hydride ion by 26 kcal. This stabilization of the hydride ion increases the lifetime of this species and potentially facilitates hydride transfer to carbon dioxide shown in eq 9.

The existent experimental data is consistent with either a concerted hydride transfer (eq 8) or an H_3O^- ion intermediate (eqs 9–11) as mechanistic possibilities. In either case, the key intermediate (or transition state) has substantial H–H bond order. This proposal contrasts with earlier proposals for nucleophilic dihydrogen activation, which focused on a free hydride ion intermediate (for example, eqs 4 and 5).

The catalytic cycle for water–gas shifting (eq 6) is closed by the carbonylation of hydroxide ion to formate ion (eq 12).

$$OH^- + CO \rightarrow HCO_2^- \qquad (12)$$

None of the reactions in eqs 7–12 require the presence of a metal center.

Lead(II) Oxide. The high-temperature reaction chemistry of solvated formate and hydroxide ion in the water–gas shift system is related to the effect of metal centers on the solution-phase hydroxide–formate-catalyzed water–gas shift reaction. A number of potential metal oxide cocatalysts were added to the homogeneous sodium formate–triethylene glycol system, and the most dramatic improvement was obtained with lead(II) oxide (5).

Lead(II) oxide dissolves in these sodium formate–triethylene glycol solutions to yield a species that exhibits a single resonance in the ^{207}Pb NMR. The addition of lead(II) oxide to the sodium formate system was found to increase the rate of water–gas shifting by nearly 3 orders of magnitude, yet the activation energy was unchanged (26 ± 1 kcal). Furthermore, two commercial water–gas shift catalysts, a high-temperature iron oxide catalyst and a low-temperature copper–zinc oxide catalyst, were compared with the homogeneous sodium hydroxide catalysts, with and without the addition of lead(II) oxide cocatalyst. Significantly, all four of the metal oxide systems were found (5) to exhibit remarkably similar activation energies: 26 ± 1 kcal for the homogeneous sodium hydroxide system, both with and without lead(II) oxide; 27 ± 0.2 kcal for the heterogeneous iron oxide catalyst; and 19 ± 0.6 kcal for the copper–zinc oxide catalyst. The mechanism for the cocatalysis by lead is currently under investigation. However, the existing activation parameters suggest that entropy factors may be important in these metal oxide systems.

Conclusions

Triethylene glycol solutions of sodium hydroxide are well-defined water–gas shift catalysts. Results with tetrabutylammonium ion demonstrate that a metal center is not necessary for catalysis of the water–gas shift reaction. Furthermore, the catalysis of the water–gas shift reaction by hydroxide ion is not a high-energy mechanistic pathway; its activation energy (26 ± 1 kcal) is not substantially different from that exhibited by a commercially used iron oxide catalyst (27 ± 0.2 kcal).

Metal centers do, however, have a dramatic effect on the overall activity of the soluble metal oxide water–gas shift system, as best demonstrated by the addition of lead(II) oxide. The nature of the beneficial effect of lead on the water–gas shift reaction catalyzed by sodium hydroxide ion is not understood at this point, but it appears that entropy factors may be important. In contrast to earlier proposals for nucleophilic dihydrogen activation, which focused on free hydride ion intermediates, both the proton dependence of dihydrogen evolution and the deuterium kinetic isotope effect argue against a free hydride ion intermediate, at least within the water–gas shift system catalyzed by hydroxide ion.

These results, in conjunction with the prior deuterium-exchange data and the catalytic hydrogenation work of Walling (19, 20), underscore the

importance of nucleophilic oxygen centers as a primary point of reactivity for the dihydrogen molecule. In addition to the important metal center, nucleophilic oxygen centers need to be considered in evaluating the reaction chemistry of metal oxide catalysts.

Acknowledgments

References

1. Halpern, J. *Adv. Catal.* **1959**, *11*, 301.
2. Kokes, R. J. *Acc. Chem. Res.* **1973**, *6*, 226.
3. Knozinger, H.; Ratnasamy, P. *Catal. Rev.–Sci. Eng.* **1978**, *17*, 31.
4. Saillard, J. Y.; Hoffmann, R. *J. Am. Chem. Soc.* **1984**, *106*, 2006.
5. Klingler, R. J.; Krause, T. R.; Rathke, J. W. *Catal. Lett.* **1989**, *3*, 347.
6. Wirtz, K.; Bonhoeffer, K. F. *Z. Phys. Chem. (Leipzig)* **1936**, *177A*, 1.
7. Claeys, Y. M.; Dayton, J. C.; Wilmarth, W. K. *J. Chem. Phys.* **1950**, *18*, 759.
8. Wilmarth, W. K.; Dayton, J. C.; Fluornoy, J. M. *J. Am. Chem. Soc.* **1953**, *75*, 4549.
9. Wilmarth, W. K.; Dayton, J. C. *J. Am. Chem. Soc.* **1953**, *75*, 4553.
10. Miller, S. L.; Rittenberg, D. *J. Am. Chem. Soc.* **1958**, *80*, 64.
11. Fluornoy, J. M.; Wilmarth, W. K. *J. Am. Chem. Soc.* **1961**, *83*, 2257.
12. Pocker, Y. *Chem. Ind. (London)* **1959**, 1383.
13. Grabowski, J. J.; De Puy, C. H.; Bierbaum, V. M. *J. Am. Chem. Soc.* **1983**, *105*, 2565.
14. Kleingeld, J. C.; Nibbering, N. M. M. *Int. J. Mass Spectrom. Ion Phys.* **1983**, *49*, 311.
15. Kleingeld, J. C.; Ingermann, S.; Jalonen, J. E.; Nibbering, N. M. M. *J. Am. Chem. Soc.* **1983**, *105*, 2474.
16. Paulson, J. F.; Henchman, M. J. *Bull. Am. Phys. Soc.* **1982**, *27*, 108.
17. Cremer, D.; Kraka, E. *J. Phys. Chem.* **1986**, *90*, 33.
18. Chalasinski, G.; Kendall, R. A.; Simons, J. *J. Chem. Phys.* **1987**, *87*, 2965.
19. Walling, C.; Bollyky, L. *J. Am. Chem. Soc.* **1961**, *83*, 2968.
20. Walling, C.; Bollyky, L. *J. Am. Chem. Soc.* **1964**, *86*, 3750.
21. Ford, P. C.; Rokicki, A. *Adv. Organomet. Chem.* **1988**, *28*, 139.
22. Pearson, R. G.; Mauermann, H. *J. Am. Chem. Soc.* **1982**, *104*, 500.
23. Shido, T.; Asakura, K.; Iwasawa, Y. *J. Catal.* **1990**, *122*, 55.
24. Melander, L.; Saunders, W. H. *Reaction Rates of Isotopic Molecules*; Wiley: New York, 1980.
25. Ozaki, A. *Isotopic Studies of Heterogeneous Catalysis*; Kodansha Ltd. and Academic Press: New York, 1977; Chapter 6.

Homogeneous Bimetallic Hydroformylation Catalysis

Two Metals Are Better Than One

Scott A. Laneman and George G. Stanley[1]

Department of Chemistry, Louisiana State University, Baton Rouge, LA 70803

Homobimetallic rhodium complexes based on the electron-rich binucleating linear tetratertiary phosphine ligand $(Et_2CH_2CH_2)(Ph)$-$PCH_2P(Ph)(CHC_2PEt_2)$ (eLTTP) are surprisingly active and selective hydroformylation catalysts. This behavior is remarkable because monometallic rhodium catalysts based on electron-rich chelating phosphine ligands are extremely poor hydroformylation catalysts. The proposed key rate-enhancing step in the bimetallic $Rh_2(eLTTP)$ catalyst system is an intramolecular hydride transfer that facilitates the elimination of the aldehyde product. This proposal has been tested by preparing model binucleating tetraphosphine ligands of the general type $Et_2PCH_2CH_2P(Ph)Y(Ph)PCH_2CH_2PEt_2$ (Y is p-xylene or propylene) to space the two metal centers apart and limit the extent of bimetallic cooperativity. These spaced bimetallic complexes, as well as related monometallic model complexes, are very poor hydroformylation catalysts. This evidence clearly points to the most dramatic example of homobimetallic cooperativity ever seen for a major catalytic process.

TRANSITION METAL DIMER AND CLUSTER SPECIES are of interest as homogeneous catalysts because of the following advantages that multimetallic systems should have over mononuclear complexes:

- the ability to form multicenter metal-to-ligand bonds to a substrate, thus assisting in the activation of that species toward further reactions;

[1]Corresponding author

- the capacity to support multielectron transfers (e.g., reduction of N_2 to NH_3) either as a transfer point or as an electron sink–reservoir;

- the potential to use M–M bonds, particularly weak ones, as "disguised" sites of coordinative unsaturation allowing direct insertion of a substrate into the M–M bond, thus eliminating the need for prior ligand dissociation to open coordination sites; and

- the use of mixed-metal systems, which offer the possibility for the selective and subsequent activation of two (or more) different substrate species.

Despite these potential advantages, only a very few dimer or cluster catalysts are known to have activities or selectivities even remotely approaching those of well-known mononuclear systems (1, 2). Considering the amount of work being done on dimer and cluster species, it might appear tempting to wonder if these types of complexes will ever display novel homogeneous catalytic behavior. Yet the enormous number of possible combinations of metal centers (different types and oxidation states), ligands, and framework geometries make it clear that the seemingly large body of work on multimetallic systems represents only the tip of the iceberg. A seminal report by Adams et al. (3) on the cluster-catalyzed amine metathesis describes a reaction that is uniquely homogeneously catalyzed by a multimetallic system. It provides strong impetus for continuing work in the area of polymetallic catalysis.

Two problems have traditionally hampered the study of polymetallic systems: the preparation of these complexes in high yields and their fragmentation under catalytically interesting conditions (e.g., medium to high pressures of CO or H_2). In the last decade, however, synthetic techniques for the rational preparation of polymetallic complexes have been developed by Stone (4, 5), Vahrenkamp (6), Richter (7), Osborn and co-workers (8, 9), Geoffroy and Gladfelter (10), and others. The unifying idea behind all of these synthetic methods is the use of suitably designed ligand systems that can act as a template for the assembly of polymetallic complexes.

Inhibition of fragmentation of dimer and cluster systems usually centers around the use of strong M–M bonds (e.g., osmium clusters, M–M multiple bonds) or bridging ligands such as bis(diphenylphosphino)methane (dppm). Strong M–M bonds, however, negate the advantage of using M–M bonds as reaction sites. Weak M–M bonds can be ideal reactive sites for interaction with substrates because the molecular orbitals (MO) associated with the M–M interaction are often the highest occupied (HOMO) and lowest unoccupied MO (LUMO).

The breaking of a M–M bond can play an important role in the activation of a substrate species. Similarly, the re-formation of the M–M bond(s) at the

end of a catalytic cycle can assist in the elimination of products and the temporary stabilization of an unsaturated catalyst. The second approach, using bridging ligands such as dppm, often fails either because the ligands do not coordinate strongly enough to stop fragmentation or because they impose metal coordination geometries that are not as reactive.

To fully exploit both template and antifragmentation concepts, we designed and synthesized a new hexatertiary phosphine ligand $(Et_2PCH_2CH_2)_2$-$PCH_2P(CH_2CH_2PEt_2)_2$ (abbreviated eHTP). This polyphosphine ligand has a number of features favoring it as a binucleating ligand system: the ability to both bridge and bichelate two transition metal centers; alkylphosphine moieties (rather than arylphosphines), which improve solubility and metal coordinating strength; and a straightforward, high-yield synthetic procedure (*11*).

As might be expected, eHTP is a powerful binucleating ligand system. Every time we have treated it with two equivalents of a simple mononuclear metal halide or carbonyl we have obtained a bimetallic system, typically in high yields (*12–17*). Although eHTP was designed to form closed-mode binuclear complexes of the general type **1a**, we have found that the open-mode complexes of the general types **1b**, **1c**, and **1d** are produced.
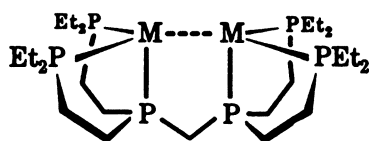
1a
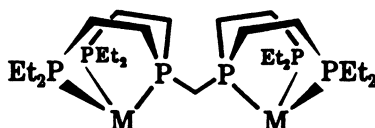
1b
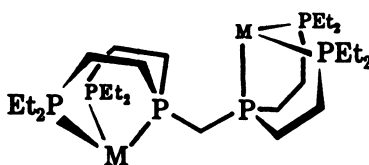
1c
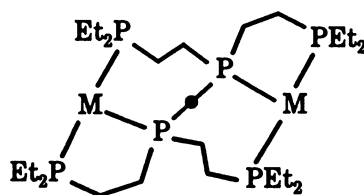
1d

The preceding work has clearly demonstrated that eHTP is a powerful and quite rugged binucleating ligand system. It confirms our choice of combining bridging and chelating functionalities into a single ligand system. One of our primary concerns with eHTP, however, was that the tridentate, bichelating nature of the ligand ties up too many coordination sites on a metal

center. As a result, for a closed-mode ligand conformation such as **1a**, access to the metal centers by a substrate molecule is essentially limited to the "top-side" of the eHTP–dimer system. Our work on Group VIII square planar complexes of eHTP also clearly showed that steric factors would prevent these M_2(eHTP) complexes from readily accessing closed-mode geometries.

A Binucleating Tetraphosphine Ligand System

One approach to reducing some of the unfavorable steric factors in eHTP is to conceptually backtrack and remove two of the chelate arms from eHTP to prepare a binucleating tetratertiary phosphine ligand of the general type $(R_2PCH_2CH_2)(R)PCH_2P(R)(CH_2CH_2PR_2)$. This ligand would still have the bridging–chelating framework of eHTP, yet would provide a considerably more open environment about the metal centers for reactions to occur.

A tetratertiary phosphine of this type is chiral at the two internal phosphorus atoms. This conformation results in both the *racemic* (*R,R; S,S*) and *meso* (*R,S*) diastereomers shown as *rac*-eLTTP and *meso*-eLTTP. We refer to this general class of ligands as LTTP (for linear tetratertiary phosphine). The chirality of this system can be a desirable feature for promoting potential enantioselective reactions, but will reduce our overall synthetic yields and lead to more difficult separations of the tetraphosphine itself.

rac-eLTTP   *meso*-eLTTP
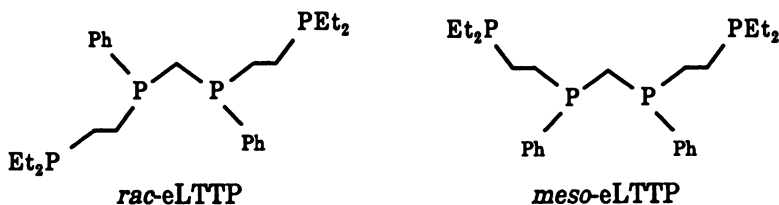
We developed a straightforward synthetic route to LTTP that is quite amenable to a wide variety of structural modifications. Our synthetic procedure for preparing the LTTP ligand $(R_2PCH_2CH_2)(Ph)PCH_2P(Ph)$-$(CH_2CH_2PR_2)$ (R is Et or Ph) is shown in Scheme I. It involves the building of the central bis(phosphino)methane unit from the reaction of KP(H)Ph with CH_2Cl_2. The Ph(H)PCH_2P(H)Ph species thus produced is isolated and then treated with 2 equiv of $R_2P(CH=CH_2)$ under free radical-catalyzed conditions (*18*) to produce LTTP (*19*).

We decided to use ethylene-linked terminal phosphines in LTTP because they simplify the synthetic procedure and give higher yields of the final tetraphosphine (88–92% isolated yields based on Ph(H)PCH_2P(H)Ph, 39–43% isolated yields based on starting PhPH_2). The presence of phenyl groups on the central P–CH_2–P bridge is a designed feature of this ligand
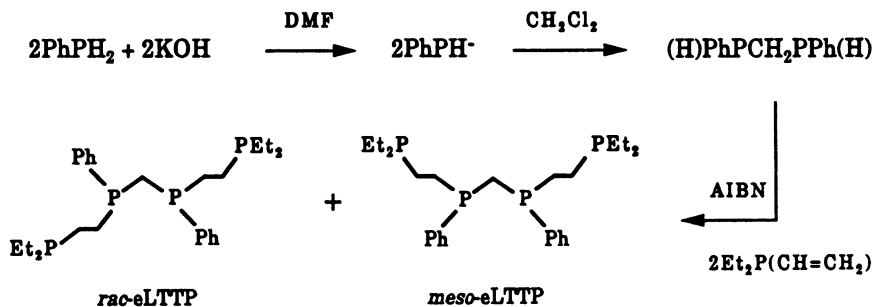
Scheme I. Synthetic procedure for preparing the LTTP ligand.

to allow more facile crystallizations of transition metal complexes. Although the all-phenyl-substituted LTTP ligand was prepared, our primary interest is in the ethyl-substituted LTTP (eLTTP) ligand. Its electron-rich alkylated terminal phosphines will coordinate strongly to transition metal centers and be far more effective at inhibiting ligand dissociation and dimer fragmentation processes.

Bimetallic Complexes Based on eLTTP

The *meso* and *racemic* diastereomers of eLTTP are powerful binucleating ligands that can both bridge and chelate two metal centers. They form complexes that will have different overall orientations of the phosphines about the two metal centers for idealized M–M bonded dimer systems. The *racemic* diastereomer of eLTTP has an *anti* orientation of the chelate rings; the *meso* diastereomer has the chelate rings directed *syn* to one another.
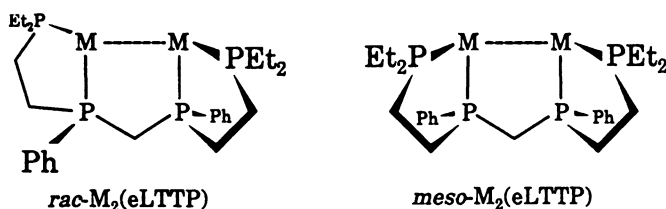
We were able to separate the two eLTTP diastereomers by reacting them with metal complexes to produce bimetallic M_2(eLTTP) systems. Then we took advantage of the differences between the *rac*-M_2(eLTTP) and *meso*-M_2(eLTTP) coordination geometries to effect separations by column chromatography or by fractional crystallizations. This approach worked particularly well for the Ni_2Cl_4(eLTTP) complexes (20). From them we can isolate pure *rac*- or *meso*-eLTTP by treatment of the appropriate diastereomerically

pure nickel complex with excess KCN in refluxing H_2O–heptane. The cyanide displaces the nickel atoms to form water-soluble $NiCN_4^{2-}$ and free eLTTP, which quantitatively extracts into the organic phase. We believe that the eLTTP ligands can also be separated directly by HPLC techniques, but have not yet been able to study this feature in detail.

The reaction of $Rh_2(\mu\text{-}Cl)_2(CO)_4$ with eLTTP produces the bimetallic Rh(I) system $Rh_2Cl_2(CO)_2(eLTTP)$ in about 40–50% yield (19). The first diastereomer of this complex to crystallize out of the tetrahydrofuran (THF) or toluene solution is the *racemic* system (*see* structure). Not too surprisingly, the *rac*-$Rh_2Cl_2(CO)_2(eLTTP)$ structure is closely related to the *rac*-$Ni_2Cl_4(eLTTP)$ system (20) with a Rh–P1⋯P1′–Rh′ torsional angle of 123° and a Rh⋯Rh separation of 5.813(2) Å. We now almost exclusively use a higher yield synthetic route to bimetallic rhodium–eLTTP complexes. It involves the use of $[Rh(norb)_2](BF_4)$ (norb is norbornadiene) as a starting material to give 80–90% isolated yields of $[Rh_2(norb)_2(eLTTP)](BF_4)_2$.

racemic-$Rh_2Cl_2(CO)_2(eLTTP)$ *meso*-$Co_2(\mu\text{-}CO)_2(CO)_2(eLTTP)$
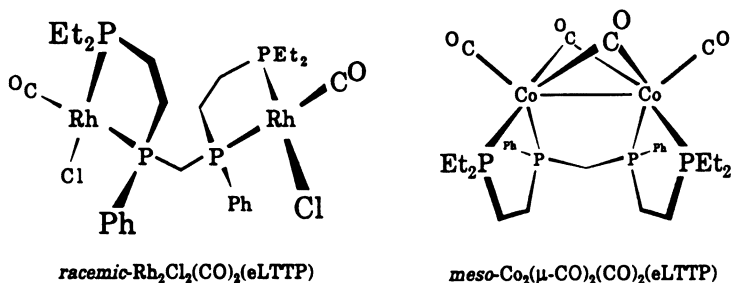
We characterized bimetallic systems based on eLTTP that formally possess M–M bonds. For example, the Co(0) dimer $Co_2(\mu\text{-}CO)_2(CO)_2(eLTTP)$ was prepared by the reaction of the Co(0) dimer system $Co_2(\mu\text{-}CO)_2(CO)_2(norb)_2$ with eLTTP (21). Single-crystal X-ray analysis on the orange crystals that initially form from the slow evaporation of a THF solution confirms the presence of *meso*-eLTTP in a cradle geometry that is bridging and chelating a Co–Co dimer. The *meso*-$Co_2(\mu\text{-}CO)_2(CO)_2(eLTTP)$ (*see* structure) molecule lies on a crystallographic mirror plane that passes through the bridging carbonyl ligands and the central methylene group of the eLTTP ligand. The Co–Co bond length of 2.513(4) Å is typical for a Co–Co single bond (22–24). The *meso*-eLTTP ligand symmetrically bridges and chelates both cobalt centers with the two five-membered chelate rings eclipsed and oriented *syn* to one another. Because of the crystallographic mirror plane, all four phosphorus atoms lie in the same plane.

Both the *rac*- and *meso*-$M_2(LTTP)$ binuclear systems have significantly less steric hindrance than the corresponding $M_2(HTP)$ complexes. They represent new geometric arrangements for phosphine ligands about two metal centers. We believe that the more open ligand environment and

rotational flexibility in these M_2(LTTP) dimers will promote a greater number of interesting reactions.

Bimetallic Hydroformylation Chemistry

Hydroformylation (also called the oxo reaction) is the chemical process of converting alkenes into aldehydes by using H_2 and CO, typically with soluble rhodium- or cobalt-based transition metal catalysts. It is the largest homogeneous catalytic process in the world, with more than 9 billion pounds of industrially important aldehydes and alcohols produced each year (25). Hydroformylation is also a reaction that is potentially well suited to bimetallic systems (26, 27).

Heck and Breslow (28), for example, proposed in 1963 that there could be an intermolecular hydride transfer in the $Co_2(CO)_8$-catalyzed hydroformylation cycle (Scheme II). Instead of adding H_2 to a Co(acyl)$(CO)_4$ species and then eliminating the product aldehyde, they suggested that another $HCo(CO)_4$ species does an intermolecular hydride transfer to the acyl spe-
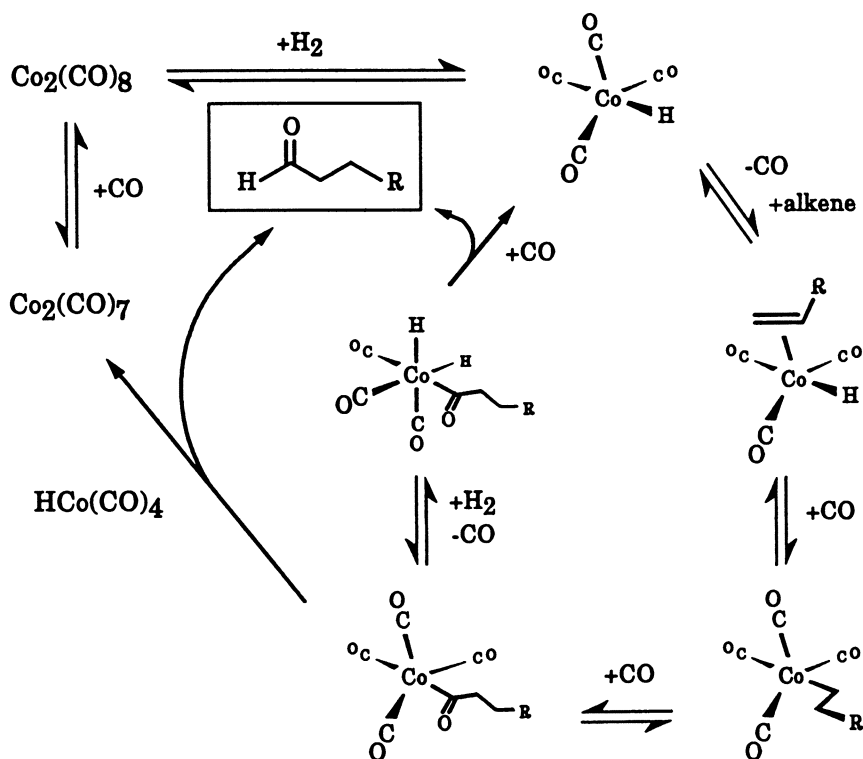
Scheme II. Heck–Breslow hydroformylation mechanism.

cies. This transfer eliminates aldehyde and forms a Co–Co bonded carbonyl system, which then goes on to react with H_2 to form 2 equiv of $HCo(CO)_4$. Initially, kinetic and high-pressure IR data supported this mechanism for cobalt-catalyzed hydroformylation (29–35), but more recently careful high-pressure IR studies (36, 37) provided strong support for the dominance of the monometallic pathway shown in Scheme II.

Mechanistic data for hydroformylation by rhodium-based catalysts such as $HRh(CO)(PPh_3)_3$ is considerably less firm about details such as direct H_2 addition or intermolecular hydride transfer from another rhodium hydride species (38). Sanger's group (39–43) demonstrated rate enhancements for hydroformylation with bimetallic rhodium catalysts. However, the linear-to-branched aldehyde selectivities are quite poor for these systems.

Several reports (44–47) have described the effects of heterobimetallic homogeneous catalysts on the rate and selectivity of hydroformylation reactions. Kovacs et al. (48), for example, proposed that the rate-limiting step in the mechanistic study of a mixed $HCo(CO)_4$–$HMn(CO)_5$ catalyst system is the bimolecular reaction of an unsaturated cobalt acyl with the manganese hydride to give a binuclear reductive elimination of the product aldehyde.

For these reasons, we examined $Rh_2(eLTTP)$-type bimetallic complexes for hydroformylation catalysis. Our reaction studies on $Rh_2(CO)_2(norb)_2$-$(eLTTP)^{2+}$ (norb is norbornadiene) show that it is a remarkable hydroformylation catalyst. The rates reported for our bimetallic complexes have all been divided by 2 to convert from a per-mole basis to a per-rhodium-atom basis. This conversion allows straightforward comparisons to monometallic catalyst systems. Table I lists the rates and selectivities of our bimetallic system and several other conventional monometallic hydroformylation catalysts for 1-hexene.

The bimetallic $Rh_2(eLTTP)$-based catalyst is quite active and shows remarkable product selectivity with a 25–30:1 linear-to-branched aldehyde ratio. This result is particularly impressive considering that we are not adding any excess phosphine ligand to our catalyst. Virtually every other commercial

Table I. Hydroformylation Catalysts for 1-Hexene

Catalyst	P:Rh[a]	Turnover (h^{-1})[b]	Linear-to-Branched (% isomer)[c]
$Rh_2(norb)_2(eLTTP)^{2+}$	0.5:1	390	>25:1 (8%)
$Rh(norb)(depmpe)^+$ [d]	1:1	10	3:1 (85%)
$HRh(CO)(PPh_3)_3$[e]	10:1	4900	4:1 (10%)
$HRh(CO)(PPh_3)_3$	958:1	875	14:1 (4%)

NOTE: Catalytic runs were done in Parr autoclaves under 60 psi of pressure, at 80 °C with acetone as the solvent. Catalyst concentration was 80 ppm.
[a]Phosphine ligand to rhodium ratio.
[b]Initial turnover number for catalytic run on a normalized per-rhodium basis.
[c]Ratio of linear-to-branched aldehyde products. The amount of alkene isomerization observed at the end of the run is given in parentheses.
[d]depmpe is $Et_2PCH_2CH_2PPhMe$.
[e]Estimated from the work of Hughes and Unruh (49).

Rh–PR$_3$ catalyst system we know of requires excess phosphine ligand to stabilize the catalyst and to give good product aldehyde selectivities. Excess phosphine (usually PPh$_3$) is required for HRh(CO)(PPh$_3$)$_3$-based systems to help improve the production of linear aldehydes, cut down on alkene isomerization, and improve the stability and lifetime of the catalyst. Even with chelating phosphines such as Ph$_2$PCH$_2$CH$_2$PPh$_2$ (dppe), excess phosphine is required to maintain catalyst stability (49). Our mainly alkylated eLTTP ligand, on the other hand, is considerably more basic and coordinates far more strongly than phenylated ligands such as PPh$_3$ or dppe.

The activity of our bimetallic system is close to that seen for the commercial HRh(CO)(PPh$_3$)$_3$ catalyst system. This activity is definitely not expected because the considerably more basic nature of the eLTTP ligand should give rise to a much slower catalyst. At 60 psi and 80 °C, the initial turnover rate for the hydroformylation of 1-hexene in acetone is 390 turnovers per hour. This rate can be compared to HRh(CO)(PPh$_3$)$_3$, with a 10:1 PPh$_3$-to-catalyst ratio, which has an average rate of 4900 turnovers per hour. Under these conditions, however, HRh(CO)(PPh$_3$)$_3$ has a linear-to-branched aldehyde selectivity of only 4:1. Increasing the PPh$_3$-to-catalyst ratio to 950:1 decreases the average rate to 875 turnovers per hour, but increases the linear-to-branched aldehyde selectivity to 14:1.

Thus, these studies indicate that our bimetallic system is only slower by about a factor of 2 (on a per-rhodium basis) relative to the current best commercial rhodium catalyst system. It has a significantly higher product selectivity and does not require any excess phosphine ligand to maintain the selectivity and stability of the catalyst. With the proper steric and electronic modifications of the substituent groups on our LTTP ligand, both the rate and selectivity of this system should increase even further.

Our bimetallic Rh$_2$(eLTTP)-based catalyst has several rather unusual features relative to results seen for monometallic Rh–PR$_3$ hydroformylation catalysts: its speed, high selectivity, and freedom from the requirement for the presence of excess phosphine to stabilize the catalyst and improve its selectivity. Why is our system so much faster than one would expect from monometallic systems? Pruett and Smith, in their early key work (50) on Rh hydroformylation catalysis, clearly showed that, for monometallic systems, increasing the basicity of the phosphine ligand resulted in a considerably less active catalyst and reduced the selectivity to linear aldehyde product. They also demonstrated that excess phosphine ligand was necessary to improve the selectivity of the catalyst.

With our eLTTP ligand system it is relatively straightforward to generate monometallic analogs that incorporate half of the eLTTP ligand. In our initial studies we used Et$_2$PCH$_2$CH$_2$PEt$_2$, depe, to act as a chelating model for eLTTP. We also prepared Et$_2$PCH$_2$CH$_2$PMePh (depmpe), shown in Scheme III, and Et$_2$PCH$_2$CH$_2$PPh$_2$ (dedppe) ligands to act as more electronically correct monometallic model ligand systems. All these model monometallic hydroformylation catalysts have very similar activities and selectivities.
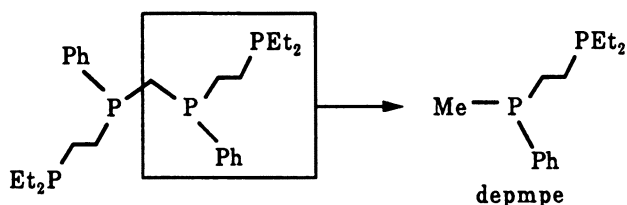
Scheme III. Preparation of depmpe.

Rh(norb)(depmpe)$^+$ is, perhaps, the monometallic complex most electronically analogous to our bimetallic Rh$_2$(norb)$_2$(eLTTP)$^{2+}$ system. It is a terrible hydroformylation catalyst (*see* Table I). It has an initial turnover frequency of 10 per hour with a product aldehyde selectivity of only 3:1 and does extensive alkene isomerization. Our bimetallic system is, therefore, a far superior catalyst relative to this electronically correct monometallic analog. We are planning to compare mono- and bimetallic catalyst systems for the hydroformylation of ethylene or propylene. The isomerization reaction will be eliminated in these systems, and a direct and more accurate comparison of the absolute hydroformylation rates can be made.

We believe that this dramatic rate enhancement is due to homobimetallic cooperativity. Specifically, it is an intramolecular hydride transfer from one metal center to the other. An intramolecular hydride transfer implies that the two rhodium centers in the bimetallic Rh$_2$(eLTTP) unit must be able to closely approach one another. The rotational flexibility of Rh$_2$(eLTTP) has been probed by performing van der Waals (VDW) energy calculations on the model complex *rac*-Rh$_2$H$_2$(CO)$_2$(eLTTP) by using the SYBYL molecular mechanics–graphic program package (*51, 52*). The results are summarized in Figure 1, which shows an expanded portion of the 360° × 360° two-dimensional VDW energy map.

The calculation shows that the *rac*-Rh$_2$H$_2$(CO)$_2$(eLTTP) complex should have a considerable amount of conformational flexibility. Most important, the VDW calculation indicates that this complex can readily access a closed-mode orientation in which the two Rh centers approach one another. This closed-mode conformation is shown in Figure 1.

The rotation of the two rhodium centers toward one another brings the hydride ligands into perfect position for bridging to the other metal center. The VDW energy calculation only measures the steric factors involved in rotations about the central methylene bridge. It knows nothing about the potential for forming chemical bonds between the hydride ligands and empty p$_z$ orbitals on the other rhodium atoms. This rotational flexibility is significant because square-planar complexes based on the more sterically hindered eHTP hexaphosphine ligand cannot form closed-mode complexes because of severe intramolecular steric interactions. This property of eHTP was one of the primary reasons for designing and preparing the LTTP ligand system.
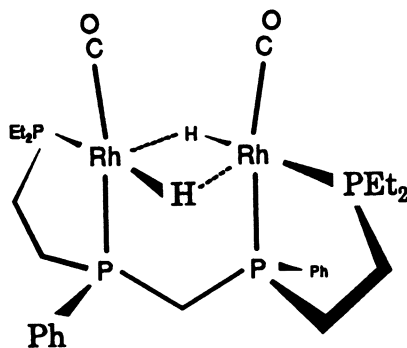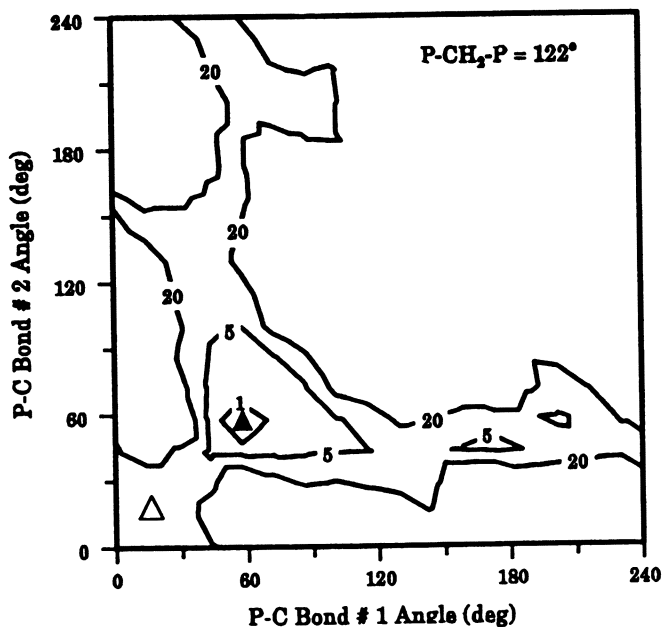
Figure 1. Top: Expanded VDW energy map for rac-Rh₂H₂(CO)₂(eLTTP) from the SYBYL molecular-modeling program. Axes represent rotation angles about the two central P–CH₂–P bonds. Contours are the relative VDW energies in kilocalories per mole. Values higher than 20 kcal mol⁻¹ are not listed. The solid triangle marks the position of the global minimum; the open triangle marks the closed-mode rotational conformation shown schematically on the bottom.

Although these VDW energy studies are quite simple, they clearly support the premise that the two rhodium atoms can approach one another and have the proper geometry for a facile hydride transfer from one Rh atom to another. In a real hydroformylation catalytic cycle we would anticipate the existence of species such as Rh(acyl)(CO)(μ-eLTTP)RhH(CO). This type

of system could also readily access a closed-mode conformation in which an intramolecular hydride transfer could occur (*see* structure **2**).

2
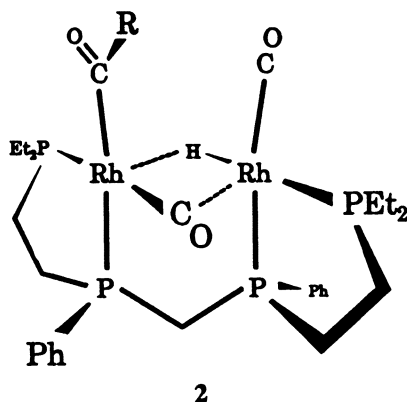
Our overall proposed mechanism for $Rh_2(eLTTP)$ bimetallic hydroformylation is shown in Scheme IV. The $Rh_2(eLTTP)$ unit essentially acts as a conventional monometallic hydroformylation catalyst until it reaches the acyl intermediate. This point is where the rotational flexibility of the eLTTP ligand comes into play and bimetallic cooperativity takes place to transfer a hydride to the acyl-bound rhodium. Reductive elimination of aldehyde product will probably then generate a Rh–Rh bonded complex that can react with H_2 to regenerate the $Rh_2H_2(CO)_2(eLTTP)$ starting catalyst.

We also prepared some bimetallic model systems in which spacer groups replace the central methylene bridge to probe the importance of having the two metal centers near one another. Bimetallic rhodium norbornadiene complexes based on *p*-xylene- and propylene-bridged tetraphosphine ligands (eLTTP–*p*-xylene and eLTTP–propyl) (*see* structures) were prepared and studied as hydroformylation catalysts. Bimetallic Rh–norbornadiene complexes based on these spaced binucleating tetraphosphine ligands are dreadful hydroformylation catalysts. Their results essentially mirror those seen for the monometallic model systems. The hydroformylation catalytic results for mono- and bimetallic complexes discussed here are summarized in Figure 2.

eLTTP-*p*-xylene   eLTTP-propyl
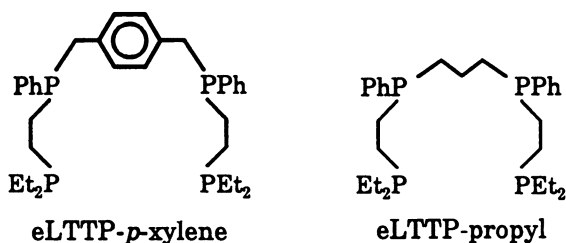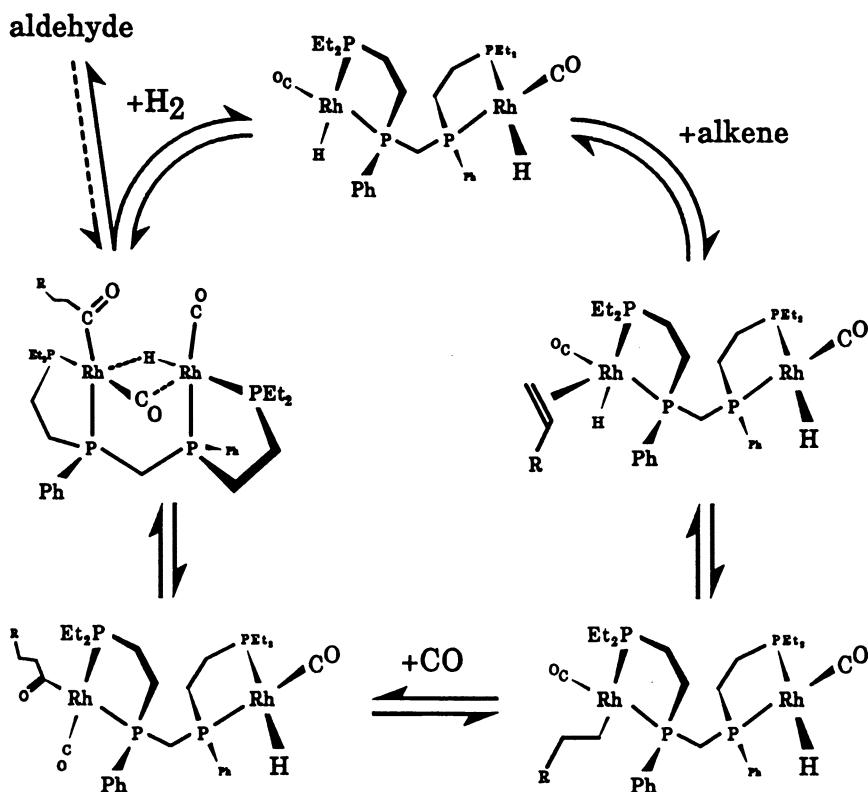
Scheme IV. Proposed mechanism for bimetallic hydroformylation.

Molecular modeling studies of the $Rh_2H_2(CO)_2$(eLTTP–*p*-xylene) and $Rh_2H_2(CO)_2$(eLTTP–propyl) catalyst systems clearly indicate that it will be very difficult, if not impossible, for the metal centers in these systems to approach one another to do an intramolecular hydride transfer. Thus the presence of the single-atom bridge in eLTTP, which constrains the two square planar rhodium centers to adopt a rotationally flexible face-to-face orientation, may well be the key design feature in the Rh_2(eLTTP) complex. This feature allows facile intramolecular hydride transfer between the metal centers and greatly enhances the rate of the hydroformylation reaction.

The second question that arises is why our system is so selective. This selectivity was an unanticipated feature of the system. A number of theories have been advanced on the origin of product selectivity in hydroformylation. Hughes and co-workers (49, 53), for example, proposed that, in order to be selective to linear aldehydes, a Rh complex must have three phosphine ligands coordinated at the instant that selectivity is determined. The selectivity step occurs when the hydride ligand adds to the coordinated alkene to give either a linear or branched alkyl moiety.
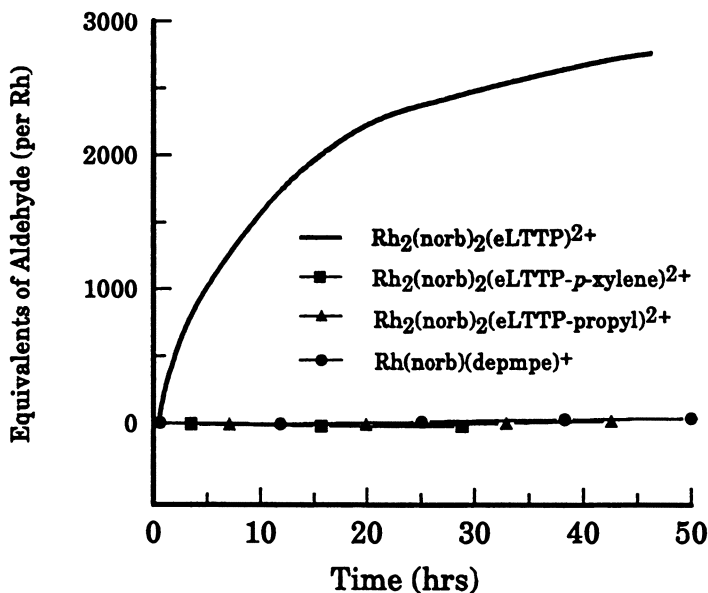
Figure 2. Results for the hydroformylation of 1-hexene at 60 psi and 80 °C with a variety of electron-rich phosphine–rhodium catalyst systems. The ligand abbreviation depmpe stands for Et₂PCH₂CH₂PPhMe.

This theory appears consistent with the fact that excess phosphine ligand is required to obtain high selectivities in virtually all Rh catalysts. It does not, however, fit our bimetallic catalyst system in which there is no extra phosphine ligand present, yet high selectivities are observed. Indeed, careful studies by Merola and co-workers (54) showed that excess phosphine is required in traditional Rh catalysts to maintain a suitable concentration of the bisphosphine species $HRh(CO)(PPh_3)_2$. Although it is less active, this species gives higher selectivities to the linear aldehyde.

We are not sure exactly why the $Rh_2(eLTTP)$ catalyst has such a high linear-to-branched aldehyde ratio. However, we believe that it is tied into the overall shape of the bimetallic $Rh_2(eLTTP)$ molecule. When an alkene adds to $Rh_2H_2(CO)_2(eLTTP)$ (the presumed active catalyst) (structure 3), it can add only to one of the outside axial rhodium coordination sites. As it coordinates to the rhodium center, the other ligands will want to bend away. Ideally, they will form a trigonal bipyramid, which is the least sterically hindered geometry. $Rh_2(eLTTP)$, however, cannot attain this geometry because the other half of this face-to-face complex limits the extent of ligand motion toward trigonal bipyramidal or square pyramidal. As the geometry reorganization about the one rhodium center is curtailed, the steric effects are maximized and the alkene insertion into the M–H bond is directed toward the anti-Markovnikov alkene position to form a linear alkyl group.

3
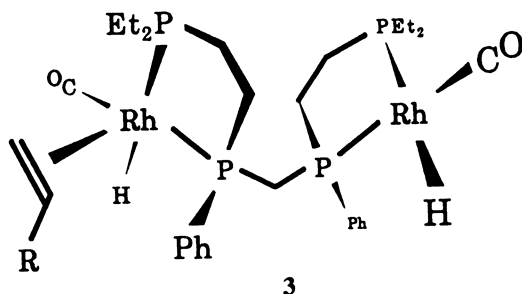
There is clearly a great deal of further work to be done in studying this system. Some of the important factors that we plan to study include

- Modification of both steric and electronic factors in eLTTP for enhancing the activity and selectivity of our bimetallic catalyst. By using somewhat less basic phosphines we may be able to increase the activity. Increasing the steric bulk of the substituent groups on the terminal phosphines should have a dramatic effect on increasing the selectivity. Use of groups that are too sterically bulky, however, may kill the hydroformylation activity and selectivity by preventing rotation into the closed-mode conformer.

- A key experiment is to separate eLTTP into pure diastereomers so we can prepare and study the hydroformylation activity and selectivity of separated *rac-* and *meso*-$Rh_2(norb)_2(eLTTP)^{2+}$ species. All the results presented here are for a 50:50 mixture of *racemic* and *meso* catalysts. Our molecular modeling studies suggest that the *racemic* diastereomer may well be the more active species. If one diastereomer is active and the other is not, then the rate data we have presented can be doubled. This step would make our eLTTP-based dirhodium catalyst about equally active (on a per-Rh basis) as the current Union Carbide $Rh–PPh_3$ commercial system. If the two diastereomers have very different activities it will, of course, be important to develop large-scale procedures to separate the two diastereomers from one another.

- If the *racemic* catalyst turns out to be the effective species, then we have the potential for resolving the *racemic* system into pure enantiomers for studying asymmetric hydroformylation catalysis of prochiral alkenes. There are very few enantioselective hydroformylation catalysts; most give enantiomeric excesses of 50% or lower.

- Although the use of less basic phosphine ligands should increase the activity of our catalyst system, they will also coordinate less strongly and lead to catalyst stability problems. We believe that a much better way to increase the activity of our system is to use heterobimetallic species. Mixed-metal systems have been shown on a number of occasions to enhance the activity of hydroformylation catalysts. We plan to study mixed Rh–Co, Rh–Ru, and, perhaps most interestingly from a commercial–economic viewpoint, Co–Ru systems based on our tetraphosphine ligand system.

- Finally, we of course need to fully explore the effects of temperature, pressure, H_2–CO ratio, solvents, and different alkenes on the hydroformylation catalysis.

Although we have additional mechanistic and kinetic studies to perform to fully test our bimetallic hydroformylation proposal, all the experimental evidence so far clearly points to the most dramatic example of homobimetallic cooperativity ever observed. This example is particularly significant because the unique properties of our bimetallic system may allow us to develop the first highly selective heterogenized hydroformylation catalyst system by linking the LTTP ligand system to a surface support. Work in this area is currently in progress in our laboratories.

Acknowledgments

References

1. Muetterties, E. L.; Krause, M. J. *Angew. Chem., Int. Ed. Engl.* **1983**, *22*, 135.
2. Johnson, B. F. G. *Transition Metal Clusters*; Wiley: New York, 1980.
3. Adams, R. A.; Kim, H.-S.; Wang, S. *J. Am. Chem. Soc.* **1985**, *107*, 6107.
4. Stone, F. G. A. In *Inorganic Chemistry: Toward the 21st Century*; Chisholm, M. H., Ed.; ACS Symposium Series 211; American Chemical Society: Washington, DC, 1983; p 383.
5. Stone, F. G. A. *Angew. Chem., Int. Ed. Engl.* **1984**, *23*, 89.
6. Vahrenkamp, H. *Adv. Organomet. Chem.* **1983**, *22*, 169.
7. Richter, F.; Vahrenkamp, H. *Angew. Chem., Int. Ed. Engl.* **1979**, *18*, 531.
8. Osborn, J. A.; Stanley, G. G. *Angew. Chem., Int. Ed. Engl.* **1980**, *19*, 1025.
9. Bahsoun, A. A.; Osborn, J. A.; Voelker, C. *Organometallics* **1982**, *1*, 1114.
10. Geoffroy, G. L.; Gladfelter, W. L. *J. Am. Chem. Soc.* **1977**, *99*, 7565.
11. Askham, F. R.; Marques, E. C.; Stanley, G. G. *J. Am. Chem. Soc.* **1985**, *107*, 3082.

12. Laneman, S. A.; Stanley, G. G. *Inorg. Chem.* **1987**, *26*, 1177.
13. Saum, S. E.; Stanley, G. G. *Polyhedron* **1987**, *6*, 1803.
14. Askham, F. R.; Maverick, A. W.; Stanley, G. G. *Inorg. Chem.* **1987**, *26*, 3963.
15. Saum, S. E.; Askham, F. R.; Fronczek, F.; Stanley, G. G. *Organometallics* **1988**, *7*, 1409.
16. Saum, S. E.; Askham, F. R.; Fronczek, F. R.; Stanley, G. G. *Polyhedron* **1988**, *7*, 1785.
17. Saum, S. E.; Fronczek, F. R.; Laneman, S. A.; Stanley, G. G. *Inorg. Chem.* **1989**, *28*, 1878.
18. DuBois, D. L.; Hyers, W. H.; Meek, D. W. *J. Chem. Soc., Dalton Trans.* **1975**, 1011.
19. Laneman, S. A.; Fronczek, F. R.; Stanley, G. G. *J. Am. Chem. Soc.* **1988**, *110*, 5585.
20. Laneman, S. A.; Fronczek, F. R.; Stanley, G. G. *Inorg. Chem.* **1989**, *28*, 1872.
21. Laneman, S. A.; Fronczek, F. R.; Stanley, G. G. *Inorg. Chem.* **1989**, *28*, 1206.
22. Swaminathan, S.; Lessinger, L. *Cryst. Struct. Commun.* **1978**, *7*, 621.
23. Jones, R. O.; Maslen, E. N. *Z. Kristallogr.* **1966**, *123*, 330.
24. Bird, P. H.; Fraser, A. R.; Hall, D. N. *Inorg. Chem.* **1977**, *16*, 1923.
25. Cf. *Reactivity and Structure Concepts in Organic Chemistry: New Syntheses with Carbon Monoxide*; Falbe, J., Ed.; Springer-Verlag: New York, 1980; Vol. 11.
26. Pino, P. *J. Organomet. Chem.* **1980**, *200*, 223.
27. Paulik, F. E. *Catal. Rev.* **1972**, *6*, 49.
28. Heck, R. F.; Breslow, D. S. *J. Am. Chem. Soc.* **1963**, *83*, 651.
29. Whyman, R. *J. Chem. Soc.* **1972**, 1375.
30. Whyman, R. *J. Organomet. Chem.* **1974**, *66*, C23.
31. Whyman, R. *J. Organomet. Chem.* **1974**, *81*, 97.
32. Whyman, R. *J. Organomet. Chem.* **1975**, *94*, 303.
33. Van Boven, M.; Alemdaroglu, N.; Penninger, J. M. L. *J. Organomet. Chem.* **1975**, *84*, 65.
34. Bianchi, M. *J. Organomet. Chem.* **1977**, *135*, 387.
35. Kaschina, W. W.; Kaznjelson, M. G.; Mischenkowa, G. N. *Z. Org. Chim.* **1978**, *14*, 877.
36. Mirbach, M. F. *J. Organomet. Chem.* **1984**, *265*, 205.
37. Moser, W. R. In *Homogeneous Transition Metal Catalyzed Reactions*; Moser, W.; Slocum, D., Eds.; Advances in Chemistry 230; American Chemical Society: Washington, DC, 1992; Chapter 1.
38. Brown, J. M.; Kent, A. G. *J. Chem. Soc., Perkin Trans. 2* **1987**, 1597.
39. Sanger, A. R. *Homogeneous Catalysis with Metal Phosphine Complexes*; Pignolet, L. H., Ed.; Plenum: New York, 1983; pp 215–237.
40. Sanger, A. R.; Schallig, L. R. *J. Mol. Catal.* **1977–1978**, *3*, 101.
41. Sanger, A. R. *J. Mol. Catal.* **1977–1978**, *3*, 221.
42. Sanger, A. R. *J. Chem. Soc., Dalton Trans.* **1977**, 120.
43. Sanger, A. R. *J. Chem. Soc., Dalton Trans.* **1977**, 1971.
44. Gelmini, L.; Stephan, D. W. *Organometallics* **1988**, *7*, 849.
45. Hidai, M.; Fukoka, A.; Koyasu, Y.; Uchida, Y. *J. Chem. Soc., Chem. Commun.* **1984**, 516.
46. Pino, P.; von Bezard, D. A. Swiss Patent 625 233, 1981.
47. Pino, P.; Consiglio, G. *Proceedings Symposium on Rhodium Homogeneous Catalysis*; Veszprem, 1978; p 98.
48. Kovacs, I.; Hoff, C. D.; Ungvary, F.; Marko, L. *Organometallics* **1985**, *4*, 1347.
49. Hughes, R. O.; Unruh, J. D. *J. Mol. Catal.* **1981**, *12*, 71.
50. Pruett, R. L.; Smith, J. A. *J. Org. Chem.* **1969**, *34*, 327.

51. TRIPOS Associates, Inc., 1699 South Hanley Rd., Suite 303, St. Louis, MO 63144.
52. Naruto, S.; Motoc, I.; Marshall, G. R.; Daniels, S. B.; Sofia, M. J.; Katzenellenbogen, J. A. *J. Am. Chem. Soc.* **1985**, *107*, 5262.
53. Hughes, O. R.; Young, D. A. *J. Am. Chem. Soc.* **1981**, *103*, 6636.
54. Oswald, A. A.; Hendriksen, D. E.; Kastrup, R. V.; Merola, J. S.; Mozeleski, E. J.; Reisch, J. C. *Phosphorus Sulfur* **1983**, *18*, 475.

Hydroformylation and Hydrogenation with Platinum Phosphinito Complexes

Piet W. N. M. van Leeuwen and Cornelis F. Roobeek

Koninklijke/Shell-Laboratorium, Amsterdam, Shell Research B.V., Postbus 3003, 1003 AA Amsterdam, Netherlands

Platinum complexes containing phosphinito ligands are moderately active hydroformylation catalysts (30–100 bar, 80–100 °C). The products consist of a mixture of alcohols and aldehydes with linearities in excess of 90%. Internal alkenes can also be hydroformylated, with linearities as high as 70%. Alkyl and acyl complex intermediates have been identified. Aldehyde reduction proceeds via metal alkoxide species rather than hydroxymethyl fragments. Aldehyde reduction can be greatly accelerated by the addition of carboxylic acids. In summary, diphenylphosphinous acid turns out to be an interesting ligand with peculiar electronic properties capable of inducing catalytic hydroformylation and hydrogenation. It may have a function in promoting the activation of dihydrogen, which seems to be a prerequisite for platinum complexes to be catalytically active.

Hydroformylation of internal alkenes to linear products is a key process for the industrial production of higher alcohols. Two metals are commercially applied, rhodium and cobalt. Of these, only cobalt is used for converting internal alkenes to terminal hydroformylation products.

Platinum is the third metal active in hydroformylation (*1–11*). Out of the plethora of known platinum (hydride) complexes, only those containing trichlorostannate as the ligand–anion show activity as hydroformylation catalysts. The classical, but still rare, example of a platinum complex active as catalyst for the hydrogenation of alkenes (*12*) also requires the presence of trichlorostannate as the ligand. Cationic complexes have been reported as active hydroformylation catalysts, yielding only branched products (*13*). A combination of the cationic character and trichlorostannate anion led to the

discovery of the conversion of internal alkenes with platinum catalysts (5), although the selectivity to alkanes was rather high (>40%).

In a preliminary communication (14, 15) we reported on the formation of platinum hydroformylation catalysts with PPh_2OH (phosphinous acids or diphenylphosphine oxide) as the ligands. Quite significantly, they are also active for internal alkenes. In this report we review some of the results of the catalytic hydroformylation studies as well as the isolation of several intermediates and hydride precursors. The synthesis, not the catalysis, of one of the hydride catalyst precursors was described earlier (16). In addition, we report on the use of a new catalyst (viz., platinum phosphinito complexes in the presence of carboxylic acids) for the hydrogenation of aldehydes. Hydrogenation of aldehydes during hydroformylation is a secondary reaction, which may well be promoted by the carboxylic acids formed by partial decomposition of the catalyst.

Catalytic Hydroformylation Reactions

In situ mixing of $Pt(1,5\text{-cod})_2$ (cod is 1,5-cyclooctadiene), PPh_2OH, and various other donor ligands led to active catalysts. Hydroformylation of 1-heptene gave rise to a high linearity and appreciable rates (see Table I, entries 1–4). When no PPh_2OH was added (entry 5) the catalytic activity was negligible. Two hydroformylation products were formed, aldehydes and alcohols. The formation of alcohols requires 2 mol of H_2, and therefore most experiments were carried out with CO and H_2 in a 1:2 ratio.

The composition of the actual catalyst cannot be derived from the ratios of PPh_3 and PPh_2OH applied and the resulting activities, although a presumably unsaturated system such as that of entry 1 seems to give the highest activity. The lowest activity for isomerization was found when more saturated platinum complexes could be formed (as in, for instance, entry 2). An excess of diphenylphosphinous acid only temporarily slows down the reaction. The excess reacts with the aldehyde product to form an α-hydroxyphosphine oxide that does not interfere with the platinum complexes. Several other ligand combinations were tested; entries 8 (with $Ph_2PCH_2CO_2H$) and 9 (with PCy_3) serve as examples.

Bidentate phosphines were reported (10, 11) to have a pronounced and accelerating effect on hydroformylation with platinum trichlorostannate catalysts. In combination with platinum phosphinito complexes, the bidentate ligands dppe, dppp, and dppb (see Table I, entries 6 and 7) led to catalysts with higher rates. However, the effect is not as spectacular as that seen with the trichlorostannate complexes.

The systems based on PPh_3 and PPh_2OH led to isolable species derived from complex 1 (Scheme I), previously reported by Roundhill et al. (16). Complexes 1a–1e can be used as the catalyst precursor; the results in this case are in line with those obtained from in situ mixing (Table I, entry 10).

Table I. Hydroformylation of 1-Heptene

Exp. No.	Catalyst[a] (mmol)	Pressure (bar)	Time (h)	% Conversion (% Linear)				
				Aldehyde	Alcohol	Alkane	Isomer	Rate[b]
1	$Pt(cod)_2$ (0.1), PPh_2OH (0.1), PPh_3 (0.1)	50	1	9.8 (>90)	8.6 (>90)	0.9	30	18
2	$Pt(cod)_2$ (0.1), PPh_2OH (0.1), PPh_3 (0.2)	50	1	2.9 (>90)	6.1 (>90)	0.2	10	9
3	$Pt(cod)_2$ (0.1), PPh_2OH (0.2)	50	1	3.6 (>90)	1.8 (>90)	2.1	80	3
4	$Pt(cod)_2$ (0.1), PPh_2OH (0.4)	50	1	1.7 (>90)	5.4 (>90)	3.6	60	7
5	$Pt(cod)_2$ (0.1), PPh_3 (0.2)	50	1	<0.1	—	—	—	—
6	$Pt(cod)_2$ (0.1), PPh_2OH (0.1), dppe (0.1)	50	1	24.0 (>90)	3.1 (>90)	0.9	33	27
7	as 6, with dppp	50	1	18.0	1.8	1.4	40	20
8	$Pt(cod)_2$ (0.1), PPh_2OH (0.1), $Ph_2PCH_2CO_2H$ (0.1)	50	1	7.9	2.2	1.5	39	10
9	$Pt(cod)_2$ (0.1), PPh_2OH (0.1), PCy_3 (0.1)	50	1	3.6	2.0	1.0	50	5
10	complex 1a (0.1)	45	1.5	7.9 (90)	9.6 (80)	1.2	27	11
11	1a (0.1) 2-heptene	45	2	2.5 (71)	0.5 (66)	4.2	NA	1.5
			4	4.5 (67)	1.2 (66)	4.5	NA	1.5
			17	8.2 (51)	9.4 (77)	5.5	NA	1
12	1a (0.1) 2-heptene	94	2.5	8.1 (55)	5.8 (73)	4.8	NA	5
			5.5	8.0 (63)	15.7 (74)	5.0	NA	5

NOTE: Reaction conditions were as follows: 100-mL autoclave; 20 mL of benzene; H_2:CO ratio of 2:1; 10 mmol of 1-heptene; 100 °C. In experiments 11 and 12, 10 mmol of 2-heptene was used as the substrate. —, not determined; NA, not applicable.
[a]cod: 1,5-cyclooctadiene; dppe: 1,2-bis(diphenylphosphino)ethane; dppp: 1,3-bis(diphenylphosphino)propane; dppb: 1,4-bis(diphenylphosphino)butane; PCy_3: tricyclohexylphosphine.
[b]Rate in moles of oxo product per mole of platinum complex per hour.

1a: L = PPh$_3$
1b: L = PMePPh$_2$
1c: L = PMe$_2$Ph
1d: L = P(n-Bu)$_3$
1e: L = PPh$_2$OH
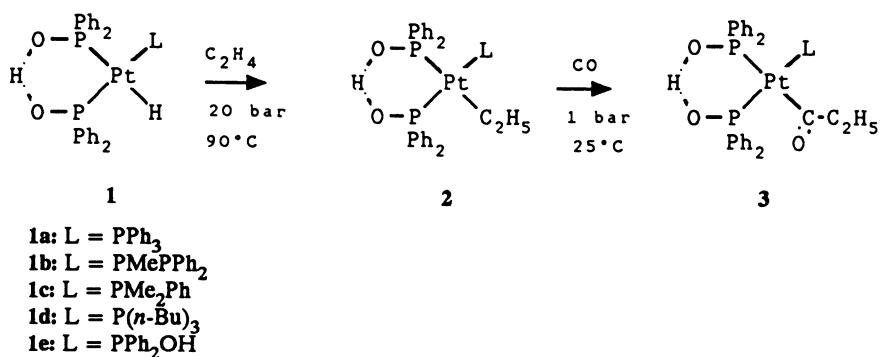
Scheme I.

So far the results are very similar to those reported for the platinum–tin catalysts; both the rates and the high selectivities for linear products are very much alike. The platinum phosphinito catalysts differ from the platinum–tin systems in two ways: the secondary reaction to alcohols attains appreciable rates and, more importantly, the present catalysts are also active in the conversion of internal alkenes. The complexes have a high activity for isomerization (*see* Table I). For the hydroformylation of terminal alkenes this activity is, in fact, a drawback. The rare combination of a high preference for the formation of terminal oxo products and an isomerization activity under carbon monoxide pressure leads to an active catalyst for the hydroformylation of internal alkenes to linear products.

In Table I, experiment 11, an average linearity as high as 70% in the oxo products is observed. Unfortunately, the hydrogenation activity also increases at the same time. This combination gives rise to less desirable alkane formation. Entries 11 and 12 clearly show that alcohols are secondary products (vide infra for a more detailed explanation), and also that alkane formation occurs mainly at the beginning of the catalytic run.

Isolation of Intermediates

Several hydrides with structures similar to 1 have been prepared and characterized (structures 1a–1e). These hydrides react with ethene under pressure (20 bar, 90 °C) to give the ethyl complexes. Intramolecular reactions with phosphinoalkenes 4 have shown that alkene insertion is a smooth reaction giving phosphaplatinacycloalkenes 5 and 6 (Scheme II) (*17*).

These chelating alkyl complexes are very robust and even resist insertion of carbon monoxide. We were not able to isolate the alkyl complexes of nonchelating alkenes other than ethene. However, the alkyl complexes could be trapped as the acyl complexes [C(O)C$_2$H$_5$, C(O)C$_3$H$_7$, and C(O)C$_7$H$_{15}$] by supplying a CO pressure to solutions of the hydride and the alkene. The

$X = -, CH_2, OC_2H_4$
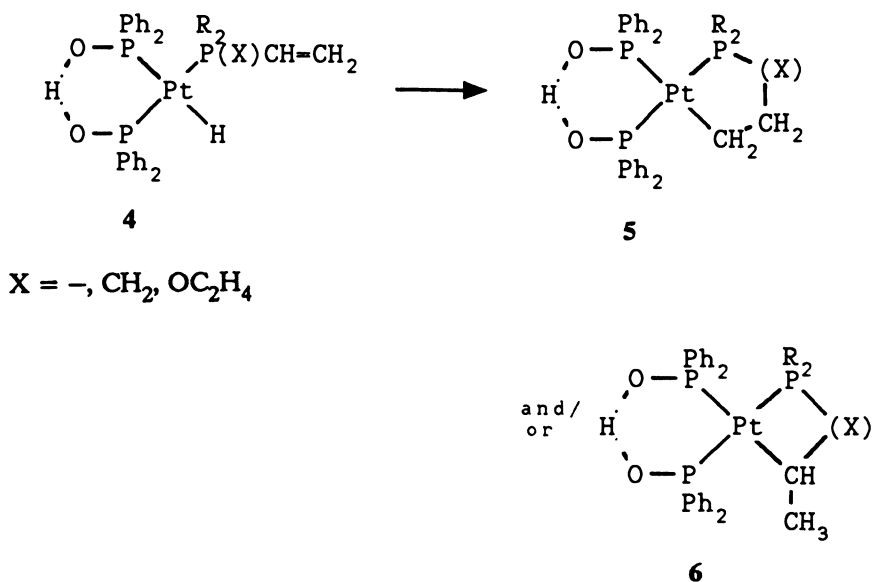
Scheme II.

ethyl complexes **2a–2e** can also be converted to the propionyl derivatives by admission of 1 bar of CO at 25 °C. Acyl complexes **3a–3e** were prepared by this method.

From consideration of the ^{1}H NMR spectra of the butyric complex **7** (Scheme III), we conclude that the linear isomer is formed exclusively, not only in the catalytic experiment but also in the stoichiometric reaction. We assume that the formation of the linear isomer of the acyl is kinetically controlled because we do not expect a large difference in stability between the linear and branched acyl complexes. In the alkyl complexes the linear isomers are most likely thermodynamically favored. Comparison of the ^{31}P NMR spectra obtained from the solutions after a catalytic hydroformylation run revealed that they are the sum of the spectra of the hydride and acyl species together with some decomposition products.
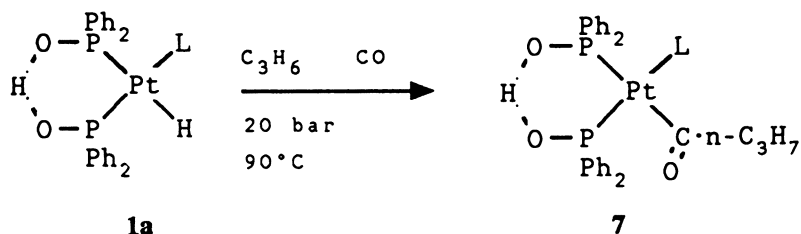
Scheme III.

Catalysts based on dppe display somewhat higher activity (entries 6 and 7, Table I) than those based on monophosphines such as PPh_3. Accordingly, we synthesized platinum hydride complexes based on dppe (or dppp) and PPh_2OH that turned out to have structure **8** (Scheme IV). The hydride **8** did not lead to ethyl complexes after reaction with ethene at 30 bar. Reaction at 85 °C under 20 bar of ethene:CO (1:1) gave the propionyl complex **9** within 0.5 h.

L = PPh_2O
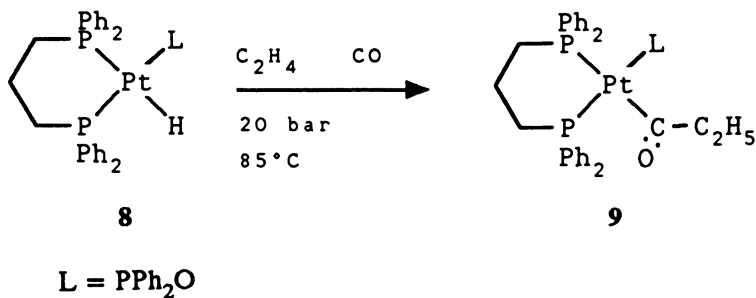
Scheme IV.

Decomposition Studies; Formation of Phosphido Species

Prolonged hydroformylation (24 h) caused complete decomposition, and a very complex ^{31}P NMR spectrum was recorded. This spectrum showed the presence of at least four species, all containing platinum dimers with a phosphido bridge. During work-up through column chromatography all were converted into **12** (Scheme V). This compound's structure was established by an X-ray determination (*18*).
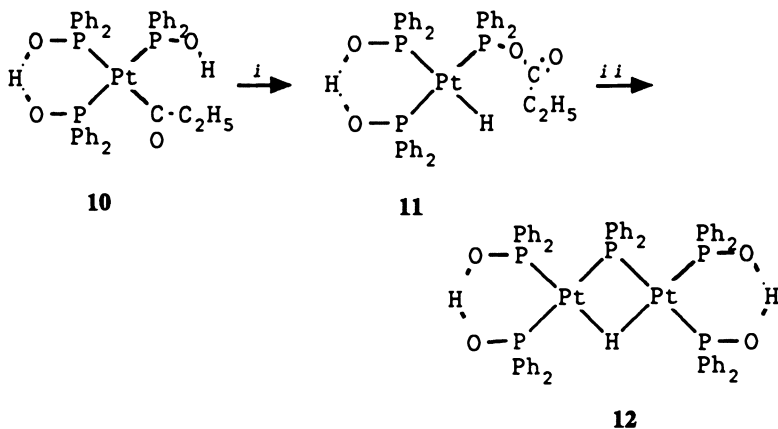
Scheme V. i: 90 °C, 20–50 bar of H_2, CO, and C_2H_4; ii: 1e added, C_2H_5COOH and PPh_2OH removed.

Decomposition of triarylphosphine to phosphido species is a common reaction often encountered in catalytic reactions using phosphine complexes of noble metals (*17*). When the present hydroformylation reaction for ethene was run for 24 h, traces of propionic acid were found instead of the decomposition products to be expected from aryl groups of the added phosphines.

^{1}H NMR analysis showed that indeed roughly one propionic acid molecule had been formed per mole of platinum dimer after work-up. From this and other evidence, it was concluded that the diphenylphosphido anion originates from diphenylphosphinous acid ("diphenylphosphine oxide"; *see* Scheme V, complexes **10–12**). This reaction is quite surprising because the phosphine–oxygen double bond is extremely stable toward cleavage. The scheme involves the formation of a mixed anhydride of a carboxylic acid and phosphinous acid. Such complexes have been observed in the reaction mixture. An alternative way to form complexes of phosphinous carboxylic acid anhydrides **11** is the treatment of phosphinous acid complexes with acetic anhydride. Indeed, addition of acetic anhydride to refluxing **1a** or **1e** in toluene gave the characteristic red color and ^{31}P NMR spectra of the dimeric complex **12** and its analogues within 15 min.

These results show that $Pt(\mu\text{-}H)(\mu\text{-}PPh_2)Pt$ is a stable bonding unit that is preferentially formed under severe conditions. In addition, we have seen that diphenylphosphinous acid can be reduced by platinum acyl complexes.

Aldehyde Reduction

The catalytic conversion of aldehydes into alcohols during the hydroformylation of alkenes suggests that the present platinum phosphinito complexes are catalysts for the reduction of aldehydes in the presence of CO. Very few known catalysts affect this reaction in the presence of CO; phosphine-modified cobalt catalysts are the most familiar example. Ruthenium and rhodium catalysts (notably in the absence of CO) have also been reported (*19, 20*).

When complex **1e** was tested as a hydrogenation catalyst for aldehydes, we accidentally found that very fast catalysts can be obtained when carboxylic acids are present in these catalyst systems (*see* Table II, entries 2 and 3). The highest rates were obtained in the absence of CO, but at 5 bar of CO the rates were acceptable (entry 8). In the hydroformylation experiments the rate of hydrogenation was only in the order of ten moles of aldehyde per mole of catalyst per hour, but this time turnover frequencies of several thousands were obtained. Even for acetone a turnover frequency of 500 mol mol^{-1} h^{-1} was found, but in the absence of acetic acid the rate of 2-propanol formation was negligible.

The addition of carboxylic acids has no rate-enhancing effect on the hydroformylation reaction. This fact was shown in a hydroformylation experiment with ethene as the substrate; the rate remained the same and the

Table II. Hydrogenation Results

Exp. No.	1e (mmol)	Acid (mmol)	i-C₃H₇COH (mmol)	Solvent (mL)	Rate[a]
1	0.02	i-C$_3$H$_7$COOH (4)	110	ethanol (20)	1000
2	0.02	i-C$_3$H$_7$COOH (9)[b]	110	toluene (20)	4500
3	0.02	i-C$_3$H$_7$COOH (9)[b]	220	none	9000
4	0.02	CH$_3$COOH (0.1)	22	toluene (20)	220
5	0.01	none	275[c]	acetone	<10
6	0.02	CH$_3$COOH (10)	275[c]	acetone	500
7	0.01	i-C$_3$H$_7$COOH (5)	220	none	2800
8	0.01	as 7, with 5 bar CO			1100

NOTE: The reaction took place in a 100-mL Hastelloy C autoclave at 95 °C and 40 bar of H$_2$.
[a]Average rate in moles of alcohol product per mole of catalyst per hour, measured over 30–50% conversion.
[b]Undistilled substrate; contains 4% isobutyric acid.
[c]With acetone as the substrate.

product was pure 1-propanol. The complexes formed with the carboxylic acids have not yet been identified. However, preliminary studies seem to indicate that the acids only play a role during the catalytic cycle without the intermediacy of any complexes.

Mechanism of Aldehyde Reduction

Two intermediates have been proposed for aldehyde reduction: alkoxide and hydroxymethyl late transition metal complexes (21–28). We now discuss the mechanism of the aldehyde hydrogenation reaction in a model compound with o-diphenylphosphinobenzaldehyde (29) as the substrate.

o-Ph$_2$PC$_6$H$_4$CHO has been employed in reactions with Vaska's complex (30) and PtCl$_2$ (31) to give oxidative addition of the aldehyde to the metal. When Pt(Ph$_2$PO)(Ph$_2$POH)$_2$H (1e) was treated with o-diphenylphosphino-benzaldehyde (32), one of the Ph$_2$POH ligands was immediately replaced. The resulting product showed that insertion of the aldehyde into the platinum hydride bond had occurred (Scheme VI). NMR spectroscopy proved that the complex formed contains a platinum alkoxide bond in a six-membered ring and not a hydroxymethyl platinum bond in a five-membered ring, although the latter would be sterically favored.
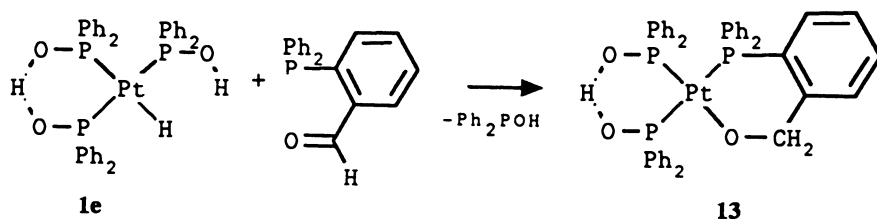
Scheme VI.

Several platinum alkoxides have been prepared (*21, 23*) via metathesis reactions, but they have never been obtained via aldehyde insertions. These reactive species are labile with respect to β-hydrogen elimination (*33*). In complex **13** the alkoxide is entropically stabilized by the chelating phosphine.

We propose that the intermediates are platinum alkoxides in the catalytic reaction as well. The role of the added carboxylic acids may well be to liberate the alcohol via protonolysis. The intermediate platinum carboxylates formed require hydrogenation to the hydride complexes and acid, but this is a facile reaction. Stronger acids have a negative effect, if any, as might be expected. Strong acids react with platinum hydrides to give platinum salts.

Weak carboxylic acids have no effect on the rate of hydroformylation because the platinum acyl bond is relatively resistant to protonolysis. Stronger acids may enhance this reaction, but hydride regeneration may again be difficult. The hydroformylation reaction has a different mechanism for dihydrogen activation. This mechanism presumably involves a direct reaction with dihydrogen and the acyl complex.

Current knowledge throws new light on the secondary aldehyde hydrogenation reaction observed during hydroformylation. We have seen that decomposition of the hydroformylation catalyst leads to the formation of carboxylic acids. It would seem that this decomposition product has a promoting effect on the aldehyde hydrogenation.

References

1. Schwager, I.; Knifton, J. F. *J. Catal.* **1976**, *45*, 256.
2. Hsu, C. Y.; Orchin, M. *J. Am. Chem. Soc.* **1975**, *97*, 3553.
3. Anderson, G. K.; Clark, H. C.; Davies, J. A. *Inorg. Chem.* **1983**, *22*, 427.
4. Anderson, G. K.; Clark, H. C.; Davies, J. A. *Organometallics* **1982**, *1*, 64.
5. Tang, S.; Kim, L. *J. Mol. Catal.* **1982**, *14*, 231.
6. Ruegg, H. J.; Pregosin, P. S.; Scrivanti, A.; Toniolo, L.; Botteghi, C. *J. Organomet. Chem.* **1986**, *316*, 233.
7. Albinati, A.; Von Guten, U.; Pregosin, P. S.; Ruegg, H. J. *J. Organomet. Chem.* **1985**, *295*, 239.
8. Scrivanti, A.; Berton, A.; Toniolo, L.; Botteghi, C. *J. Organomet. Chem.* **1986**, *314*, 369.
9. Scrivanti, A.; Cavinato, G.; Toniolo, L.; Botteghi, C. *J. Organomet. Chem.* **1985**, *286*, 115.
10. Kawabata, Y.; Hayashi, T.; Ogata, I. *J. Chem. Soc., Chem. Commun.* **1979**, 462.
11. Hayashi, T.; Kawabata, Y.; Isoyama, T.; Ogata, I. *Bull. Chem. Soc. Jpn.* **1981**, *54*, 3438.
12. Cramer, R. D.; Jenner, E. L.; Lindsey, R. V.; Stolberg, U. G. *J. Am. Chem. Soc.* **1963**, *85*, 1691.
13. Mrowca, J. J. U.S. Patent Application 3 876 672, 1975.
14. van Leeuwen, P. W. N. M.; Roobeek, C. F.; Wife, R. L.; Frijns, J. H. G. *J. Chem. Soc., Chem. Commun.* **1986**, 31.
15. van Leeuwen, P. W. N. M.; Roobeek, C. F. European Patent Application EP 82 576, 1983; *Chem. Abstr.* **1983**, *99*, 121813.

16. Beaulieu, W. B.; Rauchfuss, T. B.; Roundhill, D. M. *Inorg. Chem.* **1975**, *14*, 1732.
17. Garrou, P. E. *Chem. Rev.* **1981**, *81*, 229.
18. van Leeuwen, P. W. N. M.; Roobeek, C. F.; Frijns, J. H. G.; Orpen, A. G. *Organometallics* **1990**, *9*, 1211.
19. Strohmeier, W.; Weigelt, L. *J. Organomet. Chem.* **1978**, *145*, 189.
20. Tani, K.; Suwa, K.; Tanigawa, E.; Yoshida, T.; Okana, T.; Otsuka, S. *Chem. Lett.* **1982**, 261.
21. Bryndza, H. E.; Calabrese, J. C.; Marsi, M.; Roe, D. C.; Tam, W.; Bercaw, J. E. *J. Am. Chem. Soc.* **1986**, *108*, 4805.
22. Bernard, K. A.; Atwood, J. D. *Organometallics* **1989**, *8*, 795.
23. Bryndza, H. E.; Tam, W. *Chem. Rev.* **1988**, *88*, 1163.
24. Park, S.; Pontier-Johnson, M.; Roundhill, D. M. *J. Am. Chem. Soc.* **1989**, *111*, 3101.
25. Bryndza, H. E.; Fong, L. K.; Paciello, R. A.; Tam, W.; Bercaw, J. E. *J. Am. Chem. Soc.* **1987**, *109*, 1444.
26. Hoffman, D. M.; Lappas, D.; Wierda, D. A. *J. Am. Chem. Soc.* **1989**, *111*, 1531.
27. Kim, Y-J.; Osakada, K.; Sugita, K.; Yamamoto, T.; Yamamoto, A. *Organometallics* **1988**, *7*, 2182.
28. Arnold, D. P.; Bennett, M. A. *Inorg. Chem.* **1984**, *23*, 2110.
29. Schiemenz, G. P.; Kaack, H. *Justus Liebigs Ann. Chem.* **1973**, *9*, 1480.
30. Landvatter, E. F.; Rauchfuss, T. B. *Organometallics* **1982**, *1*, 506.
31. Rauchfuss, T. B. *J. Am. Chem. Soc.* **1979**, *101*, 1045.
32. van Leeuwen, P. W. N. M.; Roobeek, C. F.; Orpen, A. G. *Organometallics* **1990**, *9*, 2197.
33. Bennett, M. A.; Yoshida, T. *J. Am. Chem. Soc.* **1978**, *100*, 1750.

Rhodium-Catalyzed Carbonylation of Methyl Acetate

Joseph R. Zoeller[1], James D. Cloyd[1], Norma L. Lafferty[1], Vincent A. Nicely[1], Stanley W. Polichnowski[1], and Steven L. Cook[2]

[1]Research Laboratories and [2]Tennessee Eastman Acid Division, Eastman Chemical Company, Kingsport, TN 37662

In principle, the rhodium-catalyzed carbonylation of methyl acetate involves the types of transformations found in the conversion of methanol to acetic acid, namely the activation of a normally unreactive methyl group, insertion of carbon monoxide, and recombination with the initial leaving group. However, several significant differences become apparent upon switching from the well-documented aqueous methanol carbonylation to the anhydrous methyl acetate carbonylation to acetic anhydride. A mechanism based primarily upon high-pressure kinetic and infrared data is proposed. The operational and mechanistic similarities and differences involved in the carbonylation of methanol to acetic acid and the carbonylation of methyl acetate to acetic anhydride will be discussed, as well as the historical development of the process.

Aᴄᴇᴛɪᴄ ᴀɴʜʏᴅʀɪᴅᴇ ʜᴀs ʙᴇᴇɴ ɢᴇɴᴇʀᴀᴛᴇᴅ ᴄᴏᴍᴍᴇʀᴄɪᴀʟʟʏ by the thermal cracking of acetic acid to ketene and subsequent reaction with acetic acid to render acetic anhydride. The Eastman Chemical Company successfully used this process in Kingsport, Tennessee, for more than 60 years. However, our development of a commercial process for the carbonylation of methyl acetate to acetic anhydride (1) has replaced this older technology as the method of choice in the last decade.

The concept of carbonylating methyl acetate to acetic anhydride is not new; it was initially demonstrated almost 40 years ago at BASF (2). However these processes, which used Co, Ni, or Fe, were never adequate for commercial purposes. Following the success of the Rh-catalyzed carbonylation

of methanol described by Monsanto (3–8), processes demonstrating commercially viable rates finally began to appear in the patent literature in the early 1970s. Several patent applications were published in very rapid succession by Halcon (9), Ajinomoto (10), Showa Denko (11, 12), and Hoechst (13). The claims in these patents covered all Group VIII metals, but clearly favored Rh.

In a similar program we had narrowed our catalyst choices to Ni, Pd, and Rh. Negotiations with Halcon to combine our technologies ultimately resulted in the merger of research and development efforts in 1980. This agreement was followed within a year by the announcement of Eastman's intentions to construct a plant in Kingsport, Tennessee, for the carbonylation of methyl acetate to acetic anhydride. The plant bore a nameplate capacity for 225 thousand metric tons (KMT) per year of acetic anhydride. Production began in March 1983.

We have successfully operated this process, generally in excess of nameplate capacity, for more than 8 years. The plant, which can coproduce in excess of 70 KMT per year of acetic acid, uses coal as its sole source of carbon. The operation has been a resounding success, and an expansion of the facility doubled its capacity in mid-1991.

These complex plants for the conversion of coal to acetic anhydride required a myriad of creative chemical and engineering innovations to make the process commercially viable. Among these innovations was the development of an iodine-promoted rhodium catalyst system. Although it bears significant similarities to the well-known Monsanto methanol carbonylation to acetic acid (3–9), several unique requirements distinguish it from the earlier Monsanto system.

Unlike the earlier rhodium-catalyzed carbonylation of methanol, the carbonylation of methyl acetate required the addition of a salt (or salt precursor) and the addition of a reducing agent to achieve and maintain commercially viable rates (1, 14). These additional requirements, when applied to the commercially practiced aqueous methanol carbonylation, are reported to have little effect upon the catalysis (5, 15). We felt that a clear understanding of the factors affecting this catalytic process was imperative. Therefore we undertook a detailed mechanistic investigation with high-pressure kinetics and in-line high-pressure infrared spectroscopy as probes.

Experimental Procedures

Kinetic Measurements. The following procedure is typical for a kinetic run. A solution of consisting of 676.5 g (9.14 mol) of methyl acetate, 220.5 g (3.67 mol) of acetic acid, and 57 mL (130 g, 0.92 mol) of methyl iodide was added to a Hastelloy B autoclave equipped with a high-pressure condenser and a liquid sampling loop. To this mixture was added 0.62 g of $RhCl_3 \cdot XH_2O$ (2.53 mmol of Rh) and 25.39 g (0.190 mol) of anhydrous LiI. The autoclave was sealed, flushed thoroughly with nitrogen, then pressurized to 100 psi of 5% H_2 in CO,

and a flow rate of 2.0 mol h⁻¹ was established through the condenser. The reaction was heated to 190 °C. Upon reaching the desired temperature, the mixture was pressurized to 750 psi with 5% H_2 in CO and a sample was removed immediately via the sampling loop. Thereafter, the pressure was maintained by using 5% H_2 in CO as feed gas, and samples were removed every 30 min. The samples were analyzed by gas chromatography (GC). Because this reaction is reversible, rates were determined by using the method of initial rates with data up to 30% of completion.

High-Pressure Infrared Spectroscopy. A Hastelloy B autoclave with Hastelloy B plumbing throughout and heat-traced lines was equipped with a gas inlet and an outlet for a pump suitable for use under high pressure. A small portion of the reaction mixture was pumped through a loop containing a heated IR flow cell constructed from 6-mm polycrystalline MgF (Irtran 1; Eastman Kodak) or polycrystalline ZnS (Irtran 2; Eastman Kodak) windows. IR spectra were recorded with a Fourier transform infrared (FTIR) spectrometer. Results were analyzed by using a linear regression technique to remove solvent interferences (16).

Equilibrium Measurements for Metal Salts and Methyl Acetate. An acetic acid solution was prepared to attain a 1 M concentration of all of the following components: methyl acetate, acetic anhydride, p-dichlorobenzene (internal standard), and either lithium iodide or sodium iodide. A series of samples was placed in an aluminum heating block that was filled with oil to increase thermal transfer and maintained at 190 °C. Samples were removed and quenched by chilling in a cold-water bath every 30 s for the first 5 min, then every 1 min thereafter for an additional 10 min. Several samples were retained in the bath for 3 h to positively ascertain the equilibrium constant. The heating rate was determined and corrected for in all kinetic measurements. The rate constants were determined by using a published method (17).

Results and Discussion

The rhodium-catalyzed carbonylation of methyl acetate to acetic anhydride gave a selectivity of >95% after accounting for recovered methyl acetate. Modifications made after this study achieved a selectivity well in excess of 99%. The product is accompanied by the formation of low levels of ethylidene diacetate (1,1-diacetoxyethane), acetone, carbon dioxide, and methane. A typical reaction profile for the carbonylation of methyl acetate is shown in Figure 1 along with a statement of typical reaction conditions.

The thermodynamic parameters for the carbonylation of methyl acetate are much less favorable than those for the carbonylation of methanol. Calculated values of the free energy (ΔG_{298}) and heat of reaction (ΔH_{298}) at 298 K for the methyl acetate carbonylation are ΔG_{298} = –2.5 kcal mol⁻¹ and ΔH_{298} = –12.1 kcal mol⁻¹ as compared to ΔG_{298} = –17.8 kcal mol⁻¹ and ΔH_{298} = –28.8 kcal mol⁻¹, respectively, for methanol carbonylation. Because of this low thermodynamic driving force, the reaction does not go to completion. It reaches an equilibrium that is a function of temperature and carbon monoxide pressure.
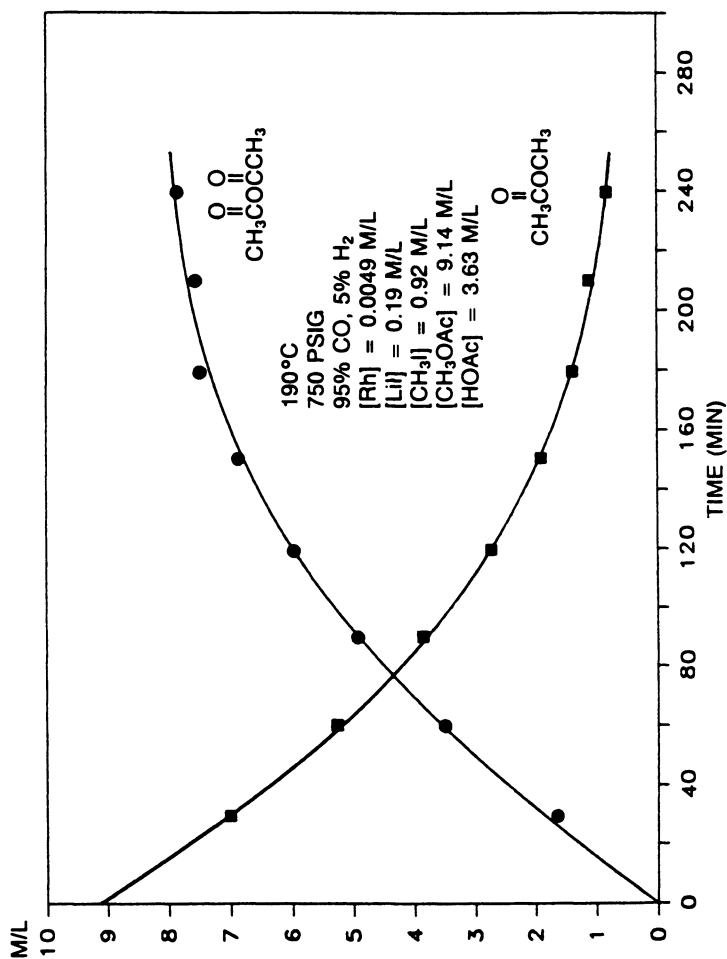
Figure 1. Typical reaction profile for the carbonylation of methyl acetate to acetic anhydride.

Our mechanistic studies utilized both high-pressure kinetics and high-pressure infrared spectroscopy. Under the conditions in Figure 1, the high-pressure infrared spectrum displayed bands at 2055 and 1984 cm^{-1} that are consistent with the formation of $Rh(CO)_2I_2^-$. This catalytically active species was identified by Monsanto during mechanistic examinations of the methanol carbonylation (3).

Our initial working mechanistic hypothesis for the methyl acetate carbonylation was a minor modification of the well-studied and well-accepted catalytic cycle for the carbonylation of methanol presented by Forster and others (3–8). The catalytic cycles for the Rh-catalyzed carbonylation of methanol and the modifications needed for adaptation to methyl acetate carbonylation are presented in Scheme I. (The required changes are indicated in parentheses.) We successfully repeated the stoichiometric reactions described by Forster (3, 6–8) for the Rh-induced conversion of methyl iodide to acetyl iodide.

Temperature Dependence. Our examination of temperature dependence strengthened the relationship between methanol carbonylation and methyl acetate carbonylation. By using the reaction composition and gas mixtures shown in Figure 1, we examined the effect of temperature between 170 and 210 °C. A log rate vs. inverse temperature (Arrhenius) plot indicated that the reaction had an energy of activation $E_a = 15.4$ kcal mol^{-1}, with an enthalpy of activation $(\Delta H^{\ddagger}) = 14.4$ kcal mol^{-1} and entropy of activation $(\Delta S^{\ddagger}) = -27$ eu. These values compared remarkably well with the reported parameters for the carbonylation of methanol: $E_a = 14.7$ kcal mol^{-1}, $\Delta H^{\ddagger} = 13.6$ kcal mol^{-1}, and $\Delta S^{\ddagger} = -32$ eu (18). These results indicate that the rate-determining step (the oxidative addition of methyl iodide to $Rh(CO)_2I_2^-$) is probably common to both processes.

The methyl acetate and methanol carbonylations apparently share a common catalytically active species- and rate-limiting step. The interesting portions of this investigation were not the similarities, but understanding the differences between the two systems. Unlike the methanol carbonylation, the methyl acetate carbonylation requires a reducing agent, such as hydrogen, and a salt (or salt precursor) to attain and sustain high reaction rates.

Hydrogen Effect. Figure 2 shows the rate of formation of acetic anhydride, with pure carbon monoxide and with 5% hydrogen in carbon monoxide as feed gas. Clearly, the addition of hydrogen removes a significant induction period and maintains a more consistent reaction rate. The induction period can vary considerably from run to run. In continuous processes the reaction rate steadily deteriorates with pure CO. With the addition of hydrogen, the reaction rate remains constant.

The high-pressure infrared spectrum using 5% hydrogen displays bands at 2055 and 1984 cm^{-1} that are consistent with the presence of $Rh(CO)_2I_2^-$.
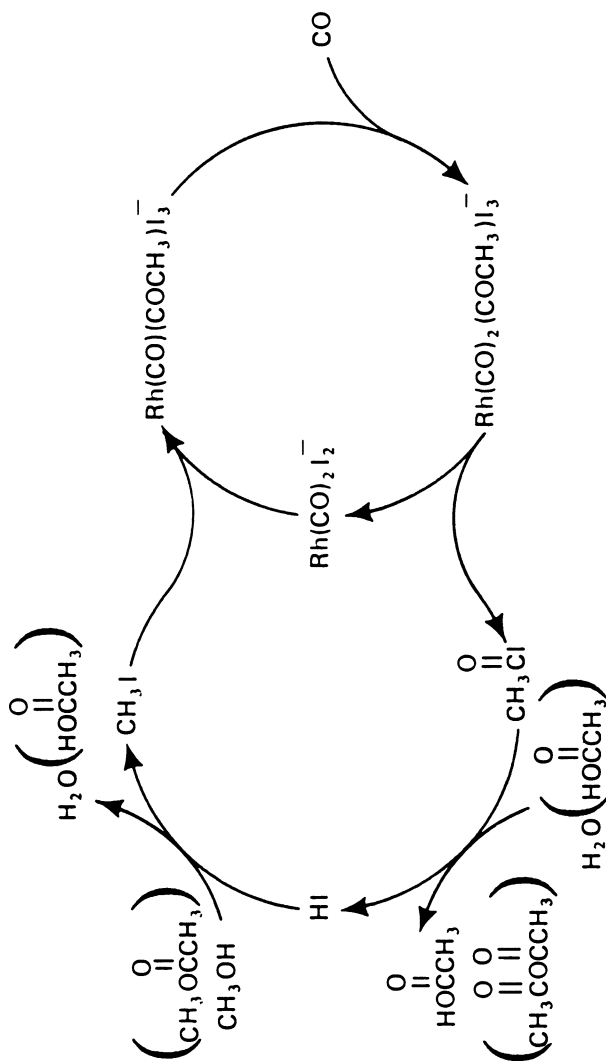
Scheme I. Mechanism for the carbonylation of methanol. The proposed changes necessary to adapt this mechanism to the carbonylation of methyl acetate are noted in parentheses.
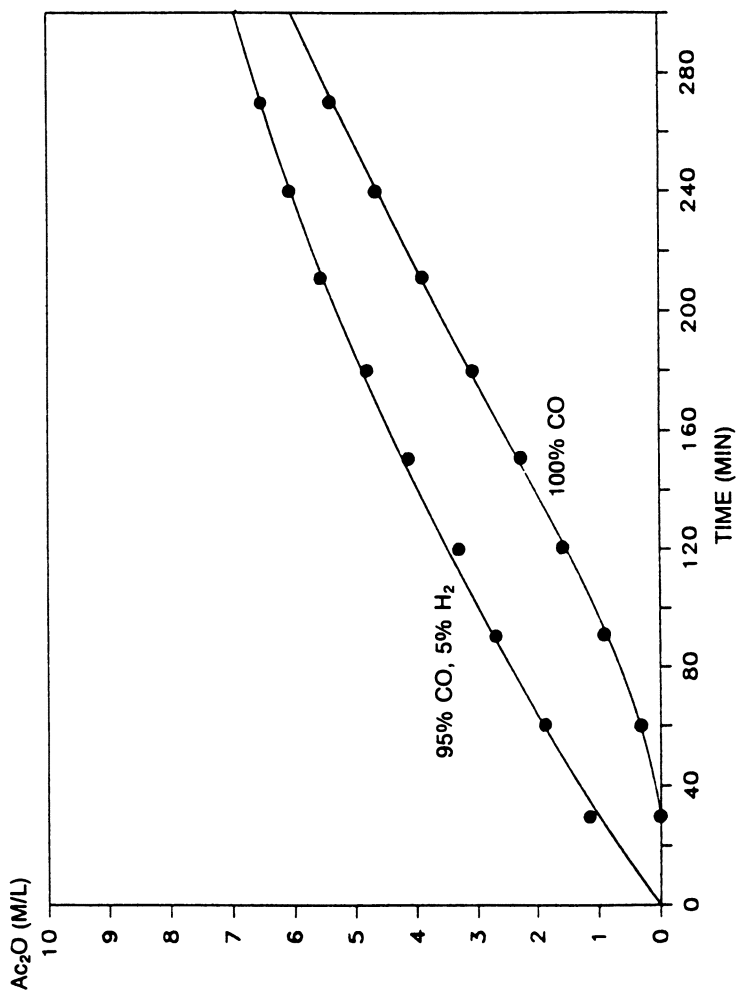
Figure 2. Effect of hydrogen on rate.

When pure CO is used, the high-pressure infrared spectrum displays the same bands with an additional band at 2087 cm^{-1}. This band indicates Rh(CO)$_2$I$_4^-$, which is inactive in the carbonylation. This peak increases as the reaction progresses. If small amounts of hydrogen are introduced into the reactor while a pure CO run is underway, the peak at 2087 cm^{-1} rapidly disappears and the rate is accelerated.

The application of high-pressure infrared spectroscopy has been reported in the related triphenylphosphine-promoted system with a pure CO feed (*19*). Our results with pure CO feeds are consistent with the published work. However, the earlier investigators were unaware of the hydrogen effect and consequently did not report any spectra under these conditions.

Iodocarbonyl complexes of rhodium are excellent catalysts for the water–gas shift reaction (*5*). Traces of water were reported to be responsible for the presence of the reduced species. The water would generally be added with the catalyst, and small quantities of water are likely to be present in the reagents. We agree with this interpretation. Addition of small amounts of water at the beginning of the reaction, before any acetic anhydride is formed, will reduce the induction period and produce a temporary rate acceleration. Once acetic anhydride formation begins, water is effectively scavenged and the accelerated rate is not maintained. The water–gas shift accounts for the lack of any required auxiliary reducing agent in methanol carbonylation because it is run in an aqueous media.

The addition of hydrogen extracts a penalty, however, as acetic anhydride is slowly hydrogenated to acetaldehyde and acetic acid. The acetaldehyde subsequently reacts with a mole of the acetic anhydride product to generate ethylidene diacetate, which constitutes the major impurity in this process. The rate of ethylidene diacetate formation was found to be a direct function of the hydrogen level.

Cationic Promoter. The second significant difference between the methanol and methyl acetate carbonylations is that the methyl acetate carbonylation requires the presence of a cation. At the outset of our efforts to identify active catalyst systems, we examined innumerable promoters. However, much of this investigation and the external reports (*19–22*) preceded our knowledge of the need for hydrogen in achieving and maintaining acceptable catalyst activity. A representative list of promoters that we reexamined after this knowledge was attained appears in Table I.

We recognized the need for a cationic promoter early in our studies. However, an understanding of the role of the cation was very slow to emerge. Our mechanistic study focused on the alkali metals, particularly lithium, because they demonstrated fast rates and were structurally simple.

Our initial kinetic measurements using lithium iodide as a promoter indicated that the reaction was a complex function of lithium iodide, methyl iodide, and rhodium. Like the Monsanto carbonylation of methanol, the rate

Table I. Comparison of Selected Cationic Promoters

Cationic Promoter	Relative Rate
None	1.0
Li$^+$	9.2
Na$^+$	6.3
Bu$_4$N$^+$	4.9
Bu$_4$P$^+$	6.0
Al^{3+}	7.4
Zn^{2+}	1.4
Mg^{2+}	5.5

NOTE: Conditions: temperature, 175–190 °C; pressure, 750 psig; feed gas composition, 5% H$_2$–95% CO; initial concentrations of feed materials: [Rh], 4.9×10^{-3} M; promoter concentration, 0.19 M; [MeI], 0.92 M; [MeOAc], 9.14 M; [AcOH], 3.63 M. The promoter was added as the iodide, except in the case of Al, where the acetate was used.

of methyl acetate carbonylation is independent of carbon monoxide pressure above 500 psi. This complex behavior contrasts with the aqueous methanol carbonylation, which is a kinetically simple reaction demonstrating first-order dependencies on rhodium and methyl iodide.

The source of this complex behavior was most clearly seen when the reaction rate was examined as a function of added lithium iodide. This comparison, using two different rhodium levels, is represented in Figure 3.

The reaction was characterized by an initial surge in the reaction rate as lithium was added, followed by a period in which the addition of more lithium iodide produced a negligible response. Next we examined the effect of the remaining two rate-determining factors at two levels of lithium iodide: 0.19 M (a region of little response to lithium) and 0.02 M (a region of high lithium response). Graphic depictions of the rate dependency on rhodium and methyl iodide at these two lithium iodide levels appear in Figures 4 and 5, respectively.

Figure 4 clearly shows a first-order reaction in rhodium at the higher lithium levels. However, at the lower lithium levels the rate is nearly independent of rhodium between 1.25 and 5.0 mM Rh.

The rate dependency upon methyl iodide, displayed in Figure 5, showed a similar pattern. At 0.02 M lithium, the reaction was nearly independent of the methyl iodide level between 0.4 and 2.0 M CH$_3$I. However, the rate was slightly less than first order (~0.86 when calculated from the plot in Figure 4) and had a nonzero intercept with respect to methyl iodide at the higher lithium levels.

Changes in Rate-Determining Step.

Initially, this behavior was rather puzzling. The results at the higher lithium levels seemed to support our original assumption that this reaction rate was related to methanol carbonylation, even though we were disturbed by the slight deviation from
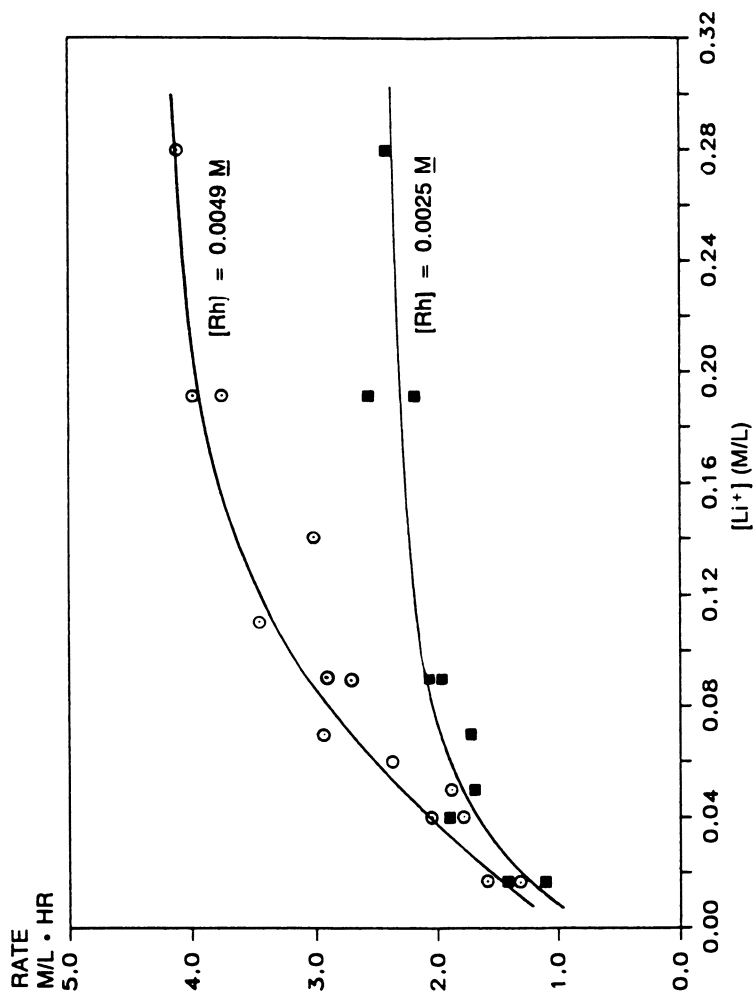
Figure 3. Effect of lithium iodide level on rate.
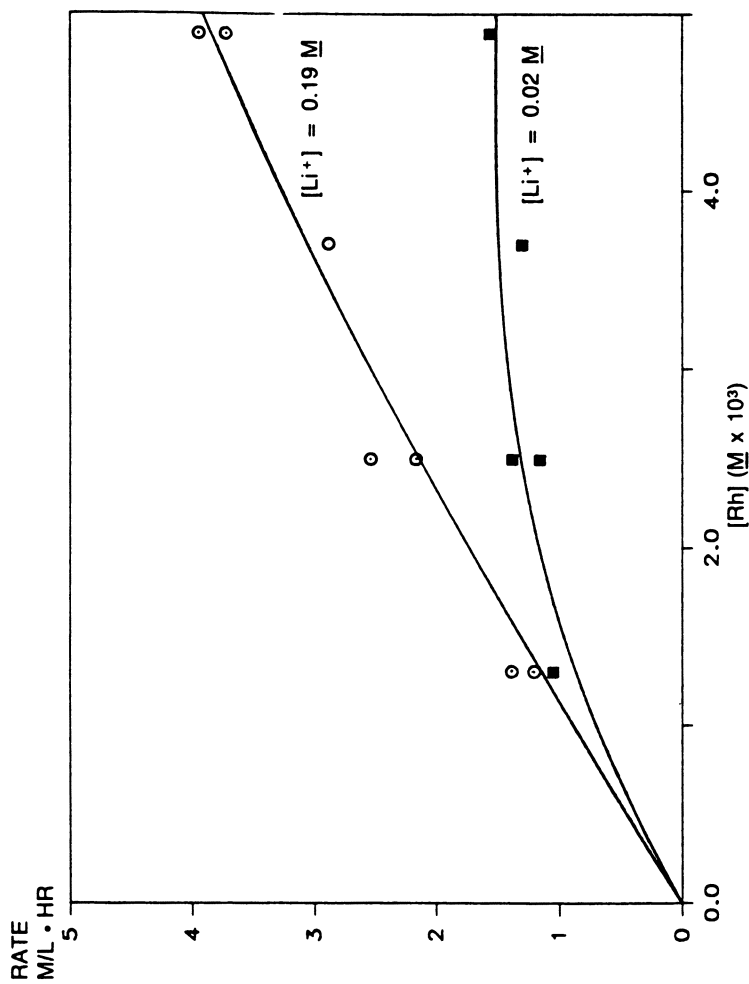
Figure 4. Dependence of rate on Rh at two Li levels.

RATE
M/L • HR

[Li⁺] = 0.19 M

[Li⁺] = 0.02 M

[CH₃I] (M/L)
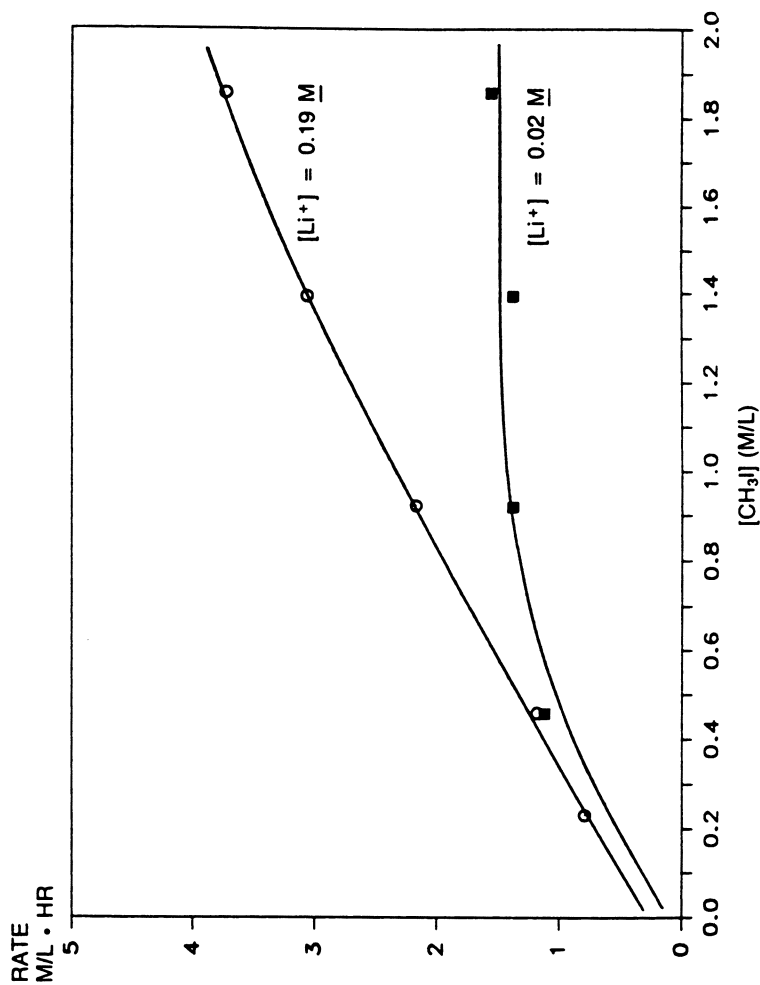
Figure 5. Dependence of rate on MeI at two Li levels.

first-order dependence with respect to methyl iodide. However, the results at the lower lithium iodide levels seemed to indicate some alteration in the rate-determining step at the lower lithium levels.

To this point there was no indication that our initial hypothetical mechanism was incorrect or incomplete. Therefore, we initially thought that the change in the rate-determining step might result from a change in the catalyst form. In the absence of sufficient iodide, the catalyst might form a mixture of $Rh(CO)_3I$ (which would be expected to be much less active) and the active catalyst, $Rh(CO)_2I_2^-$. The result would be a net rate suppression. We reexamined the high-pressure infrared spectra in the absence of Li and in the presence of low levels of Li.

In the absence of a cationic promoter and with $[Rh(CO)_2I]_2$ as a Rh source, we observed the temperature- and pressure-dependent equilibrium between $[Rh(CO)_2I]_2$ and $Rh(CO)_3I$ previously described by Morris and Tinker (23). In this solvent system, the peaks for $Rh(CO)_3I$ were located at 2086 (s) and 2063 (m) cm^{-1} and the peaks for $[Rh(CO)_2I]_2$ were located at 2099 (m), 2083 (s), and 2031 (s) cm^{-1}. However, the introduction of even small quantities of LiI (Li:Rh = 2.5:1) eliminated the peaks assignable to these neutral species. The change left a clean spectrum of $Rh(CO)_2I_2^-$, as evidenced by peaks at 1984 and 2055 cm^{-1}. This observation effectively eliminated this possibility in the mechanism.

Next we examined the high-pressure infrared behavior of the low-lithium system in the absence of hydrogen. The spectroscopic behavior mirrored the behavior at higher lithium levels, including the clean conversion of residual $Rh(CO)_2I_4^-$ to $Rh(CO)_2I_2^-$ upon the addition of hydrogen. However, at lower Li levels the conversion of all the Rh to the active $Rh(CO)_2I_2^-$ by hydrogen was no longer accompanied by an increase in reaction rate.

This loss of any kinetic correlation with the proposed active rhodium catalyst or methyl iodide indicated that the rate-limiting step at low lithium levels was not related to the rhodium species and probably was outside the rhodium cycle. Therefore, we turned our attention to the cycle involving the conversion of methyl acetate and acetyl iodide to acetic anhydride and methyl iodide.

Methyl Acetate and Acetyl Iodide Activation.

By using NMR techniques, we examined the equilibrium shown in reaction 1.

$$AcI + MOAc \rightleftarrows MI + Ac_2O \qquad (1)$$

where M is H, Li, or Na. When HI was added to acetyl anhydride, the HI was converted completely to acetyl iodide within the limits of the NMR experiment. This conversion indicated that, with HI, the equilibrium lies >99% in favor of acetyl iodide and that acetic acid is a poor scavenger of acetyl iodide. However, when lithium acetate was added to a solution of

acetyl iodide, the lithium acetate quantitatively consumed the acetyl iodide and the equilibrium lies well in favor of acetic anhydride. We concluded that, in the absence of lithium, the iodine promoter was likely to accumulate as acetyl iodide. However, the lithium salt efficiently converted the acetyl iodide to acetic anhydride.

This conversion did not completely satisfy the kinetic picture with respect to lithium. The reaction of lithium acetate with acetyl iodide, essentially instantaneous at room temperature, was too fast to account for the dependence on lithium. The sole process left was the reaction of methyl acetate with lithium iodide. We examined the equilibrium between methyl acetate and lithium iodide, shown in reaction 2, at 190 °C.

$$MeOAc + LiI \rightleftarrows MeI + AcOLi \qquad (2)$$

We determined both the equilibrium constant (K_{463} = 0.388) and a value of the forward rate constant (k_f = 8.0 ± 0.9 L mol^{-1} h^{-1}). The value of the forward rate constant indicates that when the lithium iodide level is low (e.g., LiI = 0.02 M) the reaction with lithium iodide becomes rate-limiting. Methyl iodide is then consumed faster than it can be regenerated. There is a transitional region in which the oxidative addition of methyl iodide to rhodium and the reaction of lithium iodide both enter the rate expression and would behave like a series of consecutive reactions.

Difference Between Cationic Promoters. This equilibrium (reaction 2) helped us to understand the source of the difference between cationic promoters. The kinetics of the methyl acetate carbonylation can be examined by using sodium in place of lithium. The sodium system, even at 0.2 M NaI, behaves like a low-lithium system and thus is dependent on sodium concentration over a large range. The equilibrium constant for reaction 2 if lithium is replaced by sodium is 0.0419, and the forward rate constant is 2.6 ± 0.2 L mol^{-1} h^{-1}.

Clearly, the rate of converting sodium iodide and methyl acetate to methyl iodide and sodium acetate is involved in determining the rate of sodium-promoted carbonylations. Although we have compared only sodium and lithium, we believe that the same principles would apply to comparing the remaining promoters. Estimates of the equilibrium constant for a number of iodide salts have been recorded elsewhere (2, 24).

The measurements around reaction 2 were also useful in explaining the observed deviation from first-order dependence upon added methyl iodide at higher lithium levels. If the rate of acetic anhydride formation is plotted as a function of the calculated methyl iodide levels at equilibrium, the deviation from first-order behavior at the higher lithium levels completely disappears (Figure 6).

RATE MOL/L/HR
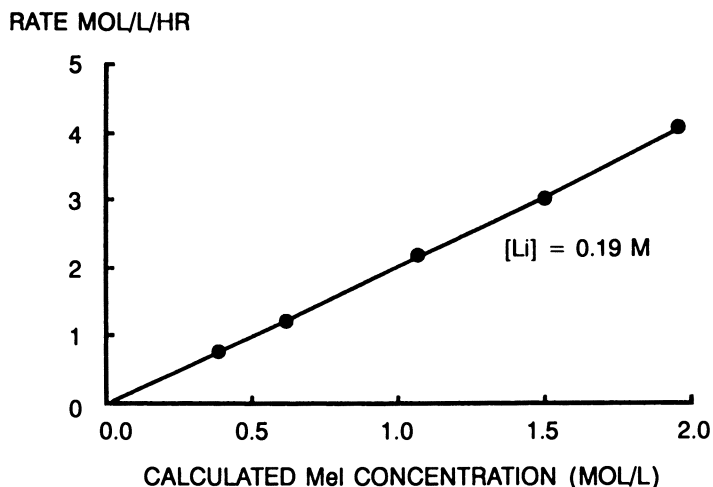
Figure 6. Dependence of rate on MeI; values were calculated at equilibrium.

Potential Role of Rhodium Dianions.   Although it seemed unlikely, considering the kinetics for lithium dependence already shown in Figure 4, we felt one more potential mechanism should be considered. We had already discounted the equilibrium between $Rh(CO)_3I$ and $Rh(CO)_2I_2^-$ because of the high-pressure infrared spectra. However, an equilibrium between $Rh(CO)_2I_2^-$ and a spectroscopically undetected $Rh(CO)_2I_3^{2-}$, which would be expected to be more nucleophilic and therefore more reactive, could be responsible for the lithium effect.

After our initial disclosure of the lithium effect (*1, 7*), workers at Celanese reexamined the effect of LiI in the methanol carbonylation by using a low-water process. They proposed the same process to explain the acceleration they observed upon the addition of lithium (*25–27*).

We tested this hypothesis by measuring the reaction rate as a function of added lithium iodide, with a constant total iodine (Figure 7). The reaction rate was not accelerated as we attained very high lithium levels, but was actually slightly suppressed with additional LiI. This slight rate decrease could be anticipated on the basis of the results of the equilibrium study for reaction 2. The higher initial levels of LiI would be expected to slightly suppress the level of methyl iodide available for the rate-limiting oxidative addition. This experiment clearly discounts the possible role of $Rh(CO)_2I_3^{2-}$.

Proposed Catalytic Cycle.   In light of the contribution the lithium-catalyzed conversion of acetyl iodide to methyl iodide makes in determining the rate, we were forced to revise our initial conjecture on the mechanism by adding a third cycle that includes the lithium reaction. This mechanism appears in Scheme II. We have left the nonlithium-catalyzed cycle in our
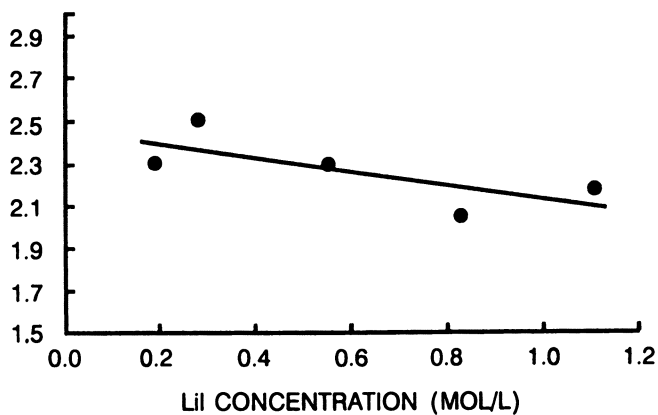
Figure 7. Dependence of rate on LiI at constant total I.
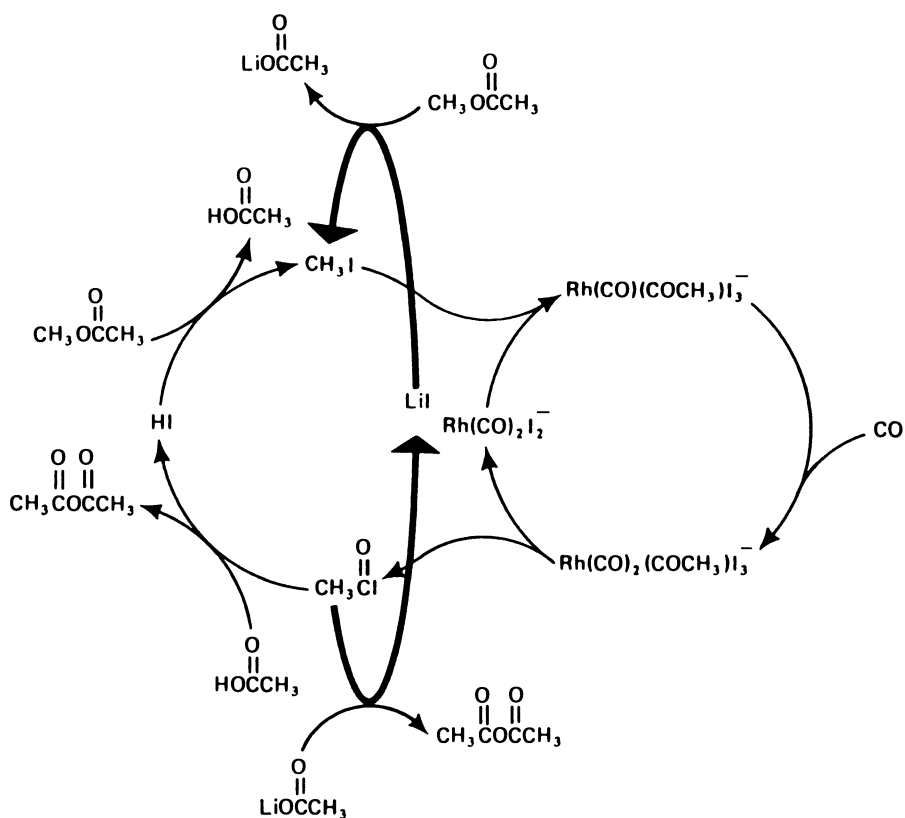
Scheme II. Proposed mechanism of the carbonylation of methyl acetate to acetic anhydride.

proposed mechanism because, with both lithium and sodium, we still obtain a finite rate ($\sim$0.4–0.8 mol L^{-1} h^{-1}) upon extrapolation to zero levels of cation. Thus, the noncation-assisted cycle is a lesser, but not a negligible, contributor to the rate.

Conclusion

We have delineated the differences between the carbonylation of methyl acetate and methanol. A summary of the effects of different parameters with high levels of lithium, along with a comparison to commercial aqueous methanol carbonylation, appears in Table II. This chapter provides substantial evidence for a mechanistic proposal involving contributions from

- a rhodium-catalyzed conversion of methyl iodide to acetyl iodide, which is identical to that delineated by Forster in the carbonylation of methanol to acetic acid;
- a cation-accelerated net conversion of acetyl iodide to methyl iodide, which represents one of the key differences between the carbonylation of methanol and the carbonylation of methyl acetate; and
- a conversion of acetyl iodide to methyl iodide, which is analogous to that already described for the methanol carbonylation.

Table II. Parameters in the Carbonylation of Methyl Acetate and Methanol

Parameter	Effect On MeOAc Carbonylation	Effect on MeOH Carbonylation
[Rh]	First order	First order
[MeI]	First order	First order
Temperature	E_a = 15.4 kcal mol^{-1}	E_a = 14.7 kcal mol^{-1}
Pressure	0 order	0 order
Hydrogen	(a) Generates and maintains Rh(I) (b) Generates ethylidene diacetate	No effect
Cation	(a) Generates anionic Rh (b) Contributes to methyl group activation by accelerating AcI consumption and displacing alkyl methyl group from the ester (c) Displays a dependence upon concentration and form of cation	No effect in commercial system (positive effect at very low water)

References

1. Polichnowski, S. W. *J. Chem. Educ.* **1986**, *63*, 206.
2. Gauthier-Lafaye, J.; Perron, R. *Methanol and Carbonylation*, (English Translation); Editions Technip: Paris, and Rhone-Poulenc Recherches: Courbevoie, France, 1987; Chapter 7.
3. Dekleva, T. W.; Forster, D. *Adv. Catal.* **1986**, *34*, 81.
4. Gauthier-Lafaye, J.; Perron, R. *Methanol and Carbonylation*; (English Translation); Editions Technip: Paris, and Rhone-Poulenc Recherches: Courbevoie, France, 1987; Chapter 6.
5. Eby, R. T.; Singleton, T. C. *Appl. Ind. Catal.* **1983**, *1*, 275.
6. Forster, D. *Adv. Organomet. Chem.* **1979**, *17*, 255.
7. Forster, D. *Ann. N. Y. Acad. Sci.* **1977**, *295*, 79.
8. Forster, D.; Hershman, A.; Morris, D. E. *Catal. Rev.–Sci. Eng.* **1983**, *23*(1 and 2), 89.
9. Halcon International, Belgian Patent 819 455, 1973.
10. Ajinomoto, Japanese Kokai 50 030 820, 1973.
11. Showa Denko, Japanese Kokai 50 042 921, 1973.
12. Showa Denko, Japanese Kokai 50 042 922, 1973.
13. Hoechst, German Offenlegungsschrift 2 450 965, 1973.
14. Eastman Kodak, U.S. Patent 4 374 070, 1983.
15. Forster, D.; Singleton, T. C. *J. Mol. Catal.* **1982**, *17*, 299.
16. Efroymson, M. A. In *Mathematical Methods for Digital Computers*; Ralston, A.; Wilf, H. S., Eds.; Wiley: New York, 1960; Volume 1, Chapter 17, p 191.
17. Dye, J. L.; Nicely, V. A. *J. Chem. Educ.* **1971**, *48*, 443.
18. Hjortkjaer, J.; Jensen, V. W. *Ind. Eng. Chem. Prod. Res. Dev.* **1976**, *15*, 46.
19. Luft, G.; Schrod, M.; Grobe, J. *J. Mol. Catal.* **1983**, *22*, 169.
20. Schrod, M.; Luft, G. *Ind. Eng. Chem. Prod. Res. Dev.* **1981**, *20*, 649.
21. Luft, G.; Ritter, G.; Schrod, M. *Chem.-Ing.-Tech.* **1982**, *54*, 758.
22. Luft, G.; Schrod, M. *J. Mol. Catal.* **1983**, *20*, 175.
23. Morris, D. E.; Tinker, H. B. *J. Organomet. Chem.* **1973**, *49*, C53.
24. Shina, H.; Hashimoto, T. *Yukagaku* **1980**, *29*, 901.
25. Smith, B. L.; Torrence, G. P.; Murphy, M. A.; Aquilo, A. *J. Mol. Catal.* **1987**, *39*, 115.
26. Murphy, M. A.; Smith, B. L.; Torrence, G. P.; Aquilo, A. *J. Organomet. Chem.* **1987**, *303*, 257.
27. Murphy, M. A.; Smith, B. L.; Torrence, G. P.; Aquilo, A. *Inorg. Chim. Acta* **1985**, *101*, L47.

Electronic Effects on the Synthesis, Structure, Reactivity, and Selectivity of Rhodium Hydroformylation Catalysts

Alexis A. Oswald[1,+], Dan E. Hendriksen[2], Rodney V. Kastrup[3], and Edmund J. Mozeleski[4]

[1]Enimont America, Inc., R&D Center, Monmouth Junction, NJ 08852
[2]Exxon Chemical Company, Baytown, TX 77522–4900
[3]Exxon Research and Engineering Company, Annandale, NJ 08801
[4]Exxon Chemical Company, Annandale, NJ 08801

Steric effects of phosphine and phosphite ligands on carbonylhydridorhodium catalysts have been considered. However, the electronic effects were not considered systematically. We studied rhodium complexes of phosphorus ligands of varying strengths of coordination via sigma donation and pi back-donation. For example, we compared complexes of Ph_3P, Ph_2PEt, $PhPEt_2$, Et_3P, and $(EtO)_3P$. In general, complexes of strongly σ-donating aliphatic phosphine ligands required a high temperature for their activation by ligand dissociation and showed a high total (normal plus iso) aldehyde selectivity. In contrast, pi back-donation by triarylphosphines and particularly by phosphite esters led to a very high normal-to-iso ratio of aldehydes derived from α-olefins but also led to more undesired olefin hydrogenation and isomerization. The results can be explained with a consistent, overall framework of rhodium hydroformylation mechanisms involving complexes of different carbonylation degrees.

TERTIARY PHOSPHINE AND PHOSPHITE ESTER COMPLEXES of rhodium hydroformylation catalysts are attractive candidates for studying electronic and steric effects on catalyst activity and selectivity. Both the electronic and steric environments of rhodium can be greatly changed by an appropriate choice of phosphorus ligands. The electronic and sometimes the steric effects

+Deceased

of phosphorus ligands will be considered here from the viewpoint of catalyst activity–selectivity and equilibrium between the two carbonylhydridorhodium catalyst precursors.

$$(R_3P)_3Rh(CO)H \rightleftarrows [(R_3P)_2Rh(CO)H] \leftrightarrows$$

$$(R_3P)_2Rh(CO)_2H \rightleftarrows [(R_3P)Rh(CO)_2H] \quad (1)$$
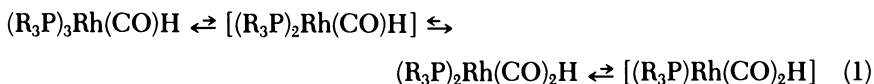
Steric effects of phosphorus ligands have been extensively studied in low-pressure rhodium hydroformylation. The electronic effects were not considered broadly and systematically. In the scientific literature, electronic effects are often described in papers devoted mainly to reaction mechanisms and stereochemistry. Sometimes electronic and steric effects cannot be clearly distinguished. Therefore, in this literature review, interrelated steric and electronic effects and mechanistic considerations are often discussed as a whole. In the area of triarylphosphine ligands, a large number of such publications are available.

Rhodium Hydroformylation Catalysts

Selectivity for Linear Aldehydes. The high selectivity of aromatic phosphine–rhodium complexes for the production of linear (n-) aldehydes via α-olefin hydroformylation has been identified as a consequence of the *trans* configuration of two rather bulky phosphorus ligands in a coordinatively unsaturated square-planar carbonylhydridorhodium species (1–3). To estimate the steric requirements of *tert*-phosphine ligands, Tolman (4) developed the cone angle concept, which has been widely used in studies of steric effects. Pruett and Smith (5) observed early that the use of even bulkier ortho-substituted triaryl phosphite ester ligands such as tris-(o-phenoxyphenyl) phosphite leads to a reduced aldehyde linearity (i.e., a decreased normal-to-iso (n:i) product ratio.

$$RCH=CH_2 \xrightarrow{CO/H_2} RCH_2CH_2CHO + RCH(CH_3)CHO \quad (2)$$

More recently Van Leeuwen and Roobeek (6, 7) showed that such bulky ligands (e.g., tris-(o-tert-butylphenyl) phosphite) have an increased activity in the hydroformylation of linear internal and branched terminal olefins. They suggested that, for steric reasons, only two highly bulky ligands could be coordinated to the same rhodium. Therefore, such ligands could increase the coordinative unsaturation of rhodium and thus lead to a higher catalyst activity.

A number of coordinatively unsaturated carbonylrhodium complexes of bulky and highly basic and branched trialkylphosphine ligands were described by Otsuka and co-workers (8–10) and by Freeman and Young (11).

Young patented the use of some such ligands (specifically tricyclohexyl-phosphine) as improved rhodium hydroformylation catalyst ligands for internal and terminal monobranched olefins at medium pressure (*12*). Rhodium complexes of bulky trialkylphosphine ligands such as tri-*sec*-butylphosphine and preferably tricyclohexylphosphine were studied by Tau as stable catalysts for the continuous low-pressure hydroformylation of 2-butene and are claimed as such in U.S. Patent 4 605 781 (*13*). The activity of these catalysts was clearly attributable to the stereochemistry rather than the basicity of the ligands.

Stereochemical Effects. Unruh, Christenson, Hughes, and Young (*14–16*) also investigated phosphine ligands for rhodium hydroformylation, mainly to observe stereochemical effects. These researchers were particularly interested in the selective rhodium hydroformylation of 1-*n*-olefins in the presence of bidentate phosphine ligands of a chelating character. However, they obtained some comparative data with monophosphine ligands as well. Unruh and co-workers (*14*, *15*) showed in a study of *m*- and *p*-phenyl-substituted bis(diphenylphosphino)ferrocene ligands that the use of the more basic aromatic phosphine ligands in rhodium hydroformylation leads to lower n:i ratios of aldehyde products. An increase of the H_2–CO pressure at constant H_2:CO ratio also resulted in lower n:i ratios (*14*). Similar results were obtained with a series of *p*-substituted triphenylphosphine ligands by Moser and co-workers (*17*).

Unruh and co-workers found little difference between the high n:i ratios (~7) of the products of the rhodium hydroformylation of 1-hexene in the presence of either excess triphenylphosphine or ethyldiphenylphosphine. Under similar conditions, a significantly lower n:i ratio (~5) was obtained in the presence of trioctylphosphine (*14*). A relatively low ratio of *n*- to *i*-aldehydes was also obtained by Bahrmann and Fell (*18*) when using tri-ethylphosphine in high-pressure rhodium hydroformylation.

Hughes and Young (*16*) suggested the formation of a more highly carbonylated rhodium complex in the presence of the more basic phosphines. They pointed to the key role of a tris(phosphine)–rhodium complex in selective hydroformylation. Their studies of the *trans*-chelated carbonylhy-dridorhodium complexes of bis(phosphine) ligands by ^{31}P NMR showed the coordination of three phosphorus moieties to one rhodium. However, they proposed a mechanism in which the active catalytic species is a carbonyl-free rhodium hydride generated from this complex via CO rather than phosphine ligand dissociation.

Working with triphenylphosphine and its *p*-substituted derivatives at a P:Rh ratio of 6.6 under 13.6 atm of H_2–CO pressure, Moser and co-workers (*17*) concluded on the basis of cylindrical internal reflectance–Fourier transform infrared (CIR–FTIR) spectroscopy studies that the main catalyst precursor was $(Ar_3P)_2Rh(CO)_2H$. They proposed that CO dissociation from this

complex provides the key reactive coordinatively unsaturated intermediate of selective rhodium hydroformylation.

Alkyldiphenylphosphine–Rhodium Complexes.

In the area of alkyldiphenylphosphine–rhodium complexes, we carried out a long-term systematic investigation (19–25) of both electronic and steric effects. These investigations included ^{31}P and ^{13}CO NMR studies under H_2–CO pressure of the catalyst systems (19–22). On the basis of results of our studies and related prior work, we proposed an overall mechanism of rhodium-complex-catalyzed hydroformylations, explaining the formation of both n- and i-aldehyde products. This mechanism was later extended to trialkylphosphines and will be discussed later.

We observed that because of their increased σ-electron donor ability (i.e., basicity) n-alkyldiarylphosphine complex catalysts are more stable and less active than triarylphosphine complexes at comparable temperatures (20–23). We also found that the n:i selectivity of branched alkyldiarylphosphine complexes and the equilibria between the major carbonylhydride complexes are very much dependent on the site and the degree of their branching (i.e., steric crowding in the vicinity of their P atoms) (22–25). Alkyldiphenylphosphine ligands branched at their α- or β-alkyl carbon atoms, including cyclohexyldiphenylphosphine, were found to form bis(phosphine)– rather than tris(phosphine)–carbonylhydridorhodium complexes under simulated hydroformylation conditions. As a consequence, they were more active catalyst ligands for hydroformylation but led to the formation of aldehyde products having lower n:i isomer ratios (25, 26).

More recently, our studies were extended to other types of phosphorus ligands. The new results to be discussed largely provide information on the electronic effects of trialkylphosphines and trialkyl phosphites.

Electron-Donor Properties.

Electron-donor properties of phosphorus ligands in transition metal complexes can best be described in terms of the basicities of the free ligands as characterized by their half neutralization potentials (HNP). A specific method of determining HNPs in reference to a standard, diphenylguanidine, was first developed by Streuli (27, 28). Essentially the same method was broadly utilized later by Thorsteinson and Basolo (29) and by Allman and Goel (30). π-Electron-accepting properties were particularly studied by Verkade (31), who mainly used phosphite esters of specific stereochemistry.

As indicated by the literature references discussed, broad correlations between the electronic properties of different types of phosphorus ligands and their catalytic behavior were not studied systematically, and the results were not obtained under comparable conditions. However, it can be concluded from the work of Bahrmann and Fell (18), Pruett and Smith (5), Unruh et al. (14, 15), Yoshida et al. (8–10), and Freeman and Young (11, 12)

that rhodium complexes of strongly basic trialkylphosphines are less active low-pressure hydroformylation catalysts than weakly basic triarylphosphines. The total aldehyde selectivity of trialkylphosphine complexes is higher, but they provide a less linear product mixture, even in the absence of steric hindrance. Triarylphosphines of different basicities were studied by many groups. It can be stated, particularly on the basis of studies by Unruh (*14*, *15*), Moser (*17*), and their co-workers, that less basic aromatic phosphines are more active and provide more linear products.

The present study of electronic effects of phosphorus ligands in rhodium hydroformylation was carried out to observe such effects in broad ranges of temperature and ligand concentration. A critical step of our hydroformylation mechanism is reversible phosphorus or CO ligand dissociation from carbonylhydridorhodium complexes to generate reactive, coordinatively unsaturated species. Such a dissociation obviously depends on the coordinative bond strength of the ligand and the temperature. High-temperature hydroformylation was of particular interest to us because the distillation of the aldehyde products is an industrially preferred method of separating them from the nonvolatile rhodium complex catalysts. With higher boiling aldehydes, more stable catalyst systems are required.

Proposed Reaction Mechanism and Ligand Effects

Before a specific discussion of the experimental results, our previously proposed rhodium hydroformylation mechanism will be generalized for phosphorus ligands. The coordination of both *tert*-phosphine and phosphite ester ligands to rhodium will be considered, together with that of CO and hydride ligands.

Our work on rhodium complex olefin hydroformylation catalysts was focused on carbonylhydridorhodium complexes of tertiary phosphine and phosphite ester ligands. A generic formula of these pentacoordinated rhodium complexes is shown by Scheme I. The trivalent phosphorus ligands are the most important structural variable, determining catalyst activity and selectivity.

CO Ligands and Catalyst Function. We postulate that the presence of at least one of the CO ligands is essential for the functioning of the catalyst (i.e., the introduction of CO into the olefin reactant). Depending on the number of CO ligands, one to three phosphorus ligands are also present in the modified complex. The presence of phosphines generally increases the strength of metal-to-CO coordination and thus allows hydroformylation catalysis at low pressure. Depending on their electronic properties and stereochemistry, phosphine ligands also have a major effect on the activity and selectivity of hydroformylation catalysts.

y = 1 - 3 $(R_3P)_y$ ── Rh ── $(CO)_{4-y}$ 4 - y = 1 - 3

For CO Stabilization | **For CO Introduction**
                                           H

Activity &   - R_3P ↓↑

Selectivity Control

                               $(R_3P)_{y-1}$ ── Rh ── $(CO)_{4-y}$
                                           |
                                           H

                                     Olefin
                                     Insertion:

                          Rh   Rh
                          | |
                  $CH_3CH_2CH_2$ CH_3CHCH_3
                          ↓   ↓
  normal $CH_3CH_2CH_2CHO$ CH_3CHCHO **Iso**
                                                    |
                                                   CH_3
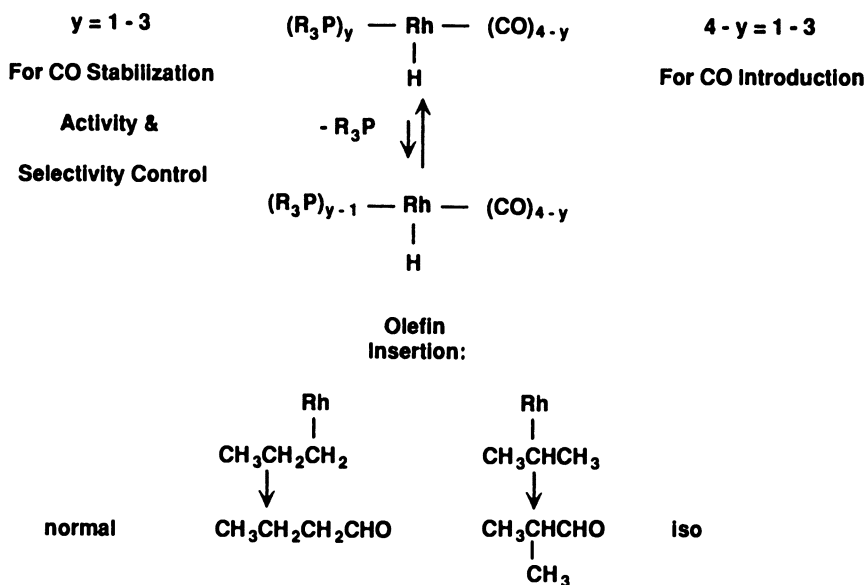
Scheme I. Generic formula of rhodium complex hydroformylation catalysts.

Scheme I shows that coordinatively unsaturated, reactive intermediates are formed via reversible dissociation reactions of such pentacoordinated carbonylhydride complexes, usually via phosphine dissociation. The resulting species can then be reversibly complexed with the olefin reactant, leading to olefin insertion into the metal hydride bond. Such an insertion results in the formation of either a normal alkyl or a secondary alkyl derivative. These derivatives in turn are converted via a series of fairly well-known reactions to n- and i-aldehyde products, respectively. We found that the key problems and opportunities in this type of catalysis are the control of reaction temperature (i.e., ligand dissociation, mainly by employing phosphines of appropriate electronic properties) and the control of n- versus i-aldehyde production (mainly via phosphine stereochemistry).

Our work confirmed that, in the absence of steric crowding, tertiary phosphine and phosphite ligands form pentacoordinate monocarbonylhydridorhodium complexes containing three coordinated phosphorus moieties. These complexes operate as selective α-olefin hydroformylation catalysts leading to a high ratio of normal to iso aldehydes. They are stabilized by excess free phosphorus ligand to form a stable catalyst reservoir for the generation of active species.

Mechanism of Hydroformylation Reaction.   Scheme II shows the mechanism of the rhodium-catalyzed hydroformylation reaction starting with the $(R_3P)_3Rh(CO)H$ complex. This complex undergoes reversible phosphorus
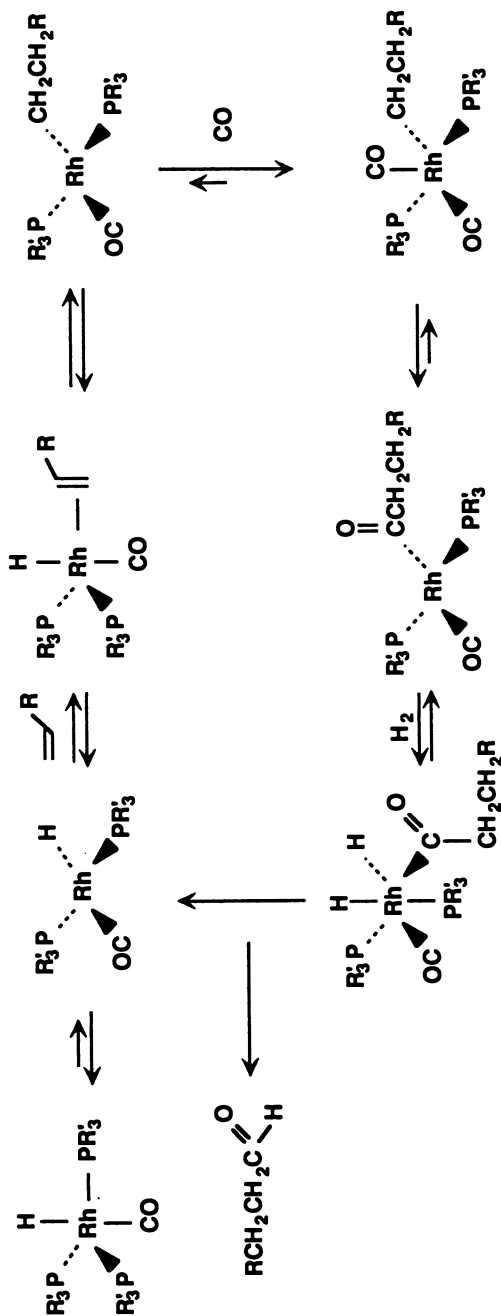
Scheme II. Mechanism of the rhodium-catalyzed hydroformylation reaction. The intermediate $L_2Rh(CO)H$ leads to linear aldehyde product.

ligand dissociation at rates dependent on the ligand and temperature employed. Such dissociations result in coordinatively unsaturated, square-planar *trans*-bisphosphine–monocarbonylhydride complexes. The reaction of such complexes with the α-olefin leads, via insertion into the Rh–H bond, to the selective formation of the key *n*-alkylrhodium intermediate. The subsequent reactions are rather well established. Reaction with CO followed by alkyl migration forms the acylrhodium compound. The latter undergoes oxidative hydrogen addition followed by aldehyde product extrusion to regenerate the initial catalyst.

The electronic and steric effects on the formation and stability of the trisphosphine–carbonylhydridorhodium precursors of selective hydroformylation catalysts are considered as illustrated by Figure 1. Molecular orbital considerations indicate that increased σ-electron donation from the phosphine—which is directly related to the basicity of the phosphine—leads to stronger bonding of both the phosphine and the CO ligands. The increased bonding to CO results from the increased flow of electrons through the rhodium to the antibonding orbitals of CO. Thus stable carbonylhydrido-rhodium complexes are formed with highly basic, tri-*n*-alkylphosphine ligands of high σ-donor ability. If the phosphorus ligand is not only donating electrons but accepting them as well, the R_3P–Rh bond strength is increased by π back-donation, but the CO–Rh bond strength is negatively affected. This is the case with weakly basic triarylphosphines and phosphites. Coordination of three phosphine ligands to the same rhodium is negatively af-

$(R_3P)_3Rh(CO)H$
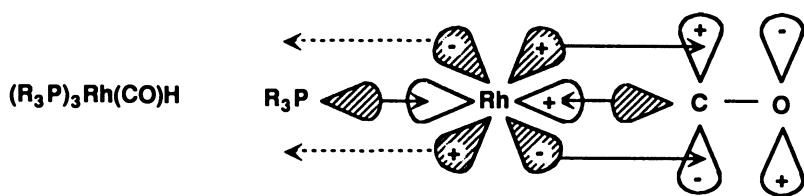
Characteristic of Phosphine	Effect on Bonding to Rhodium of	
	R_3P	CO
Electron Donation (σ)	+	+
Electron Acceptance (π)	+	-
Steric Crowding	-	+

Figure 1. Trends in bond strengths in L₃Rh(CO)H as affected by the electronic and steric properties of the phosphorus ligand.

fected by steric crowding. Thus, CO more effectively competes with bulky phosphines for multiple coordination on the rhodium.

Synthesis and NMR Studies of Catalyst Complexes

The structure, reversible dissociation, and equilibria of rhodium complex precursors of active catalyst species and their role in determining the selectivity of 1-*n*-olefin hydroformylation were developed on the basis of NMR studies under simulated hydroformylation conditions and catalysis experiments. A few of the investigations employed pure crystalline trisphosphine–carbonylhydridorhodium complexes. However, in most of the cases, halide-free carbonylhydridorhodium complexes were generated in situ, in the presence of excess stabilizing phosphorus ligand. The catalyst precursors were dicarbonylrhodium acetylacetonate and dodecacarbonyltetrarhodium.

Synthesis. Triphenylphosphine– and triphenyl phosphite–carbonylrhodium acetylacetonates (derived by reacting dicarbonylrhodium acetylacetonate acacRh(CO)$_2$, with triphenylphosphine and triphenyl phosphite, respectively) were reported as hydroformylation catalysts by Ziolkowski and co-workers (*32–34*). Our work indicated that, on reacting excess *tert*-phosphines with acacRh(CO)$_2$ in toluene solution, bis- and/or monophosphine–carbonylrhodium acetylacetonates were formed, dependent on the bulkiness of the phosphorus ligand (*23*). When these solutions were reacted with hydrogen, acetylacetonate ligand-free carbonylhydride catalyst complexes were formed, as shown by Scheme III. In the absence of steric
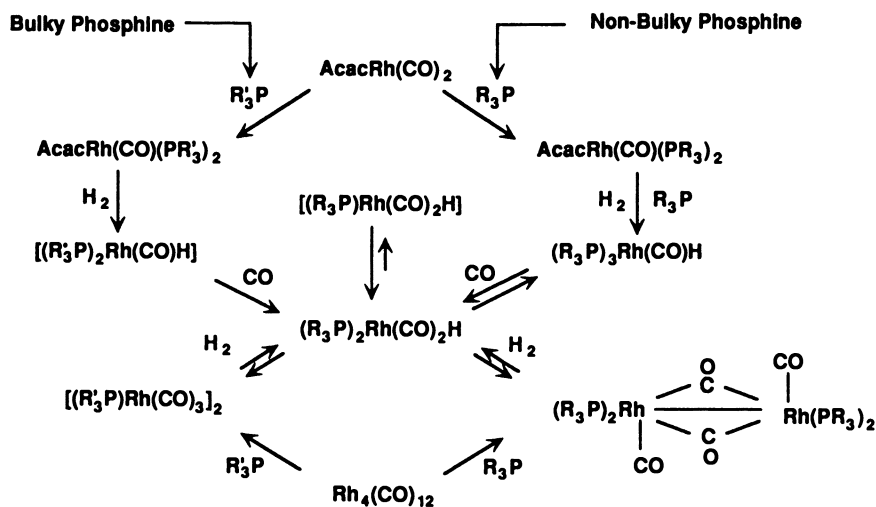
Scheme III. Key intermediates in the formation of rhodium catalysts from bulky or nonbulky phosphine ligands.

hindrance, tris(phosphine)–carbonylhydridorhodium complexes were produced in quantitative yield, even under atmospheric hydrogen pressure at ambient temperatures.

Booth et al. (35) discovered that, when dodecacarbonyltetrarhodium is reacted with equivalent or excess triphenylphosphine under CO, triphenylphosphine–carbonylrhodium dimers are formed. These dimers were successfully used as 1-alkene hydroformylation catalysts at 70 °C under 120 atm of H_2–CO pressure. In our work the carbonylrhodium dimer complex with triphenylphosphine and other sterically nondemanding *tert*-phosphine ligands was converted to the corresponding tris-(*tert*-phosphine)–carbonylhydridorhodium catalyst complex by atmospheric hydrogen in the presence of excess *tert*-phosphine ligand.

In general, the synthesis of alkyldiarylphosphine–rhodium complexes started with toluene solutions of acacRh(CO)$_2$ or Rh$_4$(CO)$_{12}$ having concentrations equivalent to 0.4% Rh. These solutions were then reacted with varying amounts of the appropriate phosphine ligand typically to provide a 9:1 P:Rh ratio and then saturated with ^{13}CO and H_2 in the 2–35-atm pressure range. All the experiments were carried out in thick-walled NMR tubes (10-mm o.d.) equipped with poly(tetrafluoroethylene) (Teflon) screw valves. ^{31}P and ^{13}C NMR spectra were obtained mostly at –30 °C with a multinuclear NMR spectrometer (JEOL FX 900). The rhodium complex structures, equilibria, and dissociation rates were primarily characterized in terms of ^{31}P and ^{13}C chemical shifts, Rh–P and P–C coupling constants, and line broadening.

The reactions studied are outlined with both bulky and nonbulky phosphines in Scheme III. The main factors in determining the structure and equilibria were steric. As such, they were discussed in some detail in a study of alkyldiphenylphosphines (23). The following discussion illustrates the electronic effects of phosphorus ligands.

NMR Studies. Carbonylhydridorhodium complexes with phosphorus ligands may have one or two carbonyl ligands coordinated to the same rhodium, as shown in Scheme IV. Due to reversible R$_3$P and CO ligand dissociation, the two coordinatively saturated carbonylhydridorhodiums are in equilibrium. In recent NMR studies of the triphenylphosphine–carbonylhydridorhodium complexes, this conclusion was confirmed by Brown and Kent (36). Bond-strength considerations indicate that the more basic σ-donating trialkylphosphines tend to form catalyst systems containing more of the dicarbonylhydridorhodium complex. Phosphine dissociation from this complex leads to nonselective monophosphine–dicarbonylhydride species. The reaction of this species with 1-butene leads to major amounts of branched valeraldehyde hydroformylation product. In contrast, the weakly basic π-bonding phosphite esters mostly form monocarbonylhydridorhodium complexes. These preferentially generate selective diphosphine–monocarbonyl-
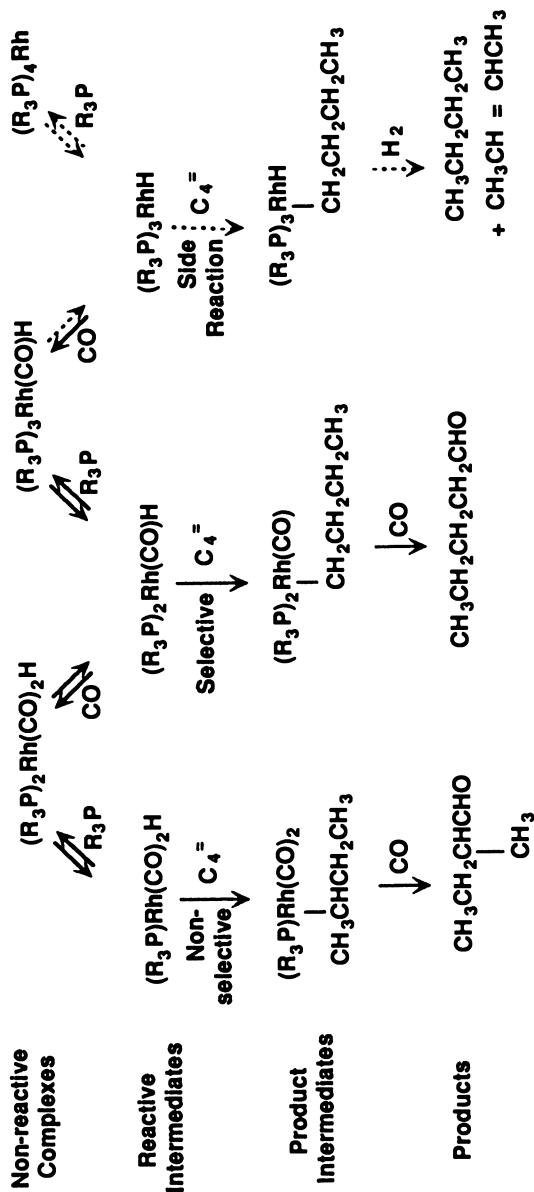
Scheme IV. Intermediates in the hydroformylation of 1-butene by rhodium–phosphine catalysts.

hydridorhodium hydroformylation catalyst species. However, they may also undergo complete CO dissociation at high temperature. This reaction results in the formation of carbonyl-free rhodium hydrides of high olefin hydrogenation and isomerization activity.

The dissociation of PR_3 and CO ligands from rhodium complexes can be studied by variable-temperature ^{31}P and ^{13}C NMR spectrometry. This capability is illustrated by Figure 2, which compares the ^{31}P proton decoupled spectra of two tris(phosphine)–carbonylhydridorhodium complexes. At -60 °C, the typical doublet signal of the phosphorus coupled to the rhodium was observed for both complexes. The doublet signal of the complex of the more basic alkyldiphenylphosphine ligand remained sharp at 35 °C; in contrast, the less basic triphenylphosphine complex exhibited a broad doublet. Further increases in the ligand exchange rates resulted in single composite signals for the Ph_3P and Ph_2PR systems at 90 and 120 °C, respectively.

Higher temperatures were clearly necessary in the Ph_2PR complex system to reach ligand exchange rates comparable to that of the Ph_3P complex. Because the increase in ligand exchange rate parallels that of complex dissociation to yield coordinatively unsaturated species, these data indicate that a comparable generation of such reactive species occurs at higher temperatures in the Ph_2PR complex systems. This conclusion suggests that higher temperatures are needed to achieve comparable hydroformylation rates when complexes of Ph_2PR are used in place of Ph_3P. On the other hand, the Ph_2PR complexes are more stable at the higher temperatures than the Ph_3P complex.

^{31}P NMR Studies.

In other experiments, trialkylphosphine complexes of rhodium were also studied by ^{31}P NMR. These experiments were done to show the effect of H_2–CO pressure on the equilibria among the various complexes formed when a mixture of 1 mol of dicarbonylrhodium acetylacetonate and 9 mol of triethylphosphine is reacted with CO and H_2. The first experiment used a toluene solution of the acetylacetonate, which was first equilibrated under 4.3 atm of ^{13}CO and then pressured with an additional 4.3 atm of H_2. Because of the resulting ^{13}CO enrichment of the complexes formed, not only the large coupling due to the rhodium but also the small coupling by the ^{13}CO could be observed. Thus the ^{31}P spectra indicated the number of CO ligands coordinated to each rhodium center.

A downfield double doublet—the phosphorus signal of carbonylhydridotris(triethylphosphine)rhodium—was observed. The structure of this complex is also supported by rhodium NMR spectroscopy. An overlapping double triplet was assigned to the corresponding bis(phosphine)–dicarbonylhydridorhodium, and a broad upfield doublet was attributed to a dicarbonylrhodium dimer complex. No rhodium dimer is present under these conditions when triphenylphosphine is used instead of triethylphosphine. The excess free phosphine shows up as a singlet at -23.4 ppm. In a second
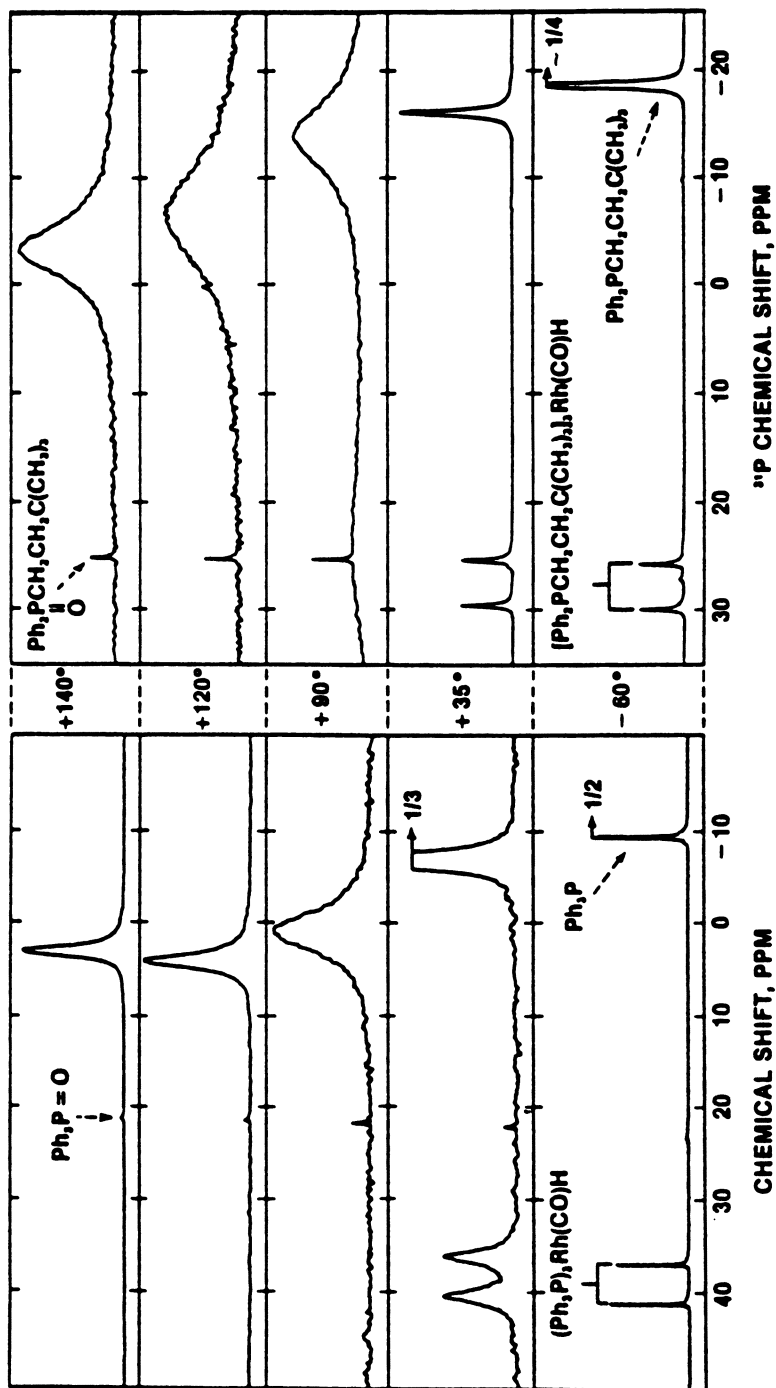
Figure 2. ^{31}P NMR study of ligand exchange at various temperatures in $(Ph_3P)_3Rh(CO)H$ and $[Ph_2PCH_2CH_2C(CH_3)_3]_3Rh(CO)H$.

experiment the pressure of the mixture was increased to about 36 atm, by a regular 1:1 mixture of H_2 and CO. This addition changed the equilibria in favor of the dicarbonylhydride complex, as expected.

^{13}C NMR Studies.   The ^{13}CO-enriched solutions of carbonylhydrido-rhodium complexes were also used for ^{13}C NMR studies. This labeling allowed the determination of the number of phosphorus ligands coordinated to one rhodium, as illustrated by Figure 3 with the triphenylphosphine ligand. The ^{13}CO complexes of Figure 3 were derived by reacting a toluene solution of tetrakis(triphenylphosphine)hydridorhodium and excess triphenylphosphine having a P:Rh ratio of 9:1 with ^{13}CO.

The resulting mixture of triphenylphosphine mono- and dicarbonylhydrides was then studied by ^{13}CO NMR spectroscopy under 0.35 and 2 atm of ^{13}CO pressure. The ^{13}C spectra in the complexed CO region show a double quartet and a double triplet for the monocarbonylhydride and dicarbonylhydride complexes, respectively. Obviously, the double quartet signal is the result of the splitting of the complexed CO signal into a quartet by the three phosphine ligands. This quartet is then further split by the rhodium to give the observed double quartet. Similarly, the double triplet signal can be clearly and unambiguously assigned to the analogous bis(phosphine)-dicarbonyl hydride. It is apparent from the signal intensities of the spectra that an increased partial pressure of free ^{13}CO leads to a change of the equilibrium between the mono- and dicarbonyl complexes, in favor of the latter.
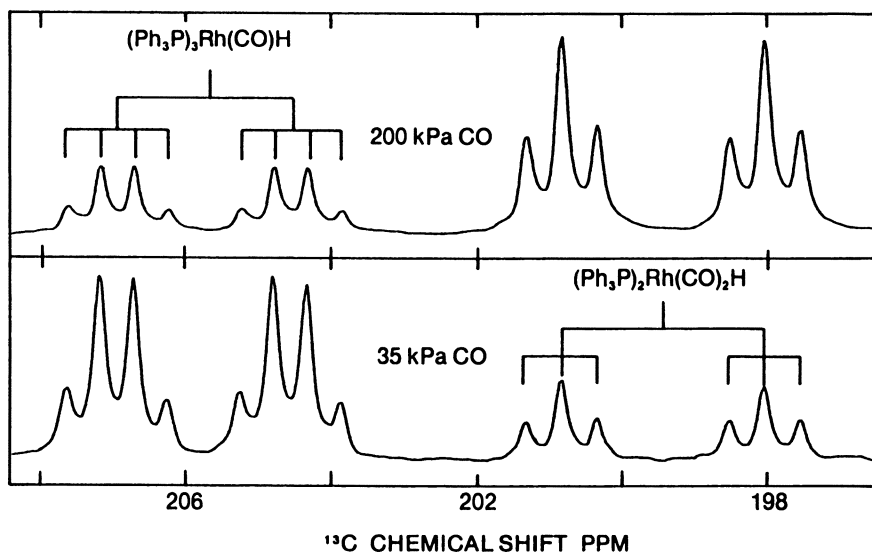
Figure 3. ^{13}C NMR study showing the equilibrium between $(Ph_3P)_3Rh(CO)H$ and $(Ph_3P)_2Rh(CO)_2H$ at two CO pressures.

Table I. Correlation of Phosphorus Ligand Bonding with Catalyst Activity and Selectivity

Phosphorus Ligand		Temp. (°C) at Equivalent Dissociation and Activity	Normalized Rate Constant[a] at 145 °C K_n ($K_{obs}/[Rh]$)	Approx. n:i Ratio of Product
Structure Type R = C_2H_5	Major Bonding			
Ph_3P	σ and π	100	200	11
Ph_2PR	σ and π	140	50	10
R_3P	σ	200	5	5
$(RO)_3P$	π	>200	2	11

[a]Experimental determinations were made under standard hydroformylation conditions: 2500 kPa, 5:1 H_2–CO, 1 M [R_3P].

Stability of Pentacoordinate Complexes. The stability and structure of the pentacoordinated carbonylhydridorhodium complexes largely depend on the strength and type of the rhodium coordination with the phosphorus ligand modifier. Therefore, we can correlate the activity and selectivity of the catalyst systems with the type of phosphine ligand. As shown in Table I, these correlations are illustrated by comparative hydroformylation experiments, which were carried out at a 1 M phosphorus ligand concentration. A triarylphosphine ligand, such as triphenylphosphine, which is both a medium σ donor and a medium π acceptor, provides a triarylphosphine complex with a significant dissociation rate at 100 °C. In a standard 145 °C hydroformylation catalysis experiment, the activity of this catalyst is high, as indicated by the normalized rate constant. The n:i selectivity is also high.

Alkyldiarylphosphine ligands have significantly increased σ-donor and somewhat reduced π-acceptor characteristics. Therefore, a higher temperature (in the range of 140 °C) is needed for their significant dissociation. Consequently, they show only about one-fourth of the activity of the triphenylphosphine-based system at 145 °C. Trialkylphosphine ligands are very strong σ donors and as such lead to very stable complexes. Therefore, at 145 °C these complexes have little activity. Because of increased bonding of CO by back-donation, these complexes tend to form multiple carbonyl complexes that lead to reduced n:i product ratios.

Finally, trialkyl phosphites are extremely strong π acceptors with negligible σ-bonding ability. As a result of the powerful back-donation, phosphites form more stable complexes than phosphines. With trialkyl phosphites, temperatures in excess of 200 °C are needed for good catalyst activity. In contrast to trialkylphosphines, these high-temperature ligands selectively form monocarbonylhydride complexes and provide a high n:i product ratio.

Catalysis Studies

The process studies of the present work were mainly carried out with 1-butene as a reactant. Use of 1-butene instead of propylene provided an

additional insight into the mechanism. In addition to the hydroformylation reactions producing *n*- and *i*-valeraldehydes, and hydrogenation producing *n*-butane, isomerization side reactions producing *cis*- and *trans*-2-butenes could also be studied, as indicated by Scheme V.

$$CH_3CH_2CH = CH_2 \xrightarrow{\ \ CO/H_2\ \ } CH_3CH_2CH_2CH_2CHO \qquad n\text{-}$$

$$\updownarrow \qquad\qquad\qquad\qquad\quad CH_3CH_2CHCHO \qquad i\text{-}$$
$$\xrightarrow{\ CO/H_2\ } \qquad\qquad\quad CH_3$$

$$CH_3CH = CHCH_3 \xrightarrow[\ \ H_2\ \ ]{} CH_3CH_2CH_2CH_2CH_3$$
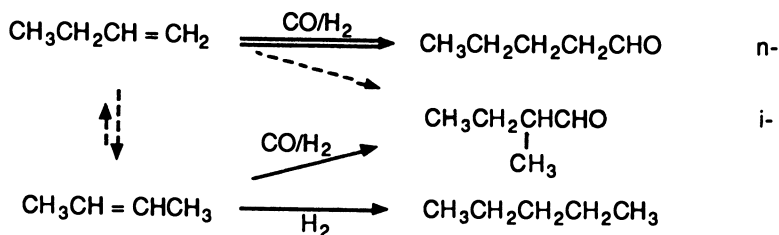
Scheme V. Products and byproducts from hydroformylation of 1-butene.

Our batch hydroformylation reactions were carried out in a 300-mL autoclave to 50% 1-butene conversion, as indicated by the CO–H_2 consumed. The rhodium concentration was selected from the range of 0.25–2.0 mM L^{-1} to achieve the desired 50% conversion in a period of 5–40 min. The phosphorus ligand concentration was in the 0.14–3.0 M range. The reaction rates showed an excellent first-order dependence on rhodium concentration. Therefore, for comparing different catalytic systems, so-called normalized rates could be calculated by dividing the observed rate constant by the Rh concentration.

In standard experiments, the starting reactant was a 20% solution of 1-butene in 2-ethylhexyl acetate plus phosphorus ligand. The initial synthesis gas reactant, used to pressure our autoclave, had a H_2–CO ratio of 5:1 or 1:1. Additional H_2–CO was added during the run to maintain the total pressure. The H_2–CO ratio of this additional feed was always adjusted slightly above one to provide extra H_2 for the hydrogenation side reaction. This adjustment maintained the original H_2–CO ratio and the original CO partial pressure during the course of the reaction. The total gas pressure was maintained by the feed gas at a value chosen from 2500 to 6900 kPa. The reaction temperature was selected in the 90–200 °C range. At the end of the reaction the products, byproducts, and reactants were all analyzed by gas–liquid chromatography.

The hydroformylation of 1-butene with triethylphosphine–rhodium catalyst systems was extensively studied to correlate the structure and equilibria of the complexes present with their activity and selectivity. The catalysis results obtained with triethylphosphine, a strong σ-donor ligand, were compared with results obtained with triphenylphosphine, which has both σ-donor and π-acceptor characteristics.

Triethylphosphine Ligand Concentrations. As shown by Table II, at first the effect of increased triethylphosphine ligand concentration was

Table II. Effect of Triethylphosphine Ligand Concentration on the Rhodium Hydroformylation of 1-Butene at Low CO Pressure

Reaction Temp. (°C)	Catalyst System			H_2–CO Ratio, Final	Rate $K_{obs}/[Rh]$ (M^{-1} min^{-1})	Reaction Time (min)	Aldehyde		Byproduct Selectivity (%)	
	Ligand		Rh Conc. (mM)				Linearity n:i	Selectivity n+i (%)	2-Butenes	Butane
	Structure	Conc. (M)								
180	Et₃P	0.14	0.25	6.76	128	21	3.35	86.1	8.4	5.5
		0.56	1.00	5.89	57	12	4.84	86.0	6.8	7.2
		1.00	1.00	6.10	38	17	5.62	86.3	6.7	7.0
		2.20	2.00	6.30	21	16	6.96	86.7	6.5	6.8
145	Ph₃P	2.20	2.00	5.20	90	4	21.50	81.0	13.5	5.5

NOTE: Reactions at 180 °C at 2500 kPa of 5:1 H_2–CO with 56/44 feed; 20 g of 1-butene; 80 g of mixture of phosphine ligand plus ethylhexyl acetate; acacRh(CO)₂ as catalyst precursor; reaction was stopped at 50% conversion.

studied at 180 °C with a 5:1 H_2–CO reactant gas under 2500 kPa of pressure. The data show that an increase of the phosphine ligand concentration from 0.14 to 2.2 M results in a decrease of rhodium catalyst activity and an increase in n-aldehyde selectivity. The activity drops to about 1/6 of the original, but the n:i ratio of aldehyde products increases from about 3.5 to 7.0. The total aldehyde selectivity, n + i, remains unchanged. The qualitative response of the catalyst to increased concentration of the triethylphosphine ligand is the same as that observed with the triphenylphosphine ligand. However, the optimum reaction temperature is much higher for the triethylphosphine-modified catalyst system. A comparison of the 180 °C data for 2.2 M triethylphosphine with those at 145 °C for 2.2 M triphenylphosphine shows similar catalyst activity. However, the triethylphosphine system provides less aldehyde linearity, about 7 versus 21, but greater aldehyde selectivity, n + i of 86.7 instead of 81.0%.

These qualitative effects of increased triethylphosphine ligand concentration on the rhodium hydroformylation rate and selectivity are observed in a broad pressure and temperature range. Similarly, the use of increased CO pressure changes the n-aldehyde selectivity in a manner attributable to a changing equilibrium between rhodium monocarbonyl hydride and dicarbonyl hydride complexes.

As shown by Table III, hydroformylation at 2500 kPa with a 1:1 rather than 5:1 ratio of H_2–CO—which increases the CO partial pressure 2.5-fold— gives similar results. In the presence of increasing excess concentration of triethylphosphine, the reaction rates similarly decrease. There is no indication of reaction inhibition or catalyst instability. In effect, reaction rates are better maintained at the higher CO partial pressure of the present series of experiments. The linearity of the aldehyde product, characterized by the n:i ratio, increases with increased phosphine concentration in the manner previously observed. However, under the presently increased CO pressure, the n:i ratios are in a lower range (2.76–4.33) than before (3.35–6.96).

Selectivity of Aldehydes.   Selectivity to total (n + i) aldehyde product is generally higher at increased CO partial pressures. In addition, selectivity to n + i aldehydes increases with the triethylphosphine ligand concentration under increased CO pressure. At 2.2 M phosphine concentration the n + i selectivity is 95%. This increased selectivity is mainly due to the more effective inhibition of 1-butene to 2-butene isomerization by higher concentration of the phosphine. At this point, the n-aldehyde selectivity at increased CO pressure is higher (77.2%) than at the lower CO pressure in Table II (75.8%). This increase in n-aldehyde selectivity, due to the greatly increased n + i %, is obtained in spite of the lower n:i ratio (4.33 versus 6.96).

A comparison of catalytic behavior of the triethylphosphine–rhodium complex catalyst system at high ligand concentration and increased CO pres-

Table III. Effect of Triethylphosphine Ligand Concentration on the Rhodium Hydroformylation of 1-Butene at Increased CO Pressure

| Reaction Temp. (°C) | Catalyst System | | | H_2–CO Ratio, Final | Rate $K_{obs}/[Rh]$ ($M^{-1} min^{-1}$) | Reaction Time (min) | Aldehyde | | Byproduct Selectivity (%) | |
| | Ligand | | Rh | | | | | | | |
	Structure	Conc. (M)	Conc. (mM)				Linearity n:i	Selectivity n+i (%)	2-Butenes	Butane
180	Et$_3$P	0.14	0.25	1.34	180	15	2.76	88.9	9.3	1.8
		0.56	0.50	1.37	52	27	3.21	92.2	5.3	2.5
		1.00	1.00	1.34	36	19	3.62	93.8	4.1	2.1
		2.20	1.50	1.33	18	27	4.33	95.0	3.2	1.8
145	Ph$_3$P	2.20	0.25	1.60	128	24	13.30	88.2	9.1	2.7

NOTE: Reactions at 180 °C at 2500 kPa of 1:1 H_2-CO with 52/48 feed; 20 g of 1-butene; 80 g of mixture of phosphine ligand plus ethylhexyl acetate; acacRh(CO)$_2$ as catalyst precursor; reaction was stopped at 50% conversion.

sure was made with the corresponding triphenylphosphine system. As shown by the last experiment in Table III, only the reaction temperature was different with the less stable triphenylphosphine complex. A comparison of the catalysis data shows the same qualitative differences that were observed at lower CO pressure. The triethylphosphine system is less active and produces a lower ratio of n- and i-aldehyde products. However, it provides significantly higher selectivity to n + i aldehydes. The choice between the two types of catalysts may depend on the market for the isoaldehyde product.

The rhodium hydroformylation of 1-butene with 5:1 H_2–CO was studied under similar conditions in the presence of phosphite ester ligands. Table IV shows the effect of the reaction temperature on catalyst activity and selectivity in the presence of 1 M triethyl phosphite. Increasing reaction temperature moderately increased the activity and the n:i selectivity of the triethyl phosphite-modified rhodium catalyst. However, there was a serious decrease in total aldehyde selectivity. At 180 °C the n + i selectivity was only 75.5%; with the triethylphosphine ligand, the comparable n + i was 86.3%. The high percentage of hydrocarbon byproducts observed with the phosphite-based catalyst is believed to be due to carbonyl-free rhodium hydride complex formation. Using triethyl phosphite as a rhodium ligand, a compromise between high activity and high total aldehyde selectivity may be the best choice. The present data suggest that such a compromise may be realized at about 160 °C.

Comparative data with triphenyl phosphite were obtained at 110 °C. Triphenyl phosphite-modified rhodium catalysts were extensively studied by several groups in the past. We found that, at low temperature, the triphenyl phosphite based catalyst system is much more active and provides a significantly higher n:i ratio of aldehyde products than the triethyl phosphite system. However, the triethyl phosphite complex leads to a much higher total aldehyde selectivity. The n + i percentage is 95.3% versus 80.7%. The low total aldehyde selectivity of the triphenyl phosphite catalyst is due to extensive 1-butene isomerization; the 2-butene selectivity is 17.1%. In the presence of triphenyl phosphite, butene isomerization becomes the dominant reaction at higher reaction temperatures.

Highly stable trialkylphosphine–rhodium complex catalysts with high total aldehyde selectivity are of particular interest for continuous hydroformylation processes using product flash-off (PFO). Figure 4 shows such a PFO operation. The process scheme shown is generally used for the hydroformylation of propylene to produce n-butyraldehyde (37, 38). This aldehyde is by far the most important oxo-chemical intermediate. During the process, the gaseous reactants are continuously introduced into a low-pressure reactor. The reaction takes place in the homogeneous solution of the rhodium complex catalyst system, and the products and unconverted reactants are continuously removed in the vapor phase. The aldehyde products are separated by condensation, and volatile unreacted reactants are recirculated. If

Table IV. Effect of Reaction Temperature on the Activity and Selectivity of the Triethyl Phosphite–Rhodium Catalyst in the Hydroformylation of 1-Butene

| Reaction Temp. (°C) | Catalyst System | | | H_2–CO Ratio, Final | Rate $K_{obs}/[Rh]$ (M^{-1} min^{-1}) | Reaction Time (min) | Aldehyde | | Byproduct Selectivity (%) | |
	Ligand Structure	Rh Conc. (mM)					Linearity n:i	Selectivity n+i (%)	2-Butenes	Butane
110	(PhO)₃P	2.5		5.03	8.8	31	12.72	80.7	17.1	2.2
110	(EtO)₃P	100.0		6.02	0.3	27	6.90	95.3	1.7	3.0
145		10.0		4.70	2.2	31	7.40	91.0	3.3	5.7
160		5.0		7.30	5.0	27	8.05	81.1	6.7	12.2
170		5.0		6.14	8.8	16	8.59	79.3	8.4	12.3
180		2.5		5.36	11.6	25	8.15	75.5	11.3	13.2
180	Et₃P	1.0		6.10	38.0	17	5.62	86.3	6.7	7.0

NOTE: Reactions at 2500 kPa of 5:1 H_2–CO with 52/48 to 56/44 feed; 20 g of 1-butene; 80 g of mixture of phosphine ligand (1 M) plus ethylhexyl acetate; acacRh(CO)₂ as catalyst precursor; reaction was stopped at 50% conversion.
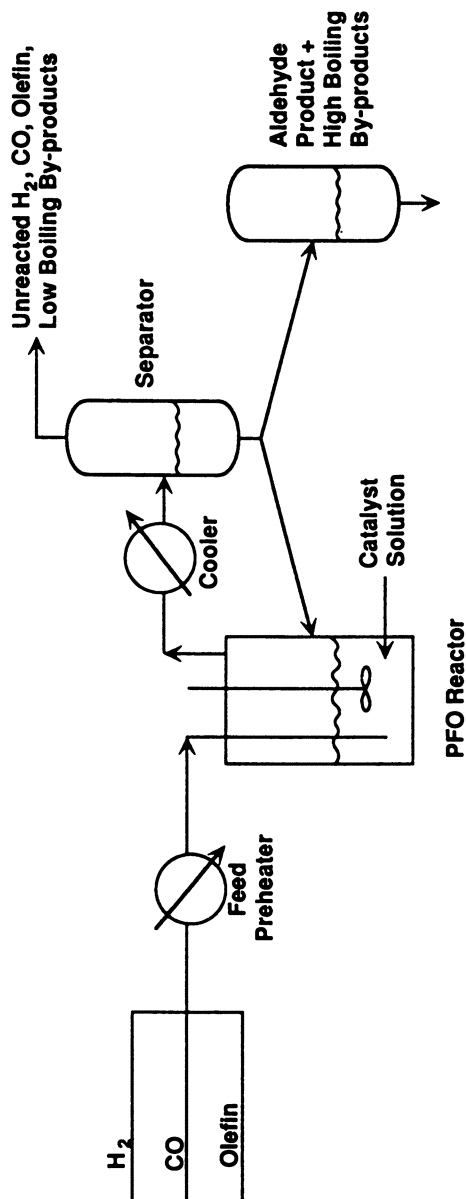
Figure 4. Continuous hydroformylation unit with continuous product flash-off (PFO).

this product flash-off or similar distillation technique is employed for the hydroformylation of higher molecular weight olefins leading to less volatile aldehyde products, the thermal stability of the complex becomes increasingly important because the product removal requires increased temperature.

Conclusions and Outlook

On the basis of the present study, we conclude that electronic effects of phosphorus ligands are an important factor in rhodium hydroformylation. We believe that strongly basic, σ-bonding trialkylphosphine ligands are potentially attractive in high-temperature rhodium hydroformylation. They are advantageous compared to triarylphosphine ligands from the viewpoint of product removal, complex stability, and ligand degradation. Their high total aldehyde product selectivity (n + i) at times is more important than their relatively low product linearity (n:i).

Nonvolatile, higher trialkylphosphines are promising ligand candidates in continuous rhodium hydroformylations using aldehyde product flash-off. Their rhodium complexes are much more stable than those of triarylphosphines because the main scrambling mechanism of aromatic phosphine degradation is not available.

From the scientific point of view, these data suggest that both the steric and electronic effects of phosphine ligands should be considered in rhodium hydroformylation. The electron donor and acceptor characteristics are important factors in determining the equilibria and dissociation of the catalytic complexes present. These in turn determine catalyst activity and selectivity.

References

1. Cornils, B. In *New Syntheses with Carbon Monoxide*; Fable, J., Ed.; Springer-Verlag: Berlin, 1980.
2. Parshall, G. W. *Homogeneous Catalysis. The Application and Chemistry of Catalysis by Soluble Transition Metal Complexes*; Wiley: New York, 1980; pp 1–47, 77–100.
3. Tolman, C. A.; Faller, J. W. In *Homogeneous Catalysis with Metal Phosphine Complexes*; Pignolet, L. H., Ed.; Plenum: London, 1983; particularly pp 81–102.
4. Tolman, C. A. *Chem. Rev.* **1977**, *77*, 319.
5. Pruett, R. L.; Smith, J. A. *J. Org. Chem.* **1969**, *34*, 327.
6. Van Leeuwen, P. W. N. M.; Roobeek, C. F. *J. Organomet. Chem.* **1983**, *258*, 343.
7. Roobeek, C. F.; Van Leeuwen, P. W. N. M. U.S. Patent 4 467 116, 1984.
8. Yoshida, T.; Okano, T.; Ueda, Y.; Otsuka, S. *J. Am. Chem. Soc.* **1981**, *103*, 3411.
9. Yoshida, T.; Okano, T.; Otsuka, S. In *Catalytic Activation of Carbon Monoxide*; Ford, P. C., Ed.; ACS Symposium Series 152; American Chemical Society: Washington, DC, 1981; p 79.
10. Yoshida, T.; Thorn, D. L.; Ibers, J. *J. Am. Chem. Soc.* **1980**, *102*, 6451.
11. Freeman, M. A.; Young, D. A. *Inorg. Chem.* **1986**, *25*, 1556.
12. Young, D. A. U.S. Patent 4 625 068, 1986.

13. Tau, K. D. U.S. Patent 4 605 781, 1986.
14. Unruh, J. D.; Christenson, J. R.; Hughes, O. R.; Young, D. A. In *Catalysis of Organic Reactions*; Moser, W. R., Ed.; Vol. 5 in *Chemical Industries*; Dekker: New York, 1981.
15. Unruh, J. D.; Christenson, J. R. *J. Mol. Catal.* **1982**, *14*, 19.
16. Hughes, O. R.; Young, D. A. *J. Am. Chem. Soc.* **1981**, *103*, 6636.
17. Moser, W. R.; Papile, C. J.; Brannon, D. A.; Weininger, S. J. *J. Mol. Catal.* **1987**, *41*, 271.
18. Bahrmann, H.; Fell, B. *J. Mol. Catal.* **1980**, *8*, 334.
19. Kastrup, R. V.; Merola, J. S.; Oswald, A. A. In *Catalytic Aspects of Metal Phosphine Complexes*; Alyea, E. C.; Meek, D. W., Eds.; Advances in Chemistry 196; American Chemical Society: Washington, DC, 1982; p 43.
20. Oswald, A. A.; Merola, J. S.; Mozeleski, E. J.; Kastrup, R. V.; Reisch, J. C. In *Phosphorus Chemistry: Proceedings of the 1981 International Conference*; Quin, L. D.; Verkade, J. G., Eds.; ACS Symposium Series 171; American Chemical Society: Washington, DC, 1981; p 503.
21. Oswald, A. A.; Hendriksen, D. E.; Kastrup, R. V.; Merola, J. S. Preprints, Division of Petroleum Chemistry, Inc., of the American Chemical Society, National Meeting, Las Vegas, NV **1982**, *27*(2), 292.
22. Oswald, A. A.; Hendriksen, D. E.; Kastrup, R. V.; Merola, J. S.; Mozeleski, E. J.; Reisch, J. C. Preprints, Division of Fuel Chemistry of the American Chemical Society, National Meeting, Seattle, WA **1983**, *28*(2), 191–208.
23. Oswald, A. A.; Hendriksen, D. E.; Kastrup, R. V.; Irikura, K.; Mozeleski, E. J.; Young, D. A. *Phosphorus Sulfur* **1987**, *30*, 237.
24. Oswald, A. A.; Jermansen, T. G.; Westner, A. A.; Huang, I. D. U.S. Patents 4 298 541, 1981; 4 450 299, 1984; 4 595 753, 1986; 4 668 809, 1987; 4 687 866, 1987; 4 687 874, 1987.
25. Oswald, A. A.; Jermansen, T. G.; Westner, A. A.; Huang, I. D. U.S. Patent 4 593 141, 1986.
26. Billig, E.; Bunning, D. L. U.S. Patent 4 283 562, 1981.
27. Streuli, C. A. *Anal. Chem.* **1960**, *32*, 985.
28. Streuli, C. A. *Anal. Chem.* **1959**, *31*, 1652.
29. Thorsteinson, E. M.; Basolo, F. *J. Am. Chem. Soc.* **1966**, *88*, 3929.
30. Allman, T.; Goel, R. G. *Can. J. Chem.* **1982**, *60*, 712.
31. Verkade, J. G. *Coord. Chem. Rev.* **1972**, *9*, 1–106, particularly pp 21–23.
32. Janecko, H.; Trzeciak, A. M.; Ziolkowski, J. J. *J. Mol. Catal.* **1984**, *26*, 355.
33. Trzeciak, A. M.; Ziolkowski, J. J. *J. Mol. Catal.* **1986**, *34*, 213.
34. Trzeciak, A. M.; Ziolkowski, J. J. *J. Mol. Catal.* **1988**, *48*, 319.
35. Booth, B. L.; Else, M. L.; Fields, R.; Haszeldine, R. N. *J. Organomet. Chem.* **1971**, *27*, 119.
36. Brown, J. M.; Kent, A. G. *J. Chem. Soc., Perkin Trans. 2* **1987**, 1597.
37. Brewester, E. A. V.; Pruett, R. L. U.S. Patent 4 247 486, 1981.
38. Bryant, D. R.; Billig, E. U.S. Patent 4 277 627, 1981.

Influence of Organophosphines on the Hydroformylation of Olefins Catalyzed by Anionic Ruthenium Clusters

Georg Süss-Fink

Institut de Chimie, Université de Neuchâtel, Avenue de Bellevaux 51, CH–2000 Neuchâtel, Switzerland

Anionic ruthenium clusters catalyze the hydroformylation of olefins with excellent chemo- and regioselectivity. Isotope-labeling studies and trapping of intermediates suggest that the catalytic reaction proceeds through the intermediacy of intact clusters. Organophosphines have a remarkable influence on the catalytic reaction. Triphenylphosphine completely blocks the catalytic activity of the ruthenium cluster. Diphenylphosphine, by contrast, enhances the catalytic activity but modifies the selectivity of the catalyst. The chemistry underlying these influences is discussed.

DISCUSSION OF TRANSITION METAL CLUSTERS as catalysts has led to controversy over whether such molecules can really be useful in catalysis. In the 1970s the goal in chemistry of transition metal clusters was to contribute significantly to the development of systematic catalysis. This movement was stimulated mainly by Johnson and Lewis (1) and the late Earl Muetterties (2).

As oligonuclear species with intermetallic bonds, metal clusters occupy the "no man's land" between mononuclear metal complexes and polynuclear metal surfaces (Chart I). Because of this intermediary position between typical homogeneous catalysts and typical heterogeneous catalysts, transition metal clusters may be a new generation of catalysts (3). The aim of research in this area is twofold: to find transition metal clusters that provide a unique

mononuclear   **oligonuclear**   **polynuclear**
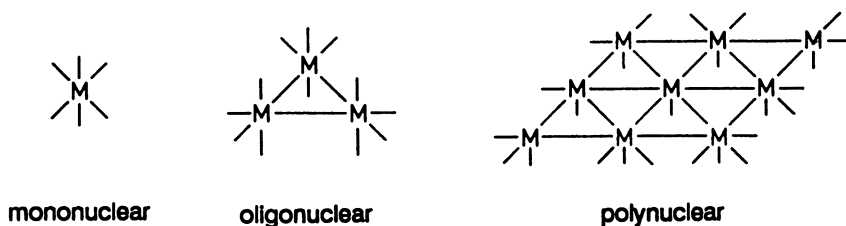
Chart I. Intermediary position of metal clusters.

catalytic potential and to find transition metal clusters that are highly selective in their catalytic applications.

Trinuclear Ruthenium Cluster Anions as Catalysts

The trinuclear cluster anion $[HRu_3(CO)_{11}]^-$ (1), which we discovered in 1979, proved to be particularly interesting in this twofold respect. It is easily accessible from carbonylruthenium and base reagents (4, 5). In recent years we and others have found a considerable number of reactions catalyzed by 1, only two of which will be mentioned here.

The unique catalytic potential of 1 expresses itself by the spirocyclization of alkyl isocyanates, which gives a surprisingly simple access to a new series of spiroheterocycles (6) (Scheme I). The high selectivity of 1 is demonstrated by the hydroformylation of propylene, which leads exclusively to C_4 aldehydes with very high regioselectivity (n:i) ratio (7) (Table I).

This chapter describes the influence of phosphines (as cocatalysts) on the catalytic activity and the selectivity of 1 for the hydroformylation of olefins.

$$5\ R-N=C=O \xrightarrow[\text{Et}_3\text{SiH} \quad \text{Et}_3\text{SiOH}]{[HRu_3(CO)_{11}]^-}$$

Yields:	R	Me	Et	^nPr	^iPr	^nBu
	%	41	43	69	22	51
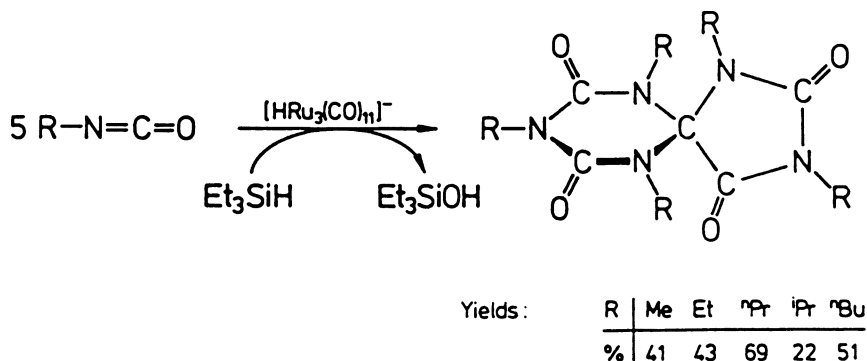
Scheme I. Spirocyclization of alkyl isocyanates in tetrahydrofuran at 120 °C.
The molar ratio of isocyanate to silane to cluster was 5000:1000:1.

Table I. Chemo- and Regioselectivity of Compound 1
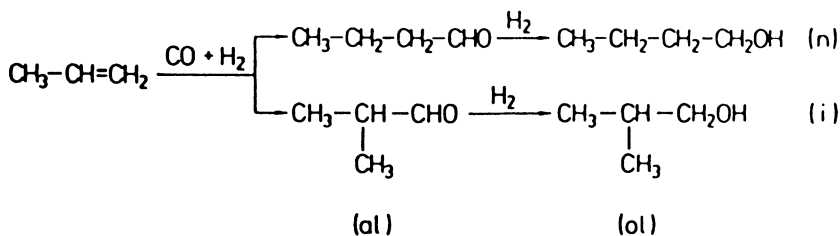
Solvent	Temperature (°C)	Chemoselectivity (Aldehyde:Alcohol)	Regioselectivity (Normal:Isopropyl)
DMF	70	100.0:0.0	94.1:5.9
DMF	80	100.0:0.0	94.0:6.0
DMF	90	100.0:0.0	93.6:6.4
Glyme	80	100.0:0.0	98.0:2.0
Diglyme	80	100.0:0.0	98.6:1.4

NOTE: The reaction took place with 0.17 mmol of $[NEt_4][HRu_3(CO)_{11}]$ in 10 mL of solution at 10 bars of total pressure.

Organophosphines as Hydroformylation Cocatalysts

The high selectivity of 1 as a hydroformylation catalyst can be best understood on the basis of a catalytic cycle involving exclusive intact trinuclear clusters as intermediates by the steric demands of a trinuclear metal framework. The catalytic cycle as proposed in Scheme II is based on the trapping of the intermediate $[Ru_3(CO)_{10}(OCEt)]^-$ by acidification of the reaction mixture with CF_3COOH and CH_3COOD to give the neutral clusters $HRu_3(CO)_{10}(OCEt)$ (8) and $DRu_3(CO)_{10}(OCEt)$, and on isotope-labeling studies with molecular deuterium as the hydroformylation component (9).

For a large number of hydroformylation catalysts, both catalytic activity and selectivity can be improved by using organophosphines as cocatalysts (10). Accordingly, we attempted to make the hydroformylation of propene, which is already highly selective in the presence of 1, chemo- and regio-specific by adding triphenylphosphine or derivatives thereof. However, the catalytic activity of 1 collapsed completely in the presence of excess PPh_3. In contrast, catalytic activity increased in the presence of PPh_2H, but this increase was accompanied by a complete change of selectivity.

These effects cannot be explained on the basis of simple phosphine substitution products of 1. Therefore, we undertook to study the rather complex reactions of 1 with PPh_3 and PPh_2H. Our goal was to elucidate the chemistry underlying the strange influences of organophosphines on the hydroformylation catalyzed by the cluster anion 1.

The reaction of 1 with triphenylphosphine was reported to give the monosubstitution product $[HRu_3(CO)_{10}(PPh_3)]$ (2) (11). This anionic species was characterized in a careful kinetic study (11, 12); however, it has never

$$CH_2=CH_2 \quad + \quad CO \quad + \quad H_2 \quad \longrightarrow \quad CH_3-CH_2-CH=O$$
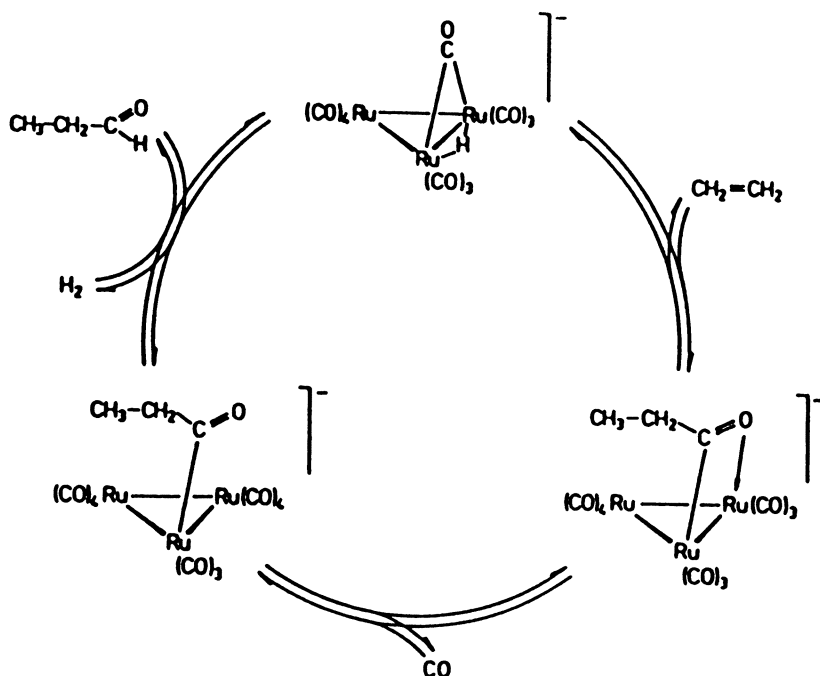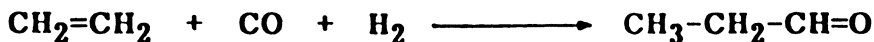
Scheme II. Proposed mechanism for hydroformylation catalyzed by [NEt₄][HRu₃(CO)₁₁] in tetrahydrofuran at 100 °C and 50 bar of pressure for 4 h. The catalytic turnover (ratio of products to catalyst) was 345 ± 5, and the catalyst recovery was 98%.

been isolated. As a catalyst, **2** should be at least as active as **1**. Therefore, the breakdown of the catalytic activity of **1** in the presence of PPh_3 cannot be caused by the formation of **2**. Rather, it must originate in transformations of the cluster that are much more complicated than the substitution of a carbonyl by a phosphine ligand.

We therefore undertook a careful ^1H NMR study of the reaction system **1**–PPh_3 (Figure 1). The monosubstitution product $[HRu_3(CO)_{10}(PPh_3)]^-$ (**2**) is formed and gives rise to a doublet hydride signal at –12.01 ppm. However, even before **1** has completely disappeared, the formation of the disubstitution product $[HRu_3(CO)_9(PPh_3)_2]^-$ (**3**) (Scheme III) is indicated by a triplet hydride signal at –11.20 ppm.

Anions **2** and **3** are not very stable. Even at 20 °C, **3** undergoes elimination of benzene and converts into the phosphine–phosphido derivative $[Ru_3(CO)_9(PPh_3)(PPh_2)]^-$ (**4**), which can be isolated and characterized as
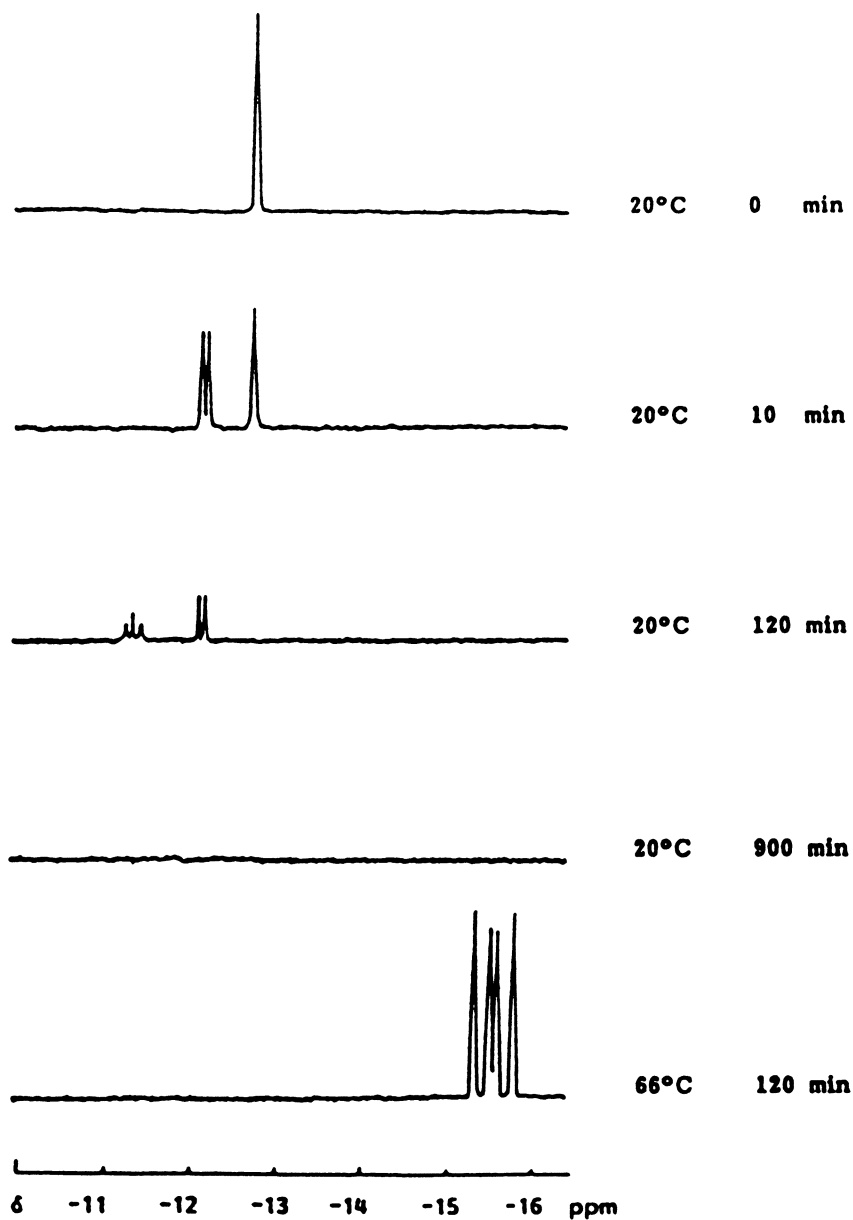
Figure 1. ¹H NMR spectra of the reaction of 0.5 mmol of [N(PPh)₃] [HRu₃(CO)₁₁] with 0.5 mmol of PPh₃ in 50 mL of tetrahydrofuran at various temperatures.

$[HRu_3(CO)_{11}]^-$

PPh$_3$

20°C

CO

$[HRu_3(CO)_{10}(PPh_3)]^-$

PPh$_3$

20°C

CO

$[HRu_3(CO)_9(PPh_3)_2]^-$

20°C

PhH

$[Ru_3(CO)_9(PPh_3)(PPh_2)]^-$

66°C

CO

$[HRu_3(CO)_8(PPh_3)(PPhC_6H_4)]^-$

isolated as
tetraethyl ammonium salt
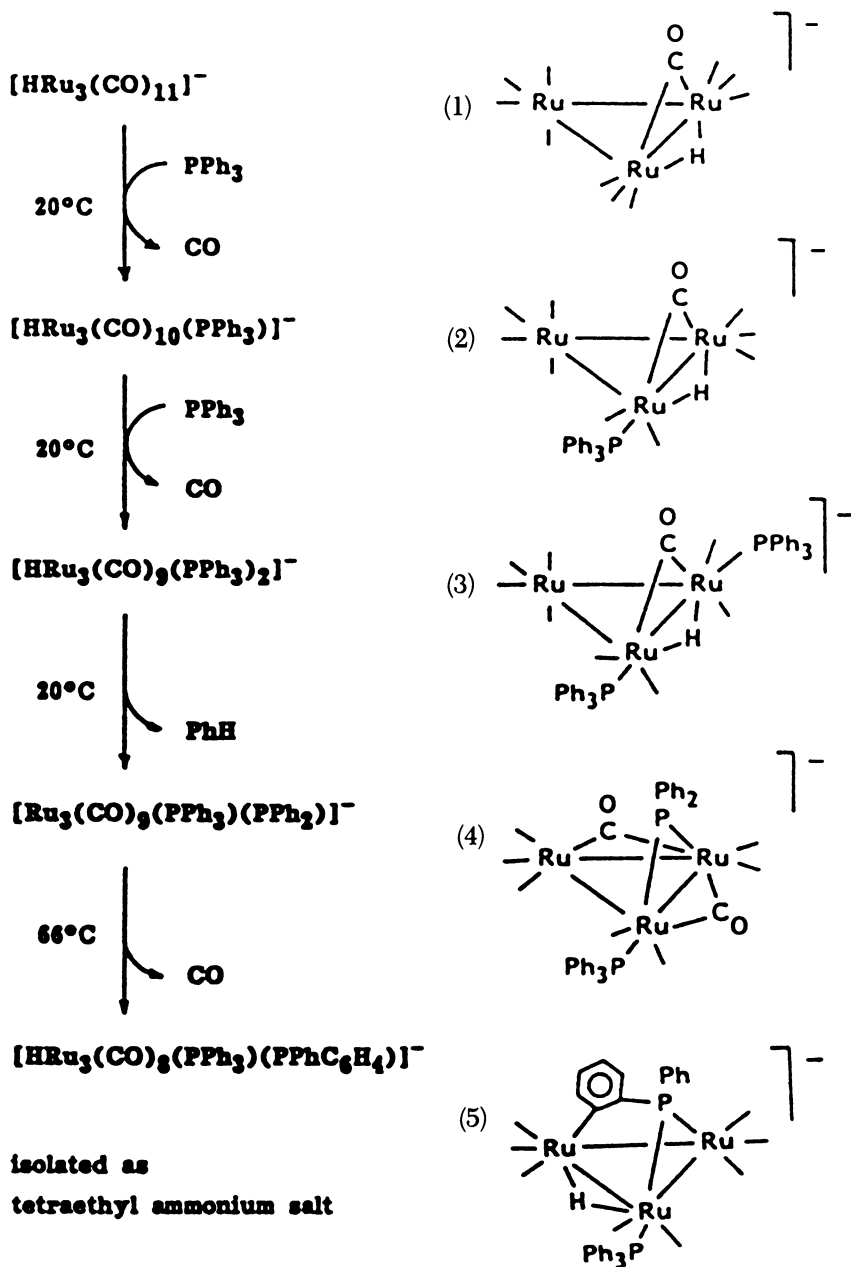
Scheme III. The reaction system 1–PPh$_3$.

bis(triphenylphosphine)iminium salt. Heating at conditions similar to those of the catalytic process converts **4** with orthometalation of one of the aromatic rings and carbonyl substitution into the anion $[HRu_3(CO)_8(PPh_3)(PPhC_6H_4)]^-$ (**5**), which was isolated as tetraethylammonium salt. The single-crystal X-ray structural analysis of **5** was performed.
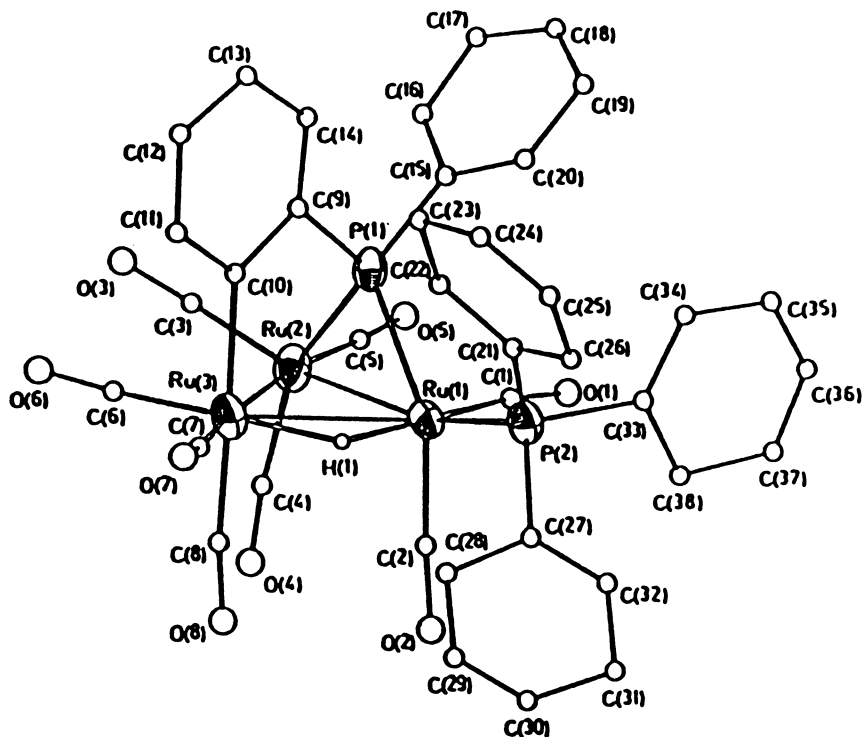
Molecular structure of **5**.

The isolation and characterization of the cluster anion **5** as the species formed from **1** and PPh_3 under catalytic conditions explains why the catalytic cycle according to Scheme II is suppressed. One of the two PPh_3 ligands coordinated initially on the metal framework undergoes benzene elimination and orthometalation to give a tripodal phosphorus–carbon handle over the triangular metal face blocking the catalytic activity of the cluster. The variable-temperature NMR spectra in fact show that **5** is a rigid cluster, the ligands of which are not fluxional.

In contrast to PPh_3, diphenylphosphine enhances the catalytic activity of the cluster anion **1**. We therefore studied the stoichiometric reaction of **1** with PPh_2H, from which we isolated the bisphosphido derivative **6** as bis(triphenylphosphine)iminium salt.

$$[HRu_3(CO)_{11}]^- + 2PPh_2H \rightarrow [HRu_3(CO)_8(PPh_2)_2]^- + H_2 + 3CO$$

$$\quad\; \textbf{1} \qquad\qquad\qquad\qquad\qquad\qquad \textbf{6}$$
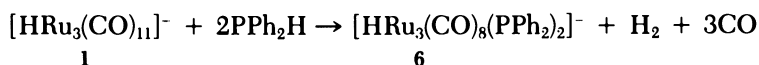
The crystal structure analysis reveals that anion **6** contains a triangular metal framework with two different Ru–Ru bonds bridged by PPh_2 ligands, which occupy different sides with respect to the Ru_3 plane. One of the phosphido-bridged Ru–Ru edges also carries the hydride bridge. The solid-state structure of compound **6** is found in solution only at low temperature. Variable-temperature NMR spectra (Figure 2) prove that **6** is fluxional in solution. These spectra are best interpreted in terms of dynamic site exchange of the hydride ligand between the two phosphido-bridged Ru–Ru bonds.

In contrast to the rigid orthometalated cluster anion **5**, the fluxional cluster anion **6** catalyzes the hydroformylation of olefins. However, the selectivity is completely changed with respect to that of **1**. Whereas **1** is
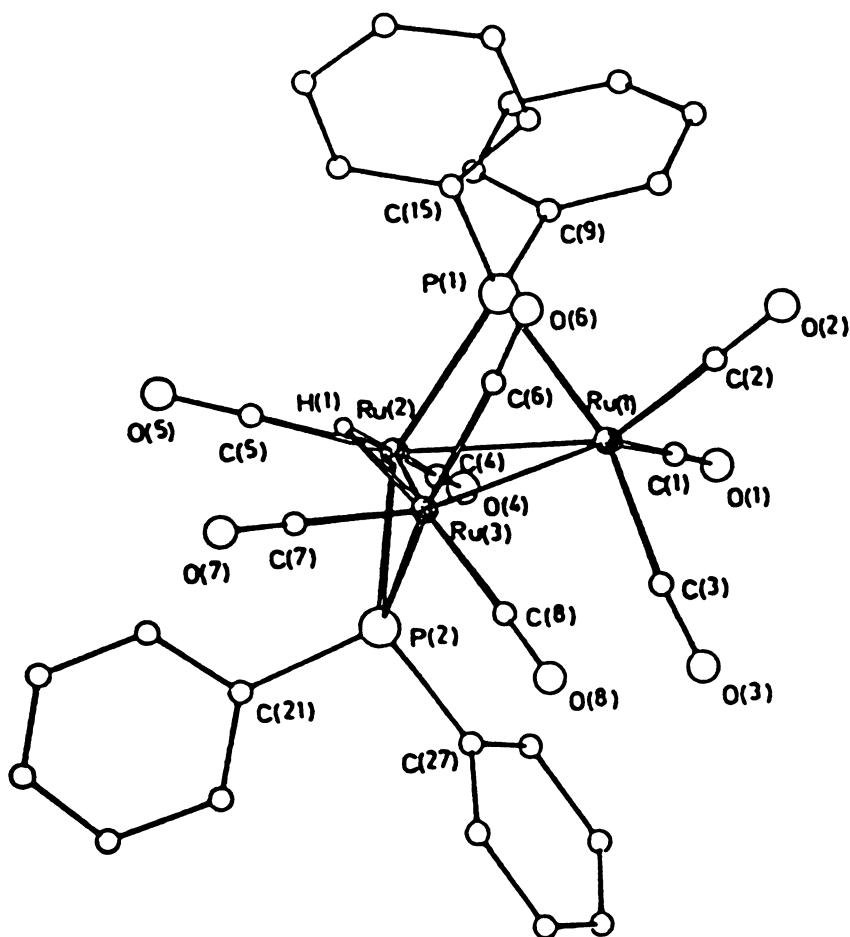
Molecular structure of **6**.

$$31P-(^1H)-NMR \qquad ^1H-NMR$$
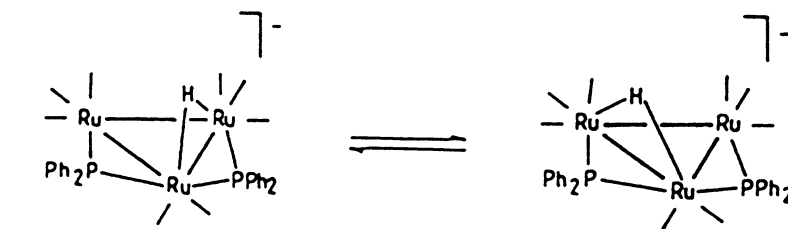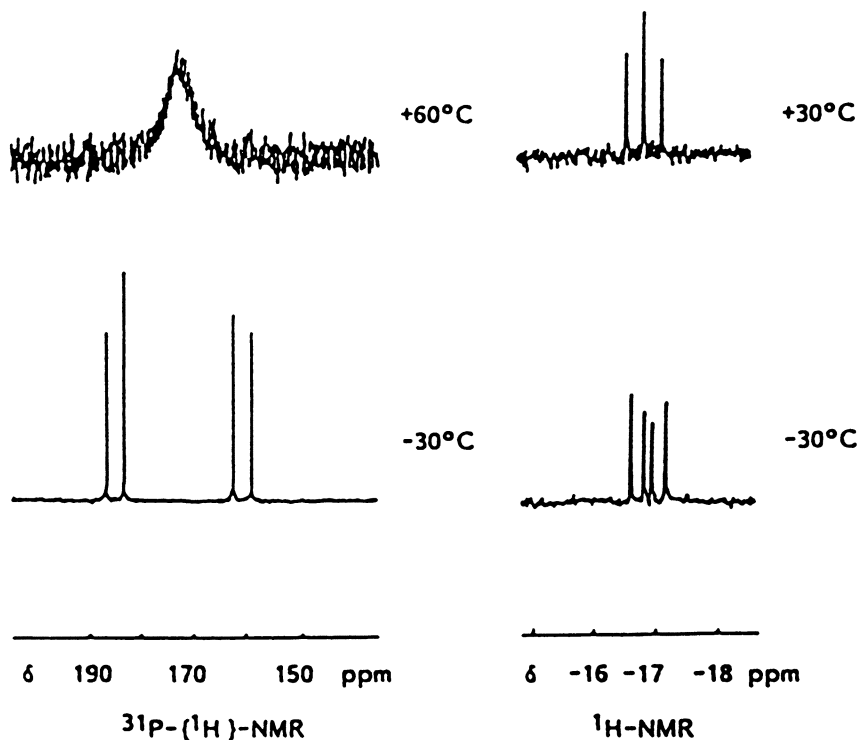
Figure 2. Variable-temperature NMR spectra of **6** *and dynamic site exchange of hydride ligand.*

extremely chemoselective for aldehydes (even chemospecific under optimum conditions), **6** provides a mixture of aldehydes, alcohols, and ketones.

For ethylene, the ratio of the aldehyde to ketone to alcohol products can be varied between 90:2:8 and 29:70:1, depending upon the ethylene partial pressure. This loss of selectivity of **1** in the presence of PPh$_2$H, accompanied by an enhancement of catalytic activity (Table II) can be explained by the formation of **6**. This cluster anion, fluxional as the parent

Table II. Hydroformylation versus Hydrocarbonylation

$$CH_2=CH_2 + CO + H_2 \rightarrow CH_3-CH_2-CH_2-CH=O$$

$$2CH_2=CH_2 + CO + H_2 \rightarrow (CH_3-CH_2)_2C=O$$

$$CH_3-CH_2-CH=O + H_2 \rightarrow CH_3-CH_2-CH_2-OH$$
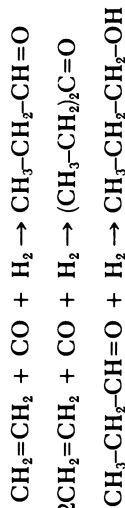
Catalyst [NEt_4]+	Temperature (°C)	Partial Pressures[a] (C_2H_4, CO, H_2)	Catalytic Turnover (Products/Catalyst)	Selectivity[b]
[HRu_3(CO)_{11}]-	100	15, 30, 20	345	99:0:1
[HRu_3(CO)_8(PPh_2)_2]-	140	15, 15, 10	1210	90:2:8
[HRu_3(CO)_8(PPh_2)_2]-	140	25, 15, 10	1240	65:30:5
[HRu_3(CO)_8(PPh_2)_2]-	140	40, 15, 10	1260	29:70:1

NOTE: All reactions took place in tetrahydrofuran for 18 h.
[a]Partial pressures are in bars.
[b]Aldehyde to ketone to alcohol ratio.

anion **1**, also catalyzed the hydroformylation of olefins. However, it proceeded by a different mechanism than that determined for **1**, which was depicted in Scheme II.

Studies to elucidate the catalytic cycle of the ethylene hydroformylation, catalyzed by phosphido derivative **6**, are under way.

Acknowledgments

References

1. Johnson, B. F. G.; Lewis, J. *Colloq. Int. C. N. R. S.* **1977**, *281*, 101; *Pure Appl. Chem.* **1975**, *44*, 43.
2. Muetterties, E. L. *Science (Washington, D.C.)* **1977**, *196*, 839; *Bull. Soc. Chim. Belg.* **1975**, *84*, 959.
3. Muetterties, E. L.; Krause, M. J. *Angew. Chem.* **1983**, *95*, 135; *Angew. Chem., Int. Ed. Engl.* **1983**, *22*, 135.
4. Süss-Fink, G. *Inorg. Synth.* **1986**, *24*, 186.
5. Johnson, B. F. G.; Lewis, J.; Raithby, P. R.; Süss(-Fink), G. *J. Chem. Soc., Dalton Trans.* **1979**, 1356.
6. Süss-Fink, G.; Herrmann, G.; Thewalt, U. *Angew. Chem.* **1983**, *95*, 899; *Angew. Chem., Int. Ed. Engl.* **1983**, *22*, 880; *Angew. Chem. Suppl.* **1983**, 1203.
7. Süss-Fink, G.; Schmidt, G. F. *J. Mol. Catal.* **1987**, *42*, 361.
8. Kampe, C. E.; Boag, N. M.; Kaesz, H. D. *J. Am. Chem. Soc.* **1983**, *105*, 2896.
9. Süss-Fink, G.; Herrmann, G. *J. Chem. Soc., Chem. Commun.* **1985**, 735.
10. Cornils, B. In *New Syntheses with Carbon Monoxide*; Falbe, J., Ed.; Reactivity and Structure, Concepts in Organic Chemistry 11; Springer-Verlag: Berlin, 1980.
11. Taube, D. J.; Ford, P. C. *Organometallics* **1986**, *5*, 99.
12. Taube, D. J.; van Eldik, R.; Ford, P. C. *Organometallics* **1987**, *6*, 125.

Selectivity Control in the Amination of Ethylene Glycol

John A. Marsella

Air Products and Chemicals, Inc., Allentown, PA 18195

We previously reported that vicinal diols react with secondary amines in the presence of soluble ruthenium and iridium catalysts at 100–125 °C to give high yields of amino alcohols and diamines. The selectivity can be modified in favor of mono- or diamination by the proper choice of metal and by varying the level of triphenylphosphine present in the reaction mixture. We now report the effect of other phosphine ligands on this catalyst system, as well as the effect of temperature on the selectivity. Stepwise progression from PPh₃ to PMe₃ indicates that both electron-donating ability and steric bulk on the ligand increase the tendency to make amino alcohol. Not surprisingly, increasing the reaction temperature causes a decrease in selectivity. However, some of the selectivity toward monoamination can be recovered by adding more phosphine ligand. Preliminary spectroscopic observations suggest that ethylene glycol binds much more strongly to Ru(II) than does methanol. This tendency explains the higher reactivity of the diol with these catalysts.

HOMOGENEOUSLY CATALYZED REACTIONS OF AMINES and alcohols that give *N*-alkylated products have been the focus of a number of reports during the past decade (*1–5*). Watanabe's group (*6–14*) has been particularly active and has demonstrated the synthesis of amino alcohols, diamines, and various heterocycles from diols and both alkyl- and arylamines. Earlier we reported (*15–19*) that ruthenium and iridium complexes catalyze the formation of either amino alcohols or diamines from ethylene glycol and secondary amines. The reactions occur with a high degree of selectivity, which can be altered in a controllable fashion by the proper choice of catalyst system.

Triphenylphosphine complexes of ruthenium, as well as $RuCl_3 \cdot xH_2O$–PPh_3 mixtures, give high selectivity to amino alcohols. In contrast, $RuCl_3 \cdot xH_2O$ by itself and iridium complexes give high selectivity to diamines. We speculated that the selectivity control stems from the existence of intermediate metal–amino alcohol complexes whose stabilities vary depending on the metal and the coordination environment (15). The ability of these soluble catalysts to control the selectivity of glycol aminations appears to be greater than that achievable with traditional heterogeneous methods (20–22) or with photocatalysis (23). Here we report further studies of these reactions, including effects of various phosphine ligands and of temperature on the selectivity obtainable with ruthenium catalysts.

Phosphines play an important role in controlling the selectivity of metal-catalyzed and metal-assisted organic reactions (24). Consistent with this condition, the selectivity of the reaction of ethylene glycol with secondary amines catalyzed by ruthenium complexes varies smoothly with the PPh_3:Ru ratio. We previously (15) defined a selectivity ratio r, which reflects the effectiveness of a catalyst for the synthesis of either **1** or **2**.

$$HOCH_2CH_2OH + HNR_2 \rightarrow HOCH_2CH_2NR_2 + R_2NCH_2CH_2NR_2$$
$$\qquad\qquad\qquad\qquad\qquad\qquad\quad \textbf{1} \qquad\qquad\qquad\qquad \textbf{2}$$

$$r = \frac{\text{selectivity to } \textbf{2}}{\text{selectivity to } \textbf{1} + \text{selectivity to } \textbf{2}}$$

We now report that this selectivity ratio is also quite sensitive to the nature of the phosphine ligand. The effect of the phosphine is dependent on both its steric and electronic properties. In the case of triphenylphosphine, the effectiveness of the ligand in controlling selectivity decreases as the reaction temperature is increased. However, this loss of selectivity can be reversed by increasing the phosphine concentration.

Effect of Phosphine on Selectivity

Table I lists several phosphines and their effects on the catalysis of the reaction of morpholine with ethylene glycol in the presence of $RuCl_3 \cdot xH_2O$. *CAUTION: Reactions run in closed systems can develop pressure from evolved H_2. A suitable means of pressure relief or containment must be provided.* The data in Table I are arranged in order of increasing selectivity to the diamination product, 1,2-bis(morpholino)ethane (**2a**). A general trend of selectivity based on phosphine cone angle (25) is not evident, although very large ligands tend to lower conversions (with the exception of $PPh(C_6F_5)_2$).

Table I. Effect of Phosphines on RuCl$_3$ · xH$_2$O-Catalyzed Reactions of Morpholine with Ethylene Glycol

Phosphine Ligand	L:Ru	Temperature (°C)	Time (h)	Conversion (%)	Total Selectivity (%)[a]	r	Cone Angle (degrees)[b]
P(p-C$_6$H$_4$F)$_3$	3.0	120	2.5	100	95	<0.01	—
PPh$_3$	3.0	120	2	95	90	0.02	145
P(p-tol)$_3$	2.9	128	2.25	100	93	0.17	145
P(C$_6$F$_5$)$_3$	2.5	120	3	22	60	>0.60	184
P(OPh)$_3$	3.2	125	2.5	13	48	0.69	128
dppm[c]	1.0	120	2	70	91	0.73	121
PPh$_2$Me	3.0	125	2.5	45	88	0.73	136
P(i-Pr)$_3$	3.8	120	2.5	12	44	0.75	160
dppe[d]	1.0	125	2	13	57	0.82	125
PPh(C$_6$F$_5$)$_2$	3.6	117	3	100	84	0.84	—
P(o-C$_6$H$_4$NMe$_2$)	2.7	120	2	37	90	0.94	—
P(o-tol)$_3$	2.9	130	2.5	48	85	0.95	194

NOTE: Typical reactions were run with 5.0 mL of ethylene glycol (5.6 g, 90 mmol), 1.0 mL of morpholine (1.0 g, 11 mmol), 0.50 mL of N-methylpyrrolidone (internal GC standard), and ca. 0.1 mmol of Ru (1 mol % based on morpholine) in a 22-mL Parr bomb.
[a] Sum of selectivity to **1** and **2**. (Because of the nature of the products and analytical difficulties, low conversions often gave a low total selectivity.)
[b] Ref 25.
[c] dppm is bis(diphenylphosphino)methane.
[d] dppe is 1,2-bis(diphenylphosphino)ethane.

In addition, 1,2-bis(diphenylphosphino)ethane (dppe), a very good chelating agent, retards the reaction significantly. In contrast, the poorer chelating agent, bis(diphenylphosphino)methane (dppm), gives a respectable conversion with selectivity favoring the diamine.

A somewhat clearer understanding of the ligand effect can be achieved by examining the results of reactions in which discrete ruthenium–phosphine complexes are used as catalysts. In general, these complexes give slightly higher conversions than the analogous catalyst systems obtained by simply mixing the ligand with $RuCl_3 \cdot xH_2O$, and distortions from in situ catalyst generation are minimized. Results obtained with various Ru(II) phosphine complexes are shown in Table II. Particularly noteworthy are the results for the complexes containing the series of ligands PMe_xPh_{3-x} ($x = 0$–3). The phosphines PPh_3, $PPhMe_2$, and PMe_3 all give higher selectivity to monoamination (low values of r). The ligand PPh_2Me stands out as an obvious exception, with diamination being slightly favored ($r > 0.5$). The tendency for diamination with this ligand is also evident in Table I. Clearly, an explanation based solely on steric factors is not satisfactory.

Our original rationalization for selectivity control was based on the presence or absence of triphenylphosphine (15). The reaction apparently proceeds through an intermediate ruthenium complex that can either dissociate amino alcohol to give monoaminated product or further aminate to give

Table II. Catalysis and Selectivity Shown by Ru(II) Complexes
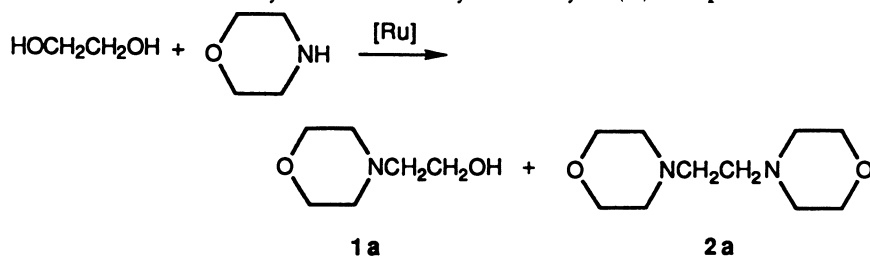
| | Conversion | Selectivity (%) | | |
Complex	(%)	1a	2a	r
$RuCl_2(PPh_3)_3$	100	84	9	0.10
$[(RuL_3)_2(\mu\text{-}Cl)_3]Cl^a$	100	36	56	0.61
$[(RuL_3)_2(\mu\text{-}Cl)_3]Cl^b$	100	76	12	0.14
$RuCl_2(PMe_3)_4$	100	91	1	0.01
$cis\text{-}RuCl_2(dppm)_2{}^c$	100	50	39	0.44
$trans\text{-}RuCl_2(dppm)_2$	100	45	46	0.51
$trans\text{-}RuCl_2(dppe)_2{}^d$	low	—	—	—
$RuCl_2(dppm)(PMePh_2)_2$	87	34	56	0.62

NOTE: Conditions are as in Table I; temperature = 120–125 °C; time = 2–2.5 h.
[a] L is $PMePh_2$.
[b] L is PMe_2Ph.
[c] 130 °C.
[d] 3.5 h.

diamine (*see* Scheme I). Clearly, a sterically hindered phosphine coordinated to the metal will destabilize other ligands present. However, it is also true that electron-rich phosphines will cause weaker binding of ligands that are largely σ-donors. Both alcohols and amines fall into this category for the later transition metals.

Thus, the selectivity control seen for the PMe_xPh_{3-x} series appears to be caused by a combination of steric and electronic factors. The greater the number of phenyl groups, the larger the steric destabilization of the intermediate amino alcohol complex. As some of the phenyl groups are replaced with methyl groups, the steric demands placed on the complex fall, but at the expense of increased electron density at the metal center, which also destabilizes the amino alcohol complex. The ligand $PMePh_2$ appears to represent an intermediate case, the ligand being neither large enough nor basic enough to favor monoamination. The result is higher selectivity to diamine. However, selectivity is also strongly dependent on the L:Ru ratio. Some of the complexes listed in Table II have L:Ru ratios of 4:1; others have ratios of 3:1.

The ability of phosphines to alter the selectivity of these reactions is not unlimited. A ligand such as tris(*ortho*-tolyl)phosphine [P(*o*-tol)₃] has a very large cone angle and might be expected to give monoamination. It is such a poor ligand, however, that it itself is only weakly complexed under catalytic conditions. The results in Table I indicate that the portion of the ruthenium with P(*o*-tol)₃ ligated to it is very likely to be inactive because of steric crowding, although the portion that is free of the ligand gives diamination.
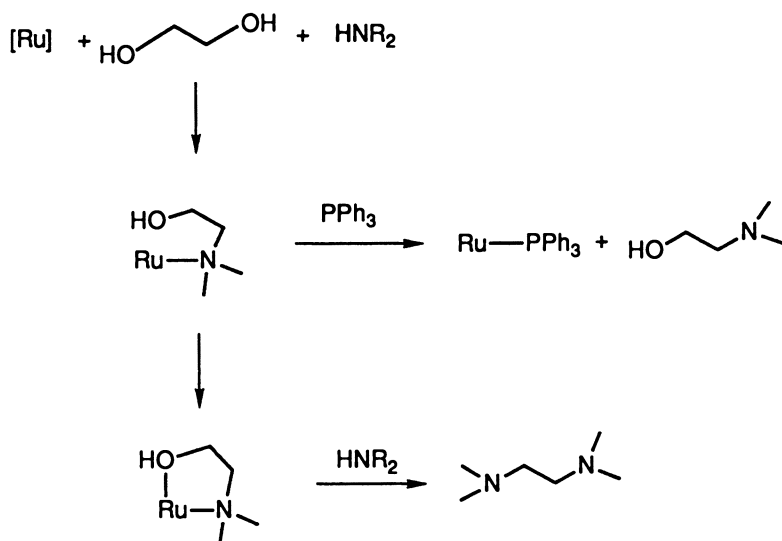
Scheme I. Ruthenium-catalyzed reaction of ethylene glycol and secondary amines.

Mixed-Ligand Systems

A particularly curious ligand effect is seen with the mixed phosphine complexes listed in Table II: $RuCl_2(dppm)(PMe_2Ph)_2$ and $RuCl_2(dppm)$-$(PMePh_2)_2$. The selectivities shown by both complexes appear to be dominated by the unidentate ligand. Coupled with the fact that the Ru–dppm systems without other phosphines present give selectivity very similar to $PMePh_2$, this fact implies that dppm is itself behaving as a unidentate ligand under reaction conditions, and the metal "sees" it only as an alkyldiphenylphosphine.

High-Temperature Reactions

As the temperature of these reactions increases, selectivity toward monoamination falls (*17*). This effect is shown in Table III for ruthenium-catalyzed reactions of morpholine and ethylene glycol in the presence of PPh_3. For a P:Ru ratio of 3 (i.e., pure $RuCl_2(PPh_3)_3$), a dramatic effect is seen going from 120 to 150 °C. Just as dramatic is the effect seen when the P:Ru ratio is increased from 3 to around 5 at both 150 and 180 °C (*see* Table IV). This ratio is very critical in determining selectivity at these higher temperatures. Below this ratio, the reaction is essentially nonselective in terms of mono-versus diamination. Above this ratio, selectivity to monoamination can again be achieved. The effect of added phosphine on higher-temperature reactions has also been reported by Bitsi et al. (*4*).

**Table III. Effect of Temperature on Selectivity
of $RuCl_2(PPh_3)_3$-Catalyzed Reactions of Ethylene Glycol
with Morpholine**

Temperature (°C)	Conversion (%)	Selectivity (%)		
		1	2	r
120	100	84	9	0.10
150	99	55	39	0.41
180	100	44	54	0.55

NOTE: Conditions are as in Table II, unless otherwise stated.

Reactions of Diethylene Glycol

Our results show the dependence of selectivity on phosphine ligands. Watanabe (*9*) reported that the activity of these types of catalyst systems is also strongly dependent on the properties of the phosphine. By using a very large number of examples, he and his co-workers showed that cyclizations of 1,5-pentanediol with primary aromatic amines proceeded well with $RuCl_3 \cdot xH_2O$ as the catalyst system, but more basic amines required more basic phosphines to achieve satisfactory conversions. Thus, the yield of *N*-

Table IV. Effect of P:Ru Ratio on Selectivity of $RuCl_2(PPh_3)_3$–PPh_3-Catalyzed Amination of Ethylene Glycol with Morpholine
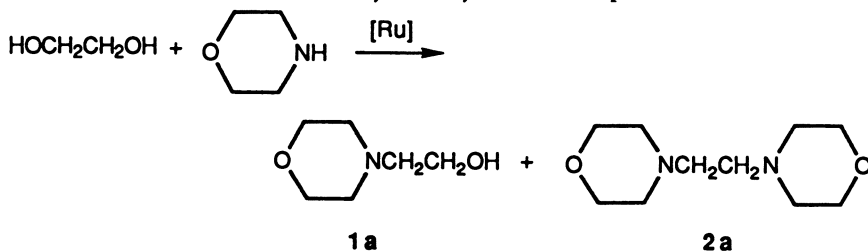
Temperature (°C)	P:Ru	Selectivity (%)		Conversion (%)	r
		1a	2a		
180	10.3	93	3	100	0.03
180	5.1	87	7	100	0.07
180	3.0	44	51	100	0.54
180	0[a]	7	76	95	0.92
150	4.6	84	16	100	0.16
150	0[a]	17	79	100	0.82
120	3.0	83	9	100	0.10
120	0[a]	15	80	100	0.84

NOTE: Conditions are as in Table I.
[a]Data for $RuCl_3 \cdot xH_2O$ as catalyst.

octylpiperidine from 1,5-pentanediol and *N*-octylamine was highest at a PBu_3:Ru ratio in the range of 2 to 3.

We have seen a related phosphine effect on the activities of our catalytic reactions, but in this case the reactivity is also related to the diol. Diethylene glycol is notably less reactive than ethylene glycol for the Ru–PPh_3 catalyst systems. The use of $RuCl_3 \cdot xH_2O$–PBu_3, however, leads to higher yields of aminated products (Table V). One explanation for this difference is that these diols can serve as chelating ligands. In a chelating mode, models show that β-hydride elimination to form an aldehydic intermediate is not favorable. [Presumably, an aldehydic-type of species—coordinated or otherwise—is necessary for amination to occur in these systems. We never directly observed such species. However, others have also surmised them to be present (5, 8).] Diethylene glycol is capable of acting as a tridentate ligand, stabilizing a chelate form relative to ethylene glycol. A very basic ligand such as PBu_3 can destabilize the chelate complex and thus allow the necessary β-hydride elimination.

Glycols as Ligands

This argument necessarily requires coordination of the alcohol. In Watanabe's work (8), they speculate that an amine complex is the active species and cite UV–visible spectroscopic data as evidence that alcohols (specifically

Table V. Reactions of Diethylene Glycol with Morpholine (mor) and Dimethylamine (DMA)
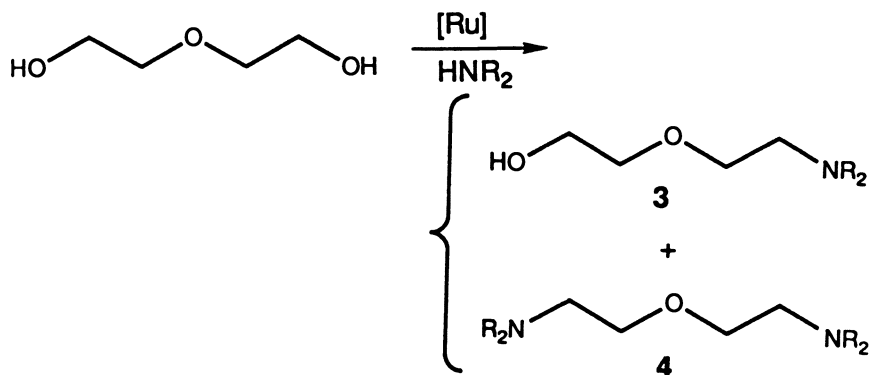
Catalyst[a]	Amine	Temperature (°C)	Selectivity		Conversion (%)
			3	4	
A	mor	115	81	—	17
A	mor	160	72	—	35
B	mor	120	81	4	37
B	mor	150	80	17	100
B	DMA	120	69	3	52
A	DMA	150	62	3	64
B	DMA	150	63	7	98

NOTE: Conditions are as in Table I unless otherwise specified.
[a]Catalyst A is $RuCl_2(PPh_3)_3$; catalyst B is $RuCl_3 \cdot xH_2O-3PBu_3$.

benzyl alcohol) do not displace phosphine from $RuCl_2(PPh_3)_3$. We, too, see no spectral changes (other than slight dilution effects) when a chloroform solution of $RuCl_2(PPh_3)_3$ (ca. 10^{-2} M) is treated with an 80-fold excess of methanol.

However, a 20-fold excess of ethylene glycol leads to an immediate color change from red-brown to pinkish. The characteristic (26) maxima at 740 and 480 nm for $RuCl_2(PPh_3)_3$ decrease in intensity, and a new absorbance at 495 nm appears. As the ^{31}P NMR spectrum of $RuCl_2(PPh_3)_3$ (27) in $CDCl_3$ disappears, free phosphine and a new sharp resonance at 54 ppm are evident. Clearly, ethylene glycol has a much higher affinity for the Ru(II) center than does either methanol or benzyl alcohol. This greater affinity accounts for the greater reactivity of ethylene glycol relative to methanol, which is almost unreactive at 120 °C. It is, however, important that the affinity not be so large as to favor too strong a chelating binding mode.

Although the experimental evidence for coordination of ethylene glycol (and by inference diethylene glycol) is quite strong, we cannot rule out the possibility that the need for a strongly basic phosphine such as PBu_3 for diethylene glycol arises from stable complex formation by the product. Tran-

sition metal complexes with amino alcohols are well known (28). It seems reasonable that an aminoethoxyethanol would bind more strongly than a simple amino alcohol. Thus, it may be that aminated products from diethylene glycol more readily poison the ruthenium catalyst than do those from ethylene glycol. The role of the PBu_3 in this case would be to regenerate a Ru–phosphine catalyst. A higher temperature is also required to achieve conversions of amines with diethylene glycol comparable to those seen with ethylene glycol.

Conclusion

The selectivity control observed in this reaction system contrasts strongly with that attainable with traditional heterogeneous alcohol amination catalyst systems. In particular, the subtle effects seen by small variations in amount and choice of ligand are striking. These catalysts offer new opportunities for the selective and efficient syntheses of highly functionalized organic compounds from readily available starting materials.

Acknowledgments

References

1. Grigg, R.; Mitchell, T. R. B.; Sutthivaiyakit, S.; Tongpenyai, N. *J. Chem. Soc., Chem. Commun.* **1981**, 611.
2. Murahashi, S.-I.; Kondo, K.; Hakata, T. *Tetrahedron Lett.* **1982**, *23*, 229.
3. Arcelli, A.; Bui-the-Khai; Porzi, G. *J. Organomet. Chem.* **1982**, *235*, 93.
4. Bitsi, G.; Schleiffer, E.; Antoni, F.; Jenner, G. *J. Organomet. Chem.* **1989**, *373*, 343.
5. Ganguly, S.; Joslin, F. L.; Roundhill, D. M. *Inorg. Chem.* **1989**, *28*, 4562.
6. Watanabe, Y.; Tsuji, Y.; Ohsugi, Y. *Tetrahedron Lett.* **1981**, *22*, 2667.
7. Watanabe, Y.; Tsuji, Y.; Ohsugi, Y.; Shida, J. *Bull. Chem. Soc. Jpn.* **1983**, *56*, 2452.
8. Watanabe, Y.; Tsuji, Y.; Ige, H.; Ohsugi, Y.; Ohta, T. *J. Org. Chem.* **1984**, *49*, 3359.
9. Tsuji, Y.; Huh, K.-T.; Ohsugi, Y.; Watanabe, Y. *J. Org. Chem.* **1985**, *50*, 1365.
10. Tsuji, Y.; Nishimura, H.; Huh, K.-T.; Watanabe, Y. *J. Organomet. Chem.* **1985**, *286*, C44.
11. Tsuji, Y.; Takeuchi, R.; Ogawa, H.; Watanabe, Y. *Chem. Lett.* **1986**, 293.
12. Tsuji, Y.; Huh, K.-T.; Watanabe, Y. *Tetrahedron Lett.* **1986**, *27*, 377.
13. Tsuji, Y.; Huh, K.-T.; Watanabe, Y. *J. Org. Chem.* **1987**, *52*, 1673.
14. Tsuji, Y.; Yokoyama, Y.; Huh, K.-T.; Watanabe, Y. *Bull. Chem. Soc. Jpn.* **1987**, *60*, 3456.
15. Marsella, J. A. *J. Org. Chem.* **1987**, *52*, 467.

16. Marsella, J. A. European Patent Application 169 547, 1986.
17. Marsella, J. A. U.S. Patent 4 680 393, 1987.
18. Marsella, J. A. U.S. Patent 4 745 190, 1988.
19. Marsella, J. A. U.S. Patent 4 855 425, 1989.
20. Winderl, S.; Haarer, E.; Corr, H.; Hornberger, P. U.S. Patent 3 270 059, 1966.
21. Barnes, C. M.; Rase, H. F. *Ind. Eng. Chem. Prod. Res. Dev.* **1981**, *20*, 399.
22. Runberg, J.; Baiker, A.; Kijenski, J. *Appl. Catal.* **1985**, *17*, 309.
23. Ohtani, B.; Osaki, H.; Nishimoto, S.-I.; Kagiya, T. *Tetrahedron Lett.* **1986**, *27*, 2019.
24. Tolman, C. A.; Faller, J. W. In *Homogeneous Catalysis with Metal Phosphine Complexes*; Pignolet, L. H., Ed.; Plenum: New York, 1983; Chapter 2.
25. Tolman, C. A. *Chem. Rev.* **1977**, *77*, 319.
26. James, B. R.; Markham, L. D. *Inorg. Chem.* **1974**, *13*, 97.
27. Hoffman, P. R.; Caulton, K. G. *J. Am. Chem. Soc.* **1975**, *97*, 4221.
28. Antelo, J. M.; Arce, F.; Rey, F.; Varela, A. *Polyhedron* **1987**, *6*, 1279.

Electronic and Steric Control

Catalytic Intramolecular Carbon–Hydrogen Insertion Reactions of Diazo Compounds

Michael P. Doyle

Department of Chemistry, Trinity University, San Antonio, TX 78212

Dirhodium(II) carboxylates and carboxamides are the most effective catalysts for intramolecular carbon–hydrogen insertion reactions that result from decomposition of diazo compounds. Cyclopentanones, β- and γ-lactams, and γ-lactones are formed from diazoketones, diazoamides, and diazoesters, respectively, in moderate to high yields and, ordinarily, with a high degree of regio- and stereocontrol. Acting as metal-stabilized carbocations, the intermediate rhodium carbenes are electrophilic reagents whose reactivities and selectivities are dependent on the electron-withdrawing capabilities of their bridging ligands. Selectivity for C–H insertion is greatly enhanced by the use of Rh₂(acetamide)₄, and chiral dirhodium(II) carboxamide catalysts offer great potential for highly enantioselective transformations.

$\mathbf{R}$HODIUM(II) CARBOXYLATES are now well-known catalysts for the remote functionalization of carbon–hydrogen bonds in carbenoid reactions of diazocarbonyl compounds (eq 1, Z = H or COOR) (*1*, *2*).

$$\tag{1}$$
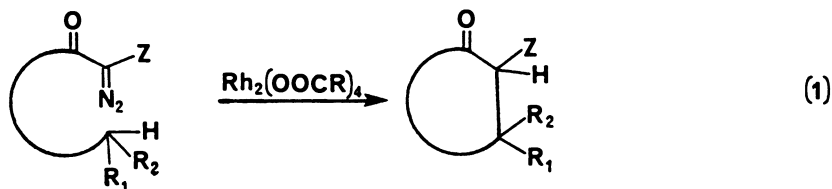
Their advantages over the more traditional copper catalysts (*3*) are well documented both in the yields of products obtained from intramolecular cyclization and in the selectivity that can be achieved from these reactions.

Indeed, rhodium(II) compounds have become the catalysts of choice for carbenoid reactions extending from cyclopropanation (4) and insertion reactions to ylide generation–rearrangement (5–8) or dipolar addition (9–11).

Rhodium(II) acetate, the catalyst most often employed for carbenoid reactions, is a binuclear compound with four bridging acetate ligands and D_{4h} symmetry (1, R = CH$_3$) (12–14).

1
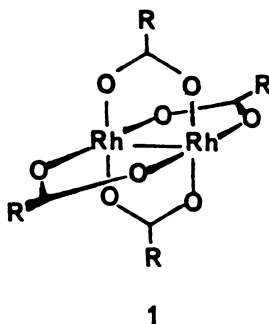
In the absence of coordinating ligands that include nitriles, alcohols, and ketones, Rh$_2$(OAc)$_4$ possesses one vacant coordination site per metal atom. When reacting as an electrophile, it undergoes addition to the diazo carbon of the reactant diazo compound (1). With diazocarbonyl compounds such as ethyl diazoacetate, this electrophilic addition takes place near –20 °C and is the rate-limiting step. Subsequent loss of dinitrogen is presumed to result in the formation of an electrophilic metal carbene that is the active intermediate in carbenoid reactions (Scheme I).
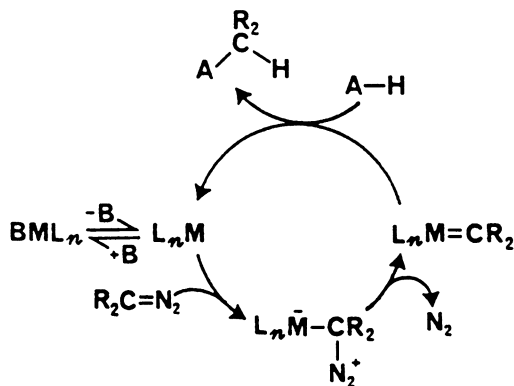
Scheme I.

Although these intermediates have not been directly observed, indirect evidence from reactivity–selectivity correlations with pentacarbonyltungsten carbenes in cyclopropanation reactions suggest their formation (15, 16).

With diazo compounds ranging from phenyldiazomethane and trimethylsilyldiazomethane to diazoacetates and diazoamides, reactions with

$Rh_2(OAc)_4$ occur at room temperature. More stable diazo compounds such as diazoacetoacetates and diazoacetoacetamides require higher temperatures for efficient catalytic dinitrogen loss and carbenoid reactions. Normally reactions are performed by controlled addition of the diazo compound to the catalyst to limit the concentration of the diazo compound and minimize carbene dimer formation (*17*).

Carbon–Hydrogen Insertion Reactions

Cyclopentanones.   The employment of $Rh_2(OAc)_4$ for intramolecular carbon–hydrogen insertion reactions with diazocarbonyl compounds evolved from the prior use of copper catalysts for these transformations (*3*). The advantages of $Rh_2(OAc)_4$ have been clearly evident. The conversion of isopimaridiene skeleton **2** into the 16-keto steroid **3** was achieved in 60% yield with $Rh_2(OAc)_4$ as the catalyst (eq 2), but poor yields of **3** were obtained when $CuSO_4$ was used (*18*).

$$(2)$$
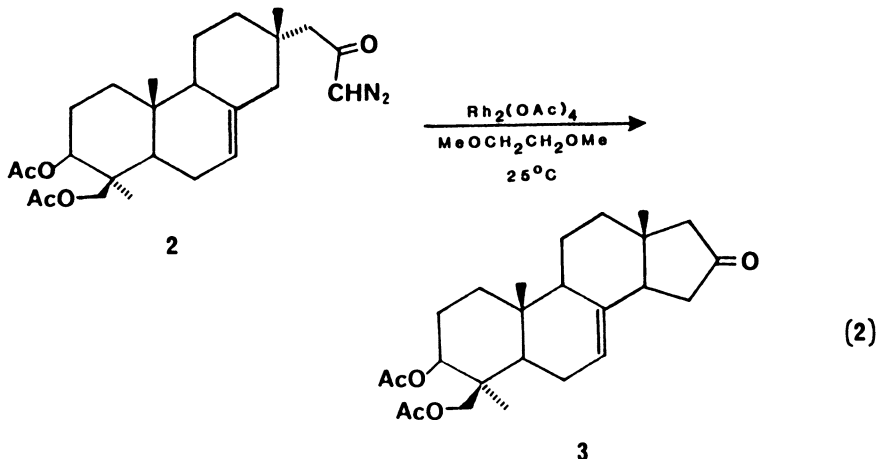
Similarly, only minor amounts of cyclopentanone products resulted from the $CuSO_4$-catalyzed decomposition of 1-diazo-2-octanone (**4**) (eq 3), where cyclohexanone formation (**6**) was also observed, or 1-diazo-4,4-dimethyl-2-pentanone (*18*).

$$(3)$$
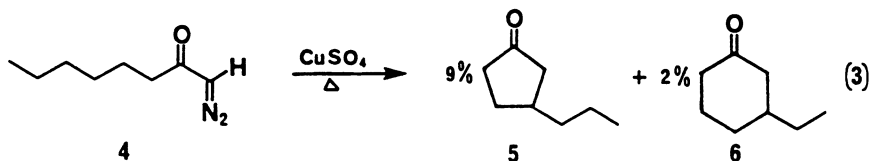
A broad selection of α-diazo-β-ketoesters, -sulfones, and -phosphonates has been transformed in moderate to good yields to the corresponding cyclopentanone derivatives with the use of $Rh_2(OAc)_4$ (e.g., eqs 4–6).

$$(4)$$

only (5)

$$(6)$$
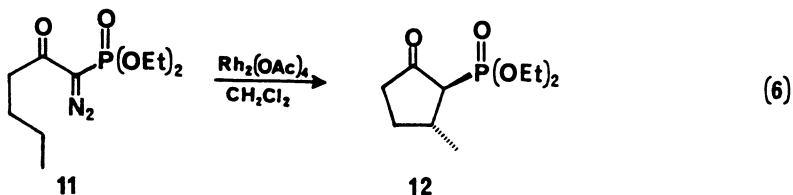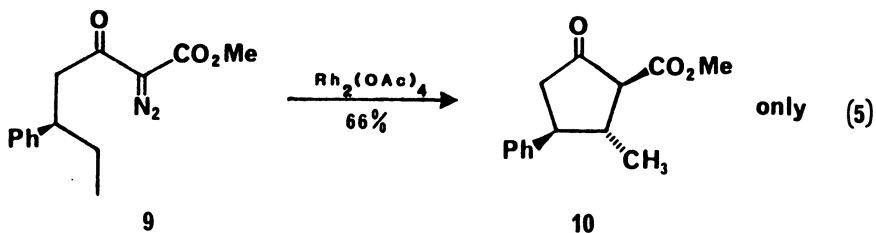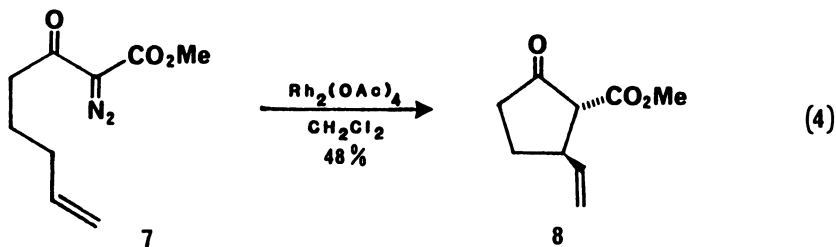
Exceptional regioselectivity and diastereoselectivity were achieved (19–23). In contrast to results obtained with $Rh_2(OAc)_4$ (eq 4), treatment of the same α-diazo-β-ketoester 7 with $CuSO_4$ produced a mixture of products with intramolecular cyclopropanation favored over carbon–hydrogen insertion (24).

Extensive investigations of competitive intramolecular carbon–hydrogen insertion reactions (Scheme II), where the two reacting bonds are at the
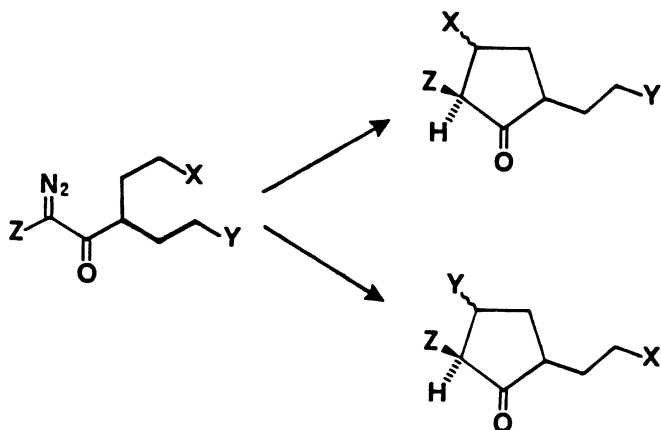
Scheme II.

same formal distance from the carbenoid center, have demonstrated that reactivity decreases according to 3° C–H > 2° C–H > 1° C–H (*21*).

Surprisingly, in view of the electronic character of the reactant metal carbene, insertion into benzylic and allylic methylene positions was found to be disfavored relative to insertion into aliphatic methylene positions. Furthermore, in one of the most dramatic demonstrations of regiocontrol by electron-withdrawing groups, Stork and Nakatani (*25*) found that an ester substituent deactivated both α- and β-methylene groups toward C–H insertion (eqs 7 and 8).

(7)

(8)
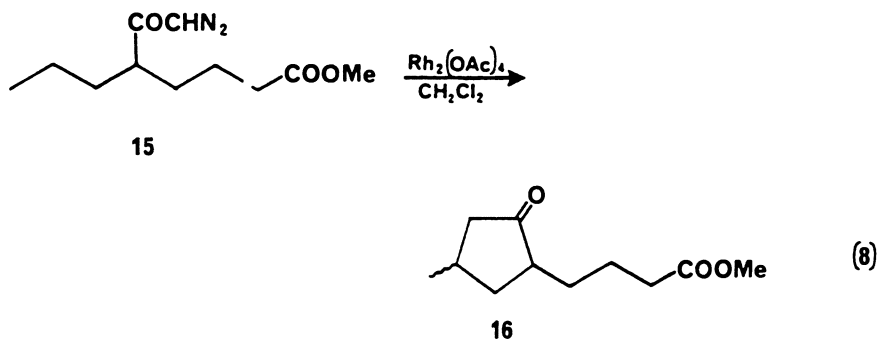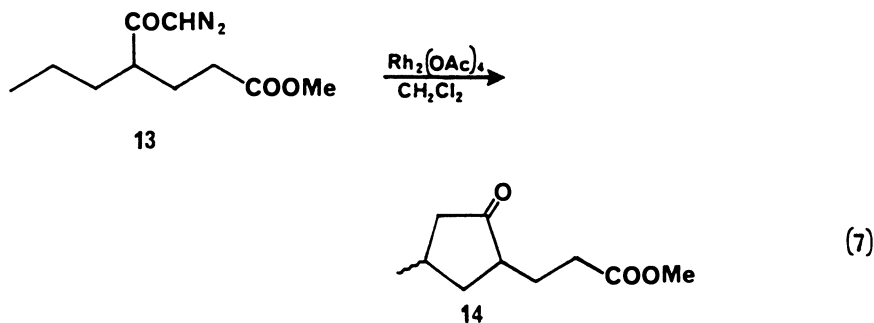
Thus, even when this intramolecular pathway is the only one possible, only carbene dimer formation is realized (*25*). Electronic preferences appear to control regioselectivity but, as will be seen (vide infra), conformational control of reaction selectivity provides a rational explanation for these results.

Despite the apparent overwhelming preference for cyclopentanone formation in $Rh_2(OAc)_4$-catalyzed C–H insertion reactions of diazo carbonyl compounds, isolated examples of preferential β- and δ-C–H insertion reactions have been reported. Whereas **17** produced both **18** and **19** in a 1.5:1.0 ratio (eq 9), only **21** was produced from the structurally similar, but more highly substituted, **20** (eq 10) (*26*).

Similarly, the δ-lactone **23** was the only insertion product isolated from the $Rh_2(OAc)_4$-catalyzed decomposition of **22** (eq 11) (*26*).

17 $\xrightarrow[\text{83\%}]{\text{Rh}_2(\text{OAc})_4}$

18   +   **19**   (9)

20 $\xrightarrow[\text{55\%}]{\text{Rh}_2(\text{OAc})_4}$

21   only   (10)

22 $\xrightarrow[\substack{\text{Freon TF} \\ \text{45\%}}]{\text{Rh}_2(\text{OAc})_4}$ **23**   (11)
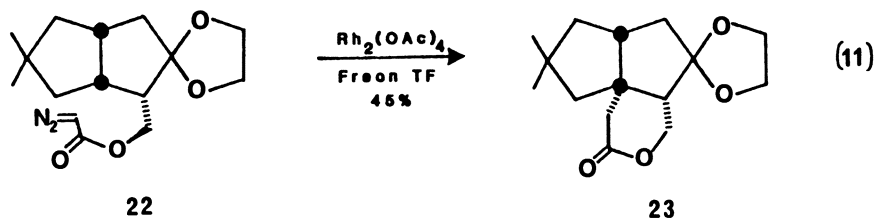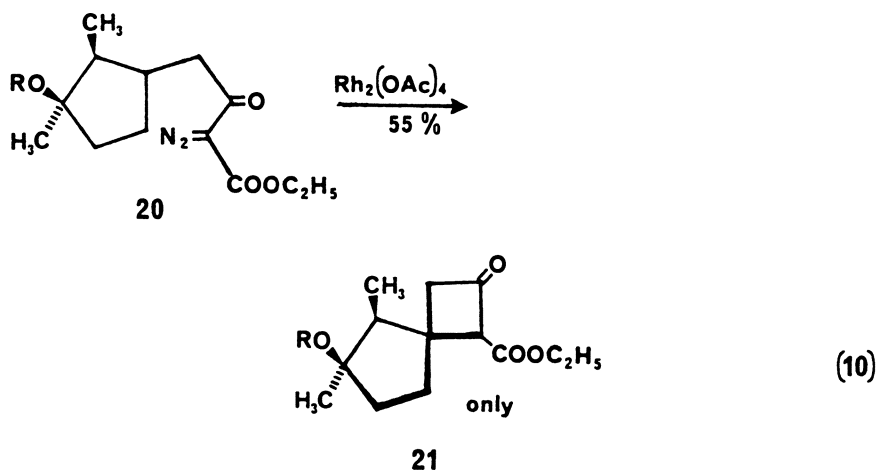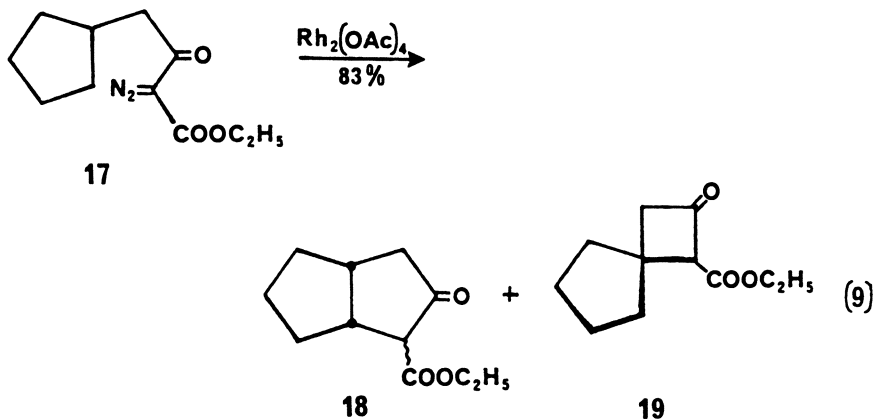
These examples suggest that subtle changes in reactant structure can have an enormous influence on reaction regioselectivity and that electronic preferences alone cannot explain the selectivity for carbon–hydrogen insertion in $\text{Rh}_2(\text{OAc})_4$-catalyzed reactions.

Lactams.   Ponsford and Southgate (27) were the first to report that $\text{Rh}_2(\text{OAc})_4$ was an effective catalyst for intramolecular carbon–hydrogen in-

sertion reactions. Diazoacetoacetamide **24** underwent $Rh_2(OAc)_4$-catalyzed decomposition at room temperature to yield β-lactam **25** in 75% yield (eq 12).

$$(12)$$
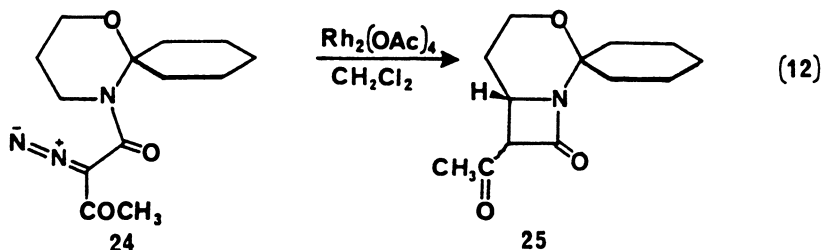
With Cu in toluene at 90 °C, **25** was formed in only 25% yield. Similar results were obtained with other 1,3-oxazines (*28, 29*) but the generality of this methodology for the synthesis of β-lactams awaited reports by Doyle and co-workers (*30, 31*). Treatment of a series of N-benzyl-N-*tert*-butyldi-azoacetoacetamides **26** ($R = CH_3CO$) with $Rh_2(OAc)_4$ (1.0 mol %) in refluxing benzene resulted in the exclusive production of *trans*-disubstituted β-lac-tams **27** in nearly quantitative yields (eq 13).

$$(13)$$
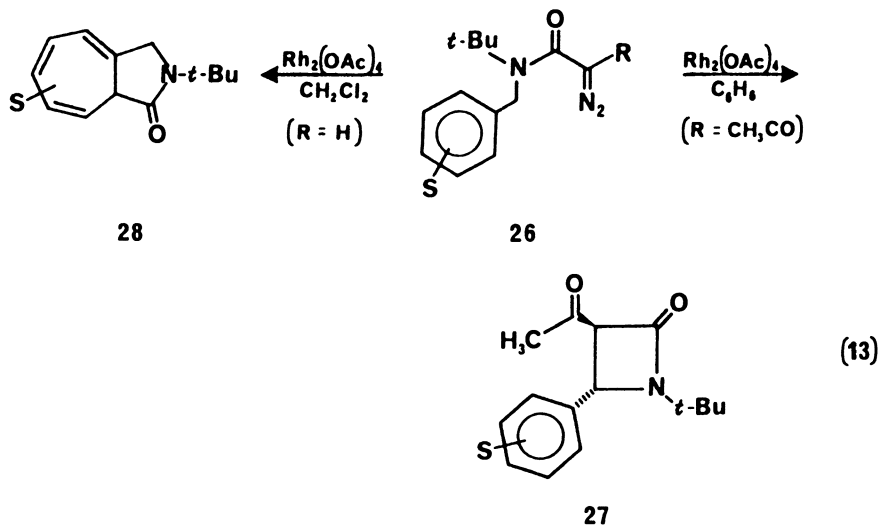
28 (%)	26	27 (%)
94	S = 3,4-di-OCH₃	95
93	m-OCH₃	90
99	H	98
89	m-Br	92
—	p-NO₂	92

NOTE: — means this experiment was not performed.

In contrast, the N-benzyl-N-*tert*-butyldiazoacetamides **26** (R = H) underwent exclusive carbene addition to the aromatic ring (**28**) when treated with a catalytic amount of $Rh_2(OAc)_4$ in dichloromethane at room temperature (*32*). The acetyl group of the diazo carbon obviously inhibits carbenoid addition to the electron-rich aromatic ring, even when substituted with two methoxy groups to enhance its nucleophilic reactivity.

The influence of the N-*tert*-butyl group is seen from results obtained with diazoacetoacetamides having smaller N-alkyl substituents. When the *tert*-butyl group of **26** (R = CH_3CO) is replaced by isopropyl, only 60% of the reaction products result from insertion into the benzylic position. The remaining 40% arise from insertion into the methine hydrogen of the isopropyl substituent. With ethyl as the N-alkyl substituent, only 17% of the reaction products result from insertion into the benzylic position. The remainder are due to insertion into the ethyl group: 60% into the primary methyl group to form the corresponding γ-lactam and 23% into the secondary methylene group.

The selectivity observed in these reactions does not appear to be a function of electronic influences by substituents on the reacting C–H bond, as was reported by Taber and Ruckle (*21*) for cyclopentanone formation by carbon–hydrogen insertion. Rather, these results can be explained by insertion into a C–H bond that is held in close proximity to the carbenoid center (**29**).

29
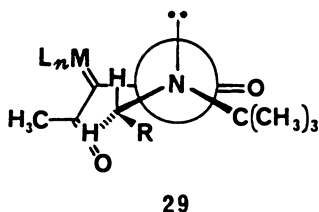
Overlap of the nitrogen nonbonded electrons with the carbonyl π-system fixes the amide conformation so that the larger nitrogen substituent is oriented toward the carbonyl group. Steric effects by the carbenoid substituents on benzylic substituents force the aryl group away from the acetyl group and coordinated metal and place the benzylic hydrogens within the reactive environment of the carbenoid center. Consistent with this interpretation, decomposition of **30** in refluxing benzene, catalyzed by $Rh_2(OAc)_4$, forms β-lactam **31**, solely as the *trans* isomer, in 96% isolated yield (eq 14) (*31*).

(14)

30   **31**
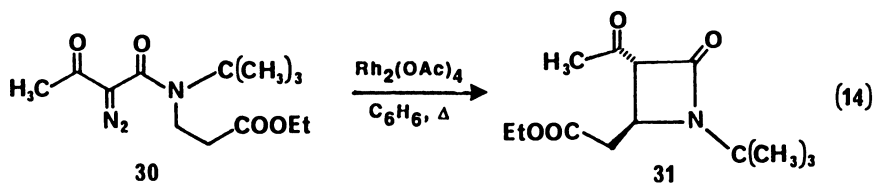
In addition, in the most convincing demonstration of conformational preferences in carbenoid insertion reactions, diazoacetoacetamide **32** undergoes high-yield conversion (89%) to the *cis*-disubstituted β-lactam **33** in rhodium(II)-perfluorobutyrate-catalyzed reactions performed in refluxing dichloromethane (eq 15) (*31*). If electronic factors controlled carbenoid C–H insertion reactions, these results would not have been anticipated on the basis of conclusions drawn from eqs 7 and 8.

$$(15)$$
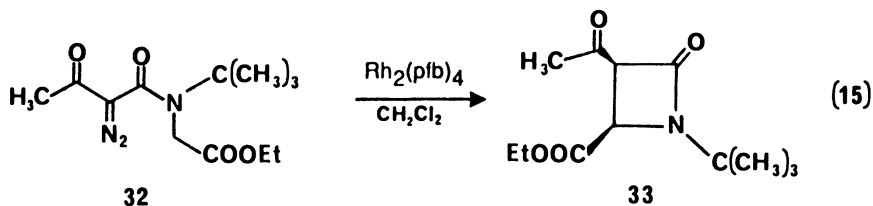
What, then, is the cause of the apparent difference between the regiocontrol observed for β-lactam formation and that for cyclopentanone formation? We believe that the metal carbenes derived from reactions of rhodium(II) carboxylates and diazo compounds should be viewed as metal-stabilized carbocations (**34a**), with their inherent stability arising from electron donation through the dirhodium framework (**34b**).
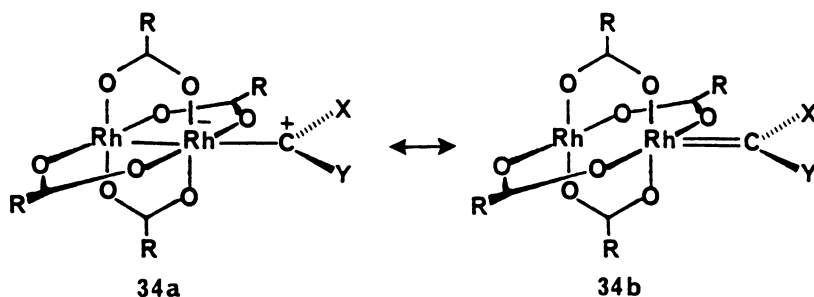
Carbon–hydrogen insertion occurs by interaction of the p-orbital on the carbenic carbon with the σ-C–H bond. It results in bond formation between the carbene carbon and both carbon and hydrogen of the reacting carbon–hydrogen bond (Scheme III).

As this bond formation progresses, the metal bound to the carbene carbon dissociates and product formation is realized. The mechanistic depiction in Scheme III also accounts for the diastereoselectivity that is observed in these reactions. Steric interactions between R and COOR' destabilize the conformation in which the R group is in the axial position. The exception appears to be the formation of the *cis*-disubstituted β-lactam in eq 15. However, in this case the C–H insertion that would have resulted
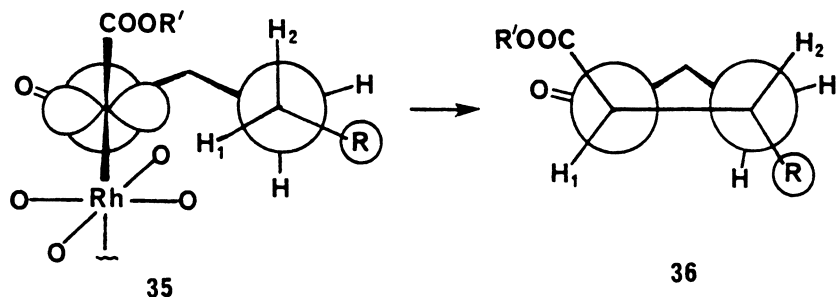
Scheme III.

in the *trans*-disubstituted β-lactam would have had to occur from a conformation in which the carboxylate group was juxtaposed against the catalyst face. Steric and stereoelectronic factors disfavor this conformation.

The cause of the apparent electronic destabilization by ester functional groups on β-C–H insertion that was reported by Stork and Nakatani (25) is probably due to repulsion of the carboxylate by the bridging ligands of the dirhodium catalyst (35). A similar explanation can be made for the apparent lower reactivity of benzylic methylene C–H bonds described by Taber and Ruckle (21). The influence of catalyst structure on selectivity is minimized too often in mechanistic considerations of catalytic reactions. However, insertion into a C–H bond α to a carboxylate group is certainly subject to electronic destabilization of the transition state leading to products. Similarly, insertion into a C–H bond α to nitrogen is subject to electronic stabilization of this state.

Application of this methodology to other aliphatic systems in which both β- and γ-C–H insertion are possible demonstrates its broad applicability for the construction of β-lactams. Rhodium(II)-acetate-catalyzed decomposition of the diazoacetoacetamides derived from diisopropylamine, dicyclohexylamine, and *trans*-2,6-dimethylpiperidine in benzene formed the corresponding β-lactam products 37–39 exclusively and in high yield: 37 (89%), 38 (100%), and 39 (90%, isomer ratio = 1.4) (30).
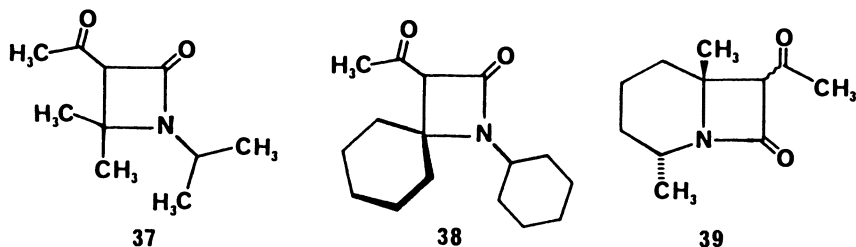
The corresponding diazoacetamides also formed β-lactam products but, in these systems, competition between β-C–H and γ-C–H insertion occurred to a limited extent (30).

As is implied from consideration of the metal-stabilized carbocation (**34**) hypothesis for carbene reactivity, significant manipulation of product distributions in catalytic transformations of diazoamides could be achieved by changing the catalyst from the indiscriminate $Rh_2(pfb)_4$ (*33, 34*) through $Rh_2(OAc)_4$ to the electronically selective $Rh_2(acam)_4$ (pfb is perfluorobutyrate, and acam is acetamide) (*4, 34*).
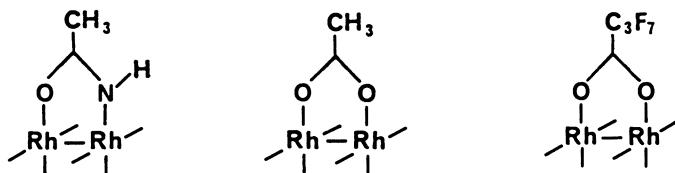
For example, decomposition of *N-tert*-butyl-*N*-(2-phenylethyl)diazoacetoacetamide (**40**, R = $COCH_3$) yields both β-lactam and γ-lactam products (Scheme IV).

Each product is formed exclusively as the *trans* diastereoisomer, and they are formed in approximately equal amounts, with $Rh_2(OAc)_4$ as the catalyst. However, use of $Rh_2(pfb)_4$ favors the β-lactam product, and $Rh_2(acam)_4$ favors formation of γ-lactam. The corresponding diazoacetamide (**40**, R = H) produces products from both γ-C–H insertion (**43**) and aromatic addition (**44**) upon catalytic decomposition. Effective control of product selectivity is achieved with the use of $Rh_2(pfb)_4$ and $Rh_2(acam)_4$. In all cases product yields are greater than 90%. Similarly, decomposition of *N-n*-butyl-*N-tert*-butyldiazoacetoacetamide (**45**, R = $COCH_3$) with these catalysts exhibits a significant catalyst-ligand-dependent variation in the relative yields for formation of β-lactam and γ-lactam products (Scheme V).

However, the corresponding diazoacetamide (**45**, R = H) formed the γ-lactam **48** with only minor amounts (2–7%) of β-lactam product, using the same set of rhodium(II) catalysts.

Relative to $Rh_2(OAc)_4$, the metal carbene derived from $Rh_2(acam)_4$ is projected to be more stable and, consequently, more susceptible to product development control in intramolecular reactions. In contrast, the metal carbene derived from $Rh_2(pfb)_4$ is less stable and more electrophilic. Therefore, it is more reactive toward electron-rich substituents, as in the formation of **44**, and less discriminate.

The conditions that favor γ-lactam formation—use of diazoacetamides rather than diazoacetoacetamides, the absence of an electron-withdrawing group at the site of insertion, and use of the less electrophilic $Rh_2(acam)_4$—signify the importance of stereoelectronic considerations in predicting the outcome of these C–H insertion reactions. β-Lactam formation is not the preferred pathway for the catalytic decomposition of diazoamides. When there is a competitive choice between β-lactam and γ-lactam production, as with **45**, the γ-lactam predominates. The reason that $Rh_2(pfb)_4$ enhances β-
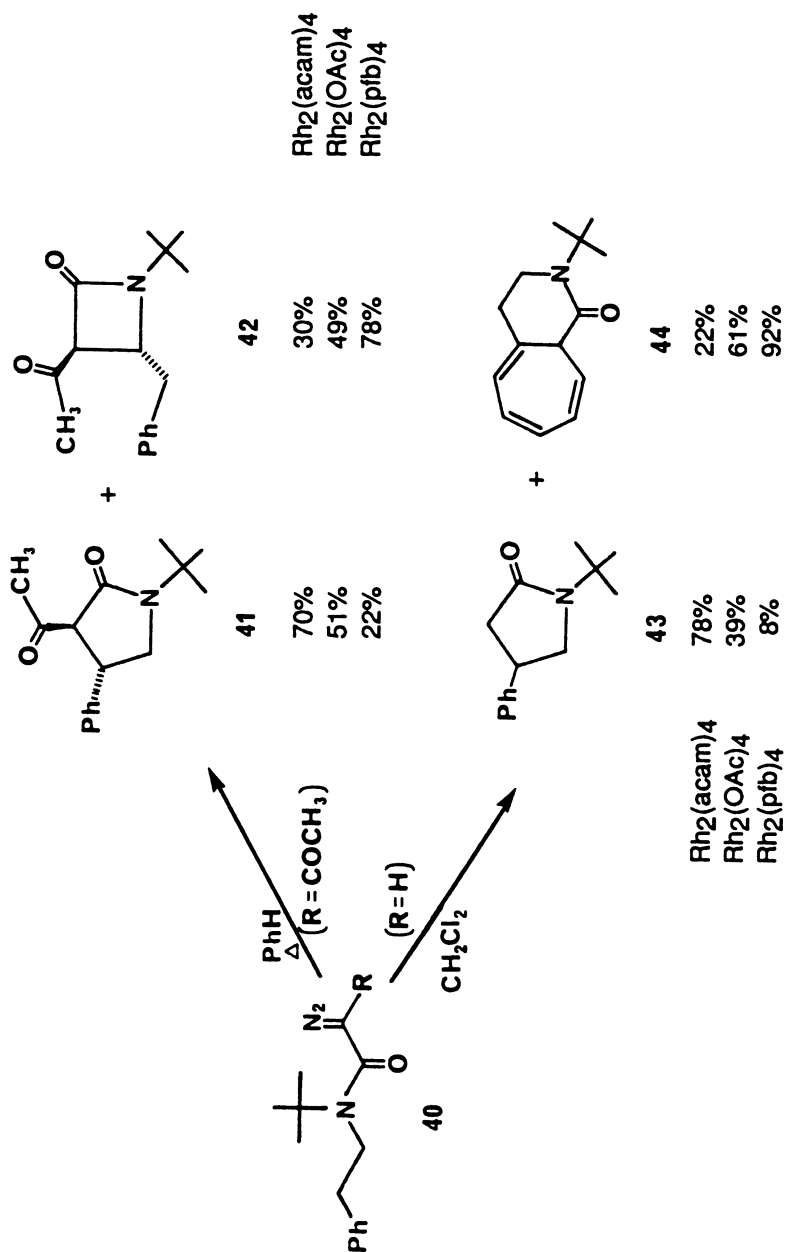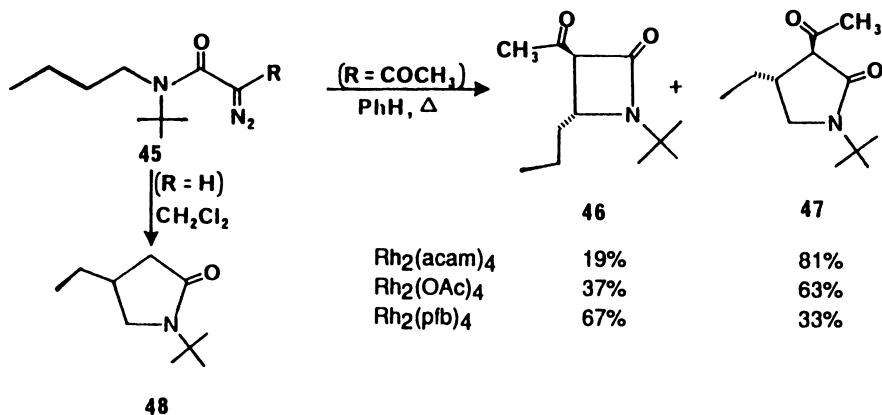
Scheme IV.

Scheme V.

lactam formation is probably the high reactivity of the intermediate metal carbene, which allows bond formation to begin at a greater distance from the C–H bond and thereby initiates relatively indiscriminate insertion.

Lactones.   In copper-catalyzed reactions, diazoacetate esters do not undergo C–H insertion to any meaningful extent (*35, 36*). Even the more viable diazomalonate esters produce γ-lactones in only low to moderate yields in the few examples that have been published (*37–39*). Cane and Thomas (*26*) reported the first example of an intramolecular C–H insertion reaction of a diazoester catalyzed by $Rh_2(OAc)_4$ (eq 11). Rather than the normally favored γ-lactone, a δ-lactone directed to the synthesis of pentalenolactone E was produced. Capitalizing on the directive influences that can be achieved by variation of the bridging ligands of rhodium(II) carboxylates and rhodium(II) carboxamides, Doyle and co-workers (*40*) reported that catalytic carbenoid decomposition of diazoesters provides a general and highly selective methodology for the synthesis of γ-butyrolactones (e.g., eq 16).

(16)
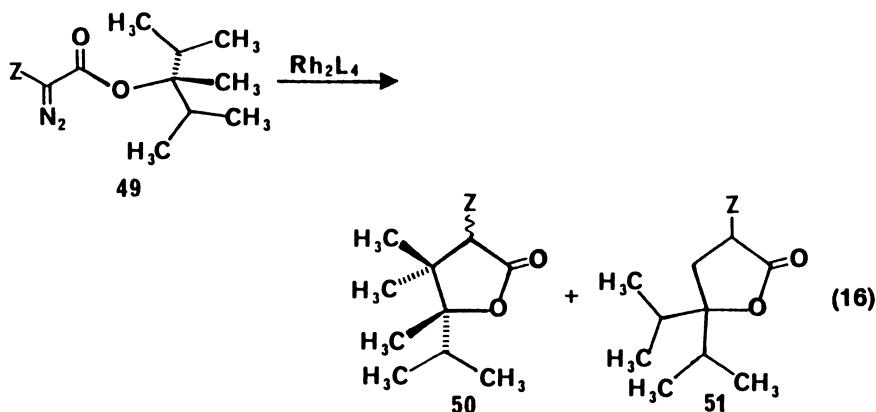
Rh_2L_4	$Z = H$ Yield (%)	Relative Yield (%)		$Z = CH_3CO$ Yield (%)	Relative Yield (%)	
		50	**51**		**50**	**51**
$Rh_2(pfb)_4$	56	32	68	45	45	55
$Rh_2(OAc)_4$	81	53	47	97	90	10
$Rh_2(acam)_4$	96	>99	<1	89	>99	<1

Indiscriminate C–H insertion occurred with the use of $Rh_2(pfb)_4$, primarily into normally unreactive 1° C–H bonds, but exceptionally high regioselectivity for insertion was achieved with the use of $Rh_2(acam)_4$. Extension of this methodology to **52** produced **53** in 85–88% yield as the sole lactone product from $Rh_2(OAc)_4$- or $Rh_2(acam)_4$-catalyzed decompositions (eq 17). Similarly, effective control of regioselectivity for C–H insertion could be achieved in the catalytic decomposition of **54** (eq 18) with the use of $Rh_2(acam)_4$.

(17)

(18)
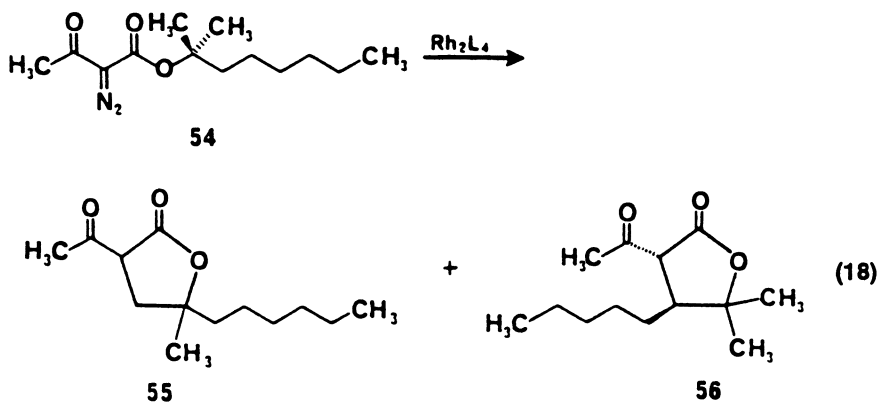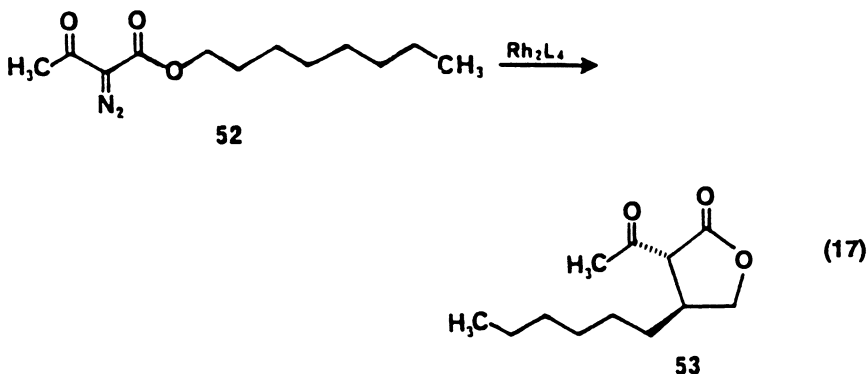
Rh_2L_4	Yield (%)	Relative Yield (%)	
		55	**56**
$Rh_2(pfb)_4$	81	63	37
$Rh_2(OAc)_4$	80	28	72
$Rh_2(acam)_4$	80	6	94

The composite results from a series of similar insertion reactions that allowed selection between 1°, 2°, and 3° C–H bonds demonstrate that the relative reactivities for these transformations are highly dependent on the catalyst. With $Rh_2(acam)_4$, relative reactivities for 1°, 2°, and 3° C–H insertion are approximately 1:40:>100, those for $Rh_2(OAc)_4$ are 1:8:54, and relative reactivities for $Rh_2(pfb)_4$ are nearly statistical. However, these relative reactivities are of no practical value in predicting the outcome of C–H insertion reactions in more complex systems where stereoelectronic or steric factors govern product formation. For example, $Rh_2(OAc)_4$-catalyzed decomposition of $(1R,2S,5R)$-$(-)$-menthyl diazoacetoacetate, **57**, resulted in the exclusive formation of bicyclic γ-lactone **58** (80% yield) with *trans* ring fusion and "*trans*" geometry for the acetyl group (eq 19).
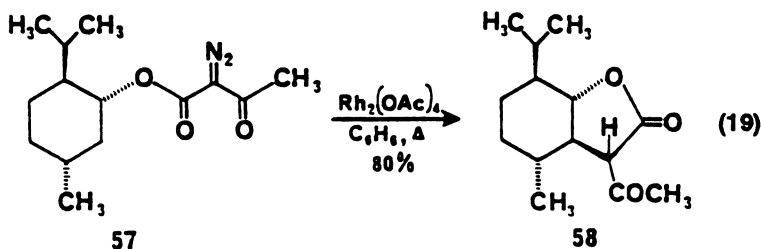
Substitution by an ether or ester oxygen apparently increases the reactivity of a C–H bond toward carbene insertion. Adams et al. (*41*) reported a high degree of regioselectivity for 3(2*H*)-furanone production in $Rh_2(OAc)_4$-catalyzed reactions (e.g., eq 20).
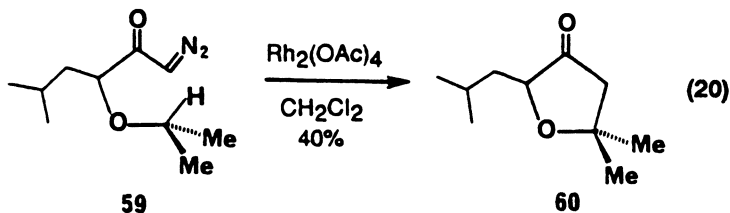
They employed this transformation in the total synthesis of (+)-muscarine (*42*). More recently, Lee et al. (*43*) reported that alkyl methyl

diazomalonates form, preferentially in several examples, β-lactones in $Rh_2(OAc)_4$-catalyzed reactions (e.g., eq 21).

(21)
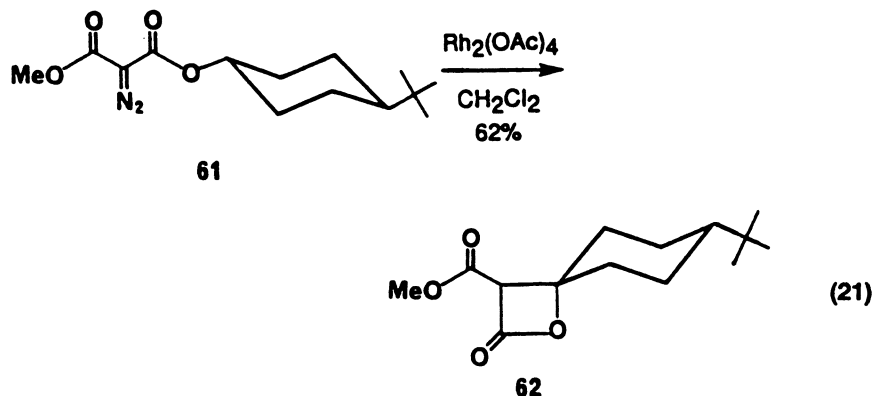
As was found with **58**, γ-lactone production is the exclusive consequence of $Rh_2(OAc)_4$-catalyzed decomposition of menthyl methyl diazomalonate.

Adams attributes the selectivity observed for 3(2H)-furanone formation to electronic influences; Lee explains β-/γ-lactone preferences as due to undefined conformational bias in the metallocarbene species. Although both factors may be important in these insertion reactions, conformational influences clearly have a central role in defining observed regioselectivities. This influence is amply demonstrated in the catalytic insertion reactions of diazoacetamides.

Summary and Future Directions

Rhodium(II) carboxylates and carboxamides clearly are effective catalysts for carbon–hydrogen insertion reactions of carbenoid intermediates formed from diazo compounds. Regiocontrol in these reactions is greatly influenced by the bridging ligands of the dirhodium(II) nucleus. Rhodium(II) acetamide offers the highest degree of selectivity, and rhodium(II) perfluorobutyrate offers the lowest selectivity in competitive insertion reactions. Further control of selectivity is anticipated with structural modifications of the bridging dirhodium(II) ligands.

Enantioselective C–H insertion reactions, which do not appear to be as feasible with chiral copper catalysts (44–47), should be optimal with the use of chiral dirhodium(II) catalysts. Indeed, by using chiral dirhodium(II) tetrakis[methyl 2-pyrrolidinone-5-carboxylates] [i.e., $Rh_2(5S\text{-}MEPY)_4$ and $Rh_2(5R\text{-}MEPY)_4$; MEPY is methyl 2-pyrrolidone-5-carboxylate], we have been able to achieve greater than 90% enantiomeric excess (ee) in intramolecular cyclopropanation reactions (48).
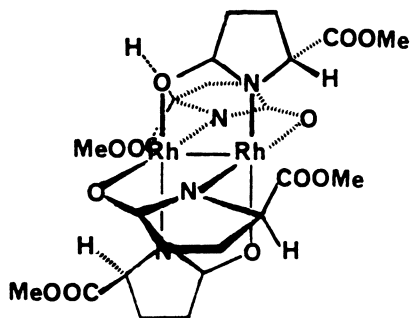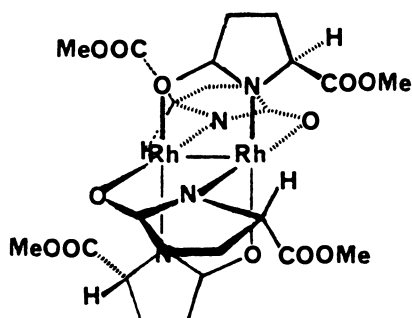
Rh$_2$(5*R*-MEPY)$_4$ Rh$_2$(5*S*-MEPY)$_4$

In preliminary results from the catalytic decomposition of **63** (R = Me, Et, or PhCH$_2$) with Rh$_2$(MEPY)$_4$ catalysts, asymmetric induction in the formation of γ-lactones **64** is at the 85–90% ee level (eq 22). Intensive efforts are underway to develop this potential.

(22)
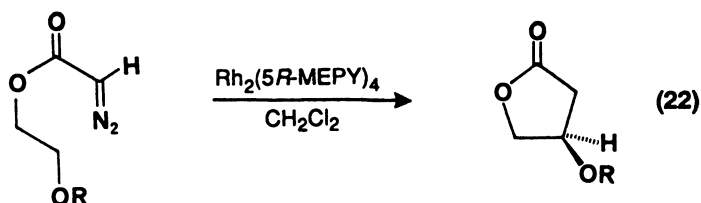
That such high enantiomeric excesses can be achieved with chiral di-rhodium(II) carboxamides, which have two nitrogen donor atoms oriented *cis* on each rhodium, clearly suggests that the dirhodium(II) ligands are not fluxional, undergoing Rh–O or Rh–N bond cleavage in response to metal carbene formation and subsequent reactions (*21*). Instead, C–H insertion is a consequence of the electrophilic character of the intermediate metal carbene. The metal stabilizes the carbocation form of the metal carbene (**34** and Scheme III), and a coordination site on the metal is not opened by association with a carbene.

Acknowledgments

References

1. (a) Doyle, M. P. *Acc. Chem. Res.* **1986**, *19*, 348; (b) Doyle, M. P. *Chem. Rev.* **1986**, *86*, 919.
2. Maas, G. *Top. Curr. Chem.* **1987**, *137*, 75.
3. Burke, S. D.; Grieco, P. A. *Org. React. (N. Y.)* **1979**, *26*, 361.
4. Doyle, M. P.; Bagheri, V.; Wandless, T. J.; Harn, N. K.; Brinker, D. A.; Eagle, C. T.; Loh, K.-L. *J. Am. Chem. Soc.* **1990**, *112*, 1906.
5. Doyle, M. P.; Bagheri, V.; Claxton, E. E. *J. Chem. Soc., Chem. Commun.* **1990**, 46.
6. Doyle, M. P.; Griffin, J. H.; Chinn, M. S.; van Leusen, D. *J. Org. Chem.* **1984**, *49*, 1917.
7. Pirrung, M. C.; Werner, J. A. *J. Am. Chem. Soc.* **1986**, *108*, 6060.
8. Roskamp, E. J.; Johnson, C. R. *J. Am. Chem. Soc.* **1986**, *108*, 6062.
9. Padwa, A.; Carter, S. P.; Nimmesgern, H. *J. Am. Chem. Soc.* **1988**, *110*, 2894.
10. Padwa, A.; Fryxell, G. E.; Zhi, L. *J. Org. Chem.* **1988**, *53*, 2875.
11. Padwa, A.; Hertzog, D. L.; Chinn, R. L. *Tetrahedron Lett.* **1989**, *30*, 4077.
12. Felthouse, T. R. *Prog. Inorg. Chem.* **1982**, *29*, 73.
13. Cotton, F. A.; Walton, R. A. *Multiple Bonds Between Metal Atoms*; Wiley: New York, 1982; p 311.
14. Boyar, E. B.; Robinson, S. D. *Coord. Chem. Rev.* **1983**, *50*, 109.
15. Doyle, M. P.; Griffin, J. H.; Bagheri, V.; Dorow, R. L. *Organometallics* **1984**, *3*, 53.
16. Doyle, M. P.; Griffin, J. H.; Conceicão, J. *J. Chem. Soc., Chem. Commun.* **1985**, 328.
17. Doyle, M. P.; van Leusen, D.; Tamblyn, W. H. *Synthesis* **1981**, 787.
18. Wenkert, E.; Davis, L. L.; Mylari, B. L.; Solomon, M. F.; da Silva, R. R.; Shulman, S.; Warnet, R. J.; Ceccherelli, P.; Curini, M.; Pellicciari, R. *J. Org. Chem.* **1982**, *47*, 3242.
19. Taber, D. F.; Petty, E. H. *J. Org. Chem.* **1982**, *47*, 4808.
20. Taber, D. F.; Petty, E. H.; Raman, K. *J. Am. Chem. Soc.* **1985**, *107*, 196.
21. Taber, D. F.; Ruckle, R. E., Jr. *J. Am. Chem. Soc.* **1986**, *108*, 7686.
22. Monteiro, H. J. *Tetrahedron Lett.* **1987**, *28*, 3459.
23. Corbel, B.; Hernot, D.; Haelters, J.-P.; Sturtz, G. *Tetrahedron Lett.* **1987**, *28*, 6605.
24. Taber, D. F.; Saleh, S. A.; Korsmeyer, R. W. *J. Org. Chem.* **1980**, *45*, 4699.
25. Stork, G.; Nakatani, K. *Tetrahedron Lett.* **1988**, *29*, 2283.
26. Cane, D. E.; Thomas, P. J. *J. Am. Chem. Soc.* **1984**, *106*, 5295.
27. Ponsford, R. J.; Southgate, R. *J. Chem. Soc., Chem. Commun.* **1979**, 846.
28. Smale, T. C. *Tetrahedron Lett.* **1984**, *25*, 2913.
29. Brown, P.; Southgate, R. *Tetrahedron Lett.* **1986**, *27*, 247.
30. Doyle, M. P.; Shanklin, M. S.; Oon, S.-M.; Pho, H. Q.; van der Heide, F. R.; Veal, W. R. *J. Org. Chem.* **1988**, *53*, 3384.
31. Doyle, M. P.; Taunton, J.; Pho, H. Q. *Tetrahedron Lett.* **1989**, *30*, 5397.
32. Doyle, M. P.; Shanklin, M. S.; Pho, H. Q. *Tetrahedron Lett.* **1988**, *29*, 2639.
33. Doyle, M. P.; Mahapatro, S. N.; Caughey, A. C.; Chinn, M. S.; Colsman, M. R.; Harn, N. K.; Redwine, A. E. *Inorg. Chem.* **1987**, *26*, 3070.
34. Doyle, M. P.; Loh, K.-L.; DeVries, K. M.; Chinn, M. S. *Tetrahedron Lett.* **1987**, *28*, 833.
35. Rando, R. R. *J. Am. Chem. Soc.* **1972**, *94*, 1629.
36. Kirmse, W.; Dietrich, H.; Bücking, H. W. *Tetrahedron Lett.* **1967**, 1833.
37. Ledon, H.; Linstrumelle, G.; Julia, S. *Tetrahedron Lett.* **1973**, 25.
38. Lowe, G.; Parker, J. *J. Chem. Soc., Chem. Commun.* **1971**, 577.

39. Ledon, H.; Linstrumelle, G.; Julia, S. *Bull. Soc. Chim. Fr.* **1973,** 2071.
40. Doyle, M. P.; Bagheri, V.; Pearson, M. M.; Edwards, J. D. *Tetrahedron Lett.* **1989,** *30,* 7001.
41. Adams, J.; Poupart, M.-A.; Grenier, L. *Tetrahedron Lett.* **1989,** *30,* 1749.
42. Adams, J.; Poupart, M.-A.; Grenier, L.; Schaller, C.; Quimet, N.; Frenette, R. *Tetrahedron Lett.* **1989,** *30,* 1753.
43. Lee, E.; Jung, K. W.; Kim, Y. S. *Tetrahedron Lett.* **1990,** *31,* 1023.
44. Aratani, T.; Yoneyoshi, Y.; Nagase, T. *Tetrahedron Lett.* **1982,** *23,* 685.
45. Aratani, T. *Pure Appl. Chem.* **1985,** *57,* 1839.
46. Fritschi, H.; Leutenegger, U.; Siegmann, K.; Pfaltz, A.; Keller, W.; Kratky, Ch. *Helv. Chim. Acta* **1988,** *71,* 1541.
47. Fritschi, H.; Leutenegger, U.; Pfaltz, A. *Helv. Chim. Acta* **1988,** *71,* 1553.
48. Doyle, M. P.; Pieters, R. J.; Martin, S. F.; Austin, R. E.; Oalmann, C. J.; Müller, P. *J. Am. Chem. Soc.* **1991,** *113,* 1423.

Cyclizations Made Easy by Transition Metal Catalysts

Barry M. Trost

Department of Chemistry, Stanford University, Stanford, CA 94305–5080

Ring construction by carbon–carbon bond formation is more versatile than methods involving carbon–heteroatom bond formation, which is limited to macroheterocycles like macrolactones. Palladium-catalyzed carbon–carbon bond formation is spectacularly successful. With palladium-catalyzed allylic alkylation, the formidable task of making medium-sized rings (8–10 members) and large rings (up to 27 members) becomes simple. Polymer-supported catalysts enable such cyclizations to occur at high concentrations (0.2–0.5 M). Even carbon–heteroatom bonds can be formed in this way. Condensations and cycloisomerizations involving terminal acetylenes as donors and acetylenes or allenes as acceptors represent a new palladium-catalyzed strategy. Application of these methods involves the syntheses of antibiotic A26771B, (–)-aspochalasin B, and models for polyene macrolides (represented by tetrin A) and for taxanes (represented by taxinine).

$\mathbf{T}$HE INCREASING IMPORTANCE IN BIOLOGY of rings larger than seven members spotlights the importance of developing practical routes to these systems. Construction of rings of three and five to seven members proceeds by straightforward application of many carbon–carbon or carbon–heteroatom bond-forming reactions to intramolecular processes. However, such an approach frequently fails for medium (8–10 members) and large (>10 members) rings. Many processes do not apply, and those that do require very special conditions such as the employment of high dilution.

The notion that a transition metal complex may serve as a template to facilitate otherwise difficult reactions led us to explore their applicability for the synthesis of medium and large rings. Impetus for such studies derives

from the growing importance of such molecular types from both theoretical and biological points of view. Materials possessing unusual electronic (e.g., the annulenes) or coordinating (host–guest chemistry) properties have such rings as their core. Natural products valued for their biological properties (from organoleptics to antibiotics and antitumor compounds) frequently are macrocycles. The extension of palladium-catalyzed bond-forming reactions to intramolecular processes has proven to be particularly successful (1).

Macrocyclization via Allylic Alkylation

The ability of palladium to chemoselectively generate a cation in the presence of an anion permits the use of charge neutralization to facilitate ring formation (eq 1).
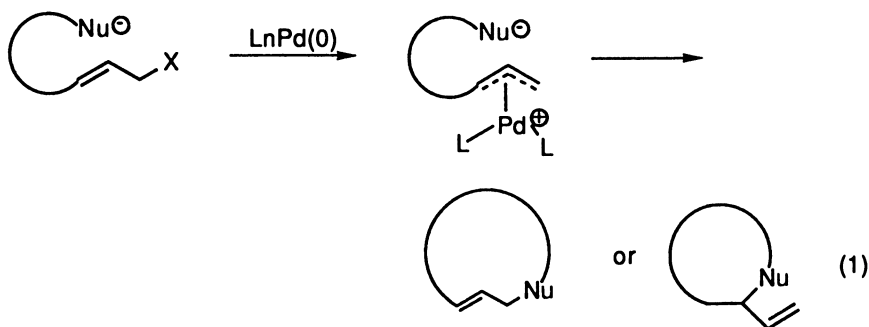
Early applications of this methodology feature the biologically important area of macrolide syntheses (2, 3). For example, the 16-membered ring of exaltolide, the fragrant constituent of angelica root oil, was obtained in 69% yield by the cyclization of eq 2 (3). Tests of ring size indicated that 12- (eq 3) (3, 4) and 10-membered rings (eq 4) (3) form with equal facility.

exaltolide
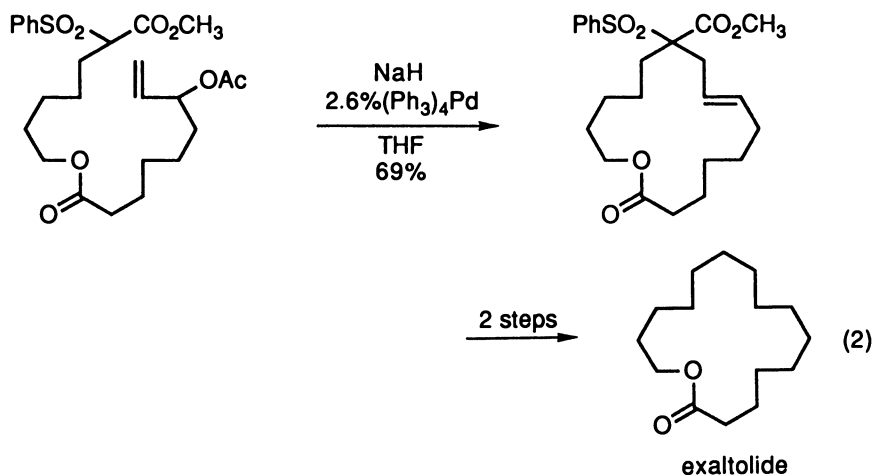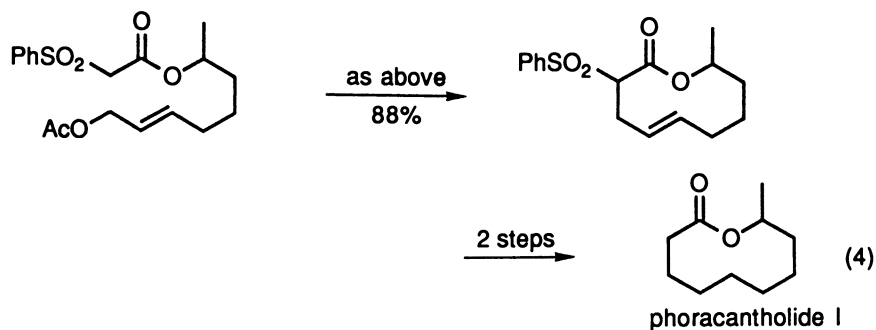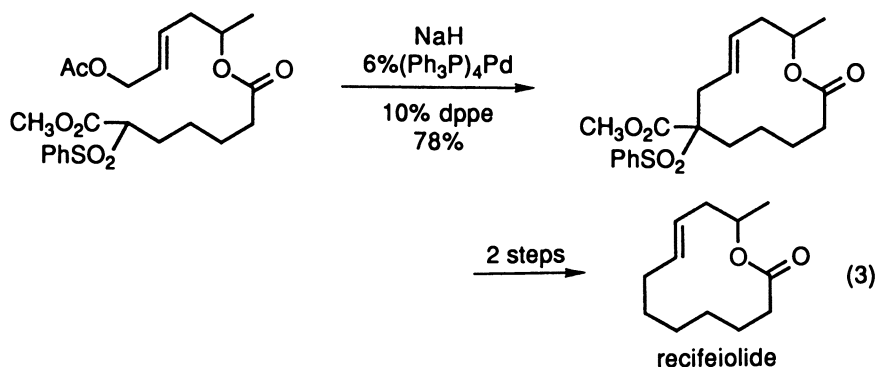
The importance of lactones led us to develop a new strategy for macro-lactonization. The strategy is outlined in eq 5, in which an alkoxyacyl anion equivalent (as shown in **1**) is envisioned as the nucleophile (5).
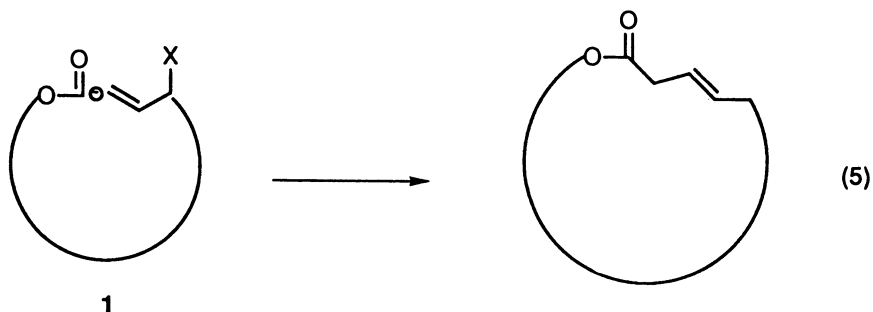
Completion of the macrolide synthesis involves silver ion assisted hy-drolysis on silica gel.

Because the pronucleophile is formed by reaction of the appropriate alcohol with chlorophenylthioacetonitrile, the latter can be viewed as a car-bonyl zwitterion equivalent (i.e., **2**).

(6)

2
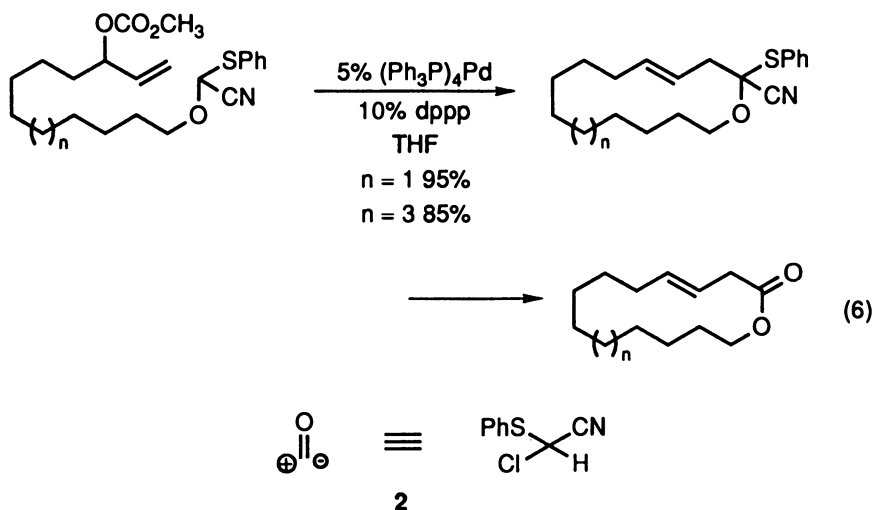
A simple illustration of this synthetic equivalence in an acyclic case is shown in eq 7.

(7)
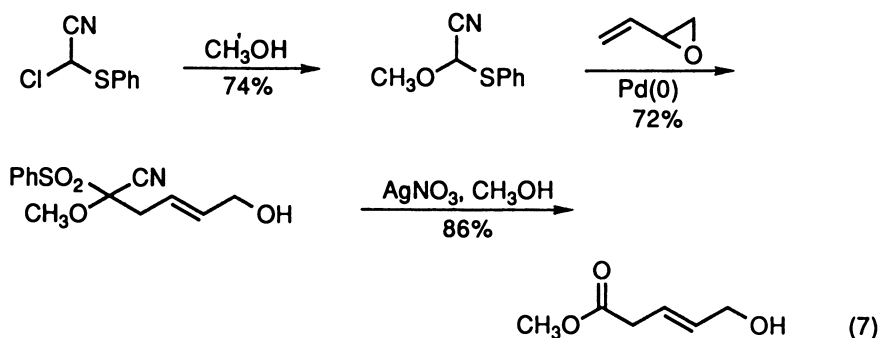
The extension of palladium-catalyzed cyclizations to eight- and nine-membered lactones has been most extraordinary. Cyclization to form six- and seven-membered rings would normally be expected to dominate. Instead, cyclization of **3** produces predominantly (94:6) the eight-membered ring. This product forms in spite of the fact that the *syn* complex **4**, which can cyclize to form only the six-membered ring product, should be preferred over the *anti* complex **5**, which is required for eight-membered ring formation (*2, 3*).

Cycloisomerizations constitute a special class of macrocyclizations. By using the principle of pseudohigh dilution, such reactions can be performed at practical concentrations. A spectacular illustration of the power of this method is the formation of the 27-membered macrolactone in 70% yield at 0.25–0.5 M (eq 9) (*6*).

(8)

(9)
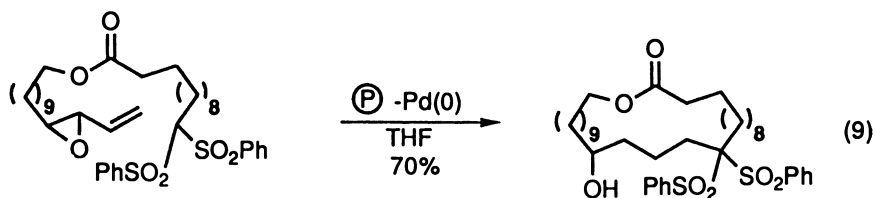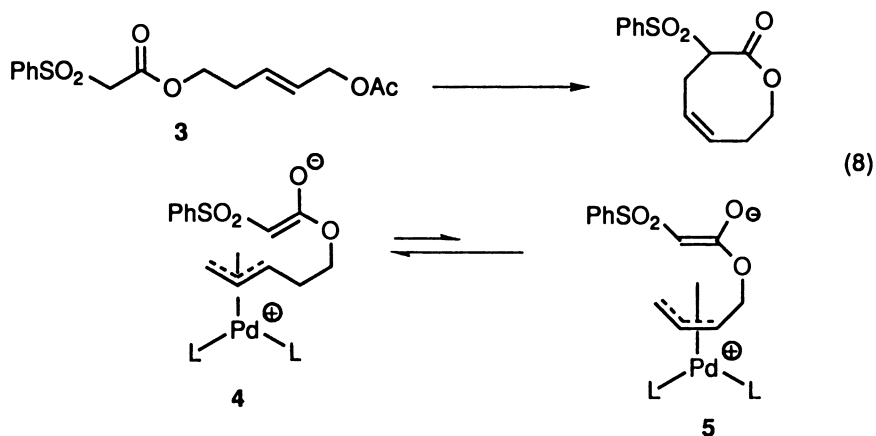
The regioselectivity of this reaction stems from the effect of the oxygen substituent (eq 10). It involves faithful translation of the stereochemistry of the leaving group into the new C–C bond with retention of configuration (7).

(10)
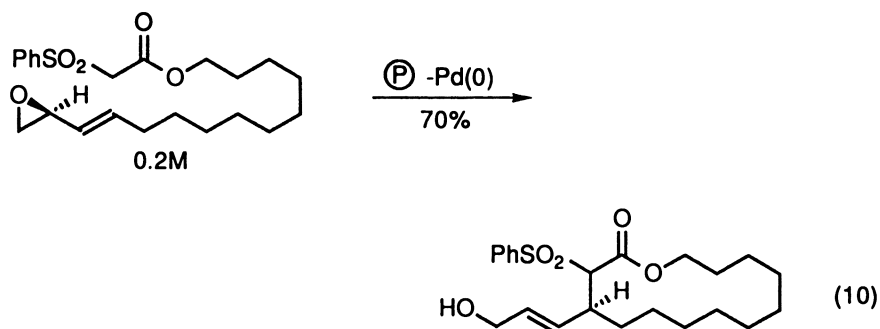
The magnitude of this regioselectivity directive effect was tested by examining the formation of medium-sized carbocyclic rings (8). By using homogeneous catalysis at 0.01 M, cyclization of **6** ($n = 2$) produces only the nine-membered ring, in spite of the fact that a seven-membered ring can form (9). On the other hand, the next lower homologue, **6** ($n = 1$), produces only the six-membered ring (9). Nevertheless, the six- versus eight-mem-

bered ring competition must be very close in this metal-catalyzed reaction, compared to the 10^5 kinetic preference for six-membered ring formation in non-metal-catalyzed reactions (eqs 8 and 11a). Furthermore, a slight change in substitution pattern in the carbocyclic precursor totally reorients reaction away from the six-membered rings to favor eight-membered ring formation (eq 11b) (10).
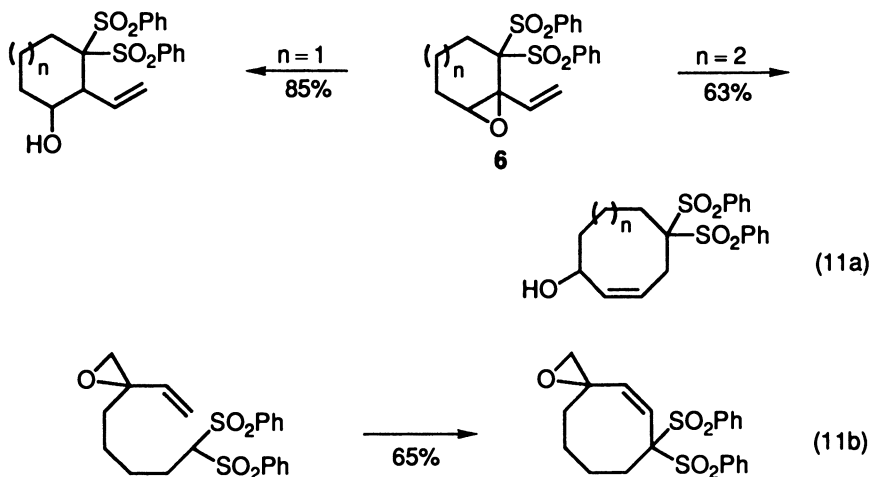
We focused on the use of carbon nucleophiles, but heteroatom nucleophiles also succeed (9). Carboxylate nucleophiles provide an alternative approach to macrolide construction with the interesting feature that the regioselectivity depends upon the reaction temperature. Thus, the sterically nondemanding oxygen nucleophile preferentially attacks the more substituted carbon at room temperature (eq 12, path a, kinetic conditions). However, it attacks the less substituted carbon at reflux (eq 12, path b, thermodynamic conditions).

Confirmation that the differences reside in kinetic versus thermodynamic factors arises from the conversion, with palladium(0) catalysts, of the 26-membered macrolactone 7 to the 28-membered one 8.

With phenols, the regioselectivity of cyclization depends upon the reaction solvent (9). In tetrahydrofuran (THF), the predominant product (2:1) of cyclization of phenol 9 arises by templating the pronucleophile to the departing epoxide oxygen to give the vicinal product 10 (eq 13).

With the use of an alcohol solvent to disrupt the hydrogen bonding between the phenol and the epoxide, the bias for attack at the carbon distal to the departing oxygen returns to form the macroether 11. In contrast to the use of carbon nucleophiles, these reactions did not succeed at high concentrations in the presence of a polymeric catalyst. Presumably this failure reflects the much higher rate of proton transfer with noncarbon atoms.

(12)

(13)
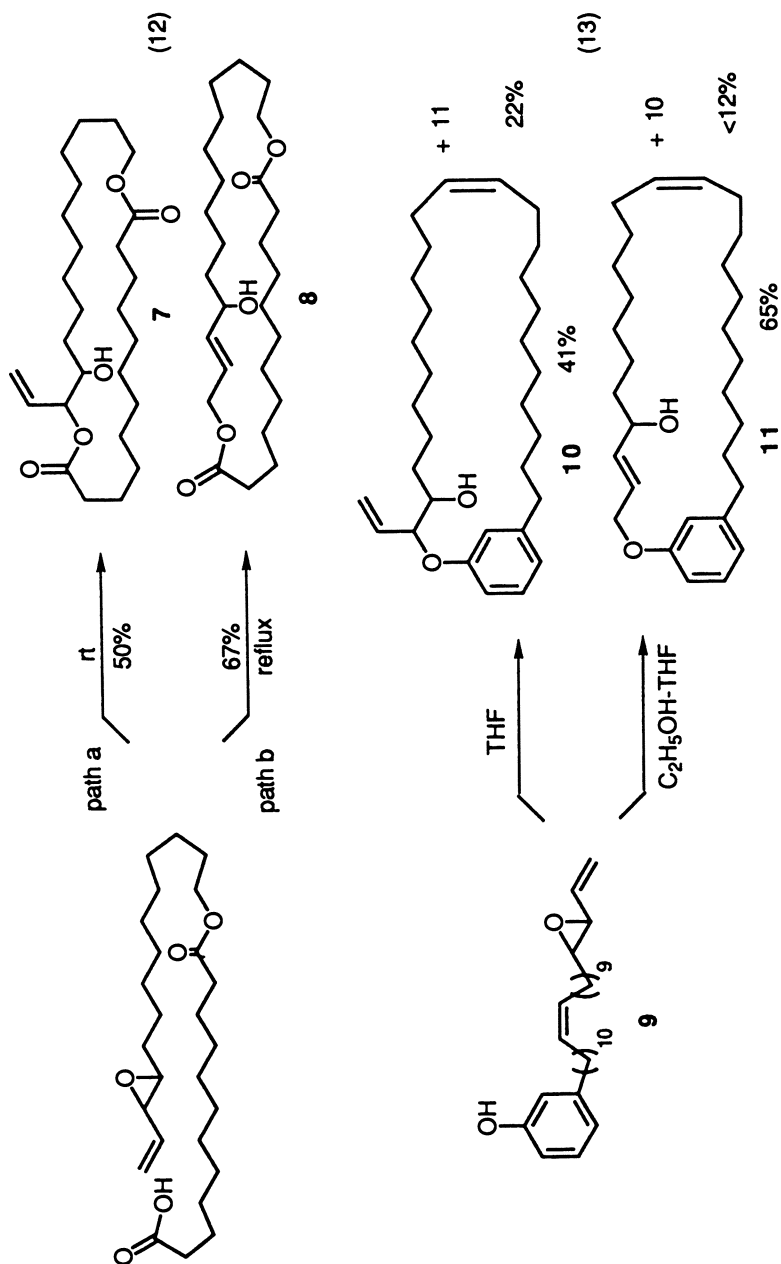
Couplings of Terminal Acetylenes

The feasibility of performing macrocyclizations at high concentrations led us to search for new condensation reactions that, when applied intramolecularly, would become cycloisomerizations. An excellent candidate stems from our development of a cross-condensation of terminal acetylenes with internal acetylenes, as exemplified in eq 14 (11–12).
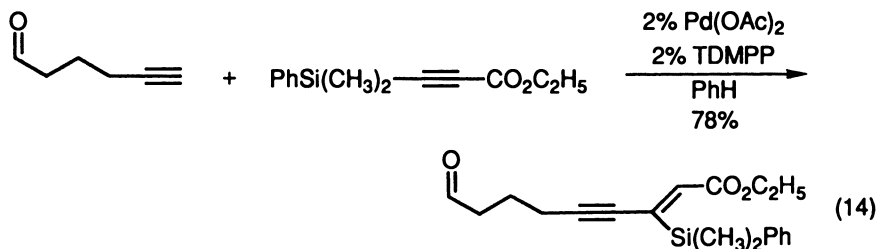
An intramolecular version of this reaction proceeds very smoothly to produce both carbocycles (eq 15) and macrolactones (eq 16) by using slow addition of the substrate to the catalyst (13).
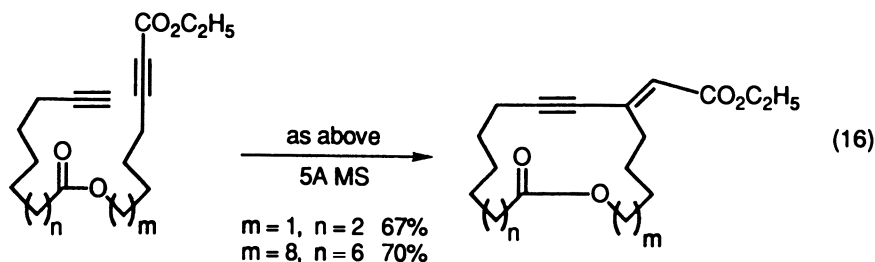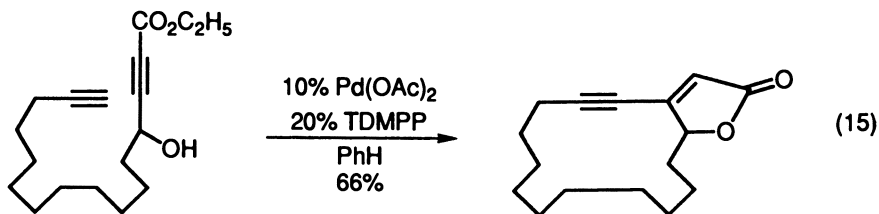
An alternative approach to the macrolactone uses the ester as the activating group for the acceptor acetylene. The yield is more modest in this cyclization (eq 17).
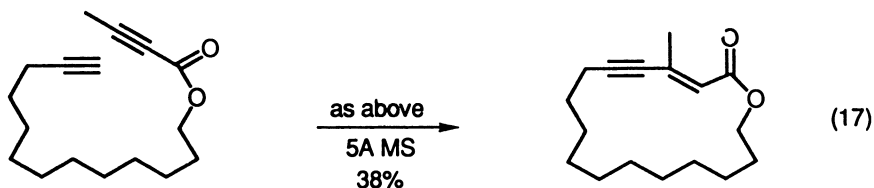
Cyclization proceeds chemoselectively, even when both acetylenes are terminal, to give 14- and 18-membered ring macrocycles (eq 18) (*14*).
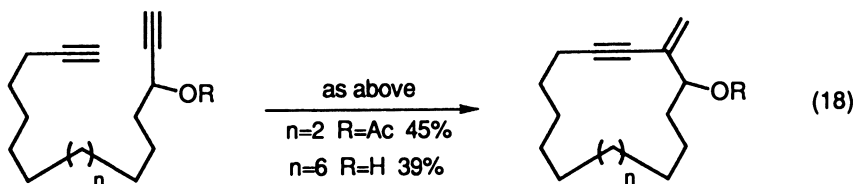
In the sequence outlined in Scheme I, considering the fact that acetylenic hydrogens exchange rapidly under these conditions, the product-determining step appears to be the intramolecular carbapalladation. The reactivity of the acceptor acetylene would be enhanced by the presence of an inductively electron-withdrawing group.
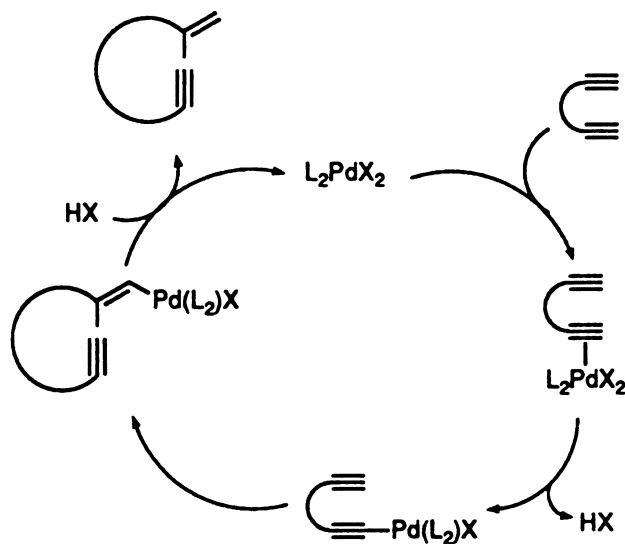
Scheme I. Mechanistic rationale of cycloisomerizations of diynes.

Extension of this concept to unsaturated acceptors other than an acetylene should be feasible. Preliminary work suggests that allenes can indeed perform such a function (*15*). The intermolecular condensation exhibits a remarkable dependence of regioselectivity of the addition on the choice of catalyst (eq 19).

Although the intramolecular version has only begun to be investigated, its feasibility has been established (eq 20) (*16*).

$$4\% \text{ Pd(OAc)}_2, \text{ TDMPP}$$
$$4\% \text{ TCPC, TDMPP}$$

(19)

| 74% | 85% | 15% |
| 53% | 6% | 94% |

$$8\% \text{ Pd(OAc)}_2, \text{ TDMPP}$$
$$25\%$$

(20)
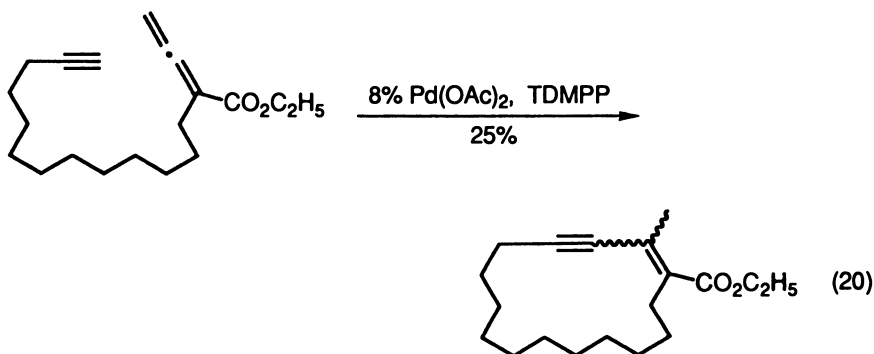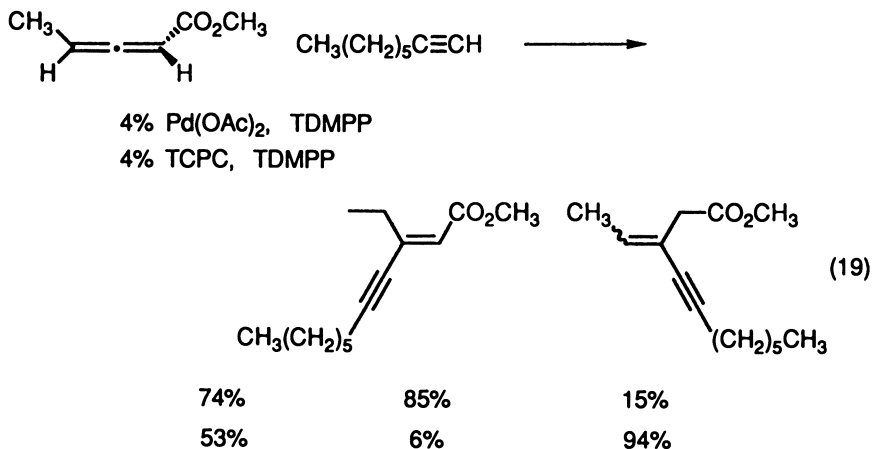
Applications Toward Natural Products

The ready access to macrocycles through palladium templates suggests extension of synthetic strategy to complex molecules. Its ready applicability has led to several simple targets in our investigation of the scope of this reaction. The ability to incorporate enol ethers in the allyl fragment permits a versatile strategy to macrocycles bearing a highly functionalized sequence, as shown in eq 21.

The synthesis of the macrolide antibiotic A26771B exemplifies this concept (eq 22) (17).

A secondary benefit of this strategy emanates from the ability of the sulfone to function as a diastereochemical relay group. By influencing the conformation of the large ring, it transmits stereochemical information from the carbon bearing the methyl group to the olefin, thereby directing the stereochemistry of introduction of the oxygen substituent.

(21)

Y = OH
Y = H

7% (ph₃P)₄Pd
dppp
84%

3 steps

(22)

antibiotic A26771B
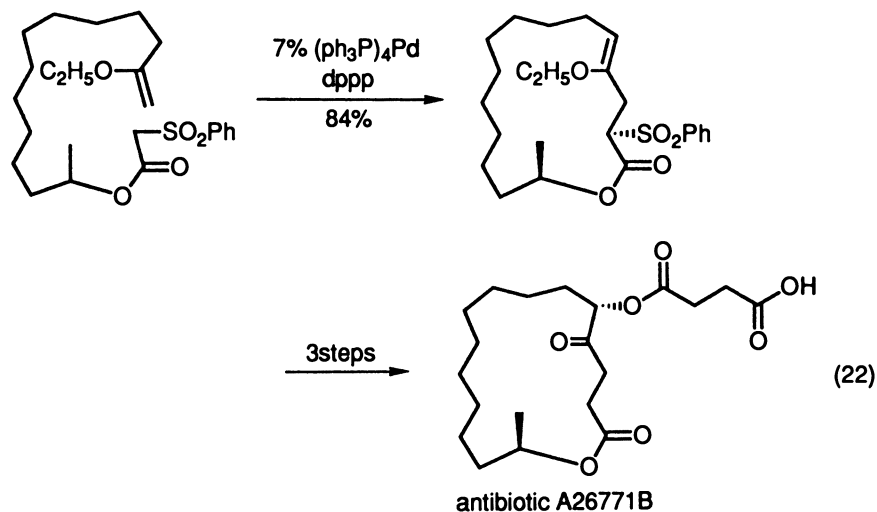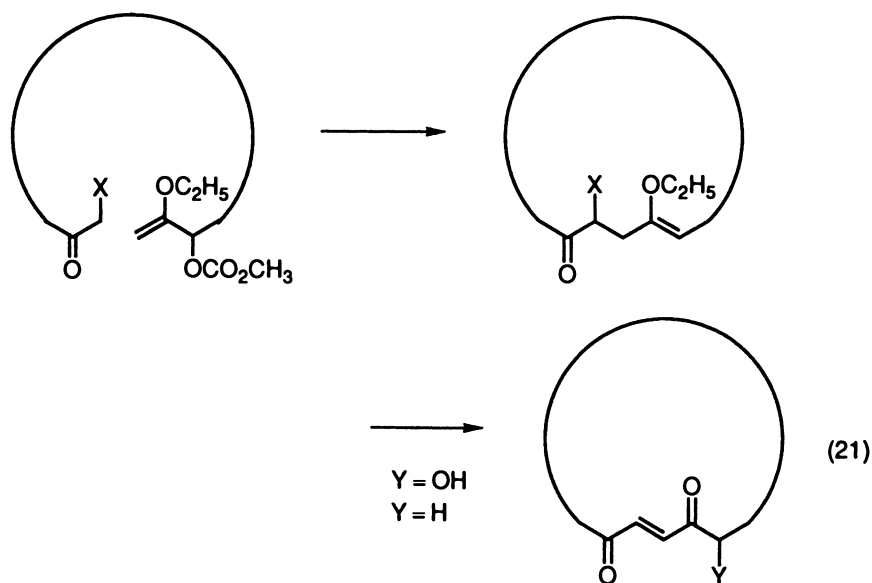
Because this method constructs the macrocycle by C–C bond formation, carbocyclic natural products can be constructed with equal facility. A synthesis of (–)-aspochalasin B benefits both by flexibility for further elaboration (as in eq 2) and by use of the phenylsulfonyl group as a stereochemical relay (eq 23) (*18*).

Cycloisomerization of the vinyl epoxides also provides a particularly advantageous juxtaposition of functionality for further elaboration. For ex-

(23)

R=OH   (-)aspochalasin   B
 =H   (-)desoxyaspochalasin B

as in eq 21

49%

2 steps
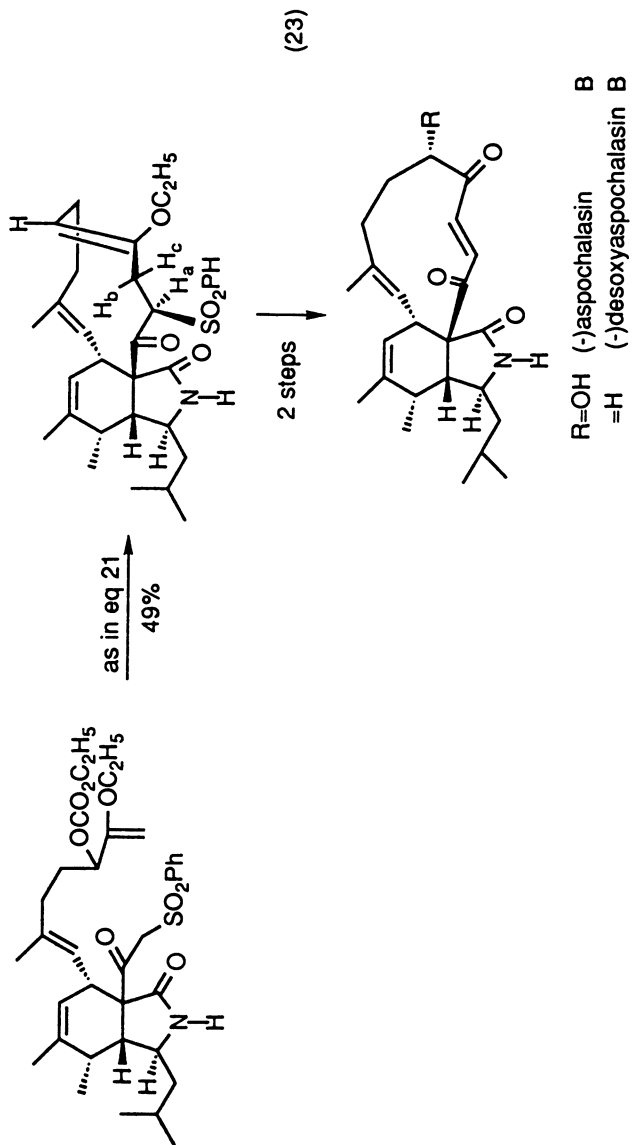
ample, model studies shown in eq 24 directed toward polyene macrolides take advantage of the presence of both an allylic sulfone and an allylic alcohol to effect a second palladium-catalyzed reaction to the tetraene (*19*).

(24)
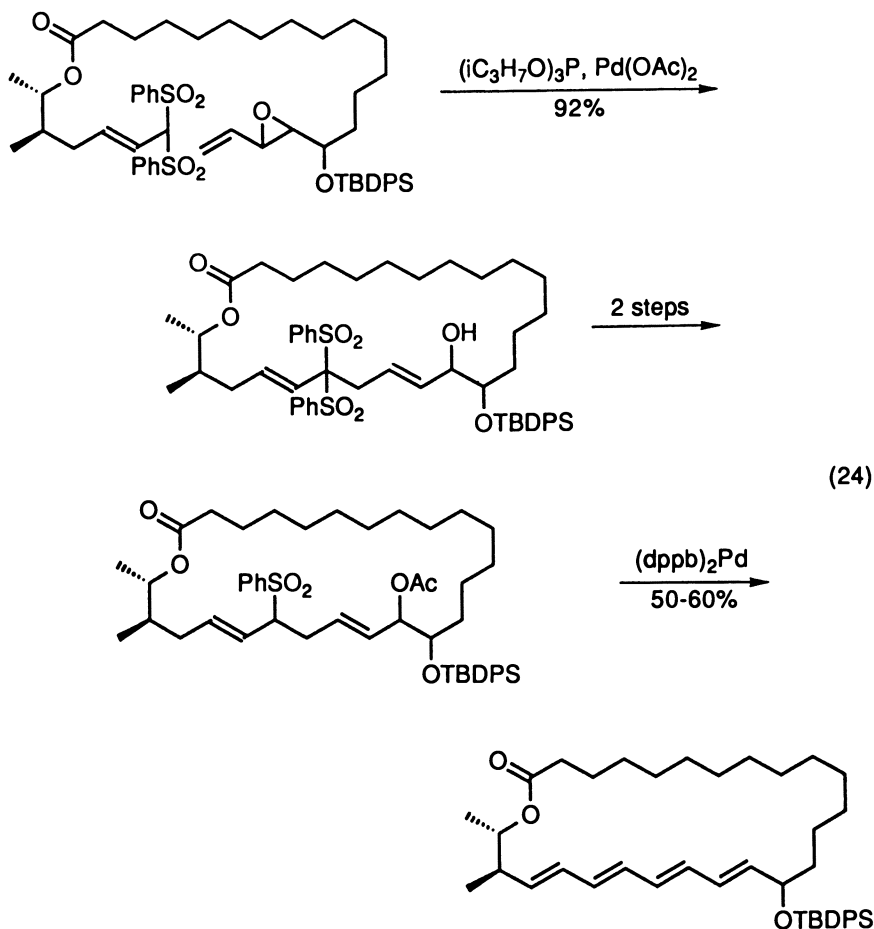
In a synthesis directed toward taxinine or taxine-I, we envision creation of the tricyclic nucleus by a transannular cyclization for which the cyclodecanone **12** becomes a logical precursor (eq 25).

As shown in eq 26, palladium-catalyzed cycloisomerization followed by ruthenium-catalyzed reductive desulfonylation readily forms the key macrocycle. This example illustrates the subtleties that can be involved in these reactions since tri-2-furylphosphine proved to be an important ligand (*20*).

R=H taxinine
OH taxine I

(25)

12

80-90%

⟶ **12** (26)
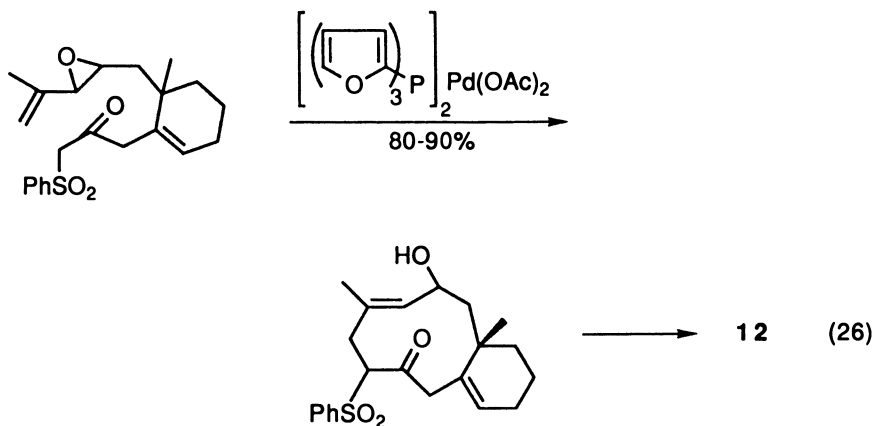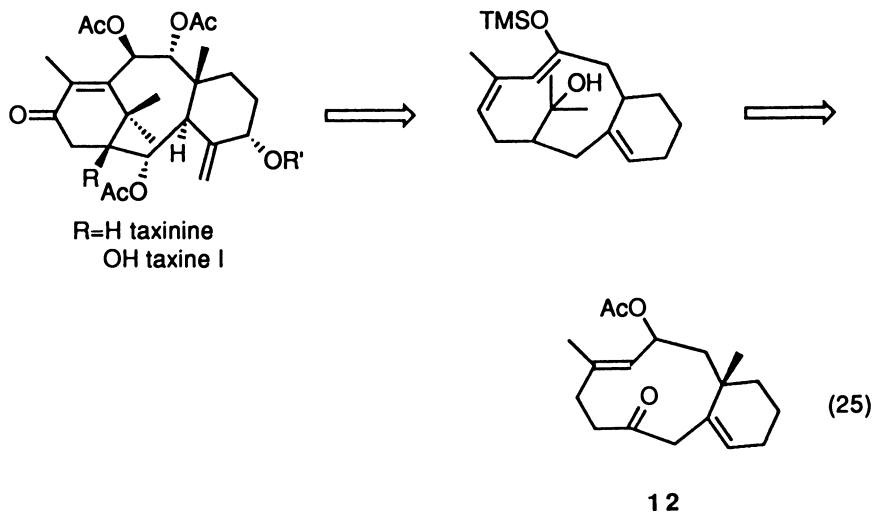
Conclusion

Transition metal controlled behavior of allyl systems dramatically facilitates formation of both medium and large rings. Thus the normal 10^3–10^5 kinetic bias in favor of seven- and six-membered rings over nine- and eight-membered rings can be reversed to favor the medium-sized rings. Variation of the substituents in and on the chain and variation of the nature of the nucleophile impart flexibility in generating both carbocycles and heterocycles. The high chemoselectivity provides excellent opportunities for complex molecule construction.

The great successes of cycloisomerizations involving π-allylpalladium intermediates require exploration to discover new types of metal-catalyzed

condensations that may translate into opportunities for large-ring construction under practical operating conditions. The ability to make large changes by varying the metal and to fine-tune subsequent behavior by varying the ligands provides tremendous opportunities for new inventions and for enhancing selectivity. Therefore these catalysts can justly be called "the chemist's enzymes".

Abbreviations in Equations

dppb	1,4-bis(diphenylphosphino)butane
dppe	1,2-bis(diphenylphosphino)ethane
dppp	1,3-bis(diphenylphosphino)propane
MSG	molecular sieve
OTBDPS	*t*-butyldiphenylsiloxy
PhH	benzene
TCPC	tetracarbomethoxypalladacyclopentadiene
TDMPP	tris(2,6-dimethoxyphenyl)phosphine
THF	tetrahydrofuran
TMSO	trimethylsiloxy

Acknowledgment

References

1. Trost, B. M. *Angew. Chem., Int. Ed. Engl.* **1989,** *28,* 1173.
2. Trost, B. M.; Verhoeven, T. R. *J. Am. Chem. Soc.* **1977,** *99,* 3867.
3. Trost, B. M.; Verhoeven, T. R. *J. Am. Chem. Soc.* **1980,** *102,* 4743.
4. Trost, B. M.; Verhoeven, T. R. *Tetrahedron Lett.* **1978,** 2275.
5. Trost, B. M.; Granja, J. *J. Am. Chem. Soc.* **1991,** *113,* 1044.
6. Trost, B. M.; Warner, R. W. *J. Am. Chem. Soc.* **1983,** *105,* 5940.
7. Trost, B. M.; dalla Cort, A., Stanford University, unpublished results.
8. *See also* Trost, B. M.; Warner, R. *J. Am. Chem. Soc.* **1982,** *104,* 6112.
9. Trost, B. M.; Brzezowski, C. M., Stanford University, unpublished results.
10. Trost, B. M.; Vos, B. A., Stanford University, unpublished results.
11. Trost, B. M.; Chan, C.; Ruhter, G. *J. Am. Chem. Soc.* **1987,** *109,* 3486.
12. Trost, B. M.; Caringi, J., Stanford University, unpublished results.
13. Trost, B. M.; Matsubara, S.; Caringi, J. *J. Am. Chem. Soc.* **1989,** *111,* 8745.
14. Trost, B. M.; Tucker, J. A., Stanford University, unpublished results.
15. Trost, B. M.; Kottirsch, G. *J. Am. Chem. Soc.* **1990,** *112,* 2816.
16. Trost, B. M.; Kottirsch, G., Stanford University, unpublished results.

17. Trost, B. M.; Brickner, S. J. *J. Am. Chem. Soc.* **1983,** *105*, 568.
18. Trost, B. M.; Ohmori, M.; Boyd, S. A.; Okawara, H.; Brickner, S. J. *J. Am. Chem. Soc.* **1989,** *111*, 8281.
19. Trost, B. M.; Hane, J. T.; Metz, P. *Tetrahedron Lett.* **1986,** *27*, 5695.
20. Trost, B. M.; Phan, L. T., Stanford University, unpublished results.

Classic Process Chemistry

New Science and New Applications

William A. Nugent, Ronald J. McKinney, Frank W. Hobbs, Jr., and Francis J. Waller

Central Research & Development Department, E. I. du Pont de Nemours and Company, P.O. Box 80328, Wilmington, DE 19880–0328

The classic process chemistry used to manufacture commodity chemicals can represent a valuable untapped resource for the synthesis of fine chemicals. This premise is illustrated with three examples. Nickel-catalyzed hydrocyanation technology, originally developed for the commodity production of adiponitrile, has been modified to provide an efficient route to a class of anti-inflammatory drugs. Perfluorinated ion-exchange polymer (PFIEP) was originally developed for caustic and chlorine production. Upon treatment with copper salts, it affords a superior cyclopropanation catalyst for the manufacture of pyrethroid insecticides. The catalytic dimerization of methyl acrylate, originally developed as an alternative route to adipic acid, provides a ready source of dimethyl (2-E)-hexenedioate. Tandem conjugate addition–cyclization of this dimer provides a simple route to 2,3-disubstituted cyclopentanones such as the 11-deoxyprostaglandins.

THE USE OF HOMOGENEOUS CATALYSIS is growing in the manufacture of "fine chemicals" such as pharmaceuticals, crop-protection chemicals, flavors, and fragrances, as documented in a series of reviews (1). In contrast to this relatively recent development, processes using homogeneous catalysis have dominated the manufacture of large-volume "commodity" organic chemicals for decades (2). To be competitive, the process chemistry used to manufacture commodities must be extremely efficient. Such processes typically result from many decades of research and optimization.

Our experience is that such venerable process chemistry can represent a valuable resource in developing new synthetic routes to fine chemicals. This chapter illustrates this contention with three examples from our recent experience.

The first example has its origins in the nickel-catalyzed addition of hydrogen cyanide to olefins. This technology is used by Du Pont to manufacture a billion pounds per year of adiponitrile. Recently developed Lewis acid additives (3) provide remarkably high regioselectivity for the anti-Markovnikov addition of HCN required in this process. Interestingly, the research challenge was to reverse this regioselectivity to provide the Markovnikov addition product. The nitrile-based route to the anti-inflammatory drug naproxen is of special interest because of the availability of stereospecific amidase enzymes that allow the nitrile to be hydrolyzed to the enantiomerically pure drug (4).

The second example is based on Du Pont's perfluorinated ion-exchange polymer (PFIEP) that has revolutionized the electrochemical production of commodity caustic and chlorine. We now report the use of PFIEP as a chemically resistant support for a highly active cyclopropanation catalyst (5).

The third example differs from the other two in that the process chemistry was never commercialized. The catalytic tail-to-tail dimerization of methyl acrylate (6) was developed as an alternative route to adipic acid based on C_3 rather than C_6 feedstocks. We harnessed this technology to provide Du Pont synthesis chemists with a convergent route to 2,3-disubstituted cyclopentanones such as the 11-deoxyprostaglandins.

Hydrocyanation Studies

The two anti-inflammatory drugs ibuprofen (7, 8) (1) and naproxen (9, 10) (2) are members of the class of 2-arylpropionic acids toward which extensive synthesis research has been directed. This level of research reflects both the economic importance of these pharmaceuticals and the fact that no existing route is fully satisfactory (11).

1   2
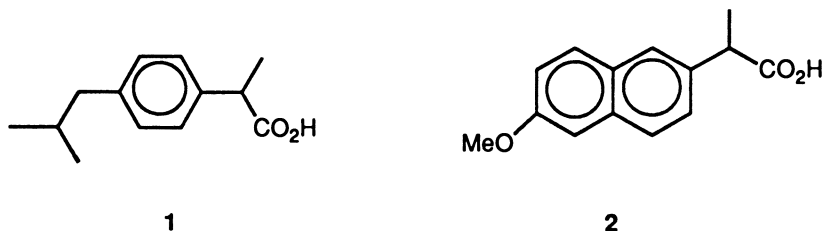
An attractive approach to these compounds involves hydrocyanation of the corresponding vinylarenes (eqs 1 and 2) followed by hydrolysis. Our

mechanistic studies of nickel-catalyzed olefin hydrocyanation (*12*) allowed us to develop the Markovnikov addition of HCN to vinylarenes as a new synthetic tool (*13*).

(1)

(2)
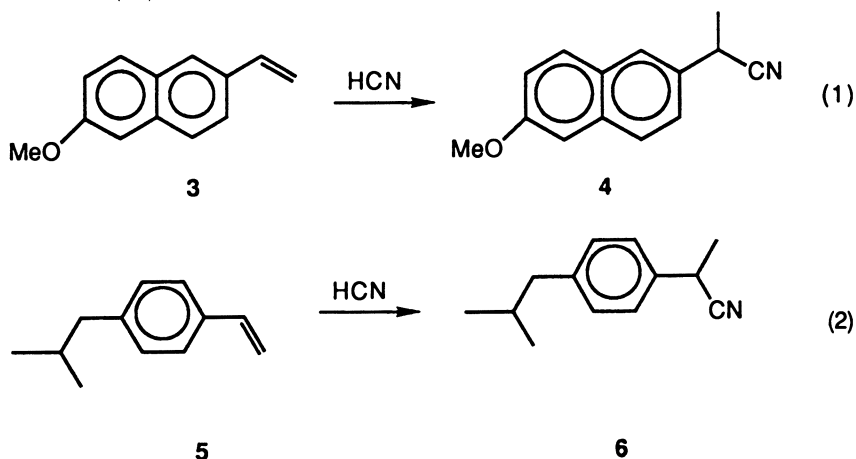
Tetrakis(tri-*p*-tolyl phosphite)nickel(0) is an effective catalyst for the regiospecific hydrocyanation of **3** to **4** at temperatures greater than 50 °C. Lewis acid promoters generally used in monoene hydrocyanation are detrimental to selectivity, increasing the anti-Markovnikov addition product. Because the degradation of the nickel catalyst is second-order in HCN concentration, the HCN is fed slowly as an $HCN-N_2$ gas mixture. This process is easily accomplished by passing a controlled flow of nitrogen gas through liquid HCN maintained at 0 °C in an ice bath, through a P_2O_5 trap, and directly into the reaction vessel. The resulting vapor is approximately 35% HCN. To suppress competing oligomerization, it is also desirable to introduce **3** gradually during the course of the reaction. By using 5 mol % Ni catalyst, **4** was routinely prepared in 90–93% isolated yield. Comparable results were obtained with 2-vinylnaphthalene.

Hydrocyanation of styrene or substituted styrenes such as **5** under similar conditions is less efficient because of extensive oligomerization even in the presence of radical inhibitors. The addition of a limited amount of Lewis acid such as zinc chloride helps to overcome this problem by increasing the rate of hydrocyanation compared to oligomerization. For example, hydrocyanation of **5** (5 mol % of Ni, 2 mol % of $ZnCl_2$, 88 °C) afforded **6** in 65–70% yield along with 8–10% of the isomeric 3-arylpropionitrile. The isomeric nitriles are readily separated by flash chromatography.

This new reaction provides a very simple route for the synthesis of a series of homologous 2-arylpropionic acids. The requisite vinylarene starting materials are readily prepared from commercially available aryl bromides by using the nickel-catalyzed cross-coupling chemistry of Kumada et al. (*14*) (eqs 3 and 4). The product nitriles are readily hydrolyzed to the correspond-

ing acids (NaOH–H$_2$O–ethylene glycol, 125 °C). The entire procedure is amenable to preparation of multigram quantities of material for biological testing.

$$\text{(structure)} + CH_2{=}CHMgBr \xrightarrow{\text{(dmpe)NiCl}_2} 3 \qquad (3)$$

$$\text{(structure)}{-}Br + \text{i-BuMgCl} \xrightarrow{\text{(dppp)NiCl}_2} 5 \qquad (4)$$
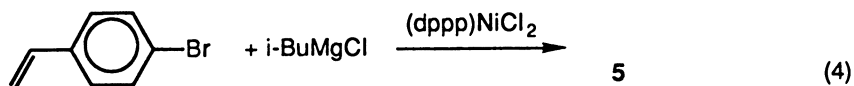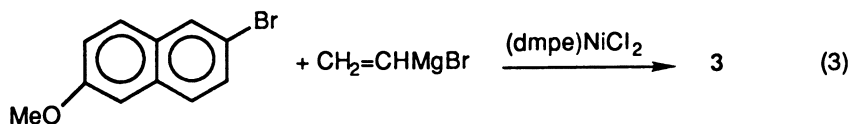
where dmpe is 1,2-bis(dimethylphosphino)ethane and dppp is 1,2-bis(diphenylphosphino)propane.

Cyclopropanation Studies

The generation of reactive carbenoid intermediates by transition metal catalyzed decomposition of α-diazocarbonyl compounds is a rapidly developing area of synthetic methodology. Addition of such species to olefins affords cyclopropane–carboxylate esters such as 7, which has been widely used in organic synthesis (15–17), and 8, the key intermediate in the manufacture of synthetic pyrethroid insecticides (18). Moreover, addition of such carbenoids to C–H and N–H bonds provides stereocontrolled access to products ranging from steroids (19) to thienamycin derivatives (20).

7   8
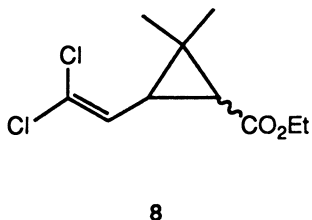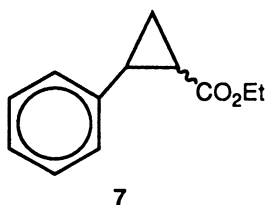
Among the known catalysts for such reactions, copper(II) trifluoromethanesulfonate (21–23) and rhodium(II) acetate (24, 25) have proven uniquely effective in a number of applications. However, in our experience, the cost of rhodium or trifluoromethanesulfonic acid is a serious constraint for applying this chemistry to large-scale syntheses. For this reason, we sought heterogenized versions of these catalysts that would be fully recoverable and reusable (26).

Du Pont's perfluorinated ion-exchange polymer consists of a perfluorinated backbone with pendant perfluorinated sulfonic acid exchangeable sites. The general structure of Du Pont's PFIEP can be represented as **9**. PFIEP powder in the potassium form is readily exchanged to PFIEP (K$^+$, M^{n+}), where M^{n+} is Cu^{2+} or Rh^{2+}

$$[(CF_2—CF_2)_n—CF—CF_2]_x$$

$$(OCF_2CF)_mOCF_2CF_2SO_3H$$

$$CF_3$$

m = 1,2,3...

9
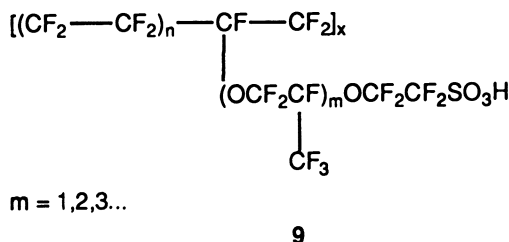
Typically, PFIEP (K$^+$) was slurried with the exchanging solution for several hours to prepare the catalysts in our study. The activity of PFIEP (K$^+$, Cu^{2+}) catalysts was comparable, whether they were prepared from copper nitrate, chloride, or acetate. A procedure utilizing PFIEP (H$^+$) and copper carbonate also provided comparable catalysts. A PFIEP (K$^+$, Rh^{2+}) catalyst was likewise prepared from PFIEP (K$^+$) and rhodium(II) acetate (CH$_2$Cl$_2$, reflux, 1 h, N$_2$ atm). Other metals have been supported on PFIEP as well (27, 28).

We examined the use of these catalysts for the synthesis of **7** and **8** from ethyl diazoacetate and styrene or 1,1-dichloro-3-methyl-1,3-butadiene, respectively. We also studied the cyclopropanation of cyclohexene to afford **10** (eq 5).

$$+ EtO_2CCHN_2 \xrightarrow{\text{catalyst}} + N_2 \qquad (5)$$

CO$_2$Et

10
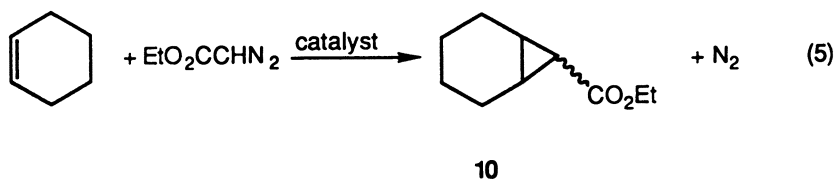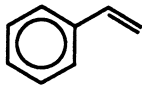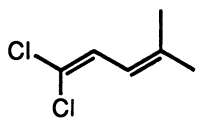
Table I summarizes our results with both our supported catalysts and the analogous homogeneous catalyst [copper(II) trifluoromethanesulfonate and rhodium(II) acetate]. Also included for comparison is a Cu^{2+} catalyst supported on Amberlyst 15, which lacks the chemically resistant perfluoroalkyl backbone of PFIEP.

Table I shows that synthetically useful yields of both **7** and **10** could be obtained by using the PFIEP-supported catalysts. In contrast to the relatively electron-rich substrates styrene and cyclohexene, significantly lower yields were observed for the electron-deficient 1,1-dichloro-4-methylpentadiene. The yield of **1** achieved by using the PFIEP (K$^+$, Cu^{2+}) catalyst

Table I. Yield of Cyclopropanes from Olefins and Ethyl Diazoacetate Using
Supported and Unsupported Catalysts

Catalyst	Styrene	Cyclohexene	1,1-Dichloro-4 methylpentadiene
PFIEP (K$^+$, Cu^{2+})	91	63	11
PFIEP (K$^+$, Rh^{2+})	51	51	14
Cu^{2+}–Amberlyst	60	57	10
Copper triflate	84	69	31
Rhodium acetate	96	85	26

NOTE: Yields (in percent) are based on ethyl diazoacetate by capillary gas liquid chromatography. All reactions involve dropwise addition of 2.0 mmol of ethyl diazoacetate in CH$_2$Cl$_2$ (12.5 mL) and olefin (12.5 mL) to 0.2 mmol of catalyst (0.5 h, 25 °C).

was slightly but reproducibly higher than that for copper(II) trifluoromethanesulfonate. Yields of both **7** and **10** were higher when the supported Cu^{2+} catalyst was used than for the supported Rh^{2+} catalyst.

Another significant difference between the supported Cu^{2+} and Rh^{2+} catalysts pertains to their behavior on repeated use. After up to 10 uses, the Cu^{2+} catalysts showed no detectable loss of copper content and no diminution of rate or selectivity. In contrast, rhodium was steadily leached from the Rh^{2+} catalyst so that the rate of cyclopropanation had become noticeably slower by the 10th run.

For runs at 25 °C higher yields were obtained when the olefinic substrate was diluted 1:1 with methylene chloride or fluorocarbon 113 (CF$_2$ClCFCl$_2$), as compared with runs in neat olefin. Alternatively, runs in neat olefin provided higher yields when carried out at slightly elevated temperature, to a maximum of ~75 °C. When tetrahydrofuran (THF) was used as cosolvent, no cyclopropanated products were formed.

Acrylate Dimerization Studies

The 2,3-disubstituted cyclopentanones include many biologically active compounds, including the 11-deoxyprostaglandins (29, 30) and the cyclopentanoid antibiotic antitumor agents such as sarkomycin (31, 32). A conceptually attractive route to these compounds begins with conjugate addition of organometallic reagents to enone **11** (33–35).

The resulting 2-carbomethoxycyclopentanones can then be transformed by standard methods into a variety of useful cyclopentanoids. However, compound **11** is unstable, difficult to prepare, and polymerizes in the pres-

$$\text{(6)}$$

11   12
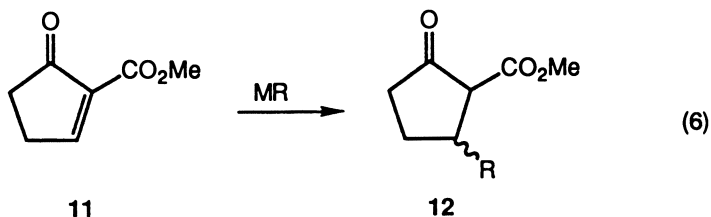
ence of many nucleophiles (*34*). It occurred to us (*36*, *37*) that eq 7, a conjugate addition–cyclization utilizing dimethyl 2-hexenedioate, **13a**, would represent an attractive alternative to eq 6.

13a

$$\left[\begin{array}{c} \text{MeO}_2\text{C} \underset{\text{R}}{\overset{(-)}{\diagdown}} \text{CO}_2\text{Me} \end{array} \right] \longrightarrow \textbf{12} \quad \text{(7)}$$
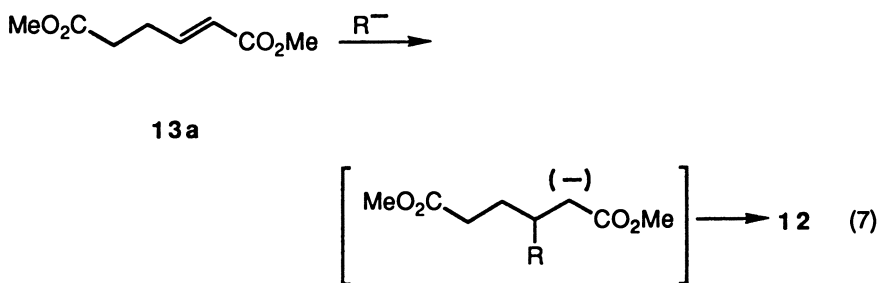
Tandem conjugate addition–cyclization reactions related to eq 7 have been reported (*38*, *39*). The practicality of this approach depends on the ready availability of **13a**. Therefore a high-yield synthesis of **13a** by dimerization of methyl acrylate was first developed.

The catalytic tail-to-tail dimerization of methyl acrylate (eq 8) has been reported (*40–43*). Unfortunately, we found that each of the known catalysts had severe limitations for the practical synthesis of **13a**. In particular, predominant formation of isomeric **13b**, limited catalyst life, or further oligomerization of product dimers were problems.

$$2\text{MeO}_2\text{CCH}{=}\text{CH}_2 \xrightarrow{\text{catalyst}} \text{MeO}_2\text{C}{\diagdown}{\diagup}{\diagdown}\text{CO}_2\text{Me} \quad \text{(8)}$$

Δ^2 isomer **13a**
Δ^3 isomer **13b**
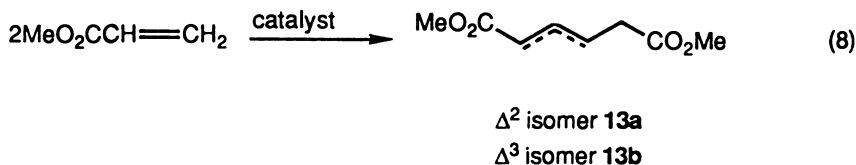
We discovered that the loosely coordinated cationic palladium complex Pd(NCMe)$_4$(BF$_4$)$_2$ (*44*, *45*) affords very high yields of **13a** under mild conditions, particularly in the presence of anhydrous LiBF$_4$. Thus, treatment of neat methyl acrylate with 0.005 equiv of palladium catalyst and 0.16 equiv of LiBF$_4$ at 40 °C for 30 h afforded after distillation a 93% yield of dimers consisting of 93–96% of the *trans* Δ^2 isomer. We found this mixture of products to be suitable for use in the subsequent addition–cyclization re-

Table II. 3-Substituted 2-Carbomethoxycyclopentanones from Conjugate Addition–Cyclization of 13a

Product	R in eq 6	Conditions	Yield[a] (%)
12a	methyl	normal[b]	76
12b	n-butyl	normal	71
12c	sec-butyl	normal	42
12d	neopentyl	normal	68
12e	vinyl	normal	42
12f	phenyl	0 °C	66
12g	methoxy-6-naphthyl	catalytic[c]	53

[a]Percent yield based on **13a**.
[b]Normal conditions indicate stoichiometric reaction of $LiCuR_2$ at –25 °C.
[c]CuCl-catalyzed reaction of Grignard reagent.

action. (The amount of palladium catalyst in these reactions can be further reduced by addition of a nonligating reoxidant such as benzoquinone or VOF_3.)

Tandem conjugate addition–cyclization of **13a** with lithium dialkylcuprates proceeds readily at –25 °C. A twofold excess of cuprate is required because an enolizable β-dicarbonyl system is produced. Isolated yields for several alkyl, vinyl, and aryl cuprates ranged from 40% to 80%, as summarized in Table II. In each case the product consists overwhelmingly of a single isomer, which NMR spectroscopy indicates is the *trans* diastereomer. In one case we extended this reaction to a copper-catalyzed Grignard reaction. Thus, the Grignard reagent from 2-bromo-6-methoxynaphthalene was added to **13** in the presence of 5% CuCl to afford cyclopentanone **12g** in 53% yield.
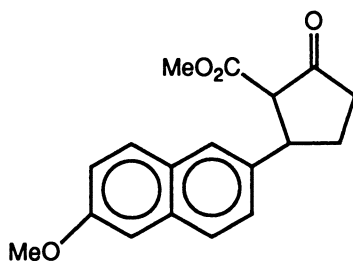
12g

The limited electrophilicity of enoate esters (*46*) imposes some limitations on the nature of the nucleophile R used in eq 7. Lithium di-*tert*-butylcuprate afforded only a low yield of the expected adduct. KCN, Et_2AlCN, 2-potassiocyclohexanone, and 2-lithio-1,3-dithiane failed to produce cyclopentanoid products.

Compounds **12** represent a general class of versatile synthetic intermediates. A wide variety of techniques exist for the subsequent alkylation (*47*) and decarboxylation (*48*) to afford the corresponding 2,3-disubstituted cyclopentanones. Moreover, 5-substituents could presumably be incorporated by means of the corresponding dianions (*49*).

Cyclopentanone **12e** was converted by Tsuji and co-workers (*50, 51*) into methyl dihydrojasmonate and 18-hydroxyestrone. The potential utility of naphthyl derivatives such as **12g** for synthesis of steroids has likewise been demonstrated (*52, 53*).

Significantly higher yields of **12e** and related 3-vinylcyclopentanones can be obtained by substituting higher-order cyanocuprates for the simple Gilman reagents used here (*37*).

Concluding Remarks

The contrast between the typical manufacturing processes for commodity chemicals versus fine chemicals represents a fascinating irony. Routes to inexpensive commodities like butyraldehyde or acetic acid routinely use homogeneous catalysts containing expensive metals like rhodium. This practice is possible because the large volume of these products justifies decades of process development and optimization. In general, the processes used to make smaller-volume compounds like pharmaceuticals and crop-protection chemicals have been less sophisticated. Industry's investment in process development for the commodities can also provide an important "leg up" in harnessing the efficiency and selectivity of transition metal catalysis for fine chemical manufacture. The examples described serve to support our contention.

References

1. Parshall, G. W.; Nugent, W. A. *CHEMTECH* **1988**, *18*, 184–190, 314–320, 376–383.
2. Parshall, G. W. *Homogeneous Catalysis*; Wiley-Interscience: New York, 1981.
3. Hall, W. T.; McKinney, R. J.; Nugent, W. A. U.S. Patent 4 774 353, 1988.
4. Cerbelaud, E.; Petre, D. Eur. Patent Application EP 0326 482 A1, 1989.
5. Nugent, W. A.; Waller, F. J. U.S. Patent 4 709 085, 1987.
6. Nugent, W. A. U.S. Patent 4 451 665, 1984.
7. Nicholson, J. S.; Adams, S. S. U.S. Patent 3 228 831, 1966.
8. Shen, T. Y. *Angew. Chem., Int. Ed. Engl.* **1972**, *11*, 460–472.
9. Harrison, I. T. U.S. Patent 3 658 858, 1972.
10. Harrison, I. T.; Lewis, B.; Nelson, O.; Rooks, W.; Roszkowski, A.; Tomolonis, A.; Fried, J. H. *J. Med. Chem.* **1970**, *13*, 203–205.
11. Giordana, C.; Castaldi, G.; Uggeri, F. *Angew. Chem., Int. Ed. Engl.* **1984**, *23*, 413–419.
12. Tolman, C. A.; McKinney, R. J.; Seidel, W. C.; Druliner, J. D.; Stevens, W. R. *Adv. Catal.* **1985**, *33*, 1–46.
13. Nugent, W. A.; McKinney, R. J. *J. Org. Chem.* **1985**, *50*, 5370.

14. Tamao, K.; Sumitani, K.; Kiso, Y.; Zembayashi, M.; Fujioka, A.; Kodama, S.; Nakajima, I.; Minato, A.; Kumada, M. *Bull. Chem. Soc. Jpn.* **1976**, *49*, 1958–1969.

15. Burger, A.; Yost, W. L. *J. Am. Chem. Soc.* **1948**, *70*, 2198–2201.

16. Borne, R. F.; Forrester, M. L.; Waters, I. W. *J. Med. Chem.* **1977**, *20*, 771–776.

17. Kaiser, C.; Weinstock, J.; Olmstead, M. P. *Org. Synth.* **1970**, *50*, 94–98.

18. (a) Holland, D.; Milner, D. J. *J. Chem. Res. Miniprint* **1979**, 3734–3746; (b) Brit. Patent 1 553 638, 1979.

19. Taber, D. F.; Raman, K. *Abstracts of Papers*, 186th National Meeting of the American Chemical Society, Washington, DC; American Chemical Society: Washington, DC, 1983; ORGN 181.

20. Andrus, A.; Heck, J. V.; Christensen, B. G.; Partridge, B. *J. Am. Chem. Soc.* **1984**, *106*, 1808–1811.

21. Salomon, R. G.; Salomon, M. F.; Heyne, T. F. *J. Org. Chem.* **1975**, *40*, 756–760.

22. Smith, A. B.; Toder, B. H.; Brance, S. J. *J. Am. Chem. Soc.* **1984**, *106*, 3995–4001.

23. Doyle, M. P.; Dorow, R. L.; Buhro, W. E.; Griffin, J. H.; Tamblyn, W. H.; Trudell, M. L. *Organometallics* **1984**, *3*, 44–52.

24. Anciaux, A. J.; Hubert, A. J.; Noels, A. F.; Petiniot, N.; Tessie, P. *J. Org. Chem.* **1980**, *45*, 695–702.

25. McKervery, M. A.; Tuladhar, S. M.; Twohig, M. F. *J. Chem. Soc., Chem. Commun.* **1984**, 129–130.

26. Nugent, W. A.; Waller, F. J. *Synth. Commun.* **1988**, 61–68.

27. Kanemoto, S.; Saimoto, H.; Oshima, K.; Nozaki, H. *Tetrahedron Lett.* **1984**, *25*, 3317–3320.

28. Waller, F. J. *Preprints of the American Chemical Society, Division of Petroleum Chemistry* **1982**, *27*, 611–613.

29. Bartmann, W.; Beck, G.; Lerch, U.; Teufel, H.; Babej, M.; Bickel, M.; Schoelkens, B.; Seeger, K. In *Chemistry, Biochemistry and Pharmacological Activity of Prostanoids*; Roberts, S. M.; Scheinmann, F., Eds.; Pergamon: Elmsford, NY, 1979; p 195.

30. Mitra, A. In *The Synthesis of Prostaglandins*; Wiley: New York, 1979; pp 337–352.

31. Umezawa, H.; Yamamoto, T.; Takeuchi, T.; Osata, T.; Okami, Y.; Yamaoka, S.; Okuda, T.; Nittak, K.; Yagishita, K.; Utuhara, R.; Umezawa, S. *Antibiot. Chemother. (Washington, D.C.)* **1954**, *4*, 514–520.

32. Wexler, B. A.; Toder, B. H.; Minaskanian, G.; Smith, A. B. *J. Org. Chem.* **1982**, *47*, 3333–3335 and references therein.

33. Marx, J. N.; Minaskanian, G. *Tetrahedron Lett.* **1979**, 4175–4178.

34. Marx, J. N.; Cox, J. H.; Norman, L. R. *J. Org. Chem.* **1972**, *37*, 4489–4491.

35. Marx, J. N.; Minaskanian, G. *J. Org. Chem.* **1982**, *47*, 3306–3310.

36. (a) Nugent, W. A.; Hobbs, F. W., Jr. *J. Org. Chem.* **1983**, *48*, 5364–5366; (b) Nugent, W. A.; Hobbs, F. W., Jr. *J. Org. Chem.* **1986**, *51*, 3376–3378.

37. Nugent, W. A.; Hobbs, F. W., Jr. *Org. Synth.* **1987**, *66*, 52–59.

38. Tanaka, K.; Uchiyama, F.; Sakamoto, K.; Inubushi, Y. *J. Am. Chem. Soc.* **1982**, *104*, 4965–4967.

39. Näf, F.; Decorzant, R.; Thommen, W. *Helv. Chim. Acta* **1975**, *58*, 1808–1812.

40. Alderson, T.; Jenner, E. L.; Lindsey, R. V. *J. Am. Chem. Soc.* **1965**, *87*, 5638–5645.

41. Barlow, M. D.; Bryant, M. J.; Haszeldine, R. N.; Mackie, A. G. *J. Organomet. Chem.* **1970**, *21*, 215–226.

42. Pracejus, H.; Krause, H.-J.; Oehme, G. *Z. Chem.* **1980**, *20*, 24.

43. Oehme, G.; Pracejus, H. *Tetrahedron Lett.* **1979**, 343–344.

44. Wayland, B. B.; Schramm, R. F. *Inorg. Chem.* **1969**, *8*, 971–976.
45. Sen, A.; Lai, T.-W. *J. Am. Chem. Soc.* **1981**, *103*, 4627–4629.
46. Posner, H. G. *Org. React. (N. Y.)* **1972**, *19*, 1–113, especially p 25.
47. House, H. O. In *Modern Synthetic Reactions*; Benjamin: Menlo Park, CA, 1972; pp 510–546.
48. Krapcho, A. P. *Synthesis* **1982**, 893–914.
49. *See* House, H. O. In *Modern Synthetic Reactions*; Benjamin: Menlo Park, CA, 1972; p 554.
50. Tsuji, J.; Kobayashi, Y.; Kataoka, H.; Takahashi, T. *Tetrahedron Lett.* **1980**, *21*, 1475–1478.
51. Tsuji, J.; Okumoto, H.; Kobayashi, Y.; Takahashi, T. *Tetrahedron Lett.* **1982**, *22*, 1357–1358.
52. Trost, B. M.; Runge, T. A. *J. Am. Chem. Soc.* **1981**, *103*, 7559–7572.
53. Posner, G.; Chapdelaine, M.; Lentz, C. *J. Org. Chem.* **1979**, *44*, 3661–3665.

Catalyzed and Noncatalyzed Hydrosilation of Organotransition Metal Acyl Complexes

Paul K. Hanna, Brian T. Gregg, D. Lawrence Tarazano, John R. Pinkes, and Alan R. Cutler

Department of Chemistry, Rensselaer Polytechnic Institute, Troy, NY 12180

Wilkinson's compound, $Rh(PPh_3)_3Cl$, catalyzes the hydrosilation of a series of organoiron acetyl complexes $Cp(L)(CO)Fe$–$COCH_3$ using dihydrosilanes (Cp is cyclopentadienyl, L is CO). Stable α-siloxyethyl complexes $FpCH(OSiHR'_2)CH_3$ [Fp is $Fe(CO)_2$-(η^5-C_5H_5)] are available from $FpCOCH_3$, whereas phosphine- and phosphite-substituted iron α-siloxyethyl intermediates promptly convert to vinyl compounds, $Cp(L)(CO)FeCH$=CH_2. Manganese acyl complexes $L(CO)_4Mn$–COR (L is CO, R is CH_3 or Ph; L is PPh_3, R is CH_3) are more effective catalysts for hydrosilating $FpCOR$ (R is CH_3 or Ph). In addition to Fp(α-siloxyalkyl) complexes, $[FpCH(CH_3)O]_2SiR'_2$ (R' is Et or Ph) and $[FpCH(CH_3)O]_3SiPh$ also are isolated and fully characterized. The manganese acyl catalysts endure (within NMR spectral detection limits) until all organoiron acyl substrate is consumed; only then do they undergo hydrosilation. Treating manganese acyls with 1 equiv of R'_3SiH or R'_2SiH_2 cleanly affords a series of α-siloxyalkyl compounds $(CO)_5Mn$–$CH(OSiMe_2Ph)CH_3$, $(CO)_5Mn$–$CH(OSiHR'_2)CH_3$, and $(CO)_5Mn$–$CH(OSiHR'_2)Ph$ (R' is Et or Ph).

T RANSITION METAL ACYL COMPLEXES function as pivotal intermediates in homogeneous catalysis processes involving carbonylation of a substrate. Cleavage of a cobalt–carbon bond in acyl–cobalt intermediates by H_2 or by a hydridocobalt complex during carbonylcobalt-catalyzed hydroformylation of alkenes, for example, affords initial aldehyde products (*1*). Hydrosilanes

also are quite reactive toward thermally labile acyl complexes; triethylsilane cleaves acyl compounds $(L)(CO)_3Co-COR$ (L is CO or PPh_3) and $(CO)_5Mn-COCH_3$ (in tetrahydrofuran (THF), 1 atm of CO) and produces aldehydes (2, 3).

Alternatively, the silane Si–H bond could add across the acyl ligand and generate α-siloxyalkyl compounds $L_xM-CH(OSiR'_3)R$. This route occasionally has been mentioned for hydrosilating labile acyl–cobalt compounds, but no definitive evidence is available (3, 4). Siloxyalkyl compounds nevertheless have resulted from combining a silyl complex $L_xM-SiR'_3$ with an aldehyde (5, 6). Gladysz et al. (7) proposed stable (trimethylsiloxybenzyl)$M(CO)_5$ examples (M is Mn or Re). (α-Siloxyalkyl)Rh(III) complexes are proposed intermediates during $Rh(PPh_3)_3Cl$-catalyzed hydrosilation of ketones (8). Two research groups reported that $Rh(PPh_3)_3Cl$ also catalyzes hydrosilation of Fp(acyl) compounds [Fp is $Fe(CO)_2-(\eta^5-C_5H_5)$] and affords stable (α-siloxyalkyl)Fp complexes (9, 10).

Developing procedures for transforming organometallic acyl complexes to isolable α-siloxyalkyl derivatives, particularly those that will subsequently carbonylate and give new acyl compounds, serves as one objective of our ongoing hydrosilation studies. In this chapter we summarize the hydrosilation chemistry of the acyl complexes FpCOR (1, R is CH_3; 2, R is Ph) and $(CO)_5Mn-COR$ (3, R is CH_3; 4, R is Ph). Differences in the reactivity of the iron and manganese acyls are immediately apparent. The manganese acyls, which are thermally labile to terminal carbonyl dissociation [although somewhat less so than are their $Co(CO)_4$ analogs (11)], directly add hydrosilanes to form α-siloxyalkyl compounds. In contrast, nonlabile Fp(acyls) are inert to free hydrosilanes under ambient conditions and require a catalyst. An intriguing outcome of our studies is that 3 and 4 function more efficiently than $Rh(PPh_3)_3Cl$ as catalysts for hydrosilating the Fp(acyls) 1 and 2.

Rh(PPh₃)₃Cl-Catalyzed Hydrosilation of Iron Acyls η⁵-C₅H₅(L)(CO)Fe–COR

The $Rh(PPh_3)_3Cl$-catalyzed hydrosilation of 1 with Et_2SiH_2 occurs rapidly in THF or in benzene between 5 °C and room temperature. The product is a stable diethylsiloxyethyl complex 5 (eq 1) (10). Workup of this reaction requires careful chromatography—fast passage down a short column of deactivated silica gel in pentane—to obtain analytically pure 5 in 85–90% yields. (Siloxyalkyl complexes generally are quite sensitive toward routine chromatographic procedures, even at lower temperatures.) Ethylidene and SiH absorptions in the ^1H and ^{13}C NMR spectra of 5 (and other siloxyethyl complexes) are particularly diagnostic.

Optimal reaction conditions entail using 2 equiv of Et_2SiH_2 and 4–5% $Rh(PPh_3)_3Cl$ to accommodate competing rhodium-catalyzed dehydrogenative coupling of Et_2SiH_2 to $Et_2(H)Si_2HEt_2$ (12). The choice of silane is critical.

$$\underset{\textbf{1}}{\overset{\displaystyle O}{\underset{OC \quad CO}{\overset{\displaystyle \|}{Fe - C}}\diagdown CH_3}} \quad + \quad \underset{R_2' = Et_2, Ph_2, PhMe}{2\ R'_2SiH_2} \quad \xrightarrow[\substack{THF\ or\ benzene \\ 0^\circ\ to\ 22^\circ\ C}]{5\%\ (PPh_3)_3RhCl}$$

$$\underset{\textbf{5}}{\overset{\displaystyle O\text{-}SiHR'_2}{\underset{OC \quad CO}{\overset{\displaystyle |}{Fe - C \cdot H}}\diagdown CH_3}} \qquad (1)$$
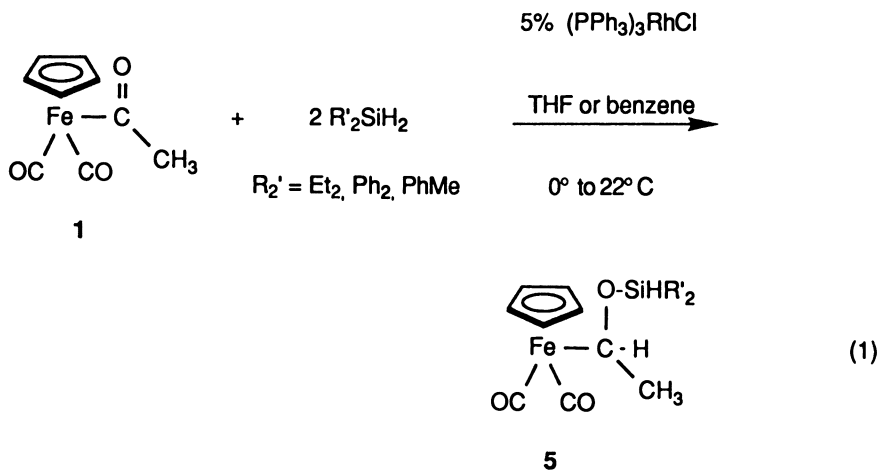
Et$_3$SiH and Me$_2$PhSiH are unreactive under these conditions, and PhSiH$_3$ overreduces **1** and **2** to FpCH$_2$CH$_3$ and FpCH$_2$Ph, respectively. Other dihydrosilanes, Ph$_2$SiH$_2$ and PhMeSiH$_2$, reacted similarly to Et$_2$SiH$_2$, but incomplete product separation from silane residues initially precluded obtaining analytically pure samples (*10*). By doing preparative size-exclusion chromatography on Bio-Rad S-X polystyrene beads (mol wt excluded 400, 200–400 mesh) in benzene, we now obtain pure samples of these Fp(α-siloxyalkyl) compounds.

We briefly investigated the scope of the Rh(PPh$_3$)$_3$Cl-catalyzed hydrosilation of Fp(acyls) with Et$_2$SiH$_2$. Iron and ruthenium acetyl complexes analogous to **1** but containing η^5-C$_5$Me$_5$ or η^5-indenyl ligands (Fe) and η^5-C$_5$H$_5$ (Cp) or indenyl (Ru) readily afford their (α-diethylsiloxy)ethyl compounds. Changing the acyl ligand on Fe(CO)$_2$Cp complexes has a much greater effect on the outcome of the hydrosilation reaction. Although linear propanoyl and butanoyl FpC(O)(CH$_2$)$_x$CH$_3$ (x is 1 or 2) are only slightly less reactive than **1**, hydrosilation reactions of the branched-chain acyls Fp-COCH(CH$_3$)$_2$ and FpCOCH$_2$CH(CH$_3$)$_2$ are sluggish. Even in the presence of more catalyst and silane, these reactions are characterized by messy workup procedures that afford impure α-siloxyalkyl products in moderate yields. Fp(benzoyl) (**2**) likewise proved to be a difficult substrate.

Phosphine- and phosphite-substituted iron acetyl compounds **6** are extremely reactive substrates, even when using only 1% Rh(PPh$_3$)$_3$Cl and either Et$_2$SiH$_2$ or Ph$_2$SiH$_2$. Vinyl complexes Cp(L)(CO)Fe–CH=CH$_2$ (**8**) (eq 2), however, are the final products. This reaction is an extremely efficient procedure for directly converting an acetyl compound to its vinyl derivative (*13*). Conducting the reactions dilute in C$_6$D$_6$ affords substantial concentrations of the α-siloxyethyl intermediates **7**, which we examined by ^{1}H, ^{13}C, and ^{31}P NMR spectroscopy. Analogous (η^5-indenyl)Fe, CpRu (L is PPh$_3$ or

$$(2)$$
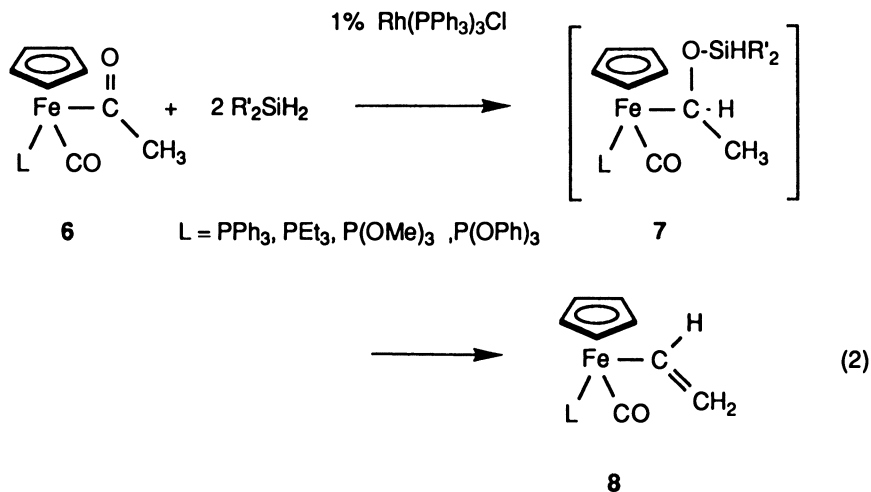
PEt$_3$), and (η^5-indenyl)Ru (L is PPh$_3$) acetyl compounds also undergo similar Rh(I)–hydrosilane catalysis.

A plausible mechanism for Rh(PPh$_3$)$_3$Cl-catalyzed hydrosilation of 1, patterned after the accepted mechanism for Rh-catalyzed ketone hydrosilation (8), appears in Scheme I. A salient intermediate is the octahedral hydrido(silyl)Rh(III) compound that results from Rh(PPh$_3$)$_2$Cl, the apparent active catalyst. It oxidatively adds R′$_2$(H)Si–H and then binds 1. Subsequent rearrangement with regioselective Si–O bond formation affords a hydrido(alkyl)Rh(III) species that reductively eliminates the product 5.

Iron acyl complexes are not ketones, however, and hydrosilation of 1 differs in at least two respects. First, PhSiH$_3$ completely reduces the acyl ligand of 1; second, hydrosilation of 6 affords vinyl compounds 8. Organic analogs of these ligand reactions during Rh-catalyzed hydrosilation of ketones are unknown, although silyl vinyl ethers [e.g., PhC(OSiR′$_3$)=CH$_2$ from PhCOCH$_3$] occasionally form (8). Both organometallic side reactions are consistent with the iron α-siloxyalkyl intermediates 5 and 7 heterolytically cleaving the α-siloxy leaving group (and eliminating a disiloxane) as a rhodium intermediate either transfers hydride to the α-carbon or deprotonates the β-site on 5 and 7. Similar organoiron ligand reactions are established (13).

Rhodium-catalyzed hydrosilation of iron acyl compounds suffers from two drawbacks as a synthetic procedure for α-siloxyalkyl complexes. First, this reaction is of limited scope. Monohydrosilanes do not work, and many Fp(acyls) react sluggishly with dihydrosilanes. Second, efficient Rh-catalyzed dehydrogenative coupling of dihydrosilanes imposes the need for excess silane and also engenders messy workup procedures. Other rhodium systems tried to date are less effective than is Rh(PPh$_3$)$_3$Cl.
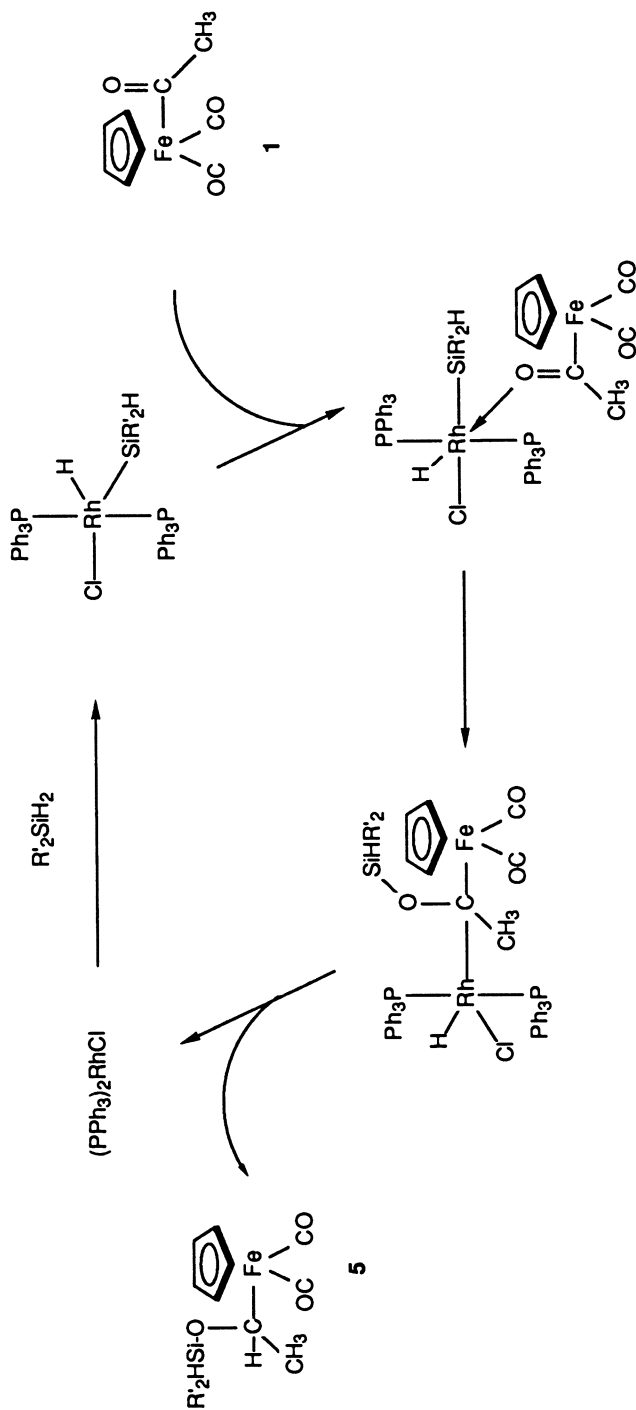
Scheme 1. Hypothesized mechanism for Rh(PPh₃)₃Cl-catalyzed hydrosilation of FpCOCH₃.

5

7
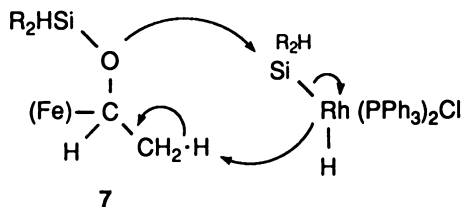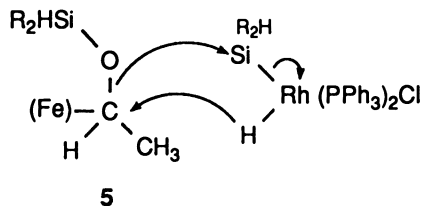
Manganese Acyl-Catalyzed Hydrosilation of Cp(CO)₂Fe–COR

Hydrosilation of **1** with monohydrosilanes is accomplished by using $(CO)_5Mn-COPh$ (**4**) as the catalyst (eq 3) (*14*). These reactions occur rapidly with only 1 equiv of silane (less than 2 h with 2–3% **4**) and afford stable, analytically pure trialkylsiloxyethyl compounds **9** in up to 90% yield after column chromatography.

$$ \tag{3} $$

9a $R'_3Si = Et_3Si$

9b $R'_3Si = Me_2PhSi$
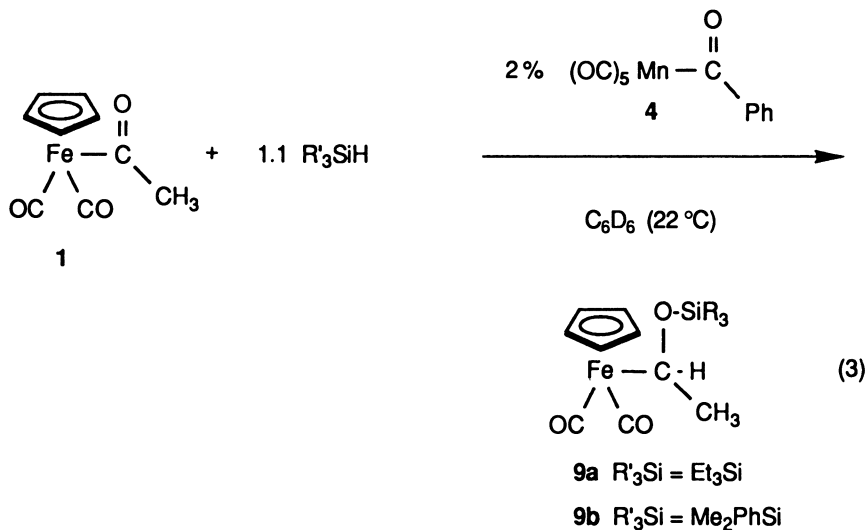
Both manganese acyl complexes $(CO)_5Mn-COR$ **3** and **4** function as catalysts for hydrosilating **1** with the more reactive dihydrosilanes, although manganese benzoyl catalysis is somewhat faster. These reactions quantita-

tively convert **1** into mixtures of mono-Fp(siloxyethyl) **5a–5b** and bis-Fp(siloxyethyl) **10a–10b** (eq 4). Typical product ratios of **5** to **10** vary between 0.8 and 1.2. Analytically pure samples of all four products were procured easily by size-exclusion chromatography. Reaction times range from less than 1 h (with Ph_2SiH_2 and **4**) to 20 h (Et_2SiH_2 and **3**) for procedures with 1.2 equiv of R'_2SiH_2, 4% **3** or **4**, and 200 mg of **1** (0.91 mmol) in 600 mg of C_6D_6.
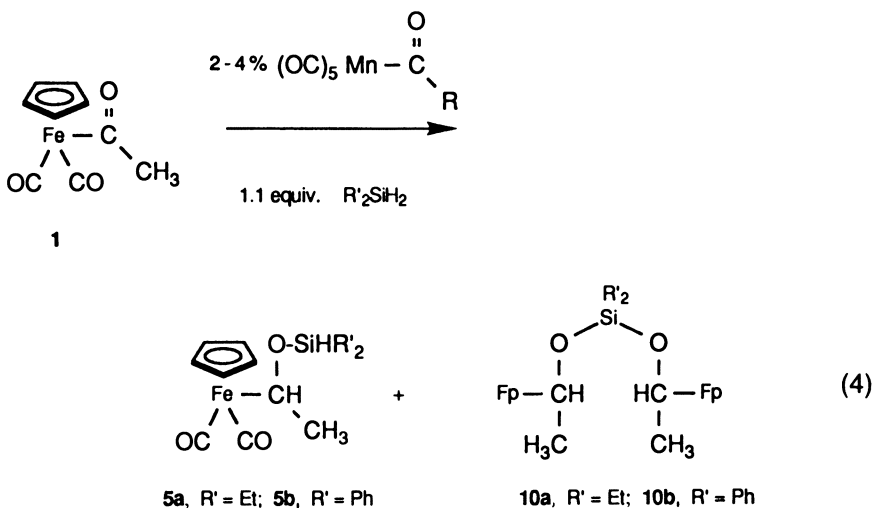
Figure 1 is a typical ^1H NMR spectral scan of a hydrosilation reaction (65% complete) involving $FpCOCH_3$ (**1**), Ph_2SiH_2, and $(CO)_5MnCOCH_3$ (**3**) as the catalyst. Significantly, this spectrum indicates a clean reaction. Only starting materials and products are present, and the manganese acetyl catalyst **3** has not undergone hydrosilation (vide infra). A singlet at δ 2.23 corresponds to **3** (the equivalent absorption for **1** appears at δ 2.39); the methyl doublet at δ 1.81 characterizes **5b**; and the two remaining methyl doublets (δ 1.95, 1.97 with J = 6.0 Hz) define **10b** as a 1:1 mixture of diastereomers. Three Cp singlets also distinguish **5b** (δ 4.12) and **10b** (δ 4.14, 4.15).

Hydrosilation of Fp(benzoyl) (**2**) requires a more active catalyst, because neither **3** nor **4** is effective even when using diphenylsilane. Fortunately $(PPh_3)(CO)_4Mn–COCH_3$ (**11**), which exists as an equilibrating *cis–trans* mixture (1:4.5) (*15*), quantitatively transforms **2** and Ph_2SiH_2 into the fully characterized siloxybenzyl product **12** (Table I).

The heightened activity of **11** as a hydrosilation catalyst carries over to the Ph_2SiH_2–Fp(acetyl) (**1**) reaction. Under comparable conditions, **11** catalyzes this hydrosilation more rapidly than does manganese benzoyl **4** (0.25 h vs. 4 h for 4% precatalyst). Even a 0.5% catalyst concentration of **11** in
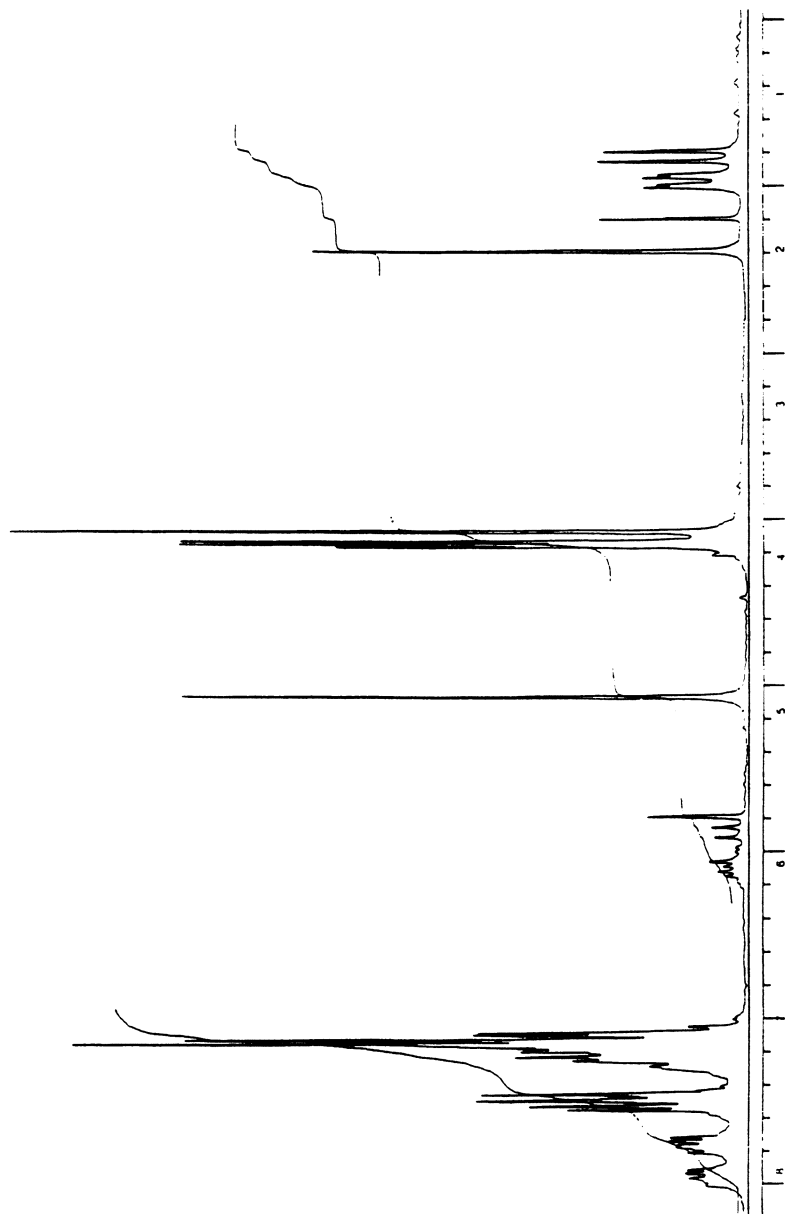
Figure 1. ¹H NMR spectrum of FpCOCH₃ (50 mg), Ph₂SiH₂ (1.2 equiv), and (CO)₅MnCOCH₃ (6 mg, 11%) in 600 mg of C₆D₆ (4 h).

Table I. Manganese Acyl Catalysts for the Ph$_2$SiH$_2$–FpCOPh Reaction
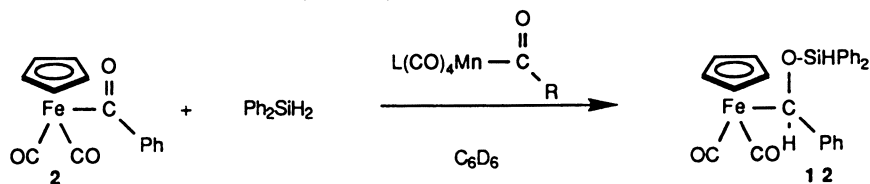
Mn–Acyl Precatalyst[a]	Reaction Time	Consumption of FpCOPh (%)
PPh$_3$(CO)$_4$Mn–COCH$_3$ (2.4%)	26 min	100[b]
(CO)$_5$Mn–COPh (2.8%)	19 h	30
(CO)$_5$Mn–COCH$_3$ (2.4%)	19 h	<10[c]
(CO)$_5$Mn–COCH$_3$ (20.2%)	2 h	<10[d]

[a][FpCOPh] = 0.67 mmol g^{-1} C$_6$D$_6$; [Ph$_2$SiH$_2$]/[FpCOPh] = 1.10.
[b]No further change occurred over 19 h; no bis-Fp adduct was formed.
[c]Starting (CO)$_5$Mn–COCH$_3$ does not add Ph$_2$SiH$_2$.
[d]Less than 10% consumption of (CO)$_5$Mn–COCH$_3$ (≥2 h).

C$_6$D$_6$ converts a 1:1.2 mixture of 1 and Ph$_2$SiH$_2$ to 5b in 5 h. Significantly, reactions employing 11 as the catalyst quantitatively generate the mono-Fp product 5b. Figure 2, another in situ ^{1}H NMR spectral scan, clearly illustrates this selectivity; residual Ph$_2$SiH$_2$ accounts for the δ 6.08 singlet (SiH).

Three observations that pertain to planning mechanistic studies have emerged from our preliminary studies on manganese acyl-catalyzed hydrosilation reactions. First, the presence of CO (1 atm) slows the catalysis. The half-life for Ph$_2$SiH$_2$ hydrosilation of 1 using 3.3% (CO)$_5$Mn–COPh (4) increases from 10 min to 1.8 h when the reaction is maintained under CO. Second, the manganese acetyl (3) remains intact during catalysis. ^{1}H and ^{2}H NMR spectral monitoring of reactions using 4–20% 3 or (CO)$_5$Mn–COCD$_3$ (3-d_3) indicates the absence of other manganese complexes or organic products derived from 3, within the detection limits of the NMR experiment, until at least 90% of the iron acyl substrate is consumed. Then 3 rapidly hydrosilates (vide infra). An extreme example of substrate blocking hydrosilation of the manganese acyl catalyst appears in Table I. Manganese acetyl 3 fails to promote Ph$_2$SiH$_2$ hydrosilation of FpCOPh (2), which in turn blocks the otherwise rapid hydrosilation of 3.

The third observation is that the acyl ligand on 3 or 4 is not a prerequisite for hydrosilation catalysis. Table II qualitatively ranks a number of Mn(CO)$_5$ complexes as Ph$_2$SiH$_2$–Et$_2$SiH$_2$ hydrosilation catalysts toward 1. Manganese alkyl complexes (CO)$_5$Mn–CH$_3$ and the siloxyethyl compounds deriving from 3 and 4 are quite efficient catalysts, in contrast to the relatively inactive manganese silyl (CO)$_5$Mn–SiMe$_3$ and dimer Mn$_2$(CO)$_{10}$. No evidence of dehydrogenative coupling of R'$_2$SiH$_2$ is found during these reactions.

A mechanism for manganese acyl-catalyzed hydrosilation of 1 resembling that outlined in Scheme I for Rh(PPh$_3$)$_3$Cl catalysis appears less attractive.
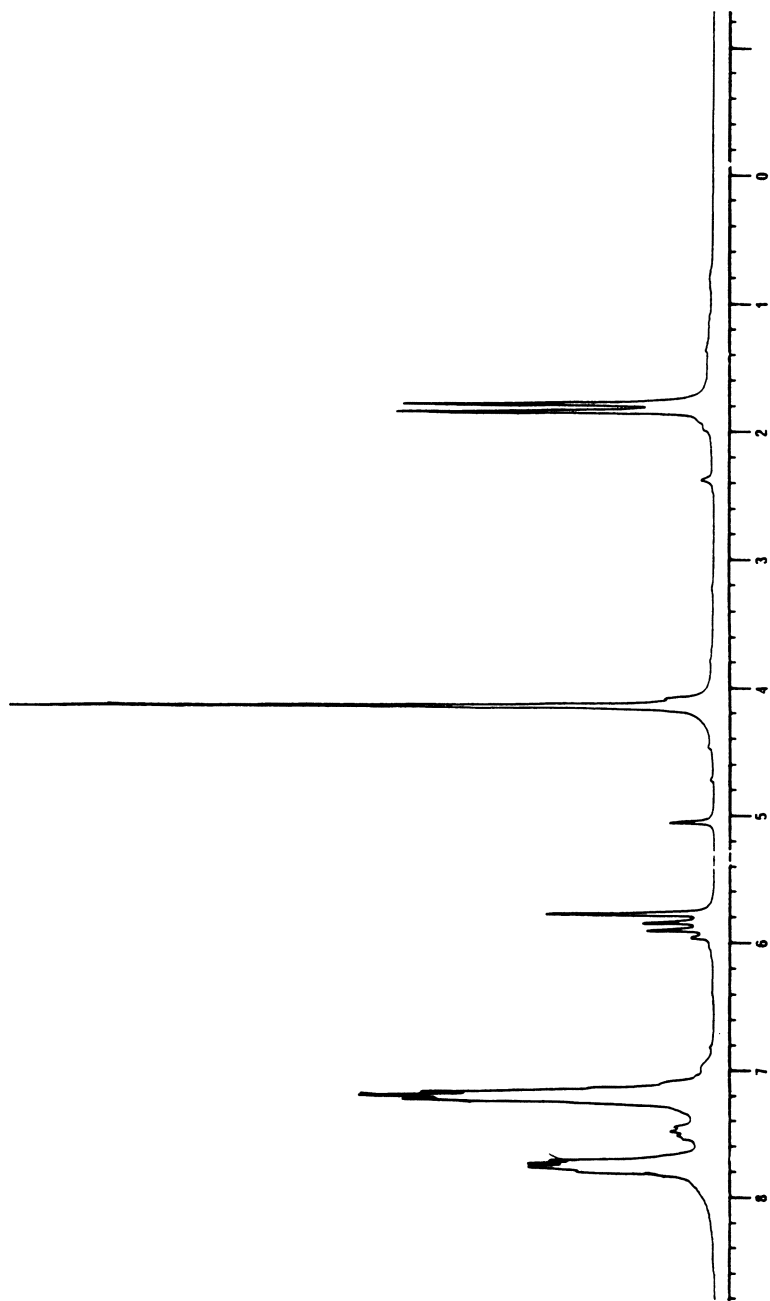
Figure 2. ^1H NMR spectrum of FpCOCH$_3$ (100 mg), Ph$_2$SiH$_2$ (1.2 equiv), and (PPh$_3$)(CO)$_4$MnCOCH$_3$ (1.4%) in 600 mg of C$_6$D$_6$ (15 min).

Table II. Manganese Catalyst Reactivity
Toward FpCOCH₃–R′₂SiH₂

	Mn precatalyst	
1	**(1.1 equiv.)**	**5a, 5b**
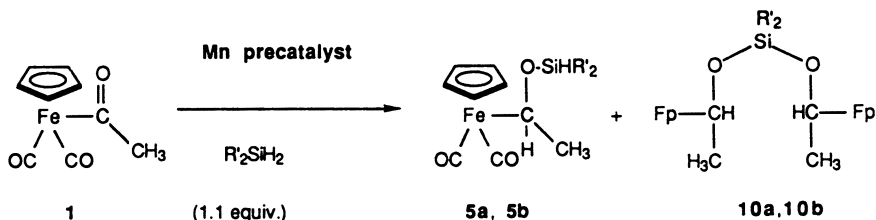
Mn Catalyst	Ph₂SiH₂	Et₂SiH₂
PPh₃(CO)₄Mn–COCH₃*a*	0.25 h	—
(CO)₅Mn–COPh	0.3 h	8 h
(CO)₅Mn–CH₃	0.5 h	8 h
(CO)₅Mn–CH(CH₃)OSiHR′₂	0.5 h	8 h
PEt₃(CO)₄Mn–COCH₃*a*	3.0 h	—
(CO)₅Mn–COCH₃	4.0 h	12 h
(CO)₅Mn–CH(Ph)OSiHR′₂	6.0 h	36 h
(CO)₅Mn–SiMe₃	6 d	20 h
Mn₂(CO)₁₀	>7 d	7 d

NOTE: All values are reaction times for consumption of FpCOCH₃.
*a*Gives only mono-Fp adduct.

The manganese precatalyst $Mn(CO)_5(COR)$ must lose two terminal carbonyls in order to simultaneously bind silane and **1** as $(CO)_3(RCO)Mn(H)(SiR'_3)$-$[O=C(CH_3)Fp]$. An alternative proposal (eq 5) is a free-radical mechanism (*16*) in which a 17-electron species **12**, resulting from hydrogen atom abstraction from the silane oxidative addition product $(CO)_4(RCO)Mn(H)$-(SiR'_3), associates **1**. The resulting 19-electron adduct, perhaps having its odd electron partially delocalized on the ligated FpCOR, can rearrange to a 17-electron manganese system **13** that shares a μ-siloxyalkylidene ligand with a Fp moiety. Subsequent hydrogen atom transfer to **13** and reductive elimination of $FpCH(OSiR'_3)R$ product then would regenerate the active catalyst $(CO)_4MnCOR$.

$$(5)$$
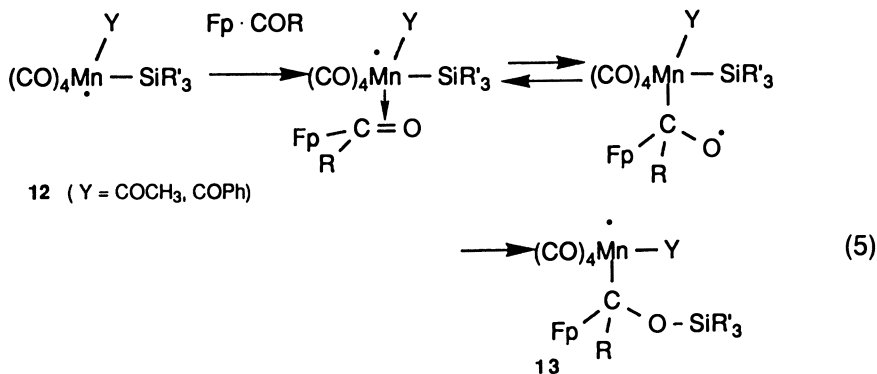
Manganese acetyl-catalyzed $PhSiH_3$ hydrosilation of **1** merits separate discussion because of the ensuing ligand reactions (eq 6) (*14*). A 1:1 mixture of **1** and $PhSiH_3$ with $(CO)_5MnCOCH_3$ (**3**) as the catalyst (4.6%) in C_6D_6 converts to a mixture of mono-**14**, bis-**15**, and tris-**16** (siloxyethyl)Fp compounds within 8 h; over an additional 4–6 h **14** and **15** transform to Fp(ethyl), as ascertained by ^1H and ^{13}C NMR spectral monitoring.

$$(6)$$
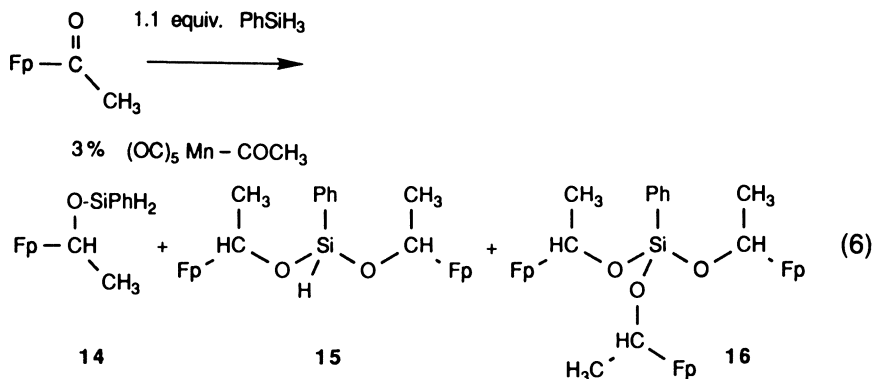
Assignments for **14** and **15** closely resemble those of the fully characterized diphenylsiloxyethyl compounds **5a** and **9a**. Isolated yields of fully characterized tris-**16** and Fp(ethyl) are 26% and 53%, respectively, after isolation by size-exclusion chromatography.

Hydrosilation of Manganese Acyls (CO)₅Mn–COR

Treatment of $(CO)_5MnCOCH_3$ (**3**) with 1 equiv of Me_2PhSiH in C_6D_6 forms the siloxyethyl compound **17** (90% yield) (eq 7), which we isolate analytically pure in 70% yield. We detect no trace of acetaldehyde, its hydrosilated product $CH_3CH_2OSiMe_2Ph$, or the independently characterized silyl complex $(CO)_5Mn–SiMe_2Ph$. In addition, we find no evidence that **17** rapidly degrades by β-elimination of $(CO)_5MnH$ (*16*).

$$(7)$$
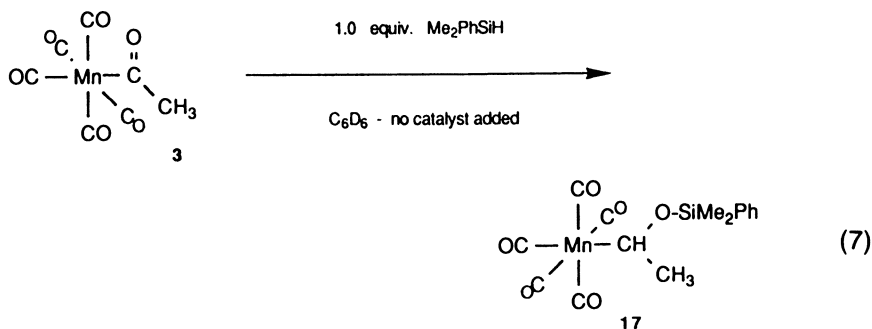
Dihydrosilanes R'_2SiH_2 (R' is Et or Ph) react rapidly with manganese acyl compounds **3** and **4** (eq 8). Between 1 and 3 equiv of Ph_2SiH_2 quantitatively produce siloxyalkyl compounds **18b–18d**, whereas diethylsilane and **3** give 1.5–2.0:1 mixtures of **18a** and **19**. We initially detect neither the manganese silyl compounds $(CO)_5Mn–SiHR'_2$ nor the organic silyl ethers $RCH_2OSiHR'_2$; ^1H and ^{13}C NMR assignments for **18** and bis-Fp **19** are very similar to those for their fully characterized Fp analogs. The manganese siloxyalkyl compounds, however, are unstable, especially in the absence of excess silane. Attempts at isolating them by using size-exclusion chromatography failed.

3 R = CH₃
4 R = Ph

18 a & b R = CH₃, R' = Et & Ph

18 c & d R = Ph, R' = Et & Ph

19
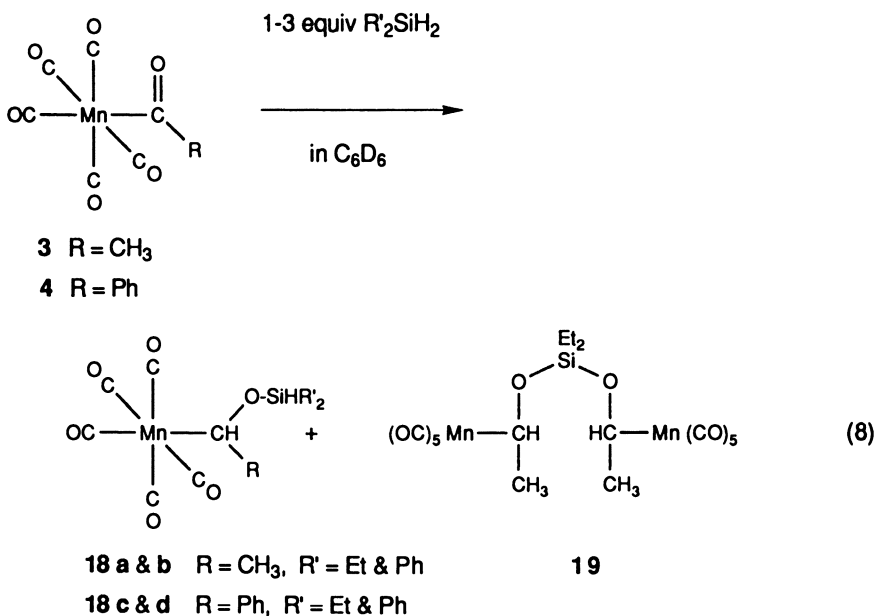
Reactions between manganese benzoyl **4** and monohydrosilanes Et_3SiH and Me_2PhSiH generate at most trace amounts of the corresponding siloxybenzyl compounds, as ascertained by ^1H and ^{13}C NMR spectral monitoring. Under a variety of experimental conditions, these silanes cleave **4** and produce the benzyl silylethers according to the stoichiometry indicated in eq 9. These (and all other silylethers mentioned) were generated quantitatively
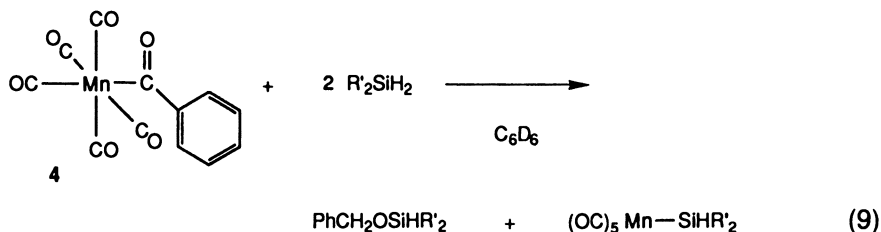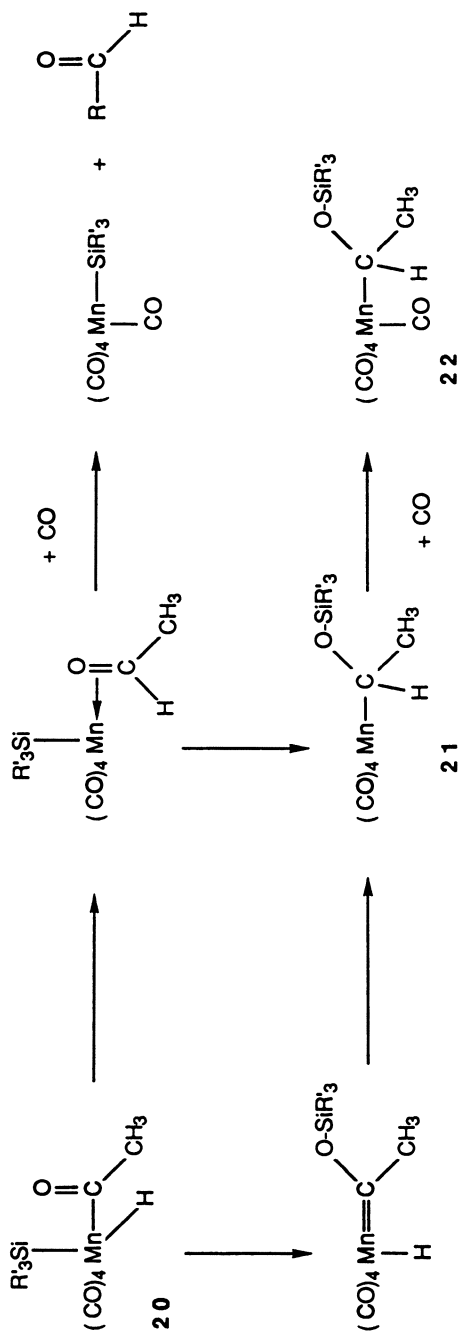
Scheme II. Pathways for intramolecular (noncatalyzed) hydrosilation of (CO)₅MnCOR.

by $(CO)_5MnCOR$-catalyzed hydrosilation of benzaldehyde (or acetaldehyde). We find certain parallels between manganese acyl-catalyzed hydrosilation of aldehydes, ketones, and $FpCOCH_3$ (1). In particular, the catalyst 3 remains intact during the substrate hydrosilation; 3 only reacts after the substrate is consumed.

The title of this chapter indicates that hydrosilation of manganese acyls 3 and 4 could be "noncatalyzed". Scheme II outlines two "traditional" intramolecular pathways, progressing via 16- and 18- electron intermediates, that account for the observed α-siloxyalkyl products 22. The initial product of oxidatively adding $R_3Si–H$ to 3 or 4 is 20. It either reductively eliminates aldehyde (ligated), which rearranges to 21, or undergoes a 1,3-silatropic shift (17) and a hydride transfer to give 21. Coordinatively unsaturated 21 then can reassociate CO (giving 22) or it can add more silane (eliminating silylether). Organic silylethers also may originate from 20, reductively eliminating free aldehyde, which then undergoes a separate catalyzed hydrosilation.

The mechanisms summarized in Scheme II are appealing, as they resemble those advanced by Murai and Seki (6) and Gladysz (5) for reactions of cobalt and manganese silyl compounds $R'_3Si–M(CO)_x$ with aldehydes and CO. It is also possible that hydrosilation of manganese acyls is catalytic in that a free-radical mechanism such as that suggested in eq 5 (with 3 or 4 replacing $FpCOCH_3$ as the substrate) operates. These mechanistic alternatives, as well as continuing synthetic studies on metal acyl hydrosilation chemistry, are under study.

Acknowledgment

References

1. Kovacs, I.; Ungvary, F.; Marko, L. *Organometallics* **1986**, 5, 209.
2. Wegman, R. W. *Organometallics* **1986**, 5, 707.
3. Kovacs, I.; Sisak, A.; Ungvary, F.; Marko, L. *Organometallics* **1988**, 7, 1025.
4. Murai, S.; Sonoda, N. *Angew. Chem., Int. Ed. Engl.* **1979**, 18, 837.
5. Gladysz, J. A. *Acc. Chem. Res.* **1984**, 17, 326.
6. Murai, S.; Seki, Y. *J. Mol. Catal.* **1987**, 41, 197.
7. Selover, J. C.; Vaughn, G. D.; Strouse, C.; Gladysz, J. A. *J. Am. Chem. Soc.* **1986**, 108, 1455.
8. Ojima, I.; Hirai, K. In *Asymmetric Synthesis*; Morrison, J. D., Ed.; Academic: New York, 1985; Vol. 5, p 103.
9. Akita, M.; Mitani, O.; Moro-oka, Y. *J. Chem. Soc., Chem. Commun.* **1989**, 527.
10. Crawford, E. J.; Hanna, P. K.; Cutler, A. R. *J. Am. Chem. Soc.* **1989**, 111, 6891.
11. Kovacs, I.; Hoff, C. D.; Ungvary, F.; Marko, L. *Organometallics* **1985**, 4, 1347.

12. Chang, L. S.; Corey, J. Y. *Organometallics* **1989**, *8*, 1855, and references therein.
13. Cutler, A. R.; Hanna, P. K.; Vites, J. C. *Chem. Rev.* **1988**, *88*, 1363.
14. Hanna, P. K.; Gregg, B. T.; Cutler, A. R. *Organometallics* **1991**, *10*, 31.
15. Kraihanzel, C. S.; Maples, P. K. *Inorg. Chem.* **1968**, *7*, 1806.
16. Gregg, B. T.; Hanna, P. K.; Crawford, E. J.; Cutler, A. R. *J. Am. Chem. Soc.* **1991**, *113*, 384.
17. Brinkman, K. C.; Blakeney, A. J.; Krone-Schmidt, W.; Gladysz, J. A. *Organometallics* **1984**, *3*, 1325.

Reduction of Methanol by Tetracarbonylcobalt Anion Assisted by Carbon Dioxide and Cobalt Cation

Giuseppe Fachinetti and Tiziana Funaioli

Dipartimento di Chimica e Chimica Industriale, University of Pisa, via Risorgimento 35, I–56126 Pisa, Italy

Fundamental electron-transfer reactions involving CH_3OH and $Co_2(CO)_8$ are investigated. In a fully disproportionated CH_3OH solution of $Co_2(CO)_8$, in the presence of CO_2, a CH_3OH reduction by $Co(CO)_4^-$ occurs, under the intervention of the highly polarizing Co^{2+} cations. In tetrahydrofuran as solvent under carbon monoxide atmosphere, the CH_3O^- nucleophile formed gives rise to the Co(I) species tetracarbonyl(methoxycarbonyl)cobalt. Under low carbon monoxide pressure, this Co(I) species disproportionates to $Co(OCH_3)_2$ and $Co_2(CO)_8$. Catalytic amounts of $Co_2(CO)_8$ activate the carbonylation reaction of $Co(OCH_3)_2$ to dimethyl carbonate and tetracarbonyl(methoxycarbonyl)cobalt.

CARBONYL(METHOXYCARBONYL)COBALTS are believed to be key intermediates in important industrial and laboratory catalytic processes performed in CH_3OH solutions of $Co_2(CO)_8$, namely olefin carbalkoxylation (*1, 2*) and CH_3OH carbonylation (*3*) or homologation (*4*). This assumption is justified by the chemical properties of preformed tetracarbonyl(alkoxycarbonyl)-cobalts. Nevertheless, the generation of these intermediates in CH_3OH solutions of $Co_2(CO)_8$ requires the O–H bond activation of the CH_3OH molecule, an elementary step that is still to be demonstrated in these solutions.

We recently observed an O–H bond activation of the H_2O molecule in a fully disproportionated $Co_2(CO)_8$ wet ethereal solution (*5*). Such an activation consists of a Co^{2+}-assisted reduction of H_2O (to H_2 and nucleophile

hydroxide) by $Co(CO)_4^-$. We have now found that in a fully disproportionated CH_3OH solution of $Co_2(CO)_8$ in the presence of CO_2, the O–H bond activation of the CH_3OH molecule consists of Co^{2+}- and CO_2-assisted CH_3OH reduction to H_2 and nucleophile methoxide by $Co(CO)_4^-$.

Experimental Details

All manipulations were carried out by standard Schlenk techniques under prepurified argon. Methanol was distilled from $Mg(OCH_3)_2$, and tetrahydrofuran (THF) was distilled from $LiAlH_4$. $Co_2(CO)_8$ was purchased from Strem Chemicals and sublimed (38 °C, 0.1 mm Hg) prior to use. IR spectra were recorded on a Perkin Elmer model 283 instrument (0.1 mm CaF_2 cell).

$Co_2(CO)_8$ (3 g, 8.77 mmol) was dissolved in 50 mL of CH_3OH and stirred until gas evolution ceased. The resulting pink solution was transferred in a 120-mL rocking steel autoclave and charged with CO_2 up to 15 atm. After 4 h at 100 °C, gas chromatographic (GC) analysis revealed the presence of H_2 and CO in the gas phase. After they were cooled, the gases were vented out and a 10-mL portion of the solution was treated with a slight excess of bis(triphenylphosphine)iminium chloride (PPNCl). The quantitative precipitation of $Co(CO)_4^-$ yielded colorless crystals of $PPNCo(CO)_4$ (1.095 g, 1.54 mmol, 88% yield). By potentiometric back titration of the mother liquor, 1.63 meq of base (methyl carbonate) was determined. Anhydrous $CoCl_2$ (30 mg) was added to the remaining solution (40 mL). Upon evacuation, the 1615-cm^{-1} methyl carbonate band disappeared. The evacuation of the solution was prolonged until dryness, leaving a solid residue that was dissolved in 40 mL of THF. The resulting dark green solution was transferred again in the 120-mL autoclave, pressurized with 80 atm of CO, and kept at 80 °C for 4 h. After the solution cooled, the gases were vented out. $CH_3OC(O)Co(CO)_4$ and $Co_2(CO)_8$ were quantitatively determined by measuring the infrared absorbances of the reaction mixture at 1684 and 1857 cm^{-1}.

Discussion

As a consequence of the complete disproportionation reaction (6) (eq 1), a 0.15 M CH_3OH solution of $Co_2(CO)_8$ soon becomes pink and its IR spectrum in the CO stretching region shows only the 1910-cm^{-1} band of the unperturbed $Co(CO)_4^-$.

$$\frac{3}{2} Co_2(CO)_8 \xrightarrow{CH_3OH} [Co(CH_3OH)_n]^{2+} + 2Co(CO)_4^- + 4CO \qquad (1)$$
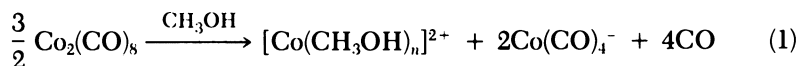
When this solution is warmed in a closed vessel at about 100 °C under an Ar atmosphere, cobalt metal and CO are formed. Presumably, intermediates of such a Co(II)–Co(–I) synproportionation are endothermic $Co^{2+}, Co(CO)_4^-$ homonuclear ion pairs (7, 8). However, when the same solution is warmed to 100 °C under 15 atm of CO_2, metal formation is suppressed and both H_2 and CO evolve. The IR spectrum of the solution shows the 1910-cm^{-1} band of unreacted $Co(CO)_4^-$ and a new absorption (1615

cm^{-1}), which was attributed to the methyl carbonate ion acting as bidentate ligand for Co^{2+} cations (9). CO and H$_2$ were detected in the evolved gases. Quantitative determination of methyl carbonate and of unreacted Co(CO)$_4^-$ indicates the stoichiometry of eq 2.

$$[Co(CH_3OH)_n]^{2+} + 2Co(CO)_4^- \begin{array}{c} \xrightarrow{\text{100 °C,}\ \text{Ar}} 3Co + 8CO \\ \xrightarrow[\substack{\text{100 °C,} \\ \text{15 atm,} \\ CO_2}]{} \frac{3}{2}[CoO_2COCH_3]^+ + \\ \frac{3}{2}Co(CO)_4^- + \frac{3}{4}H_2 + 2CO \end{array} \qquad (2)$$
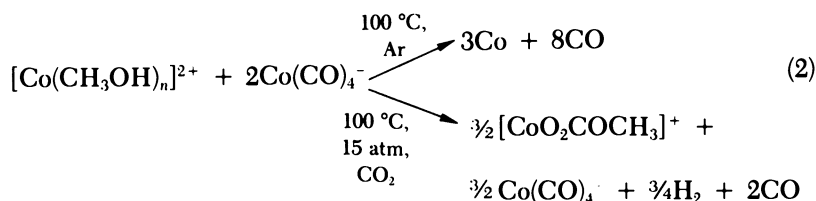
Thus, CO$_2$ assists the CH$_3$OH reduction by Co(CO)$_4^-$. Highly polarizing Co^{2+} cations also play a crucial role in the reaction. Neither H$_2$ nor methyl carbonate was formed when a 0.2 M solution of NaCo(CO)$_4$ in CH$_3$OH, pressurized with CO$_2$ at 15 atm, was warmed to 100 °C.

These results can be rationalized in terms of proton transfer from Co^{2+}-coordinated CH$_3$OH to Co(CO)$_4^-$. In the absence of CO$_2$ the acid–base equilibrium is far to the left. In the presence of CO$_2$ the formation of bidentate methyl carbonate ligand increases the steady-state concentration of HCo(CO)$_4$, whose decomposition accounts for the observed products (eq 3).

$$[(CH_3OH)_nCoO-H]^+ + Co(CO)_4^- \xrightarrow{CO_2}$$
$$\underset{CH_3}{|}$$
$$[(CH_3OH)_nCoO_2COCH_3]^+ + HCo(CO)_4 \rightarrow$$
$$\frac{1}{2}H_2 + \frac{1}{2}Co_2(CO)_8 \qquad (3)$$
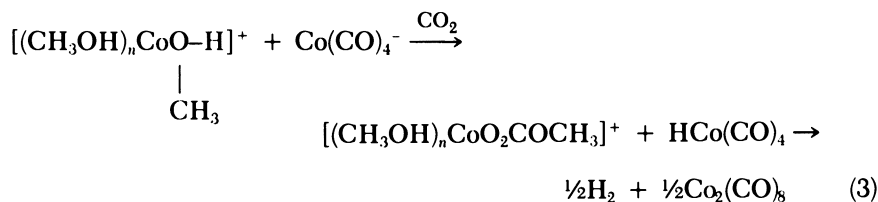
This finding constitutes a rare case in which a CO$_2$ effect on electron transfers occurring in a carbonyl metal solution has been singled out. Furthermore, we have found that in the presence of catalytic amounts of halide ions, [CoO$_2$COCH$_3$]$^+$ is in equilibrium with [CoOCH$_3$]$^+$. Thus, a solution containing an equimolar mixture of CH$_3$O$^-$ and Co(CO)$_4^-$ (as counteranions of Co^{2+}) was obtained on evacuating CO$_2$.

Investigation of the carbonylation reaction of a solution containing Co^{2+}, CH$_3$O$^-$, and Co(CO)$_4^-$ (1:1:1 molar ratio) confirmed that the Co^{2+}-, CO$_2$-assisted reduction of CH$_3$OH by Co(CO)$_4^-$ can constitute a step toward the formation of CH$_3$OC(O)Co(CO)$_4$. In CH$_3$OH the carbonylation to methyl formate masks the reaction of the cobalt-containing species. Therefore THF was used as solvent instead of CH$_3$OH. This change of solvent alters the solution from pink to deep green. Correspondingly, IR analysis of the THF

solution shows a characteristic pattern of four bands at 2042 (m), 1978 (s), 1952 (vs), and 1940 (vs) cm^{-1}. This pattern suggests the presence of a dimeric alkoxo-bridged $[CoOCH_3]^+, Co(CO)_4^-$ homonuclear ion pair of the $[(OC)_4CoCo(OR)L]_2$ type (10). The THF solution containing the $[(OC)_4CoCo(OCH_3)THF]_2$ dimer can be carbonylated at 80 °C under carbon monoxide pressure (P_{CO}) of 80 atm. Under these conditions tetracarbonyl(methoxycarbonyl)cobalt [ν(CO) in THF: 2118 (m), 2054 (s), 2043 (vs), 2032 (vs), and 1684 (m) cm^{-1}] and $Co_2(CO)_8$ were formed in substantially quantitative yields according to the stoichiometry of eq 4.

$$[(OC)_4CoCo(OCH_3)THF]_2 \xrightarrow[\text{THF, 80 °C}]{\text{CO, 80 atm}}$$

$$2CH_3OC(O)Co(CO)_4 + Co_2(CO)_8 \quad (4)$$
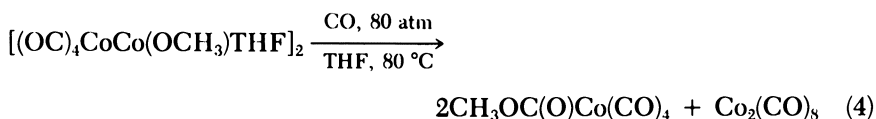
The formation of tetracarbonyl(methoxycarbonyl)cobalt according to this reaction sequence (Scheme I) suggests a plausible pathway for the formation of carbonyl(methoxycarbonyl)cobalts as intermediates in catalytic processes carried out in CH_3OH solutions of $Co_2(CO)_8$. The highly polarizing Co^{2+} cations and CO_2 assist the CH_3OH reduction by $Co(CO)_4^-$. The synproportionation reaction induced by high CO pressure gives the Co(I) species $CH_3OC(O)Co(CO)_4$, presumably through a dimeric, alkoxo-bridged, $[CoOCH_3]^+, Co(CO)_4^-$ homonuclear ion pair.

The formation of $CH_3OC(O)Co(CO)_4$ at 80 °C (eq 4) is rather surprising because this compound has been reported to undergo thermal decomposition at room temperature (11). As a matter of fact, IR investigations under various CO pressures, gas volumetric measurements, and the characterization of the solid product $Co(OCH_3)_2$ indicate that the thermal decomposition of $CH_3OC(O)Co(CO)_4$ actually occurs according to the P_{CO}-dependent equilibrium in eq 5. That fact was confirmed by reacting a mixture of preformed $Co(OCH_3)_2$ (12) and $Co_2(CO)_8$ in a 2:1 molar ratio with CO at 80 °C and 80 atm pressure. IR analyses of the resulting solution showed that $CH_3OC(O)Co(CO)_4$ was the unique product of the carbonylation reaction.

$$2CH_3OC(O)Co(CO)_4 \xrightleftharpoons{\text{THF}} Co(OCH_3)_2 + \frac{1}{2} Co_2(CO)_8 + 6CO \quad (5)$$

Thus, $Co(OCH_3)_2$, which does not react with CO even under drastic conditions (13), is carbonylated to $CH_3OC(O)Co(CO)_4$ in the presence of the stoichiometric amount of $Co_2(CO)_8$ as electron source.

A completely different carbonylation of $Co(OCH_3)_2$ was observed when only catalytic amounts of $Co_2(CO)_8$ were added to a suspension of $Co(OCH_3)_2$ in THF. In this case, CO itself acts as reducing agent, and both dimethyl

$$6Co_2(CO)_8 \xrightarrow{\ CH_3OH,\ -CO\ } 4[Co(CH_3OH)_n]^{2+} + 8CO$$

$$\downarrow \begin{array}{c} CO_2 \\ -CO \end{array}$$

$$3H_2 + 6[(CH_3OH)_{n-1}CoO_2COCH_3]^+ + 6\ Co(CO)_4^-$$

$$-CO_2,[X]^- \ \big\updownarrow\ +CO_2$$

$$6[(CH_3OH)_{n-1}CoOCH_3]^+ + 6Co(CO)_4^-$$

$$THF \ \big\updownarrow\ CH_3OH$$

$$[(OC)_4CoCo(OCH_3)THF]_2$$

$$\downarrow CO$$

$$6CH_3OC(O)Co(CO)_4 + 3Co_2(CO)_8$$

$$-CO \ \big\updownarrow\ +CO$$

$$3Co(OCH_3)_2 + 3\backslash2Co_2(CO)_8$$

$$\downarrow [Co_2(CO)_8],\ CO$$

$$3\backslash2CH_3OC(O)OCH_3 + 3CH_3OC(O)Co(CO)_4$$
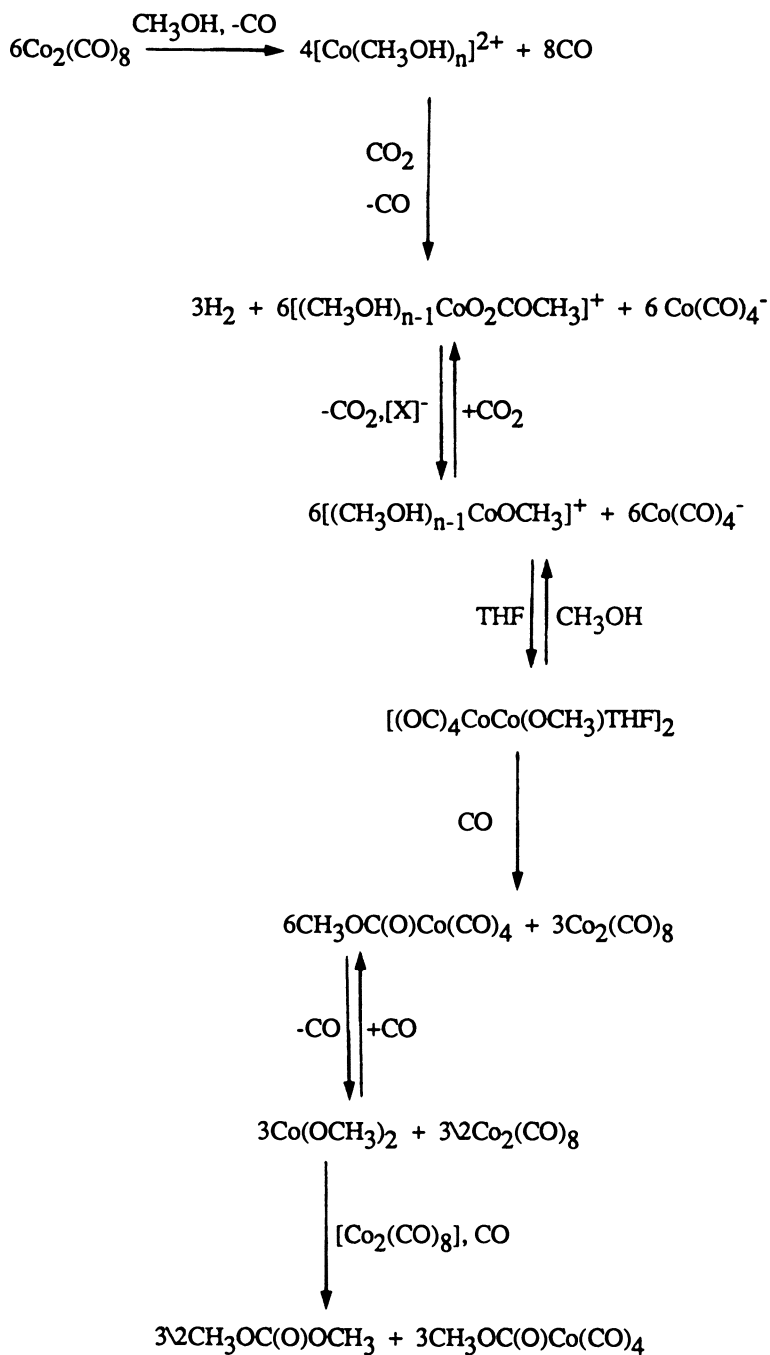
Scheme I. Some C₁ chemistry in CH₃OH solutions of Co₂(CO)₈.

carbonate and $CH_3OC(O)Co(CO)_4$ were formed in substantially quantitative yields (eq 6).

$$2Co(OCH_3)_2 + 11CO \xrightarrow[\text{80 °C, 80 atm}]{Co_2(CO)_8}$$

$$CH_3OC(O)OCH_3 + CH_3OC(O)Co(CO)_4 \quad (6)$$
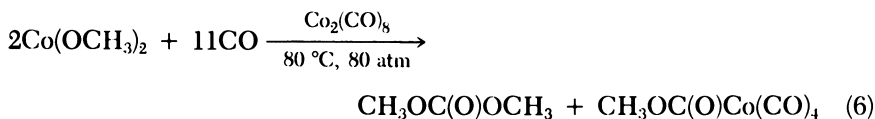
According to Scheme I, the summation of the elementary steps leading to dihydrogen and dimethyl carbonate gives the overall stoichiometry of eq 7.

$$2CH_3OH + CO \xrightarrow{Co_2(CO)_8, CO_2} H_2 + CH_3OC(O)OCH_3 \quad (7)$$
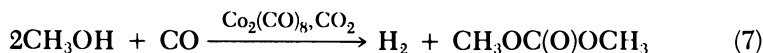
The formation of dimethyl carbonate according to reaction 6 can be tentatively attributed to the reductive elimination of dimethyl carbonate from a tricarbonylbis(methoxycarbonyl)cobaltate anion. This hypothesis is substantiated by the fact that we found the alkali metal salts of tricarbonylbis(methoxycarbonyl)cobaltate to reductively eliminate dimethyl carbonate at room temperature (14) (eq 8).

$$\{[CH_3OC(O)]_2Co(CO)_3\}^- \xrightarrow[\text{20 °C}]{THF} CH_3OC(O)OCH_3 + Co(CO)_4^- \quad (8)$$
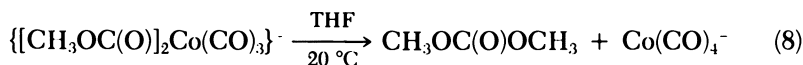
Scheme I reports some fundamental electron-transfer reactions that can be useful for a better understanding of known catalytic processes. In general, our findings indicate that, in metal carbonyl chemistry, transition metal cations formed in disproportionation reactions of neutral carbonyls are highly reactive species (15–17).

Acknowledgments

References

1. Milstein, D.; Huckaby, J. L. *J. Am. Chem. Soc.* **1982**, *104*, 6150.
2. Milstein, D. *Acc. Chem. Res.* **1988**, *21*, 428.
3. Ungváry, F.; Markó, L. *Organometallics* **1983**, *2*, 1608.
4. Bartik, T.; Krümmling, T.; Markó, L.; Pályi, G. *Gazz. Chim. Ital.* **1989**, *119*, 307.
5. Funaioli, T.; Biagini, P.; Fachinetti, G. *Inorg. Chem.* **1990**, *29*, 1440.
6. Hieber, W.; Mühlbauer, F.; Ehmann, A. *Chem. Ber.* **1932**, *65*, 1090.

7. Fachinetti, G.; Fochi, G.; Funaioli, T. *J. Organomet. Chem.* **1986**, *301*, 91.
8. Fachinetti, G.; Fochi, G.; Funaioli, T.; Zanazzi, P. F. *Angew. Chem., Int. Ed. Engl.* **1987**, *26*, 680.
9. Yamamoto, T.; Kubota, M.; Yamamoto, A. *Bull. Chem. Soc. Jpn.* **1980**, *53*, 680.
10. Funaioli, T.; Biagini, P.; Zanazzi, P. F.; Fachinetti, G. *Gazz. Chim. Ital.* **1991**, *121*, 321.
11. Tasi, M.; Pályi, G. *Organometallics* **1985**, *4*, 1523.
12. Adams, R. W.; Bishop, E.; Martin, R. L.; Winter, G. *Aust. J. Chem.* **1966**, *19*, 207.
13. Saegusa, T.; Tsuda, T.; Isayama, K. *J. Org. Chem.* **1970**, *35*, 2976.
14. Fachinetti, G.; Funaioli, T.; Masi, D.; Mealli, C. *J. Organomet. Chem.* **1991**, *417*, C32.
15. Fachinetti, G.; Funaioli, T.; Marcucci, M. *J. Organomet. Chem.* **1988**, *353*, 393.
16. Fachinetti, G.; Fochi, G.; Funaioli, T.; Zanazzi, P. F. *J. Chem. Soc., Chem. Commun.* **1987**, 89.
17. Mealli, C.; Proserpio, D. M.; Fachinetti, G.; Funaioli, T.; Fochi, G.; Zanazzi, P. F. *Inorg. Chem.* **1989**, *28*, 1122.

The Activation of Carbon–Oxygen Bonds

Approaches to the Catalytic Deoxygenation of Phenols by CO

J. Ni and C. P. Kubiak[1]

Department of Chemistry, Purdue University, West Lafayette, IN 47907

*The deoxygenation of allyl oxides and aryl oxides by CO in the complexes Pt(dppe)(OR)$_2$ [R is C$_3$H$_5$, C$_6$H$_5$, p-Me$_2$NC$_6$H$_4$, p-MeC$_6$H$_4$, p-MeSC$_6$H$_4$, or p-ClC$_6$H$_4$; dppe is bis(diphenylphosphino)ethane] was investigated with the goal of developing catalysts for the deoxygenation of phenols by CO. The allyloxy complex Pt(OC$_3$H$_5$)$_2$(dppe), **1**, reacts with CO in benzene to produce the η^3-allyl complex [Pt(η^3-C$_3$H$_5$)(dppe)]$^+$ (**2**), CO$_2$, and free allyl alcohol. The aryl complexes Pt(OAr)$_2$(dppe) incorporate CO into both Pt–OAr bonds to give the bis(aryloxycarbonyl) complexes Pt(dppe)[C(O)OAr]$_2$. The bis(aryloxycarbonyl) complexes effect deoxygenation of one aryl oxide ligand under CO to give CO$_2$, ArC(O)OAr, and Pt(dppe)(CO)$_2$, **5**. In a competing pathway, orthometallation of the aryloxycarbonyl ligand and ArOH elimination occurs to yield unprecedented metallolactones, Pt(dppe)[C(O)OC$_6$H$_3$R]. The competing pathways may be controlled by CO pressure. The X-ray structure of the metallolactone Pt(dppe)[C(O)OC$_6$H$_4$], **6**, was determined. Trapping studies indicate that a benzyne intermediate is formed under phenoxide deoxygenation conditions. Complex **6** is thermally stable and photochemically reactive, but is not the source of benzyne. A mechanism involving a Pt(IV) benzyne intermediate is proposed for the platinum-mediated deoxygenation of phenols by CO.*

$\mathbf{T}$HE DEOXYGENATION OF PHENOLS is a conceptually simple but unusually difficult chemical transformation that is important in organic synthesis (*1–9*)

[1]Corresponding author

and commercial coal liquefaction (*10–17*). The phenolic C–O bond energy of 103 kcal mol^{-1} is as strong as a benzene C–H bond and over 10 kcal mol^{-1} stronger than the C–O bonds of methanol and ethanol.

$$D(\text{C-O}) = 103 \text{ kcal/mol}$$
$$D(\text{O-H}) = 85 \text{ kcal/mol}$$
$$D(\text{C-H}) \le 103 \text{ kcal/mol}$$
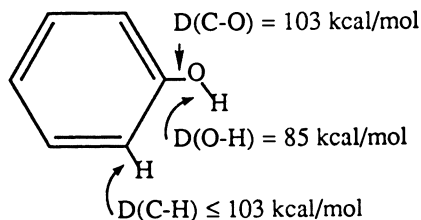
The rupture of aryl carbon–oxygen bonds is often a key step in the synthesis of a variety of natural products. Pterocarpans, for example, which are contained in the naturally occurring phytoalexins and display important biological activity, are synthesized via deoxygenation of a phenolic functional group (*18*).

Numerous attempts to discover general methods for the cleavage of aryl carbon–oxygen bonds include direct reduction (*4, 5*), reduction of phenolic ethers or esters (*19–23*), and conversion via thiophenols (*8*). The high-energy ultraviolet photodeoxygenation of phenol in the presence of $EtAlCl_2$ has also been reported (*9*). Most of these stoichiometric organic methods have limited applications. Many organic compounds simply decompose below the temperatures required for phenol reduction, and selectivities are generally low when other reducible functional groups are present.

Catalytic methods for the hydrodeoxygenation (HDO) of phenols involve supported transition metal oxides, such as $Mo-\gamma-Al_2O_3$, $Ni-Mo-\gamma-Al_2O_3$, $Co-Mo-\gamma-Al_2O_3$, $Fe_2O_3-SiO_2$ (*10–17*). Typical phenol hydrodeoxygenation conditions involve hydrogen pressures in excess of 100 atm and temperatures in excess of 200 °C. Arene ring hydrogenation generally competes with phenol deoxygenation under these conditions; the coproduct, water, impairs the activity of catalysts (*10–17*). This chapter reports initial studies aimed at achieving the catalytic deoxygenation of phenols via the unprecedented use of the $CO-CO_2$ couple (eq 1).

$$\langle \rangle\text{-OH (l)} + \text{CO (g)} \rightleftharpoons \langle \rangle\text{-H (l)} + CO_2 \text{ (g)} \qquad (1)$$

$$\Delta G^{\circ}_{298} = -20.7 \text{ kcal/mol}$$
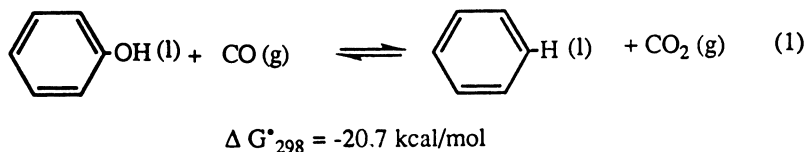
Experimental Section

Materials and Physical Measurements. All manipulations were performed under an atmosphere of dry N_2. Solvents were reagent grade and were distilled

from the appropriate drying agents. All solvents were deoxygenated prior to use. All high-pressure reactions were carried out in pressure-valve NMR tubes (Wilmad Glass Co.). Carbon monoxide was research purity, and hydrogen was extra dry (Matheson Gas Company). The complex $PtCl_2(dppe)$ [dppe is bis(diphenylphosphino)ethane] was prepared by a modified published procedure (24).

Infrared spectra were recorded on a Fourier transform infrared (FTIR) spectrometer (Perkin-Elmer 1710) equipped with a Perkin-Elmer 3600 data station. ^1H NMR spectra were recorded on a Gemini 200 spectrophotometer and $^{31}P\{^1H\}$ NMR spectra on a Varian XL-200 spectrophotometer. ^1H and ^{31}P NMR chemical shifts were referenced to internal tetramethylsilane (TMS) and external 85% H_3PO_4, respectively.

Gas chromatograms were recorded on a Carle analytical gas chromatograph. High-pressure liquid chromatography (HPLC) experiments were performed on a Varian 5000 liquid chromatograph equipped with a Varian 2050 variable λ detector and a Perkin-Elmer LCI-100 laboratory computing integrator. The column used was Econosphere C_{18}, 5 μm, 4.6 mm $\times$ 25 cm, manufactured by Alltech/Applied Science. The mobile phase was H_2O (A) and CH_3CN (B), with ratios programmed: 40–90% B in 12 min, 90–100% B in 8 min, hold at 100% B for 5 min, 100–40% B in 10 min, hold at 40% B for 5 min. The flow rate was 1.5 mL min^{-1}, and products were detected at 254 nm.

Preparation of NaOC$_3$H$_5$.   Sodium allyl oxide was prepared by mixing 5 mL of allyl alcohol with 0.25 g of sodium hydride in 25 mL of benzene for 18 h at room temperature under N_2. Care was taken to adequately vent the evolved H_2. The reaction was concentrated in vacuo, and the product was precipitated as a white solid with hexanes. The mixture was then filtered. ^1H NMR (δ): 5.75 (m, 1 H), 5.05 (d, 1 H), 4.95 (d, 1 H), 3.85 (d, 2 H) ppm.

Deoxygenation of Pt(OC$_3$H$_5$)$_2$(dppe) (1) and Preparation of [Pt(η^3-CH$_2$CHCH$_2$)(dppe)](PF$_6$) (2).   Sodium allyl oxide (0.0325 g, 0.406 mmol) and PtCl$_2$(dppe) (0.09 g, 0.135 mmol) were combined under N_2 in a 25-mL Schlenk flask at -78 °C in 7 mL of allyl alcohol and 10 mL of benzene. The reaction slurry was stirred at this temperature for 3 h and then warmed to 0 °C. The pale yellow solution was then cannula-filtered through a fine frit into a 50-mL Schlenk flask. This reaction flask was placed under 1 atm of dry CO. The reaction flask was stirred at room temperature for 15 min and then heated to 55 °C. The reaction was followed by gas chromatography to monitor the evolution of CO_2. After 3 days the evolution of CO_2 had ceased. Approximately 1 equiv of CO_2 had been formed in the reaction process. The resulting reaction mixture was again cannula-filtered through a fine frit into a 50-mL Schlenk flask. The solvent was removed in vacuo, and the resulting yellow oily solid was taken up in a solution of 8-mL of MeCN containing NaPF$_6$ (0.40 mmol). The solvent was removed in vacuo, and the resulting pale yellow solid was dissolved in CH_2Cl_2. This solution was filtered. The filtrate was concentrated, and the product was precipitated by the addition of diethyl ether. A pale yellow solid resulted (0.04 g, 40%). $^{31}P\{^1H\}$ NMR (CD_2Cl_2) (δ): 47.97 [J (P–Pt), 3711 Hz], 144.1 (m, PF$_6^-$); ^1H NMR (CD_2Cl_2) (δ): 7.6 (m, 20 H, dppe-C_6H_5), 5.2 (m, 1 H, CH$_2$CHCH$_2$), 3.0 (m, 4 H, CH$_2$CHCH$_2$), 2.6 (m, 4 H, PCH$_2$CH$_2$P). These spectroscopic data agree well with those reported in the literature for [Pt(η^3-CH$_2$CHCH$_2$)(dppe)](PF$_6$) (25).

Preparation of NaOAr.   To a suspension of NaH (1.000 g, 41.67 mmol) in tetrahydrofuran (THF) was added a solution of PhOH (3.9167 g, 41.67 mmol)

in THF. The reaction solution was stirred for 1 h before being filtered. Then the filtrate was concentrated under reduced pressure, and hexane was added to produce white solid NaOPh in 90% yield. Other sodium aryl oxides were prepared by the same procedure.

Preparation of Pt(OPh)$_2$(dppe) (3). To a suspension of PtCl$_2$(dppe) (0.2000 g, 0.3 mmol) in THF was added a solution of NaOPh (0.0733 g, 0.63 mmol, 5% excess) in THF. After 2 h the solution was filtered, the filtrate was concentrated, and hexane was added to produce a pale yellow solid. The solid was isolated and washed with Et$_2$O to obtain Pt(OPh)$_2$(dppe) (3) in 86% yield. ^{31}P{^{1}H} NMR (THF–C$_6$D$_6$): δ 26.45 [J (P–Pt), 3549 Hz].

Other Pt(OAr)$_2$(dppe) complexes (Ar is p-C$_6$H$_4$Cl, p-C$_6$H$_4$SMe, p-C$_6$H$_4$Me, p-C$_6$H$_4$OMe, or p-C$_6$H$_4$NMe$_2$) were prepared by the same method as 3. The complexes and their ^{31}P{^{1}H} NMR (THF–C$_6$D$_6$) chemical shifts (δ) are as follows:

- Pt(O-p-C$_6$H$_4$Cl)$_2$(dppe): 27.42 [J (P–Pt), 3557 Hz].
- Pt(O-p-C$_6$H$_4$SMe)$_2$(dppe): 27.22 [J (P–Pt), 3565 Hz].
- Pt(O-p-C$_6$H$_4$Me)$_2$(dppe): 25.74 [J (P–Pt), 3540 Hz].
- Pt(O-p-C$_6$H$_4$NMe$_2$)$_2$(dppe): 25.85 [J (P–Pt), 3531 Hz].

Reaction of Pt(OPh)$_2$(dppe) (3) with CO. CO (100 psi) was introduced into a pressure-valve NMR tube containing a solution of Pt(OPh)$_2$(dppe) (3, 0.015 g) in a mixture of the solvents THF and C$_6$D$_6$ (volume 3:1). The solution was then heated to 75 °C, and the reaction was monitored by ^{31}P{^{1}H} NMR spectroscopy. The formation of Pt[C(O)OPh]$_2$(dppe), 4, was observed first. Then as the reaction proceeded, the formation of Pt(dppe)(CO)$_2$, 5, and Pt(COOC$_6$H$_4$)(dppe), 6, was observed. When ^{31}P{^{1}H} NMR spectra indicated the complete consumption of Pt(OPh)$_2$(dppe) and Pt[C(O)OPh]$_2$(dppe), the reaction was stopped. The reaction solution was transferred to a flask and the solvents were removed under reduced pressure. The resulting residue was extracted with Et$_2$O four times, and all the Et$_2$O extract was combined for HPLC experiments. HPLC indicated the formation of the deoxygenation product PhCOOPh together with PhOH. The formation of PhCOOPh and PhOH was also confirmed by FTIR spectroscopy. The carbon dioxide eliminated in the reaction was detected by gas chromatography.

- Pt[C(O)OPh]$_2$(dppe) (4): ^{31}P{^{1}H} NMR (THF–C$_6$D$_6$): δ 38.73 [J (P–Pt), 1918 Hz].
- Pt(CO)$_2$(dppe) (5): ^{31}P{^{1}H} NMR (THF–C$_6$D$_6$): δ 24.03 [J (P–Pt), 3124 Hz].
- IR (THF): ν(CO) 1990(s), 1948(s) cm^{-1}.

Synthesis of Pt(COOC$_6$H$_4$)(dppe) (6). Complex 3 (0.05 g) was employed in the reaction with CO. When ^{31}P{^{1}H} NMR spectra indicated the complete consumption of 3 and 4, the reaction was stopped. The reaction solution was transferred to a flask, and the solvents were removed. The residue was washed with C$_6$D$_6$ (0.2 mL) three or four times, then with ether to afford Pt(COOC$_6$H$_4$)(dppe), 6, as an off-white solid. ^{31}P{^{1}H} NMR (THF–C$_6$D$_6$): δ 46.06 (P$_A$), 44.20 (P$_B$) [AB, J (AB), 9.3 Hz; J (Pt–P$_A$), 2083 Hz; J (Pt–P$_B$), 2044 Hz]. ^{1}H NMR (CD$_2$Cl$_2$): δ 8.4–6.35 (m, 24 H), 2.37 (s, 4 H). IR (KBr) ν(CO): 1680 cm^{-1}, IR(THF) ν(CO): 1698 cm^{-1}. Complex 6 was also characterized by X-ray diffraction.

Benzyne Trapping with Furan.   The reaction of **3** with 100 psi of CO was carried out in a mixture of the solvents furan and C_6D_6 (volume 3:1), as described. The organic products were analyzed by HPLC as PhOH, PhCOOPh, and 1-naphthol.

Reaction of 6 with CO and H_2.   A solution of **6** in THF–C_6D_6 (volume 3:1) was placed under 100 psi of CO. The solution was heated at 75 °C for 3 weeks. $^{31}P\{^1H\}$ NMR spectroscopy indicated no reaction.
A solution of **6** in THF–C_6D_6 (volume 3:1) was placed under 100 psi of H_2. The solution was heated at 75 °C for 9 days. $^{31}P\{^1H\}$ NMR spectroscopy indicated no reaction.

Photolysis of 6.   A solution of **6** in THF was photolyzed in a 1-cm UV cell and irradiated (λ >290 nm) with an Oriel 1000 W Xe–Hg lamp. A bright yellow compound $Pt(OC_6H_4CO)(dppe)$ was formed exclusively. $^{31}P\{^1H\}$ NMR (THF): δ 38.83 (P_A), 30.58 (P_B) [AB, J (AB), 9.8 Hz; J (Pt–P_A), 1454 Hz; J (Pt–PB), 4204 Hz]. IR (THF) ν(CO): 1625 cm^{-1}. These data are in agreement with literature values for the complex $Pt(OC_6H_4CO)(dppe)$ (*20*).

Crystal Data Collection and Reduction.   Suitable crystals of **6** were obtained by diffusion of Et_2O into CH_2Cl_2 solution. Complex **6** crystallized in space group $P\,2_1/n$ (No. 14) with lattice constants $a = 12.155(2)$ Å, $b = 13.527(2)$ Å, $c = 17.417(2)$ Å, $\beta = 99.50(1)°$, $V = 2824(1)$ Å^3, $Z = 4$, $d_{calcd} = 1.678$ g cm^{-3} for the formula $PtP_2O_2C_{33}H_{28}$. Crystal dimensions were $0.40 \times 0.24 \times 0.15$ mm. Intensity data were collected at 20 °C by the θ–2θ scan method in the range $4° \leq 2\theta \leq 45°$ on Enraf-Nonius CAD4 diffractometer. A total of 3875 unique data were collected over the following h, k, and l limits: –13 to 12, 0 to 14, and 0 to 18, respectively. The structure was solved by MULTAN–least squares–Fourier methods and was refined to R and R_w values of 0.033 and 0.038 for 343 variables and 2373 observations with integrated intensities (I) $> 3.0\sigma(I)$. All programs were from the Enraf-Nonius SDP package.

Discussion

Insertions of CO into the metal–oxygen bonds of several late transition metal alkoxide and aryl oxide complexes have been reported (*26–34*). The resulting alkoxycarbonyl and aryloxycarbonyl complexes generally appear to be quite stable, with the exception of an allyloxycarbonylcobalt complex, $Co[C(O)OC_3H_5](CO)_4$, which undergoes thermal decarboxylation to produce $Co(\eta^3\text{-}C_3H_5)(CO)_3$ (*26*).

Deoxygenation.   We observed similar deoxygenations of the allyloxy groups of the complex $Pt(OC_3H_5)_2(dppe)$, **1** (*35*). Treatment of a benzene solution of **1** with CO affords the known η^3-allyl complex [Pt(η^3-C_3H_5)(dppe)]$^+$ (**2**), CO_2, and free allyl alcohol according to eq 2.
Treatment of **1** with CO and D_2O led to deoxygenation of 1 equiv of allyl alcohol and elimination of the other. Under these conditions, in which excess CO is present, reduction of Pt(II) to $Pt(CO)_2(dppe)$ also occurs (eq 3).

$$(2)$$

$$(3)$$
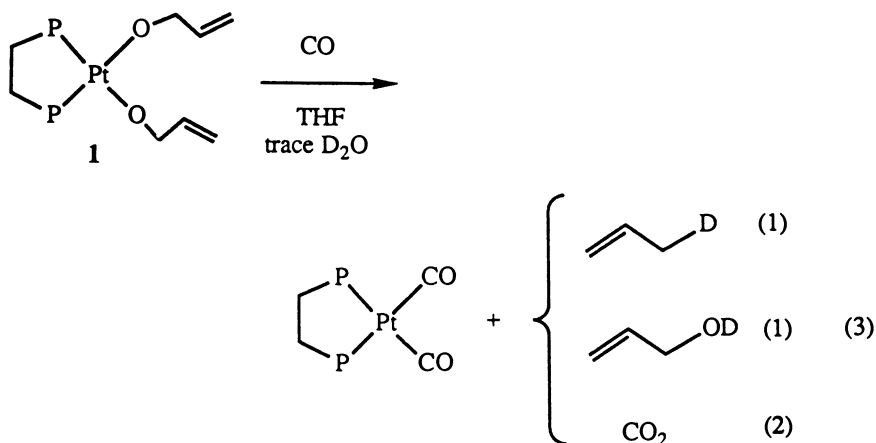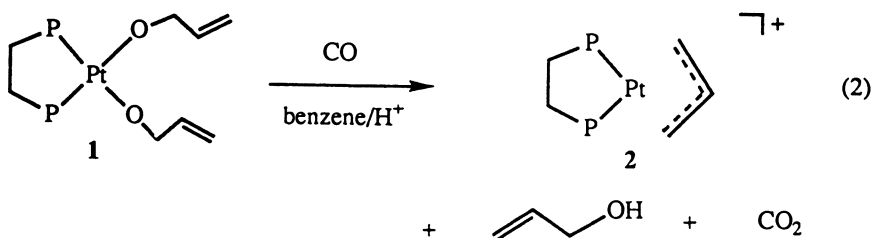
Our results for the complex $Pt(OC_3H_5)_2(dppe)$, **1**, together with the earlier work of Tasi and Palyi (**26**) on $Co[C(O)OC_3H_5](CO)_4$ suggest that allyloxycarbonyl complexes formed by the insertion of CO into metal–oxygen bonds of metal allyloxy complexes are capable of undergoing β-allyl migration–decarboxylation (eq 4).

$$(4)$$
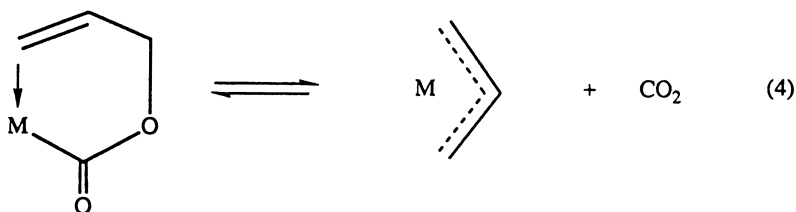
At this juncture we decided to explore the possibility of extending the use of CO as the oxygen-atom acceptor for the deoxygenation of phenols. However, the simple migration of an aryl group of an aryloxycarbonyl ligand to the metal center is not a particularly promising transformation. Only complexes of the late transition metals are expected to be strong candidates as catalysts for the deoxygenation of phenols by CO because only these metals form metal–oxygen bonds that are sufficiently weak for CO insertion

to occur. In the d^8 platinum group metal complexes, the vacant p_z orbitals contribute to strong electrophilicity; the phenolic hydroxyl group activates the *ortho*-positions toward electrophilic substitution.

Aryloxycarbonyls.   Orthometallation of aryloxycarbonyls of platinum group metal complexes appears likely. The orthometallation of aryloxycarbonyls is not necessarily a dead end, however. The resulting metallolactones may, under appropriate circumstances, decarboxylate to produce a benzyne hydride intermediate that ultimately would produce the same phenyl complex one would expect from simple phenyl migration (Scheme I).
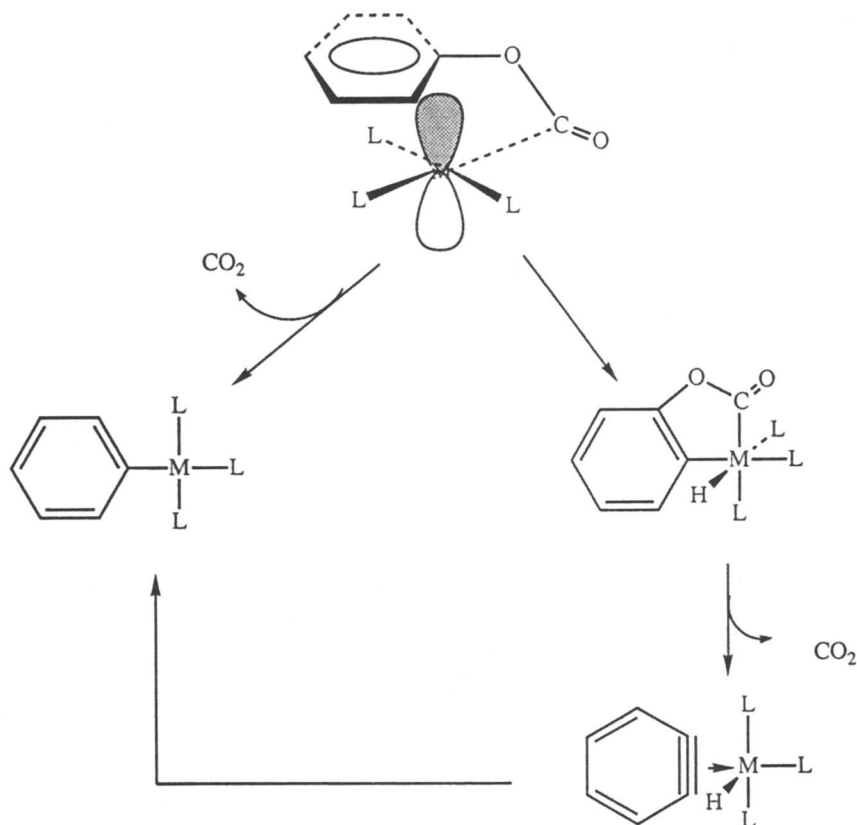
Scheme I.

Treatment of $PtCl_2$(dppe) with NaOPh produces $Pt(OPh)_2$(dppe), **3**. Complex **3** is indefinitely thermally stable in solution at 75 °C, in contrast to the corresponding alkoxide complex $Pt(OMe)_2$(dppe), which decomposes by β-H elimination (*36*). Complex **3** inserts 2 equiv of CO to form a new bis(aryloxycarbonyl) complex, $Pt[C(O)OPh]_2$(dppe), **4** (eq 5).
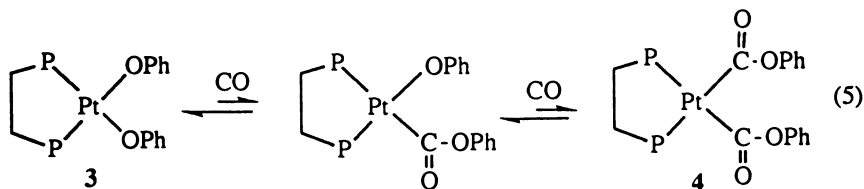
The CO insertion requires moderately high temperatures and pressures. At 25 °C and 100 psi, only starting complex 3 is evident after 1 h by $^{31}P\{^{1}H\}$ NMR spectroscopy. After the sample is heated in a high-pressure NMR tube to 75 °C for 1 h, some formation of 4 is observed. The fraction of 4 formed increases with initial CO pressures. The rapid reverse reaction prevented us from isolating 4. However, the identity of 4 is established by $^{31}P\{^{1}H\}$ NMR spectra, particularly by the excellent agreement between the structurally sensitive phosphorus–platinum coupling constants, J (Pt–P), for 4 and Pt[C(O)OMe]$_2$(dppe) (31). Complex 4 is significantly less stable thermodynamically than the alkoxide complex Pt[C(O)OMe]$_2$(dppe), which is also formed reversibly but at much lower temperatures and CO pressures (31). Complex 4 also appears to be significantly less stable than several cobalt (26) and iridium (27) aryloxycarbonyl complexes. The formation of bis(aryloxycarbonyls) related to 4 is strongly dependent on the basicity of the starting phenoxide. The bis(aryl oxide) complexes Pt(OAr)$_2$(dppe) (Ar is p-ClC$_6$H$_4$, p-MeSC$_6$H$_4$, p-MeC$_6$H$_4$, and p-Me$_2$NC$_6$H$_4$) all insert CO, similar to 3 + CO → 4. The extent of CO insertion to form Pt[C(O)OAr]$_2$(dppe) at fixed temperatures and CO pressures follows the order:
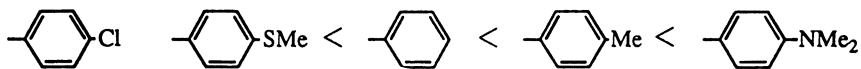
Continued reaction of 3 with CO (100 psi) proceeds with the ultimate formation of two platinum-containing products, 5 and 6.
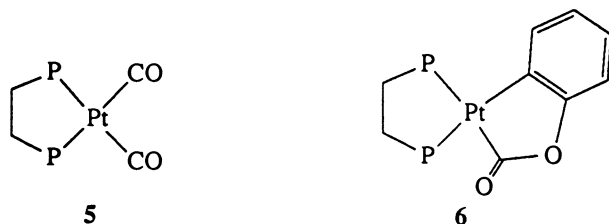
Benzyne Intermediate. The organic products are CO$_2$, phenyl benzoate, and phenol. The appearance of phenyl benzoate and CO$_2$ together implies that a phenoxy group has been deoxygenated by CO. A key finding is that a benzyne intermediate is required for phenoxide deoxygenation by

3. When the reaction of 3 with CO is carried out in furan, the organic products are 1-naphthol, phenol, and significantly reduced quantities of phenyl benzoate. The 1-naphthol is a known isomerization product of 1,4-epoxy-1,4-dihydronaphthalene, the furan adduct of benzyne (37). Biphenylene and triphenylene were not observed. These results are consistent with the formation of a benzyne intermediate, but not with the formation of free benzyne. Initially our search for a source of benzyne centered on the potential decarboxylation of the metallolactone complex, 6.

Complex 6 has been isolated from reaction mixtures and characterized by X-ray crystallography (38). An ORTEP diagram of complex 6 is presented in Figure 1, together with selected bond distances and angles. The molecule contains the first example of a five-membered *ortho*-phenyl metallolactone (7), apparently formed by orthometallation of a phenoxycarbonyl group. Complex 6 may be viewed as the product of "abnormal" insertion of CO_2
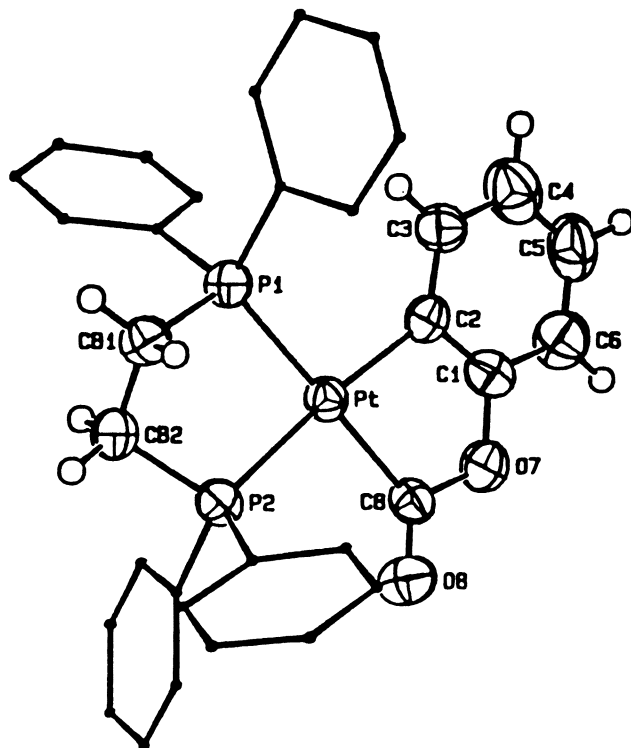
Figure 1. ORTEP drawing of 6. Selected bond lengths in angstroms (and angles in degrees): Pt–P-1, 2.305 (3); Pt–P-2, 2.290 (3); Pt–C-2, 2.06 (1); Pt–C-8, 2.06 (1); C-1–C-2, 1.38 (2); C-1–O-7, 1.37 (1); O-7–C-8, 1.41 (1); O-8–C-8, 1.16 (1); P-1–Pt–P-2, 84.9 (1); P-1–Pt–C-2, 100.3 (3); P-2–Pt–C-8, 93.3; C-2–Pt–C-8, 81.5 (4); C-2–Cl–O-7, 121 (1); C-1–O-7–C-8, 115.0 (9); and Pt–C-8–O-7, 112.2.
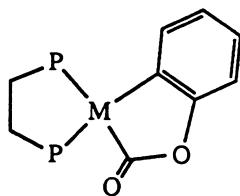
Metallolactone

7
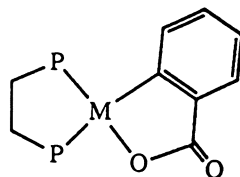
Metallobenzoate

8

into a putative platinum benzyne complex Pt(C$_6$H$_4$)(dppe). It differs in connectivity from the CO$_2$ adducts of transition metal benzyne complexes, which generally exist as metallocyclobenzoates **8** (*33, 39*).

However, the implication that complex **6** is an intermediate on the pathway to a benzyne intermediate has been eliminated on the basis of the following facts:

- Complex **6** is indefinitely stable at 75 °C in the presence of excess phenol and CO (100 psi);

- Complex **6** is inert in the presence of H$_2$ (100 psi).

Complex **6** is photosensitive, but not with respect to decarboxylation and the formation of a benzyne intermediate. UV irradiation (λ <300 nm) of tetrahydrofuran (THF) solution of **6** leads to the efficient 1,2 migration of CO according to eq 6 to produce the known complex Pt[o-C(O)C$_6$H$_4$O](dppe) (*40*).
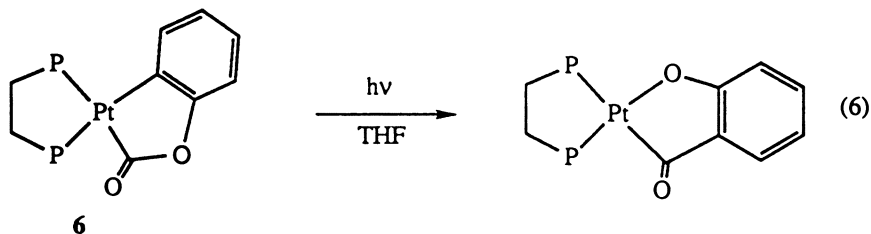
$$\text{(6)}$$

6

Thus none of the chemistry or photochemistry of **6** is consistent with formation of a benzyne intermediate. However, a benzyne intermediate does appear to be involved in the formation of phenyl benzoate, as suggested by our trapping studies with furan.

Our observations concerning the deoxygenation of phenoxide from **3** by CO can be summarized as follows:

- Insertions of CO into both Pt–OPh bonds of **3** are reversible processes.

- The product of phenoxide deoxygenation is phenyl benzoate.

- Benzyne trapping experiments suggest that a benzyne complex is an intermediate required for phenyl benzoate formation; however, the metallolactone product **6** is not the source of benzyne or phenyl benzoate.

- The relative yields of metallolactone **6** versus phenyl benzoate and **5** can be controlled by CO pressure. Low CO pressures favor **6**. High pressures favor **5** and phenyl benzoate.

- We also find that Pt(Ph)$_2$(dppe) is inert with respect to insertion of both CO and CO$_2$ under the reaction conditions employed (75 °C, 100 psi of CO; 75 °C, 35 psi of CO$_2$) for formation of phenyl benzoate.

Metallolactone Intermediate.   We therefore propose that CO$_2$ elimination and benzyne formation occur from a Pt(IV) metallolactone intermediate. The metallolactone intermediate on the pathway to phenol deoxygenation is produced in the high CO pressure regime where the bis(aryloxycarbonyl), **4**, is the predominant species in solution. Our proposed mechanism for the formation of diaryl esters from aryloxy groups and CO is presented in Scheme II.

The intermediate Pt(IV) metallolactone appears to be essential for the deoxygenation process. The stability of this intermediate with respect to reductive elimination of aryl formate enables deoxygenation. We suggest that this process occurs by subsequent decarboxylation, benzyne intermediate formation, and the formation of an aryl aryloxycarbonyl intermediate that eliminates the observed organic product: C$_6$H$_5$C(O)OC$_6$H$_5$.

The elimination of diaryl esters in our proposed mechanism requires comment in light of the lack of literature precedents for this reaction. Bennett and Rokicki (*30*) and Bryndza (*32*) reported that insertion of CO into the Pt–O bond occurs in preference to insertion into the Pt–C bond of Pt(dppe)(C$_6$H$_9$)(OMe) (*30*) and Pt(dppe)Me(OMe) (*32*) to give methoxycarbonylplatinum(II) complexes Pt(dppe)R(COOMe). These complexes, however, show no tendency to undergo reductive elimination of the corresponding esters. The observation is not contradictory to the mechanism proposed here because these workers did not carry out the reductive elimination study of Pt(dppe)R(COOMe) at high temperature, with high CO pressure for an
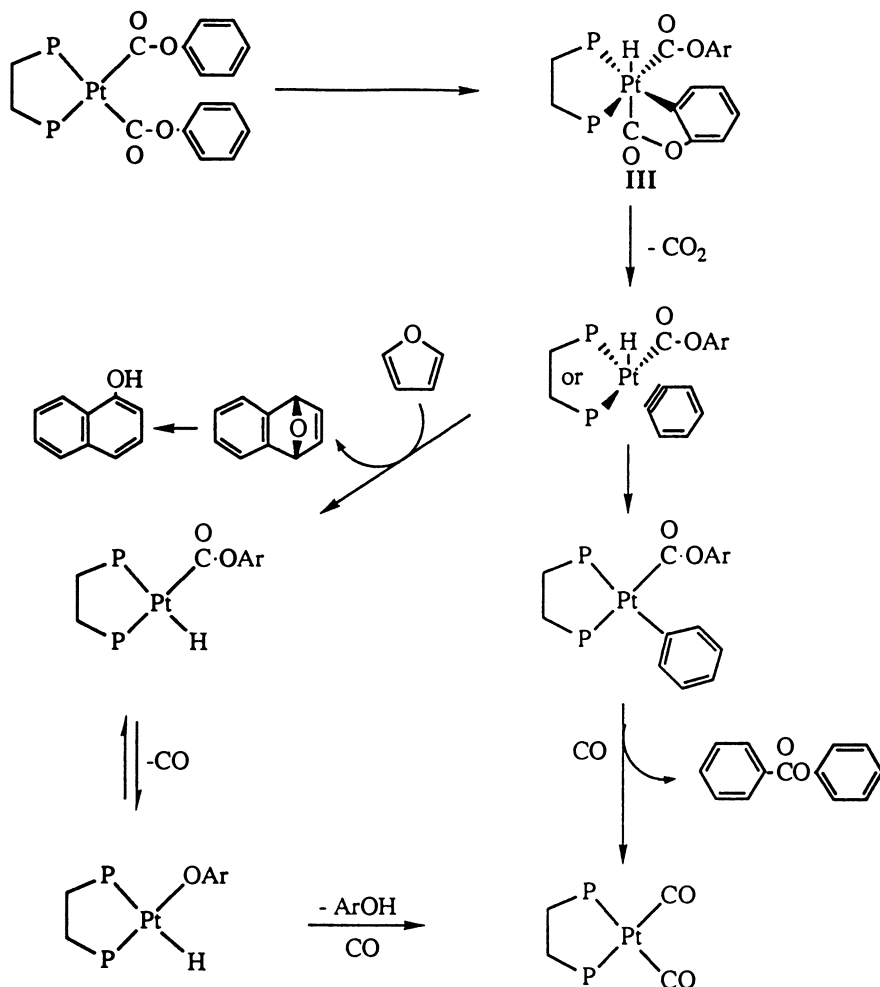
Scheme II.

extended period of time. Reductive elimination of carboxylate esters at Ni(II) and Pd(II) centers was reported by Kim et al. (28) and Bennett and Schwemlein (33). Reductive elimination of diaryl esters in the Pt(dppe) system for phenol deoxygenation by CO is reasonable.

Conclusions

The deoxygenation of phenols by CO is a viable process. Metallolactones, created via late transition metal orthometallation of aryloxycarbonyl ligands, may provide the essential low-energy pathway for elimination of CO_2, for-

mation of a benzyne hydride intermediate, and thereby formation of the phenyl group. In the present Pt(OAr)$_2$(dppe) system the phenyl group produced by phenol deoxygenation is eliminated with an aryloxycarbonyl ligand to yield phenyl benzoates. For this reason we are focusing our ongoing efforts on systems that contain one aryl oxide, and thus have no possibility of reductive elimination of the phenyl group before the elimination of free arenes.

Acknowledgments

References

1. Peterson, G. A.; Kunng, F.; McCallum, J. S.; Wulff, W. D. *Tetrahedron Lett.* **1987**, *28*, 1381.
2. Linders, J. T. M.; Lie, T. S.; Maat, L. *Bull. Soc. Chim. Belg.* **1988**, *97*, 463.
3. Lu, X.; Zhu, J. *Synthesis* **1987**, 726.
4. Gross, M. E.; Lankelma, H. P. *J. Am. Chem. Soc.* **1951**, *73*, 3439.
5. Moulton, W. N.; Wade, C. G. *J. Org. Chem.* **1961**, *26*, 2528.
6. Koelsch, C. F.; Lindquist, R. M. *J. Org. Chem.* **1956**, *21*, 657.
7. Hussey, B. J.; Johnstone, R. A. W.; Entwistle, I. D. *Tetrahedron* **1982**, *38*, 3775 and references therein.
8. Newman, M. S.; Karnes, H. A. *J. Org. Chem.* **1966**, *31*, 3980.
9. Furukawa, J.; Omura, K. *Tetrahedron Lett.* **1973**, 2631.
10. *Coal Conversion Technology*; Pelofsky, A. H., Ed.; ACS Symposium Series 110; American Chemical Society: Washington, DC, 1979.
11. *Coal Liquefaction Fundamentals*; Whitehurst, D. D., Ed.; ACS Symposium Series 139; American Chemical Society: Washington, DC, 1980.
12. *Upgrading Coal Liquids*; Sullivan, R. F., Ed.; ACS Symposium Series 156; American Chemical Society: Washington, DC, 1981.
13. Weigold, H. *Fuel* **1982**, *61*, 1021.
14. Vogelzang, M. W.; Li, C. L.; Schuit, G. C. A.; Gates, B. C.; Petrakis, L. *J. Catal.* **1983**, *84*, 170.
15. (a) Li, C. L.; Xu, Z. R.; Cao, Z. A.; Gates, B. C.; Petrakis, L. *AIChE J.* **1985**, *31*, 170; (b) Shabtai, J.; Nag, N. K.; Massoth, F. E. *J. Catal.* **1987**, *104*, 413.
16. Furimsky, E.; Mikhlin, J. A.; Jones, D. Q.; Adley, T.; Baikowitz, H. *Can. J. Chem. Eng.* **1986**, *64*, 982.
17. Hunska, M. K. *Polyhedron* **1986**, *5*, 233.
18. Engler, T. A.; Combrink, K. D.; Reddy, J. P. *J. Chem. Soc., Chem. Commun.* **1989**, 454.
19. Pelletier, S. W.; Locke, D. M. *J. Org. Chem.* **1958**, *23*, 131.
20. Johnstone, R. A. W.; McLean, W. N. *Tetrahedron Lett.* **1988**, *29*, 5553.
21. Echavarren, A. M.; Stille, J. K. *J. Am. Chem. Soc.* **1987**, *109*, 5478.
22. Chen, Q.; Yang, Z. *Tetrahedron Lett.* **1986**, *27*, 1171.
23. Cacchi, S.; Ciattini, P. G.; Morera, E.; Ortar, G. *Tetrahedron Lett.* **1986**, *27*, 5541.
24. Anderson, G. K.; Lumetta, G. J. *Inorg. Chem.* **1987**, *26*, 1518.

25. Boag, N. M.; Green, M.; Spencer, J. L.; Stone, F. G. A. *J. Chem. Soc., Dalton Trans.* **1980**, 1208.
26. Tasi, M.; Palyi, G. *Organometallics* **1985**, *4*, 1523.
27. Rees, W. M.; Churchill, M. R.; Fettinger, J. C.; Atwood, J. D. *Organometallics* **1985**, *4*, 2179.
28. Kim, Y. J.; Osakada, K.; Sugita, K.; Yamamoto, T.; Yamamoto, A. *Organometallics* **1988**, *7*, 2182 and references therein.
29. Michelin, R. A.; Napoli, M.; Ros, R. *J. Organomet. Chem.* **1979**, *175*, 239.
30. Bennett, M. A.; Rokicki, A. *J. Organomet. Chem.* **1983**, *244*, C31.
31. Bryndza, H. E.; Kretchmar, S. A.; Tulip, T. H. *J. Chem. Soc., Chem. Commun.* **1985**, 977.
32. Bryndza, H. E. *Organometallics* **1985**, *4*, 1686.
33. Bennett, M. A.; Schwemlein, H. P. *Angew. Chem., Int. Ed. Engl.* **1989**, *28*, 1296.
34. Alcock, N. W.; Platt, A. W. G.; Pringle, P. G. *Inorg. Chim. Acta* **1987**, *128*, 215.
35. Banta, G. D. M.S. Thesis, Purdue University, 1989.
36. Bryndza, H. E.; Calabrese, J. C.; Marsi, M.; Roe, D. C.; Tam, W.; Bercaw, J. E. *J. Am. Chem. Soc.* **1986**, *108*, 4805.
37. Gilchrist, T. L.; Graveling, F. J.; Rees, C. W. *J. Chem. Soc. C* **1971**, 977.
38. Ni, J.; Fanwick, P. E.; Kubiak, C. P. *J. Am. Chem. Soc.* **1992**, *114*, in press.
39. Kolomnikov, I. S.; Lobeeva, T. S.; Gorbachevskaya, V. V.; Aleksandrov, G. G.; Struckhov, Y. T.; Volpin, M. E. *J. Chem. Soc., Chem. Commun.* **1971**, 972.
40. Motschi, H.; Pregosin, P. S.; Ruegger, H. *J. Organomet. Chem.* **1980**, *193*, 397.

High-Velocity Palladium Catalysis

Timothy L. Friebe[1], John R. Johnson[1], Damian J. Krysan[1], Peter B. Mackenzie[1,3], and Michal Sabat[2]

[1]Department of Chemistry, Northwestern University, Evanston, IL 60208
[2]Department of Chemistry, University of Virginia, Charlottesville, VA 22903

Enal-derived 2-ethenyl-1,3-dioxolanones undergo exceptionally fast palladium-catalyzed reactions with sodium tetraphenylborate. Turnover rates as high as 660 min^{-1} have been observed in the presence of suitable palladium(II) and palladium(0) catalyst precursors, including [(μ-chloro)(1,2,3-η^3-2-propen-1-yl)palladium(II)]$_2$, bis-(acetonitrilo)dichloropalladium(II), and tris(dibenzylideneacetone)-dipalladium(0). An allylpalladium mechanism is proposed on the basis of model studies of the stoichiometric and catalytic reaction chemistry of isolable allylnickel and allylpalladium analogs of the proposed reaction intermediates. Possible explanations for the high reaction velocities are discussed.

WHAT ARE REASONABLE UPPER LIMITS for the rates of oxidative addition, transmetallation, and reductive elimination in palladium-catalyzed cross-coupling reactions? We had occasion to address this question recently as part of our studies of the palladium-catalyzed chemistry of optically active 2-alkenyl-1,3-dioxolanones (1–4). The investigation led to the observation of an apparent case of remarkably fast catalysis, the mechanism and implications of which are the subject of this chapter.

The original impetus for our research in this area derived from our interest in the synthetically important problem of enantioselective conjugate addition (5–7). Our approach, developed in more detail elsewhere (3, 4), was to explore optically active 2-alkenyl-1,3-dioxolanones as enal equivalents for palladium-catalyzed allylation-type reactions (Scheme I). We hoped to achieve the equivalent of conjugate addition through a sequence of acetalization, palladium-catalyzed S$_N$2' substitution, and aqueous acid hydrolysis of the resultant alkyl enol ether products.

[3]Corresponding author

Scheme 1.
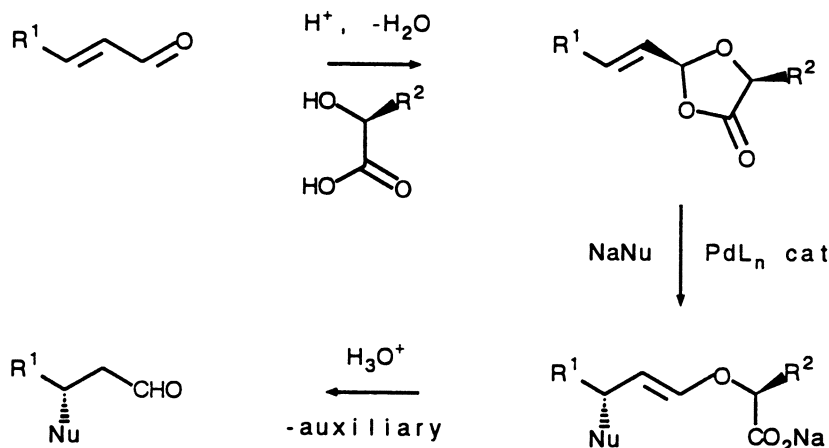
Reaction of *cis*-2-propenyl derivative **1a** with sodium tetraphenylborate in the presence of bis[(μ-chloro)(1,2,3-η³-2-propen-1-yl)palladium(II)], **2a**, as a catalyst precursor gave a 78% yield of (*E*)-enol ether **3a**, isolated as the sodium carboxylate salt (eq 1) (3, 4).

$$(1)$$
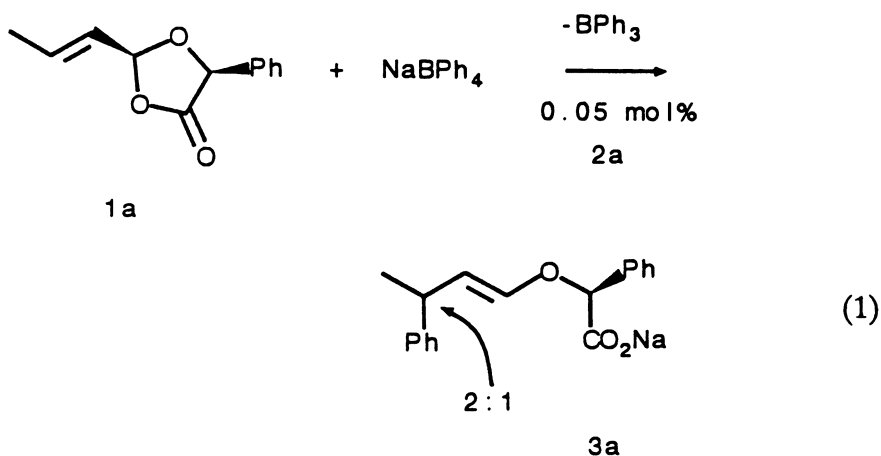
Although a success in terms of yield, regioselectivity, and double bond stereoselectivity, this reaction was a failure as a diastereoselective method. The ratio of chiralities at the newly formed chiral center was only 2:1, corresponding to a 36% enantiomeric excess (ee) after hydrolysis. Given that analogous palladium-catalyzed allyl acetate reactions are generally highly stereospecific (8), the surprising overall nonstereospecificity of this reaction prompted us to examine the underlying reaction chemistry in more detail.

To simplify analysis of the reaction products, our studies focused on the 2-ethenyl derivatives **1b–1e**, which do not give rise to a new chiral center upon conjugate addition. Similar overall chemistry was observed (eq 2, Table I). However, it quickly became apparent that we were observing remarkably rapid turnover rates. Addition of 0.5 mol % of **2a** on a 10-g scale reaction resulted in the ejection of the contents of the flask as the heat of reaction caused the dichloromethane reaction solvent to reflux violently (3, 4).

(2)
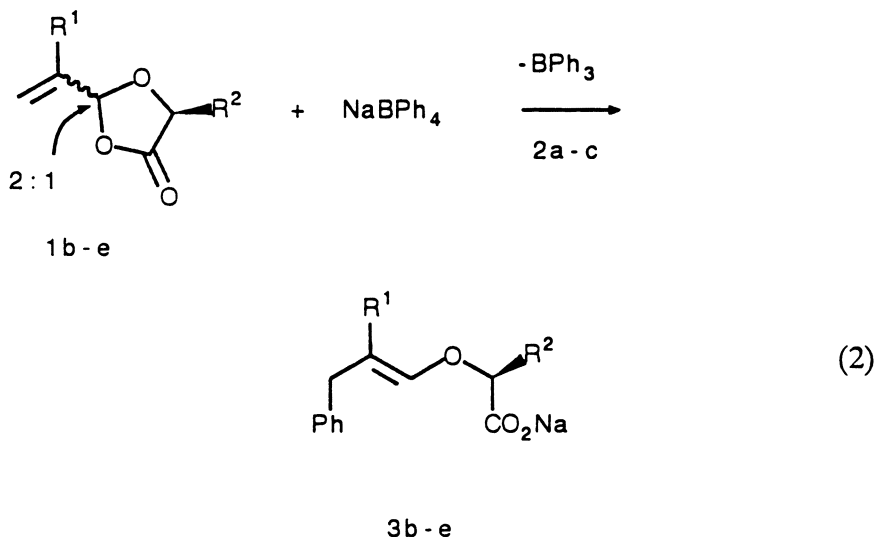
Subsequent study showed that as little as 0.001 mol % of bis(aceto-nitrile)palladium dichloride, **2b**, was sufficient to give complete reaction in 2.5 h at 65 °C in chloroform. Indeed, substrate-to-catalyst ratios as high as

Table I. Palladium-Catalyzed Conjugate Addition Reactions

Entry	Compound	R^1	R^2	Catalyst[a]	Product	% Yield[b]
1	**1b**	H	Ph	**2a** (0.05)	**3b**	66
2	**1b**	H	Ph	**2b** (0.001)[c]	**3b**	70[d]
3	**1b**	H	Ph	**2c** (0.4)[e]	**3b**	64[d]
4	**1c**	H	Cy[f]	**2a** (0.1)	**3c**	48
5	**1d**	Me	Ph	**2a** (0.05)	**3d**	54
6	**1e**	H	Me	**2a** (0.25)	**3e**	45

NOTE: All reactions were conducted in CH_2Cl_2 unless otherwise noted. Yields and reaction times are unoptimized. The reaction temperature was 25 °C, except for Entry 2 when it was 65 °C. The reaction time was 14 h, except for Entry 2 when it was 2.5 h.
[a]Catalyst precursor with mol % in parentheses.
[b]Isolated purified yield (unless otherwise noted).
[c]Reaction was conducted in $CHCl_3$.
[d]Crude yield.
[e]Reaction was conducted in CH_3CN.
[f]Cy is cyclohexyl.

500,000:1 were successfully employed. This corresponds to 10^2–10^4 less catalyst than is required for the vast majority of palladium-catalyzed reactions.

In light of the far-reaching importance of palladium catalysis in organic synthesis, this observation excited our interest and prompted us to pose some mechanistically related questions.

Experimental Section

A typical procedure for sodium tetraphenylborate reactions is as follows. A three-necked flask equipped with a condenser and a nitrogen inlet was charged with (2R,S,5S)-2-ethenyl-5-phenyl-1,3-dioxolan-4-one (1.25 g, 6.57 mmol) and sodium tetraphenylborate (2.25 g, 6.57 mmol). The flask was evacuated and refilled with nitrogen, then fitted with a mechanical stirrer and septum. Chloroform (4.5 mL) was added, and stirring was initiated. Upon addition of a $CHCl_3$ solution of $[(\eta^3\text{-}C_3H_5)PdCl]_2$ (0.00120 g in 0.5 mL, 0.05 mol %, prepared under nitrogen) to the stirring mixture, the mixture became increasingly viscous. After several hours it turned black. After 14 h the solvent was removed under vacuum. The solid was washed with ether (3 × 20 mL, washes removed via filter-paper-tipped cannula). After drying, 1.67 g of a light grey powder was obtained. Recrystallization (to remove unreacted sodium tetraphenylborate) from MeOH–CH_3CN gave analytically pure sodium (2S)-2-phenyl-2-[(E)-3-phenylpropenyloxy]ethanoate (1.26 g, 66% yield). All new compounds were characterized by ^1H and ^{13}C NMR spectroscopy and by satisfactory elemental analysis or high-resolution mass spectrometry.

Determining If the Reactions Are Palladium-Catalyzed

The palladium catalyst precursor is certainly required in the sense that no reaction is observed in its absence. However, this observation alone did not preclude the possibility that the palladium(II) compound was actually only initiating the reaction. Such would be the case if, for example, the palladium(II) reacted with sodium tetraphenylborate to generate triphenylboron, which in turn acted as a Lewis acid catalyst to promote conjugate addition. Alternatively, the palladium(II) could be envisaged as generating organic radicals that would promote a free radical chain mechanism similar to that involved in the addition of trialkylboron reagents to conjugated enones (9).

Control experiments that disfavor both of these possibilities include the following (3, 4).

- In the absence of palladium catalyst, triphenylboron (1 eq) had no effect.
- When 1 mol % of bis(acetonitrilo)dichloropalladium(II), **2b**, was reacted with sodium tetraphenylborate (1 equiv) in the absence of 2-ethenyl-1,3-dioxolanone, the mixture immediately turned black, and a flocculent black precipitate began to form. This

mixture was catalytically inactive, as evidenced by the lack of any reaction upon addition of **2b** within ~1 min. It is reasonable that a palladium-catalyzed reaction involving a monoatomic palladium catalyst (or a small palladium cluster) should be shut down by allowing the palladium to aggregate to form bulk palladium metal. However, it is not obvious why a hypothetical boron-centered Lewis acid would so rapidly decompose under such conditions.

- In addition to the palladium(II) catalyst precursors, tris(dibenzylidene)dipalladium(0), **2c**, was also observed to serve as an effective catalyst precursor. Unlike the reactions involving palladium(II) catalyst precursors, in which either triphenylboron or tetraphenylborate radical formation could reasonably be proposed as an initiation step, it is difficult to see how this palladium(0) complex would serve to initiate either Lewis acid-catalyzed or free radical chain chemistry. In combination with the model reaction studies described here, we take these results to indicate that the reactions are, indeed, palladium-catalyzed.

Reaction Steps

The a priori expectation was that these reactions would proceed via an allylation mechanism (Scheme II) similar to that established for analogous palladium-catalyzed reactions of allyl carboxylates (8). (The ancillary ligands L_n are not specified but can only be drawn from the solvent and from the

Scheme II.
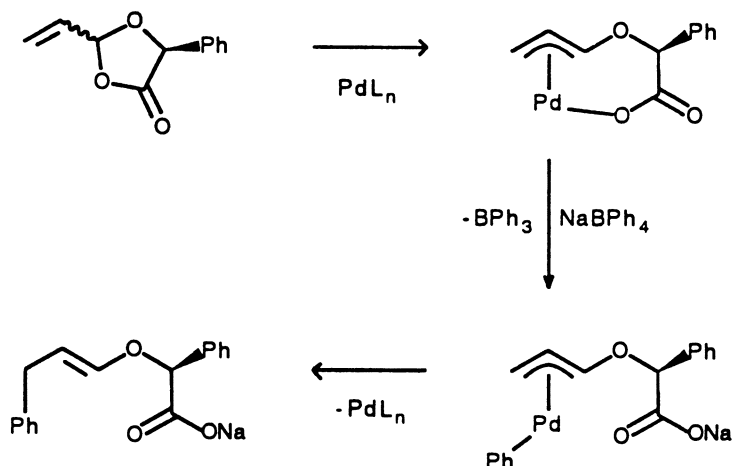
donor atoms or groups shown. All species are assumed to be ligated by sufficient numbers of ancillary ligands so as to maintain a 12–16 e⁻ count at all times.)

According to this mechanism, a palladium(0) species would coordinate and then oxidatively add the 2-ethenyl-1,3-dioxolanone to give an allylpalladium(II) carboxylate intermediate. Transmetallation of a phenyl ring from boron to palladium would then give an (allyl)(phenyl)palladium(II) intermediate. Subsequent reductive elimination would join the two carbon fragments and return the catalyst to the palladium(0) state.

With regard to the details of the transmetallation step, initial η^6-tetraphenylborate complex formation, followed by a boron-to-palladium phenyl group transfer (via an electrophilic aromatic substitution-type mechanism), would seem reasonable. Albano et al. (*10*) crystallographically characterized an isoelectronic η^6-(tetraphenylborate)rhodium(I) complex. They observed that it underwent subsequent reaction with carbon dioxide to give a rhodium benzoate derivative, presumably via initial boron-to-rhodium phenyl-group transfer (Scheme III).

Although ample precedent exists for such a mechanism, more direct support was sought through attempts to isolate and study the putative intermediates. These efforts have not yet resulted in the isolation or even

cf. **Albans et al.:**

$$[\text{PhCO}_2\text{Rh}(\text{diphos})]_2$$
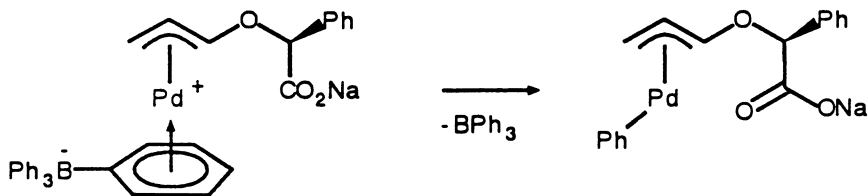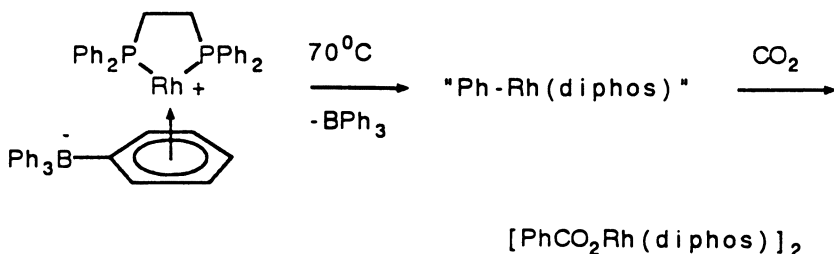
Scheme III.

spectroscopic detection of the exact species. However, several close analogs have been isolated and studied. For example, reaction of bis(1,5-cyclooctadiene)nickel(0) with **1c** yields allylnickelcarboxylate **4a** (Scheme IV; Cy is cyclohexyl) (*1*). Although it is highly insoluble and therefore not subject to recrystallization to analytical purity, **4a** has nonetheless been securely characterized by ^{1}H NMR, ^{13}C magic-angle spinning solid-state NMR, IR, and mass spectroscopy (the calculated isotopomeric distribution being observed for the expected dimeric formulation), and by derivatization to afford the fully characterized silyl ester derivative **5a**.

4a

5a
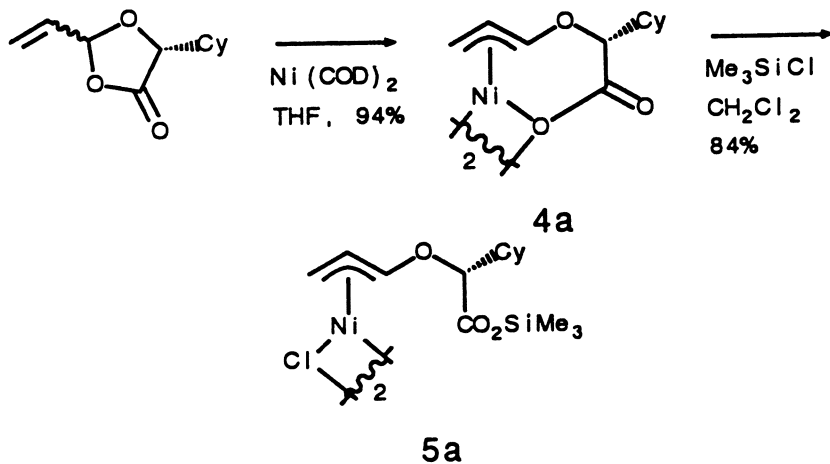
Scheme IV.

The X-ray crystal structure of **5a** (*4*) (Figure 1) establishes the π-allyl nature of this complex. It also shows evidence of significant overlap of the allyl oxygen substituent with the allyl π-system (Table II): the C-1–O-1 bond distance is only 1.373 (6) Å, the C-1–O-1–C-4 angle is 114°, and the allyl C-1 terminus is 0.06 (1) Å further from the metal than the allyl C-3 terminus. The implied distortion toward a C-3-bound η^1-allyl bonding mode is consistent with a least-motion rationale for the tetraphenylborate reaction regioselectivity, wherein phenyl-group transfer to the C-3 terminus is preferred over transfer to the C-1 terminus.

Complex **5a** is a versatile synthetic intermediate, coupling with both halocarbon electrophiles (eq 3, R is aryl, alkenyl, or alkyl) (*1*) and with
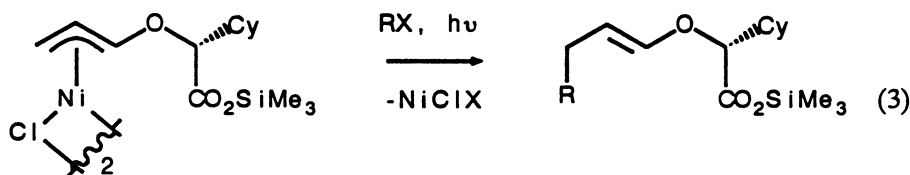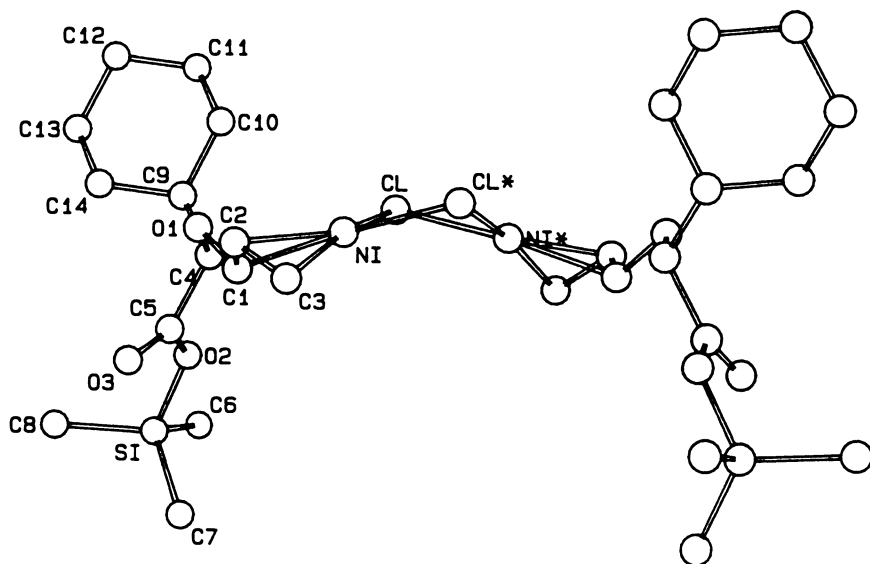
Figure 1. An ORTEP representation of the X-ray crystal structure of the allylnickel chloride dimer **5a**. Ni–C-1 = 2.044 (5) Å; Ni–C-2 = 1.968 (5) Å; Ni–C-3 = 1.980 (5) Å; C-1–O-1 = 1.373 (6) Å; angle C-1–O-1–C-4 = 114.1 (4)°.

Table II. Palladium-Catalyzed Organotin Coupling Reactions

Entry	R^1	R^2	$RSnR^3_3$	% Yield	E:Z
1	H	Me	$H_2C=CHSnBu_3$	91[a]	93:7
2	H	Cy	$H_2C=C(OEt)SnBu_3$	49[a]	95:5
3	H	Me	$PhSnMe_3$	65[a]	92:8
4	Me	Cy	$PhSnMe_3$	53[b]	94:6

[a]5 mol % **2b**.
[b]2.5 mol % **2c**.

organotin nucleophiles (eq 4, R is H, alkenyl, or alkynyl) (4) to afford the corresponding (E)-enol ethers.

$$RSnBu_3$$
$$-ClSnBu_3$$
$$-Ni\,(0)$$

$$(4)$$
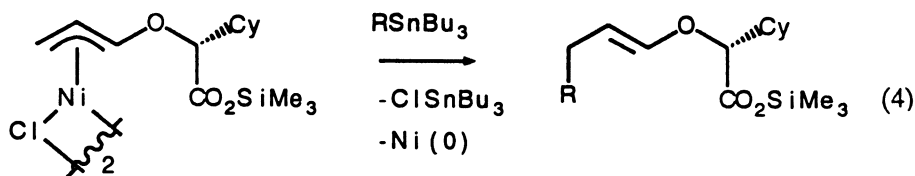
The latter reactions presumably proceed via (allyl)(R)nickel(II) inter-mediates similar to those involved in the catalytic tetraphenylborate chem-istry. Inasmuch as nickel(0) is generated as a coproduct, the success of these

stoichiometric reactions implied that catalytic organotin coupling chemistry might be possible. Subsequent investigations established that reactions of this type proceed under the influence of either nickel or palladium catalysts (eq 5, Table II) (3, 4). A soluble chloride anion source was found to be required for the reactions, with lithium chloride preferred because the resultant lithium carboxylate salts are dependably crystalline.

$$\text{(structure)} + RSnR^3{}_3 / LiCl \xrightarrow[\text{Pd cat}]{-ClSnR^3{}_3} \text{(product)} \qquad (5)$$
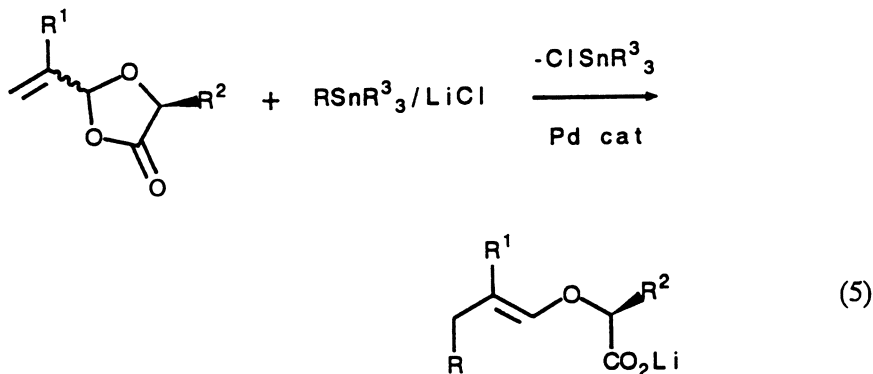
These reactions are not unusually fast and require the standard 1–5 mol % catalyst precursor. Nonetheless, they are important as models for tetraphenylborate chemistry. In seeking closer analogies, we also investigated whether the allylnickel reagents would serve as intermediates in organoborate coupling reactions. Tetraphenylborate itself has not yet been observed to react under nickel-catalyzed conditions. However, sodium methoxytriphenylborate does give conjugate addition-type chemistry (eq 6).

$$\text{(structure)} + NaBPh_3OMe \xrightarrow[\substack{Ni(COD)_2 \\ 10 \text{ mol\%}}]{-BPh_2OMe} \text{(product)} \qquad (6)$$

$$45\%$$
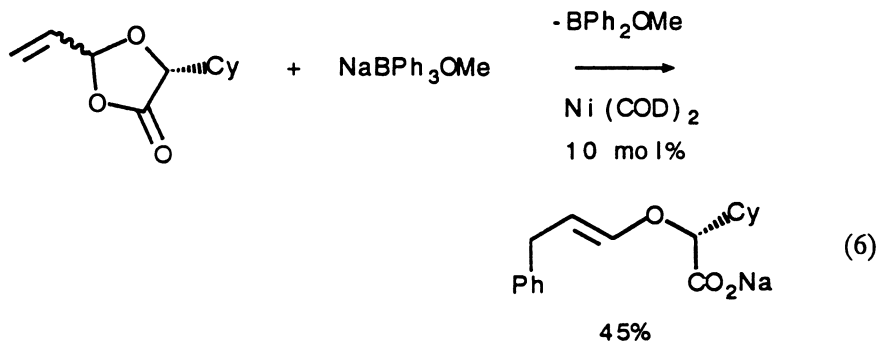
Nickel chemistry thus serves to establish the plausibility of the proposed palladium-catalyzed tetraphenylborate chemistry. In seeking yet more direct evidence, we recently developed a novel "bait and switch" approach to the synthesis of relevant allylpalladium complexes. In this strategy the 2-ethenyl-1,3-dioxolanone is first converted to allylnickel derivative **5a** and then transferred to palladium upon reaction with 1 equiv of **2b** (Scheme V) (4). A near-
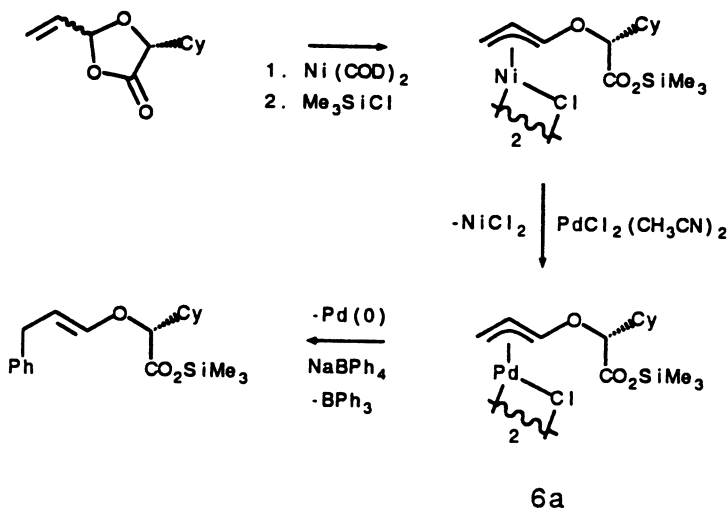
Scheme V.

quantitative crude yield of allylpalladium complex **6a** is observed. The isolated crystalline yield is lower (~50%), in part because of the high solubility of this complex. Subsequent reaction with sodium tetraphenylborate yields palladium metal and the corresponding (*E*)-enol ether. A similar reaction is observed with vinyltributyltin, modeling exactly the transmetallation and reductive elimination steps of the catalytic organotin coupling reactions.

To exactly model the tetraphenylborate reactions, however, we require the allylpalladium carboxylate, rather than the silyl ester derivative. In pursuit of this elusive species, we recently attempted bait and switch experiments with the allylnickel carboxylate and **2b**. Nickel dichloride and a highly insoluble organopalladium product were produced (4). The insolubility of the latter product has thus far hampered its purification and characterization. However, it has been converted to silyl ester derivative **6a** by treatment with chlorotrimethylsilane. The identification of this species as the sought-after allylpalladium carboxylate is supported by the observation that attempted dissolution in a highly coordinating solvent (e.g., dimethyl sulfoxide) results in immediate decomposition to 2-ethenyl-1,3-dioxolanone and a palladium metal mirror. We are continuing efforts to further characterize this apparently highly reactive species to better evaluate its suitability as an intermediate in the catalytic tetraphenylborate chemistry.

Reaction Speed

A combination of factors is likely to be responsible for the speed of these reactions. First, 2-ethenyl-1,3-dioxolanones are very reactive. They contain

both an alkene functionality, which allows for initial π-complexation to the catalyst center, and a relatively weak allylic carbon–oxygen bond that is further activated by anomeric effects. Both factors are likely to promote rapid oxidative addition. Second, the transmetallation step is likely to be especially rapid by virtue of the "ligand-poor" reaction conditions and the special characteristics of the tetraphenylborate anion. Inasmuch as the organoborate reagent is obviously a very poor nucleophile, it is undoubtably important that there not be any good donor ligands present to compete with the tetraphenylborate for a coordination site at palladium.

In agreement with this analysis, the reactions are fastest in chloroform or dichloromethane, despite the very low solubility of sodium tetraphenylborate in these solvents. They are slower by approximately a factor of 10 in acetonitrile and by roughly an additional factor of 10 in acetone (3). Furthermore, whereas tris(dibenzylideneacetone)dipalladium is an effective catalyst precursor, no reaction is observed when using tetrakis(triphenylphosphine)palladium(0) (3). It may also be significant that tetraphenylborate coordination would be expected to be favored by attractive electrostatic interactions between the positively charged palladium and the negatively charged tetraphenylborate (cf. Scheme III). Finally, the actual boron-to-palladium phenyl-group transfer step may be especially facile by virtue of the availability of an electrophilic aromatic substitutionlike pathway. Model experiments wherein sodium tetraphenylborate is reacted with either 2a or 6a are certainly fast reactions. They are completed within seconds at 25 °C in the former case and require less than 5 min in the latter case (4).

Lack of Stereospecificity of the cis-2-Propenyl-1,3-dioxolanone Reaction

Control experiments (3, 4) have shown that the triphenylboron coproduct, which is actually a quite weak Lewis acid, is nonetheless strong enough to very rapidly equilibrate the initially near-pure *cis*-dioxolanone to afford ca. 2:1 *cis–trans* mixture under reaction conditions. The overall lack of stereospecificity may therefore simply reflect this equilibration.

The observed 2:1 ratio of epimeric enol ethers corresponds to the expected overall inversion of configuration, starting from a 2:1 *cis–trans* mixture. Significantly, when this reaction is interrupted at 10% completion, the epimer ratio is ca. 3:1 (3). Relatively little triphenylboron has been formed at that point, and there has been less time for equilibration. Therefore, this ratio is consistent with the idea that triphenylboron equilibration of the starting stereochemistry is competitive with the desired allylpalladium chemistry. The possibility that a stereospecific reaction can be achieved by using organometallic nucleophiles that give rise to less Lewis acidic coproducts is under investigation.

Conclusion

The weight of the evidence supports an allylpalladium mechanism for these reactions. All of the steps involved are remarkably rapid, with the slowest step corresponding to a turnover rate of 660 min^{-1} at 65 °C. Inasmuch as the steps involved are similar to those involved in many other synthetically important reactions, it is of considerable interest to try to understand why these reactions are so fast. Several possible reasons have been identified here. We are now moving to test these ideas in other systems.

Acknowledgment

References

1. Krysan, D. J.; Mackenzie, P. B. *J. Am. Chem. Soc.* **1988,** *110,* 6273–6274.
2. Faunce, J. A.; Friebe, T. L.; Grisso, B. A.; Losey, E. N.; Sabat, M.; Mackenzie, P. B. *J. Am. Chem. Soc.* **1989,** *111,* 4508.
3. Friebe, T. L. Ph.D. Dissertation, Northwestern University, 1990.
4. Friebe, T. L.; Johnson, J. R.; Krysan, D. J.; Sabat, M.; Mackenzie, P. B. unpublished results.
5. Soai, K.; Hayasaka, T.; Ugajin, S. *J. Chem. Soc., Chem. Commun.* **1989,** 516.
6. Mangeney, P.; Alexakis, A.; Normant, J. F. *Tetrahedron Lett.* **1987,** *28,* 2363.
7. Fujiwara, J.; Fukutani, Y.; Hasegawa, M.; Maruoka, K.; Yamamoto, H. *J. Am. Chem. Soc.* **1984,** *106,* 5004.
8. Trost, B. M.; Verhoeven, T. R. In *Comprehensive Organometallic Chemistry*; Wilkinson, G.; Stone, F. G. A.; Abel, E. W., Eds.; Pergamon: Oxford, 1982; Vol. 8, p 799.
9. Brown, H. C.; Midland, M. M. *Angew. Chem., Int. Ed. Engl.* **1972,** *11,* 692.
10. Albano, P.; Aresta, M.; Manassaro, M. *Inorg. Chem.* **1980,** *19,* 1069.

Hydrosilylation

A "Homogeneous" Reaction Really Catalyzed by Colloids

Larry N. Lewis, Nathan Lewis[1], and Richard J. Uriarte[2]

General Electric Research and Development, P.O. Box 8, Schenectady, NY 12301

The evidence for the intermediacy of colloids in the hydrosilylation reaction is reviewed. Data are presented to support the fact that reactions catalyzed by the active catalyst Pt[(vinyl)Me₂SiOSiMe₂- (vinyl)] (Karstedt's catalyst) form colloids. Analytical electron microscopy (AEM) and high-resolution electron microscopy (HREM) confirm the formation of colloids. Additional evidence comes from analysis of X-ray absorption near-edge spectroscopy (XANES) measurements, which show that Pt reduction occurs upon reaction of Karstedt's catalyst with (EtO)₃SiH and that Pt is in a new environment.

$\mathbf{T}$HE HYDROSILYLATION REACTION (eq 1) has been known since the 1940s but has received considerable attention since Speier's pioneering work using H_2PtCl_6–i-PrOH "homogeneous" catalysts (*1–5*). Chalk and Harrod's (*6, 7*) mechanistic work and proposals, which became accepted in the literature (*8*), were based on the intermediacy of molecular compounds.

$$R_3SiH + R^1\diagup\!\!\!\diagdown \xrightarrow{\text{cat}} R_3Si\diagup\!\!\diagdown\!\!\diagup^{R^1} \qquad (1)$$

In 1986 we reported (*9*) that strong evidence implicated colloids as important intermediates in the catalytic cycle of hydrosilylation. For example, if CODPtCl₂ (COD is 1,5-cyclooctadiene) was reacted with excess

---

[1]Current address: Knolls Atomic Power Laboratory, Niskayuna, NY 12309
[2]Current address: GE Silicone, Waterford, NY 12188

$(EtO)_3SiH$ in CH_2Cl_2, a Pt colloid formed after about 1 h with release of H_2 (eq 2).

$$CODPtCl_2 + (EtO)_3SiH \xrightarrow{CH_2Cl_2}$$

$$[Pt(0)]_x + H_2\uparrow + ClSi(OEt)_3 + cyclo\text{-}C_8H_{14} + cyclo\text{-}C_8H_{16} \quad (2)$$
colloid 1
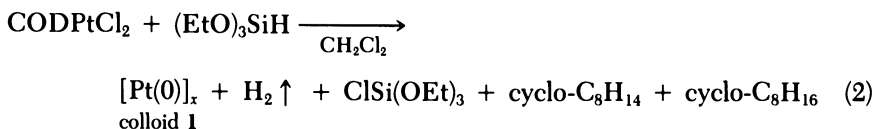
The colloidal product, identified by analytical electron microscopy (AEM), was more active than $CODPtCl_2$ itself. An induction period was observed in the hydrosilylation reaction catalyzed by $CODPtCl_2$. However, no induction period was noted when colloid 1 was used as a catalyst. The length of the induction period corresponded to the time it took to form colloid 1 from $CODPtCl_2$.

This chapter addresses recent results that further support Pt colloids as intermediates in the Pt-catalyzed hydrosilylation reaction. AEM, high-resolution electron microscopy (HREM), and X-ray absorption near-edge spectroscopy (XANES) were employed to analyze the Pt colloids.

Experimental Procedures

General Information. AEM analyses were performed on an analytical electron microscope (Hitachi H–600–1 instrument) operated at 100 kV and equipped with an energy-dispersive X-ray detector [EEG Ortec Si(Li)]. HREM was performed on an electron microscope (Philips EM 430 instrument) operated at 300 kV. The XANES measurements were made at Brookhaven National Laboratory National Light Source; zero energy was taken at the L_{III} edge of platinum metal (by using Pt foil) at 11,568.4 eV with electron energy of 2.5 GeV. Data were collected in the fluorescence mode, and normalized plots of the near edge were produced by using published procedures (10).

NMR spectra were recorded on one of two NMR spectrometers (Varian XL 300 spectrometer, ^{13}C, ^{29}Si, and ^{195}Pt at 75.43, 59.3, and 64.12 MHz, respectively, or on a GE QE–300 instrument, ^{13}C at 75.48 MHz).

Pt Catalyst. Catalyst solutions were either the complex of divinyltetramethyldisiloxane (DVTMDS, *see* structure), Pt(DVTMDS)$_x$ ("Karstedt" catalyst in xylene, available from Petrarch systems as PC 072); or Pt(DVTMDS)$_x$ in neat DVTMDS made by following a modification of a published procedure (11, 12). H_2PtCl_6 (5 g, 39.4% Pt, 10 mmol) was combined with 5 mL of EtOH and DVTMDS (50 g, 0.27 mol) and heated at 60 °C with stirring for 4–6 h. A
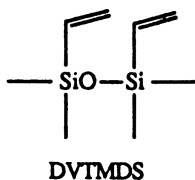
DVTMDS

homogeneous orange solution was obtained, to which solid NaHCO$_3$ (1.7 g, 70.8 mmol) was added. After an additional 1 h of stirring, the mixture was filtered and the precipitate was washed with two 10-g aliquots of DVTMDS. A yellow liquid was obtained, 2.27% Pt by analysis. The xylene solution of Pt(DVTMDS)$_x$ or the Pt(DVTMDS)$_x$ in neat DVTMDS previously described had identical ^{195}Pt NMR resonances at –6148 ppm upfield from Na$_2$PtCl$_6$. In addition, concentrates of this solution were obtained by vacuum distilling (30 °C, 0.5 mm Hg pressure) a portion of the DVTMDS. ^{13}C NMR spectra of these concentrated mixtures showed the presence of bound DVTMDS, on the basis of the appearance of an upfield set of resonances from 55–59 ppm versus 131.89 and 139.62 ppm for the vinyl portion of free DVTMDS.

Hexene Reactions.   In a typical run, 3,3′-dimethyl-1-butene (*t*-hexene, 1.38 mL, 10.8 mmol) was combined with a xylene solution of Karstedt catalyst (2.7 μL, 0.7 mmol) and decane (internal standard, 0.2 mL, 1.03 mmol). Addition of Et$_3$SiH (1.72 mL, 10.8 mmol) initiated the reaction; a yellow color was noted after about 2 min at ambient temperature. NMR data are as follows:

$$(\text{CH}_3\text{CH}_2)_3\text{SiCH}_2\text{CH}_2\text{C}(\text{CH}_3)_3$$
$$\ \ \ \text{a}\ \ \ \ \ \text{b}\ \ \ \ \ \ \ \ \ \text{c}\ \ \ \ \ \text{d}\ \ \ \text{e}\ \ \ \text{f}$$
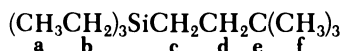
^{13}C: 37.76 (d), 31.04 (f), 28.73 (e), 7.38 (b), 5.02 (c), and 3.18 (a) ppm
^{29}Si: 7.58 ppm, single isomer

Results and Discussion

Colloid Synthesis and Structure.   In 1989 we described the synthesis and structure of platinum group metal colloids from metal halide salts and alkoxysilane [e.g., PtCl$_4$ + Me$_2$(EtO)SiH (13)]. AEM and HREM analyses of these colloids showed (for Pt) that 1–5-nm diameter platinum crystallites formed (Figure 1).

The work described and recent mechanistic work (14, 15) showed that the most active catalyst precursors for hydrosilylation were those that could most easily form colloids. Thus the most active catalysts were Pt(O) complexes with olefin ligands. Conversely, Pt(II) complexes with strongly binding ligands such as phosphines were the least active. An example of one of the most active catalyst precursors was the Karstedt catalyst (12, 16).

As we (13) and others (16) showed, the Karstedt catalyst is a mixture of compounds, but the main component is the *n* = 0 compound. The Karstedt catalyst is referred to as "solution A" in the Chandra work (16).

$$\left(\diagdown\!\!=\!\!-\overset{|}{\underset{|}{\text{Si}}}(\text{OSi})_n\overset{|}{\underset{|}{\text{OSi}}}-\diagup\!\!=\diagdown \right)_2\text{Pt}$$

Karstedt catalyst, n=0-9

Figure 1. HREM for the Pt colloid formed between $PtCl_4$ and $Me_2(EtO)SiH$; 1–5-nm particles are evident. Also evident are diffraction fringes of the (111) planes. (Reproduced from reference 13. Copyright 1989 American Chemical Society.)

The reaction of an orange xylene Karstedt catalyst solution with $(EtO)_3SiH$ resulted in instantaneous formation of a black solution (eq 3).

$$(3)$$

AEM analysis confirmed that platinum colloids formed. XANES was used to analyze the platinum reactant and product of eq 3. In general, the area under the near-edge curve (white line) is related to the metal oxidation state. The electronic dipole transitions at the Pt L_{III} edge are from $2p^{3/2}$ core level to the empty 5d state ($\Delta J = 0 \pm 1$, where ΔJ corresponds to the difference between the excited state and ground state; J is the total angular momentum quantum number.) Therefore the peak intensity or "white line"

is proportional to the d-electron vacancies (*17*, *18*). As shown in Figure 2, the reaction product, colloid **2**, was more "reduced" than the starting Karstedt catalyst. Figure 2 shows that there is a lower white-line area for colloid **2** than for Karstedt. In addition, the change in fine structure observed after the edge in going from Karstedt to colloid **2** suggested that Pt was in a different environment in colloid **2** than in Karstedt catalyst.
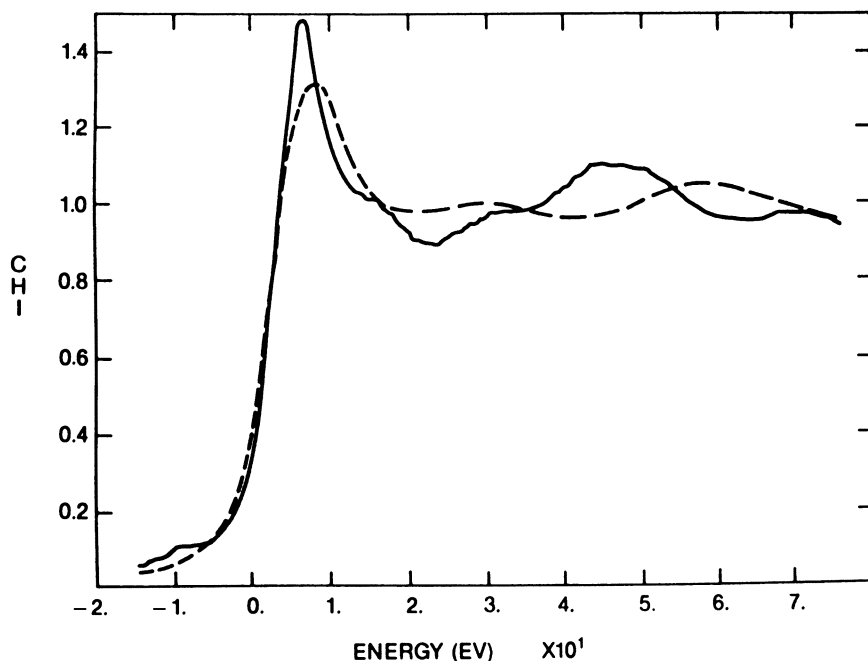
*Figure 2. Near-edge spectra for Karstedt catalyst (solid line) and colloid **2**, eq 3 (dashed line).*

Figure 3 compares the near-edge region for colloids **1** and **2**. Although two different Pt starting materials were used to form colloids **1** and **2** (PtCl$_4$ and Pt(DVTMDS)$_x$, respectively), colloids with equivalent white-line areas were obtained. The fine-structure region suggests a different environment around Pt in colloids **1** and **2**, however.

Platinum Colloids from Actual Catalyzed Reactions.

AEM and HREM were used to analyze the Pt product from hydrosilylation reactions catalyzed by Karstedt catalyst. Et$_3$SiH was reacted with *n*-hexene (eq 4) or *t*-hexene (eq 5) in the presence of about 100 ppm of Pt as Karstedt catalyst.

$$CH_2=CH(CH_2)_3CH_3 + Et_3SiH \xrightarrow[\text{Karstedt}]{} \underset{\text{10\%, colorless}}{Et_3Si(CH_2)_5CH_3} \qquad (4)$$
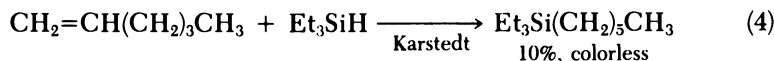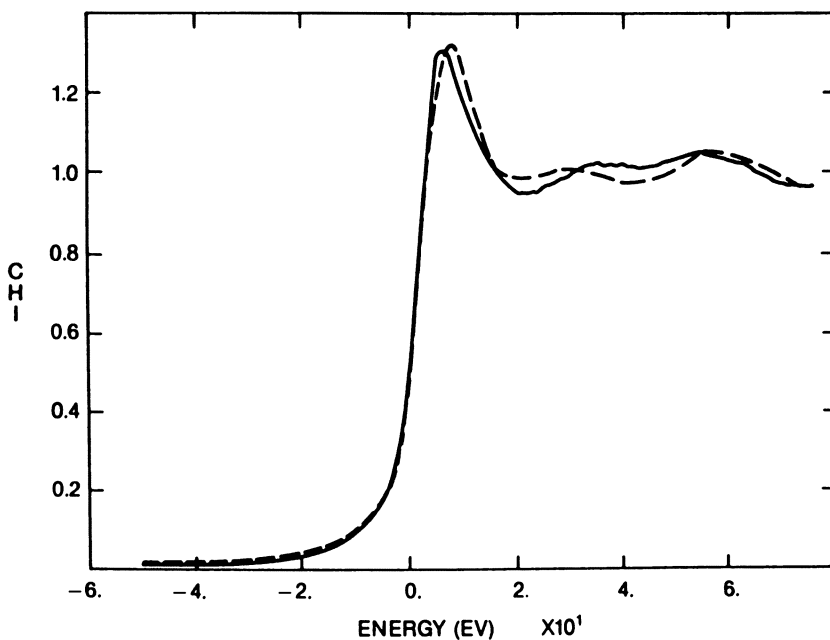
Figure 3. Comparison of the near-edge regions for colloid 1 (solid line) and colloid 2 (dashed line).

$$CH_2=CHC(CH_3)_3 + Et_3SiH \xrightarrow[\text{Karstedt}]{} \underset{\text{100\%, colorless}}{Et_3SiCH_2CH_2C(CH_3)_3} \quad (5)$$
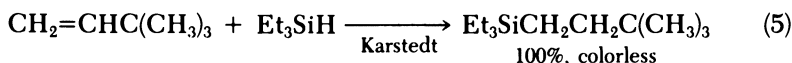
Equations 4 and 5 show that high conversion to product occurred for t-hexene in 17 h at ambient temperature, but that only 10% conversion occurred in the n-hexene reactions under the same conditions.

The morphology of the colloids formed from eqs 4 and 5 were different. AEM analysis of the reaction solution from eq 4 (Figure 4) showed that amorphous-looking agglomerates of Pt-containing material were present. The inset to Figure 4 (HREM) showed that the amorphous clump contained 1.5–2.0-nm Pt crystallites. The particles exhibited fringes that corresponded to the spacing of the (111) planes of platinum (9). AEM analysis (Figure 5) of the reaction solution of eq 5 showed that there was a lower degree of agglomeration of the Pt particles but that the individual Pt crystallites (HREM inset) were larger, 2.2–2.8 nm, than those from eq 4. As in Figure 4, the particles in Figure 5 exhibited the (111) planes attributed to crystalline Pt. In addition, an electron-diffraction pattern obtained from this sample indexed to crystalline platinum. The larger individual particles of Figure 5 presumably gave rise to the yellow appearance in eq 5 vis-a-vis the colorless solution of eq 4.
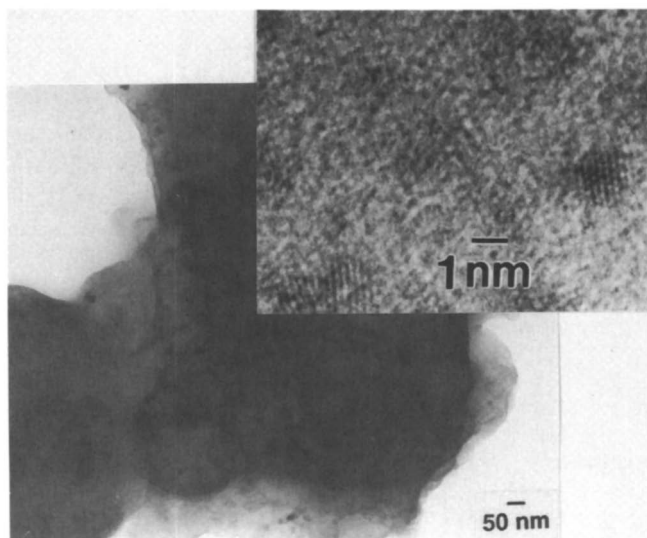
Figure 4. AEM image of the reaction solution from eq 4, n-hexene + Et₃SiH, catalyzed by Karstedt catalyst. Inset shows HREM image. The fringes correspond to the (111) planes of crystalline Pt. (Reproduced with permission from reference 18. Copyright 1991 Academic Press.)
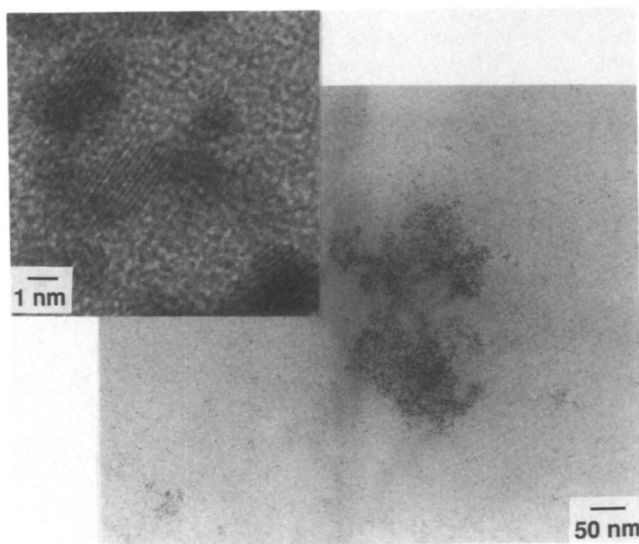
Figure 5. AEM image of the reaction solution from eq 5, t-hexene + Et₃SiH catalyzed by Karstedt catalyst. Inset shows HREM image. (Reproduced with permission from reference 18. Copyright 1991 Academic Press.)

Summary

The combination of XANES and AEM–HREM showed that colloidal platinum formed from Karstedt catalyst reactions with the SiH functionality either directly or in a hydrosilylation reaction catalyzed by Karstedt catalyst. The colloid formed was more reduced than the starting complex. It is proposed that this reduction step is the commonly observed induction period in hydrosilylation. The morphology of the colloid formed was controlled by the reagents of the reaction. It is not known whether the differences in the two colloids of Figures 4 and 5 were due to the differences in steric or electronic factors between n-hexene and t-hexene or to both.

Acknowledgments

References

1. Ojima, I. In *The Chemistry of Organic Silicon Compounds*; Patai, S.; Rappoport, Z., Eds.; Wiley: New York, 1989; p 1479.
2. Armitage, D. A. In *Comprehensive Organometallic Chemistry*; Wilkinson, G.; Stone, F. G. A.; Abel, E. W., Eds.; Pergamon: Oxford, 1982; Vol. 2, p 117.
3. Speier, J. L. *Adv. Organomet. Chem.* **1979**, *17*, 407.
4. Lukeviks, E.; Belyakova, Z. V.; Pomeransteva, M. G.; Voronkov, M. G. *J. Organomet. Chem. Libr.* **1977**, *5*, 1.
5. Eaborn, C.; Bott, R. W. In *The Bond to Carbon*; MacDiarmid, A. G., Ed.; Dekker: New York, 1968; Vol. 1.
6. Harrod, J. F.; Chalk, A. J. In *Organic Synthesis via Metal Carbonyls*; Wender, I.; Pino, P., Eds.; Wiley: New York, 1977; p 673.
7. Chalk, A. J.; Harrod, J. F. *J. Am. Chem. Soc.* **1965**, *87*, 16.
8. Collman, J. P.; Hegedus, L. S. *Principles and Applications of Organotransition Metal Chemistry*; University Science Books: Mill Valley, CA, 1980; pp 384ff.
9. Lewis, L. N.; Lewis, N. *J. Am. Chem. Soc.* **1986**, *108*, 7228.
10. Wong, J.; Lytle, F. W.; Messmer, R. P.; Maylotte, D. H. *Phys. Rev. B: Condens. Matter* **1984**, *30*, 5587.
11. Karstedt, B. D. U.S. Patent 3 775 452, 1973.
12. Ashby, B. A.; Modic, F. J. U.S. Patent 4 288 345, 1981.
13. Lewis, L. N.; Lewis, N. *Chem. Mater.* **1989**, *1*, 106.
14. Lewis, L. N. *J. Am. Chem. Soc.* **1990**, *112*, 5998.
15. Lewis, L. N.; Uriarte, R. J. *Organometallics* **1990**, *9*, 621.
16. This complex is referred to as "Solution A" in Chandra, G.; Lo, P. Y.; Hitchcock, P. B.; Lappert, M. F. *Organometallics* **1987**, *6*, 191.

17. (a) Lytle, F. W.; Greegor, R. B.; Marques, E. C.; Biebesheimer, V. A.; Sand-strom, D. R.; Horsley, J. A.; Via, G. H.; Sinfelt, J. H. In *Catalyst Characterization Science*; Deviney, M. L.; Gland, J. L., Eds.; ACS Symposium Series 288; American Chemical Society: Washington, DC, 1985; p 280. (b) Lytle, F. W.; Via, G. H.; Sinfelt, J. H. In *Synchrotron Radiation Research*; Winick, H.; Doniach, S., Eds.; Plenum: New York, 1980; p 401.
18. Lewis, L. N.; Uriarte, R. J.; Lewis, N. *J. Catal.* **1991**, *127*, 67.

Catalytic Synthesis of Polymethylsilsesquioxanes

Richard M. Laine[1,3], Jeffrey A. Rahn[1,4], Kay Youngdahl Blohowiak[1], and John F. Harrod[2]

[1]Department of Materials Science and Engineering, University of Washington, Seattle, WA 98195
[2]Department of Chemistry, McGill University, Montreal H3A 2A7, Canada

Dimethyltitanocene, Cp_2TiMe_2, will promote the redistribution of $-[MeHSiO]_x-$ oligomers to produce a polymethylsilsesquioxane copolymer of the type $-[MeHSiO]_{0.3}[MeSi(O)_{1.5}]_{0.7}-$. The mechanism for this redistribution is suggested to involve σ-bond metathesis promoted by a Ti(IV) species. The structural evolution of the copolymer on heating to 1000 °C is followed by using solid-state ^{29}Si NMR spectroscopy. Thermogravimetric analysis (TGA) experiments and chemical analysis are used to support the NMR results. The Cp_2TiMe_2-derived catalyst also promotes alcoholysis of the Si–H bonds in the copolymer. This reaction produces alkoxy derivates, $-[Me(RO)SiO]_{0.3}[MeSi(O)_{1.5}]_{0.7}-(R$ is Me, Et, n-Pr, or n-Bu). Furthermore, this catalyst will also polymerize the oligosilazanes $-[MeHSiNH]_x-$ or $-[H_2SiNMe]_x-$, but only if some $-[MeHSiO]_x-$ is present. The ceramic yields of the copolymers $-[MeHSiO]_x-:-[MeHSiNH]_x-(with 1:1, 1:3, 1:9, and 1:18 ratios) are much higher than yields found for the pure polysilazane.

S~ILSESQUIOXANES~ REPRESENT A UNIQUE and poorly studied subset of polyalkylsiloxanes. This statement is true despite the fact that they offer many exceptional properties. For example, silsesquioxanes, $RSi(O)_{1.5}$, because of their need to form three Si–O–Si bonds, assume regular polyhedral shapes such as that shown in structure 1 for octamethyloctasilsesquioxane (*1*).

[3]Corresponding author: Department of Materials Science and Engineering, University of Michigan, Ann Arbor, MI 48109–2136
[4]Current address: Department of Chemistry, Eastern Washington University, Cheney, WA 99004

These polyhedral shapes have geometries very similar to those found for silica and its derivatives. Feher and co-workers (2, 3) used this similarity as the basis for developing molecular models of silica surfaces. The regular geometry also contributes to such properties as high-temperature stability (1) and high hardness (4). Octamethyloctasilsesquioxane is stable in air to 415 °C, at which temperature it sublimes.

Polysilsesquioxanes appear to have cage rather rather than ladder structures (5). The polymer is formed by the opening of a polyhedral edge, as suggested for polymethylsilsesquioxane (see structure 2).

1   2
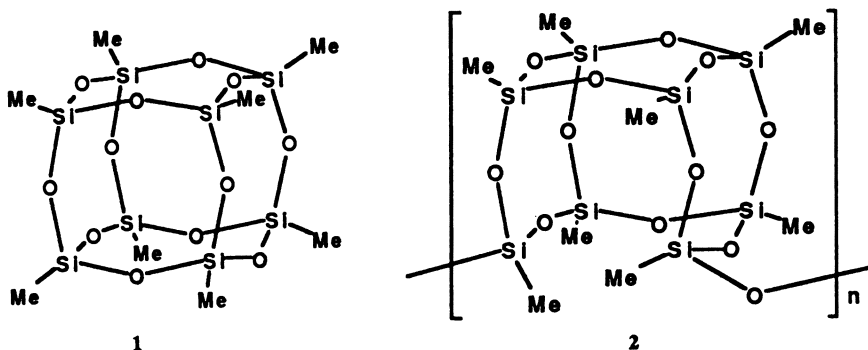
Polymethylsilsesquioxane, $-[MeSi(O)_{1.5}]_x-$, is stable to temperatures above 500 °C in air and to at least 600 °C in nitrogen. The phenyl derivative is reported to be stable to 800 °C (1). The cage structure is useful for making microporous materials (6).

Polymethylsilsesquioxanes have been used as protective polymer coatings in the electronics industry (7) and as precursors to silica and $SiO_{4-x}C_x$ glasses (Scheme I) (8–10).

From an engineering standpoint, these materials offer exceptional properties that should lead to widespread applications. Unfortunately, their propensity for forming gels makes it extremely difficult to prepare useful, processable quantities of any given material. Until recently, the only method of preparing silsesquioxanes was via hydrolysis of the alkyltrichloro- or trialkoxysilane (Scheme II) (1, 2, 6).

Separation of the polyhedral- or polyalkylsilsesquioxane from the reaction mixture is extremely difficult. Isolable yields of these compounds are quite poor, typically ranging from 15 to 30%. Consequently, the discovery (11) that titanium will catalyze the redistribution of alkoxysilanes under extremely mild conditions (reaction 1) suggested that it might be possible to synthesize polysilsesquioxanes via a similar route that would eliminate the need for a hydrolytic synthesis (reaction 2).

$$3MeHSi(OEt)_2 \xrightarrow{\text{<0.1 mol \% } Cp_2TiMe_2/RT} MeSiH_3 + 2MeSi(OEt)_3 \quad (1)$$

900°C/O$_2$

1200°C/N$_2$

70% SiO$_2$, 20% SiC and 10% C

Scheme I.

MeSiCl$_3$ + H$_2$O

Catalyst

+

Scheme II.

$$-[MeHSiO]_n- \xrightarrow{\text{<0.1 mol \% Cp}_2\text{TiMe}_2/\text{RT}} MeSiH_3 + -[MeSi(O)_{1.5}]_x- \quad (2)$$
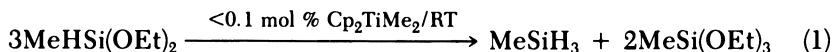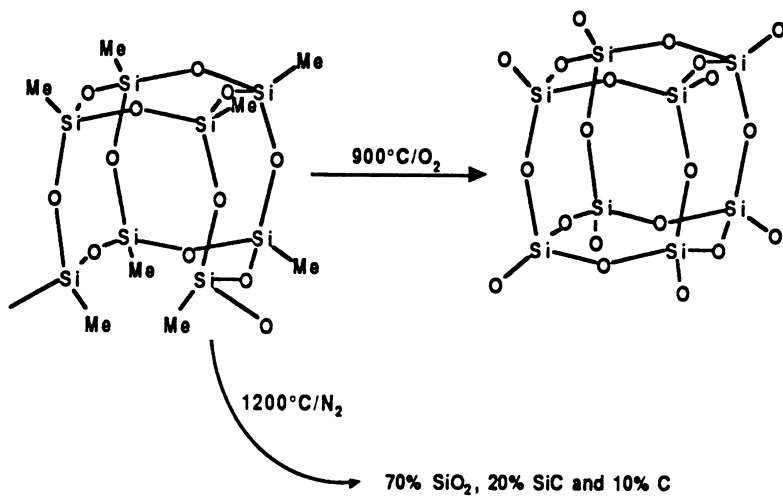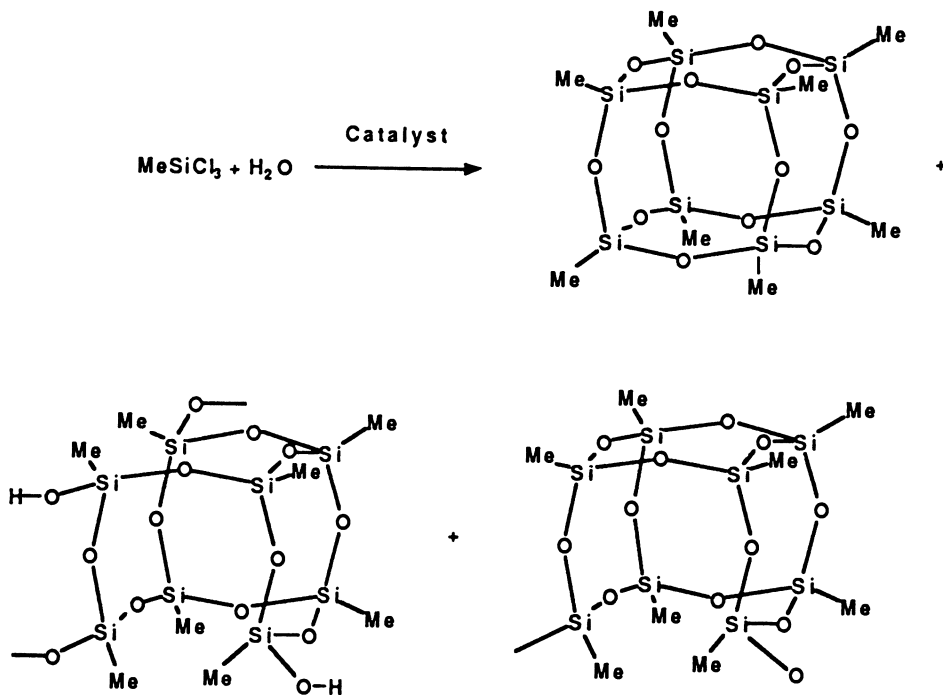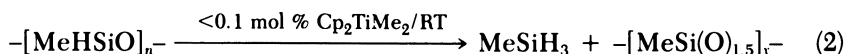
where Cp_2TiMe_2 is dimethyltitanocene and RT is room temperature.

Indeed, this reaction works very effectively. The following discussion is an overview of our recent efforts to prepare and characterize the resulting polymers and their properties. The information presented here includes data previously published elsewhere (12, 13).

Results and Discussion

Neat mixtures of either cyclic $-[MeHSiO]_n-$ ($n = 4$ or 5) or linear oligomeric $Me_3Si-[MeHSiO]_n-H$ (number-average molecular weight, M_n ~2000 daltons) with 0.2 mol % $(\eta^5-C_5H_5)_2TiMe_2$ turn royal blue (under N_2 at 20 °C) following an induction period of ~15 min. $MeSiH_3$ evolves rapidly with stirring. In 5–7 min the solution becomes extremely viscous; it gels in 10–15 min. Solid-state ^{29}Si NMR spectroscopy indicates that the final gel consists of a copolymer of approximate composition $-[MeHSiO]_{0.3}[MeSi(O)_{1.5}]_{0.7}-$. The induction period that precedes reaction appears to involve free radical promoted decomposition of $(\eta^5-C_5H_5)_2TiMe_2$. This reaction generates the true catalyst.

Soluble product can be obtained by dilution with toluene. Thus, reaction in a fivefold excess (with respect to added $-[MeHSiO]_n-$) of toluene gives a stable solution after 72 h of reaction. Reactions attempted with less than a fivefold excess of toluene lead inevitably to the formation of a gel.

Thin films cast from the resulting copolymer–toluene solution exhibit moderate elastomeric properties and excellent adhesion to glass, carbon, and metal surfaces; they can be heated without significant changes in properties to 250 °C. Above this temperature the polymer becomes increasingly brittle; however, no visible degradation occurs up to approximately 400 °C.

Because of our continuing interest in polymer precursors to ceramics, we followed the structural evolution of the $Me_3Si-[MeHSiO]_n-H$-derived copolymer during heating to 1000 °C by using solid-state ^{29}Si NMR spectroscopy (Figure 1). At room temperature, the Me_3Si (3%) and $Me(OH)Si$ (4%) end caps of the original oligomer appear, together with peaks for $-[MeHSiO]_n-$ (30%) and $-[MeSi(O)_{1.5}]_x-$ (70%). Thermogravimetric and chemical analysis (9) support the NMR results. Both methods indicate that most of the starting monomer is either volatilized or undergoes further redistribution such that by 400 °C only the pure polymethylsilsesquioxane remains. In the NMR results, the sharp singlet of the $[MeSi(O)_{1.5}]$ silicon is present even at 600 °C. It becomes severely broadened as the polymer is transformed into a glass at 800 °C (13).

Nearly identical copolymer compositions are obtained from the copolymer generated in toluene solution, as determined following solvent re-
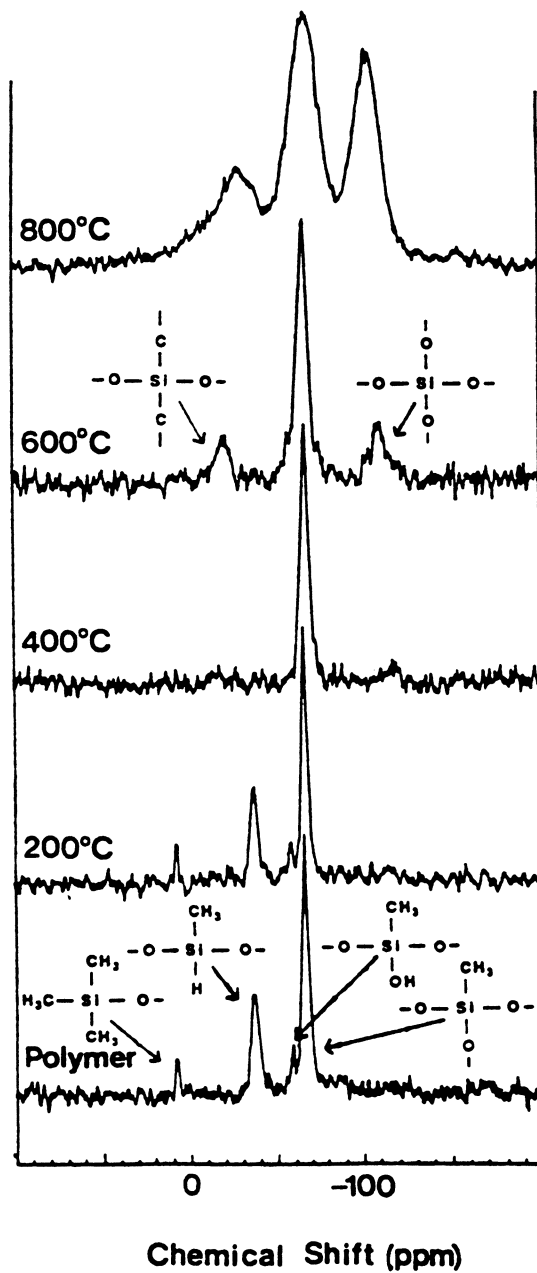
Figure 1. Chemical evolution of Me₃Si–[MeHSiO]ₙ–H-derived copolymer during heating to selected temperatures below 1000 °C by using solid-state ²⁹Si NMR spectroscopy.

moval. The composition, established by solution NMR spectroscopy, is confirmed by the chemical analysis (Found: C, 19.4%; H, 5.4%; Si, 41.5%; Calc. $-[MeHSiO]_{0.3}[MeSi(O)_{1.5}]_{0.7}-$: C, 18.5%; H, 5.1%; Si, 43.1%). Given the relatively simple ^{29}Si NMR results, the copolymer structure is assumed to be that shown in Scheme III. However, other polyhedral silsesquioxane structural units may also form in the copolymer.
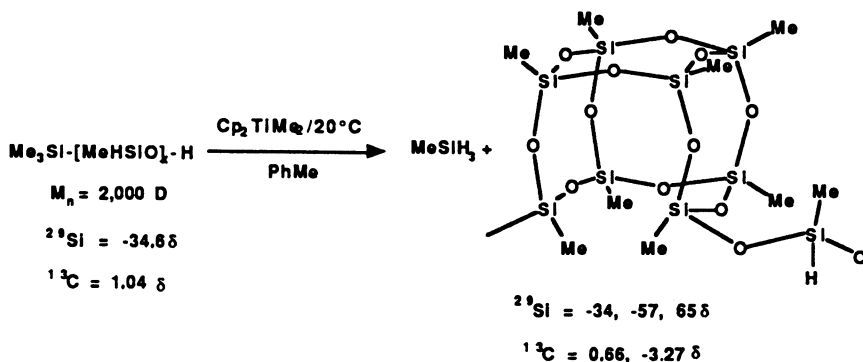
Scheme III.

Catalytic redistribution of hydridosiloxanes by transition metals was first reported by Curtis and Epstein (*14*). They discovered that iridium complexes promoted redistribution of $H-[Me_2SiO]_x-SiMe_2H$ and proposed the type of mechanism shown in Scheme IV.
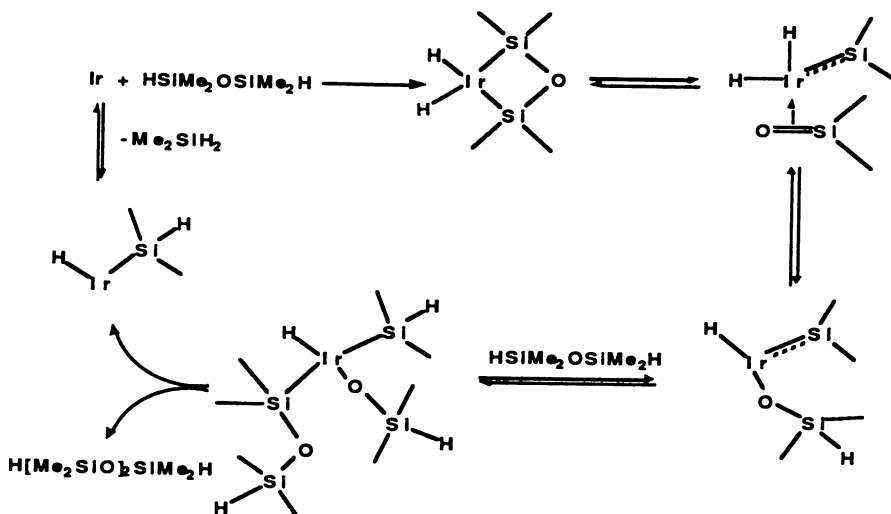
Scheme IV.

On the basis of work by Woo and Tilley (*15*) on the reactions of d^0 metals with silanes, we believe that a different mechanism is operating here. This mechanism probably involves σ-bond metathesis promoted by a Ti(IV) species generated by decomposition of $(\eta^5\text{-}C_5H_5)_2TiMe_2$. The mechanism shown in Scheme V is based on the work of Woo and Tilley (*15*). However, substantiation must await detailed kinetic studies.
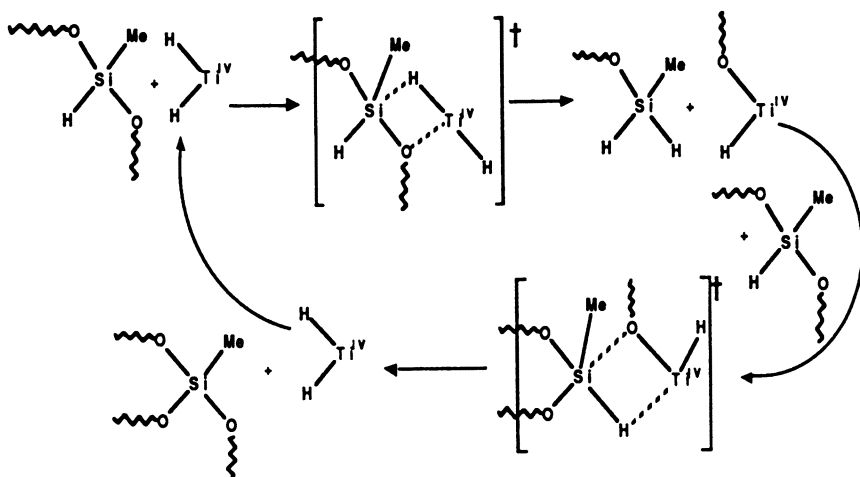
Scheme V.

We propose a Ti(IV) catalytic process, despite the royal blue color of the reaction (which is typical of Ti(III) compounds) and despite our having isolated Ti(III) complexes (*16*) in related systems. Our choice of Ti(IV) is based on the following discovery.

The copolymer $-[MeHSiO]_{0.3}[MeSi(O)_{1.5}]_{0.7}-$ still retains Si–H groups that are susceptible to further modification by either hydrosilylation or alcoholysis. Therefore, we explored the possibility of changing the copolymer rheological characteristics by reaction with alcohols. Addition of alcohols to the toluene reaction solution at any time during the course of the reaction leads to very effective alcoholysis of the copolymer (Scheme VI).

The addition of MeOH leads to a rapid color change from royal blue to yellow-orange and extremely rapid (almost violent) evolution of hydrogen. The reaction is complete within the time of addition. The other alcohols are less reactive, with the *n*-BuOH reaction taking 1–2 days at room temperature.

Once the solvent is removed, the methoxy derivative will become gel-like in hours to days, depending on the temperature of the room. The *n*-butoxy derivative, in contrast, is much less susceptible to gelling. It will remain a viscous liquid for periods of up to 1 week. 1-Propanol solutions of the *n*-propoxy derivative (25 wt%) will remain stable almost in-
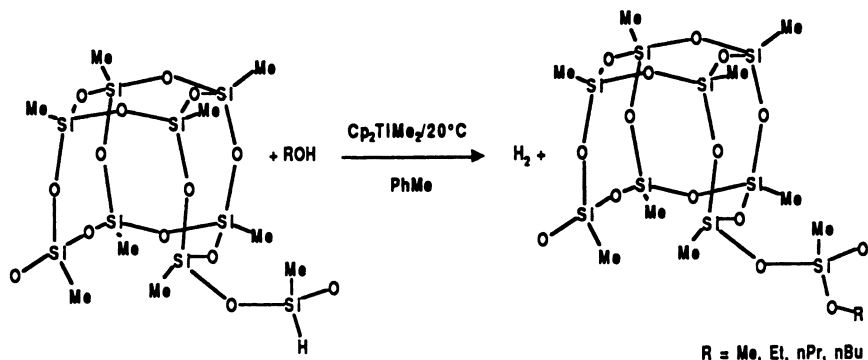
Scheme VI.

definitely. NMR characterization indicates the formation of –[Me(RO)-SiO]$_{0.3}$[MeSi(O)$_{1.5}$]$_{0.7}$– and confirms the initial copolymer composition (*13*). These polymers are actually a masked form of –[MeSi(O)$_{1.5}$]$_x$–. Addition of water leads to hydrolysis of the SiOR bond, and water can be used to cause thermosetting.

The yellow-orange color is typical of a Ti(IV) catalyst and, when coupled with Woo and Tilley's work (*15*), suggests that a Ti(IV) species also promotes the redistribution reaction.

Polysilazane Polymerizations

The success of this catalyst system (*17*) suggested that it might also be used for the catalytic polymerization of polysilazane oligomers such as –[Me-HSiNH]$_x$– or –[H$_2$SiNMe]$_x$–. This application would offer an alternative to the ruthenium catalysts that we previously used to form tractable silicon nitride preceramic polymers. To our surprise, neither oligomer underwent catalytic redistribution when mixed with (η^5-C$_5$H$_5$)$_2$TiMe$_2$, despite the fact that the catalyst reacted and some small amount of gas (presumably CH$_4$) evolved coincident with the reaction.

This result was disappointing. However, we attempted to catalyze redistribution of –[MeHSiO]$_x$– in the presence of –[MeHSiNH]$_x$– to explore the possibility of trapping the –[MeHSiNH]$_x$– oligomer in the resulting silsesquioxane gel. We used ceramic yield as a measure of our success. Thus, Figure 2 shows thermogravimetric analysis (TGA) results for the copolymer derived from –[MeHSiO]$_x$– (74–78% ceramic yield at 900 °C in N$_2$), pure –[MeHSiNH]$_x$– (37% ceramic yield at 900 °C in N$_2$), and a 1:1 mixture of –[MeHSiO]$_x$–:–[MeHSiNH]$_x$–. If the 1:1 mixture were to act simply as a physical mixture, then the ceramic yields for the combination should be the arithmetic mean or 56%. Instead, the ceramic yield is ~72% (Figure 2). This yield suggests that we were successful in trapping the silazane in the interstices of the polymethylsilsesquioxane gel.
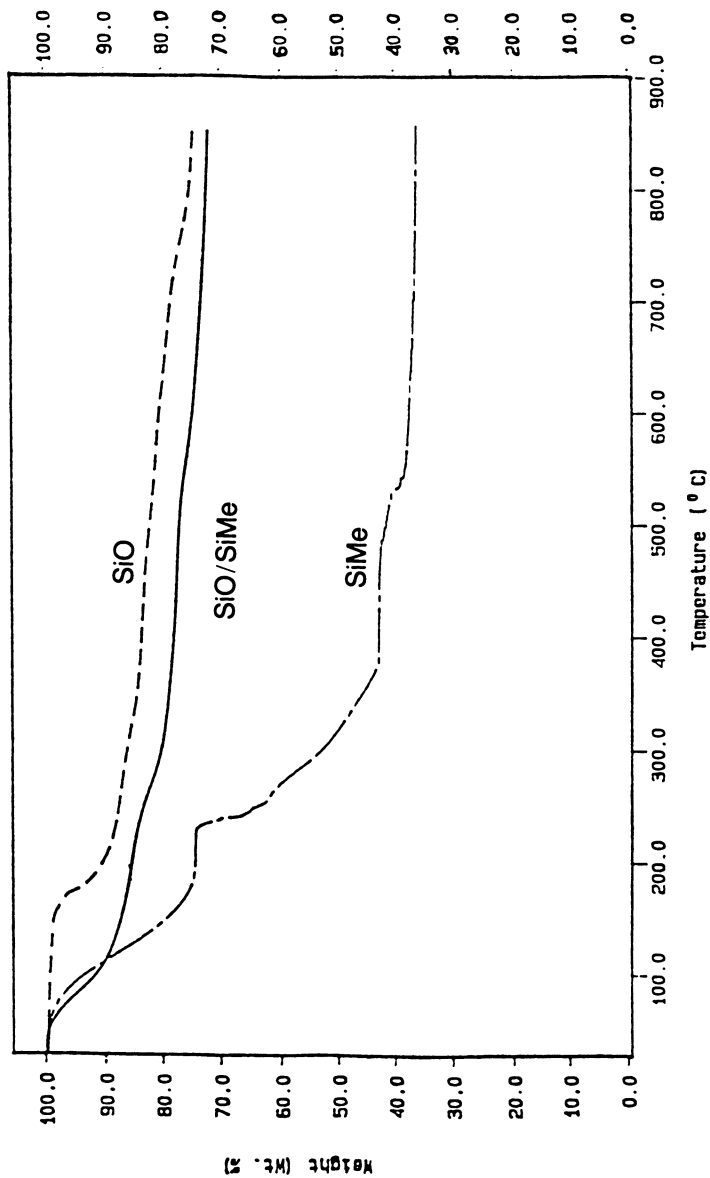
Figure 2. Thermogravimetric analysis of −[MeSi(O)$_{1.5}$]$_x$−, −[MeHSiNH]−, and a 1:1 copolymer of −[MeHSiNH]− and −[MeSi(O)$_{1.5}$]$_x$− pyrolyzed under N$_2$ at a heating rate of 5 °C/min.

An alternative explanation is that, in the presence of hydridosiloxane, the catalyst is capable of catalyzing redistribution of polysilazanes. To test this possibility, we changed the siloxane-to-silazane ratio. Table I shows that as the ratio is changed from 1:1 to 1:3 to 1:18, the reaction continues to occur and the ceramic yields stay high (relative to pure polysilazane). The resulting ceramic products begin to look like the ceramic products obtained from pure –[MeHSiNH]$_x$–. Our preliminary conclusion is that titanium-catalyzed redistribution of –[MeHSiNH]$_x$– requires the presence of some quantity of hydridosiloxane as cocatalyst (17).

Table I. Apparent Ceramic Compositions for Selected Polysilazanes, Polymethylsilsesquioxane, and Various Mixtures

Polymer	Ceramic Yield	Apparent Ceramic Composition		
		Si$_3$N$_4$	SiC	C$_{(excess)}$
MeHSiNH	37	64	25	10
H$_2$SiNMe	63	75	—	18
MeHSiO	78	70 SiO$_2$	20	10
1:1 MeHSiO/MeHSiNH	72	31	20	10
1:3 MeHSiO/MeHSiNH	64	43	20	10
1:9 MeHSiO/MeHSiNH	64	53	22	10
1:18 MeHSiO/MeHSiNH	63	62	19	11

NOTES: Data are given as mol %. Pyrolyzed to 900 °C in nitrogen. Heating rate, 5 °C per min. Apparent ceramic compositions are calculated assuming Si is the limiting element. N is the limiting element when –[H$_2$SiNMe]$_x$– is the preceramic.

The apparent compositions reported in Table I are a form of bookkeeping and are not truly indicative of the actual nature of the SO$_{4-x}$C$_x$ glass (13). However, these compositions are adequate for describing the selectivity to ceramic products, at 900 °C, obtained by pyrolysis of –[MeHSiNH]$_x$– and –[H$_2$SiNMe]$_x$–. The siloxane–silazane mixtures are perhaps better treated as mixtures of silicon oxynitride (Si$_2$ON$_2$ and SO$_{4-x}$C$_x$ or Si$_2$ON$_2$ and silicon nitride–carbide), depending on the percentage of initial hydridosiloxane.

Conclusions

Titanium-catalyzed redistribution of –[MeHSiO]$_x$– provides a useful route to tractable, processable methylhydridosiloxane–methylsilsesquioxane copolymers. The Ti catalyst active in the redistribution reaction will also promote alcoholysis of the resultant copolymers to produce alkoxy derivatives. Such derivatives display equivalent (or slightly better) high-temperature stability and more controllable rheology than the starting copolymer.

Cp$_2$TiMe$_2$ will not catalyze the polymerization of pure –[MeHSiNH]$_x$–. However, in the presence of small amounts of hydridosiloxane it is an active catalyst precursor. It permits catalytic redistribution that leads to a high ceramic yield silicon nitride precursor.

Acknowledgments

We thank the Strategic Defense Sciences Office, Office of Naval Research, for support through ONR contract No. N00014–88–K–0305. R. M. Laine thanks IBM Corporation for partial support of this work. R. M. Laine and J. F. Harrod thank NATO for a travel grant.

References

1. Voronkov, M. G.; Lavrent'yev, V. I. *Top. Curr. Chem.* **1982**, *102*, 199.
2. Feher, F. J.; Newman, D. A.; Walzer, J. F. *J. Am. Chem. Soc.* **1989**, *111*, 1741.
3. Feher, F. J. *J. Am. Chem. Soc.* **1986**, *108*, 3850.
4. Data sheet on GE polyalkylsilsesquioxane (PALS) coatings distributed by General Electric Company.
5. Frye, C. L.; Klosowski, J. M. *J. Am. Chem. Soc.* **1971**, *93*, 4599.
6. Shea, K. J.; Loy, D. A. *Chem. Mater.* **1989**, *1*, 572.
7. January, J. R. U.S. Patent 4 472 510, 1986.
8. White, D. A.; Oleff, S. M.; Boyer, R. D.; Budringer, P. A.; Fox, J. R. *Adv. Ceram. Mater.* **1987**, *2*, 45.
9. White, D. A.; Oleff, S. M.; Fox, J. R. *Adv. Ceram. Mater.* **1987**, *2*, 53.
10. Baney, R. In *Ultrastructure Processing of Ceramics, Glasses, and Composites*; Wiley: New York, 1983; pp 245–255.
11. Harrod, J. F.; Xin, S.; Aitken, C.; Mu, Y.; Samuel, E. Presented at the International Conference on Silicon Chemistry, St. Louis, MO, June 1986.
12. Rahn, J. A.; Laine, R. M.; Zhang, Z. F. Symposium on Polymer-Based Molecular Composites Proceedings of the Materials Research Society **1990**, *171*, 31.
13. Laine, R. M.; Youngdahl, K. A.; Babonneau, F.; Hoppe, M. L.; Zhang, Z. F.; Harrod, J. F. *Chem. Mater.* **1990**, *2*, 464.
14. Curtis, M. D.; Epstein, P. S. *Adv. Organomet. Chem.* **1981**, *19*, 213.
15. Woo, H. G.; Tilley, T. D. *J. Am. Chem. Soc.* **1989**, *110*, 3757.
16. Harrod, J. F. In *Transformation of Organometallics into Common and Exotic Materials: Design and Activation*; Laine, R. M., Ed.; Martinus Nijhoff: Amsterdam, 1988; NATO ASI Series E: Applied Science 141; p 103.
17. Youngdahl, K. A.; Hoppe, M. L.; Laine, R. M.; Harrod, J. F. *Proc. 4th Int. Conf. Ultrastructure Ceram., Glasses, Composites*; Uhlmann, D.; Ulrich, D. R., Eds.; in press.

Model Systems for Catalytic Reactions

Peter M. Maitlis, Futai Ma, Jesus Martinez, Peter K. Byers, Isabel Saez, and Glenn J. Sunley

Department of Chemistry, The University, Sheffield S3 7HF, England

Models for various C–C, C–C–C, and C–C–C–C coupling reactions have been developed, based on results from labeling studies of thermal or oxidative decomposition of the di- and mono-alkyldi-μ-methylenedirhodium complexes [$C_5Me_5Rh(\mu\text{-}CH_2)R$]$_2$ and {[$C_5Me_5Rh(\mu\text{-}CH_2)$]$_2R(L)$}$^+$. Decomposition of the vinyl complex [$C_5Me_5Rh(\mu\text{-}CH_2)(CH{=}CH_2)$]$_2$ leads to very facile methylene–vinyl coupling. These results have led to a proposal for a new mechanism for promoted Fischer–Tropsch polymerization over surfaces, in which the chain carriers are surface alkenyls, not alkyls. The reaction starts at a surface vinyl, formed from a methylene and a methyne. Evidence is presented supporting this mechanism for reactions of CO–H$_2$ over rhodium–ceria catalysts. When $^{13}C_2H_3$ [from labeled Si($^*C_2H_3$)$_4$] is added to a CO–H$_2$ gas stream over Rh–CeO$_2$–SiO$_2$, there is significant incorporation of $^{13}C_2$, and very little of $^{13}C_1$, into the C$_3$ and C$_4$ products. Thus vinyl can be efficiently incorporated into, and can therefore be a key participant in, Fischer–Tropsch polymerization.

DEVELOPMENT OF HIGH-YIELD SYNTHETIC ROUTES to the di-μ-methylenedirhodium complexes **1** [$C_5Me_5Rh(\mu\text{-}CH_2)R$]$_2$ (*1*, *2*), **2** {[$C_5Me_5Rh(\mu\text{-}CH_2)$]$_2R(L)$}$^+$ (*3*), and **3** {[$C_5Me_5Rh(\mu\text{-}CH_2)$]$_2(L)_2$}$^{2+}$ (*34*) (R is alkyl; L is CO, MeCN, etc.) has allowed an exploration of the organic chemistry of dinuclear complexes. We have been especially interested in the reactivity of alkyls and bridging methylenes and their relevance to catalytic C–C coupling and related processes.

Organic Chemistry of Di-μ-methylenedirhodium Complexes

When **1** (R is Me) is decomposed, either thermally (300–350 °C) or oxidatively [Ir(IV) or Fe(III), 20–50 °C], the main organic products are propene and

methane. Labeling experiments using 1 (R is $^{13}CH_3$) showed that the propene was derived from the coupling of two methylenes and one Rh–methyl from one molecule.

The oxidative decomposition of 1 (R is CD_3) led to the formation of $CD_2{=}CHCDH_2$ (>75%). Other D-labeling experiments showed that the methane derives largely from Rh–methyl and μ-methylene hydrogen. This information led to the proposal of a very detailed mechanism for these processes (Scheme I) (5, 6). A key feature is intermediate **A**, which results from a two-electron oxidation of 1 and the simultaneous loss of methane. Internal migration of CD_3 onto μ-CH, followed by a β-elimination of D to Rh, accompanies the formation of Rh-σ-vinyl, which couples with μ-CH_2. This reaction gives Rh-σ-allyl, which reductively eliminates with Rh–D to produce $CD_2{=}CHCDH_2$.
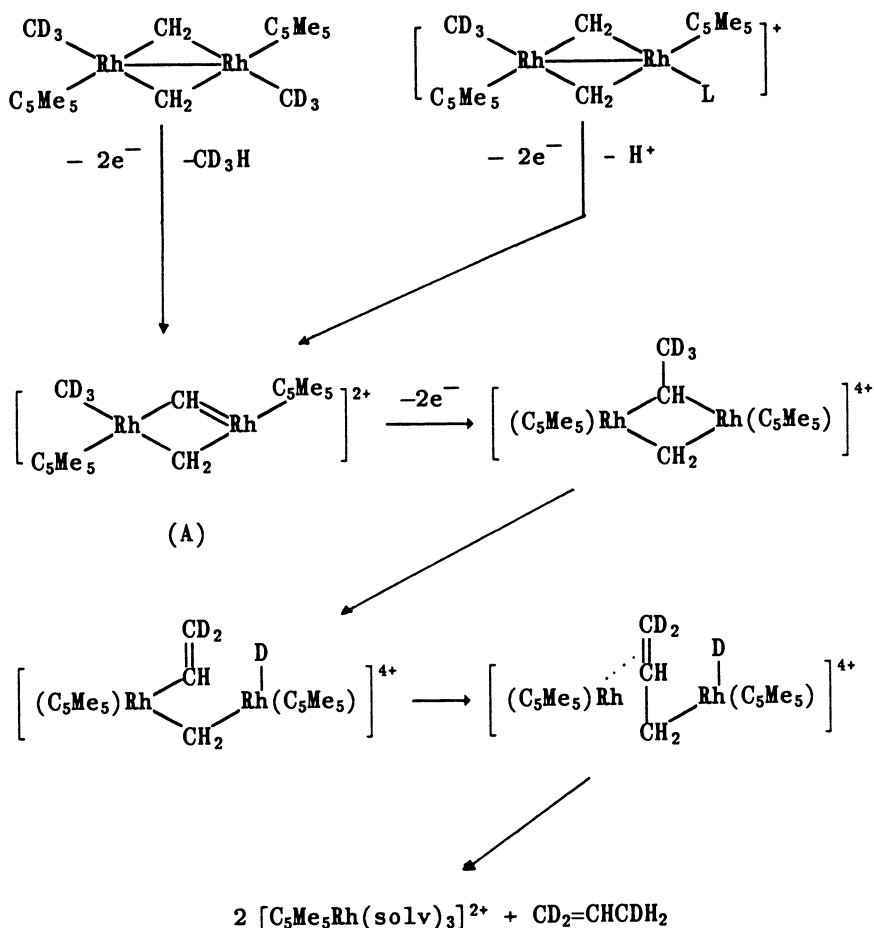
Scheme I. Proposed mechanism for the formation of propene-d_3 from complex 1 (R is CD_3) or 3 (R is DC_3).

A rather similar and even more facile reaction occurs with the cationic complex **2** (R is Me; L is MeCN), where virtually the only organic product is propene (*7*). The alkyl homologs of **1** and **2** (R is ethyl, propyl, etc.) behave similarly (*7*).

Divinyl complex **4**, prepared as illustrated in Scheme II from **1** via dichloride **3**, underwent coupling between vinyl and methylene very easily and cleanly. Thermal decomposition gave propene (88%) and methane (8%). Even reaction with HCl (or HBr) at low temperatures in toluene gave propene (*8, 9*). Silver salts (e.g., $AgBF_4$) oxidatively coupled methylene and vinyl, easily and essentially quantitatively, to give η^3-allyl complex **5** (*9*).

A further interesting transformation is provided by the reaction of the dicarbonyl dication $[\{C_5Me_5Rh(\mu\text{-}CH_2)(CO)\}_2]^{2+}$ (or its equivalent, the diester $[\{C_5Me_5Rh(\mu\text{-}CH_2)(CO_2Me)\}_2]$). In methanol in the presence of Fe(III) they yield methyl acrylate, $CH_2=CHCO_2Me$ (*10*). Again a C–C–C coupling has taken place, but this time the product is an oxygenate.

A New Model for Fischer–Tropsch Reactions

These results led to the development of a new model for the Fischer–Tropsch polymerization (Scheme III) (*11, 12*). The first steps, the formation of surface carbide, surface methyne (CH), and surface methylene (CH_2), are generally accepted features of most mechanisms (*13–16*). However, our model breaks new ground in its treatment of the subsequent C–C bond-formation reactions. The first step is postulated to be a combination of a surface CH and a surface CH_2 to give a surface vinyl ($-CH=CH_2$). Surface vinyls then react with surface methylenes to give allyls, which isomerize to surface alkenyls, which can then add further methylene, etc. The sequence is terminated by the reaction of a surface alkenyl with surface H to give the olefin product.

Organometallic reactions on clusters give models for the first stage (CH plus CH_2 to vinyl) (*17*). Although vinylic species have not yet been unambiguously identified on metal surfaces (*18, 19*), kinetic evidence for the intermediacy of a surface vinyl during the dehydrogenation of chemisorbed ethylene to surface ethylidyne on Pt(111) has been reported (*20*).

$$CHD=CD_2 \text{ (ads)} \rightarrow \text{(surface)}-CD=CD_2 \rightarrow \text{(surface)}C-CD_3$$
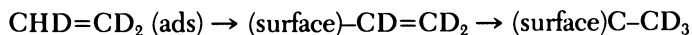
If, as we suggest, surface vinyls (and surface alkenyls) are very reactive intermediates, it is not surprising that they are difficult to detect. This scheme allows ready explanations for

- the formation of α-olefins as the primary products,
- the fact that the amounts of C_2 products formed are often anomalous by comparison with the higher hydrocarbons (they arise, in this scheme, by different routes), and

(1)   (2)

(3)

(4)

(5)
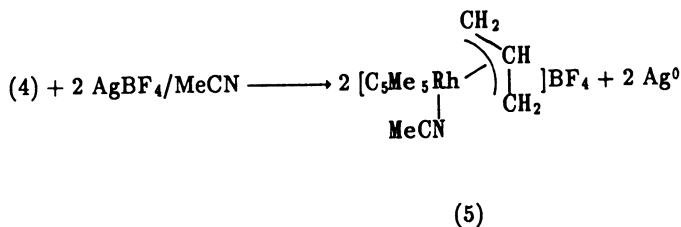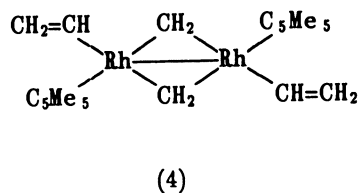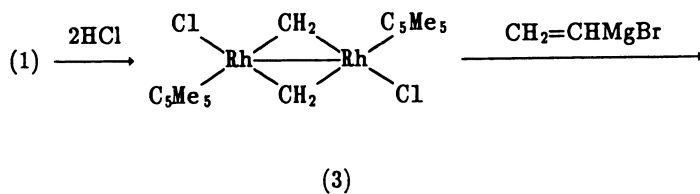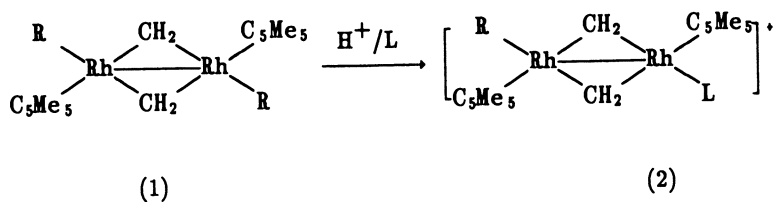
Scheme II. Routes used for the synthesis of the dirhodium-di-μ-methylene complexes 1–4 and the decomposition of 4 to 5.
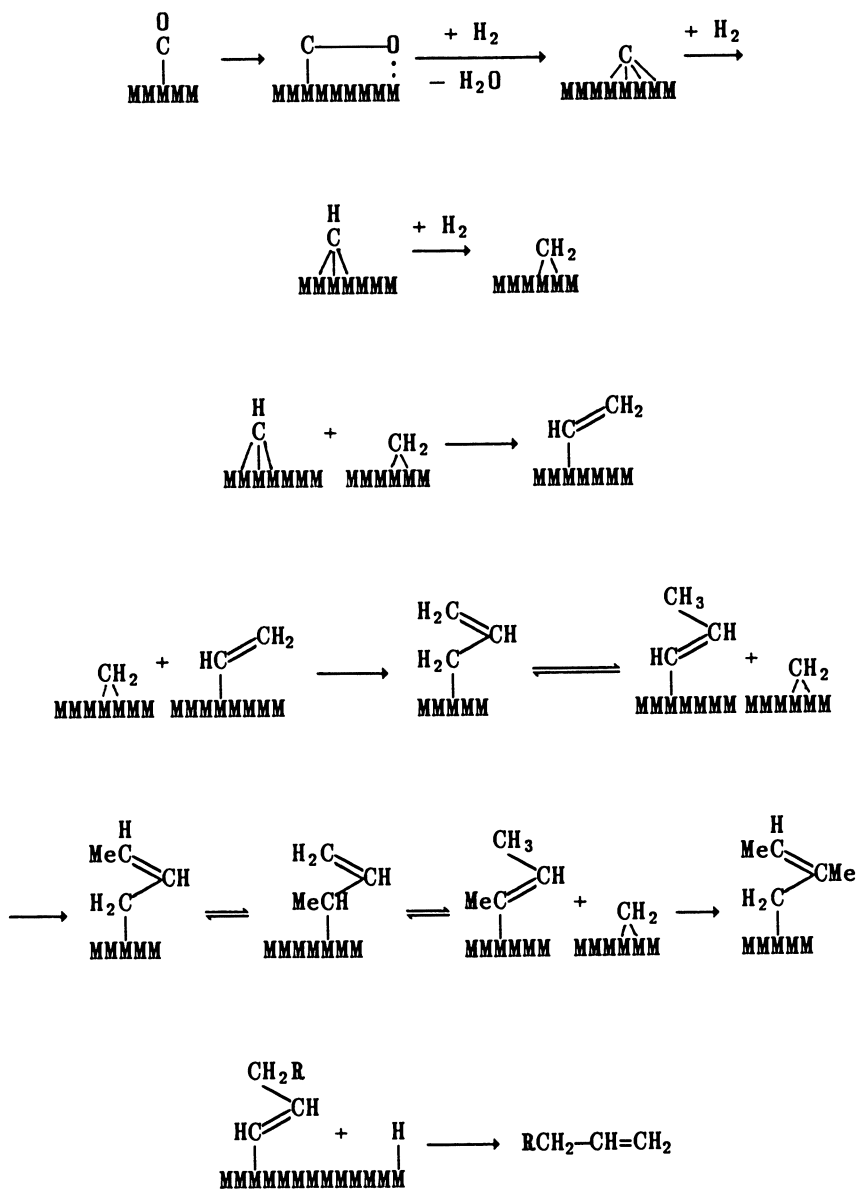
Scheme III. New model for Fischer–Tropsch polymerization. M is monomer.

- the formation of some branched (methyl) hydrocarbons in addition to the normal straight-chain hydrocarbons. Allyls isomerize easily; chain growth can occur at either end, but is easier at an unsubstituted carbon.

Other attempts to answer some of these points have not been totally successful (21–23). For example, most previous Fischer–Tropsch mechanisms require surface alkyls to undergo β-elimination of hydride to give alkenes. That must occur under strongly hydrogenating conditions, so such a step is unexpected, to say the least. To see whether the suggested Fischer–Tropsch mechanism has any validity, we began experiments to test the hypothesis. We therefore studied some reactions in which a $CO-H_2$ mixture (1:2) was passed over supported rhodium.

Experimental Procedures

Labeled Tetravinylsilane. Tetravinylsilane was prepared by a modified literature procedure (24). Labeled vinyl Grignard was made by reacting a 1:1 mixture of vinyl bromide ($^{12}C_2H_3Br$, 0.5 g) and labeled vinyl bromide (99% $^{13}C_2H_3Br$, Matheson of Canada, 0.5 g) with magnesium (0.22 g) in dry tetrahydrofuran (THF) under nitrogen. The reaction was initiated with a trace of 1,2-dibromoëthane. The vinyl Grignard was then treated with silicon tetrachloride (0.24 g) in pentane (3.4 cm³) and gently refluxed (24). Workup gave a solution of labeled tetravinylsilane in THF. The pure labeled $Si(*C_2H_3)_4$ was obtained by preparative GC. Mass spectroscopic and NMR analysis (^1H and ^{13}C) showed that the sample prepared contained 44% $^{13}C_2H_3$.

Preparation of Rhodium and Ceria on Silica Catalyst and Its Use. The rhodium (4 wt %) and ceria (9 wt %) on silica catalyst was prepared by the incipient wetness method. Silica gel (Davisil, grade 645, 60–100 mesh) was successively impregnated with (a) an acidic aqueous solution of cerium(IV) and dried (200 °C), and (b) a methanol solution of rhodium trichloride hydrate. The catalyst was dried at 120 °C in air. It was then transferred to a reactor tube and activated by a temperature-programmed reduction in flowing hydrogen gas (4 °C min⁻¹ to 400 °C). It was held at 400 °C for 4 h and then cooled in hydrogen gas. Carbon monoxide and hydrogen (1:2) were premixed and allowed to flow through the catalyst (1 g, in a fixed-bed microreactor, 6 × 350 mm) at 250 °C, 1 atm, and at a flow rate of 300 cm³ h⁻¹, for 2 h. This procedure led to equilibrium, after which tetravinylsilane (0.5 μL) was injected into the gas stream via a septum. Separate experiments showed that the gases deriving from this pulse exited into a collecting sample tube (25 cm³) after 3 min (15 cm³).

The gases were collected in the sample tube and analyzed by gas chromatography and gas chromatography–mass spectrometry (GC–MS) (Poropak Q; Carlo–Erba chromatograph; Kratos MS–25 mass spectrometer). They were also quantified by reference to authentic samples. The data are presented in Tables I and II.

Table I. Products from Fischer–Tropsch Reactions over Rhodium

Catalyst	CH_4	C_2H_6	C_3	C_4	C_5
Rh (5%)–SiO$_2$	70	6	12	8	5
Rh (5%)–SiO$_2$–Si(Vi)$_4$	60	16	12	9	3
Rh (4%)–SiO$_2$–CeO$_4$	71	12	10	5	2
Rh (4%)–SiO$_2$–CeO$_r$–Si(Vi)$_4$	48	31	10	9	2

NOTE: All values are given in percents. In all cases, only a trace of MeCHO was found. Vi is C_2H_3.

Table II. Labeling Found in Gases from $CO–H_2–Si(^{13}C_2H_3)_n(^{12}C_2H_3)_{4-n}$

Gas	$^{12}C_n$	$^{12}C_{n-1}{}^{13}C_1$	$^{12}C_{n-2}{}^{13}C_2$
Rh–ceria–silica at 250 °C			
Ethane	55	5	40
Propane	80	5	15
Propene	85	5	10
Butene[a]	70	5	20
Rh–silica at 250 °C			
Ethane	50	10	40
Propane	95	3	2
Propene	97	3	
Butene	95	4	1

NOTE: All values are given in percents.
[a] 5% $^{12}C_1{}^{13}C_3H_8$ was found.

First Tests of the Alkenyl Chain-Growth Reaction Mechanism

Although rhodium is generally better at promoting methanation than Fischer–Tropsch reactions, in the presence of various oxide promoters (for example, Ce, La, Mo, Th, Ti, and V) its activity toward the formation of higher hydrocarbons is substantially enhanced. In addition, such catalysts also show some selectivity toward oxygenates (especially ethanol) (25–30). In these preliminary studies we used two catalysts, one with a 5% loading of rhodium on silica (Rochester–McQuire). The other, also made by the incipient wetness method, contained Rh (4%) and CeO$_2$ (9%) on silica. Table I shows the products identified over these catalysts.

To test the hypothesis, tetravinylsilane, $Si(CH=CH_2)_4$, was chosen as a source of vinyl; silicon-containing byproducts should have little effect on the reaction. In some experiments reported in the literature (for example, references 31–33), ethylene (or propene) added to Fischer–Tropsch reaction streams gave somewhat ambiguous results; that is, only small changes in Fischer–Tropsch products were usually seen, and hydroformylation products often dominated. To avoid ambiguity, we used double ^{13}C labeling in our experiments.

Baseline experiments were carried out both with and without the addition of unlabeled tetravinylsilane. Addition of the pulse of $Si(CH=CH_2)_4$ slightly deactivated the catalyst and increased the amount of ethane formed, but appeared to have no other effect on the course of the reaction.

To make the required material, $^{13}C_2H_3MgBr$, diluted with an equal amount of normal $^{12}C_2H_3MgBr$, was reacted with $SiCl_4$. The product, labeled $Si(*C_2H_3)_4$, contained a statistical mixture of $Si(^{13}C_2H_3)_n(^{12}C_2H_3)_{4-n}$ ($n = 0-4$). Pulses of 0.5 μL of this $Si(*C_2H_3)_4$ were introduced into a Fischer–Tropsch gas stream passing through the catalyst (1 atm, 250 °C). The product gases were collected and analyzed by GC–MS for isotopic content.

The data from the reactions with labeled tetravinylsilane are presented in Table II. The values for ethane reflect the hydrogenation of $Si(*C_2H_3)_4$ and show approximately the amount of doubly labeled $^{13}C_2H_6$ expected. The labels in the propene, propane, and butene from the reaction of Rh–SiO$_2$ are not significantly different from natural abundance. This fact indicates only small incorporation of vinyl into these products over that catalyst.

A dramatic difference is shown in the results from the Rh–ceria–silica experiment. The amount of ^{13}C present in the C_3 and C_4 products is close to that expected for natural abundance. However, the amount of $^{13}C_2$ for propene, propane, and butene is very much higher (by ca. 4 orders of magnitude) than natural abundance would predict. This result indicates that labeled vinyl has been incorporated directly into these products (34).

Blank tests showed that tetraethylsilane (SiEt$_4$), injected under similar conditions, had no effect on the reaction at all. It passed straight through the catalyst without reacting, in both the presence and the absence of H$_2$–CO. Thus the reaction we find with vinyl [from $Si(CH=CH_2)_4$] does not occur with ethyl. At this admittedly early stage of the work, we draw the conclusion that, at least in some cases, vinyl can be efficiently incorporated into, and can therefore participate in, Fischer–Tropsch polymerization.

Vinyl incorporation has so far only been found in the Rh–CeO$_2$ experiments. Thus it seems that this type of oligomerization is promoted by a mild cooxidizing site. This result mirrors the model experiments described. The coupling reactions of the ligands in dinuclear complexes 1–4 are very significantly improved with a cooxidant.

Work on other organometallic models, both dinuclear and mononuclear (35–37), and detailed analysis of Fischer–Tropsch kinetics (38) is providing further support for the ideas presented here.

The term "Fischer–Tropsch" refers to a group of processes, not just a single reaction. The products obtained from CO–H$_2$ reactions under different conditions could arise by various routes. For example, the hydrocarbon and oxygenate products from a Fischer–Tropsch reaction over K-promoted iron catalysts have been shown to arise by separate paths (39).

To summarize, model studies have shown that methylenes couple very easily with vinyls (alkenyls) in dirhodium complexes. Labeling studies indicate that a related mechanism, the essential step of which is a coupling of surface methylenes with surface vinyls (or alkenyls), is also useful for understanding at least some Fischer–Tropsch polymerization reactions over rhodium metal. Work is in progress to define these Fischer–Tropsch reactions further and to find out the extent to which such processes occur in other metal systems.

Acknowledgments

References

1. Isobe, K., Vazquez de Miguel, A.; Bailey, P. M.; Okeya, S.; Maitlis, P. M. *J. Chem. Soc., Dalton Trans.* **1983**, 1441.
2. Vazquez de Miguel, A.; Gomez, M.; Isobe, K.; Taylor, B. F.; Mann, B. E.; Maitlis, P. M. *Organometallics* **1983**, 2, 1724.
3. Okeya, S.; Meanwell, N. J.; Taylor, B. F.; Isobe, K.; Vazquez de Miguel, A.; Maitlis, P. M. *J. Chem. Soc., Dalton Trans.* **1984**, 1453.
4. Isobe, K.; Okeya, S.; Meanwell, N. J.; Smith, A. J.; Adams, H.; Maitlis, P. M. *J. Chem. Soc., Dalton Trans.* **1984**, 1215.
5. Saez, I. M.; Meanwell, N. J.; Nutton, A.; Isobe, K.; Vazquez de Miguel, A.; Bruce, D. W.; Okeya, S.; Andrews, D. G.; Ashton, P. B.; Johnstone, I. R.; Maitlis, P. M. *J. Chem. Soc., Dalton Trans.* **1986**, 1565.
6. Saez, I. M.; Meanwell, N. J.; Taylor, B. F.; Mann, B. E.; Maitlis, P. M. *J. Chem. Soc., Chem. Commun.* **1987**, 361.
7. Saez, I. M.; Andrews, D. G.; Maitlis, P. M. *Polyhedron* **1988**, 7, 827.
8. Martinez, J.; Gill, J. B.; Adams, H.; Bailey, N. A.; Saez, I. M.; Maitlis, P. M. *Can. J. Chem.* **1989**, 67, 1698.
9. Martinez, J.; Gill, J. B.; Adams, H.; Bailey, N. A.; Saez, I. M.; Sunley, G. J.; Maitlis, P. M. *J. Organomet. Chem.* **1990**, 394, 583.
10. Saez, I. M.; Andrews, D. G.; Maitlis, P. M. *J. Organomet. Chem.* **1987**, 334, C17.
11. Martinez, J.; Adams, H.; Bailey, N. A.; Maitlis, P. M. *J. Chem. Soc., Chem. Commun.* **1989**, 286.
12. Maitlis, P. M. *Pure Appl. Chem.* **1989**, 61, 1747.
13. Slivinskii, E. V.; Voitsekhovenskii, Yu. P. *Russ. Chem. Rev. (Engl. Transl.)* **1989**, 58, 57.
14. Anderson, R. B. *The Fischer–Tropsch Synthesis*; Academic: London, 1984.
15. Roeper, M. In *Catalysis in C₁ Chemistry*; Keim, W., Ed.; Reidel: Dordrecht, 1983.

16. Sheldon, R. A. *Chemicals from Synthesis Gas*; Reidel: Dordrecht, 1983.
17. Davies, D. L.; Parrott, M. J.; Sherwood, P.; Stone, F. G. A. *J. Chem. Soc., Dalton Trans.* **1987**, 1201.
18. Sheppard, N.; De La Cruz, C. *React. Kinet. Catal. Lett.* **1987**, 35, 21.
19. Sheppard, N. *Annu. Rev. Phys. Chem.* **1988**, 39, 589.
20. Zaera, F. *J. Am. Chem. Soc.* **1989**, 111, 4240.
21. McCandlish, L. E. *J. Catal.* **1983**, 83, 362.
22. Hoel, E. L.; Ansell, G. B.; Leta, S. *Organometallics* **1984**, 3, 1633; **1986**, 5, 585.
23. Hoel, E. L. *Organometallics* **1986**, 5, 587.
24. Rosenberg, S. D.; Walburn, J. J.; Stankovitch, J. D.; Balint, A. E.; Ramsden, H. E. *J. Org. Chem.* **1957**, 22, 1200.
25. Union Carbide. Belg. Patent 824 822, 1975.
26. Ichikawa, M. *J. Chem. Soc., Chem. Commun.* **1978**, 566.
27. Ichikawa, M. *Tailored Metal Catalysts*; Reidel: Dordrecht, 1985; p 183.
28. Gysling, H. J.; Monnier, J.; Apai, G. *J. Catal.* **1987**, 103, 407.
29. Yu-Hua, D.; De-An, C.; Khi-Rui, T. *Appl. Catal.* **1987**, 35, 77.
30. Kieffer, R.; Kiennemann, A.; Rodriguez, M.; Bernal, S.; Rodriguez-Izquierdo, J. M. *Appl. Catal.* **1988**, 42, 77.
31. Watson, P. R.; Somorjai, G. A. *J. Catal.* **1981**, 72, 347.
32. Thivolle-Cazat, J. *Appl. Catal.* **1986**, 24, 211.
33. Kip, B. J.; Hermans, E. G. F.; van Wolput, J. H. M. C.; Haermans, N. M. A.; van Grondelle, J.; Prins, R. *Appl. Catal.* **1987**, 35, 109.
34. Ma, F.; Sunley, G. J.; Saez, I. M.; Maitlis, P. M. *J. Chem. Soc., Chem. Commun.* **1990**, 1279.
35. Doherty, N. M.; Howard, J. A. K.; Knox, S. A. R.; Terrill, N. J.; Yates, M. I. *J. Chem. Soc., Chem. Commun.* **1989**, 638.
36. Colborn, R. E.; Dyke, A. F.; Gracey, B. P.; Knox, S. A. R.; MacPherson, K. A.; Mead, K. A.; Orpen, A. G. *J. Chem. Soc., Dalton Trans.* **1990**, 761.
37. Gibson, V. C.; Parkin, G.; Bercaw, J. E. *Organometallics* **1991**, 10, 220.
38. Santilli, D. S.; Castner, D. G. *J. Energy Fuels* **1989**, 3, 8.
39. Miller, D.; Moskovits, M. *J. Am. Chem. Soc.* **1989**, 111, 9250.

Active Sites in Soluble Ziegler Polymerization Catalysts Generated from Titanocene Halides and Organoaluminum Lewis Acids

J. J. Eisch and K. R. Caldwell

Department of Chemistry, State University of New York at Binghamton, Binghamton, NY 13902

By means of X-ray single-crystal data the Ti–C and Ti–Cl bond lengths in trimethylsilylmethyltitanocene chloride (11) have been determined. The operation of σ-hyperconjugation in this compound leads to an unusual shortening of the Ti–C bond. In solution the observed shifts in the ^1H NMR signals of the CH_2 or the cyclopentadienyl (Cp) groups of 11 are attributed to varying degrees of coordinative solvation of the titanium center or hydrogen bonding at the chlorine center. Such inherent polarity of the Ti–Cl bond in 11 has been found to be sharply accentuated by the introduction of a Lewis acid, $AlCl_2R$. By monitoring such reaction mixtures by ^1H, ^{13}C, and ^{27}Al NMR spectroscopy, direct evidence is obtained for the generation of the alkyltitanocenium ion, Cp_2RTi^+, and $AlCl_4^-$. Such combinations of 11 and Lewis acid are effective catalysts for the polymerization of ethylene, and Me_3Si fragments from 11 are found in the resulting polyethylene. These findings support the thesis that Cp_2RTi^+ ions are the active polymerization sites in such Ziegler catalyst systems.

T HE NATURE OF OLEFIN POLYMERIZATION CATALYSTS formed from combinations of titanium halides and alkylaluminum halides has remained the subject of controversy (1) since the epoch-making discoveries of Ziegler et al. (2) and of Natta et al. (3) some 35 years ago. Much of the difficulty in

understanding the molecular basis for such Ziegler–Natta catalysis lies in the heterogeneous character of the subvalent titanium halides generated by reduction of $TiCl_4$ with the aluminum alkyl (4). For this reason, mechanistic studies have often employed a soluble ethylene polymerization catalyst, which results from the interaction of titanocene dichloride and alkylaluminum halides (4).

First introduced by Breslow and Newburg (5), this system has been shown to contain tetravalent titanium in the active catalyst (6, 7), as well as cationic titanocene ions (8). It exhibits accelerated polymerization of ethylene in dipolar halocarbons, CH_nCl_{4-n}, over that shown by aromatic hydrocarbons (9). Furthermore, equilibrium and kinetic (10) studies have demonstrated that the catalyst components, Cp_2TiCl_2 (1, Cp is cyclopentadienyl) and $RAlCl_2$ (2), are not themselves the active catalyst partners. Rather, they are converted into the active catalyst (4, eq 1), which to an undetectable extent is in equilibrium with a 1:1 complex (3) of 1 and 2.

$$Cp_2TiCl_2 \quad + \quad RAlCl_2 \quad \rightleftharpoons \quad 3 \quad \rightleftharpoons \quad 4 \qquad (1)$$
$$\quad 1 \qquad\qquad\qquad 2$$
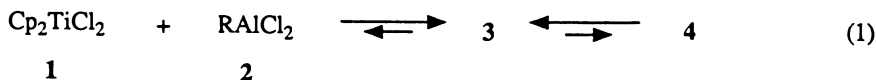
What the structures of 3 and 4 might be was unknown. Hence, nothing certain could be concluded about the relative roles of the titanium and aluminum centers in such Ziegler polymerization.

Our approach to clarifying the mechanism of Ziegler ethylene polymerization has been to attempt the isolation or chemical interception of intermediates 3 and 4 and to elucidate the structures of the crystalline products (11). Especially for 4, which exists at equilibrium in low concentrations, chemical trapping proved to be the only feasible way to identify its structure. With the assumption that 4 contained either a Ti–C or an Al–C bond into which the ethylene units were inserted during polymerization, we searched for a surrogate for ethylene that would readily perform the first insertion but, because of steric hindrance, would not undergo a further insertion. Polymerization thus would not ensue so that the initial insertion product 6 might then be isolated and its structure determined. After considerable evaluation of potential ethylene surrogates (12), we found trimethylphenylethynylsilane (5) to be an eminently suitable trapping agent (eq 2).

$$R-M \quad + \quad Ph-C\equiv C-SiMe_3 \quad \xrightarrow{\text{fast}}$$
$$\quad 4 \qquad\qquad\quad 5$$

$$\begin{array}{c} Ph \diagdown \qquad \diagup SiMe_3 \\ C=C \qquad\qquad \xrightarrow[\text{slow}]{\text{very}} \quad \text{polymer} \qquad (2) \\ R \diagup \qquad \diagdown M \\ \qquad 6 \end{array}$$
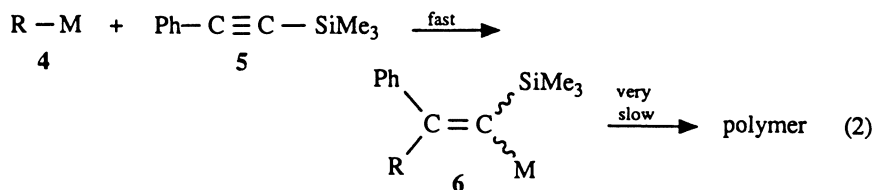
Thus, by admixing Cp_2TiCl_2 and $MeAlCl_2$ (2a) in chloroform, we isolated crystalline 3a and showed by X-ray crystallography that it was a monochloro

bridged complex. Similarly, the interaction of 1, 2a, and 5 in chloroform led to the precipitation of 6a.

3a

6a
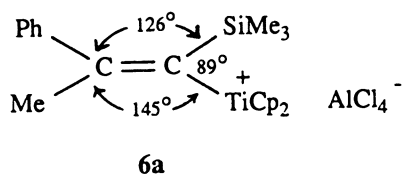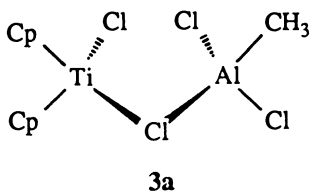
The bridging Ti–Cl bond in **3a** is only about 0.20 Å longer than the nonbridging Ti–Cl bond, and the Si–C–Ti angle in **6a** is astonishingly acute, 89° (*11*).

From the structure of **6a** one can deduce that the surrogate of ethylene, **5**, has undergone a stereoselective and regioselective insertion into **4** and that therefore **4** must be methyltitanocenium(IV) tetrachloroaluminate. The sequence of equilibria leading from the catalyst components **1** and **2a** is therefore shown in eqs 3–5.

$$Cp_2TiCl_2 \; + \; MeAlCl_2 \; \rightleftarrows \; Cp_2Ti \overset{Cl}{\underset{Cl}{\diagdown}} AlMeCl_2 \tag{3}$$

1   **2a**   **3a**

$$\textbf{3a} \; \rightleftarrows \; Cp_2Ti \overset{Me}{\underset{Cl}{\diagdown}} AlCl_3 \tag{4}$$

                                     7a

$$\textbf{7a} \; \overset{S}{\rightleftarrows} \; Cp_2TiMe^+ \quad AlCl_4^- \tag{5}$$

                                         4
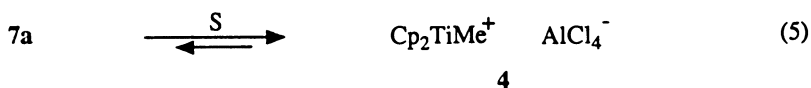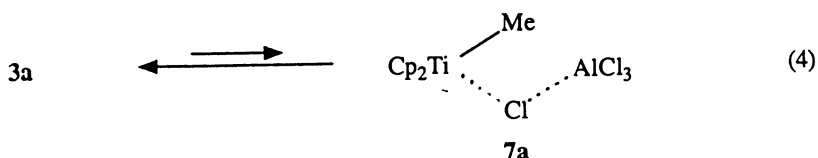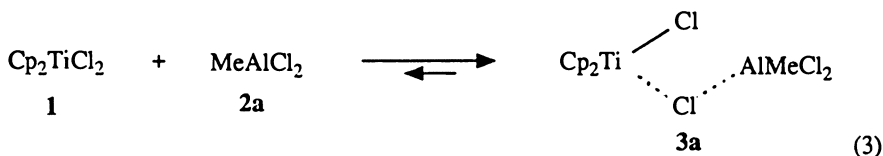
The active catalyst center is the titanocenium ion in **4**. This fact explains the following experimentally observed characteristics of this catalyst system:

- the necessity of tetravalent titanium (*6, 7*);
- the formation of titanium cations (*8*);
- the accelerating effect of polar aprotic solvents (CH_nCl_{4-n}) on the polymerization, compared with that of aromatic hydrocarbons (*9*), whereby such polar solvents (S) would aid the necessary ionization postulated in eq 5;

- the retarding or inhibiting effect of Lewis bases on the polymerization or carbotitanation by **4**, because the cationic site would thereby be solvated;
- the equilibria and kinetics of complexes formed between **1** and **2** (*10, 11*); and
- the stereoselectivity and regioselectivity with which **4** adds to phenylethynylsilane **5**.

As to this last point, Cp_2TiMe^+ would be expected to attack the methyne carbon α to Me_3Si preferentially, because the transition state **8a** can be stabilized by Si–C bond σ-hyperconjugation (**8b**) (*11, 13*).
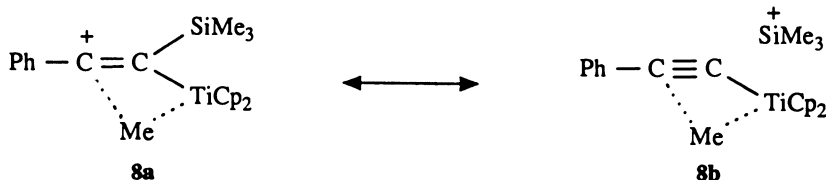
The stereoselective addition of the methyl *syn* to the Cp_2Ti group would likewise be favored by the bridging transfer of the methyl between the titanium and the β-methyne carbon (**8a**).

Remarkably, the stabilizing electronic effect of the Me_3Si group on a β carbenium ion (**8a**) overrides the destabilizing steric repulsion of the large Me_3Si and Cp_2Ti groups for each other and, in spite of this, places them on the same carbon in **6a**. Furthermore, this stabilizing influence of the Me_3Si group to a positive charge β to it is manifest also in the structure of **6a** itself. Examination of the actual bond angles about the formally sp^2 carbon α to Ti reveals that the expected C_1–C_2–Ti angle of ~120° has widened to 145°. The change brings the bulky Me_3Si and Cp_2Ti surprisingly closer to each other. Although an agostic (bonding interaction of the methyl group's hydrogens with the titanium center) attraction might be responsible for a change in angle, no experimental data (such as Si–C–H bond lengths) are available to support such a view. A more straightforward explanation is that Si–C bond hyperconjugation with a vacant 4p orbital of the titanocenium cation may change the hybridization at C_1 toward sp (**6**).
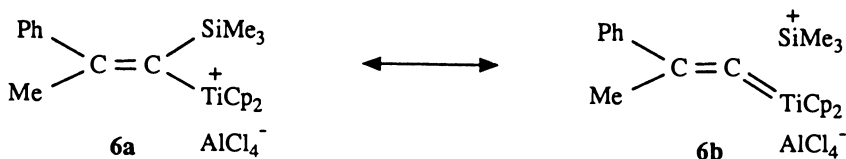
In our continuing studies of this soluble Ziegler catalyst system, therefore, we investigated the equilibria connected with the formation of the methyltitanocene chloride (**9**) from **1** and **2a** (eq 4, as its complex with $AlCl_3$) and its ionization into the methyltitanocenium cation (**10**). Our previous studies had shown how effective a Me_3Si group can be in stabilizing a β positive charge. Therefore, we used trimethylsilylmethyltitanocene chloride (**11**) in our work, in the hope that its corresponding cation (**12**) would be sufficiently more stabilized to permit its direct observation.

$$Cp_2Ti\overset{CH_3}{\underset{Cl}{\big<}} \qquad Cp_2\overset{+}{Ti}-CH_3 \qquad Cp_2Ti\overset{SiMe_3}{\underset{Cl}{\big<}}CH_2 \qquad Cp_2\overset{+}{Ti}-CH_2{\big\diagup}^{SiMe_3}$$

$$\mathbf{9} \qquad\qquad\qquad \mathbf{10} \qquad\qquad \mathbf{11} \qquad\qquad\qquad \mathbf{12}$$
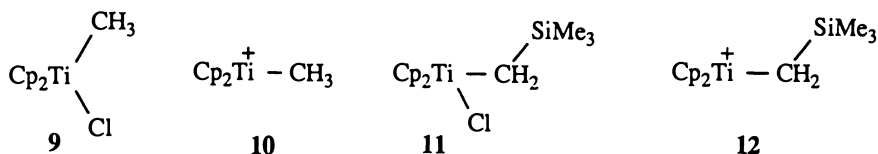
Experimental Details

General Techniques and Instrumentation.   All reactions were carried out under argon with standard inert-atmosphere techniques (*14, 15*). Manipulations of the titanocene derivatives and the methylaluminum chlorides or aluminum chlorides were designed to protect these oxygen- or moisture-sensitive reagents from contamination and decomposition (*14*). Solvents and reagents were purified with similar methodology (*14*). NMR analyses were performed on a Bruker model AM-360 instrument. The ^1H, ^{13}C, and ^{27}Al NMR spectra were recorded at 360.5, 90.6, and 93.9 MHz, respectively. The ^1H and ^{13}C chemical shifts were measured relative to solvent and are reported relative to tetramethylsilane. The ^{27}Al chemical shifts are reported relative to external $AlCl_3 \cdot 6D_2O/D_2O$. Mass spectral (MS) data were obtained on a Hewlett Packard model MS/902 CIS instrument. Infrared spectra were recorded on a Perkin-Elmer model 1420 ratio-recording infrared spectrometer.

Chlorobis(η^5-2,4-cyclopentadien-1-yl)trimethylsilylmethyltitanium, $Cp_2Ti(Cl)$-$CH_2Si(CH_3)_3$, was prepared by a modification of a published procedure (*16*). Trimethylsilylmethylmagnesium chloride in Et_2O (25 mL, 0.90 M, 22 mmol, 1.1 equiv; Aldrich) was added with stirring over a 20-min period to a solution of Cp_2TiCl_2 (4.98 g, 20.0 mmol) in CH_2Cl_2 at ambient temperature. The reaction was allowed to continue for 2.0 h. A ^1H NMR analysis of a sample of the reaction mixture showed 99% conversion to product.

The solvent was removed in vacuo, and the residue was redissolved in toluene (250 mL). The suspension was filtered through a glass frit with a Celite 450 pad (an industrial grade of diatomaceous earth). The filtrate was concentrated to about 125 mL and then kept at –10 °C for several days. The mother liquor was withdrawn via a cannula from the flask containing the orange-red crystalline product. The product was washed with 25 mL of cold hexane and then dried in vacuo for 1.0 h. Yield: 3.41 g (11.3 mmol, 56.5%); mp 147.1–148.7 °C (under Ar).

Chlorobis(η^5-2,4-cyclopentadien-1-yl)methyltitanium, $Cp_2Ti(Cl)CH_3$, was prepared by a modification of published methods (16, 17). Titanocene dichloride (4.82 g, 19.4 mmol) was dissolved in 250 mL of CH_2Cl_2. The solution was cooled to about –20 °C (CCl_4–dry ice bath). Methylmagnesium chloride in tetrahydrofuran (6.6 mL of a 2.95 M solution, 20 mmol, 1.0 equiv; Aldrich) was added over a 20-min period with stirring. After an additional 60 min of stirring at –20 °C, the reaction mixture was allowed to warm to ambient temperature. Solvent was removed via rotary evaporation. The solid residue was pulverized and then extracted with three 250-mL portions of hexane (previously dried by stirring with silica gel and activated Linde Type 4A molecular sieves for at least 4 h).

The solution containing the product was filtered, and hexane was removed via rotary evaporation. The red-orange product was dried in vacuo for 4 h at 25 °C. Additional $Cp_2Ti(Cl)CH_3$ was isolated by further extraction of the solid residue. Isolated yield: 1.83 g (8.1 mmol, 42%); mp 150–155 °C (decomp., under Ar).

Complex Formation.   The reactions of Cp_2TiRCl with $AlCl_3$ were effected by the addition of $AlCl_3$ to a solution containing the alkyltitanium compound at the desired temperature; rapid stirring ensured rapid reaction of the heterogeneous mixture. The reactions of Cp_2TiRCl with $MeAlCl_2$ were typically carried out by the rapid addition (via a cannula) of a solution of $MeAlCl_2$ in the reaction solvent to a vigorously stirred solution of the organotitanium compound. Initial concentrations of the Ti compound were in the 0.01–0.3 M range. Upon reaction with the Lewis acid, the initially orange-red solutions turned deep red, maroon, or brown-red. Samples were withdrawn via a cannula and analyzed by NMR spectroscopy.

Ethylene Polymerizations.   Solutions of $Cp_2Ti(Cl)CH_2Si(CH_3)_3$ (0.32 g, 1.1 mmol) in 50 mL of $CHCl_3$ or $Cl(CH_2)_2Cl$ were treated with 1.0 equiv of $AlCl_3$ or $MeAlCl_2$ at 0 °C. The dark red, homogeneous solutions were transferred to a 250-mL Fischer & Porter pressure bottle containing a magnetic stirring bar. The bottle was pressurized to 30 psig of ethylene at 0 °C. Polymerizations were allowed to proceed, with stirring, for 1.5 h. The reactions were quenched by the addition of 100 mL of 0.5 N aqueous HCl. The polymer was isolated from the aqueous–organic interface, washed with acetone, dried, weighed, and analyzed by MS and IR spectroscopy.

Results

Structure of Methyltitanocene Chloride (9) and Trimethylsilylmethyltitanocene Chloride (11).

Both of these compounds were previously described and were readily prepared from titanocene dichloride and the appropriate alkylmagnesium chloride. We were very interested in detailed X-ray structural data, which could not be found in the literature. Structure determinations of both compounds were attempted but a successful X-ray analysis proved possible only with 11; crystal disorder in 9 prevented a refinement of the Ti–Me bond distance (18). However, the bond distance between titanium and the formally sp^3-hybridized carbon of the groups in bis(η^5-cyclopentadienyl) bis(η^1-cyclopentadienyl)titanium is 2.332 Å.

In light of this value, the observed titanium–methylene bond in tri-methylsilylmethyltitanocene chloride (**11**), which involves a formally sp^3-hybridized carbon and has a value of 2.166 Å, must be considered as markedly shortened by the presence of the Me_3Si group on the α-carbon. This bond shortening may be a manifestation of σ-bond hyperconjugation (cf. **6a** and **6b**).
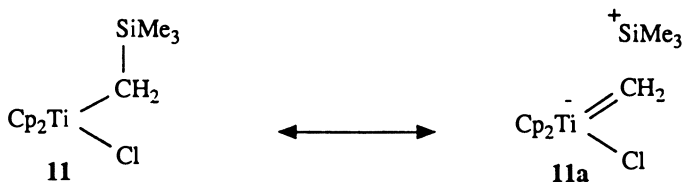
Some further commentary on the precisely known structure of **11** is in order. A stereoscopic view of **11** and important bond angles and distances are provided in Figure 1. A space-filling molecular model is given in Figure 2. Noteworthy characteristics in the structure of **11** are the abnormally large $Ti–CH_2–Si$ angle (137°), the *anti* conformation of the Me_3Si groups with respect to the Ti–Cl bond, and a $Ti–CH_2$ bond length (2.166 Å) more in keeping with a π-bonded $Ti–CH_2$ system than a simple σ-bonded Ti–C linkage, as in Cp_2TiPh_2 (2.27 Å) or $Cp_2Ti(\eta^1\text{-}Cp)_2$ (2.33 Å).

To learn what effect the polarity of the solvent might have on the chemical shifts of the CH_2 and Cp protons in the ^1H NMR spectrum of **11**, a series of halocarbon, aromatic, and dipolar coordinating solvents was investigated. The results are tabulated in Table I. The data indicate that solvent polarity has a decided, but not necessarily linear, effect on both chemical shifts. As will be discussed later in this chapter, solvation of the titanium or chlorine center may influence the polarization of the Ti–Cl bond (eq 6).

HS = hydrogen-bonding solvent

S = donor solvent

δ^+, δ^- = partial charges

$$\tag{6}$$
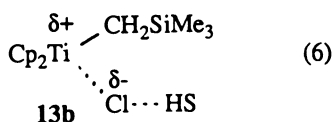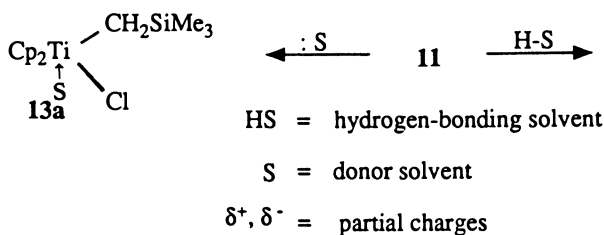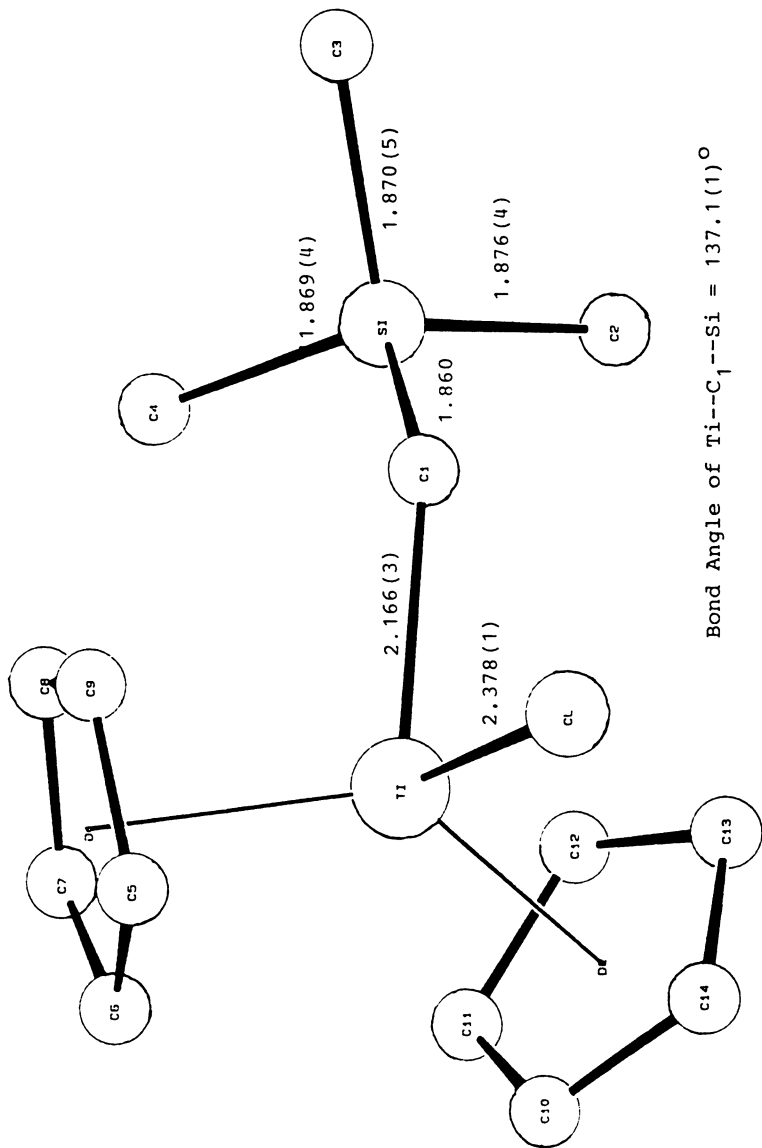
Figure 1. Stereoscopic view of trimethylsilylmethyltitanocene chloride (11) with important bond angles and distances.
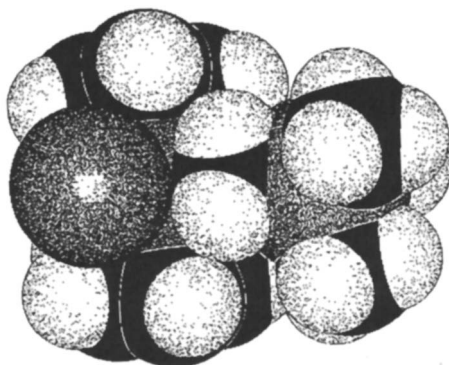
Figure 2. Space-filling Stuart–Briegleb molecular model of trimethylsilyl-methyltitanocene chloride (11).

Table I. Solvent Dependence of the ¹H NMR Chemical Shifts of Cp₂Ti(Cl)CH₂SiMe₃

Solvent	Dipole Moment (D)[a]	δ, Cp[b]	δ, CH₂[b]
Halocarbon			
CCl₄	0	6.24	2.02
CDCl₃	1.01	6.32	2.25
CH₂Cl₂	1.60	6.31	2.16
CH₂ClCH₂Cl	2.06	6.32	2.12
Aromatic			
C₆H₆	0	5.88	2.14
1,3,5-Me₃C₆H₃	0	5.80	1.90
C₆H₅CD₃	0.36	5.85	2.04
C₆H₅Cl	1.69	6.08	2.13
1,2-C₆H₄Cl₂	2.50	6.16	2.11
Dipolar Aprotic			
(CD₃)₂CO	2.88	6.41	2.02
CD₃CN	3.44	6.37	2.09
(CD₃)₂SO	3.90	6.40	1.96
OP(NMe₂)₃	5.54	6.49	1.83

[a] Gas-phase dipole moment, from the *CRC Handbook of Chemistry and Physics*, 58th ed., 1977.
[b] All values are chemical shifts relative to Me₄Si in parts per million.

Interaction of Trimethylsilylmethyltitanocene Chloride (11) and Aluminum Chlorides. Compound 11 was treated with 1 equiv of $AlCl_3$ in a variety of solvents at different temperatures. Multinuclear NMR measurements were made by the Fourier transform technique. Of particular interest with ^1H and ^{13}C spectra were the positions of the signals for the CH_2 and Cp groups. Spectral data for these measurements are compiled in Table II. Most informative were the ^{27}Al NMR spectra of 11 with $AlCl_3$, which were measured at –23 °C in 1,2-dichloroethane. Within a minute of admixing, four peaks were evident in the ^{27}Al spectrum [δ (%, peak width at half height in hertz)]: 103.3 (51; 268), 99.1 (4; 26), 98.1 (10; 63), and 66 (35; 3200). With time the broad peak at 66 Hz grew at the expense of the peak at 103.3 Hz. The peak at 103 Hz is most likely the $AlCl_4^-$ ion (19).

Table II. Chemical Shifts Observed by Interaction of $Cp_2Ti(Cl)CH_2SiMe_3$ with Me_nAlCl_{3-n}

Me_nAlCl_{3-n}	^1H, Cp	^1H, CH_2	$^{27}Al^a$
No Me_nAlCl_{3-n}	5.88 (PhH)	2.14	—
$AlCl_3$ (1 equiv)	6.05 (PhH)	3.01	—
	6.19[b] (PhH)	—	—
No Me_nAlCl_{3-n}	6.32 ($CDCl_3$)	2.26	—
$AlCl_3$ (1 equiv)	6.51 ($CDCl_3$)	3.04	—
	6.64[b] ($CDCl_3$)	—	—
No Me_nAlCl_{3-n}	5.88 (PhH)	2.14	—
$MeAlCl_2$ (1 equiv)	5.98 (PhH)	2.92	—
No Me_nAlCl_{3-n}	6.32 ($CDCl_3$)	2.26	—
$MeAlCl_2$ (1 equiv)	6.42 ($CDCl_3$)	2.70	—
No Me_nAlCl_{3-n}	6.33 (CH_2ClCH_2Cl)	2.12	—
$AlCl_3$ (1 equiv)	6.53 (CH_2ClCH_2Cl)	—[c]	103.3 (51)
	6.69[b] (CH_2ClCH_2Cl)		99.1 (3)
			98.1 (10)
			65.8 (35)

NOTE: All values are relative to Me_4Si in parts per million. Dashes mean no data are available for these cases.
[a] A solution of $AlCl_3$ in D_2O was used as an external reference.
[b] Signal is attributable to the formation of some Cp_2TiCl_2.
[c] Because 90% of 11 was converted to Cp_2TiCl_2 under these conditions (signal at 6.69 ppm), only 10% of the proposed cation, $Cp_2TiCH_2SiMe_3^+$, was present.

The new methylene ^1H NMR peak in the reaction mixture at 3.01 ppm (C_6H_6, $CDCl_3$, or CH_2Cl_2) or at 4.08 ppm (toluene) is most likely due to the $Me_3Si–CH_2$ group adjacent to a titanocenium cation. In the ^{13}C NMR spectrum the carbon signals for Cp, CH_2, and CH_3 in 11 at 115.6, 79.8, and 2.8 ppm appeared after reaction with $AlCl_3$ at 117.2 and 2.8 ppm; the former signal at 79.8 ppm disappeared. After long reaction times ^1H and ^{13}C NMR signals characteristic of $Cp_2TiCl_2 \cdot Me_3SiCH_2AlCl_2$ (15) were observed (^1H: 6.64, –0.07, and –0.61; ^{13}C: 120.7, 0.1 ppm) (eq 7).

$$
\underset{\textbf{11}}{Cp_2Ti{\Big<}\overset{\overset{\textstyle SiMe_3}{|}}{\underset{Cl}{CH_2}}} \quad \xrightarrow{\;AlCl_3\;} \quad \underset{\textbf{14}\quad AlCl_4^-}{Cp_2\overset{+}{Ti}-CH_2\overset{SiMe_3}{\diagup}} \quad \longrightarrow
$$

$$
\underset{\textbf{15}}{Cp_2Ti{\Big<}\overset{\textstyle Cl}{\underset{Cl}{\cdots}}{\Big>}\underset{}{AlCl_2}\overset{CH_2SiMe_3}{\overset{|}{}}} \tag{7}
$$
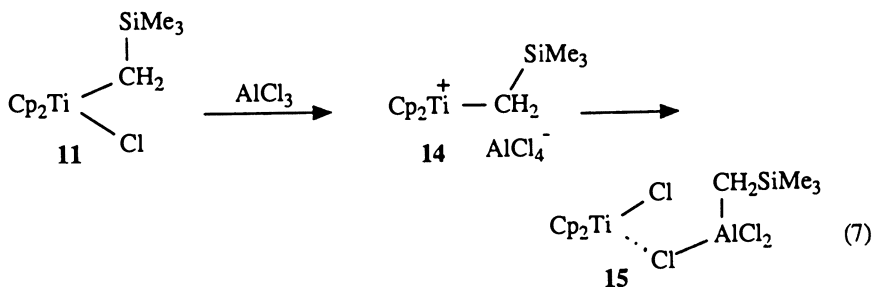
When compound **11** was treated with 1 equiv of MeAlCl$_2$ in benzene or in CDCl$_3$, the methylene protons in **11** were shifted downfield (2.14 → 2.92 in C$_6$H$_6$ and 2.26 → 2.70 ppm in CDCl$_3$). In both cases, a considerable proportion of Cp$_2$TiCl$_2$ was formed with time (eq 8).

$$
\underset{\textbf{11}}{Cp_2Ti{\Big<}\overset{\overset{\textstyle SiMe_3}{|}}{\underset{Cl}{CH_2}}} \quad \xrightarrow{\;MeAlCl_2\;} \quad \underset{\textbf{16}\quad AlMeCl_3^-}{Cp_2\overset{+}{Ti}-CH_2\overset{SiMe_3}{\diagup}} \quad \longrightarrow
$$

$$
Cp_2Ti{\Big<}\overset{\textstyle Cl}{\underset{Cl}{\cdots}}{\Big>}\underset{}{AlMeCl}\overset{CH_2SiMe_3}{\overset{|}{}} \tag{8}
$$
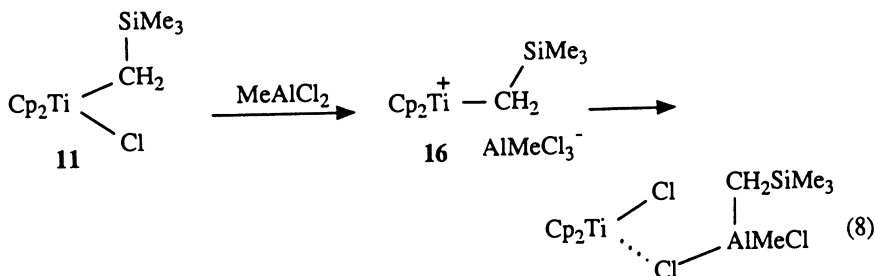
Interconversions with the Titanocene Dichloride–Methylaluminum Dichloride System.

Spectroscopic monitoring (*10*) and X-ray crystallography (*11*) have established that, in chloroform, **1** and **2a** form a bridged complex (**3a**). By admixing MeAlCl$_2$ with **1** with different solvents and in different ratios, evidence was sought on whether other 1:1 complexes could be generated and whether the equilibrium suggested in eq 4 could be driven to the right for detection of Cp$_2$TiMeCl. Furthermore, it was hoped that by admixing Cp$_2$TiMeCl and AlCl$_3$, the equilibrium hypothesized in eq 4 could be approached from the reverse direction.

Although **3a** is the main complex formed between **1** and **2a** in chloroform solution, the same two components in benzene solution show the presence of 75% of **3a**, 20% of uncomplexed Cp$_2$TiMeCl (**17**), and 5% of what may be Cp$_2$Ti$^+$Me AlCl$_4^-$ (**18**) (eq 9).

In benzene the methyl protons of **3a**, **17**, and **18** occur at –0.01, 0.87, and 1.20 ppm, respectively. The Cp protons are exhibited at 5.89, 5.89 (broad), and 5.68 ppm (*20*).

$$Cp_2TiCl_2 \quad + \quad MeAlCl_2 \quad \longrightarrow$$

$$Cp_2Ti \underset{Cl}{\overset{Cl}{<}} \cdots AlMeCl_2 \quad + \quad Cp_2Ti \underset{Cl}{\overset{Me}{<}} \qquad (9)$$
$$\textbf{3a} \qquad\qquad \textbf{17}$$

$$Cp_2TiMe^+ AlCl_4^-$$
$$\textbf{18}$$
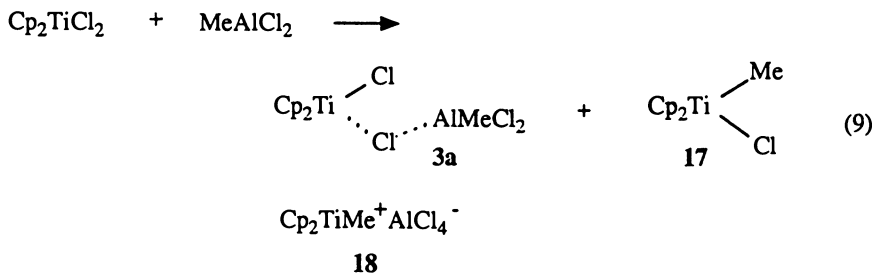
From mixtures of **1** and **2a** in benzene a brownish-red solid could be separated, which upon dissolution in $CHCl_3$ yielded a ^1H NMR spectrum exhibiting the benzene peak (7.33 ppm) and the Cp_2TiCl_2 peak (6.51 ppm) in a 1:1 ratio. In addition, weak peaks in the Me–Al region (–0.57, –0.02, and –0.57 ppm) were observed. Thus it appears that **3a** or an isomer (**3a′**) forms a weak π-complex with benzene.

$$Cp_2Ti \overset{+}{\underset{C_6H_6}{<}} \overset{Cl}{\phantom{<}} AlMeCl_3^- \qquad or \qquad Cp_2Ti \overset{+}{\underset{C_6H_6}{<}} \overset{Me}{\phantom{<}} AlCl_4^-$$

3a (solvate)   **3a′** (solvate)
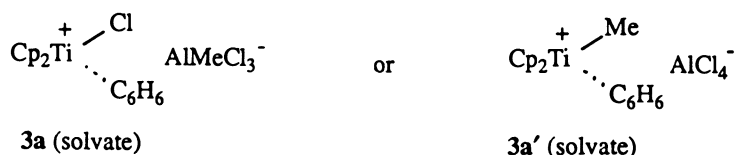
Admixing methyltitanocene chloride and $AlCl_3$ in 1:1 ratio in $CHCl_3$ gave mainly complex **3a**. This product shows that the equilibrium in eq 4 lies preponderantly to the left (^1H NMR signals in the product: Cp, 6.89; Me, –0.31 ppm). Admixing methyltitanocene chloride (**17**) with 1 equiv of $MeAlCl_2$ at 25 °C in $CDCl_3$ gave as the principal product a titanocene derivative whose CH_3 group had been shifted downfield from that in **17** (^1H: 0.82 → 1.13; ^{13}C: 50.3 → 59.5 ppm), as had its Cp group (^1H: 6.26 → 6.71; ^{13}C: 115.7 → 117.6 ppm). These shifts are consistent with ion-pair formation (**19**) (eq 10).

$$Cp_2Ti \overset{Me}{\underset{Cl}{<}} \xrightarrow{MeAlCl_2} Cp_2Ti \overset{+}{\underset{ClAlMeCl_2^-}{<}} \overset{Me}{\phantom{<}} \longrightarrow$$
$$\textbf{17} \qquad\qquad\qquad \textbf{19}$$

$$Cp_2TiCl_2 \quad + \quad Me_2AlCl \qquad (10)$$
$$\textbf{1}$$
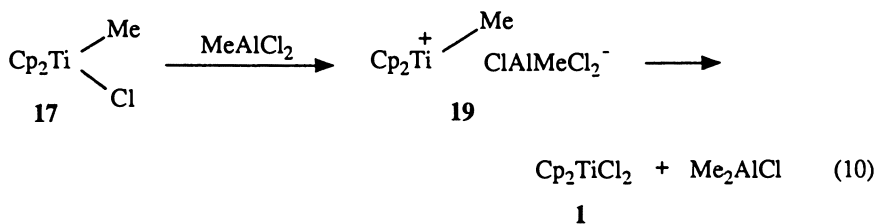
With time, again titanocene dichloride is a major product. Adding acetonitrile reforms 25% of **17**, 44% of **1**, and 31% of other cyclopentadienyltitanium products.

Polymerization of Ethylene with Trimethylsilylmethyltitanocene Chloride and an Aluminum Chloride Cocatalyst.   Compound 11, combined with either aluminum chloride in 1,2-dichloroethane or methylaluminum chloride in chloroform, was found to be an effective catalyst system for the polymerization of ethylene at 0 °C and at pressures of 30 psig. Turnover numbers of 175 per mmol of titanium per hour were observed for $AlCl_3$, and 245 per mmol of titanium per hour were observed for $MeAlCl_2$.

The resulting polyethylene had the following properties:

- mp 135–139 °C;
- infrared absorption bands consistent with those characteristic of high-density linear polyethylene: 2920, 2860, 1477, 1466, 1370, 1248, 728, and 717 (cm^{-1}); and
- mass spectrum (deep insertion at 70 eV) displaying fragments containing the Me_3Si end groups and between 22 and 25 ethylene units.

Thus, highly linear polyethylene containing trimethylsilyl end groups is produced by catalysts employing compound 11.

Discussion

The relative shortening of the titanium–methylene bond length in angstroms in 11, compared with the titanium–η^1 carbon distance in $Cp_2Ti(\eta^1-Cp)_2$, can be attributed to σ-bond hyperconjugation (20b–20c) operative in the crystalline state. The polar titanium–chlorine bond would further enhance this effect (20a).
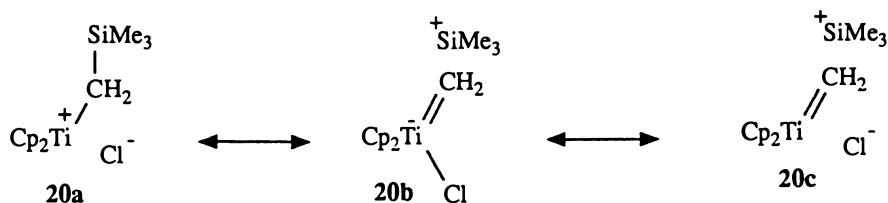
Even in solution, the changes in the ^1H NMR chemical shifts as a function of the donor or polar character of the solvent indicate that the electron-deficient titanium (20a) may undergo coordination with stronger n- or π-donors dimethyl sulfoxide and hexamethylphosphoramide or toluene and mesitylene, as shown in Table I, thereby increasing the electron density about titanium and shifting the CH_2 signal to higher magnetic field. The effects of n- and π-donors on the chemical shift of the Cp protons seems to be opposite: n-donors deshield while π-donors shield such protons. A

Stuart–Briegleb model of **11** (Figure 1) shows that such solvent coordination would have to occur from the flank of the Ti–Cl bond *anti* to the CH_2SiMe_3 group (**20e**).

With such relatively weakly coordinating solvents as the haloalkanes, the downfield chemical shift exhibited by the CH_2 signal does not correlate with dipole moment but is the greatest for chloroform. Because of the known acidity of $H–CCl_3$, this result suggests that hydrogen bonding may be operative in enhancing the Ti–Cl bond polarization (**20a**) and hence in deshielding the CH_2 protons (**20f**).

From the crystal structure of the adduct, $Cp_2TiCl_2 \cdot MeAlCl_2$, it is known that the Lewis acidic $MeAlCl_2$ coordinates with the already polarized Ti–Cl bond and stretches it by a further 0.16 Å. A similar effect would be expected upon treating methyltitanocene chloride (**9**) or its trimethylsilyl derivative (**11**) with such Lewis acids as $AlCl_3$ or $MeAlCl_2$. In these cases, the stretching of the Ti–Cl bond by the Ti—Cl—$AlCl_2R'$ interaction should be even greater because the CH_3 or CH_2SiMe_3 group can release electron density to the developing positive charge on titanium (**21a**).
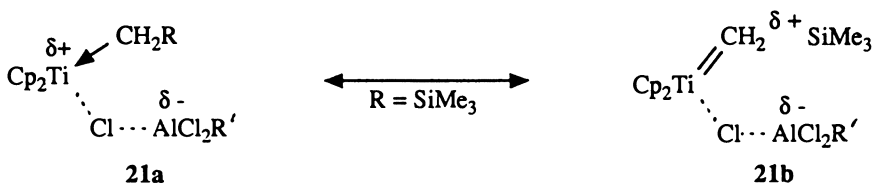
Again, by σ-bond hyperconjugation the trimethylsilyl derivative (**21b**) should be better able to sustain such developing positive charge. Such interactions should lead to downfield shifts in the ${}^1H$ NMR signals of the CH_3 or CH_2 groups, and indeed, shifts in the magnitude of $+0.8$ to $+2.0$ ppm have been observed.

The further crucial aspect of such interactions is whether the Ti–Cl bond is completely severed by such Lewis acids and whether a titanocenium cation is thereby formed. Although significant downfield shifts in ${}^1H$ signals of the CH_3 group in **9** and of CH_2 group in **11** are caused by Lewis acids, it cannot be concluded whether such shifts arise from an adjacent positively polarized titanium (**22a**) or from a titanocene cation (**22b**).

$$\text{Cp}_2\text{Ti} \overset{\displaystyle \text{CH}_2\text{SiMe}_3}{\underset{\displaystyle \text{Cl} \cdots \text{AlCl}_3}{\big/}}$$

22a

or

$$\text{Cp}_2\text{Ti} \overset{\displaystyle \text{CH}_2\text{SiMe}_3}{\underset{\displaystyle +}{\big/}} \quad \text{Cl}_4\text{Al}^-$$

22b
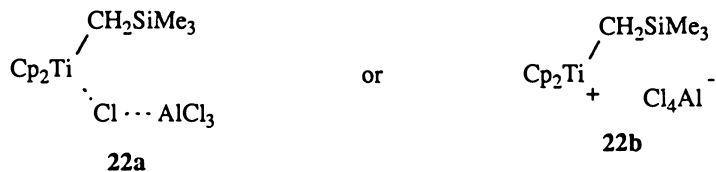
However, when the interaction of trimethylsilyl derivative 11 with $AlCl_3$ at −23 °C in 1,2-dichloroethane was monitored by ^{27}Al NMR spectroscopy, the major ^{27}Al signal initially was at 103.3 ppm. This value is exactly that previously reported for the tetrachloroaluminate anion (19). Thus, for 11 there is no doubt that the Ti–Cl bond is ruptured completely by the electrophilic $AlCl_3$ and that the titanocenium ion pair 22b is generated. Having thus established that such cations are generated in this case, one can readily trace the reason for such cation stabilization to the same σ-bond hyperconjugation already evident in the neutral trimethylsilyl derivative itself (20a–20c).

Such titanocenium cations have been postulated to be the active catalyst in the Ziegler polymerization of ethylene in homogeneous media. Therefore, one would expect combinations of the trimethylsilyl derivative and $AlCl_3$ to cause polymerization of ethylene. Further, Me_3SiCH_2 end groups should appear in the resulting polyethylene. Both expectations were fulfilled by experiment. Compound 11 by itself was inactive in polymerization but immediately became active when $AlCl_3$ was added. Any donor solvent or Lewis base (ethers or amine) that vitiated the action of the Lewis acid also destroyed the catalytic activity. As to the resulting high-density linear polyethylene produced, mass spectral measurements of the solid by direct insertion into the ionization chamber readily revealed the presence of the Me_3Si group and its fragmentation peaks.

A remaining significant question for the titanocenium cations detected in this study is the nature of their ion-pairing and solvation. This matter is under active investigation.

Acknowledgments

References

1. Boor, J., Jr. *Ziegler–Natta Catalysis and Polymerization*; Academic: New York, 1979; p 670.
2. Ziegler, K.; Holzkamp, E.; Breil, H.; Martin, H. *Angew. Chem.* **1955**, *67*, 541.
3. Natta, G.; Pino, P.; Carradini, P.; Danusso, F.; Mantica, E.; Mazzanti, G.; Moraglio, G. *J. Am. Chem. Soc.* **1955**, *77*, 1708.
4. Eisch, J. J.; Boleslawski, M. P.; Piotrowski, A. M. *Transition Metals and Organometallics as Catalysts for Olefin Polymerization*; Kaminsky, W.; Sinn, H., Eds.; Springer-Verlag: Berlin, 1988; p 371.
5. Breslow, D. S.; Newburg, N. R. *J. Am. Chem. Soc.* **1957**, *79*, 5072.
6. Long, W. P. *J. Am. Chem. Soc.* **1959**, *81*, 5312.
7. Breslow, D. S.; Newburg, N. R. *J. Am. Chem. Soc.* **1959**, *81*, 81.
8. Dyachkovskii, F. S. *Visn. Mol. Soedin* **1965**, *7*, 114.
9. Eisch, J. J.; Galle, J. E.; Piotrowski, A. M. *Transition Metal Catalyzed Polymerizations: Alkenes and Dienes*; Quirk, R. P., Ed.; Harwood Academic: New York, 1983; Part B, p 799.
10. Fink, G.; Zoller, W. *Makromol. Chem.* **1981**, *182*, 3265.
11. Eisch, J. J.; Piotrowski, A. M.; Brownstein, S. K.; Gabe, E. J.; Lee, F. L. *J. Am. Chem. Soc.* **1985**, *107*, 7219.
12. Eisch, J. J.; Manfre, R. J.; Komar, D. A. *J. Organomet. Chem.* **1978**, *159*, C13.
13. Hanstein, W.; Berwin, H. J.; Trayler, J. G. *J. Am. Chem. Soc.* **1970**, *92*, 829.
14. Eisch, J. J.; King, R. B. *Organometallic Syntheses*; Academic: New York, 1981; Part I.A.
15. Brown, H. C. *Organic Synthesis via Boranes*; Wiley: New York, 1975; Chapter 9.
16. Jeffery, J.; Lappert, M. F.; Luong-Thi, N. T.; Webb, M.; Atwood, J. L.; Hunter, W. E. *J. Chem. Soc., Dalton Trans.* **1981**, 1593.
17. Waters, J. A.; Mortimer, G. A. *J. Organomet. Chem.* **1970**, *22*, 417.
18. Krüger, C.; Werner, S. Max-Planck-Institut für Kohlenforschung, Mülheim (Ruhr), Germany, unpublished results.
19. Nöth, H.; Rürlander, R.; Wolfgardt, P. *Z. Naturforsch.* **1982**, *37b*, 29.
20. Eisch, J. J.; Pombrik, S. I. State University of New York at Binghamton, unpublished results, 1990.

Homogeneous Chromium Catalysts for Olefin Polymerization

K. H. Theopold, R. A. Heintz, S. K. Noh, and B. J. Thomas

Department of Chemistry and Biochemistry and Center for Catalytic Science and Technology, University of Delaware, Newark, DE 19716

Chromium-based heterogeneous catalysts are widely used for the polymerization of ethylene. We prepared a class of paramagnetic chromium(III) alkyls, which serve as models for the active sites of commercially used catalysts (Phillips catalyst, Union Carbide catalyst). A wide variety of cationic, neutral, or anionic complexes containing the pentamethylcyclopentadienyl ($Me_5Cp, Cp*$) ligand and one, two, or three alkyl groups were prepared and characterized structurally and by magnetic measurements. Cationic $Cp*Cr(THF)_2CH_3]^+BPh_4^-$ (THF is tetrahydrofuran) and neutral $Cp*Cr[CH_2Si(CH_3)_3]_2$ were found to polymerize ethylene at ambient pressure and room temperature or below ($-40\ °C$). The polyethylene exhibited relatively low molecular weights and narrow dispersities. A comparison was made between the reaction of $[Cp*(dmpe)Cr^{III}CH_3]^+PF_6^-$ and $Cp*(dmpe)Cr^{II}CH_3$ with ethylene (dmpe is 1,2-bis(dimethylphosphino)ethane). The chromium(III) alkyl gave polyethylene, but the chromium(II) alkyl yielded mostly propene. This contrast suggested that $+III$ is the active oxidation state of chromium-based catalysts. Finally, $Cp*(py)Cr(CH_3)(O$-t-$Bu)$ catalyzes the ring-opening metathesis polymerization (ROMP) of norbornene. This activity indicates formation of a chromium–methylene complex.

THE COORDINATION POLYMERIZATION OF SMALL OLEFINS (such as ethylene and propene) is arguably the most important industrial process involving organometallic intermediates (*1–3*). Despite a large research effort and much practical progress since the original discoveries by Ziegler (*4*) and Natta (*5*),

a detailed understanding of the reaction mechanisms and the factors that determine activity and selectivity of the polymerization catalysts remains elusive.

Among the transition metals that catalyze the polymerization of olefins, chromium occupies a prominent position. Broadly speaking, two classes of chromium-based heterogeneous catalysts are used commercially. The so-called Phillips catalyst (6) is prepared by depositing CrO_3 on silica, followed by activation with hydrogen. On the other hand, Union Carbide developed catalysts formed by treatment of silica with low-valent organometallic compounds, most notably chromocene (Cp_2Cr, Cp is cyclopentadienyl) (7, 8). Questions about the chemical nature of the active site(s), the oxidation state of the active chromium, and the mechanism of initiation have been the subject of a long-standing debate, which continues to this day.

The study of organometallic compounds of chromium in solution can make a valuable contribution to the understanding and rational modification of these heterogeneous catalysts. However, much of the known organometallic chemistry of chromium concerns low-valent carbonyl derivatives and diamagnetic complexes with 18-electron configurations. Such molecules are unlikely candidates for modeling highly reactive (coordinatively unsaturated) and oxide-supported chromium alkyls. Open-shell molecules (paramagnetic organometallic compounds or "metallaradicals") may be more reactive and thus more appropriate models for catalytic intermediates. With this possibility in mind, we are exploring the reactivity of a class of paramagnetic chromium(III) alkyls. Herein we summarize our recent results in the synthesis and characterization of paramagnetic chromium alkyls and their reactions with olefins.

Synthesis

Chart I shows a juxtaposition of the presumed active site of the Union Carbide catalysts ($Cp_2Cr–SiO_2$) with various molecules prepared in our laboratory (9–13). The active site has been described as "an adsorbed, divalent chromium species which is still bonded to one cyclopentadienyl ligand" (7). We will ignore for now the contentious question of oxidation state. The well-characterized molecules shown in Chart I are apparently good homogeneous structural models of the catalyst. They have in common the cyclopentadienyl ligand, an alkyl group, and a variety of ancillary ligands that substitute for the attachment to the silica support. All the compounds shown contain chromium in the formal + III oxidation state and are thus paramagnetic.

Crystal structure determinations and magnetic susceptibility measurements were used extensively to characterize this class of organometallic compounds. For example, Figure 1 shows the crystal structure and the magnetic behavior of $[CpCr(CH_3)(\mu\text{-}Cl)]_2$ (9). The structural studies generally feature pseudooctahedral coordination of chromium centers. The metal

(e.g. R = CH$_2$Si(CH$_3$)$_3$)   (e.g. R = Me)
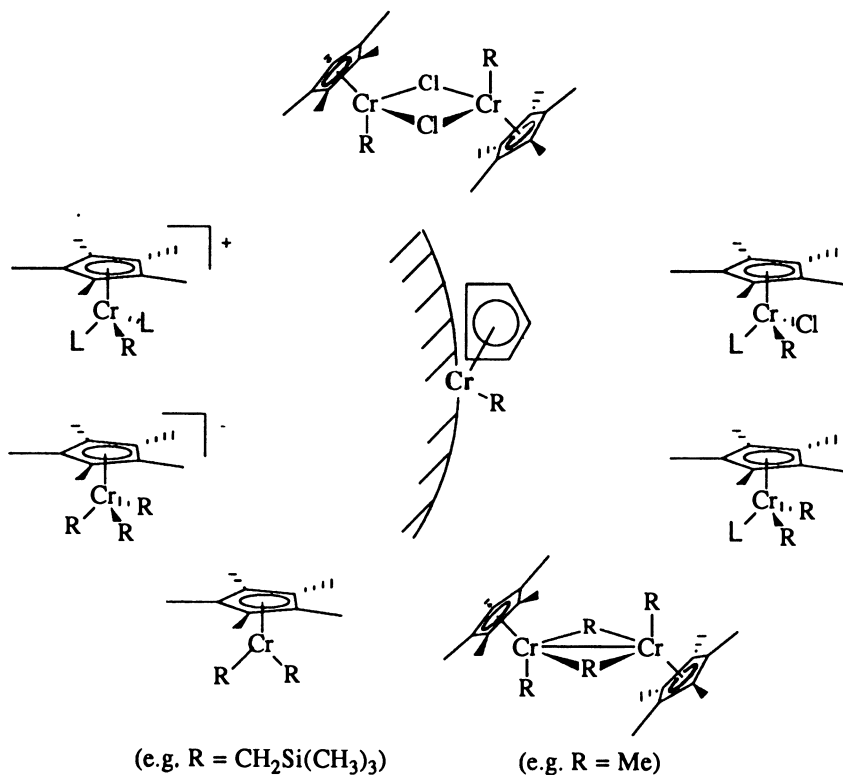
Chart 1. Presumed active site of Union Carbide catalysts juxtaposed with molecules prepared in our laboratory.

usually exhibits a 15-electron configuration, but in some cases 13-electron compounds have been isolated or observed. Mononuclear complexes invariably have temperature-independent effective magnetic moments consistent with three unpaired electrons (d^3, $\mu_{eff} \geq 3.8$ μ_B; μ_{eff} is the effective magnetic moment and μ_B is the Bohr magneton). However, in polynuclear complexes with bridging ligands, the chromium centers exhibit antiferromagnetic coupling and metal–metal bonding.

Chromium–chromium pairs with cooperative interactions between neighboring metal atoms have been invoked to explain certain features of the Phillips catalyst. Related molecular complexes may serve as precedent for postulated intermediates and allow testing of their catalytic activity. Scheme I shows a series of conversions of extremely electron-deficient dinuclear chromium complexes with bridging hydrocarbon fragments (*11*). The three-center–two-electron methyl bridges lead to metal–metal bonding due to core levels, which is reflected in unusually short Cr–Cr distances and low magnetic moments. Figure 2 depicts the molecular structures of
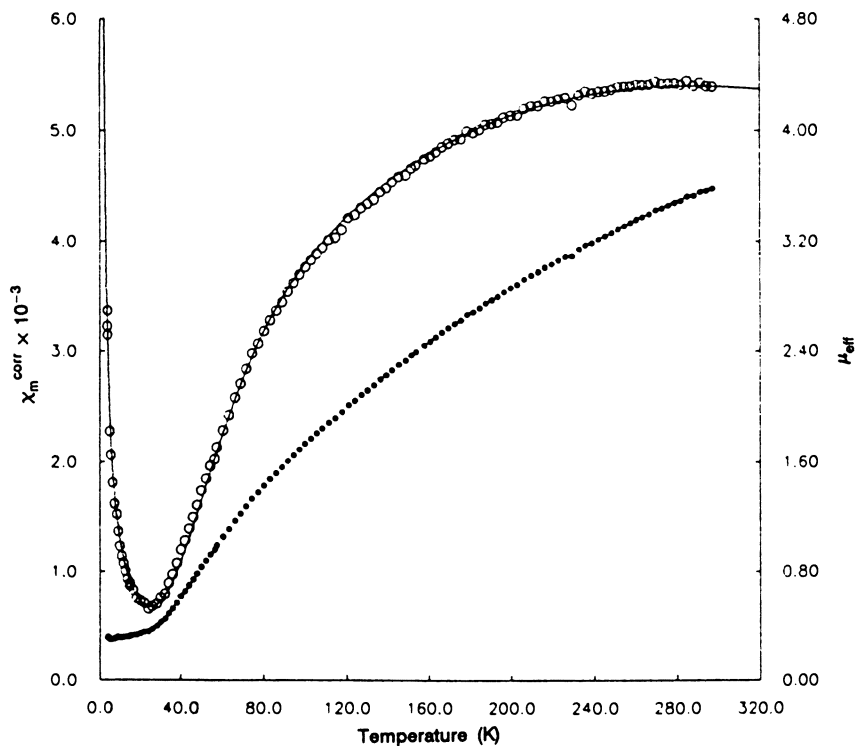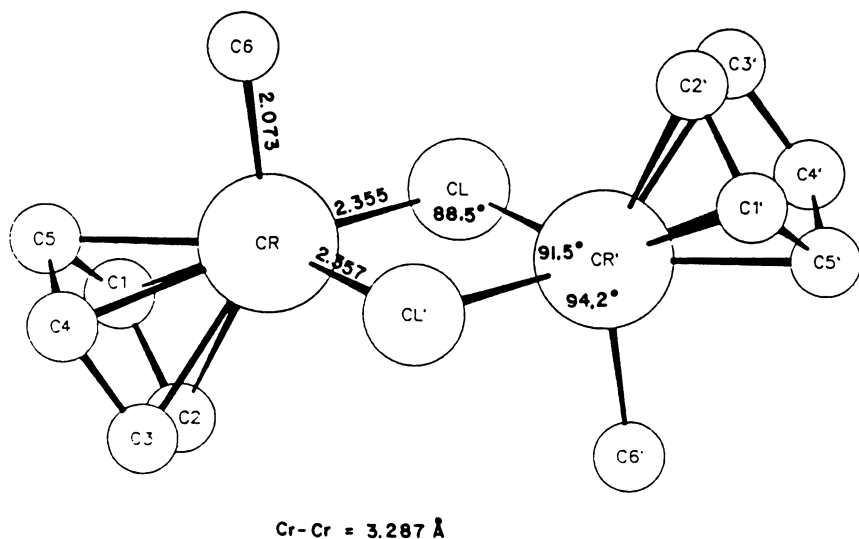
Figure 1. The molecular structure and temperature dependence of the molar magnetic susceptibility (χ_m, open circles) and the effective magnetic moment (μ_{eff}, filled circles) of $[Cp(CH_3)Cr(\mu\text{-}Cl)]_2$.
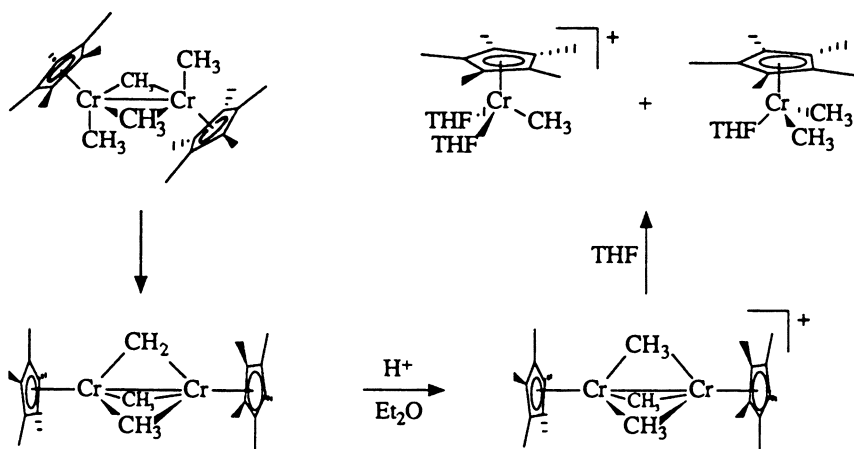
Scheme I.

$[Cp*(CH_3)Cr(\mu\text{-}CH_3)]_2$ and $[Cp*Cr(\mu\text{-}CH_3)]_2(\mu\text{-}CH_2)$. The former catalyzes the polymerization of ethylene, albeit slowly; the latter does not react with ethylene at ambient temperature. These molecules are highly unusual in the sense that they exhibit metal–metal bonds between octahedral Cr(III) ions.

Most of the compounds shown in Chart I actually show little or no catalytic activity for ethylene polymerization. Despite their low electron count, they are coordinatively saturated and must dissociate a ligand to enable binding and subsequent insertion of ethylene. Thus we prepared compounds containing weakly bound ligands. Abstraction of halide from $[Cp*Cr(CH_3)(\mu\text{-}Cl)]_2$ in tetrahydrofuran (THF) solution or protonation of $Cp*(THF)Cr(CH_3)_2$ with $HNEt_3{}^+BPh_4{}^-$ in the same solvent yielded the cationic alkyl complex $[Cp*Cr(THF)_2(CH_3)]^+BPh_4{}^-$ (*12, 13*). The two THF ligands are bound strongly enough to allow isolation and indeed structural characterization of the complex (Figure 3). However, some THF dissociates in CH_2Cl_2 solution, leaving a coordinatively unsaturated chromium alkyl in equilibrium with the coordinatively saturated precursor.

Polymerization Catalysis

$[Cp*Cr(THF)_2(CH_3)]^+BPh_4{}^-$ (4.5 mM in CH_2Cl_2) catalyzed the polymerization of ethylene at room temperature and 1.0–1.5 atm of pressure. Ethylene uptake measurements showed a brief rise in activity, followed by a period of rapid polymerization and eventually deactivation of the catalyst. Typical yields were 1.5 g of polyethylene per 60 mg of catalyst, corresponding to an average of 600 turnovers. The time from the onset of polymerization to complete deactivation was approximately 1 h, and at the point of highest
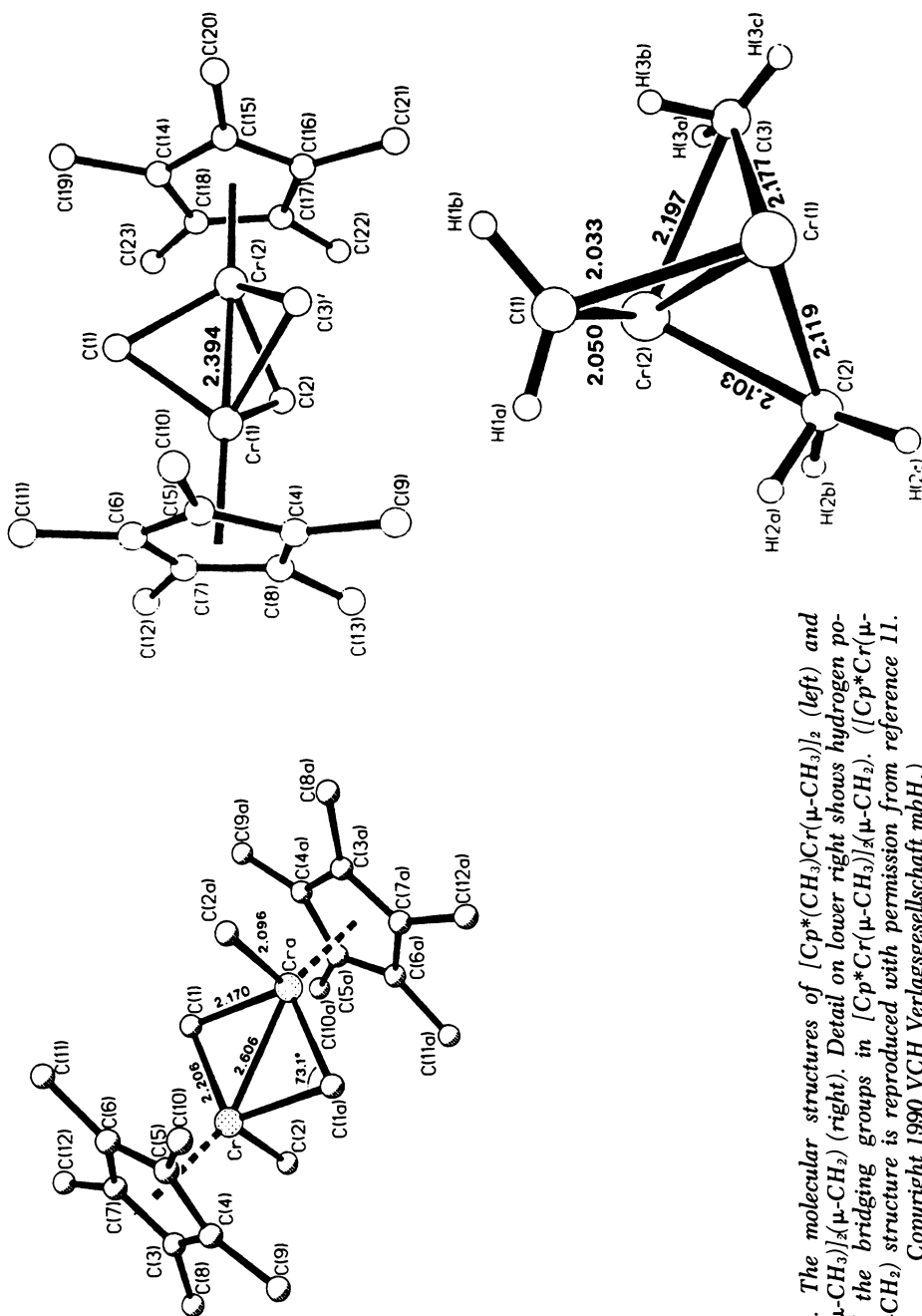
Figure 2. The molecular structures of [Cp*(CH₃)Cr(μ-CH₃)]₂ (left) and [Cp*Cr(μ-CH₃)]₂(μ-CH₂) (right). Detail on lower right shows hydrogen position of the bridging groups in [Cp*Cr(μ-CH₃)]₂(μ-CH₂). ([Cp*Cr(μ-CH₃)]₂(μ-CH₂) structure is reproduced with permission from reference 11. Copyright 1990 VCH Verlagsgesellschaft mbH.)
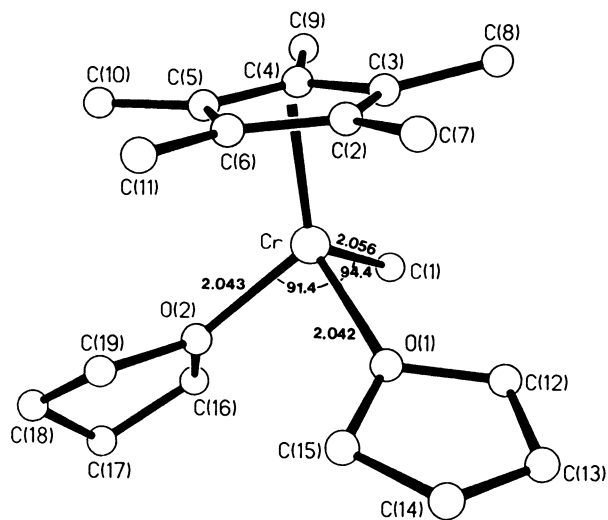
Figure 3. [Cp*Cr(THF)₂CH₃]⁺ BPh₄⁻ (tetraphenylborate counterion omitted for clarity).

activity the turnover frequency was ~0.7 s^{-1} (assuming all chromium was active). The rate of polymerization was decreased dramatically by addition of THF, presumably because of a shift of the dissociation equilibrium (eq 1).
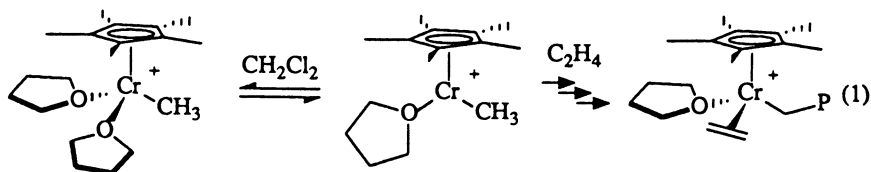
The equilibrium constant for this dissociation was estimated by NMR experiments to be $K_{eq} = 1 \times 10^{-3}$ M at 20 °C. During the course of the polymerization the color of the solution slowly changed from red-brown to purple. Attempts to isolate a chromium-containing complex from spent catalyst solutions were unsuccessful. The polyethylene was isolated by filtration, washed with CH_2Cl_2, and dried under vacuum before characterization. It

had a slight pink coloration, indicating some level of residual chromium. The IR spectrum of the polymer was indistinguishable from that of authentic high-density polyethylene. Its melting range was 135–140 °C. Table I lists the result of molecular weight determinations by gel permeation chromatography (GPC) and branching data from ^{13}C NMR spectroscopy. The molecular weights were low and their distributions M_w/M_n were relatively narrow (M_w is weight-average molecular weight; M_n is number-average molecular weight; M_w/M_n is polydispersity).

Table I. Polyethylene Characterization

$P_{ethylene}$ (atm)	Temperature (°C)	Added THF (equiv)	M_w	M_n	M_w/M_n	Branching ($R/1000\ CH_2$)
1.5	20	—	33,760	17,520	1.93	?
1.5	10	—	47,240	20,160	2.34	4.0
1.5	0	—	77,070	16,740	4.60	0
1.5	20	1	23,020	14,310	1.61	?
1.5	20	3	24,370	14,970	1.63	2.6
1.1	>25	—	19,320	10,280	1.88	?

NOTE: Polyethylene was produced by the reaction of 60 mg of [Cp*Cr(THF)$_2$Me]$^+$BPh$_4^-$ in 20 mL of CH$_2$Cl$_2$, 4.5 × 10^{-3} M.

The cationic nature of [Cp*Cr(THF)$_2$(CH$_3$)]$^+$BPh$_4^-$ nicely complemented the emerging notion that positively charged alkyls comprise the active sites of Ziegler–Natta catalyst preparations based on Group 4 elements (*14–19*). However, cationic nature is apparently not a requirement. We subsequently found another compound (i.e., the neutral dialkyl Cp*Cr[CH$_2$Si(CH$_3$)$_3$]$_2$) that is an even more active catalyst for the polymerization of ethylene.

Because of the steric bulk of the trimethylsilylmethyl ligands—and by contrast to [Cp*Cr(CH$_3$)$_2$]$_2$—this compound is monomeric even in the solid state. Its effective magnetic moment is temperature-independent, and the value of μ_{eff} (4.0 μ_B) is consistent with three unpaired electrons. In this complex chromium exhibits a 13-electron configuration and has an open coordination site for binding of ethylene. Pentane solutions of Cp*Cr[CH$_2$Si(CH$_3$)$_3$]$_2$ rapidly polymerized ethylene at temperatures as low as –42 °C. Polymer molecular weights (M_w 20,100–143,000) and dispersities (M_w/M_n 2.98–7.06) were similar to the samples prepared with the cationic catalyst. Neither of the two catalysts polymerize propene, although some lower oligomers are apparently formed in the reaction with [Cp*Cr(THF)$_2$(CH$_3$)]$^+$BPh$_4^-$.

Active Oxidation State

The valence state of the active site of chromium-based catalysts has been the subject of much controversy. Oxidation states between +II and +V

have been suggested. Our results prove that chromium in its ubiquitous and very stable +III oxidation state catalyzes the polymerization of ethylene. However, in light of the credit generally given to divalent chromium on heterogeneous catalysts, we thought it worthwhile to find out what effect reduction would have on our catalysts.

Figure 4 depicts the cyclic voltammogram of a THF solution of [Cp*(dmpe)CrCH$_3$]$^+$PF$_6^-$ [dmpe is 1,2-bis(dimethylphosphino)ethane]. The complex exhibits a reversible reduction wave at ca. -2.0 V vs. the Cp$_2$Fe$^+$-Cp$_2$Fe couple. Chemical reduction with Na–Hg yielded the neutral Cr(II) alkyl Cp*(dmpe)CrCH$_3$, which could be isolated and structurally characterized by X-ray diffraction. The availability of constitutionally identical Cr(III) and Cr(II) alkyls allowed a direct comparison of the catalytic activity of chromium in both oxidation states.

Reaction of ethylene with [Cp*(dmpe)CrCH$_3$]$^+$PF$_6^-$ required elevated temperatures (because of the greater coordinating power of the dmpe ligand), but at 90 °C reaction ensued and yielded polyethylene. Cp*(dmpe)CrCH$_3$, on the other hand, reacted with ethylene at room temperature. However, the major product of this reaction was propene; no polyethylene was formed. Apparently ethylene inserts into the chromium–carbon bond, but β-hydrogen elimination of propene is more facile than continued insertions. These results clearly suggest that +III is the more appropriate oxidation state for the active site of chromium-based polymerization catalysts.

Ring-Opening Metathesis Polymerization

Olefin polymerization catalysts are closely related chemically to metathesis catalysts. The former depend on reactive metal alkyl moieties; the latter feature an interplay between metal alkylidenes and metallacyclobutanes. A long-standing problem of the olefin metathesis reaction has been the incompatibility of the traditional early metal catalysts with heteroatom substituents (especially those containing oxygen) of functionalized olefins. A possible path to the solution of this problem is the search for less oxophilic (i.e., late transition metal) catalysts. We thus began an investigation into the possibility of preparing chromium(III) alkylidenes for use as metathesis catalysts.

A well-precedented route to metal alkylidenes utilizes α-hydrogen abstraction from metal alkyls. We found that Cp*(py)Cr(CH$_3$)(O-*t*-Bu) (py is pyridine) catalyzes the ring-opening metathesis polymerization (ROMP) (20–24) of norbornene. Heating of a toluene solution of this complex with a large excess of norbornene to ~60 °C gave a high yield of polymer (>85% isolated). Scheme II depicts the proposed mechanism of this reaction. The key feature is the generation of the coordinatively unsaturated chromium methylene complex by deprotonation of a methyl group with the internal base *tert*-butoxide (i.e., an α-abstraction).
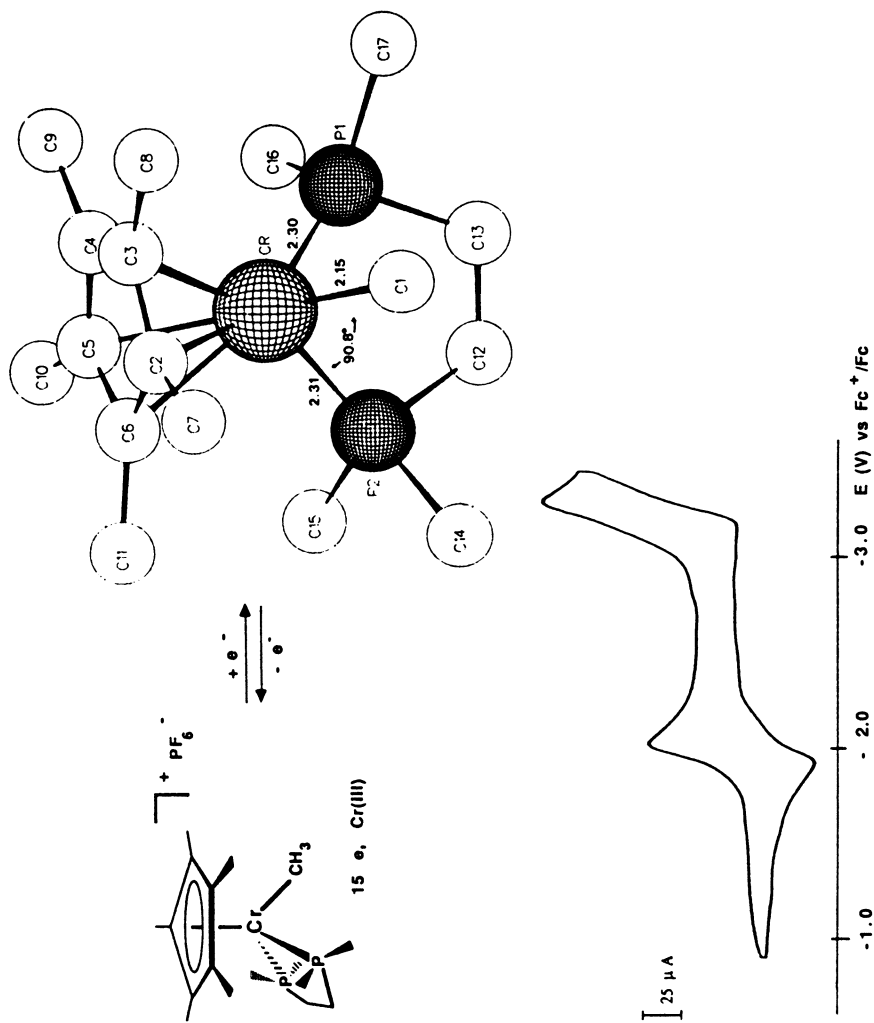
Figure 4. Cyclic voltammogram of [Cp*Cr(dmpe)CH₃]⁺PF₆⁻ in THF (bottom) and the molecular structure of neutral Cp*Cr(dmpe)CH₃ (top right).
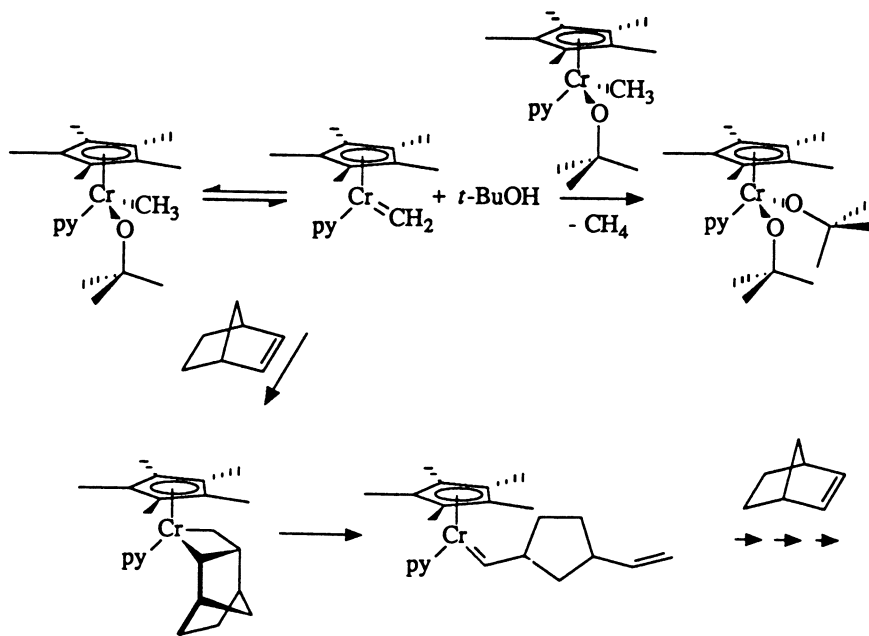
Scheme II.

The evidence for this event includes the observed formation of methane and $Cp^*(py)Cr(O\text{-}t\text{-}Bu)_2$ (from the reaction of the catalyst precursor with the liberated *tert*-butyl alcohol) as well as the catalytic activity. The decomposition of $Cp^*(py)Cr(CH_3)(O\text{-}t\text{-}Bu)$ to the active catalyst is a slow reaction that continues over the whole course of the polymerization. The polymer would thus be expected to show a broad molecular weight distribution, and GPC measurements confirmed this expectation $(M_w/M_n = 7.3)$.

The potential importance of this observation lies in the way the catalyst is generated (i.e., by breaking of a metal–oxygen bond). If chromium-based metathesis catalysts can be developed, they may be expected to be less sensitive to oxygen functionalities. Thus, they may be used in the metathesis and ROMP catalysis of functionalized olefins.

References

1. *Transition Metal Catalyzed Polymerizations*; Quirk, R. P., Ed.; Cambridge University Press: Cambridge, 1988.
2. Karol, F. J. *Catal. Rev.–Sci. Eng.* **1984**, *26*, 557.
3. Sinn, H.; Kaminsky, W. *Adv. Organomet. Chem.* **1980**, *18*, 99.
4. Ziegler, K.; Holzkamp, E.; Breil, H.; Martin, H. *Angew. Chem.* **1955**, *67*, 541.
5. Natta, G.; Pino, P.; Carradini, P.; Danusso, F.; Mantica, E.; Mazzanti, G.; Moraglio, G. *J. Am. Chem. Soc.* **1955**, *77*, 1708.

6. Clark, A. *Catal. Rev.* **1969**, *3*, 145.
7. Karol, F. J.; Karapinka, G. L.; Wu, C.; Dow, A. W.; Johnson, R. N.; Carrick, W. L. *J. Polym. Sci., Polym. Chem. Ed.* **1972**, *10*, 2621.
8. Karol, F. J.; Brown, G. L.; Davison, J. M. *J. Polym Sci., Polym. Chem. Ed.* **1973**, *11*, 413.
9. Richeson, D. S.; Hsu, S.-W.; Fredd, N. H.; Van Duyne, G.; Theopold, K. H. *J. Am. Chem. Soc.* **1986**, *108*, 8273.
10. Noh, S. K.; Sendlinger, S. C.; Janiak, C.; Theopold, K. H. *J. Am. Chem. Soc.* **1989**, *111*, 9127.
11. (a) Noh, S. K.; Heintz, R. A.; Janiak, C.; Sendlinger, S. C.; Theopold, K. H. *Angew. Chem.* **1990**, *102*, 805; (b) *Angew. Chem., Int. Ed. Engl.* **1990**, *29*, 775.
12. Thomas, B. J.; Theopold, K. H. *J. Am. Chem. Soc.* **1988**, *110*, 5902.
13. Thomas, B. J.; Noh, S. K.; Schulte, G. K.; Sendlinger, S. C.; Theopold, K. H. *J. Am. Chem. Soc.* **1991**, *113*, 893.
14. Eisch, J. J.; Piotrowski, A. M.; Brownstein, S. K.; Gabe, E. J.; Lee, F. L. *J. Am. Chem. Soc.* **1985**, *107*, 7219.
15. Jordan, R. F.; Bajgur, C. S.; Willett, R.; Scott, B. *J. Am. Chem. Soc.* **1986**, *108*, 7410.
16. Jordan, R. F.; LaPointe, R. E.; Bajgur, C. S.; Echols, S.; Willett, R. *J. Am. Chem. Soc.* **1987**, *109*, 4111.
17. Gassman, P. G.; Callstrom, M. R. *J. Am. Chem. Soc.* **1987**, *109*, 7875.
18. Taube, R.; Krukowka, L. *J. Organomet. Chem.* **1988**, *347*, C9.
19. Hlatky, G. G.; Turner, H. W.; Eckman, R. R. *J. Am. Chem. Soc.* **1989**, *111*, 2728.
20. Calderon, N. *J. Macromol. Sci., Rev. Macromol. Chem.* **1972**, *C7(1)*, 105.
21. Katz, T. J.; Lee, S. J.; Shippey, M. A. *J. Mol. Catal.* **1980**, *8*, 219.
22. Gilliom, L.; Grubbs, R. H. *J. Am. Chem. Soc.* **1986**, *108*, 733.
23. Wallace, K. C.; Schrock, R. R. *Macromolecules* **1987**, *20*, 450.
24. Schrock, R. R.; Feldman, J.; Cannizzo, L. F.; Grubbs, R. H. *Macromolecules* **1987**, *20*, 1172.

Author Index

Affiliation Index

Subject Index

C

¹³C NMR studies
  carbonylhydridorhodium complexes, 408
  equilibrium at two CO pressures, 408*f*
Cage structure, polysilsesquioxanes, 554–555
Carbene addition, aromatic ring, 450
Carbene insertion, substitution by an ether
     or ester oxygen, 457
Carbenoid intermediates, generation, 482
Carbenoid reactions
  active intermediates, 444
  insertion, conformational preferences, 451
Carbocyclic rings, regioselectivity, 467–468
Carbon–carbon bonds, formation reactions,
     567
Carbon dioxide, reduction of methanol,
     507–513
Carbon–hydrogen activation
  Rh(I) photocatalysis, 110*f*
  trimethylphosphine complex, 108
Carbon–hydrogen bond(s), activation in
     alkanes and other organic molecules,
     211–220
Carbon–hydrogen bond functionalization,
     mercury-photosensitized, 197–210
Carbon–hydrogen insertion reactions
  catalytic intramolecular, 443–461
  cyclopentanones, 445–448
  diastereoselectivity, 446
  lactams, 448–455
  lactones, 455–458
  regioselectivity, 446
Carbon–hydrogen oxidative addition
  homogeneous catalysis, 182
  preferred active species, 186
Carbon monoxide
  activation by metalloradicals, 249–259
  monomeric tetramesitylrhodium(II)
     complex, 254
  one-electron activation, 250
  problems with spectroscopy, 25
  rhodium complexes, 25–28
Carbon–oxygen bonds
  activation, 515–528
  bond energy, 516
  methods for cleavage, 516
Carbonyl
  decay kinetics, 115
  dissociation energies, 78
  dissociation from HCo(CO)₄, 77–78
  energy of dissociation from CoH(CO)₄,
     305
  energy profile for insertion into Co–CH₃
     bond, 84*f*
  formation of basic magnesium iodides, 317
  π-acceptor ligands, 87–88
  reversible migratory insertion into
     alkyl–metal bond, 112

Carbonyl complexes
  infrared spectroscopic data, 299*f,t*
  spectral data, 300*t*
Carbonyl compounds, reduction, 193*t*
Carbonyl dissociation, carbonyl-free
     rhodium hydrides, 406
Carbonyl exchange
  radical mechanism, 38
  rate constants, 37–39
  temperature stability under pressure, 38
Carbonyl ligands, catalyst function, 399–400
Carbonyl photodissociation
  laser flash photolysis, 113
  methane matrix, 114
Carbonyl stretching frequencies, rhodium
     and cobalt complexes, 27–28
Carbonylation
  benzene, 185–189
  C–H bond of hydrocarbons, 185–189
  catalyzed by transition metal complexes,
     277–296
  diversion to reductive carbonylation, 324
  lithium-promoted, 384–390
  mechanism, 325*f*
  methanol, mechanism, 382*f*
  methyl acetate
     kinetics, 378–380*f*, 385–389
     rhodium-catalyzed, 377–394
  methyl acetate and methanol, parameters,
     393*t*
  methyl acetate to acetic anhydride,
     proposed mechanism, 392*f*
  reduction of CH₃OH by Co(CO)₄⁻, 509
  sodium-promoted, 390
  temperature dependence, 381
  yields of secondary reactions of aldehydes,
     188*t*
Carbonylation–homologation, 1-butanol and
     ethanol, 310–321
Carbonylmanganese compounds,
     unsaturated mononuclear, 112–117
Carbonyl(methoxycarbonyl)cobalts,
     formation and thermal decomposition,
     510
Carbonylrhodium, intensity of IR bands, 12
Carbonylruthenium species
  CO stretching frequencies, 315*f*
  interaction of clusters with metal oxide
     surfaces, 313
  oxides as heterogeneous promoters,
     309–321
Carbonyltriruthenium clusters
  infrared difference spectrum of transients,
     111*f*
  laser flash photolysis, 110–112
  reactions, 113*f*
  reactivities, 109–112
Carboxylic acids
  asymmetric hydrogenation, 130–131
  role in catalytic reaction, 375

Cobalt—*Continued*
  reduction of methanol, 507–513
  role in oxidation of cyclohexanone,
    100–102
  uncontracted triple-ζ Slater-type orbitals,
    basis set for shells, 76
Cobalt–carbon bond, cleavage, 491
Cobalt catalysis, reductive carbonylation of
  methanol, 323
Cobalt-catalyzed hydroformylation
  mechanism, 75, 76*f*
  olefins, reaction mechanism, 13–15
  product formation, 86
Cobalt(II) porphyrin, reactions with CO,
  252–253
Colloids
  active catalyst precursors, 543
  intermediacy in hydrosilation, 541–549
Competitive reactions
  different substrates, 59
  epoxidation
    olefin pairs, 157–161
    picnic-basket porphyrins, 158*f*
    reactivity pattern, 161
    results, 160*t*
  ^{1}H NMR spectra of hydrogenation, 59*f*
  polarization decay, 60
  trapping, transient CO species, 116*f*
Conjugate addition–cyclization reactions,
  485–486*t*
Construction material, high-pressure IR
  cells, 21
Coordination compound, intermediate
  within the catalytic cycle, 8
Coordination geometries, M–M bonded
  dimer systems, 353–355
Coordination strength, σ donation and π
  back donation, 395
Coordinatively unsaturated species,
  temperature dependence, 406
Cooxidant, coupling reactions of ligands, 572
Copper
  catalyst behavior on repeated use, 484
  catalytic activity, 483–484
  Grignard reaction, 486
  tandem conjugate addition–cyclization,
    486
Coupling constant, spin density, 254
Covalent bonding, carbonyl carbon
  rehybridization, 253
Cross-dimerization, cyclohexane and
  trioxane, 202
Crystal(s)
  CIR reactors, 3
  fragility, 5–6
  polishing, 6
Crystallization, CIR reactor analyses, 12–13
Cubane reaction, oxidative addition at a
  tertiary C–H bond, 217

Cyclizations, transition metal catalysts,
  463–478
Cyclohexane
  carbonyl decay kinetics, 115*f*
  reactivities of rhodium(I) phosphine
    intermediates, 108–109
  wavelength of irradiation, 189
Cyclohexanone
  kinetic model, 101–102
  O_2 oxidation, 99–103
  oscillations in the absence of Br$^-$ ion, 102
  redox potential
    dissolved O_2 concentrations, 99–100
    visible absorbance, 100*f*
  ring-opening reactions, 101*f*
  stages in oxidation reaction, 100
Cycloisomerizations
  acetylenes, 470–472
  p-allylpalladium intermediates, 476–477
  diynes, mechanistic rationale, 471*f*
  special class of macrocyclizations, 466–467
  vinyl epoxides, 473
Cyclooctane, dehydrogenation, 190
Cyclopentanones
  asymmetric hydrogenation, 138–140
  carbon–hydrogen insertion reactions,
    445–448
  synthesis, 484–487
Cyclopropanation studies, 482–484
Cyclopropane, yield from olefins and ethyl
  diazoacetate, 484*t*
Cylindrical internal-reflectance reactors
  (CIR)
  advantages and disadvantages, 5–6
  cross-sectional diagram, 5*f*
  experimental procedure, 6–7
  photograph, 4*f*
  reaction-monitoring techniques, 3–18
Cytochrome P-450
  catalytic cycle, 154–155
  metalloporphyrin models, 156*f*

D

d-electron vacancies, platinum colloids, 545
DANTE pulse sequence, magnetization
  transfer technique, 42
Decomposition, prolonged
  hydroformylation, 372–373
Dehydroamino acids, hydrogenation, 144
Dehydrodimer, saturated functionalized
  substrates, 205
Dehydrogenation
  alkanes, 190–194
  driving force, 190
  rate-determining step, 191
Density functional method, application to
  organometallic substances, 77

Lithium
    carbonylation reaction spectra, 389
    methyl acetate and acetyl iodide
        activation, 389–390
    tandem conjugate addition–cyclization,
        486
Lithium effect
    carbonylation catalytic cycle, 391–393
    potential mechanism, 391
Lithium iodide
    complex role as promoter, 384–385
    rate-determining factors, 385
    rate of carbonylation, 386*f*

M

M–M bonds, value as reaction sites, 350
Macrocycle, C–C bond formation, 473
Macrocycle applications, natural products,
    472–476
Macrocyclization
    acetylenes, 470–472
    allylic alkylation, 464–469
Macrolide syntheses, exaltolide, 464
Magnesium oxide, promoters, 314–317
Magnetization transfer
    advantages and disadvantages, 41
    DANTE pulse sequence, 42
    examples, 43–45
    exchange broadening of resonances, 37
    inversion transfer, 41–42
    slow exchange in discrete equilibria,
        41–45
    temperature range, 41
Manganese acyl catalysts
    activity, 499*t*, 501*t*
    hydrosilation, 491
Manganese acyl-catalyzed hydrosilation,
    496–505
Manganese picnic-basket porphyrin
    catalysts, 153–162
Mechanistic studies, model substrate, 224
Mercury photosensitization
    alkane dimerization, 203–204
    C–H bond functionalization, 197–210
    dimerization, 197
    formation of H atoms, 204
    functionalized product, 201–203
    heteroatom-substituted species, 200–201
    mechanism, 198–199
    quenching by H_2 gas, 204
    reaction rate, 206
    vapor-phase selectivity, 199–200
Meso and *racemic* diastereomers, eLTTP,
    353
Metal carbenes
    C–H insertion, 451
    comparative stability, 453

Metal carbonyl stretching frequencies,
    rhodium and cobalt complexes, 27–28
Metal catalyst, role in oxidative addition,
    64–67
Metal clusters, intermediary position,
    419–420*f*
Metal formyl complexes, decarbonylation
    reaction, 83
Metal hydride bond, olefin insertion, 400
Metal oxide complexes, hydrogen activation,
    337–348
Metal oxide systems, water–gas shift, 347
Metal phosphine catalysts, selectivity, 203
Metallolactone(s)
    formation of phenol groups, 526–527
    formation pathways, 515
Metallolactone complex
    deoxygenation of phenols, 525–526
    source of benzyne, 523–524
    structure, 523*f*
Metalloradicals
    activation, structural and spin density
        changes, 252
    activation of CO, 249–259
    definition, 250
Metathesis catalysts, chromium(III)
    alkylidenes, 599
Methanol
    $Co_2(CO)_8$ solutions, reactions, 511*f*
    reduction by tetracarbonylcobalt anion
        assisted by carbon dioxide and cobalt
        cation, 507–513
    rhodium-catalyzed reductive
        carbonylation, 323–336
Methyl acetate
    activation, 390
    homologation to ethyl acetate, 321
    rhodium-catalyzed carbonylation, 377–394
Methyl acrylate, catalytic tail-to-tail
    dimerization, 485
Methyl iodide, rate dependence at two Li
    levels, 388*f*
Methyl migration, 83, 113
Methylenes, coupling with vinyls in
    dirhodium complexes, 573
Methyltitanocene chloride, structure,
    580–583
Methyltitanocenium cation
    experimental details of formation, 579–580
    soluble Ziegler catalyst system, 579
Migratory insertion
    activation barrier, 83
    alkyl into Co–CO bond, 81–85
    functionalized molecules, 215
    solvent effects, 113
    transient complexes, 333–334
Mixed-metal catalyst
    Co–Rh, 279, 289–294
    synergistic effects, 279–280, 290

Publication Date: March 1, 1992 | doi: 10.1021/ba-1992-0230.ix002

Pressure stabilization, reactive species, 36–40
Process chemistry, new science and new applications, 479–489
Product distribution, function of ruthenium concentration, 327f
Product flash-off
  continuous hydroformylation processes, 414–417
  continuous hydroformylation unit, 416f
Promoters
  carbonylruthenium iodide systems, 310
  comparison of rates, 385t
  magnesium oxide, 314–317
  selectivities, change with time, 319
  soluble and insoluble aluminum compounds, 310–314
Propene-d_3, proposed mechanism for formation, 566f
cis-2-Propenyl-1,3-dioxolanone reaction, stereospecificity, 539
Propylene carbonate, selectivities during styrene hydroformylation, 265
Propylene hydride
  ^{1}H NMR assignments, 44f
  magnetization transfer, 43–44
Proton source, water–gas shift, 344–345
Proton transfer, CH_3OH to $Co(CO)_4^-$, 509
Protonation, intermediate monohydride species, 62
Puckering, chelate ring, 148–150
Pyrrole ^{1}H line broadening, temperature dependence, 255–256f

Q

Quaternization, resistance of diphosphine complexes, 329

R

Racemization, chloride anion, 268
Radical(s), reaction of alkanes with Hg*, 208
Radical mechanism, carbonyl exchange, 38
Radicallike pathway in benzene, metalloformyl complex, 253
Rate constants, carbonyl exchange, 37–39
Reaction conditions, dependence on structures, 131
Reaction mechanism
  cobalt-catalyzed hydroformylation of olefins, 13–15
  palladium-catalyzed carbonylation of aryl halides, 9–10
  phosphine-modified rhodium-catalyzed hydroformylation of olefins, 11–13
  studies using CIR–FTIR reactors, 7
Reaction-monitoring techniques, OFCIR reactors, 16–17
Reaction order, method of initial rates, 330–332
Reaction parameters, variation, 8

Reaction rates, effect of ligand, 11
Reactive intermediates
  identification and characterization, 24–28
  oxidative addition, 213
Reactive species, pressure stabilization, 36–40
Reactivity patterns, metalloradicals with small molecules, 250
Reactor geometry, mercury photosensitization, 199–200
Reductive carbonylation
  ligand environment, 324
  methanol
    experimental procedure, 325–326
    rhodium-catalyzed reductive carbonylation, 323–336
  product distribution, 326t
Reductive elimination
  acetyl iodide, 324
  hydrogenolysis of Rh–carbon and formation of Rh(I)–hydride, 334
Regiocontrol
  bridging ligands of dirhodium(II) nucleus, 458
  electron-withdrawing groups, 447
Regioselectivity
  amide-directed chelation control, 279
  carbon–hydrogen insertion reactions, 446
  carbonylation of C–H bond, 187
  cycloisomerization, 467–468
  dehydrogenative silylation and vinylation of toluene, 194
  effective control, 456
  effects of phosphine ligands, 285
  functionalized reactions, 222–223
  1-heptanal with Pt–Sn system, 263
  1-hexene with platinum, 261
  ligand effect on linear aldehyde, 264t
  nature of solvent and ligand, 265
  reaction temperature, 468
  silylformylation and hydrosilylation, 290–291
  wavelength of irradiation, 187
Rehybridization
  carbonyl carbon, 254
  formyl radical, 257
Relative reactivities, insertion reactions, 457
Remote sensing, optical-fiber coupled high-pressure reactors, 3
Reorganization energy, rehybridization of carbonyl unit, 257
Reversibility, oxidative addition, 213
Reversible reduction wave, chromium catalyst, 599
Rhodium
  asymmetric hydroformylation, 274
  carbonylation of benzene, 185–189
  catalyst behavior on repeated use, 484
  catalyst combinations in synthesis gas chemistry, 28–29

Rhodium—*Continued*
catalyst for carbenoid reactions, 443–444
catalytic activity, 483–484
coupling of surface methylenes with surface
    vinyls, 573
electrochemical reduction of organometallic
    complexes, 261
eLTTP complex, rotational and
    conformational flexibility, 358
formation of higher hydrocarbons, 571
functionalization of C–H bonds in carbenoid
    reactions, 443–461
hydroformylation catalysts, 277–296
hydrosilation of iron acyls, 492–496
lithium effect on reaction rate, 389
olefin hydroformylation, 266–272
organic chemistry of di-μ-
    methylenedirhodium complexes,
    565–567
overall reaction selectivity, 327
performance as a catalyst, 324
potential role of dianions, 391
rate dependence at two Li levels, 387f
reductive carbonylation of methanol, 334
sterically hindered geometry, 362
water–gas shift reaction, 384
Rhodium catalysts, formation from bulky or
    nonbulky phosphine ligands, 403f
Rhodium-catalyzed reactions
carbonylation
    experimental procedures, 378–379
    methyl acetate, 377–394
    selectivity, 379
    thermodynamic parameters, 379
hydroformylation reaction, mechanism,
    400–403
oxo study, CIR in situ analyses, 11–13
reductive carbonylation of methanol,
    323–336
Rhodium complex hydroformylation catalysts
generic formula, 400f
phosphorus ligands, 399
Rhodium concentration, reaction rate
    variation, 331
Rhodium-containing species, reactions with
    carbon monoxide and dihydrogen, 25–28
Rhodium hydroformylation
1-butene
    phosphite ester ligands, 414–415t
    triethylphosphine ligand, 413t
ligand effects, 399–400
mechanism, 400–403
spectra, 271f
Rhodium hydroformylation catalysts
alkyldiphenylphosphine–rhodium
    complexes, 398
electron-donor properties, 398–399
electronic effects on synthesis, structure,
    reactivity, and selectivity, 395–418

Rhodium hydroformylation catalysts—
    Continued
selectivity for linear aldehydes, 396–397
stereochemical effects, 397–398
Rhodium(I) phosphine intermediates
flash photolysis studies, 106–109
reaction dynamics, 107f
Rhodium(II) porphyrin, reactions with CO,
    253–258
Rhodium(II) porphyrin derivatives, carbon
    monoxide activation, 249
Ring construction, carbon–carbon bond
    formation, 463–478
Ring-opening metathesis polymerization, 591,
    599–601
Ring oxidation, 226
Ring slippage, sapphire NMR tube, 40
Rotational flexibility
eLTTP complex, 358
single-atom bridge in eLTTP, 361
Ruthenium
addition to rhodium catalyst, 323
anionic clusters, 419–429
catalyst combinations in synthesis gas
    chemistry, 28–29
cycloisomerization followed by reductive
    desulfonylation, 475
homogeneous catalysts, 72
homologation of methanol to ethanol, 327
hydrogenation catalysts, 60–64
selectivity of triphenylphosphine
    complexes, 434
Ruthenium-catalyzed reactions
ethylene glycol and secondary amines, 437f
ethylene glycol with morpholine, effect of
    temperature on selectivity, 438t
morpholine with ethylene glycol, effect of
    phosphines, 435t
Ruthenium cluster anion, molecular structure,
    isolation, and characterization, 425–429
Ruthenium complexes, catalysis and
    selectivity, 436t
Ruthenium-containing species, reaction with
    dihydrogen, 24–28

S

Safety
organic–O_2 oxidations, 95
sapphire NMR tubes, 36
Sapphire NMR tubes
catalytic reactions under moderate
    pressure, 33–40
development, 35–36
intermolecular hydroacylation, 39
operation, 36
ring slippage, 40
safety, 36
Sarcosinate specialty surfactants, 238–239f

Triphenylphosphine
  ¹H NMR spectra, 423*f*
  trinuclear ruthenium cluster anions,
    reaction system, 424*f*

U

Unstable molecules, identification and
  characterization, 24–28

V

van der Waals energy map, SYBYL
  molecular-modeling program, 359*f*
Vapor-phase selectivity, mercury
  photosensitization, 199–200
Vapor-pressure biasing, skewed product mix,
  202
Vapor-selectivity effect, photochemical setup,
  199–200
Vibrational spectroscopy, homogeneously
  catalyzed reactions, 20
Vinyl
  complexes from iron acetyl compounds,
    493–494
  Fischer–Tropsch products, 571–572
  metal surfaces, 567

W

Water–gas shift
  activation barrier for catalysis, 339
  catalysis, 337–348
  cation reactivity, 340
  equilibrium, 339
  intermediate substances, 346
  involvement of proton source, 344–345
  iodocarbonyl complexes of rhodium, 384

Water–gas shift—*Continued*
  iron oxide, 340
  kinetic order in sodium formate, 342*f*
  metal centers, 347
  pentacarbonyliron, 340
Wavelength of irradiation
  cyclohexane, 189
  methyl selectivity of alkanes, 189
  regioselectivity, 187
Weitekamp proposal, parahydrogen-induced
  polarization, 50
White line, d-electron vacancies in platinum
  colloids, 544–545
Wilkinson's compound, hydrosilation of
  organoiron acetyl complexes, 491
Window materials, high-pressure IR cells, 22

X

Xenon, inert solvent, 217
p-Xylene
  electrochemical oscillations, 103
  O_2 oxidation, 103

Z

Zeolite(s), catalysts in the petroleum industry,
  154
Zeolite formation, monitoring techniques, 7
Zeolite synthesis, corrosive acidic conditions,
  6
Ziegler–Natta catalysis, molecular basis,
  575–576
Ziegler polymerization catalysts, active sites,
  575–590
Ziegler polymerization of ethylene,
  titanocenium cations, 589